frontiers | Research Topics

The Impacts of anthropogenic activity and climate change on the formation of harmful algal blooms (HABs) and its ecological consequence

Edited by
Zhangxi Hu, Aifeng Li, Zhun Li and
Margaret R. Mulholland

Published in
Frontiers in Marine Science
Frontiers in Microbiology

ISSN 1664-8714
ISBN 978-2-8325-4727-4
DOI 10.3389/978-2-8325-4727-4

About Frontiers

Frontiers is more than just an open access publisher of scholarly articles: it is a pioneering approach to the world of academia, radically improving the way scholarly research is managed. The grand vision of Frontiers is a world where all people have an equal opportunity to seek, share and generate knowledge. Frontiers provides immediate and permanent online open access to all its publications, but this alone is not enough to realize our grand goals.

Frontiers journal series

The Frontiers journal series is a multi-tier and interdisciplinary set of open-access, online journals, promising a paradigm shift from the current review, selection and dissemination processes in academic publishing. All Frontiers journals are driven by researchers for researchers; therefore, they constitute a service to the scholarly community. At the same time, the *Frontiers journal series* operates on a revolutionary invention, the tiered publishing system, initially addressing specific communities of scholars, and gradually climbing up to broader public understanding, thus serving the interests of the lay society, too.

Dedication to quality

Each Frontiers article is a landmark of the highest quality, thanks to genuinely collaborative interactions between authors and review editors, who include some of the world's best academicians. Research must be certified by peers before entering a stream of knowledge that may eventually reach the public - and shape society; therefore, Frontiers only applies the most rigorous and unbiased reviews. Frontiers revolutionizes research publishing by freely delivering the most outstanding research, evaluated with no bias from both the academic and social point of view. By applying the most advanced information technologies, Frontiers is catapulting scholarly publishing into a new generation.

What are Frontiers Research Topics?

Frontiers Research Topics are very popular trademarks of the *Frontiers journals series*: they are collections of at least ten articles, all centered on a particular subject. With their unique mix of varied contributions from Original Research to Review Articles, Frontiers Research Topics unify the most influential researchers, the latest key findings and historical advances in a hot research area.

Find out more on how to host your own Frontiers Research Topic or contribute to one as an author by contacting the Frontiers editorial office: frontiersin.org/about/contact

The impacts of anthropogenic activity and climate change on the formation of harmful algal blooms (HABs) and its ecological consequence

Topic editors

Zhangxi Hu — Guangdong Ocean University, China

Aifeng Li — Ocean University of China, China

Zhun Li — Korea Research Institute of Bioscience and Biotechnology (KRIBB), Republic of Korea

Margaret R. Mulholland — Old Dominion University, United States

Citation

Hu, Z., Li, A., Li, Z., Mulholland, M. R., eds. (2024). *The impacts of anthropogenic activity and climate change on the formation of harmful algal blooms (HABs) and its ecological consequence*. Lausanne: Frontiers Media SA.

doi: 10.3389/978-2-8325-4727-4

Table of contents

05 Editorial: The impacts of anthropogenic activity and climate change on the formation of harmful algal blooms (HABs) and its ecological consequence
Zhangxi Hu, Aifeng Li, Zhun Li and Margaret R. Mulholland

09 Effects of Algal Blooms on Phytoplankton Composition and Hypoxia in Coastal Waters of the Northern Yellow Sea, China
Xiaohong Sun, Zhao Li, Xueyan Ding, Guanglei Ji, Lei Wang, Xiaotong Gao, Qige Chang and Lixin Zhu

19 Inhibitory Effect of Isolated Bacteria from the Phycosphere of *Levanderina fissa* on the Growth of Different Microalgae
Yali Tang, Changliang Xie, Xiaotong Jin, Zhaohui Wang and Ren Hu

31 A Large Silicon Pool in Small Picophytoplankton
Yuqiu Wei and Jun Sun

38 Distribution of Dinoflagellate Cysts in Surface Sediments From the Qingdao Coast, the Yellow Sea, China: The Potential Risk of Harmful Algal Blooms
Zhaohui Wang, Yuning Zhang, Mingdan Lei, Shuanghui Ji, Jiazhuo Chen, Hu Zheng, Yali Tang and Ren Hu

49 A Decade of Time Series Sampling Reveals Thermal Variation and Shifts in *Pseudo-nitzschia* Species Composition That Contribute to Harmful Algal Blooms in an Eastern US Estuary
Katherine M. Roche, Alexa R. Sterling, Tatiana A. Rynearson, Matthew J. Bertin and Bethany D. Jenkins

60 Consistency between the ichthyotoxicity and allelopathy among strains and ribotypes of *Margalefidinium polykrikoides* suggests that its toxins are allelochemicals
Huijiao Yang, Christopher J. Gobler and Ying Zhong Tang

70 Application of modified clay in intensive mariculture pond: Impacts on nutrients and phytoplankton
Lianbao Chi, Yu Ding, Liyan He, Zaixing Wu, Yongquan Yuan, Xihua Cao, Xiuxian Song and Zhiming Yu

84 Ecological health evaluation of rivers based on phytoplankton biological integrity index and water quality index on the impact of anthropogenic pollution: A case of Ashi River Basin
Zhenxiang Li, Chao Ma, Yinan Sun, Xinxin Lu and Yawen Fan

100 An environmentally friendly material for red tide algae removal: Performance and mechanism
Zhengyu Liu, Zhiming Yu, Xihua Cao, Wenbin Jiang, Yongquan Yuan and Xiuxian Song

113 Full-length transcriptome analysis of the bloom-forming dinoflagellate *Akashiwo sanguinea* by single-molecule real-time sequencing
Tiantian Chen, Yun Liu, Shuqun Song, Jie Bai and Caiwen Li

125 Effects of the neurotoxin β-*N*-methylamino-*L*-alanine (BMAA) on the early embryonic development of marine shellfish and fish
Yilei Fu, Aifeng Li, Jiangbing Qiu, Wenhui Yan, Chen Yan, Lei Zhang and Min Li

136 Isolation and characterization of a high-efficiency algicidal bacterium *Pseudoalteromonas* sp. LD-B6 against the harmful dinoflagellate *Noctiluca scintillans*
Junyue Wang, Xueyao Yin, Mingyang Xu, Yifan Chen, Nanjing Ji, Haifeng Gu, Yuefeng Cai and Xin Shen

147 Phytoplankton community structure in the Western Subarctic Gyre of the Pacific Ocean during summer determined by a combined approach of HPLC-pigment CHEMTAX and metabarcoding sequencing
Quandong Xin, Xiaohan Qin, Guannan Wu, Xiaokun Ding, Xinliang Wang, Qingjing Hu, Changkao Mu, Yuqiu Wei, Jufa Chen and Tao Jiang

160 Comparative effects of temperature and salinity on growth of four harmful *Chattonella* spp. (Raphidophyceae) from tropical Asian waters
Wai Mun Lum, Setsuko Sakamoto, Koki Yuasa, Kazuya Takahashi, Koyo Kuwata, Taketoshi Kodama, Tomoyo Katayama, Chui Pin Leaw, Po Teen Lim, Kazutaka Takahashi and Mitsunori Iwataki

176 Investigation of phytoplankton community structure and formation mechanism: a case study of Lake Longhu in Jinjiang
Yongcan Jiang, Yi Wang, Zekai Huang, Bin Zheng, Yu Wen and Guanglong Liu

frontiers | Frontiers in Marine Science

TYPE Editorial
PUBLISHED 26 March 2024
DOI 10.3389/fmars.2024.1397744

OPEN ACCESS

EDITED AND REVIEWED BY
Eva Sintes,
Spanish Institute of Oceanography (IEO), Spain

*CORRESPONDENCE
Zhangxi Hu
huzx@gdou.edu.cn
Aifeng Li
lafouc@ouc.edu.cn
Zhun Li
lizhun@kribb.re.kr
Margaret R. Mulholland
mmulholl@odu.edu

RECEIVED 08 March 2024
ACCEPTED 18 March 2024
PUBLISHED 26 March 2024

CITATION
Hu Z, Li A, Li Z and Mulholland MR (2024) Editorial: The impacts of anthropogenic activity and climate change on the formation of harmful algal blooms (HABs) and its ecological consequence.
Front. Mar. Sci. 11:1397744.
doi: 10.3389/fmars.2024.1397744

Editorial: The impacts of anthropogenic activity and climate change on the formation of harmful algal blooms (HABs) and its ecological consequence

Zhangxi Hu[1]*, Aifeng Li[2]*, Zhun Li[3]* and Margaret R. Mulholland[4]*

[1]College of Fisheries, Guangdong Ocean University, Zhanjiang, China, [2]Key Laboratory of Marine Environment and Ecology, Ocean University of China, Ministry of Education, Qingdao, China, [3]Biological Resource Center/Korean Collection for Type Cultures (KCTC), Korea Research Institute of Bioscience and Biotechnology, Jeongeup, Republic of Korea, [4]Department of Ocean and Earth Sciences, Old Dominion University, Norfolk, VA, United States

KEYWORDS

phytoplankton, metabarcoding, dinoflagellate, diatom, toxicity

Editorial on the Research Topic
The impacts of anthropogenic activity and climate change on the formation of harmful algal blooms (HABs) and its ecological consequence

Recent decades have witnessed a marked increase in the intensity of human activities, including agriculture, aquaculture, and manufacturing, leading to significant environmental repercussions (Smith and Schindler, 2009; Lu et al., 2021; Priya et al., 2023). These activities have resulted in the excessive discharge of nutrients, notably nitrogen (N) and phosphorus (P), into riverine systems, which subsequently transport these nutrients to estuaries and coastal seas (Seitzinger and Sanders, 1997; Liu et al., 2020; Voss et al., 2021; Yu et al., 2021; Beusen et al., 2022). The resultant nutrient composition shift towards a dominance of organic over inorganic nutrients has significant implications for aquatic ecosystems (Hébert et al., 2023). Eutrophication in estuarine and coastal waters has been exacerbated by an excess of nutrient runoff, a situation that is predicted to worsen (Sinha et al., 2017). Concurrently, climate change, characterized by increased atmospheric and aquatic CO_2 levels and rising temperatures, has had profound impacts on biological processes within marine ecosystems, further complicating the challenges posed by eutrophication (Brierley and Kingsford, 2009; Boyd et al., 2013; Brandenburg et al., 2019; Fu et al., 2024).

The frequency, severity, and duration of harmful algal blooms (HABs) in coastal and estuarine waters worldwide has shown a troubling increase, and is responsible for negative wildlife and human health effects, ecological disasters, and significant economic losses (Anderson et al., 2021; Sakamoto et al., 2021; Yu et al., 2023). Understanding the causative mechanisms and the ecological consequences of HABs is crucial due to the considerable ecological, economic, and societal ramifications (Anderson et al., 2021; Yu et al., 2023). Alterations in nutrient content, notably the increase in organic nutrient loads, coupled with

climate change, significantly affects the growth, species composition, toxin production, and toxicity of HAB-forming species (Gobler et al., 2017; Brandenburg et al., 2019; Gobler, 2020; Raven et al., 2020). The persistence of HABs in an anthropogenically altered marine environment necessitates a comprehensive understanding of phytoplankton diversity, growth, physiology, allelochemicals, toxins, and toxicity of harmful algae, alongside the exploration of mitigation strategies.

Seven studies in our Research Topic focused on the diversity of resting cysts and phytoplankton in both marine and freshwater environments. Wang et al. investigated dinoflagellate cysts, particularly the distributions of toxic and harmful species along the Qingdao coast of the Yellow Sea, China, and analyzed the relationship between contents of biogenic elements and cysts. They identified a total of 32 cyst taxa, including 23 autotrophic and 9 heterotrophic taxa, among them, 17 of the cyst types identified were formed by HAB-causing species. The redundancy analysis demonstrated the influence of biogenic elements on cyst assemblages, and explained why the three sea areas examined, each with different degrees of human disturbance, showed different dinocyst assemblages and abundance. Roche et al. used amplification of the *Pseudo-nitzschia*-specific 18S-5.8S rDNA internal transcribed spacer region 1 (ITS1) in plankton samples and high throughput sequencing to characterize *Pseudo-nitzschia* species composition over a decade in Narragansett Bay, including eight years before the 2016–17 fisheries closures and two years following, and found that several species now recur as year-round residents in Narragansett Bay (*P. pungens* var. *pungens*, *P. americana*, *P. multiseries*, and *P. calliantha*). Various other species increased in frequency after 2015, and some appeared for the first time during the closure period. *Pseudo-nitzschia australis*, a species prevalent along the US West Coast and known for high domoic acid (DA) production, was not observed in Narragansett Bay until the 2017 closure but has been present in several years since the closures. Annual differences in *Pseudo-nitzschia* community composition were correlated with physical and chemical conditions, predominantly water temperature. Sun et al. investigated the phytoplankton community and its association with physicochemical properties in coastal waters of the northern Yellow Sea in 2016. These authors identified 39 taxa belonging to 4 phyla and 24 genera. Diatoms and dinoflagellates were the dominant groups. An algal bloom dominated by *Thalassiosira pacifica* occurred in March, effecting a shift in diatom-dinoflagellate dominance; notably dinoflagellates dominated throughout the summer but switched to diatom dominance again in September. Hypoxic zones (<2 $mg{\cdot}L^{-1}$) developed in bottom waters in August, with minimum dissolved oxygen (DO) of 1.30 $mg{\cdot}L^{-1}$, as a result of the diatom bloom in March. The effects of algal blooms on phytoplankton composition and hypoxia could have a cascading effect on fisheries sustainability and aquaculture in nearshore waters of the northern Yellow Sea. Xin et al. identified eight major marine phytoplankton assemblages, cryptophytes, pelagophytes, prymnesiophytes, diatoms, and chlorophytes using CHEMTAX analyses, and 149 species belonging to 96 genera of 6 major groups (diatoms, prymnesiophytes, pelagophytes, chlorophytes, cryptophytes, and dinoflagellates) by metabarcoding sequencing in the Western Subarctic Gyre during the summer of 2021.Sixteen out of the 97 identified species were annotated as potentially harmful algal species, e.g., *Heterocapsa rotundata*, *Karlodinium veneficum*, *Aureococcus anophagefferens*, etc. Nutrient concentrations were more important in shaping the phytoplankton community than temperature and salinity.

Two more works focused on freshwater ecosystems. Jiang et al. investigated the species composition and spatial distribution with respect to environmental factors in Lake Longhu, China, in July of 2020. They identified a total of 68 phytoplankton species belonging to 7 phyla, in which Chlorophyta, Bacillariophyta and Cyanophyta contributed more to the total cell density, while Chlorophyta and Cryptophyta contributed more to the total biomass. The parameters including pH, water temperature, nitrate, nitrite, and chemical oxygen demand were the main environmental factors affecting the composition of phytoplankton communities in Lake Longhu. Li et al. investigated the phytoplankton community in the Ashi River Basin (ASRB), Harbin, China, between April and October 2019, and identified 137 phytoplankton species belonging to seven phyla. They selected five critical ecological indices (Shannon-Wiener index, total biomass, percentage of motile diatoms, percentage of stipitate diatom, and diatom quotient) to evaluate the biological integrity of phytoplankton in the Ashi River Basin, and concluded that P-IBI (Phytoplankton Index of Biological Integrity) was a reliable tool to assess the relationship between phytoplankton communities and habitat and environmental conditions in that system. Their findings contribute to the ecological monitoring and protection of rivers impacted by anthropogenic pollution.

Four studies made significant contributions to our understanding of HAB physiology: one characterized the transcriptome of a species known to form HABs; another investigated the growth physiology of four harmful raphidophyte species; a third examined the interactions between bacteria and algae; and the fourth reviewed existing research on the impact of picophytoplankton on the carbon (C) and silicon (Si) cycles. Chen et al. used single-molecule real-time (SMRT) sequencing technology to characterize the full-length transcript in *Akashiwo sanguinea*, a harmful algal species commonly observed in estuarine and coastal waters around the world. In total, 83.03 Gb SMRT sequencing clean reads were generated, 983,960 circular consensus sequences (CCS) with average lengths of 3,061 bp were obtained, and 81.71% (804,016) of CCS were full-length non-chimeric reads (FLNC). Furthermore, 26,461 contigs were obtained after being corrected with Illumina library sequencing, with 20,037 (75.72%) successfully annotated in the five public databases. This work provides a sizable insight into gene sequence characteristics of *A. sanguinea*, and provides an important reference resource for *A. sanguinea* draft genome annotation. Lum et al. compared the growth responses to temperature and salinity for four harmful raphidophyte species that coexist in the tropical waters, *Chattonella malayana*, *C. marina*, *C. subsalsa*, and *C. tenuiplastida*, using unialgal cultures grown at ten temperatures (ranging 13.0–35.5°C) and five salinities (ranging 15–35) to better understand how these factors might regulate their distribution in the environment. They found that their growth rates with respect to optimal temperature were 28.0, 30.5, 25.5, and 30.5°

C, respectively, and that growth rate maxima with respect to salinity were similar for *C. subsalsa* and *C. malayana* (30), and for *C. marina* and *C. tenuiplastida* (25). The high adaptability of *C. subsalsa* to a wide range of temperatures and salinities suggests it is highly competitive in a range of environments. The ability of *C. marina* to thrive in colder waters compared to other species likely contributes to its wide distribution in the temperate Asian waters. The narrow and warmer temperature window in which *C. malayana* and *C. tenuiplastida* grew well suggests they are well suited and growth and distribution are more limited. This study provides a physiological basis for the relative occurrences and bloom potential of *Chattonella* spp. in Asia. Tang et al. isolated and identified a cultivable bacterium (*Alteromonas* sp.) coexisting with *Levanderina fissa* by the gradient dilution method and investigated the characteristics of the bacterial interactions with three diatom species (*Chaetoceros curvisetus*, *Skeletonema dohrnii*, and *Phaeodactylum tricornutum*) and three dinoflagellate species (*Scrippsiella acuminata*, *Karenia mikimotoi*, and the host alga), and found that *Alteromonas* sp. had significant inhibitory effects on the growth of all the algal species except its host (*L. fissa*). However, all the algal species tested, especially their natural hosts, showed significant stimulatory effects on the growth of *Alteromonas* sp. This study implies a highly complicated and variable interaction between phycosphere bacteria and their host alga. Picophytoplankton have been found to have significant silica (Si) accumulation, a finding which provides a new insight into the interaction of the marine carbon (C) and Si cycles and questions whether large diatoms (>2 μm) dominate the Si cycle. Wei and Sun found there were few studies on the physiology and ecology of picophytoplankton, especially regarding their potential roles in the biogeochemical Si cycle. These authors extensively reviewed past studies regarding the influence of picophytoplankton on the C and Si cycles, used this as the basis for conducting targeted studies on the picophytoplankton Si pool and its regulation. This work also provides a theoretical framework for further study of the role of small cells in the global ocean Si cycle and the coupling of C and Si cycles.

Two studies focused on the effects of algal toxin(s) and allelochemical(s) on other organisms. Yang et al. investigated the ability of 10 strains of *Margalefidinium polykrikoides* with different geographic origins and ribotypes to cause mortality in two strains of the dinoflagellate, *Akashiwo sanguinea* (allelopathy), and the sheepshead minnow, *Cyprinodon variegatus* (toxicity). Results showed that the potency of allelopathy against both strains of *A. sanguinea* and toxicity to the fish were significantly correlated across strains of *M. polykrikoides*. They concluded that the major allelochemicals and toxins of *M. polykrikoides* are identical chemicals, an ecological strategy that may be more energetically efficient than the separate synthesis of toxins and allelochemicals as has been reported for other HABs. Fu et al. investigated the effects of neurotoxin β-N-methylamino-L-alanine (BMAA) on the early development of embryos of mussel *Mytilus galloprovincialis*, oyster *Magallana gigas*, and marine medaka *Oryzias melastigma*. Results demonstrated that the embryonic development of mussels and oysters were significantly inhibited when BMAA concentrations were above 0.65 μM and 5.18 μM, respectively. The shell growth of mussel embryos was also markedly inhibited by BMAA at concentrations ≥ 0.65 μM. A sustained and dose-dependent decrease in heart rate was apparent in marine medaka embryos at 9-days post fertilization following BMAA exposure. This study contributes to our knowledge regarding the sublethal effects of BMAA on early embryonic development of marine bivalves and medaka.

Lastly, three studies explored the biological and chemical methods for controlling species that cause HABs. Wang et al. isolated a strain of algicidal bacterium *Pseudoalteromonas* sp. strain LD-B6 with high efficiency against *Noctiluca scintillans*, the highest algicidal activity reached 90.5%, and the algicidal activity of *Pseudoalteromonas* sp. was influenced by the density of *N. scintillans*. This bacterium could also lyse other algal species. This work provides a candidate algicidal bacterium against *N. scintillans* blooms. Chi et al. introduced a modified clay (MC) method to regulate the nutrients and phytoplankton community in *Litopenaeus vannamei* ponds. Compared to the control, they found that in the MC-regulated pond, there were reduced concentrations of both organic and inorganic nutrients and a distinct change in the phytoplankton community composition, with green algae becoming the most abundant phytoplankton species. This study provides new insights into an effective treatment for managing water quality and maintaining sustainable mariculture. Liu et al. compared the removal capacity of polydimethyl diallyl ammonium chloride (PDMDAAC) modified clay (MP) and hexadecyl trimethyl ammonium bromide (HDTMA) modified clay (MH) on the HAB-forming species *Prorocentrum donghaiense*. They found that PDMDAAC could remove microalgae at a low dose (2 mg/L) and quickly clarify the water by significantly enhancing the flocculation of algae onto the clay. This study provides support for the development of organic-modified clay.

In summary, the papers in this Research Topic contribute new insights into the effects of anthropogenic activities and climate change on the composition of phytoplankton communities in marine and freshwater ecosystems. They delve into the ecological physiology of species that form harmful algal blooms (HABs), the roles of allelochemicals, and the toxins and toxicity produced by harmful algae, as well as exploring methods for controlling HABs through both biological and chemical strategies. These studies offer valuable contributions to our understanding of ecosystem complexities and the impact of human activities on HAB-forming species. Moreover, this topic highlights the urgent need for further research on HAB species and their adverse effects on various trophic levels within aquatic ecosystems, alongside mitigation strategies for these impacts in both marine and freshwater environments.

Author contributions

ZH: Writing – review & editing, Writing – original draft, Funding acquisition, Conceptualization. AL: Writing – review & editing, Validation. ZL: Writing – review & editing, Validation. MM: Writing – review & editing, Validation.

Funding

The author(s) declare financial support was received for the research, authorship, and/or publication of this article. ZH acknowledges funding by the Program for Scientific Research Start-up Funds of Guangdong Ocean University (grant number 060302022201). AL thanks the special foundation for Taishan Scholar of Shandong Province. ZL thanks the Korea Research Institute of Bioscience and Biotechnology (KRIBB) and Research Initiative Program (KGM5232423). MM thanks the NOAA ECOHAB and MERHAB programs for support.

Acknowledgments

We thank authors of the papers published in this Research Topic for their valuable contributions and the referees for their rigorous review.

Conflict of interest

The authors declare that the research was conducted in the absence of any commercial or financial relationships that could be construed as a potential conflict of interest.

The author(s) declared that they were an editorial board member of Frontiers, at the time of submission. This had no impact on the peer review process and the final decision.

Publisher's note

References

Anderson, D. M., Fensin, E., Gobler, C. J., Hoeglund, A. E., Hubbard, K. A., Kulis, D. M., et al. (2021). Marine harmful algal blooms (HABs) in the United States: History, current status and future trends. *Harmful Algae* 102, 101975. doi: 10.1016/j.hal.2021.101975

Beusen, A. H. W., Doelman, J. C., Van Beek, L. P. H., Van Puijenbroek, P. J. T. M., Mogollón, J. M., Van Grinsven, H. J. M., et al. (2022). Exploring river nitrogen and phosphorus loading and export to global coastal waters in the shared Socio-economic pathways. *Global Environ. Change* 72, 102426. doi: 10.1016/j.gloenvcha.2021.102426

Boyd, P. W., Rynearson, T. A., Armstrong, E. A., Fu, F., Hayashi, K., Hu, Z., et al. (2013). Marine phytoplankton temperature versus growth responses from polar to tropical waters-outcome of a scientific community-wide study. *PloS One* 8, e63091. doi: 10.1371/journal.pone.0063091

Brandenburg, K. M., Velthuis, M., and Van De Waal, D. B. (2019). Meta-analysis reveals enhanced growth of marine harmful algae from temperate regions with warming and elevated CO_2 levels. *Global Change Biol.* 25, 2607–2618. doi: 10.1111/gcb.14678

Brierley, A. S., and Kingsford, M. J. (2009). Impacts of climate change on marine organisms and ecosystems. *Curr. Biol.* 19, R602–R614. doi: 10.1016/j.cub.2009.05.046

Fu, X., Qin, J., Ding, C., Wei, Y., and Sun, J. (2024). Effect of increased pCO_2 and temperature on the phytoplankton community in the coastal of Yellow Sea. *Sci. Total Environ.* 918, 170520. doi: 10.1016/j.scitotenv.2024.170520

Gobler, C. J. (2020). Climate change and harmful algal blooms: Insights and perspective. *Harmful Algae* 91, 101731. doi: 10.1016/j.hal.2019.101731

Gobler, C. J., Doherty, O. M., Hattenrath-Lehmann, T. K., Griffith, A. W., Kang, Y., and Litaker, R. W. (2017). Ocean warming since 1982 has expanded the niche of toxic algal blooms in the North Atlantic and North Pacific oceans. *Proc. Natl. Acad. Sci.* 114, 4975–4980. doi: 10.1073/pnas.1619575114

Hébert, M.-P., Soued, C., Fussmann, G. F., and Beisner, B. E. (2023). Dissolved organic matter mediates the effects of warming and inorganic nutrients on a lake planktonic food web. *Limnology Oceanography* 68, S23–S38. doi: 10.1002/lno.12177

Liu, Q., Liang, Y., Cai, W., Wang, K., Wang, J., and Yin, K. (2020). Changing riverine organic C:N ratios along the Pearl River: Implications for estuarine and coastal carbon cycles. *Sci. Total Environ.* 709, 136052. doi: 10.1016/j.scitotenv.2019.136052

Lu, M., Zou, Y., Xun, Q., Yu, Z., Jiang, M., Sheng, L., et al. (2021). Anthropogenic disturbances caused declines in the wetland area and carbon pool in China during the last four decades. *Global Change Biol.* 27, 3837–3845. doi: 10.1111/gcb.15671

Priya, A. K., Muruganandam, M., Rajamanickam, S., Sivarethinamohan, S., Gaddam, M. K. R., Velusamy, P., et al. (2023). Impact of climate change and anthropogenic activities on aquatic ecosystem – A review. *Environ. Res.* 238, 117233. doi: 10.1016/j.envres.2023.117233

Raven, J. A., Gobler, C. J., and Hansen, P. J. (2020). Dynamic CO_2 and pH levels in coastal, estuarine, and inland waters: Theoretical and observed effects on harmful algal blooms. *Harmful Algae* 91, 101594. doi: 10.1016/j.hal.2019.03.012

Sakamoto, S., Lim, W. A., Lu, D., Dai, X., Orlova, T., and Iwataki, M. (2021). Harmful algal blooms and associated fisheries damage in East Asia: Current status and trends in China, Japan, Korea and Russia. *Harmful Algae* 102, 101787. doi: 10.1016/j.hal.2020.101787

Seitzinger, S. P., and Sanders, R. W. (1997). Contribution of dissolved organic nitrogen from rivers to estuarine eutrophication. *Mar. Ecol. Prog. Ser.* 159, 1–12. doi: 10.3354/meps159001

Sinha, E., Michalak, A. M., and Balaji, V. (2017). Eutrophication will increase during the 21st century as a result of precipitation changes. *Science* 357, 405–408. doi: 10.1126/science.aan2409

Smith, V. H., and Schindler, D. W. (2009). Eutrophication science: where do we go from here? *Trends Ecol. Evol.* 24, 201–207. doi: 10.1016/j.tree.2008.11.009

Voss, M., Asmala, E., Bartl, I., Carstensen, J., Conley, D. J., Dippner, J. W., et al. (2021). Origin and fate of dissolved organic matter in four shallow Baltic Sea estuaries. *Biogeochemistry* 154, 385–403. doi: 10.1007/s10533-020-00703-5

Yu, L., Gan, J., Dai, M., Hui, C. R., Lu, Z., and Li, D. (2021). Modeling the role of riverine organic matter in hypoxia formation within the coastal transition zone off the Pearl River Estuary. *Limnology Oceanography* 66, 452–468. doi: 10.1002/lno.11616

Yu, Z., Tang, Y., and Gobler, C. J. (2023). Harmful algal blooms in China: History, recent expansion, current status, and future prospects. *Harmful Algae* 129, 102499. doi: 10.1016/j.hal.2023.102499

frontiers | Frontiers in Marine Science

ORIGINAL RESEARCH
published: 20 May 2022
doi: 10.3389/fmars.2022.897418

Effects of Algal Blooms on Phytoplankton Composition and Hypoxia in Coastal Waters of the Northern Yellow Sea, China

Xiaohong Sun[1], Zhao Li[2]*, Xueyan Ding[1], Guanglei Ji[3], Lei Wang[4], Xiaotong Gao[4], Qige Chang[1] and Lixin Zhu[1]*

[1] Marine College, Shandong University, Weihai, Weihai, China, [2] School of Municipal and Environmental Engineering, Shandong Jianzhu University, Jinan, China, [3] Fisheries Development Service Department, Weihai Ocean Development Research Institute, Weihai, China, [4] Jihongtan Reservoir Management Station, Shandong Water Diversion Project Operation and Maintenance Center, Qingdao, China

OPEN ACCESS

Edited by:
Zhangxi Hu, Chinese Academy of Sciences (CAS), China

Reviewed by:
Duncan A. Purdie, University of Southampton, United Kingdom
Yuqiu Wei, Chinese Academy of Fishery Sciences (CAFS), China

***Correspondence:**
Xiaohong Sun
sunxiaohong@sdu.edu.cn
Zhao Li
lizhao19@sdjzu.edu.cn

Specialty section:
This article was submitted to Aquatic Microbiology, a section of the journal Frontiers in Marine Science

Received: *22 March 2022*
Accepted: *21 April 2022*
Published: *20 May 2022*

Citation:
Sun X, Li Z, Ding X, Ji G, Wang L, Gao X, Chang Q and Zhu L (2022) Effects of Algal Blooms on Phytoplankton Composition and Hypoxia in Coastal Waters of the Northern Yellow Sea, China. Front. Mar. Sci. 9:897418. doi: 10.3389/fmars.2022.897418

Summer hypoxia and harmful algal bloom occurred sometimes in the nearshore of the northern Yellow Sea in recent years. Based on seven multidisciplinary investigations conducted from March to November 2016, except for April and October, the phytoplankton community and its association with ambient seawater physicochemical parameters in coastal waters of the northern Yellow Sea were comprehensively examined. In total, 39 taxa belonging to 4 phyla and 24 genera were identified. Diatoms and dinoflagellates were the dominant groups, which accounted for 64.1% and 30.8% of total species, respectively. An algal blooming event dominated by the diatom (*Thalassiosira pacifica*) occurred in March, which affects the shifting of diatom–dinoflagellate dominance. A notable dinoflagellate dominance occurred especially in surface water throughout the whole summer but changed to diatom dominance again from September. Hypoxic zones (<2 mg l^{-1}) were observed in the bottom water in August, with minimum dissolved oxygen (DO) of 1.30 mg l^{-1}. This low DO zone in August was clearly associated with the diatom blooming event (*Thalassiosira pacifica*) in March, as diatoms in surface waters sank into bottom waters and decomposed by the microbial community resulting in oxygen consumption. After the early-spring diatom bloom, thermohaline stratification occurred and prevented exchanges of dissolved oxygen, which eventually led to hypoxia in bottom waters. The effects of algal blooms on phytoplankton composition and hypoxia could have a cascaded effect on the fishery sustainability and aquaculture in nearshore waters of the northern Yellow Sea.

Keywords: phytoplankton, diatom, dinoflagellate, algal bloom, hypoxia

INTRODUCTION

Coastal waters are regions that are influenced by strong land–ocean interactions (Frigstad et al., 2020); they account for only a small portion of the ocean surface area (7%–8%) but are responsible for 25% of the global ocean primary production (Smith and Hollibaugh, 1993). Compared with open sea ecosystems, coastal waters are under substantial pressure and have become ecologically

fragile regions in recent decades (Regnier et al., 2013; Fennel and Testa, 2019). Under the combined influences of climate change and human activities, coastal areas are more vulnerable to eutrophication, harmful algal blooms, and hypoxia (Bianchi and Allison, 2009; He and Silliman, 2019; Wei et al., 2020). As a feedback, hypoxia can influence fundamental biological and biochemical processes (Turner et al., 2008; Breitburg et al., 2018) and affect pelagic organisms from plankton to fish (O'Connor and Whitall, 2007; Breitburg et al., 2009; Roman et al., 2012; Bausch et al., 2019), which would destroy the potential functioning of the fragile coastal ecosystem. Phytoplankton is the main source of primary production and plays a key role in estuary ecosystems, which could be reflected by the variation of composition diversity and abundance (Falkowski and Woodhead, 1992). Previous studies have shown that the spring bloom is the period with the highest annual primary production and sinking of organic matter to the sediment; thereafter, the fate of this organic matter is a key driver for material fluxes, affecting ecosystem functioning and eutrophication feedback loops (Spilling et al., 2018). The potential functioning of the coastal ecosystem strongly depends on the quantity and quality of phytoplankton.

The Yantai nearshore ecosystem is located in the western portion of the northern Yellow Sea, where it is close to the Yantai-Weihai fishing ground and affected by typical anthropogenic activities such as sewage discharge and aquaculture. Similar to other coastal waters that are severely impacted by anthropogenic activities, our study area has also been suffering from serious eutrophication, jellyfish blooms, and hypoxia (Dong et al., 2012; Wang et al., 2012; Sun et al., 2015; Zhang et al., 2018; Yang et al., 2020). Since 2013, hypoxia was reported to cover approximately 54.0 km^2 and cause mass mortality of the benthos species, such as sea cucumbers, abalones, and scallops, thus leading to huge economic and ecological losses. Bottom-layer hypoxia was also observed in the summers of most of the subsequent years (Yang et al., 2018; Zhang et al., 2018) in this studied area. Previous studies showed that phytoplankton blooms and their subsequent decomposition are important biological factors leading to oxygen depletion and hypoxia in Changjiang estuary and its adjacent waters (Wang, 2009; Chi et al., 2021). The diatom-dominated community sediments rapidly, having higher sinking rates, and contributes more carbon flux to the bottom waters during algal blooms (Guo et al., 2016; Li et al., 2018). Thus, it is important to understand the phytoplankton community composition and spatial and temporal changes, to assess algal bloom effects on shifting of diatom–dinoflagellate dominance, and on subsequent deoxygenation in coastal waters of northern Yellow Sea, China.

From March to November 2016, seven multidisciplinary investigations were conducted in the northern Shandong Peninsula, North Yellow Sea, China. The main goal of this study is to identify phytoplankton species (populations) associated with environmental factors to analyze the potential effects of spring diatom bloom on subsequent dinoflagellate dominance and formation of hypoxia. It is hypothesized that degradation of organic matter derived from diatom blooms is the cause of the formation of hypoxia.

2 MATERIALS AND METHODS

2.1 Study Area and Cruise

The Yantai coast in the northern Yellow Sea covers an area of 423 km^2 with a 118-km-long coastline, including Muping marine ranching (MR), Yantai–Weihai fishing ground (FG), and Sishili bay (SB). SB is a typical half-closed coastal bay affected by anthropogenic activities, such as harbor pollution and wastewater discharge from domestic, industrial, and agriculture areas (Wang et al., 2012). MR is an important aquaculture breeding base. The hydrological conditions of temperature, salinity, and water column stratification exhibit a seasonal cycle, leading to complex spatial–temporal heterogeneity in the phytoplankton community in the study area (Yang et al., 2020). Therefore, seven cruises were carried out from March to November 2016, except for April and October, in coastal waters of the northern Yellow Sea (121.51°E–122.03°E, 37.46°N–37.63°N). Thirty-five stations, with a sampling depth from 11 to 25 m, were established to include all representative areas within the domain. The locations of sampling stations are presented in **Figure 1** and **Table 1**.

2.2 Sampling and Processing

The profiles of temperature, salinity, and DO were recorded by the CTD device (RBRmaestro, Ottawa, Canada; RBR temperature and salinity probes, and a Model AADI DO optode). Discrete water samples were collected from standard depths, i.e., surface, 5 m, 10 m, 20 m, and 2 m above bottom, using 12-l Niskin bottles (KC Denmark Ltd., Silkeborg, Denmark) at each station. For analysis of phytoplankton assemblage, aliquots of 250-ml seawater samples were preserved with buffered formalin (2% final concentration). Following the methodology described by Utermöhl (1958), 10–25 ml of the subsamples was settled in a Hydro-bios chamber for 24 h, then identified and enumerated under an inverted light microscope (IX71, Olympus, Japan) at ×200 or ×400 magnification (Tomas, 1997). The lower size limit of resolution for this analysis was ~5μm.

2.3 Data Analysis

The diversity of phytoplankton assemblages was demonstrated by the Shannon–Weiner diversity index (H', log base 2) (Sun and Liu, 2003). The dominant phytoplankton species were determined according to the McNaughton index (Y), which is calculated as follows:

$$Y = \frac{n_i}{N} \times f_i$$

where n_i is the total abundance of species i, N is the total abundance of all species, and f_i is the frequency of species i in all samples. Values of $Y < 0.02$, indicate that the species is not dominant.

The DO saturation of each sample was calculated based on the Weiss equation (Pytkowicx, 1971).

$$\text{DO Saturation} = \frac{\text{DO}}{\text{DO}'} \times 100\,\%$$

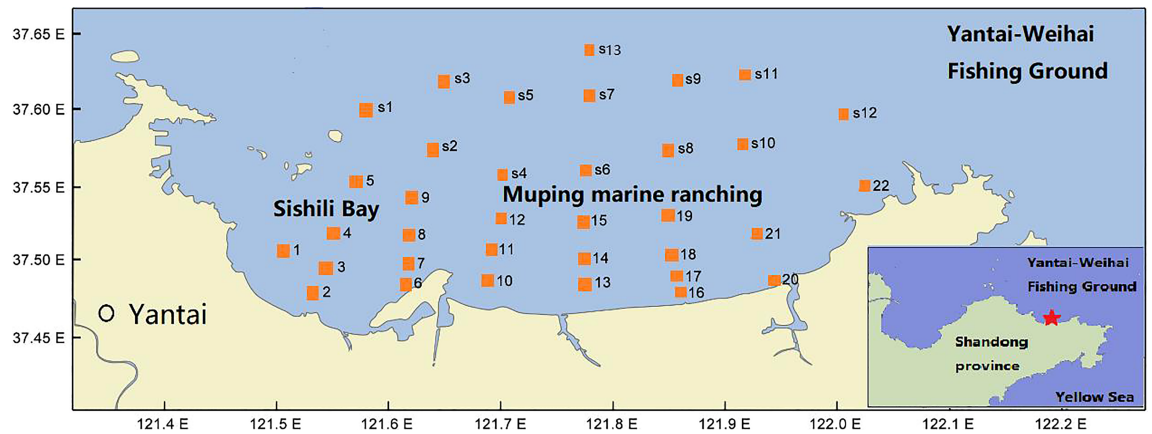

FIGURE 1 | Location of sampling stations in the northern Yellow Sea, China.

TABLE 1 | The sampling date and station numbers of environmental and biological parameters during each cruise.

Sampling date	Temperature	Salinity	DO	Phytoplankton
March 13, 2016	28	28	28	21
May 23, 2016	39	39	39	34
June 22, 2016	42	42	42	30
July 12, 2016	42	42	42	36
August 15, 2016	43	43	43	34
September 14, 2016	38	38	38	33
November 17, 2016	27	27	27	21

In the equations, DO′ is the equilibrium saturation concentration in water under certain environmental conditions and DO is the measured concentration.

2.4 Statistical Analysis

One-way analysis of variance (ANOVA) was applied to compare the parameters in different sampling sites, with the significant level of p set at 0.05. Pearson correlation analysis was conducted to access the relationships between phytoplankton abundance and environmental factors. A Kruskal–Wallis test was performed to reveal differences of phytoplankton in non-hypoxia and hypoxia zones. All statistical tests were conducted with the SPSS (Version 20.0 for Windows, SPSS Inc., La Jolla, CA, USA). The horizontal distributions of each parameter were plotted using Surfer 16 (Golden Software LLC, Golden, CO, USA). The variations in the phytoplankton abundance were conducted with OriginPro 2021 software.

3 RESULTS

3.1 Environmental Factors

3.1.1 Temporal Variation of Temperature and Salinity

Water temperature showed strong monthly variation in the study area, and variations of water temperature in bottom were consistent with the surface layer (**Figure 2**). Water temperature was highest in August, with the average of 25.38 ± 0.91°C, and lowest in March, with the average of 3.38 ± 0.51°C in the surface layer. There were small differences in water temperature of the surface layer between June and July, with the average of 19.23 ± 0.99°C and 20.84 ± 1.65°C, respectively. The averaged salinity was lower in summer than the other seasons, and salinity in the surface layer was lower than that in the bottom layer especially from March to August (**Figure 3**). In the surface layer, the lowest salinity occurred in August with the average of 31.31 ± 0.15. On the whole, the mean temperature in surface water was higher than that in bottom water from March to August ($p < 0.001$). Similarly, surface salinity was lower than bottom salinity from March to August ($p < 0.05$ in March, $p < 0.001$ in other months). No differences in surface salinity and bottom salinity were detected in September and November ($p > 0.05$).

3.1.2 Spatial Distribution of Temperature and Salinity

As a typical half-closed coastal bay, the study area was affected by wastewater discharge from domestic, open sea waters and melting snow, which together leads to the different variations of salinity from coastal to offshore waters. In March, the temperature and salinity were lower in the coastal water than those in the outer part (**Figure 2**, **3**). In May, the temperature and salinity increased from coastal to offshore waters. The relatively higher salinity and lower temperature distributed offshore in June and remained until August especially in bottom water. The

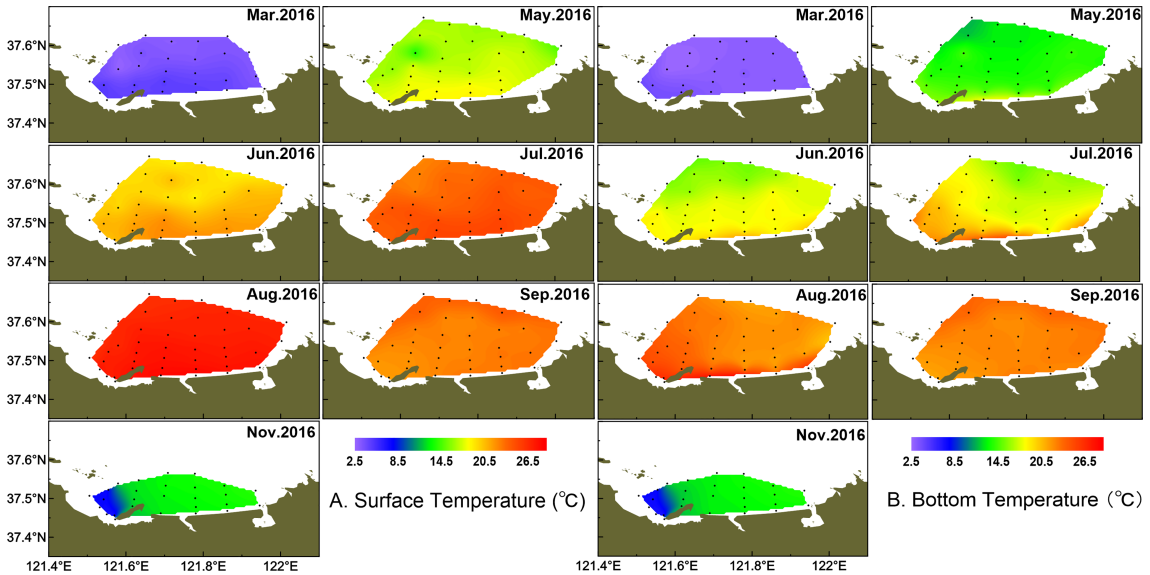

FIGURE 2 | Temporal and spatial distribution of temperature (°C) in surface **(A)** and bottom **(B)** water.

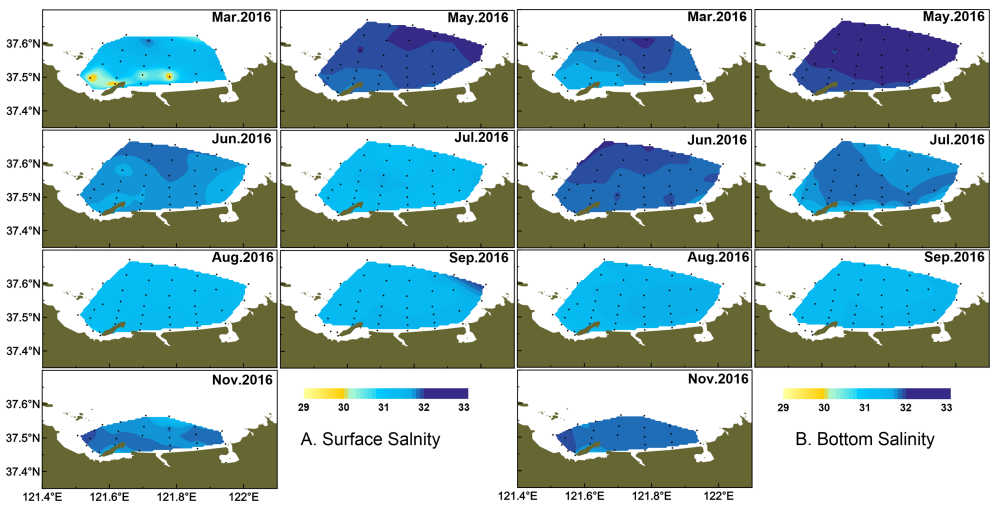

FIGURE 3 | Temporal and spatial distribution of salinity in surface **(A)** and bottom **(B)** water.

temperature and salinity were homogeneous from September in both surface and bottom waters. However, the relatively lower temperature and higher salinity occurred from the inner bay (the west of studied area) in November.

3.2 Phytoplankton Assemblage

3.2.1 Species Composition

During the seven cruises, a total of 39 taxa belonging to 4 phyla and 24 genera were identified. Diatoms and dinoflagellates were the dominant groups, which accounted for 64.1% and 30.8% of total species, respectively. In general, diatoms were dominant in March, most of which were chain-forming diatoms such as *T. pacifica* and *Paralia sulcata*. Dinoflagellates became dominant from May to August in surface water (**Figure 4**), while the species amounts of Chrysophyta and Euglenophyta were low in all cruises.

3.2.2 Dominant Species

The top 10 dominant phytoplankton species (or genera) are listed in **Figure 4A**, including six diatom and four dinoflagellate species during the study period. Chain-forming diatoms, such as *T. pacifica*, *P. sulcate*, and *Skeletonema costatum*, were the most

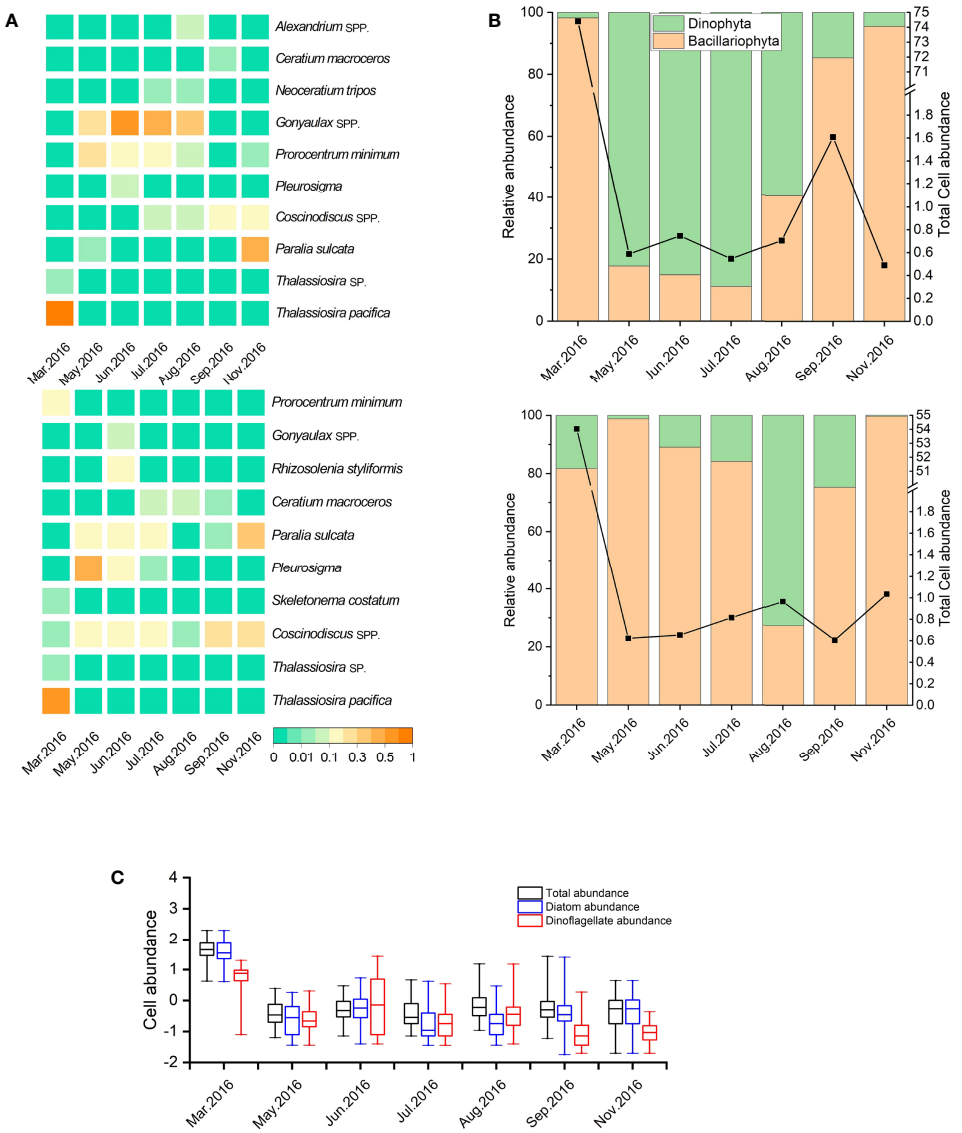

FIGURE 4 | Variation in the dominance (*Y*) of phytoplankton species (or genera) in the study area **(A)**; variation in relative abundance of diatoms and dinoflagellates in study area **(B)**. The upper and bottom capture represent surface and bottom water, respectively. Variation in cell abundance of total phytoplankters, diatoms, and dinoflagellates (all data were transformed logarithmically [log10 (x)] before analyses; the bottom and top of the box represent the lower and upper quartiles, respectively. The band near the middle of the box represents the medium; the ends of the whisker represent the maximum and minimum values, respectively) **(C)**.

common dominant species in the study area. In March, *T. pacifica* showed exclusive dominance ($Y = 0.91$). *P. sulcata* was another dominant diatom in this nearshore area except in March and August, and its highest dominance occurred in November in the whole water. *Coscinodiscus* spp. were the dominant diatoms in bottom water and higher than in surface water from March to June. *Prorocentrum minimum* presented higher dominance in surface water from May to August and was the only dominant dinoflagellate in March in bottom water. *Gonyaulax* spp. maintained the highest dominance from June to August in surface water ($Y = 0.35$–0.66). *Neoceratium tripos* was dominant in both surface and bottom waters in July and August and was the dinoflagellate species with the highest dominance in August, whereas *Alexandrium* spp. showed a relatively high dominance ($Y = 0.07$) only in August in surface water.

3.2.3 Temporal and Spatial Distribution of Phytoplankton

The relative abundance of Bacillariophyta and Dinophyta is shown in **Figure 4B**. The ratio of diatom peaked in March, but the ratio of dinoflagellates in bottom water exhibited a higher value than that in surface water. The ratio of dinoflagellates increased greatly from May to June, with the maximum of 89.97%, and maintained a relatively high abundance until August in surface water. From

September, the ratio of diatoms began to increase in both surface and bottom waters, with high ratios more than 96.77% in November. The total abundance of phytoplankton, diatoms, and dinoflagellates is shown in **Figure 4B**, and the abundance transformed logarithmically [log10 (x)] is shown in **Figure 4C**. After a relatively high abundance in March, the total of phytoplankton abundance showed low from May to August in both surface and bottom waters and then increased to a weaker peak in September in surface water.

The spatial distribution of total phytoplankton is shown in **Figure 5**. The phytoplankton abundance was relatively higher at station 6 (maximum at 2.01×10^5 cells l^{-1} in surface water) in March, with the diatom blooming event dominated by *T. pacifica* (this blooming threshold was determined based on "People's Republic of China Marine Industry Standard: HY-T069-2005_Technical specification for red tide monitoring"). In May~June, the phytoplankton presented patches with higher abundance from northern offshore areas to coastal waters. In July, the phytoplankton cell abundance remained high in northern areas but decreased in August. In September, the phytoplankton cell abundance concentrated in the northwest and thereafter phytoplankton maintained low abundance but only concentrated in the east part of the study area in November.

3.3 Low DO and Hypoxia

The DO concentration of the study area exhibited both spatial variation and seasonal fluctuation (**Figure 6**). The DO concentration in surface water was significantly higher than that in bottom water from March to August ($p < 0.05$ in July, $p < 0.001$ in other months), but there was no significant difference in September and November. In March and May, the DO concentrations in surface water waters were relatively high, ranging from 6.48 to 11.89 mg l^{-1}, while a relatively low DO zone (minimum at 4.86 mg l^{-1}) appeared in bottom water in May, which centered in the west part of the coastal area. The DO saturation ranged from 75.1% to 94.0% in March and 61.7% to 93.5% in May. The averaged DO increased slightly in June especially in surface water, while the low DO zones in bottom water expanded, with a DO concentration decreased to 4.10 mg l^{-1} in the center. The low DO zone expanded continuously from the west to east parts in July, with the lowest DO (<4.0 mg l^{-1}) formed around stations 4–7 and a lower DO (< 6.0 mg l^{-1}) distributed in most coastal areas in bottom water. In August, waters with low DO (<4.0 mg l^{-1}) almost covered all parts of the study area in bottom water and the DO concentrations of five coastal stations (stations 6–8 and stations 12–13) reached the hypoxia level (1.31–1.77 mg l^{-1}). The minimum of DO saturation was 16.2% at station 7. In September, the hypoxia zone was relieved and low DO (minimum to 3.54 mg l^{-1}) was only observed in the offshore area. The low DO zone disappeared in November, and the DO concentration in the bottom water increased to saturation in the west part of the study area. Overall, the low DO zone in the bottom water from June to August distributed at the same stations where diatom abundance was high in March (stations 6 and 7).

4 DISCUSSION

Summer oxygen depletion and even hypoxia in the northern mariculture areas of the Shandong Peninsula have been observed since 2013 (Liu et al., 2014; Zhai et al., 2014). In the present study, low DO (<3 mg l^{-1}) or hypoxic zones (<2 mg l^{-1}) were observed in bottom waters in August 2016. The low DO zone almost covered the whole of the survey area, with DO reaching its minimum of 1.31 mg l^{-1}. The low DO zone in bottom water in August was clearly associated with the high phytoplankton cell abundance of surface waters in March. Previous studies have indicated that the formation of the hypoxic zone is closely related to the oxygen utilization by the particulate organic matter

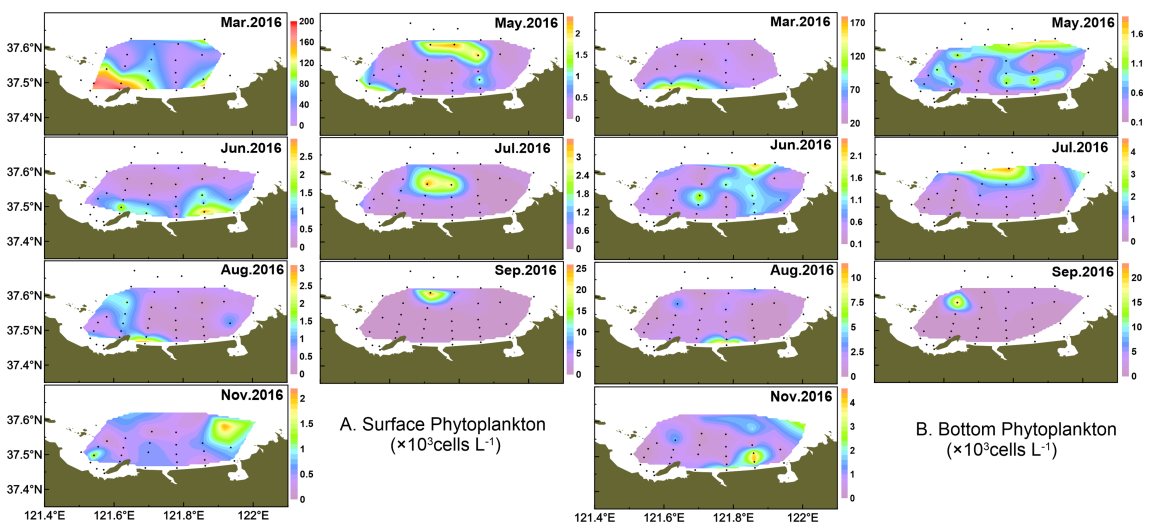

FIGURE 5 | Temporal and spatial distribution of phytoplankton in surface **(A)** and bottom **(B)** water.

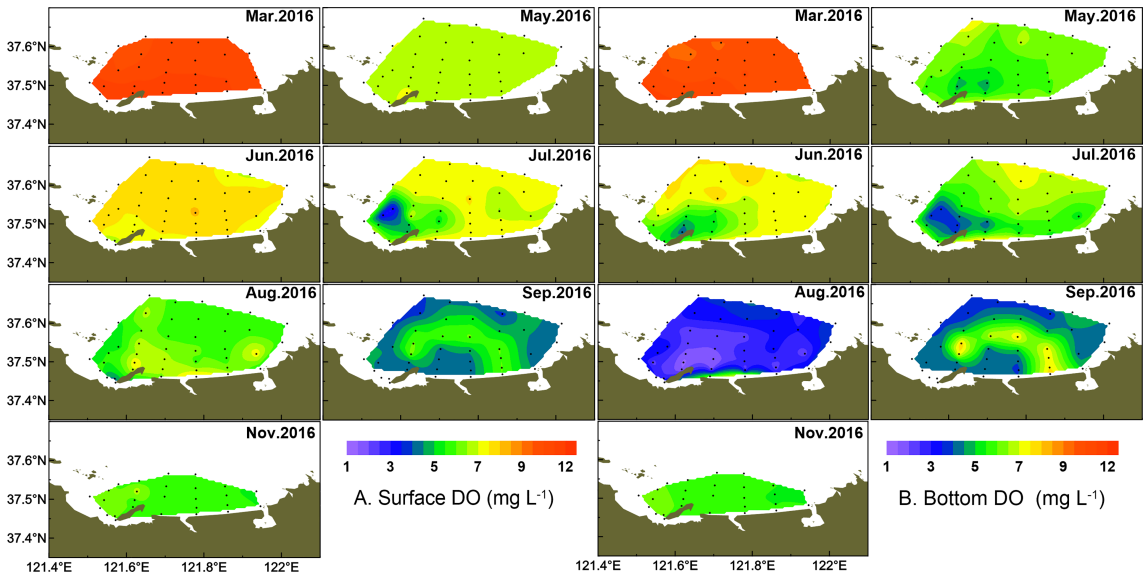

FIGURE 6 | Temporal and spatial distribution of DO (mg L^{-1}) in surface **(A)** and bottom **(B)** water.

(Rabouille et al., 2008; Li et al., 2011), and the photosynthesis of surface phytoplankton is the main source of organic matter (Wei et al., 2007). In this study, a diatom bloom dominated by *T. pacifica* broke out in March, which could provide an organic carbon source. When algal mass sank to the bottom and decomposed by microbial community eventually, low DO and even hypoxia formed in bottom waters (Li et al., 2018; Chi et al., 2021).

4.1 The Correlation Between Algal Blooms and Low DO

Hypoxia has been widely observed in various estuaries and coastal and gulf regions, including the Gulf of Mexico, Chesapeake Bay, the Baltic Sea, and the Changjiang (Yangtze River) Estuary (Chen et al., 2007; Breitburg et al., 2009; Conley et al., 2011; Carstensen et al., 2014). Previous studies have shown that phytoplankton communities dominated by diatoms with higher sinking rates contribute more particulate organic matter to the bottom waters during algal blooms and may thus be more closely associated with bottom hypoxia in the Changjiang Estuary (Yangtze River) and its adjacent waters (Guo et al., 2016; Li et al., 2018). In addition, studies have shown that the spring diatom bloom could be followed by seasonal DO reduction in coastal areas (Egge and Aksnes, 1992). Besides, 40%–60% of annual carbon fixation takes place during the spring bloom in the most eutrophicated region of the Baltic Sea. When the fixed carbon sinks to the bottom, seasonal hypoxia occurred (Spilling et al., 2018).

In this study, the relationships between the numerical abundance of dinoflagellates and diatoms in surface and bottom water and the environmental factors in the corresponding layer from May to November are shown in **Table 2**. Results showed the significant negative relationship between surface diatom abundance and surface DO concentration ($p < 0.05$, $r^2 = -0.86$), similar with the result between bottom dinoflagellate abundance and bottom DO concentration ($p < 0.01$, $r^2 = -0.92$). It is worth noting that the relatively high Chl *a* values in the surface water appeared right in the region with low DO in the bottom water (Yang et al., 2020). Particularly, the spatial distribution of the hypoxic area in August was consistent with the zone of diatom blooms in March, which provided a clue of DO consumption resulting from organic matter degradation during an algal bloom period. Phytoplankton bloom could be the primary contribution to dissolved organic matter (DOM) and dissolved organic carbon (DOC) (Wei et al., 2007; Fan et al., 2018; Zhang et al., 2018). The origin and dynamics of DOM were studied in the same cruise in the study area. The results showed that DOM mainly produced *in situ*, indicating that *in situ* diatom blooms were the resource of DOM (Zhang et al., 2018).

Degradation of organic matter is known to be a major factor contributing to the development of hypoxia (Wang et al., 2016; Su et al., 2017). In approximately the same study area, the microbial diversity in bottom water was significantly higher in summer, and *Bacteroidetes* was higher in August, which was the important organic-aggregate-associated bacteria during phytoplankton bloom (Wang et al., 2022). This may be due to that planktonic algae multiplied in spring and then sank to the bottom, increasing the influx of organic matter to the seabed in August. Besides, bacterial oxidation of sulfur compounds is known to occur extensively in the sediments under oxygen minimum zones and sulfate-reducing bacteria could indirectly promote phosphate release through organic matter mineralization (Diaz and Rosenberg, 2008; Sinkko et al., 2011). As one of sulfate-reducing bacteria, *Pseudomonas* could cause phosphate release. In the study area, *Pseudomonas* with higher abundance was found in the bottom in August, which indirectly proves that microbial decomposition accelerates the oxygen consumption in summer (Wang et al., 2022).

TABLE 2 | Pearson's correlation coefficient of the relationship between abundance of diatoms or dinoflagellates and environmental parameters in surface (S) and bottom (B) water from May to November.

	Surface		Bottom	
Classes	**Diatoms**	**Dinoflagellates**	**Diatoms**	**Dinoflagellates**
Temperature	0.05	0.51	-0.82*	0.72
Salinity	-0.18	-0.07	0.51	-0.68
Dissolved oxygen (DO)	-0.86*	0.77	0.589	-0.92**

*$P < 0.05$, **$P < 0.01$.

Moreover, studies in dissolved inorganic nutrients in the same cruise also showed that dissolved silicon (DSi) was mainly generated by sediment release, accounting for 94.2% in this area, and DSi increased from June onward, reaching a maximum in August (Yang et al., 2020). The results suggested that variation of DSi associated with DO consumption in the bottom, indicating that the mineralization of the settled diatom could contribute to deoxygenation. Therefore, the formation of hypoxia was related to the quick sinking and subsequent mineralization of diatom blooms in the study area.

In addition, stratification of the water column has also been shown be an important factor contributing to hypoxia (Wiseman et al., 1997; Murphy et al., 2011; Hamidi et al., 2015). In the study area, temperature and salinity stratification appeared from June to September. In November, the temperature and salinity distributed vertical homogeneity with adequate water exchange. Water column stratification influences the replenishment of oxygen by restricting exchanges between near-bottom waters and surface waters. Moreover, the organic matters derived from diatom blooms sinking below the pycnocline led to more oxygen depletion in near-bottom waters in summer. Therefore, both the diatom bloom as a biological factor and the thermohaline stratification as a hydrological factor could affect the formation of hypoxia. To further reveal the contribution of phytoplankton blooms sinking to the organic carbon and DO reduction in the hypoxia zone, sediment traps together with the evaluation of carbon flux could be conducted in further investigations.

4.2 Shifting of Diatom-Dinoflagellate Dominance After Early-Spring Bloom

An increasing trend in dinoflagellate abundance has been detected throughout the Baltic Sea in recent decades, and *Peridiniella catenata* (syn. *Gonyaulax catenata*) dominated in the phytoplankton community during phytoplankton bloom in the end of April (Lignell et al., 1993; Wasmund and Uhlig, 2003; Klais et al., 2011; Hajdu et al., 2000; Stoecker et al., 2017). In this study, the relative abundance of dinoflagellate reached the highest value in May and remained in high abundance until July, after the early-spring diatom bloom (**Figure 4**). In particular, the dominance of *Gonyaulax* spp. was 0.66 in June, while the diatom species even had no dominance in May ($Y < 0.02$).

During the investigation, the spatial distribution of surface nutrients exhibited an obvious seaward gradient, and the nutrients were higher in the inshore zones than in the offshore zones, especially DIN and DIP (Sun et al., 2021), leading to the higher phytoplankton abundance off coastal waters in March. However, terrestrial input was not the primary source of DSi to the study area (Liu et al., 2006), as sediment was the main source of DSi (Sun et al., 2021). In the study area, DSi increased in June with the degradation of settled diatom and reached to a maximum in August (Yang et al., 2020). This variation of DSi was consistent with shifting of diatoms–dinoflagellates, which decreased after the diatom blooming but reached maximum supporting diatom dominance to the first in September. Therefore, early-spring diatom bloom could result in dinoflagellate dominance in subsequent months and restoration of diatom dominance with release of DSi after sedimentation.

In addition to the effects of nutrients, many other factors could contribute to dinoflagellate dominance in the nearshore area of the northern Yellow Sea. Changes in mixing conditions, stratification, and wind-induced cyst resuspension have all been invoked to explain the dinoflagellate increase in the Baltic Sea (Kremp, 2001; Klais et al., 2011; Lips et al., 2011; Sildever et al., 2017). As cysts of the dominant dinoflagellates, *Gonyaulax* spp. and *Alexandrium* spp. have been shown to be dominant in Yellow Sea sediments (Liu et al., 2012; Wu et al., 2018); the potential effects of cyst germination on dinoflagellate dominance especially during the deoxygenation period should be focused in future to explain the shifting of diatom–dinoflagellate in nearshore water of the northern Yellow Sea.

5 CONCLUSIONS

Diatoms and dinoflagellates are the dominant groups, and diatom blooms occurred nearshore (station 6) in March. Hypoxic zones (<2 mg l^{-1}) were observed in bottom waters in August. The low DO zone in bottom waters in August was clearly associated with the high phytoplankton cell abundance of surface waters in March. Degradation of organic matter derived from diatom blooms is essential to the formation of low DO and shifting of diatom–dinoflagellate dominance. Moreover, water-column stratification, which occurred from May to August, could also be an important factor contributing to hypoxia. Moreover, water-column stratification, which occurred from May to August, could also be an important factor contributing to DO decrease and dinoflagellate dominance. Therefore, further *in situ* studies are needed for a better understanding of hypoxia and algal blooms in this typical

nearshore area, to assure the health of aquaculture in Muping marine ranching and sustainability in fishery resource zones nearby.

DATA AVAILABILITY STATEMENT

The original contributions presented in the study are included in the article/supplementary material. Further inquiries can be directed to the corresponding authors.

AUTHOR CONTRIBUTIONS

XS contributed in conceptualization, methodology, and writing. ZL contributed in the application of statistical and writing of the draft. XD contributed in conducting the research and investigation process. GJ contributed in conducting the research and investigation process. LW contributed in project administration. XG contributed in project administration. QC contributed in data curation. LZ contributed in application of statistical to analyze the study data. All authors contributed to the article and approved the submitted version.

FUNDING

This study was financially supported by the National Key Research and Development Program of China (Grant No. 2018YFC1407501); the National Natural Science Foundation of China (NSFC) (Grant No. 41806152); Science Foundation of Shandong Jianzhu University (XNBS1937).

ACKNOWLEDGMENTS

The authors are grateful to Professor Jianmin Zhao, for sharing his program cruise to us, and Zhang Fan, student at Shandong University, for participation in the cruises and in counting phytoplankton samples.

REFERENCES

Bausch, A. R., Juhl, A. R., Donaher, N. A., and Cockshutt, A. M. (2019). Combined Effects of Simulated Acidification and Hypoxia on the Harmful Dinoflagellate *Amphidinium Carterae*. *Mar. Biol.* 166 (80), 1–19. doi: 10.1007/s00227-019-3528-y

Bianchi, T. S., and Allison, M. A. (2009). Large-River Delta-Front Estuaries as Natural "Recorders" of Global Environmental Change. *Proc. Natl. Acad. Sci.* 106 (20), 8085.e8092. doi: 10.1073/pnas.0812878106

Breitburg, D., Hondorp, D. W., Davias, L. A., and Diaz, R. J. (2009). Hypoxia, Nitrogen, and Fisheries: Integrating Effects Across Local and Global Landscapes. *Annu. Rev. Mar. Sci.* 1, 329–349. doi: 10.1146/annurev.marine.010908.163754

Breitburg, D., Levin, L. A., Oschlies, A., Gregoire, M., Chavez, F. P., Conley, D. J., et al. (2018). Declining Oxygen in the Global Ocean and Coastal Waters. *Science.* 359 (6371), 46. doi: 10.1126/science.aam7240

Carstensen, J., Andersen, J. H., Gustafsson, B. G., and Conley, D. J. (2014). Deoxygenation of the Baltic Sea During the Last Century. *Proc. Natl. Acad. Sci. U.S.A.* 111 (15), 5628–5633. doi: 10.1073/pnas.1323156111

Chen, C. C., Gong, G. C., and Shiah, F. K. (2007). Hypoxia in the East China Sea: One of the Largest Coastal Low-Oxygen Areas in the World. *Mar. Environ. Res.* 64, 399–408. doi: 10.1016/j.marenvres.2007.01.007

Chi, L., Song, X., Ding, Y., Yuan, Y., Wang, W., Cao, X., et al. (2021). Heterogeneity of the Sediment Oxygen Demand and its Contribution to the Hypoxia Off the Changjiang Estuary and Its Adjacent Waters. *Mar. Pollut. Bull.* 172, 112920. doi: 10.1016/j.marpolbul.2021.112920

Conley, D. J., Carstensen, J., Aigars, J., Axe, P., Bonsdorff, E., Eremina, T., et al. (2011). Hypoxia Is Increasing in the Coastal Zone of the Baltic Sea. *Environ. Sci. Technol.* 45 (16), 6777–6783. doi: 10.1021/es201212r

Diaz, R. J., and Rosenberg, R. (2008). Spreading Dead Zones and Consequences for Marine Ecosystems. *Science.* 321, 926–929. doi: 10.1126/science.1156401

Dong, Z., Liu, D., Wang, Y., Di, B., Song, X., Shi, Y., et al. (2012). A Report on a Moon Jellyfish Aurelia Aurita Bloom in Sishili Bay, Northern Yellow Sea of China in 2009. *Aquat. Ecosyst. Health* 15 (2), 161–167. doi: 10.1080/14634988.2012.689583

Egge, J. K., and Aksnes, D. L. (1992). Silicate as Regulating Nutrient in Phytoplankton Competition. *Mar. Ecol. Prog. Ser.* 83 (2-3), 281–289. doi: 10.3354/meps083281

Falkowski, P. G., and Woodhead, A. D. (1992). Primary Productivity and Biogeochemical Cycles in the Sea. *Plenum. Press.* 43. doi: 10.1007/978-1-4899-0762-2

Fan, X., Cheng, F., Yu, Z., and Song, X. (2018). The Environmental Implication of Diatom Fossils in the Surface Sediment of the Changjiang River Estuary (CRE) and Its Adjacent Area. *J. Oceanol. Limnol.* 37 (2), 552–567. doi: 10.1007/s00343-019-8037-9

Fennel, K., and Testa, J. M. (2019). Biogeochemical Controls on Coastal Hypoxia. *Annu. Rev. Mar. Sci.* 11, 105–130. doi: 10.1146/annurev-marine-010318-095138

Frigstad, H., Kaste, Y., Deininger, A., Kvalsund, K., Christensen, G., Bellerby, R. G. J., et al. (2020). Influence of Riverine Input on Norwegian Coastal Systems. *Front. Mar. Sci.* 7. doi: 10.3389/fmars.2020.00332

Guo, S., Sun, J., Zhao, Q., Feng, Y., Huang, D., Liu, S., et al. (2016). Sinking Rates of Phytoplankton in the Changjiang (Yangtze River) Estuary: A Comparative Study Between *Prorocentrum Dentatum* and *Skeletonema Dorhnii* Bloom. *J. Mar. Syst.* 154, 5–14. doi: 10.1016/j.jmarsys.2015.07.003

Hajdu, S., Edler, L., Olenina, I., and and Witek, B.. (2000). Spreading and Establishment of the Potentially Toxic Dinoflagellate *Prorocentrum Minimum* in the Baltic Sea. *Int. Rev. Hydrobiol.* 85 (5-6), 561–575. doi: 10.1002/1522-2632(200011)85:5/6<561

Hamidi, S. A., Bravo, H. R., Klump, J. V., and Waples, J. T. (2015). The Role of Circulation and Heat Fluxes in the Formation of Stratification Leading to Hypoxia in Green Bay, Lake Michigan. J. *Great. Lake. Res.* 41 (4), 1024–1036. doi: 10.1016/j.jglr.2015.08.007

He, Q., and Silliman, B. R. (2019). Climate Change, Human Impacts, and Coastal Ecosystems in the Anthropocene. *Curr. Biol.* 29 (19), R1021–R1035. doi: 10.1016/j.cub.2019.08.042

Klais, R., Tamminen, T., Kremp, A., Spilling, K., and Olli, K. (2011). Decadal-Scale Changes of Dinoflagellates and Diatoms in the Anomalous Baltic Sea Spring Bloom. *PloS One* 6 (6), e21567. doi: 10.1371/journal.pone.0021567

Kremp, A. (2001). Effects of Cyst Resuspension on Germination and Seeding of Two Bloom-Forming Dinoflagellates in the Baltic Sea. *Mar. Ecol. Prog. Ser.* 216, 57–66. doi: 10.3354/meps216057

Lignell, R., Heiskanen, A. S., Kuosa, H., Gundersen, K., Kuuppoleinikki, P., Pajuniemi, R., et al. (1993). Fate of a Phytoplankton Spring Bloom: Sedimentation and Carbon Flow in the Planktonic Food Web in the Northern Baltic. *Mar. Ecol. Prog. Ser.* 94 (3), 239–239. doi: 10.3354/meps094239

Lips, U., Lips, I., Liblik, T., Kikas, V., Altoja, K., Buhhalko, N., et al. (2011). Vertical Dynamics of Summer Phytoplankton in a Stratified Estuary (Gulf of Finland, Baltic Sea). *Ocean. Dynam.* 61 (7), 903–915. doi: 10.1007/s10236-011-0421-8

Li, Z., Song, S., Li, C., and Yu, Z. (2018). The Sinking of the Phytoplankton Community and Its Contribution to Seasonal Hypoxia in the Changjiang (Yangtze River) Estuary and Its Adjacent Waters. *Estuar. Coast. Shelf. Sci.* 208, 170–179. doi: 10.1016/j.ecss.2018.05.007

Liu, G., Cai, X., Tong, F., Wang, L., and Zhang, X. (2014). Investigation of Massive Death of Sea Cucumber in Artificial Reef Zone of Shuangdao Bay, Weihai. *Fish. Inform. Strateg.* 29, 122–129. doi: 10.13233/j.cnki.fishis.2014.02.020

Liu, Y. H., Liu, X. J., Xing, Y. H., Jin, Y., Ma, Y. Q., and Liu, X. B. (2006). Analysis of the Water Quality in the Sea Area of Sishili Bay of Yantai in 2003. *Trans. Oceanol. Limnol.* 3, 93–97. doi: 10.13984/j.cnki.cn37-1141.2006.03.014

Liu, D., Shi, Y., Di, B., Sun, Q., Wang, Y., Dong, Z., et al. (2012). The Impact of Different Pollution Sources on Modern Dinoflagellate Cysts in Sishili Bay, Yellow Sea, China. *Mar. Micropaleontol.* 84-85, 1–13. doi: 10.1016/j.marmicro.2011.11.001

Li, X., Yu, Z., Song, X., Cao, X., and Yuan, Y. (2011). The Seasonal Characteristics of Dissolved Oxygen Distribution and Hypoxia in the Changjiang Estuary. *J. Coast. Res.* 27, 52–62. doi: 10.2112/JCOASTRES-D-11-00013.1

Murphy, R. R., Kemp, W. M., and Ball, W. P. (2011). Long-Term Trends in Chesapeake Bay Seasonal Hypoxia, Stratification, and Nutrient Loading. *Estuar. Coast.* 34 (6), 1293–1309. doi: 10.1007/s12237-011-9413-7

O'Connor, T., and Whitall, D. (2007). Linking Hypoxia to Shrimp Catch in the Northern Gulf of Mexico. *Mar. Pollut. Bull.* 54 (4), 460–463. doi: 10.1016/j.marpolbul.2007.01.017

Pytkowicx, R. M. (1971). On the Apparent Oxygen Utilization and the Preformed Phosphate in the Oceans. *Limnol. Oceanogr.* 16 (1), 39–42. doi: 10.4319/lo.1971.16.1.0039

Rabouille, C., Conley, D. J., Dai, M. H., Cai, W. J., Chen, C., Lansard, B., et al. (2008). Comparison of Hypoxia Among Four River-Dominated Ocean Margins: The Changjiang (Yangtze), Mississippi, Pearl, and Rhone Rivers. *Cont. Shelf. Res.* 28, 1527–1537. doi: 10.1016/j.csr.2008.01.020

Regnier, P., Friedlingstein, P., Ciais, P., Mackenzie, F. T., Gruber, N., Janssens, I. A., et al. (2013). Anthropogenic Perturbation of the Carbon Fluxes From Land to Ocean. *Nat. Geosci.* 6 (8), 597–607. doi: 10.1038/NGEO1830

Roman, M. R., Pierson, J. J., Kimmel, D. G., Boicourt, W. C., and Zhang, X. (2012). Impacts of Hypoxia on Zooplankton Spatial Distributions in the Northern Gulf of Mexico. *Estuar. Coast.* 35 (5), 1261–1269. doi: 10.1007/s12237-012-9531-x

Sildever, S., Kremp, A., Enke, A., Buschmann, F., Maljutenko, I., and Lips, I. (2017). Spring Bloom Dinoflagellate Cyst Dynamics in Three Eastern Sub-Basins of the Baltic Sea. *Cont. Shelf. Res.* 137, 46–55. doi: 10.1016/j.csr.2016.11.012

Sinkko, H., Lukkari, K., Jama, A. S., Sihvonen, L. M., Sivonen, K., Leivuori, M., et al. (2011). Phosphorus Chemistry and Bacterial Community Composition Interact in Brackish Sediments Receiving Agricultural Discharges. *PloS One* 6, e21555. doi: 10.1371/journal.pone.0021555

Smith, S. V., and Hollibaugh, J. T. (1993). Coastal Metabolism and the Oceanic Organic Carbon Balance. *Rev. Geophys.* 31, 75–89. doi: 10.1029/92RG02584

Spilling, K., Olli, K., Lehtoranta, J., Kremp, A., Tedesco, L., Tamelander, T., et al. (2018). Shifting Diatom-Dinoflagellate Dominance During Spring Bloom in the Baltic Sea and its Potential Effects on Biogeochemical Cycling. *Front. Mar. Sci.* 5. doi: 10.3389/fmars.2018.00327

Stoecker, D. K., Hansen, P. J., Caron, D. A., and Mitra, A. (2017). Mixotrophy in the Marine Plankton. *Annu. Rev. Mar. Sci.* 9, 311–335. doi: 10.1146/annurev-marine-010816-060617

Su, J., Dai, M., He, B., Wang, L., Gan, J., Guo, X., et al. (2017). Tracing the Origin of the Oxygen-Consuming Organic Matter in the Hypoxic Zone in a Large Eutrophic Estuary: The Lower Reach of the Pearl River Estuary, China. *Biogeosciences* 14 (18), 4085–4099. doi: 10.5194/bg-14-4085-2017

Sun, X., Dong, Z., Zhang, W., Sun, X., Hou, C., Liu, Y., et al. (2021). Seasonal and Spatial Variations in Nutrients Under the Influence of Natural and Anthropogenic Factors in Coastal Waters of the Northern Yellow Sea, China. *Mar. Pollut. Bull.* 175, 113171. doi: 10.1016/j.marpolbul.2021.113171

Sun, J., and Liu, D. (2003). The Application of Diversity Indices in Marine Phytoplankton Studies. *Acta Oceanol. Sin.* 26, 62–75. doi: 10.3321/j.issn:0253-4193.2004.01.007

Sun, S., Zhang, F., Li, C., Wang, S., Wang, M., Tao, Z., et al. (2015). Breeding Places, Population Dynamics, and Distribution of the Giant Jellyfish *Nemopilema Nomurai* (Scyphozoa: Rhizostomeae) in the Yellow Sea and the East China Sea. *Hydrobiologia* 754 (1), 59–74. doi: 10.1007/s10750-015-2266-5

Tomas, C. R. (1997). *Identifying Marine Phytoplankton* (New York: Academic Press), 1–858.

Turner, R. E., Rabalais, N. N., and Justic, D. (2008). Gulf of Mexico Hypoxia: Alternate States and a Legacy. *Environ. Sci. Technol.* 42 (7), 2323–2327. doi: 10.1021/es071617k

Utermöhl, H. (1958).). Zur Vervolkommung Der Quantitative Phytoplankton-Methodik. *Mitt. Int. Ver. Theor. Angew. Limnol.* 9, 1–38. doi: 10.1080/05384680.1958.11904091

Wang, B. (2009). Hydromorphological Mechanisms Leading to Hypoxia Off the Changjiang Estuary. *Mar. Environ. Res.* 67 (1), 53–58. doi: 10.1016/j.marenvres.2008.11.001

Wang, H., Dai, M., Liu, J., Kao, S., Zhang, C., Cai, W., et al. (2016). Eutrophication-Driven Hypoxia in the East China Sea Off the Changjiang Estuary. *Environ. Sci. Technol.* 50 (5), 2255–2263. doi: 10.1021/acs.est.5b06211

Wang, L., Liang, Z., Guo, Z., Cong, W., Song, M., Wang, Y., et al. (2022). Response Mechanism of Microbial Community to Seasonal Hypoxia in Marine Ranching. *Sci. Tot. Environ.* 811, 152387. doi: 10.1016/j.scitotenv.2021.152387

Wang, Y., Liu, D., Dong, Z., Di, B., and Shen, X. (2012). Temporal and Spatial Distributions of Nutrients Under the Influence of Human Activities in Sishili Bay, Northern Yellow Sea of China. *Mar. Pollut. Bull.* 64 (12), 2708–2719. doi: 10.1016/j.marpolbul.2012.09.024

Wasmund, N., and Uhlig, S. (2003). Phytoplankton Trends in the Baltic Sea. *ICES. J. Mar. Sci.* 60 (2), 177–186. doi: 10.1016/S1054-3139(02)00280-1

Wei, H., He, Y., Li, Q., Liu, Z., and Wang, H. (2007). Summer Hypoxia Adjacent to the Changjiang Estuary. *J. Mar. Syst.* 67, 292–303. doi: 10.1016/j.jmarsys.2006.04.014

Wei, Q., Wang, B., Zhang, X., Ran, X., Fu, M., Sun, X., et al. (2020). Contribution of the Offshore Detached Changjiang (Yangtze River) Diluted Water to the Formation of Hypoxia in Summer. *Sci. Tot. Environ.* 764, 142838. doi: 10.1016/j.scitotenv.2020.142838

Wiseman, W., Rabalais, N. N., Turner, R. E., Dinnel, S. P., and MacNaughton, A. (1997). Seasonal and Interannual Variability Within the Louisiana Coastal Current: Stratification and Hypoxia. *J. Mar. Syst.* 12 (1-4), 237–248. doi: 10.1016/S0924-7963(96)00100-5

Wu, H., Luan, Q., Guo, M., Gu, H., Zhai, Y., and Tan, Z. (2018). Phycotoxins in Scallops (Patinopecten Yessoensis) in Relation to Source, Composition and Temporal Variation of Phytoplankton and Cysts in North Yellow Sea, China. *Mar. Poll. Bull.* 135, 1198–1204. doi: 10.1016/j.marpolbul.2018.08.045

Yang, B., Gao, X., and Xing, Q. (2018). Geochemistry of Organic Carbon in Surface Sediments of a Summer Hypoxic Region in the Coastal Waters of Northern Shandong Peninsula. *Cont. Shelf. Res.* 171, 113–125. doi: 10.1016/j.csr.2018.10.015

Yang, B., Gao, X., Zhao, J., Lu, Y., and Gao, T. (2020). Biogeochemistry of Dissolved Inorganic Nutrients in an Oligotrophic Coastal Mariculture Region of the Northern Shandong Peninsula, North Yellow Sea. *Mar. Poll. Bull.* 150, 110693. doi: 10.1016/j.marpolbul.2019.110693

Zhai, W. D., Zheng, N., Huo, C., Xu, Y., Zhao, H. D., Li, Y. W., et al. (2014). Subsurface pH and Carbonate Saturation State of Aragonite on the Chinese Side of the North Yellow Sea: Seasonal Variations and Controls. *Biogeosciences* 11, 1103–1123. doi: 10.5194/bg-11-1103-2014

Zhang, Y., Gao, X., Guo, W., Zhao, J., and Li, Y. (2018). Origin and Dynamics of Dissolved Organic Matter in a Mariculture Area Suffering From Summertime Hypoxia and Acidification. *Front. Mar. Sci.* 5. doi: 10.3389/fmars.2018.00325

Conflict of Interest: The authors declare that the research was conducted in the absence of any commercial or financial relationships that could be construed as a potential conflict of interest.

Publisher's Note: All claims expressed in this article are solely those of the authors and do not necessarily represent those of their affiliated organizations, or those of the publisher, the editors and the reviewers. Any product that may be evaluated in this article, or claim that may be made by its manufacturer, is not guaranteed or endorsed by the publisher.

frontiers | Frontiers in Marine Science

ORIGINAL RESEARCH
published: 25 May 2022
doi: 10.3389/fmars.2022.908813

Inhibitory Effect of Isolated Bacteria from the Phycosphere of *Levanderina fissa* on the Growth of Different Microalgae

Yali Tang, Changliang Xie, Xiaotong Jin, Zhaohui Wang* and Ren Hu**

Department of Ecology, Jinan University, Guangzhou, China

Levanderina fissa (formerly *Gyrodinium instriatum*) frequently causes blooms in the Pearl River Estuary and has few advantages in interspecific competition with other bloom-forming algal species. Phycosphere bacteria, which closely interact with algal cells, may play an ecologically functional role in the population dynamics and bloom occurrence. To test this hypothesis, we isolated and identified cultivable bacteria coexisting in different growth stages of *L. fissa* by the gradient dilution method and investigated the characteristics of the bacterial interactions with three diatom species (*Chaetoceros curvisetus*, *Skeletonema dohrnii*, and *Phaeodactylum tricornutum*) and three dinoflagellate species (*Scrippsiella acuminata*, *Karenia mikimotoi*, and the host algae) after screening for functional bacteria. One of the isolated bacterial strains, Lf7, which was phylogenetically identified as an *Alteromonas* species, showed significant inhibitory effects on different algal species except its host. Moreover, all algal species, especially their hosts, showed significant stimulatory effects on bacterial Lf7 growth. These results indicate that the phycosphere bacterium Lf7 may play some ecological roles in the competition between its host alga *L. fissa* and other phytoplankton. The study also highlights the complicated interactions between phycosphere bacteria and host algae.

Keywords: algicidal bacteria, phycosphere, harmful algal bloom, growth, algae-bacteria interactions

OPEN ACCESS

Edited by:
Zhangxi Hu,
Guangdong Ocean University, China

Reviewed by:
Xinfeng Dai,
Ministry of Natural Resources, China
Arief Rachman,
National Research and Innovation Agency, Indonesia

****Correspondence:***
Zhaohui Wang
twzh@jnu.edu.cn
Yali Tang
litangyali@163.com
Ren Hu
thuren@jnu.edu.cn

Specialty section:
This article was submitted to Aquatic Microbiology, a section of the journal Frontiers in Marine Science

Received: *31 March 2022*
Accepted: *27 April 2022*
Published: *25 May 2022*

Citation:
Tang Y, Xie C, Jin X, Wang Z and Hu R (2022) Inhibitory Effect of Isolated Bacteria from the Phycosphere of Levanderina fissa on the Growth of Different Microalgae. Front. Mar. Sci. 9:908813. doi: 10.3389/fmars.2022.908813

1 INTRODUCTION

The phycosphere is the planktonic analogue of the rhizosphere in plants (Seymour et al., 2017). Phytoplankton–bacteria relationships in this microenvironment can span mutualism, antagonism, parasitism, and competition, indicating a multifarious and highly sophisticated ecological function of phycosphere bacteria (Cole, 1982; Findlay and Patil, 1984; Amin et al., 2012; Seymour et al., 2017; Höger et al., 2021). Competitive or antagonistic relationships of phycosphere bacteria and phytoplankton have been mostly extensively studied, including their competition for inorganic nutrients (Bratbak and Tingstad, 1985), algicidal abilities of bacteria (Mayali and Azam, 2004; Umetsu et al., 2019), and defense mechanisms of phytoplankton (Teplitski et al., 2004; Rajamani et al., 2011; Stien et al., 2016). Their mutualism associations were recently revealed and proposed to be more prevalent than antagonism (Xie et al., 2013; Buchan et al., 2014; Calatrava et al., 2018).

Some studies have described the phycosphere bacteria of certain algae as friends with benefits (Amin et al., 2009; Kim et al., 2014; Johansson et al., 2019). For example, several clades of *Marinobacter* ubiquitously found in close association with dinoflagellates and coccolithophores produce an unusually lower affinity dicitrate siderophore, vibrioferrin, which increased algal iron uptake of a representative dinoflagellate partner, *Scrippsiella trochoidea*, >20-fold (Amin et al., 2009). When *Rhizobium* sp., the most prevalent and dominant bacterium isolated from *Chlorella vulgaris*, was cocultured with green algae, it increased the algal cell count by approximately 72% (Kim et al., 2014). Several phycosphere bacterial strains (*Arenibacter algicola* strain SMS7, *Marinobacter salarius* strain SMR5, *Sphingorhabdus flavimaris* strain SMR4y, *Sulfitobacter pseudonitzschiae* strain SMR1, *Yoonia vestfoldensis* strain SMR4r and *Roseovarius mucosus* strain SMR3) stimulate the growth of the diatom partner *Skeletonema marinoi* under different environmental conditions, for example, low iron concentrations and high and low temperatures (Johansson et al., 2019). Symbiotic bacteria may also provide the host with vitamins and organic acids, including amino acids and siderophores, and are essential to the growth of their host (Croft et al., 2005; Amin et al., 2009; Sandhya and Vijayan, 2019). Moreover, these kinds of phycosphere bacteria are well adapted to a narrow range of compounds secreted by their algal host, forming an exclusively specific association with the host algae (Bell, 1984; Schäfer et al., 2002; Sapp et al., 2007; Sison-Mangus et al., 2014; Palacios et al., 2022). This may not be the only way phycosphere bacteria benefit their algal hosts. Our laboratory isolated several phycosphere bacteria that showed inhibitory activity against algal species other than their host (Wang et al., 2021).

Levanderina fissa (formerly *Gyrodinium instriatum*) has frequently caused blooms in the Pearl River Estuary in the past two decades, for example, blooms in Shenzhen Bay in 1998, 2003, and 2007 (Wang et al., 2001; Zhu et al., 2004; SOA, 2008); Lingding Bay in 2002 (Wang et al., 2003); and Zhuhai coastal waters in 2009 (Wang et al., 2011). However, blooms caused by this species elsewhere were rare and were observed only in the Gulf of Guayaquil in Ecuador (Jimenéz, 1993); Hakozaki Fishing Port of Japan (Nagasoe et al., 2006; Nagasoe et al., 2010); and Bahia de Acapulco, Mexico (Gárate-Lizárraga et al., 2013). Our previous study showed that *L. fissa* had few advantages in interspecific competition with three other algal bloom-forming species, namely, *Skeletonema dohrnii* (Bacillariophyceae), *Prorocentrum micans* (Dinophyceae), and *Chattonella marina* (Raphidophyceae), using pure, sterilized cultures (Wang et al., 2021). Thus, we suspect that phycospheric bacteria may play an ecological function role by promoting the growth or competition of *L. fissa*. To test this hypothesis, we isolated and identified cultivable bacteria coexisting in different growth stages of *L. fissa* by the gradient dilution method and obtained an isolate with an inhibitory effect on algal growth by screening experiments with *C. curvisetus*. We also cocultured the isolate Lf7 at different inoculation doses with three diatom species, *Chaetoceros curvisetus*, *Skeletonema dohrnii*, and *Phaeodactylum tricornutum*, as well as three dinoflagellate species, *Scrippsiella acuminata*, *Karenia mikimotoi*, and *L. fissa*, to determine their effects on these commonly dominant phytoplankton species in the Pearl River Estuary. Our research will provide insight into the ecological function of phycosphere bacteria on algal growth, interspecies competition, and bloom formation.

2 MATERIALS AND METHODS

2.1 Isolation of Bacterial Strains from the Phycosphere of *Levanderina fissa*

2.1.1 Microalgal Culture

Levanderina fissa (GenBank accession no. ITS: KF435124) was isolated in October 2009 during a bloom in the Pearl River Estuary, South China Sea. The cultures were maintained in autoclaved (121°C, 20 min) f/2 medium (Guillard, 1975). Algal cells at the exponential phase were incubated in 250 mL Erlenmeyer flasks containing 100 mL of sterilized f/2 medium. The medium was made with artificial sea salt (Red Coral Sea, nutrient-free formula) with a salinity of 30-31 and pH of 7.9 ± 0.1. Microalgal cultures were maintained in an incubator at 20 ± 1°C and illuminated with 100 μmol photon/m^2·s cool-white fluorescent illumination with a dark:light cycle of 12:12 h.

2.1.2 Isolation of Cultivable Bacteria in the Phycosphere

Samples were aseptically collected at five growth phases of *L. fissa*, that is, the lag growth phase, the logarithmic growth phase, the stationary phase, and the early and late decline phases. One milliliter of each culture was suspended in 9 mL of Zobell 2216E marine medium (Su et al., 2007) to a dilution of 10^{-1}. Zobell 2216E marine medium was prepared using artificial seawater. These suspensions were further diluted in the same way to dilutions of 10^{-2}-10^{-6}. A 0.1 mL aliquot of the dilutions of 10^{-3}-10^{-6} was spread onto Zobell 2216E agar plates, and the plates were incubated at 28°C for 5-7 days. Visually distinct bacterial colonies were subcultured on fresh Zobell 2216E agar plates and incubated for 5-7 days. The step was repeated three to four times to obtain purified bacterial colonies.

There were 32 bacterial isolates collected from cultures of *L. fissa*. The bacterial isolates were then identified based on sequencing of the V3 region of the 16S rRNA gene. Twelve different phylotypes were obtained after removing the duplicate rRNA gene sequences. The isolated bacteria were labelled Lf1 to Lf12. The sequences were submitted to the International Nucleotide Sequence Database Collaboration at NCBI (GenBank accession nos. KF444158-KF444169). The bacterial phylotypes belonged to Alphaproteobacteria, Gammaproteobacteria, Bacteroidetes, and Actinobacteria (**Table 1** and **Figure 1**)

2.2 Effects of Bacteria on the Growth of Different Microalgal Taxa

2.2.1 Antibacterial Treatment of Microalgal Cultures

The clonal strains of the six phytoplankton species, including three diatom species, *C. curvisetus* (GenBank accession no.: MW793400), *S. dohrnii* (GenBank accession no.: MW795694), and *P. tricornutum* (GenBank accession no.: MW793395), and three dinoflagellate species, *K. mikimotoi* (GenBank accession

TABLE 1 | The identities of bacteria isolated from phycosphere of *Levanderina fissa* and their phylogenetically most related sequences from EzTaxon database based on partial 16S rRNA gene sequences.

Strain code	GenBank accession no.	Phylum	Class	Family	Genus	Closest relatives	GenBank accession no.	Similarity (%)
Lf1	KF444165	Alphaproteobacteria	Rhodobacterales	Rhodobacteraceae	*Pseudooceanicola*	*Pseudooceanicola antarcticus*	OBEA01000013	99
Lf2	KF444164		Rhizobiales	Stappiaceae	*Roseibium*	*Roseibium marinum*	AY628423	99
Lf3	KF444162		Rhodobacterales	Rhodobacteraceae	*Ruegeria*	*Ruegeria pomeroyi*	CP000031	97
Lf4	KF444163					*Ruegeria atlantica*	CYPU01000053	99
Lf5	KF444159		Rhodospirillales	Rhodospirillaceae	*Rhodospirillum*	*Rhodospirillum rubrum*	CP000230	90
Lf6	KF444160		Sphingomonadales	Erythrobacteraceae	*Erythrobacter*	*Erythrobacter litoralis*	JMIX01000006	99
Lf7	KF444158	Gammaproteobacteria	Alteromonadales	Alteromonadaceae	*Alteromonas*	*Alteromonas macleodii*	CP003841	99
Lf8	KF444161				*Marinobacter*	*Marinobacter salsuginis*	EF028328	100
Lf9	KF444169		Pseudomonadales	Moraxellaceae	*Acinetobacter*	*Acinetobacter counvalinii*	KT997472	98
Lf10	KF444168	Actinobacteria	Actinomycetales	Micrococcaceae	*Arthrobacter*	*Arthrobacter crystallopoietes*	FNKH01000002	99
Lf11	KF444167	Bacteroidetes	Flavobacteriales	Flavobacteriaceae	*Winogradskyella*	*Winogradskyella poriferorum*	AY848823	100
Lf12	KF444166				*Robiginitalea*	*Robiginitalea biformata*	CP001712	92

no.: MW793400), *S. acuminata* (GenBank accession no.: MW793402), and *L. fissa*, were isolated between 2005 and 2009 from southern Chinese coastal waters and maintained in f/2 media (for diatoms) or in f/2 media without silicon (for dinoflagellates).

The stock cultures were treated with a mixture of antibiotics to destroy the external bacteria before the experiments. First, 10 μg/mL penicillin (final concentration) was added to 100 mL of *C. curvisetus* culture in the exponential phase and incubated for 24 h. Then, 10 mL of the penicillin-treated culture was inoculated into 100 mL of fresh f/2 medium with 10 μg/mL streptomycin sulfate and incubated for another 24 h, followed by treatment with 10 μg/mL kanamycin sulfate. The antibacterial treatment cultures were maintained in sterilized f/2 medium for the experiments.

2.2.2 Bacterial Isolation and Counting

Bacterial isolates were maintained in a Zobell 2216 marine agar plate after removing the repeated isolates by cross-comparison with the results of the rRNA gene sequences. Before the experiment, bacterial colonies were transferred to liquid Zobell 2216 medium, cultivated on a 28°C, 200 r/min shaking table for 8-10 h, and then gradually acclimated to 20°C within 2 h.

The bacterial concentration was determined by measuring the colony-forming unit (CFU) number on Zobell 2216E agar medium. Each distinct bacterial colony was counted in the plate of suitable colonies (30-300), and the concentration of each bacterium (CFU/mL) was obtained according to the dilution factor.

2.2.3 Screening of the Bacterial Strains

The effects of the 12 bacterial isolates on the growth of different microalgal taxa were screened by *C. curvisetus*. Liquid bacterial cultures of the 12 isolates in exponential phase were added to the exponential *C. curvisetus* cultures. The inoculation rate was 0.1% (v/v), and the initial bacterial concentration was 7.5×10^7 CFU/mL in the cocultures. Cultures in f/2 medium (f/2) and with the same volume of liquid Zobell 2216E medium (BC) were used as the negative controls. Algal cultures were cultivated under the same conditions as outlined in Section 2.1.1. All experiments were carried out in sterile 24-well tissue culture plates. The experiment was conducted for 5 days covering the whole exponential phase and reaching the stationary phase for *C. curvisetus*, and cell numbers were counted every day. The algal cell numbers were counted daily during the incubation period. The cell counts were performed in a cell counting chamber by placing 0.05-0.1 mL of culture into the chamber, fixing with a drop of Lugol's fixative, and observing under an inverted microscope (Leica DMIRB) at a magnification of 200×. Each sample was counted more than three times until the differences in cell counts were less than 10%. When *C. curvisetus* always showed negative growth with lower cell densities than initial cell densities, the maximum cell density was recorded as 0. All experiments were conducted in triplicate.

2.2.4 Effects of Bacterial Strain Lf7 on the Growth of Microalgal Taxa

The results of the screening test showed that the bacterial strain Lf7 had the strongest inhibitory effect on the growth of *C. curvisetus*. Therefore, Lf7 was selected as the bacterial strain to study its effects

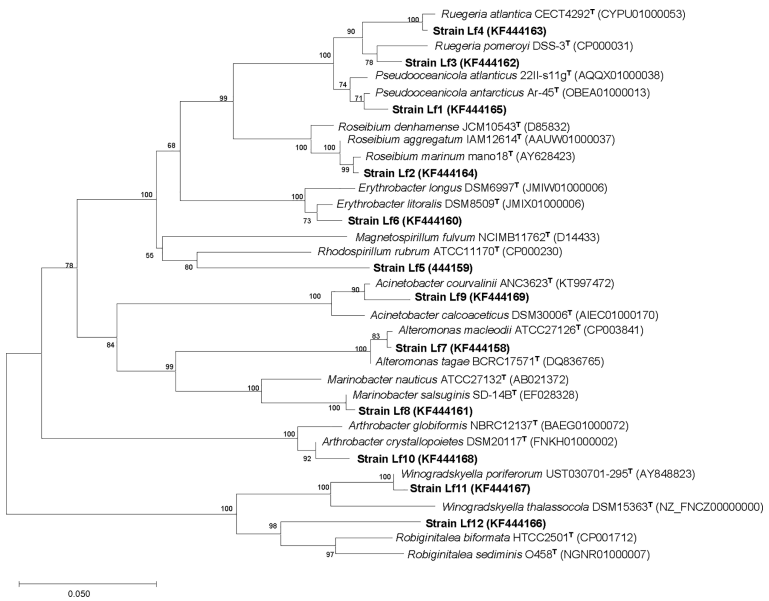

FIGURE 1 | Neighbor-joining tree, showing the phylogenetic position of bacterial strains isolated from phycosphere of *Levanderina fissa* and type strains of most phylogenetically related taxa (type species included) based on partial 16S rRNA gene sequences. GenBank accession numbers are given. Bootstrap analysis was made with 1000 resamplings; percentages of support are shown at nodes, Bar, 5% sequence divergence.

on the growth of the six different phytoplankton taxa. Four bacterial concentrations were set in the experiment, which were 7.5×10^7, 7.5×10^6, 7.5×10^5, and 7.5×10^4 CFU/mL, with an inoculation rate of 0.1% (v/v). The experiment was conducted for 6 days to cover the whole exponential phase and reach the stationary phase for the algae, and algal cell numbers and bacterial concentrations were measured every day. The initial cell densities of different microalgal taxa were set differently according to their cell sizes to obtain similar initial biomasses. The size of the microalgal taxa is described in **Supplementary Table S1**. The experiment was conducted for 6 days to cover the whole exponential phase and reach the stationary phase for the algae according to our former lab experience, and algal cell numbers and bacterial concentrations were measured every day.

This additional experimental design is the same as that in Section 2.2.3.

2.3 Data and Statistical Analysis

2.3.1 Phylogenetic Analysis

Analysis of the 16S rRNA gene sequence was performed using the software package MEGA, version 3.1 (Kumar et al., 2004). The model of Jukes and Cantor (1969) was used to compute the evolutionary distance, based on which a phylogenetic tree was constructed using the neighbor-joining method (Saitou and Nei, 1987), with a bootstrap analysis derived from 1000 replications. Sequence similarity was calculated using pairwise alignment obtained from the EzTaxon database (Chun et al., 2007).

2.3.2 Inhibitory Effect

The effects of bacterial strains on the growth of algal cells are expressed as the relative maximum cell number (%), which is defined as the maximum/final cell number in each experimental regime compared to the maximum/final cell number obtained in the f/2 medium (f/2). When cell numbers in the test group were always lower than the initial density, indicating that no active growth occurred, neither the maximum cell number (cells/mL) nor the relative maximum cell number (%) was calculated.

2.3.3 Maximum Specific Growth Rate

The specific growth rate (μ, divisions/d) of algal cells was calculated every day during the experimental period using the following equation:

$$\mu(\text{divisions/d}) = (\text{Ln}N_2 - \text{Ln}N_1)/(t_2 - t_1) \quad (1)$$

where N_2 and N_1 are cell density values at times t_2 and t_1, respectively. The maximum specific growth rate (μ_{max}) is defined as the maximum value of μ during the experiment.

2.3.4 Statistics

The mean and standard deviation (SD) were calculated for each treatment from three independent replicate cultures. The means and standard deviations of all data were calculated and graphed. Repeated measures ANOVA was used to compare growth curves of different treatments. One-way ANOVA with *post hoc* (Tukey test) analysis was conducted for multiple comparisons of the maximum specific growth rate, relative maximum cell density, and maximum bacterial concentration. Statistical analyses were performed using SPSS 25.0, and differences were considered significant when $p < 0.05$. Detailed statistical information is shown in the **Supplementary Tables**.

3 RESULTS

3.1 Bacteria Isolation from the Phycosphere of *Levanderina fissa*

The growth of *C. curvisetus* in the coculture of the 12 bacterial strains isolated from the phycosphere of *L. fissa* is shown in **Figure 2**. The cell density increased gradually in the f/2 medium and reached a maximum of 1.71×10^5 cells/mL at Day 5. The cell density in the BC control, which was supplemented with bacterial medium, increased and peaked at Day 2, with a maximum of 1.67×10^5 cells/mL. As shown in **Figure 2A**, most bacteria had no significant inhibition of the growth of *C. curvisetus*, and only two strains (Lf4 and Lf7) showed significant inhibitory effects ($p < 0.01$). The cell density of *C. curvisetus* decreased rapidly after the addition of the bacterial strain Lf7 and dropped to 2.2×10^4 cells/mL at Day 5, which was only 16.9% of the inoculation density. The growth of algal cells was significantly inhibited in the first 3 days after the addition of the bacterial strain Lf 4 ($p < 0.01$), and then the cell density increased at Day 4 and Day 5; however, it was still lower than the inoculation density. The cell densities of *C. curvisetus* in cocultures with Lf7 and Lf4 were always lower than the inoculation densities. Moreover, the maximum cell densities in the cocultures with the other 10 bacterial strains were significantly higher than those of the f/2 and BC media ($p < 0.05$, **Figure 2B**). Moreover, only *C. curvisetus* inoculated with strain Lf7 showed a negative maximum specific growth rate (**Figure 2C**). The results of the screening experiment suggested that the bacterial strain Lf7 had the most obvious growth inhibition on *C. curvisetus*. Therefore, Lf7, identified as the Gammaproteobacteria *Alteromonas* species based on a partial sequence of the 16S rRNA gene (**Table 1** and **Figure 1**), was selected for further experiments.

3.2 Effects of Bacterial Strain Lf7 on the Growth of *Chaetoceros curvisetus*

The growth curves of *C. curvisetus* in different experimental treatments were similar, except for the highest bacterial inoculation group (7.5×10^7 CFU/mL). The curves initiated at a 1–2-day lag period, then a 2–3-day rapid growth period, followed by a slow increase or a slight decrease in cell density (**Figure 3A**). Significant growth inhibition occurred only in culture with 7.5×10^7 CFU/mL bacterium Lf7, in which cell numbers deceased steadily and were always lower than the incubation number (**Figure 3A**). As shown in **Figure 4A**, the maximum cell density in the BC culture was 95.7% compared to that in the f/2 medium, while the relative maximum cell densities were over 100% (106-133%) in cultures with bacterial addition at concentrations of 7.5×10^4-7.5×10^6 CFU/mL. The algal cells showed no effective growth after adding bacteria at a concentration of 7.5×10^7 CFU/mL, and the maximum cell density was the inoculation density. The maximum specific growth rate of *C. curvisetus* showed a negative value when inoculated with 7.5×10^7 CFU/mL bacterium Lf7, indicating negative growth throughout the whole experimental period (**Figure 4B**).

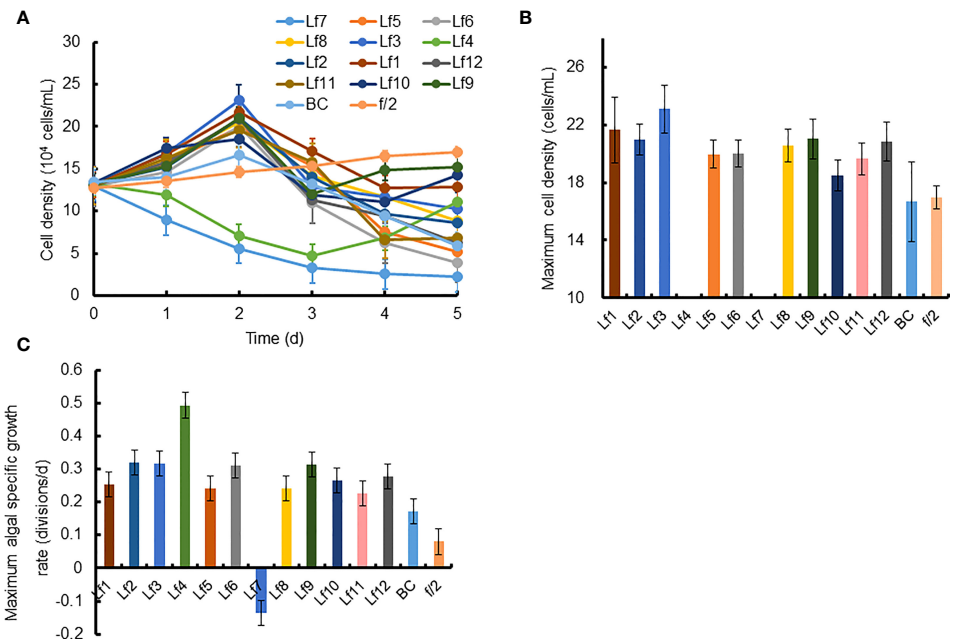

FIGURE 2 | The growth of *Chaetoceros curvisetus* in the co-culture of bacterial strains isolated from the phycosphere of *Levanderina fissa* including **(A)** Growth curve, **(B)** maximum cell density, and **(C)** maximum specific growth rate. The maximum cell densities were not shown in Lf4 and Lf7, whose cell numbers were always lower than the initial cell numbers during the experiment. Lf1-Lf12: Cultures addition of the 12 bacterial strains Lf1-Lf12, BC: Culture addition of the liquid Zobell 2216E medium, f/2: Growth in f/2 medium.

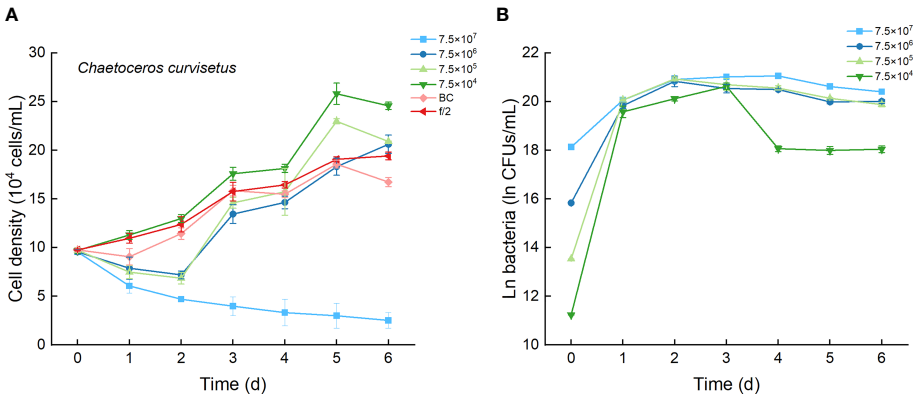

FIGURE 3 | The growth of *Chaetoceros curvisetus* in the co-cultures with different inoculum dose of bacterial strain Lf7 (7.5×10^4-7.5×10^7 CFUs/mL). **(A)** Growth curves of *C. curvisetus* in co-cultures with Lf7, **(B)** Lf7 abundances in the algal cultures.

In the coculture system, bacteria grew well and showed maximum abundances at 2 to 4 days (**Figure 3B**). The bacterial concentration in the group with the highest bacterial inoculum dose maintained the longest growing period (4 days). In all groups with different bacterial inoculum doses, the maximum bacterial concentration showed no significant difference, ranging from 8.7×10^8-1.42×10^9 CFU/mL (**Figure 4C**).

3.3 Effects of the Bacterial Strain Lf7 on the Growth of *Skeletonema dohrnii*

The cell densities of *S. dohrnii* with f/2 medium were significantly higher than those with bacterial medium. The cell densities of *S. dohrnii* inoculated with strain Lf7 were significantly lower than those inoculated with either f/2 medium or bacterial medium (**Figure 5A**). The density dropped to 15-24% of the initial

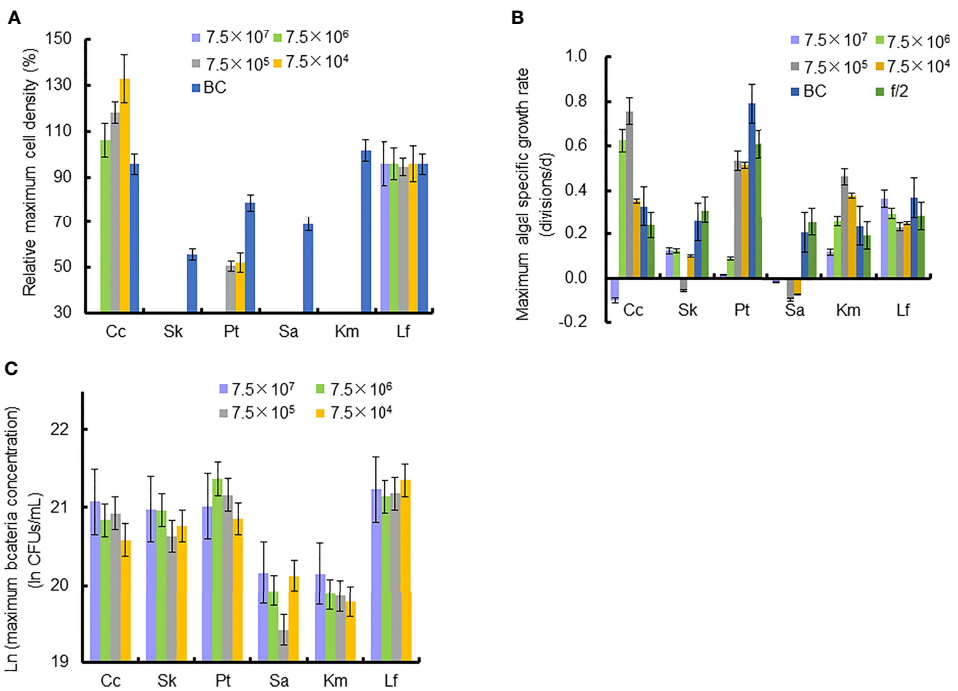

FIGURE 4 | Relative maximum algal cell density, maximum algal specific growth rate, and bacteria concentration in co-cultures of six microalgal taxa with the bacterial strain Lf7 during the six days incubation. **(A)** Relative maximum algal cell density, **(B)** maximum algal specific growth rate, **(C)** maximum Lf7 concentration in the algal cultures. Cc, co-culture of *Chaetoceros curvisetus* with Lf7; SK, co-culture of *Skeletonema dohrnii* with Lf7; Pt, co-culture of *Phaeodactylum tricornutum* with Lf7; Sa, co-culture of *Scrippsiella acuminata* with Lf7; Km, co-culture of *Karenia mikimotoi* with Lf7; Lf, co-culture of *Levanderina fissa* with Lf7.

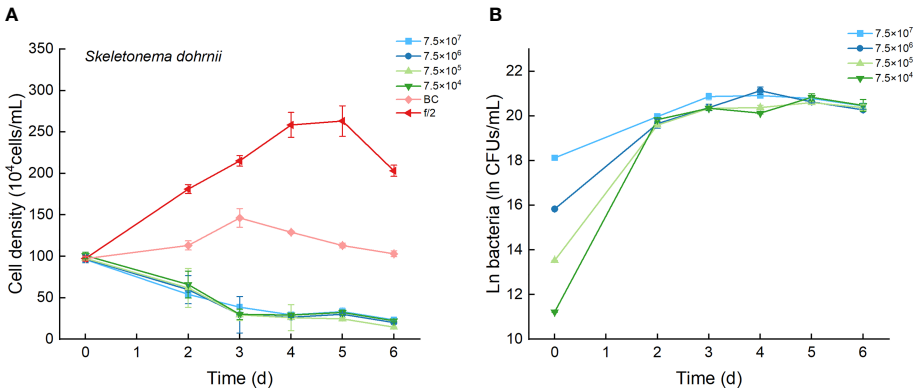

FIGURE 5 | The growth of *Skeletonema dohrnii* in the co-cultures with different concentrations of bacterial strain Lf7 (7.5×10^4-7.5×10^7 CFUs/mL). **(A)** Growth curves of *S. dohrnii* in co-cultures with Lf7, **(B)** Lf7 concentration in the algal cultures.

inoculation densities, indicating a strong inhibitory effect of the bacterial strain Lf7 on the growth of the algae *S. dohrnii*. The maximum specific growth rate of *S. dohrnii* showed a negative value when inoculated with 7.5×10^5 CFU/mL bacterium Lf7, indicating negative growth throughout the whole experimental period (**Figure 4B**).

The bacterial concentration increased significantly to 9.1×10^8-1.29×10^9 CFU/mL, showing no significant differences between groups with different bacterial inoculum doses (**Figure 5B**).

3.4 Effects of Bacterial Strain Lf7 on the Growth of *Phaeodactylum tricornutum*

As the control, *P. tricornutum* with f/2 experienced a lag phase within two days, reached maximum cell densities on the fourth day, and maintained a high cell density from Day 5 to Day 6 (**Figure 6A**). At a high inoculation dose of bacteria (7.5×10^7 and 7.5×10^6 CFU/mL), the growth of *P. tricornutum* was strongly inhibited, with a decline of 90% cell density within 3 days. Afterward, the cell density of this algae decreases slowly and remains low in such a coculture condition. Whether at a low inoculation dose of bacteria (7.5×10^4 and 7.5×10^5 CFU/mL) or under additions of bacterial medium, the growth of *P. tricornutum* showed a similar growth pattern: cell densities decreased within 2 days and gradually increased to maximum values on Day 4. The cell densities of *P. tricornutum* with high inoculation doses of strain Lf7 were significantly lower than those with either low inoculation doses of strain Lf7 or bacterial medium. The maximum specific growth rate of *P. tricornutum* showed a value close to zero when inoculated with 7.5×10^4 CFU/mL bacterium Lf7, indicating almost no growth throughout the whole experimental period (**Figure 4B**).

When cocultured with *P. tricornutum*, CFUs of strain Lf7 increased significantly (**Figure 6B**). The highest bacterial concentration occurred on Day 2 when the growth of this algae was strongly suppressed. The bacterial concentration increased to $1.14\text{-}1.9\times10^9$ CFU/mL by the end of

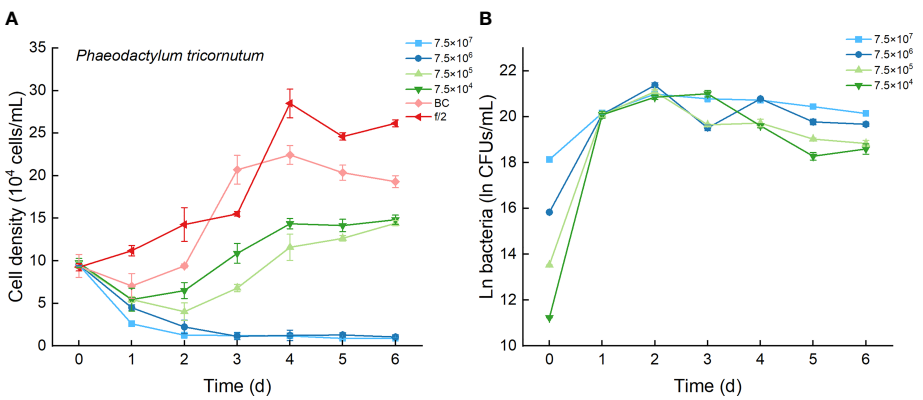

FIGURE 6 | The growth of *Phaeodactylum tricornutum* in the co-cultures with different concentrations of bacterial strain Lf7 (7.5×10^4-7.5×10^7 CFUs/mL). **(A)** Growth curves of *P. tricornutum* in co-cultures with Lf7, **(B)** Lf7 concentration in the algal cultures.

the experiment, showing no significant differences between groups with different bacterial inoculum doses ($p > 0.05$).

3.5 Effects of Bacterial Strain Lf7 on the Growth of *Scrippsiella acuminata*

As the control, the cell densities of *S. acuminata* with additions of f/2 medium and bacterial medium showed no significant differences. The cell densities of *S. acuminata* at all inoculation doses of Lf7 declined dramatically (**Figure 7A**), indicating a strong inhibitory effect of Lf7 on *S. acuminata*. Moreover, the concentration of strain Lf7 increased under the coculture conditions, with maximum values within 2.7-5.7×10^8 CFU/mL from Day 3 to Day 4 (**Figure 7B**). The maximum specific growth rate of *S. acuminata* showed a negative value at all inoculation doses of the bacterium Lf7, indicating negative growth throughout the whole experimental period for all the coculture treatments (**Figure 4B**). Among the three diatoms used in the coculture experiments, Lf7 showed the lowest maximum concentration when cocultured with *S. acuminata* (**Figure 4C**).

3.6 Effects of the Bacterial Strain Lf7 on the Growth of *Karenia mikimotoi*

As the control, the cell densities of *K. mikimotoi* with additions of f/2 medium and bacterial medium showed no significant differences in their growth curves ($p > 0.1$, **Figure 8A**). Only the maximum specific growth rate of *K. mikimotoi* cocultured with 7.5×10^6 CFU/mL bacterium Lf7 was significantly lower than that of the control (*P. tricornutum* cultured with f/2 or BC) (all $p < 0.05$, **Figure 4B**). However, the cell densities of *K. mikimoto* at all inoculation doses of Lf7 declined dramatically on the first day and were maintained at a low density, reaching 42-68% of the inoculum dose. Lf7 showed inhibitory effects on the growth of *K. mikimotoi* under the addition of all bacterial concentrations (**Figure 8A**).

The concentration of strain Lf7 under coculture conditions with *K. mikimotoi* was also similar to that with *S. acuminata* and significantly lower than that with other diatoms, reaching maximum values within 2.7-5.7×10^8 CFU/mL ($p < 0.01$, **Figures 4C**, **8B**).

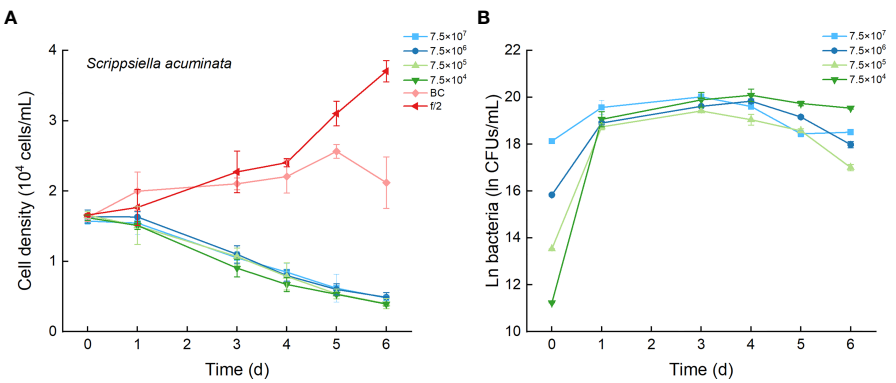

FIGURE 7 | The growth of *Scrippsiella acuminata* in the co-cultures with different concentrations of bacterial strain Lf7 (7.5×10^4-7.5×10^7 CFUs/mL). **(A)** Growth curves of *S. acuminata* in co-cultures with Lf7, **(B)** Lf7 concentration in the algal cultures.

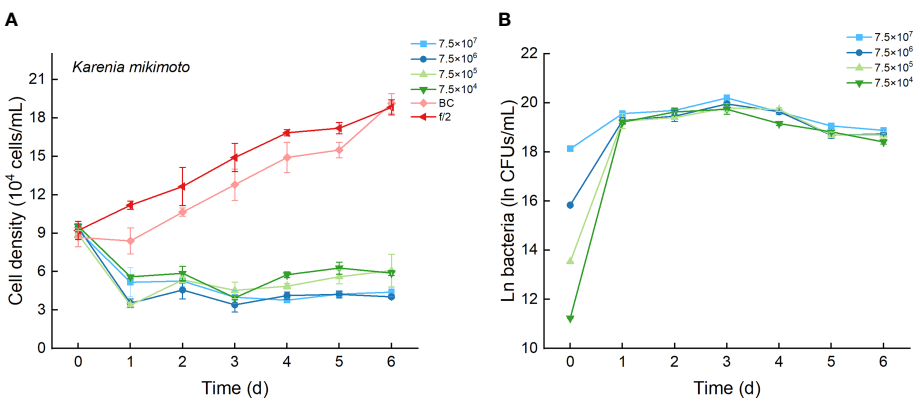

FIGURE 8 | The growth of *Karenia mikimotoi* in the co-cultures with different concentrations of bacterial strain Lf7 (7.5×10^4-7.5×10^7 CFUs/mL). **(A)** Growth curves of *K. mikimotoi* in co-cultures with Lf7, **(B)** Lf7 concentration in the algal cultures.

3.7 Effects of Bacterial Strain Lf7 on the Growth of *Levanderina fissa*

Regardless of treatments (whether with different inoculation doses of bacteria or under additions of different media), the cell densities of *L. fissa* increased to a maximum value at Day 5 (**Figure 9A**). Although the daily maximum specific growth rate occurred differently between several of the two treatments (p <0.05, **Figure 4B**), the growth curves showed no significant differences (p > 0.05), indicating that the growth of *L. fissa* was not inhibited by Lf7. However, the concentration of strain Lf7 in coculture conditions with *L. fissa* reached maximum values within 1.52-1.87×10^9 CFU/mL, with the highest average values among those of strain Lf7 in coculture conditions with all algal species in this experiment (**Figures 4C**, **9B**).

4 DISCUSSION

The study isolated and identified a total of 12 strains of cultivable bacteria coexisting in different growth stages of *L. fissa* by the gradient dilution method. Only strain Lf7, identified phylogenetically as an *Alteromonas* species using a partial 16S rRNA gene sequence, showed a significant inhibitory effect on different algal species except its host, and its growth was promoted by coculture with the host algae *L. fissa*.

Alteromonas species are frequently reported as phycosphere bacteria with two opposite interacting actions with their host (Meyer et al., 2017; Cao et al., 2021). These bacteria can directly cause the lysis of their host algae by producing β-glucosidase and chitinase (Imai et al., 1995; Wang et al., 2010; Lin et al., 2013; Umetsu et al., 2019). Shi et al. (2018) isolated an algicidal bacterium (FDHY-03) from a bloom of *Prorocentrum donghaiense* and found the characteristics of its action against *P. donghaiense* by digesting cell wall polysaccharides from the megacytic growth zone. 16S rRNA gene sequence analysis placed this strain in the genus *Alteromonas*. The beneficial effects of *Alteromonas* species on their hosts have also been reported (Ferrier et al., 2002; Sandhya and Vijayan, 2019). By examining how the entire transcriptome of *Isochrysis galbana* changed when it was cocultured with *A. macleodii* isolated from its phycosphere, Cao et al. (2021) revealed transcriptome changes, including notable increases in transcripts related to photosynthesis, carbon fixation, oxidative phosphorylation, ribosomal proteins, biosynthetic enzymes, and transport processes, as well as the depletion of transcripts encoding DNA repair enzymes, superoxide dismutase (SOD), and other stress-response proteins. Taken together with the lab-enhanced growth of *I. galbana* by coculturing with *A. macleodii*, the presence of *A. macleodii* enhanced photosynthesis and biosynthesis of *I. galbana* and protected it from stress, especially oxidative stress.

Our isolated Lf7 showed neither direct beneficial nor inhibitory effects on its host, as discussed above. However, the strain showed different inhibitory effects on the growth of five other tested algal species, including *K. mikimotoi*, *S. acuminata*, *P. tricornutum*, *C. curvisetus*, and *S. dohrnii*. All five algal species occurred in the Pearl River Estuary. Except for *the model diatom Phaeodactylum tricornutum*, the other four were reported as bloom species elsewhere (Shikata et al., 2008; Begum et al., 2015; Tse and Lo, 2017; Li et al., 2019). *L. fissa* blooms are frequent in the Pearl River Estuary, while the phenomenon is not common worldwide (Jimenéz, 1993; Nagasoe et al., 2006; Nagasoe et al., 2010; Gárate-Lizárraga et al., 2013). *L. fissa* showed few advantages in interspecific competition with three other algal bloom-forming species, *Skeletonema dohrnii* (Bacillariophyceae), *Prorocentrum micans* (Dinophyceae), and *Chattonella marina* (Raphidophyceae), using pure, sterilized cultures in previous research (Wang et al., 2021). Thus, the reason *L. fissa* outcompeted other algae in the Pearl River Estuary and other limited places might be a key factor explaining the frequent blooms. Wang et al. (2017) proposed the assumption that the ability to dissolve organic phosphorus utilization of *L. fissa* offers this species a competitive advantage in the phytoplankton community. In this study, our results hint at another possible explanation that bacteria associated with *L. fissa* might have some ecological roles in its competition with other phytoplankton.

Mutualism associations often refer to a serious chemical exchange between phytoplankton and phycosphere bacteria; for example, diatoms secrete the amino acid tryptophan, which is

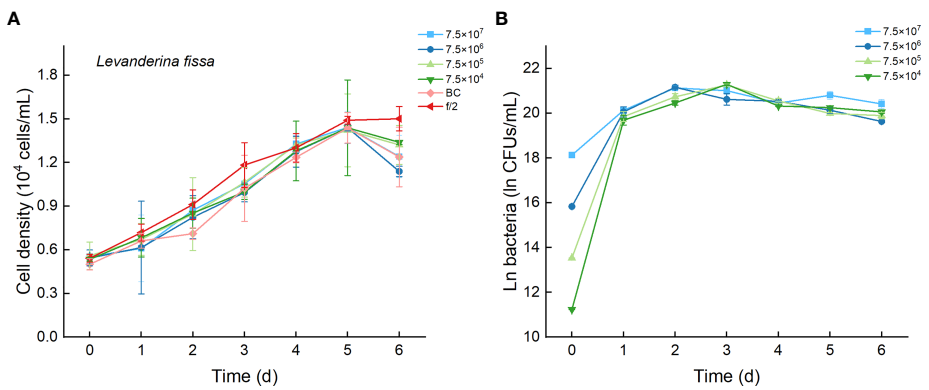

FIGURE 9 | The growth of *Levanderina fissa* in the co-cultures with different concentrations of bacterial strain Lf7 (7.5×10^4-7.5×10^7 CFUs/mL). **(A)** Growth curves of *L. fissa* in co-cultures with Lf7, **(B)** Lf7 concentration in the algal cultures.

converted by the bacterium into the hormone indole-3-acetic acid (IAA) (increasing bacterial growth simultaneously), which is then transferred from the bacterium back to the diatom to promote its cell division (Amin et al., 2015). Both bacteria and phytoplankton benefited from direct mutualism associations. *In our study, the growth of that bacterium benefited most from the original host L. fissa* among all tested algae. It is a common case that phycosphere bacteria are more adapted to a narrow range of compounds secreted by their algal host (Bell, 1984; Schäfer et al., 2002; Sapp et al., 2007; Sison-Mangus et al., 2014). Even though strain Lf7 showed no promoting effect on the growth of *L. fissa*, the inhibitory effect of strain Lf7 on other algae may lead to a competing advantage of its host. This may indicate complicated interactions between phycosphere bacteria and their host algae, which needs further lab studies.

In conclusion, by isolating and identifying cultivable bacteria coexisting in different growth stages of *Levanderina fissa* and subsequently monitoring the growth status of bacteria and microalgae in cocultural conditions, we obtained the bacterial strain Lf7 (taxonomically belonging to *Alteromonas* species), which showed inhibitory effects on the growth of five different microalgae (*K. mikimotoi*, *S. acuminata*, *P. tricornutum*, *C. curvisetus*, and *S. dohrnii*). We suspect that phycosphere bacteria Lf7 might have some ecological roles in the competition between its host algae *L. fissa* and other phytoplankton.

DATA AVAILABILITY STATEMENT

The original contributionspresented in the study are included in the article/**Supplementary Material**, further inquiries can be directed to the corresponding authors.

AUTHOR CONTRIBUTIONS

In this paper, ZW and RHvconceived and designed the experiments; CX and XJ contributed to data acquisition and analysis; YT contributed to drafting the manuscript. All authors approved the final submitted manuscript.

FUNDING

This study was funded by the National Natural Science Foundation of China (No. 42076141 and No. 32071566), Natural Science Foundation of Guangdong Province (No. 2022A1515011074), and Key Program of Marine Economy Development (Six Marine Industries) Special Foundation of Department of Natural Resources of Guangdong Province (No. GDNRC[2021]37).

ACKNOWLEDGMENTS

We are grateful for the work of numerous participants who collected and analyzed samples during the periodof experiment.

SUPPLEMENTARY MATERIAL

The Supplementary Material for this article can be found online at: https://www.frontiersin.org/articles/10.3389/fmars.2022.908813/full#supplementary-material

REFERENCES

Amin, S. A., Green, D. H., Hart, M. C., Kuepper, F. C., Sunda, W. G., and Carrano, C. J. (2009). Photolysis of Iron–Siderophore Chelates Promotes Bacterial-Algal Mutualism. *P. Natl. Acad. Sci. U.S.A.* 106, 17071–17076. doi: 10.1073/pnas.0905512106

Amin, S. A., Hmelo, L. R., Van Tol, H. M., Durham, B. P., Carlson, L. T., Heal, K. R., et al. (2015). Interaction and Signalling Between a Cosmopolitan Phytoplankton and Associated Bacteria. *Nature* 522, 98–101. doi: 10.1038/nature14488

Amin, S. A., Parker, M. S., and Armbrust, E. V. (2012). Interactions Between Diatoms and Bacteria. *Microbiol. Mol. Biol. Rev.* 76, 667–684. doi: 10.1128/MMBR.00007-12

Begum, M., Sahu, B. K., Das, A. K., Vinithkumar, N. V., and Kirubagaran, R. (2015). Extensive *Chaetoceros Curvisetus* Bloom in Relation to Water Quality in Port Blair Bay, Andaman Islands. *Environ. Monit. Assess.* 187, 1–14. doi: 10.1007/s10661-015-4461-2

Bell, W. H. (1984). Bacterial Adaptation to Low-Nutrient Conditions as Studied With Algal Extracellular Products. *Microb. Ecol.* 10, 217–230. doi: 10.1007/BF02010936

Bratbak, G., and Tingstad, T. F. (1985). Phytoplankton-Bacteria Interactions: An Apparent Paradox? Analysis of a Model System With Both Competition and Commensalism. *Mar. Ecol. Progr. Ser.* 25, 23–30. doi: 10.1016/0198-0254(86)91170-2

Buchan, A., LeCleir, G. R., Gulvik, C. A., and González, J. M. (2014). Master Recyclers: Features and Functions of Bacteria Associated With Phytoplankton Blooms. *Nat. Rev. Microbiol.* 12, 686–698. doi: 10.1038/nrmicro3326

Calatrava, V., Hom, E. F., Llamas, Á., Fernández, E., and Galván, A. (2018). OK, Thanks! A New Mutualism Between *Chlamydomonas* and Methylobacteria Facilitates Growth on Amino Acids and Peptides. *FEMS Microbiol. Lett.* 365, fny021. doi: 10.1093/femsle/fny021

Cao, J. Y., Wang, Y. Y., Wu, M. N., Kong, Z. Y., Lin, J. H., Ling, T., et al. (2021). RNA-Seq Insights Into the Impact of *Alteromonas Macleodii* on *Isochrysis Galbana*. *Front. Microbiol.* 12. doi: 10.3389/fmicb.2021.711998

Chun, J., Lee, J. H., Jung, Y., Kim, M., Kim, S., Kim, B. K., et al. (2007). EzTaxon: A Web-Based Tool for the Identification of Prokaryotes Based on 16S Ribosomal RNA Gene Sequences. *Int. J. Syst. Evol. Microbiol.* 57, 2259–2261. doi: 10.1099/ijs.0.64915-0

Cole, J. J. (1982). Interactions Between Bacteria and Algae in Aquatic Ecosystems. *Annu. Rev. Ecol. Syst.* 13, 291–314. doi: 10.2307/2097070

Croft, M. T., Lawrence, A. D., Raux-Deery, E., Warren, M. J., and Smith, A. G. (2005). Algae Acquire Vitamin B12 Through a Symbiotic Relationship With Bacteria. *Nature* 438, 90–93. doi: 10.1038/nature04056

Ferrier, M., Martin, J. L., and Rooney-Varga, J. N. (2002). Stimulation of *Alexandrium Fundyense* Growth by Bacterial Assemblages From the Bay of Fundy. *J. Appl. Microbiol.* 92, 706–716. doi: 10.1046/j.1365-2672.2002.01576.x

Findlay, J. A., and Patil, A. D. (1984). Antibacterial Constituents of the Diatom *Navicula Delognei*. *J. Nat. Prod.* 47, 815–818. doi: 10.1021/np50035a010

Gárate-Lizárraga, I., Sevilla-Torres, G., Alvarez-Anorve, M., Aguirre-Bahena, F., Violante-Gonzalez, J., and Rojas-Herrera, A. (2013). First Record of Red Tide Caused by *Gyrodinium Instriatum* (Dinophyceae: Gymnodiniales) in Bahía De Acapulco, Guerrero. *Cicimar. Oceánides* 28, 43–47. doi: 10.37543/oceanides.v28i1.120

Guillard, R. R. L. (1975). "Culture of Phytoplankton for Feeding Marine Invertebrates," in *Culture of Marine Invertebrate Animals*. Eds. W. L. Smith and M. H. Chanley (New York: Plenum Press), 29–60. doi: 10.1007/978-1-4615-8714-9_3

Höger, A. L., Griehl, C., and Noll, M. (2021). Infection With Intracellular Parasite *Amoeboaphelidium Protococcarum* Induces Shifts in Associated Bacterial Communities in Microalgae Cultures. *J. Appl. Phycol.* 33, 2863–2873. doi: 10.1007/s10811-021-02542-9

Imai, I., Ishida, Y., Sakaguchi, K., and Hata, Y. (1995). Algicidal Marine Bacteria Isolated From Northern Hiroshima Bay, Japan. *Fish. Sci.* 61, 628–636. doi: 10.1577/1548-8446(1995)020<0016:TPUOFH>2.0.CO;2

Jimenéz, R. (1993). "Ecological Factors Related to Gyrodinium Instriatum Bloom in the Inner Estuary of the Gulf of Guayaquil," in *Toxic Phytoplankton Blooms in the Sea*. Eds. T. Smayda and Y. Shimizu. (Netherlands: Elsevier B.V.) pp. 257–262.

Johansson, O. N., Pinder, M. I., Ohlsson, F., Egardt, J., Töpel, M., and Clarke, A. K. (2019). Friends With Benefits: Exploring the Phycosphere of the Marine Diatom *Skeletonema Marinoi*. *Front. Microbiol.* 10. doi: 10.3389/fmicb.2019.01828

Jukes, T. H., and Cantor, C. R. (1969). "Evolution of Protein Molecules," in *Mammalian Protein Metabolism*, vol. 3 . Ed. H. N. Munro (New York: Academic Press), 21–132.

Kim, B. H., Ramanan, R., Cho, D. H., Oh, H. M., and Kim, H. S. (2014). Role of *Rhizobium*, a Plant Growth Promoting Bacterium, in Enhancing Algal Biomass Through Mutualistic Interaction. *Biomass Bioenerg.* 69, 95–105. doi: 10.1016/j.biombioe.2014.07.015

Kumar, S., Tamura, K., and Nei, M. (2004). MEGA3: Integrated Software for Molecular Evolutionary Genetics Analysis and Sequence Alignment. *Brief Bioinform.* 5, 150–163. doi: 10.1093/bib/5.2.150

Lin, J., Zheng, W., Tian, Y., Wang, G., and Zheng, T. (2013). Optimization of Culture Conditions and Medium Composition for the Marine Algicidal Bacterium *Alteromonas* Sp. DH46 by Uniform Design. *J. Ocean. U. China* 12, 385–391. doi: 10.1007/s11802-013-2153-5

Li, X., Yan, T., Yu, R., and Zhou, M. (2019). A Review of *Karenia Mikimotoi*: Bloom Events, Physiology, Toxicity and Toxic Mechanism. *Harmful Algae* 90, 101702. doi: 10.1016/j.hal.2019.101702

Mayali, X., and Azam, F. (2004). Algicidal Bacteria in the Sea and Their Impact on Algal Blooms. *J. Eukar. Microbiol.* 51, 139–144. doi: 10.1111/j.1550-7408.2004.tb00538.x

Meyer, N., Bigalke, A., Kaulfuss, A., and Pohnert, G. (2017). Strategies and Ecological Roles of Algicidal Bacteria. *FEMS Microbiol. Rev.* 41, 880–899. doi: 10.1093/femsre/fux029

Nagasoe, S., Kim, D. I., Shimasaki, Y., Oshima, Y., Yamaguchi, M., and Honjo, T. (2006). Effects of Temperature, Salinity and Irradiance on the Growth of the Red Tide Dinoflagellate *Gyrodinium Instriatum* Freudenthal Et Lee. *Harmful Algae* 5, 20–25. doi: 10.1016/j.hal.2005.06.001

Nagasoe, S., Shikata, T., Yamasaki, Y., Matsubara, T., Shimasaki, Y., Oshima, Y., et al. (2010). Effects of Nutrients on Growth of the Red-Tide Dinoflagellate *Gyrodinium Instriatum* Freudenthal Et Lee and a Possible Link to Blooms of This Species. *Hydrobiology* 651, 225–238. doi: 10.1007/s10750-010-0301-0

Palacios, O. A., López, B. R., and de-Bashan, L. E. (2022). Microalga Growth-Promoting Bacteria (MGPB): A Formal Term Proposed for Beneficial Bacteria Involved in Microalgal-Bacterial Interactions. *Algal. Res.* 61, 102585. doi: 10.1016/j.algal.2021.102585

Rajamani, S., Teplitski, M., Kumar, A., Krediet, C. J., Sayre, R. T., and Bauer, W. D. (2011). N-Acyl Homoseine Lactone Lactonase, AiiA, Inactivation of Quorum-Sensing Agonists Produced by *Chlamidomonas Reinhardtii* (Chlorophyta) and Characterization of aiiA Transgenic Algae. *J. Phycol.* 47, 1219–1227. doi: 10.1111/j.1529-8817.2011.01049.x

Saitou, N., and Nei, M. (1987). The Neighbor-Joining Method: A New Method for Reconstructing Phylogenetic Trees. *Mol. Biol. Evol.* 4, 406–425. doi: 10.1093/oxfordjournals.molbev.a040454

Sandhya, S. V., and Vijayan, K. K. (2019). Symbiotic Association Among Marine Microalgae and Bacterial Flora: A Study With Special Reference to Commercially Important *Isochrysis Galbana* Culture. *J. Appl. Phycol.* 31, 2259–2266. doi: 10.1007/s10811-019-01772-2

Sapp, M., Schwaderer, A. S., Wiltshire, K. H., Hoppe, H. G., Gerdts, G., and Wichels, A. (2007). Species-Specific Bacterial Communities in the Phycosphere of Microalgae? *Microb. Ecol.* 53, 683–699. doi: 10.1007/s00248-006-9162-5

Schäfer, H., Abbas, B., Witte, H., and Muyzer, G. (2002). Genetic Diversity of 'Satellite'bacteria Present in Cultures of Marine Diatoms. *FEMS Microbiol. Ecol.* 42, 25–35. doi: 10.1016/S0168-6496(02)00298-2

Seymour, J. R., Amin, S. A., Raina, J. B., and Stocker, R. (2017). Zooming in on the Phycosphere: The Ecological Interface for Phytoplankton–Bacteria Relationships. *Nat. Microbiol.* 2, 1–12. doi: 10.1038/nmicrobiol.2017.65

Shi, X., Liu, L., Li, Y., Xiao, Y., Ding, G., Lin, S., et al. (2018). Isolation of an Algicidal Bacterium and its Effects Against the Harmful-Algal-Bloom Dinoflagellate *Prorocentrum Donghaiense* (Dinophyceae). *Harmful Algae* 80, 72–79. doi: 10.1016/j.hal.2018.09.003

Shikata, T., Nagasoe, S., Matsubara, T., Yoshikawa, S., Yamasaki, Y., Shimasaki, Y., et al. (2008). Factors Influencing the Initiation of Blooms of the Raphidophyte Heterosigma akashiwo and the Ciatom Skeletonema costatum in a Port in Japan. *Limnol. Oceanogr.. 53*, 2503—2518. doi: 10.4319/lo.2008.53.6.2503

Sison-Mangus, M. P., Jiang, S., Tran, K. N., and Kudela, R. M. (2014). Host-Specific Adaptation Governs the Interaction of the Marine Diatom, Pseudo-Nitzschia and Their Microbiota. *ISME J.* 8, 63–76. doi: 10.1038/ismej.2013.138

SOA (State Oceanic Administration People's Republic of China) (2008) *Bulletin of Marine Environmental Quality in Shenzhen City in 2007*. Available at: http://www.soa.gov.cn/zwgk/hygb/zghyhjzlgb/201212/t20121206_21225.html.

Stien, D., Sanchez-Ferandin, S., and Lami, R. (2016). Quorum Sensing and Quorum Quenching in the Phycosphere of Phytoplankton: A Case of Chemical Interactions in Ecology. *J. Chem. Ecol.* 42, 1201–1211. doi: 10.1007/s10886-016-0791-y

Su, J. Q., Yang, X. R., Zheng, T. L., Tian, Y., Jiao, N. Z., Cai, L. Z., et al. (2007). Isolation and Characterization of a Marine Algicidal Bacterium Against the Toxic Dinoflagellate *Alexandrium Tamarense*. *Harmful Algae* 6, 799–810. doi: 10.1016/j.hal.2007.04.004

Teplitski, M., Chen, H., Rajamani, S., Gao, M., Merighi, M., Sayre, R. T., et al. (2004). *Chlamydomonas Reinhardtii* Secretes Compounds That Mimic Bacterial Signals and Interfere With Quorum Sensing Regulation in Bacteria. *Plant Physiol.* 134, 137–146. doi: 10.1104/pp.103.029918

Tse, S., and Lo, S. (2017). Comparative Proteomic Studies of a *Scrippsiella Acuminata* Bloom With its Laboratory-Grown Culture Using a ^{15}N-Metabolic Labeling Approach. *Harmful Algae* 67, 26–35. doi: 10.1016/j.hal.2017.05.009

Umetsu, S., Kanda, M., Imai, I., Sakai, R., and Fujita, M. J. (2019). Questiomycins, Algicidal Compounds Produced by the Marine Bacterium *Alteromonas* Sp. And Their Production Cue. *Molecules* 24, 4522. doi: 10.3390/molecules24244522

Wang, Z., Guo, X., Qu, L., and Lin, L. (2017). Effects of Nitrogen and Phosphorus on the Growth of *Levanderina Fissa*: How it Blooms in Pearl River Estuary. *J. Ocean U. China* 16, 114–120. doi: 10.1007/s11802-017-3080-7

Wang, H. K., Huang, L. M., Huang, X. P., Song, X. Y., Wang, H. J., Wu, N. J., et al. (2003). A Red Tide Caused by *Gyrodinium Instriatum* and its Environmental Characters in Zhujiang River Estuary. *J. Trop. Environ.* 22, 55–62. doi: 10.1007/BF02860423

Wang, Z. H., Jiang, S., Gu, Y. G., Kang, W., Feng, J., Lin, L. C., et al. (2011). Effects of *Cochlodinium* Bloom in Pearl River Estuary in China on the Growth of Other Harmful Algal Bloom Species. *J. Shenzhen U. Sci. Engi.* 28, 553–558. doi: 10.3969/j.issn.1000-2618.2011.06.015

Wang, X., Li, Z., Su, J., Tian, Y., Ning, X., Hong, H., et al. (2010). Lysis of a Red-Tide Causing Alga, *Alexandrium Tamarense*, Caused by Bacteria From its Phycosphere. *Biol. Control* 52, 123–130. doi: 10.1016/j.biocontrol.2009.10.004

Wang, Z., Qi, Y., Yin, Y., Jiang, T., and Xie, L. (2001). Studies on the Cause and the Occurrence Reasons of a *Gyrodinium Instriatum* Red Tide in Shenzhen Bay in Spring of 1998. *Mar. Sci.* 25, 47–49. doi: 10.3969/j.issn.1000-3096.2001.05.015

Wang, Z., Wang, C., Li, W., Wang, M., and Xiao, L. (2021). Interspecies Competition Between *Scrippsiella Acuminata* and Three Marine Diatoms: Growth Inhibition and Allelopathic Effects. *Aquat. Toxicol.* 237, 195878. doi: 10.1016/j.aquatox.2021.105878

Xie, B., Bishop, S., Stessman, D., Wright, D., Spalding, M. H., and Halverson, L. J. (2013). *Chlamydomonas Reinhardtii* Thermal Tolerance Enhancement Mediated by a Mutualistic Interaction With Vitamin B12-Producing Bacteria. *ISME J.* 7, 1544–1555. doi: 10.1038/ismej.2013.43

Zhu, X., Yi, B., Dong, Y., and Yan, L. (2004). A Primary Study on One of the 'Bilateral' Red Tide at Chi Bay of Pearl River Estuary. *Mar. Environ. Sci.* 23, 41–44. doi: 10.3969/j.issn.1007-6336.2004.04.011

Conflict of Interest: The authors declare that the research was conducted in the absence of any commercial or financial relationships that could be construed as a potential conflict of interest.

Publisher's Note: All claims expressed in this article are solely those of the authors and do not necessarily represent those of their affiliated organizations, or those of the publisher, the editors and the reviewers. Any product that may be evaluated in this article, or claim that may be made by its manufacturer, is not guaranteed or endorsed by the publisher.

frontiers | Frontiers in Microbiology

REVIEW
published: 09 June 2022
doi: 10.3389/fmicb.2022.918120

A Large Silicon Pool in Small Picophytoplankton

Yuqiu Wei[1,2] *and Jun Sun*[3,4]*

[1]Key Laboratory of Sustainable Development of Marine Fisheries, Ministry of Agriculture and Rural Affairs, Yellow Sea Fisheries Research Institute, Chinese Academy of Fishery Sciences, Qingdao, China, [2]Laboratory for Marine Fisheries Science and Food Production Processes, Pilot National Laboratory for Marine Science and Technology, Qingdao, China, [3]Research Center for Indian Ocean Ecosystem, Tianjin University of Science and Technology, Tianjin, China, [4]State Key Laboratory of Biogeology and Environmental Geology, China University of Geosciences, Wuhan, China

Marine picophytoplankton (<2 μm) play a key role in supporting food web and energy flow in the ocean, and are major contributors to the global marine carbon (C) cycle. In recent years, picophytoplankton have been found to have significant silica (Si) accumulation, a finding which provides a new sight into the interaction of marine C and Si cycles and questions the overwhelming role of large diatoms (>2 μm) in the Si cycle. As picophytoplankton have high cell abundance and wide distribution in the open ocean, exploring their influences on the C and Si cycles as well as other element cycles are becoming new scientific hotspots. However, there are still few studies on the physiology and ecology of picophytoplankton, especially their potential roles in the biogeochemical Si cycle at present. Thus, it is necessary to accurately evaluate and quantify the contributions of picophytoplankton to the C and Si cycles, and to further understand their C and Si sinking mechanisms. In this review, we expect to have a novel understanding of picophytoplankton Si pool and regulation mechanism by conducting targeted studies on these scientific issues. This also provides a premise foundation and theoretical framework for further study of the role of small cells in the global ocean Si cycle and the coupling of C and Si cycles.

Keywords: biogeochemical cycles, silicon cycle, carbon cycle, Si accumulation, picophytoplankton

OPEN ACCESS

Edited by:
Zhangxi Hu,
Guangdong Ocean University, China

Reviewed by:
Baoli Wang,
Tianjin University, China
Yantao Liang,
Ocean University of China, China

***Correspondence:**
Jun Sun
phytoplankton@163.com

Specialty section:
This article was submitted to Aquatic Microbiology, a section of the journal Frontiers in Microbiology

Received: *12 April 2022*
Accepted: *26 May 2022*
Published: *09 June 2022*

Citation:
Wei Y and Sun J (2022) A Large Silicon Pool in Small Picophytoplankton. Front. Microbiol. 13:918120. doi: 10.3389/fmicb.2022.918120

INTRODUCTION

Among phytoplankton the large diatoms (>2 μm), a dominant group that are generally prevalent in coastal eutrophic ecosystems (Cermeño et al., 2005; Carstensen et al., 2015), contribute significantly to the biogenic silica (bSi) production and global primary production (Nelson et al., 1995; Brzezinski et al., 1998; Chai et al., 2007; Krause et al., 2011). These photosynthetic protists can absorb dissolved silicic acid to form their siliceous cell walls (Hecky et al., 1973; Bidle and Azam, 1999), and produce approximately 100–140 Tmol Si $year^{-1}$ for the global ocean (Nelson et al., 1995). In addition, these large diatoms are one of the major primary producers in the ocean and are able to contribute up to ~25% of global carbon (C) fixation, although they are not dominant in oligotrophic oceans (Armbrust et al., 2004; Kale and Karthick, 2015). Aspects of their life history, notably their siliceous cell walls and high sinking rates, make them also important to the export of C and Si to depth, owing to density-driven particle sedimentation (Kemp et al., 2006; Ragueneau et al., 2006; Tréguer et al., 2018). As such,

the marine Si cycle is intimately tied to the C cycle through the biotic action of large diatoms, such as growth, reproduction, and metabolism (Huang and Daboussi, 2017). Collectively, large diatoms are thought to be the primary organisms responsible for the export of Si to the ocean interior and one important group of primary producers in the global marine ecosystems (Armbrust et al., 2004; Ragueneau et al., 2006; Tréguer et al., 2018). In some cases, the presence of other siliceous organisms (e.g., Silicoflagellates and Rhizarians) would likely reduce the proportional importance of large diatoms to total bSi standing stocks (Biard et al., 2018; Hendry et al., 2018). However, a fundamental knowledge about the role of biota in marine Si cycle is that large diatoms overwhelmingly dominate the bSi standing stocks in the open ocean (**Figure 1**).

In recent years, regional bSi measurements have revealed that large diatoms have a disproportionately high contribution to bSi standing stock and Si export relative to their contribution to total phytoplankton biomass (Brzezinski et al., 2011; Krause et al., 2017), particularly in the mid-ocean oligotrophic gyres where diatom biomass and Si production rates are among the lowest in the ocean. For example, similar studies carried out in the equatorial Pacific (110–140°W) have led to a revised estimate of diatom bSi standing stock, as only 2%–31% of bSi pool was associated with living large diatoms (Krause et al., 2010). The implication is that the marine bSi pool may be not entirely originate from the large diatoms, and may be associated with a previously unexplored source of Si in the ocean. Surprisingly, Baines et al. (2012) have revealed that the widely distributed marine picocyanobacterium *Synechococcus* can accumulate substantial amounts of Si, a finding which may interpret the disproportionately high contributions of large diatoms to primary production and organic matter export. Also, Leblanc et al. (2018a) have demonstrated that some small diatoms (e.g., *Minidiscus*), which belong to the picoplanktonic size-class, may play a role in marine systems. However, as a result of their small size and slow sinking rate, these picophytoplankton (e.g., *Synechococcus* and small diatoms) have long been considered to represent a negligible fraction of the C and Si transport from the surface into the deep ocean (Buesseler, 1998). Until recently, some studies in oligotrophic areas have suggested that picophytoplankton are also important in transporting organic matter to the depth (Richardson and Jackson, 2007). It is well known that picophytoplankton are abundant in many oligotrophic oceans (Buitenhuis et al., 2012; Flombaum et al., 2013; Visintini et al., 2021), hence the role for picophytoplankton in the Si cycle would be more prominent in oligotrophic environments where large diatoms are in low biomass (**Figure 1**).

A series of theoretical arguments based on laboratory experiments and field studies have provided evidence for a role for small picophytoplankton in the Si cycle, showing that these ubiquitous small cells accumulate significant amounts of Si, exert a previously unrecognized influence on the oceanic Si cycle, and may further enhance Si export to depth (Baines et al., 2012; Tang et al., 2014; Krause et al., 2017; Leblanc et al., 2018b; Wei et al., 2021a,b). For instance, size-fractionated bSi measurements by Baines et al. (2012) and Krause et al. (2017) in the Sargasso Sea showed that the bSi standing stocks within the <3 μm size fraction averaged 16–20 and 14% of the total, respectively. Leblanc et al. (2018b) revealed a non-negligible contribution of the pico-sized fraction to bSi standing stocks (11%–26%) in the tropical South Pacific. Our

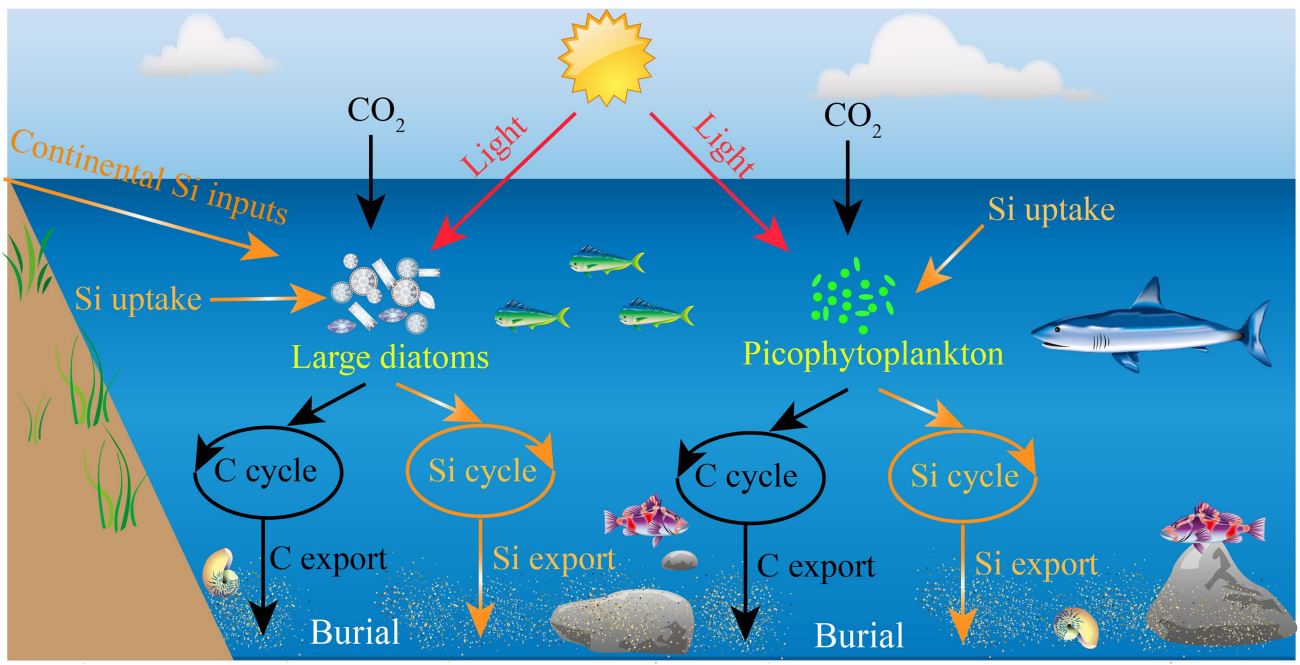

FIGURE 1 | Schematic view of the significance of large diatoms and picophytoplankton in the marine C and Si cycles.

earlier works in the oligotrophic eastern Indian Ocean and western Pacific Ocean have also shown that the pico-sized fraction was 49%–65% of the total bSi pool and 43% of the total bSi production rates, respectively (Wei et al., 2021a,b). Accordingly, we speculate that this previously unexplored Si source of marine picophytoplankton may be important to Si cycling in the open ocean, although the genetic and metabolic mechanisms of Si accumulation by *Synechococcus* are unknown, particularly for the form and precise location of the Si. Given this hypothesis, with this review, we discussed recent findings that small picophytoplankton may have a quantitatively significant contribution to both bSi pool and its rate of production for the global ocean. We hope this review will provide some inspirations for researchers to explore the mechanistic role of these fascinating small cells in the biogeochemical Si cycle, as well as providing a novel context of biological and ecological functions to those interested in marine Si cycle.

THE ROLE OF LARGE DIATOMS IN MARINE C AND Si CYCLES

Terrestrial dissolved silicic acid (DSi) through rivers and atmospheric deposition are eventually transported to the ocean. The DSi is subsequently absorbed by large diatoms to construct their cell walls, becoming an essential nutrient for diatom growth, metabolism and reproduction. Furthermore, the biological silicate, as an effective pH buffer for intracellular metabolism of diatoms, contributes to more absorption of CO_2, which in turn encourages the large diatoms to carry out more efficient photosynthesis. Thus, large diatoms account for ~25% of the total global C sequestration, and play an important role in the regulation of atmosphere CO_2 as well as global climate change (Field et al., 1998; Ragueneau et al., 2000; Jin et al., 2006). Due to the density-driven particle deposition, large diatoms have long been thought to be responsible for the transport of organic matter to the deep ocean (~1.5–2.8 Gton C $year^{-1}$; Treguer et al., 1995; Armstrong et al., 2001). Altogether, large diatoms dominate the Si absorption, metabolism, conversion, and deposition in the ocean, and closely combine the Si cycle with the C cycle, which plays an important role in the start-up and continuity of the marine biological pump (Ragueneau et al., 2006).

The process by which different phytoplankton convert CO_2 from the atmosphere into organic C through photosynthesis and send it to the deep ocean is called the "biological C pump." In this process, Si plays an irreplaceable role in the primary production and output dominated by large diatoms. Thus, the biogeochemical cycles of C and Si are closely coupled through the growth and metabolism of large diatoms, and the "biological C pump" in the ocean is called the "biological Si pump" (Raven and Falkowski, 1999). For example, studies on long-term algal blooms and nutrient status in different nearshore areas have reported that higher N and P inputs increase the C biomass of large diatoms and simultaneously result in increased Si deposition rates (Officer and Ryther, 1980). In recent years, however, studies in some oligotrophic areas have found that the C biomass of large diatoms is relatively low, but compared with the low C biomass, the Si storage and output flux are very high. The implication is that the production and output of C and Si are obviously unbalanced in these areas, i.e., the decoupling phenomenon (Assmy et al., 2013). For example, approximately 50%–75% of the Si around Antarctica is buried in deep-sea sediments, whereas large diatoms contribute only 2%–38% of the total phytoplankton C biomass (Hedges and Keil, 1995). Similarly, a large number of sediment trap data have shown a poor correlation between the C and Si flux of large diatoms in the ocean (Klaas and Archer, 2002). Although there are other siliceous organisms (e.g., silicoflagellates and Rhizarians) in the ocean that can absorb Si, their species and abundance in the ocean are very small, their growth and sedimentation rates are very low, and their contribution to offshore silicon stock, production, and output is negligible compared to that of large diatoms. Therefore, these non-diatom siliceous groups are not the main cause of the imbalance between the production and output of C and Si. So what accounts for the imbalance between the production and output of C and Si in these oligotrophic areas?

ADVANCE IN THE ROLE OF PICOPHYTOPLANKTON IN OCEAN Si CYCLING

Up to date, it is generally believed that large diatoms transport dissolved Si from the surface to the deep ocean, dominating the global ocean Si cycle and becoming the main bridge between the oceanic C and Si cycles (Raven and Falkowski, 1999). As discussed above, it is difficult to explain the imbalance between the production and output of C and Si in the ocean (especially in oligotrophic areas) from the perspective of "only diatoms." Interestingly, *Synechococcus* are found to accumulate substantial amounts Si, and their cells have different Si/P and Si/S ratios. Given the phylogenetic and taxonomic similarities between *Synechococcus* and *Prochlorococcus* (Kent et al., 2019), it is possible that *Prochlorococcus* also can accumulate Si, but they are too small (~0.6 μm) to detect their intracellular Si content. Regardless of the morphology of Si in these picocyanobacteria, if *Prochlorococcus* can accumulate Si, their high abundance and worldwide distribution suggest that they would have an important effect on the oceanic Si cycle. In addition, recent studies have shown that there are a large number of small diatoms genus *Minidiscus* in the picoplanktonic size-class, which may have important implications for the marine Si cycle (Leblanc et al., 2018a). Meanwhile, there is accumulating evidence that marine picophytoplankton are the important contributors of primary productivity in oligotrophic waters, and their contribution to the export of organic particles to the deep ocean could not be ignored (Richardson and Jackson, 2007). The discovery of picophytoplankton Si accumulation is likely to change the absolute role of large diatoms in the global marine Si cycle and provides us with a new perspective to link the interaction of C and Si cycles.

In some cases, the Si concentration in *Synechococcus* cells can exceed that of large diatoms, the indication being that picocyanobacteria may have a previously unrecognized and important impact on the ocean's Si cycle (Baines et al., 2012). Thereafter, a series of studies on Si accumulation in picophytoplankton have explored the potential impact of these small cells on the ocean Si cycle. For example, Tang et al. (2014) have found that Si can be deposited on extracellular polymeric substance (EPS) associated with decomposing *Synechococcus*, which is similar to the micro-blebs observed in the deep ocean in morphology and composition. So the EPS-Si produced by the *Synechococcus* decomposition may be the precursors of the micro-blebs that may be important to Si cycling and may further enhance export of picophytoplankton to the deep ocean. Ohnemus et al. (2016) have measured the intracellular Si content of the North Atlantic, and revealed that the intracellular Si content of *Synechococcus* varied greatly, ranging from 1 to 4,700 amol Si cell^{-1}. Subsequently, they have provided evidence that the variation of intracellular Si content with depth may be related to the difference of dominant clades in different water layers. Brzezinski et al. (2017) have reported that the growth rate of *Synechococcus* is not affected by the concentration of Si in culture. However, they also proposed that there are two Si pools, i.e., soluble and insoluble, in the cells of *Synechococcus*, and speculated that soluble Si would likely bind to organic ligands. Krause et al. (2017) have analyzed the Si stock and production rate of the pico-sized fraction in the Sargasso Sea, and average bSi stock and production rate accounted for 14 and 16% of the total, respectively, indicating that the picophytoplankton accounted for a large proportion of the total bSi stock and production. They also estimated the contribution of *Synechococcus* to the total pico-sized bSi standing stock (~15%) and production rate (~55%), suggesting that more than half of the Si production of picophytoplankton is likely to originate from *Synechococcus*. Ohnemus et al. (2018) have explored the chemical form of Si in the *Synechococcus* cells, and revealed that *Synechococcus* Si was spectroscopically different from the opal-A precipitated by large diatoms. Leblanc et al. (2018b) have shown that the contribution of picophytoplankton to the total bSi stocks could not be overlooked (about 11%–26% of the total bSi stocks) in the tropical South Pacific, and have also highlighted the importance of Si uptake by *Synechococcus* in the ocean.

Since Baines et al. (2012) first discovered the Si accumulation of *Synechococcus*, there have been a series of reports on the contribution of marine picophytoplankton to bSi standing stocks and production in different oligotrophic waters (e.g., the Eastern Pacific, North Atlantic, and South Pacific). Although the absorption mechanism and environmental regulation mechanism of picophytoplankton Si accumulation are not clear at present, their Si accumulation contributes significantly to the bSi standing stock (11%–50%) and production (~55%) in different water layers (Ohnemus et al., 2016; Krause et al., 2017; Wei et al., 2021a,b). Conceivably, Si accumulation by picophytoplankton may affect their growth and metabolism, and then regulate their photosynthetic C fixation and biological C pump. More importantly, these small cells may promote the sinking of particulate matter, and all organic C contained therein through their dense siliceous cells or extracellular EPS-Si into the ocean without entering the recycling process (Tang et al., 2014; Wei et al., 2022). This potential sinking process is likely to combine the Si cycle with the C cycle, making it a new bridge connecting the interactions of the oceanic C and Si cycles. Taken together, the Si accumulation of picophytoplankton not only changes our previous understanding that large diatoms mainly control the global oceanic C and Si cycles, but also plays an important role in the sequestration of C and Si in the ocean.

SIGNIFICANT CONTRIBUTION OF PICOPHYTOPLANKTON TO Si BUDGETS

Based on our previous studies in the oligotrophic open oceans, it is concluded that marine picophytoplankton could represent on average ~50% of total bSi standing stocks, which is a significant contribution (Wei et al., 2021a,b). In the Sargasso Sea, the picophytoplankton generally contributed measurable, and at times significant proportion of both the total bSi standing stocks (9%–24%) and production rates (1%–37%; Baines et al., 2012; Krause et al., 2017). Likewise, Leblanc et al. (2018b) have revealed a non-negligible contribution of the picophytoplankton to bSi stocks and production rates in the tropical South Pacific, representing 11–26 and 11–32%, respectively, of the total. As a result, these strong evidences suggest the need to evaluate the contribution of picophytoplankton to global ocean Si cycle, which may be more prominent in oligotrophic gyres where large diatoms are in low abundance. A revised global contribution of only 13 Tmol Si yr.$^{-1}$ gross Si production in the mid-ocean gyres has been estimated by Nelson et al. (1995) and Brzezinski et al. (2011), i.e., ~5%–7% of the budget calculated for the global ocean of 240 Tmol Si year^{-1}. The range in the calculation of the global bSi production rates for mid-ocean gyres is of 0.2–1.6 mmol m^{-2} day^{-1} (Nelson et al., 1995). Our previously measured production rates in the nutrient-depleted Indian Ocean for picophytoplankton (1.1–2.2 mmol m^{-2} day^{-1}) may increase the contribution of the oligotrophic waters to global bSi productivity (Wei et al., 2021b). The implication is that marine picophytoplankton, which is likely to have been included in previous analyses, may contribute even more to total bSi standing stocks and production rates of the world ocean, especially in nutrient-poor waters.

However, Krause et al. (2017) have put forward a different assumption and suggested an important role for diatom-derived bSi detritus in the pico-sized fraction. In other words, the contributions of small fragments from large diatom frustules or other siliceous microphytoplankton may increase the measurable bSi standing stock of picophytoplankton, as the preponderance of the total Si pool in the ocean is detrital and not associated with living cells. The implication is that picophytoplankton have a small contribution to total bSi stocks, which may be masked by a dynamic Si pool driven by large diatoms. This different assumption appears to be invalidated, because (*i*) there is surprising similarity in morphology and composition between EPS-Si and micro-blebs (a group of marine

detritus enriched in Si) and thus EPS-Si may be a precursor of micro-blebs, whereas newly produced EPS-Si may most likely originate from picocyanobacteria (Tang et al., 2014); (*ii*) Tang et al. (2014) have provided evidence that *Synechococcus*-derived bSi standing stock accounts for 50% of the bSi inventory in the surface water, thus implying that half of the bSi in the surface water may originate from *Synechococcus*; (*iii*) our earlier work has revealed that the contribution of the pico-sized fraction to total Si uptake rates is really surprising, ~44%, thus can provide insight into the significant picophytoplankton contribution to Si pool (Wei et al., 2021b); and (*iv*) some small diatoms (e.g., *Minidiscus*) are globally overlooked but play a role in the marine Si cycle (Leblanc et al., 2018a). Therefore, we suggest that the source of potential Si detritus in small size fraction may originate mostly from picophytoplankton in the ocean.

Based on our previous data in the eastern Indian Ocean (Wei et al., 2021b), we made a rough estimate for the global oceanic bSi standing stock, production rate, and export flux of picophytoplankton, although such a global estimate for these small cells had significant uncertainty. The estimated results provided a global picophytoplankton bSi standing stock of 1.55–3.85 Tmol Si based on the derived Si/C ratio (i.e., ~0.035). Leblanc et al. (2012) have previously reported a first-order estimate of the diatom C biomass for the global ocean, ranging from 444 to 582 Tg C, which converts to about 3–4 Tmol Si. Thus, the estimated global bSi stock of picophytoplankton here is similar to that of large diatoms. Furthermore, we also implied a global productivity range of picophytoplankton between 78 and 194 Tmol Si $year^{-1}$, which is about 32%–80% of the total global annual ocean bSi production estimate (~240 Tmol Si $year^{-1}$; Nelson et al., 1995; Brzezinski et al., 2011). Richardson and Jackson (2007) have suggested that the average C export flux of picophytoplankton in oligotrophic waters is ~6.21 mmol m^{-2} day^{-1}, accounting for ~50% of the total C export flux. Converting picophytoplankton C to Si export flux, using the above derived Si:C ratio (~0.035), provides an estimated global picophytoplankton Si export flux of 0.22 mmol m^{-2} day^{-1}, accounting for ~55% of the global annual ocean Si flux. Altogether, these results suggest an important role for small-sized plankton in the marine Si cycle at regional and global scales, but those calculations have large uncertainty due to the lack of data, and hence more data are necessary to better understand the spatial extent of the picophytoplankton role in the global Si cycle.

FUTURE PERSPECTIVES

The biological importance of picophytoplankton in the biogeochemical cycles is even more intriguing under climate change scenarios, as the result of several studies that predict shifts toward smaller species as oceans warm. Along with the discovery of Si accumulation by picocyanobacteria, their influence could be substantially larger in various aquatic ecosystems now and in future. Meanwhile, this discovery has also strong implications for the marine C and Si cycles. Hence, this review highlights the significant advances that have been made in the past decade toward improving our understanding of Si accumulated by picophytoplankton, and their ecological and biogeochemical impacts on the Si cycle. Although this review fills some identified knowledge gaps, there are three main aspects that still need to be addressed in the future: (*i*) our understanding of the factors controlling the magnitude and variability in the pico-sized contribution to both total bSi stocks and its rate of production is not enough; (*ii*) the physiological and/or biological mechanisms of Si accumulation by picocyanobacteria are not clear; and (*iii*) the picophytoplankton Si export associated with possible pathways has not been established.

AUTHOR CONTRIBUTIONS

JS conceived the original idea and defined the manuscript content. YW wrote the paper. All authors contributed to the article and approved the submitted version.

FUNDING

This work was financially supported by the Project funded by China Postdoctoral Science Foundation (2021M703590), the Shandong Postdoctoral Innovation Talent Support Program (SDBX2021014), the National Nature Science Foundation of China grants (41876134), the Central Public-interest Scientific Institution Basal Research Fund, YSFRI, CAFS (20603022022010), the Qingdao Postdoctoral Applied Research Project, and the State Key Laboratory of Biogeology and Environmental Geology, China University of Geosciences (GKZ21Y645).

REFERENCES

Armbrust, E. V., Berges, J. A., Bowler, C., Green, B. R., Martinez, D., Putnam, N. H., et al. (2004). The genome of the diatom *Thalassiosira pseudonana*: ecology, evolution, and metabolism. *Science* 306, 79–86. doi: 10.1126/science.1101156

Armstrong, R. A., Lee, C., Hedges, J. I., Honjo, S., and Wakeham, S. G. (2001). A new, mechanistic model for organic carbon fluxes in the ocean based on the quantitative association of POC with ballast minerals. *Deep-Sea Res. II Top. Stud. Oceanogr.* 49, 219–236. doi: 10.1016/S0967-0645(01)00101-1

Assmy, P., Smetacek, V., Montresor, M., Klaas, C., Henjes, J., Strass, V. H., et al. (2013). Thick-shelled, grazer-protected diatoms decouple ocean carbon and silicon cycles in the iron-limited Antarctic circumpolar current. *Proc. Natl. Acad. Sci.* 110, 20633–20638. doi: 10.1073/pnas.1309345110

Baines, S. B., Twining, B. S., Brzezinski, M. A., Krause, J. W., Vogt, S., Assael, D., et al. (2012). Significant silicon accumulation by marine picocyanobacteria. *Nat. Geosci.* 5, 886–891. doi: 10.1038/ngeo1641

Biard, T., Krause, J. W., Stukel, M. R., and Ohman, M. D. (2018). The significance of giant Phaeodarians (Rhizaria) to biogenic silica export in the California current ecosystem. *Glob. Biogeochem. Cycles* 32, 987–1004. doi: 10.1029/2018GB005877

Bidle, K. D., and Azam, F. (1999). Accelerated dissolution of diatom silica by marine bacterial assemblages. *Nature* 397, 508–512. doi: 10.1038/17351

Brzezinski, M. A., Krause, J. W., Baines, S. B., Collier, J. L., Ohnemus, D. C., and Twining, B. S. (2017). Patterns and regulation of silicon accumulation in Synechococcus spp. *J. Phycol.* 53, 746–761. doi: 10.1111/jpy.12545

Brzezinski, M. A., Krause, J. W., Church, M. J., Karl, D. M., Li, B., Jones, J. L., et al. (2011). The annual silica cycle of the North Pacific subtropical gyre.

Deep-Sea Res. I Oceanogr. Res. Pap. 58, 988–1001. doi: 10.1016/j.dsr.2011.08.001

Brzezinski, M. A., Villareal, T. A., and Lipschultz, F. (1998). Silica production and the contribution of diatoms to new and primary production in the central North Pacific. *Mar. Ecol. Prog. Ser.* 167, 89–104. doi: 10.3354/meps167089

Buesseler, K. O. (1998). The decoupling of production and particulate export in the surface ocean. *Glob. Biogeochem. Cycles* 12, 297–310. doi: 10.1029/97GB03366

Buitenhuis, E. T., Li, W. K., Vaulot, D., Lomas, M. W., Landry, M. R., Partensky, F., et al. (2012). Picophytoplankton biomass distribution in the global ocean. *Earth System Sci. Data* 4, 37–46. doi: 10.5194/essd-4-37-2012

Carstensen, J., Klais, R., and Cloern, J. E. (2015). Phytoplankton blooms in estuarine and coastal waters: seasonal patterns and key species. *Estuar. Coast. Shelf Sci.* 162, 98–109. doi: 10.1016/j.ecss.2015.05.005

Cermeño, P., Marañón, E., Rodríguez, J., and Fernández, E. (2005). Large-sized phytoplankton sustain higher carbon-specific photosynthesis than smaller cells in a coastal eutrophic ecosystem. *Mar. Ecol. Prog. Ser.* 297, 51–60. doi: 10.3354/meps297051

Chai, F., Jiang, M. S., Chao, Y., Dugdale, R. C., Chavez, F., and Barber, R. T. (2007). Modeling responses of diatom productivity and biogenic silica export to iron enrichment in the equatorial Pacific Ocean. *Glob. Biogeochem. Cycles* 21:GB3S90. doi: 10.1029/2006GB002804

Field, C. B., Behrenfeld, M. J., Randerson, J. T., and Falkowski, P. (1998). Primary production of the biosphere: integrating terrestrial and oceanic components. *Science* 281, 237–240. doi: 10.1126/science.281.5374.237

Flombaum, P., Gallegos, J. L., Gordillo, R. A., Rincón, J., Zabala, L. L., Jiao, N., et al. (2013). Present and future global distributions of the marine Cyanobacteria Prochlorococcus and Synechococcus. *Proc. Natl. Acad. Sci.* 110, 9824–9829. doi: 10.1073/pnas.1307701110

Hecky, R. E., Mopper, K., Kilham, P., and Degens, E. T. (1973). The amino acid and sugar composition of diatom cell-walls. *Mar. Biol.* 19, 323–331. doi: 10.1007/BF00348902

Hedges, J. I., and Keil, R. G. (1995). Sedimentary organic matter preservation: an assessment and speculative synthesis. *Mar. Chem.* 49, 81–115. doi: 10.1016/0304-4203(95)00008-F

Hendry, K. R., Marron, A. O., Vincent, F., Conley, D. J., Gehlen, M., Ibarbalz, F. M., et al. (2018). Competition between silicifiers and non-silicifiers in the past and present ocean and its evolutionary impacts. *Front. Mar. Sci.* 5:22. doi: 10.3389/fmars.2018.00022

Huang, W., and Daboussi, F. (2017). Genetic and metabolic engineering in diatoms. *Philos. Trans. Royal Soc. B Biol. Sci.* 372:20160411. doi: 10.1098/rstb.2016.0411

Jin, X., Gruber, N., Dunne, J. P., Sarmiento, J. L., and Armstrong, R. A. (2006). Diagnosing the contribution of phytoplankton functional groups to the production and export of particulate organic carbon, CaCO3, and opal from global nutrient and alkalinity distributions. *Glob. Biogeochem. Cycles* 20:GB2015. doi: 10.1029/2005GB002532

Kale, A., and Karthick, B. (2015). The diatoms. *Resonance* 20, 919–930. doi: 10.1007/s12045-015-0256-6

Kemp, A. E. S., Pearce, R. B., Grigorov, I., Rance, J., Lange, C. B., Quilty, P., et al. (2006). Production of giant marine diatoms and their export at oceanic frontal zones: implications for Si and C flux from stratified oceans. *Glob. Biogeochem. Cycles* 20:GB4S04. doi: 10.1029/2006GB002698

Kent, A. G., Baer, S. E., Mouginot, C., Huang, J. S., Larkin, A. A., Lomas, M. W., et al. (2019). Parallel phylogeography of Prochlorococcus and Synechococcus. *ISME J.* 13, 430–441. doi: 10.1038/s41396-018-0287-6

Klaas, C., and Archer, D. E. (2002). Association of sinking organic matter with various types of mineral ballast in the deep sea: implications for the rain ratio. *Glob. Biogeochem. Cycles* 16, 63-1–63-14. doi: 10.1029/2001GB001765

Krause, J. W., Brzezinski, M. A., Baines, S. B., Collier, J. L., Twining, B. S., and Ohnemus, D. C. (2017). Picoplankton contribution to biogenic silica stocks and production rates in the Sargasso Sea. *Glob. Biogeochem. Cycles* 31, 762–774. doi: 10.1002/2017GB005619

Krause, J. W., Nelson, D. M., and Brzezinski, M. A. (2011). Biogenic silica production and the diatom contribution to primary production and nitrate uptake in the eastern equatorial Pacific Ocean. *Deep-Sea Res. II Top. Stud. Oceanogr.* 58, 434–448. doi: 10.1016/j.dsr2.2010.08.010

Krause, J. W., Nelson, D. M., and Lomas, M. W. (2010). Production, dissolution, accumulation, and potential export of biogenic silica in a Sargasso Sea mode-water eddy. *Limnol. Oceanogr.* 55, 569–579. doi: 10.4319/lo.2010.55.2.0569

Leblanc, K., Arístegui, J., Armand, L., Assmy, P., Beker, B., Bode, A., et al. (2012). A global diatom database–abundance, biovolume and biomass in the world ocean. *Earth System Sci. Data* 4, 149–165. doi: 10.5194/essd-4-149-2012

Leblanc, K., Cornet, V., Rimmelin-Maury, P., Grosso, O., Hélias-Nunige, S., Brunet, C., et al. (2018b). Silicon cycle in the tropical South Pacific: contribution to the global Si cycle and evidence for an active pico-sized siliceous plankton. *Biogeosciences* 15, 5595–5620. doi: 10.5194/bg-15-5595-2018

Leblanc, K., Queguiner, B., Diaz, F., Cornet, V., Michel-Rodriguez, M., Durrieu de Madron, X., et al. (2018a). Nanoplanktonic diatoms are globally overlooked but play a role in spring blooms and carbon export. *Nat. Commun.* 9:953. doi: 10.1038/s41467-018-03376-9

Nelson, D. M., Tréguer, P., Brzezinski, M. A., Leynaert, A., and Quéguiner, B. (1995). Production and dissolution of biogenic silica in the ocean: revised global estimates, comparison with regional data and relationship to biogenic sedimentation. *Glob. Biogeochem. Cycles* 9, 359–372. doi: 10.1029/95GB01070

Officer, C. B., and Ryther, J. H. (1980). The possible importance of silicon in marine eutrophication. *Mar. Ecol. Prog. Ser.* 3, 83–91. doi: 10.3354/meps003083

Ohnemus, D. C., Krause, J. W., Brzezinski, M. A., Collier, J. L., Baines, S. B., and Twining, B. S. (2018). The chemical form of silicon in marine Synechococcus. *Mar. Chem.* 206, 44–51. doi: 10.1016/j.marchem.2018.08.004

Ohnemus, D. C., Rauschenberg, S., Krause, J. W., Brzezinski, M. A., Collier, J. L., Geraci-Yee, S., et al. (2016). Silicon content of individual cells of Synechococcus from the North Atlantic Ocean. *Mar. Chem.* 187, 16–24. doi: 10.1016/j.marchem.2016.10.003

Ragueneau, O., Schultes, S., Bidle, K., Claquin, P., and Moriceau, B. (2006). Si and C interactions in the world ocean: importance of ecological processes and implications for the role of diatoms in the biological pump. *Glob. Biogeochem. Cycles* 20:GB4502. doi: 10.1029/2006GB002688

Ragueneau, O., Tréguer, P., Leynaert, A., Anderson, R. F., Brzezinski, M. A., DeMaster, D. J., et al. (2000). A review of the Si cycle in the modern ocean: recent progress and missing gaps in the application of biogenic opal as a paleoproductivity proxy. *Glob. Planet. Chang.* 26, 317–365. doi: 10.1016/S0921-8181(00)00052-7

Raven, J. A., and Falkowski, P. G. (1999). Oceanic sinks for atmospheric CO2. *Plant Cell Environ.* 22, 741–755. doi: 10.1046/j.1365-3040.1999.00419.x

Richardson, T. L., and Jackson, G. A. (2007). Small phytoplankton and carbon export from the surface ocean. *Science* 315, 838–840. doi: 10.1126/science.1133471

Tang, T., Kisslinger, K., and Lee, C. (2014). Silicate deposition during decomposition of cyanobacteria may promote export of picophytoplankton to the deep ocean. *Nat. Commun.* 5, 1–7. doi: 10.1038/ncomms5143

Tréguer, P., Bowler, C., Moriceau, B., Dutkiewicz, S., Gehlen, M., Aumont, O., et al. (2018). Influence of diatom diversity on the ocean biological carbon pump. *Nat. Geosci.* 11, 27–37. doi: 10.1038/s41561-017-0028-x

Treguer, P., Nelson, D. M., Van Bennekom, A. J., DeMaster, D. J., Leynaert, A., and Quéguiner, B. (1995). The silica balance in the world ocean: a reestimate. *Science* 268, 375–379. doi: 10.1126/science.268.5209.375

Visintini, N., Martiny, A. C., and Flombaum, P. (2021). Prochlorococcus, Synechococcus, and picoeukaryotic phytoplankton abundances in the global ocean. *Limnol. Oceanog. Lett.* 6, 207–215. doi: 10.1002/lol2.10188

Wei, Y., Sun, J., Chen, Z., Zhang, Z., Zhang, G., and Liu, X. (2021a). Significant contribution of picoplankton size fraction to biogenic silica standing stocks in the Western Pacific Ocean. *Prog. Oceanogr.* 192:102516. doi: 10.1016/j.pocean.2021.102516

Wei, Y., Sun, J., Li, L., and Cui, Z. (2022). Synechococcus silicon accumulation in oligotrophic oceans. *Limnol. Oceanogr.* 67, 552–566. doi: 10.1002/lno.12015

Wei, Y., Wang, X., Gui, J., and Sun, J. (2021b). Significant Pico-and Nanoplankton contributions to biogenic silica standing stocks and production rates in the oligotrophic eastern Indian Ocean. *Ecosystems* 24, 1654–1669. doi: 10.1007/s10021-021-00608-w

Conflict of Interest: The authors declare that the research was conducted in the absence of any commercial or financial relationships that could be construed as a potential conflict of interest.

Publisher's Note: All claims expressed in this article are solely those of the authors and do not necessarily represent those of their affiliated organizations, or those of the publisher, the editors and the reviewers. Any product that may

be evaluated in this article, or claim that may be made by its manufacturer, is not guaranteed or endorsed by the publisher.

frontiers | Frontiers in Marine Science

ORIGINAL RESEARCH
published: 22 June 2022
doi: 10.3389/fmars.2022.910327

Distribution of Dinoflagellate Cysts in Surface Sediments From the Qingdao Coast, the Yellow Sea, China: The Potential Risk of Harmful Algal Blooms

Zhaohui Wang, Yuning Zhang, Mingdan Lei, Shuanghui Ji, Jiazhuo Chen, Hu Zheng, Yali Tang* and Ren Hu**

Department of Ecology, College of Life Science and Technology, Jinan University, Guangzhou, China

OPEN ACCESS

Edited by:
Aifeng Li,
Ocean University of China, China

Reviewed by:
Pengbin Wang,
Ministry of Natural Resources, China
Pingping Shen,
Yantai University, China

****Correspondence:***
Zhaohui Wang
twzh@jnu.edu.cn
Yali Tang
litangyali@163.com
Ren Hu
thuren@jnu.edu.cn

Specialty section:
This article was submitted to Aquatic Microbiology, a section of the journal Frontiers in Marine Science

Received: *01 April 2022*
Accepted: *23 May 2022*
Published: *22 June 2022*

Citation:
Wang Z, Zhang Y, Lei M, Ji S, Chen J, Zheng H, Tang Y and Hu R (2022) Distribution of Dinoflagellate Cysts in Surface Sediments From the Qingdao Coast, the Yellow Sea, China: The Potential Risk of Harmful Algal Blooms. Front. Mar. Sci. 9:910327. doi: 10.3389/fmars.2022.910327

Surface sediments were collected from three sea areas of the Qingdao coast, the Yellow Sea, China, namely, the inner Jiaozhou Bay, the Laoshan coast, and the Amphioxus Reserve area in November to December 2017. Dinoflagellate cysts were observed in the sediments, focusing on the distribution of toxic and harmful species. Contents of biogenic elements were analyzed to reveal their relationships to cysts. A total of 32 cyst taxa were identified, including 23 autotrophic and 9 heterotrophic taxa. Cyst concentrations ranged from 83.3 to 346.5 cysts/g D Wt with an average of 210.7 cysts/g D Wt. Generally, cysts of autotrophic dinoflagellates dominated in sediments from the Qingdao coast with proportions of 41.05%–90.25%. There were no dominant group in cyst assemblages; cysts of Protoperidiniaceae, Suessiales, and Calciodinelloideae showed similar contributions. Cyst assemblages were quite different in the inner Jiaozhou Bay reflected by the lower species richness, diversity, and cyst concentration. Results from the redundancy analysis (RDA) demonstrated the influence of biogenic elements on cyst assemblages, which explained well why the three sea areas with different degrees of human activities showed different dinocyst storages. Notably, 17 harmful algal bloom (HAB) dinoflagellate cysts were identified in this study, including cysts of those producing toxins that may damage human health and marine animals. Some of these cysts occurred widely and dominantly in this study, such as cysts of *Gonyaulax spinifera*, *Azadinium trinitatum*, *Scrippsiella acuminata*, and *Biecheleria halophila*, suggesting the potential risk of HABs in the Qingdao coastal area.

Keywords: dinoflagellate cysts, sediment, harmful algal bloom, Qingdao Coast, the Yellow Sea, biogenic elements

INTRODUCTION

Dinoflagellates are the second largest group of marine phytoplankton and also an important group of toxic and harmful algal bloom (HAB) species (Gomez, 2012). HABs affect marine organisms negatively, degrade the environment, cause severe economic losses, and, in some cases, threaten human health (Hallegraeff et al., 2003). HABs only concern about 5% of marine phytoplanktonic

species (Zingone and Enevoldsen, 2000), of which dinoflagellates represent 75% (Smayda, 1997). Many dinoflagellate species form resting cysts during their life cycles, which thicken cell walls and sink to the sea floor as part of marine sediments (Bravo and Figueroa, 2014). Resting cysts can survive in benthic sediments for decades or even centuries due to their thick, tolerant walls (Ellegaard and Ribeiro, 2018). Dinoflagellate cysts (hereafter referred to as dinocysts) help the population survive from the harsh environment, and the germination of cysts provides large amounts of vegetative cells to the water column. Therefore, dinocysts are considered as the "seed bank" for the occurrence of HAB (Anderson et al., 2014; Castaneda-Quezada et al., 2021). Although only 10%–20% of dinoflagellates can form resting cysts, many toxic and HAB species are cyst-forming, especially those causing recurrent blooms (Genovesi-Giunti et al., 2006; Bravo and Figueroa, 2014). The distribution of dinocysts in sediments provides essential information in giving early warnings of the presence of toxic species and possible continuing recurrence of HABs in a given area (Anderson et al., 2014; Joyce et al., 2015; Sidabutar and Srimariana, 2021).

The coastal zone is the most active area of human activity, provides abundant resources, and has high ecological value and environmental functions. However, many coastal environments have been suffering from environmental degradation, decline in biodiversity, and bio-invasion such as the rapid economic development, population expansion, and overexploitation of marine resources (Yu et al., 2019). Qingdao is located in northeastern China, southeast of Shandong Peninsula, and east of the Yellow Sea. It is the economic center of Shandong Province and functions as an important international port, a modern marine industry zone, an international shipping hub in Northeast Asia, and a maritime sports base. Qingdao City covers an area of 758.16 km^2 with a population of 9.50 million in 2019. Due to the rapid increase of economic development and population size as well as the increase of aquaculture, the pollution level in Qingdao coastal waters has been increasing recently (Yuan et al., 2018). The degradation of water quality results in the frequent occurrence of algal blooms. A total of 36 algal blooms occurred in the coastal areas of Qingdao between 1990 and 2017, of which more than 80% occurred in Jiaozhou Bay (Zhou et al., 2020). Though intensive surveys have been carried out to investigate phytoplankton community in Jiaozhou Bay during the past 50 years (reviewed by Liu and Chen, 2021), dinocysts have been barely reported (Li et al., 2017).

In order to understand the effects of human activities on the distribution of dinocysts and the potential of HABs in the Qingdao coast, surface sediments were sampled from three different function sea areas of the Qingdao coast in this study, namely, a eutrophic enclosed bay (the inner Jiaozhou Bay), a conservation area (the Qingdao Amphioxus Reserve area), and a scenic and aquacultural area (the Laoshan coast). Biogenic elements including total organic carbon (TOC), organic matter (OM), total nitrogen (TN), total phosphorus (TP), and biogenic silicon (BSi) were analyzed, and the relationships between dinocysts and biogenic elements were discussed. The purposes of this study were to compare dinocyst composition among the three sea areas with different degrees of human activities, and to discuss the distribution of cysts of HAB dinoflagellates in sediments from the Qingdao coast.

MATERIALS AND METHODS

Study Areas and Sediment Collection

Qingdao is located in the southeast of the Shandong Peninsula, which borders the Yellow Sea in the east and the south. Surface sediments were collected in three sea areas along the Qingdao coast, i.e., the inner Jiaozhou Bay (JZ, J1–J4), the Laoshan coast (LS, L1–L9), and the Qingdao Amphioxus Reserve area (AR, A1–A4) (**Figure 1**). Jiaozhou Bay, in the northwest of the center

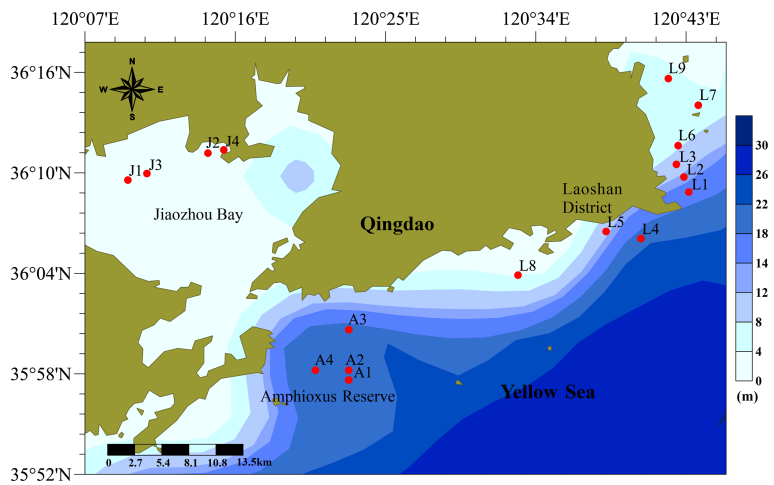

FIGURE 1 | Sampling stations in the Qingdao coastal sea area. Stations J1–J4 are in the inner Jiaozhou Bay, stations A1–A4 are in the Amphioxus Reserve area, and stations L1–L9 are in the Laoshan coast.

Qingdao City, is a large semi-closed bay connected to the Yellow Sea by a narrow bay mouth. Jiaozhou Bay has multiple functions (port, transportation, and aquaculture). The Laoshan coast is located in the eastern part of Qingdao City and surrounds the famous tourist attraction, the Laoshan Scenic Area. There are a lot of aquaculture farms in the Laoshan coast. The Amphioxus Reserve area is located in the southern part of Qingdao City, just outside the mouth of Jiaozhou Bay and close to the Qingdao Port. The Amphioxus Reserve area was established in August 2004 to protect wild amphioxus population and its habitat.

Surface sediments were collected from seventeen stations in the three sea areas using a Peterson grab between November and December 2017. The top 2 cm of sediments was sampled with a polyethylene spatula and sealed in a polyethylene bag, and then stored at −20°C for further treatment. All sediment samples were processed after transporting to the lab within 24 h.

Analyses of Biogenic Elements

Sediments for biogenic elements analysis were dried in an oven at 40°C until a constant weight was reached, and the water content of the sediments was calculated. The dried sediments were ground gently with an agate mortar and pestle, sieved through a 100-μm mesh for homogenization, and stored in sealed glass vials. In order to reduce the influence of external contamination on biogenic elements, sediment processing was carried out in a clean cupboard. All vessels were washed and soaked in acid for more than 24 h, and then fully rinsed with distilled water and dried before re-used. Total organic carbon (TOC) and total nitrogen (TN) were measured by a Perkin-Elmer 2400 Series II CHNS/O Analyzer (Perkin Elmer Inc., USA). Total phosphorus (TP) was measured using the potassium persulfate digestion method (Thien and Myers, 1992). Organic matter (OM) was determined by ignition loss in a muffle furnace (SG-XL1200, Honglang, Shanghai, China). Biogenic silica (BSi) was measured by the molybdate blue spectrophotometric method after removing the carbonates and organics by 1 mol/L HCl and 10% H_2O_2 and digested using 0.5 mol/L Na_2CO_3 solution (Mortlock and Froelich, 1989). The quality assurance/quality control (QA/QC) was assessed by the analyses of blank reagents and five replicates of the certified reference material (Offshore Marine Sediment, GBW 07314). The analytical precision was controlled to within 5% for biogenic elements.

Identification and Counting of Dinocysts

Approximately 5 g of wet sediments was weighted for dinocyst observation, placed in a beaker mixed with 50 ml of filtered seawater, and then sonicated for 60 s in a water bath. The sonicated materials were successively sieved through 125- and 10-μm sieves, and the slurry remaining on the 10-μm sieve with grain sizes between 10 and 125 μm was collected and filled to a final volume of 10 ml with filtered seawater, and then fixed with 3% formalin. An aliquot of 0.5–1 ml of treated sample was placed on a 1-ml counting chamber and diluted with appropriate distilled water. Dinocysts were identified and counted with an inverted light microscope (Nikon ECLIPSE) at 400× magnification according to Matsuoka and Fukuyo (2000) and Zonneveld and Pospelova (2015). At least 100 cysts were counted in each sample. Cyst concentration was expressed by the numbers of cyst per gram of dry sediments (cysts/g D Wt).

Data and Statistical Analyses

The sampling map was drawn by the software Sufer13.0. The Shannon–Wiener diversity index (*H'*), Pielou's Evenness index (*J*), and the correlation analysis (CA) between the cysts and biogenic elements were calculated by the SPSS 20.0 software. The bar charts and line charts were drawn by Excel 2016. Venn diagram was drawn using the Venn Diagram function package of the software R4.1.0. The bubble chart of cysts arranged by their average abundance was drawn using the ggplot2 function package of R4.1.0. The vegan function package of R4.1.0 was used to standardize the cyst data, and the vegdist function was used to calculate the Bray–Curtis distance, and then a cluster diagram was drawn by the gclus and plot function packages of R4.1.0 based on the Bray–Curtis distance. A detrended correspondence analysis (DCA) was first achieved to test the character of variability in the dinocyst assemblages. The length of the first DCA gradient was 0.78 standard deviations for our dataset, which justified the further use of the redundancy analysis (RDA). DCA and RDA were performed using Canoco 5 software.

RESULTS

Species Composition of Dinocysts

A total of 32 dinocyst taxa were identified in the surface sediments from the Qingdao coast, namely, 9 taxa in Gonyaulacales, 4 taxa in Calciodinelloideae, 1 taxon in Suessiales, 7 taxa in Gymnodiniales, 8 taxa in Protoperidiniaceae, and 3 taxa in genus *Azadinium* (Dinophyceae incertae sedis) (**Table 1**). The species richness identified at each station ranged between 6 and 23 taxa, and only 4 core species were shared among all stations (**Figure 2A**). The species richness in the inner Jiaozhou Bay (JZ) was 13 taxa, and 25 taxa were identified in the other two sea areas, the Laoshan coast (LS) and the Amphioxus Reserve area (AR), respectively (**Table 1**). Only 11 species were shared among the three sea areas (**Figure 2B**). No unique species occurred in JZ, while 6 unique species were recorded in the other two sea areas (**Figure 2B**). The Shannon–Wiener diversity index (*H'*) ranged from 1.37 to 2.63, and values of Pielou's Evenness index (*J*) were between 0.69 and 0.89 (**Figure 3A**). JZ had the lowest cyst diversity with an average *H'* value of 1.57, while the average *H'* values in LS and AR were 2.07 and 2.28, respectively. The mean values of the evenness index (*J*) were similar in the three sea areas, ranging from 0.79 to 0.82 (**Figure 3B**).

Notably, 17 cysts of the potentially toxic/harmful and/or bloom dinoflagellates were detected in this study (**Table 1**), including the paralytic shellfish poisoning (PSP) producers *Alexandrium andersonii*, *A. minutum*, *A. tamarense*, and *Gymnodinium catenatum*; the yessotoxin (YTX) producers *Gonyaulax spinifera*, *Lingulodinium polyedra* and *Protoceratium reticulatum*; the Azaspiracid shellfish poisoning (AZP) producer *Azadinium poporum*; and cysts of other bloom species (*Biecheleria halophila*, *Gonyaulax fragilis*, *Gymnodinium corollarium*, *Gy. impudicum*, *Gy. microreticulatum*, *Levanderina fissa*, *Pseudocochlodinium profundisulcus*, *Scrippsiella acuminata*, and *S. masanensis*). There were 10, 16, and 15 bloom species recorded

TABLE 1 | Information and distribution of dinoflagellate cysts in surface sediments from the Qingdao coast.

Taxonomy	Species identified	Harmful effects	JZ	LS	AR
Gonyaulacales	*Alexandrium andersonii*	HAB/PSP (Taylor et al., 2003)	+	+	+
	Alexandrium minutum	HAB/PSP (Taylor et al., 2003)			+
	Alexandrium tamarense	PSP (Hallegraeff, 1993)	+	+	+
	Gonyaulax fragilis	HAB/Mucilage (Balkis et al., 2011)		+	
	Gonyaulax scrippsae				+
	Gonyaulax spinifera	HAB/YTX (Taylor et al., 2003)	+	+	+
	Lingulodinium polyedra	HAB/YTX (Taylor et al., 2003)	+	+	
	Protoceratium reticulatum	HAB/YTX (Taylor et al., 2003)	+	+	+
	Sourniaea diacantha				+
Calciodinelloideae	*Ensiculifera carinata*		+	+	+
	Scrippsiella acuminata	Bloom (Taylor et al., 2003)	+	+	+
	Scrippsiella erinaceus			+	
	Scrippsiella masanensis	Bloom (Lee et al., 2019)		+	+
Suessiales	*Biecheleria halophila*	HAB (Kremp et al., 2005)	+	+	+
Gymnodiniales	*Gymnodinium catenatum*	HAB/PSP (Taylor et al., 2003)		+	+
	Gymnodinium corollarium	Bloom (Sundström et al., 2009)	+	+	+
	Gymnodinium impudicum	Bloom (Taylor et al., 2003)		+	+
	Gymnodinium microreticulatum	Bloom (Taylor et al., 2003)	+	+	+
	Levanderina fissa	HAB (Taylor et al., 2003)	+	+	+
	Pseudocochlodinium profundisulcus	HAB/Ichthyotoxic (Hu et al., 2021)		+	+
	Polykrikos schwartzii				+
Protoperidiniaceae	*Diplopsalis* sp.			+	
	Diplopsalopsis ovata				+
	Islandinium minutum		+		+
	Oblea acanthocysta			+	
	Protoperidinium avellane			+	
	Protoperidinium conicum			+	
	Protoperidinium denticulatum				+
	Protoperidinium monovelum		+	+	+
Dinophyceae incertae sedis	*Azadinium dalianense*			+	+
	Azadinium poporum	HAB/AZP (Krock et al., 2012)		+	+
	Azadinium trinitatum			+	+
Cyst richness	32		13	25	25

+: Occurrence in the three sea areas, JZ, the inner Jiaozhou Bay; LS, the Laoshan Coast; AR, the Amphioxus Reserve area; HAB, Harmful algal bloom species; PSP, Paralytic shellfish poisoning; YTX, Yessotoxin; AZP, Azaspiracid shellfish poisoning.

in JZ, LS, and AR, respectively, nine of which occurred in all of the three sea areas.

Structure of Cyst Assemblages

Dinoflagellates have autotrophic and heterotrophic lifestyles, in which Gonyaulacales, Calciodinelloideae, Suessiales, and *Azadinium* (Dinophyceae incertae sedis) are autotrophic dinoflagellates, Gymnodiniales have both autotrophic and heterotrophic ones, and all of Protoperidiniaceae are heterotrophic. A total of 23 taxa of cysts of autotrophic dinoflagellates and 9 taxa of heterotrophic dinoflagellates were identified. The heterotrophic dinoflagellates included 7 taxa in Protoperidiniaceae and cysts of *Polykrikos Schwartzii* in Gymnodiniales. Generally, cysts of autotrophic dinoflagellates dominated in sediments from the Qingdao coast (**Figure 4A**), and the percentage proportions of autotrophic dinoflagellate cysts ranged from 41.05% to 90.25%, with an average of 76.48%. The percentages of autotrophic cysts in the three sea areas showed a gradually increasing trend from JZ to AR, from 60.44% in JZ to 79.36% in LS, and 86.04% in AR, while those of heterotrophic cysts showed an opposite trend (**Figure 4B**).

Relative abundances of dinocyst groups in each station andsea area are illustrated in **Figures 4C, D**, respectively. There were no dominant groups in cyst assemblages, and Protoperidiniaceae, Suessiales, and Calciodinelloideae showed similar contributions with the average relative abundances of 23.45%, 21.75%, and 20.52%, respectively, followed by cysts in Gonyaulacales (17.66%) and Gymnodiniales (11.24%) (**Figure 4C**). Cyst composition varied in different sea areas (**Figure 4D**). Cyst assemblages in JZ were dominated by Protoperidiniaceae (averagely 39.56%), followed by the Calciodinelloideae (26.71%). Cysts in Suessiales slightlydominated in LS with an average proportion of 26.69%, and cysts in Protoperidiniaceae, Calciodinelloideae, and Gonyaulacales made similar contributions to the overall cyst assemblages with proportions of 15.54%–20.64%. Cysts in Gonyaulacales, Calciodinelloideae, Suessiales, and Gymnodiniales equally contributed to cyst assemblages in AR with a relative abundance of ca. 20%, and cysts in Protoperidiniaceae and *Azadinium* accounted for 13.66% and 6.81%, respectively.

Cyst Abundance and Distribution

Cyst concentrations ranged from 83.3 to 346.5 cysts/g D Wt with an average of 210.7 cysts/g D Wt, with the highest at station L6 and the lowest at station J3 (**Figure 5**). Lower cyst concentrations were recorded in JZ, ranging between 83.3 and 165.8 cysts/g D Wt, with an average of 127.2 cysts/g D Wt. Cyst concentrations

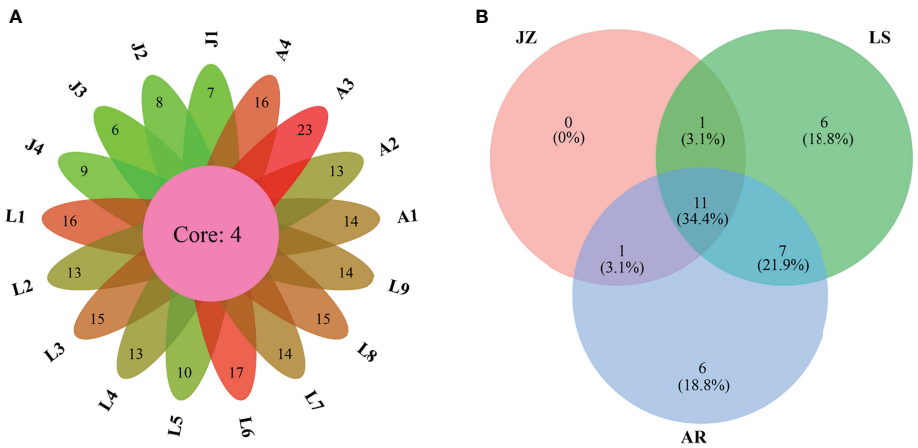

FIGURE 2 | Venn diagrams highlighting the degree of overlap of dinocyst taxa among the seventeen samples **(A)** and among the three sea areas **(B)**. JZ, the inner Jiaozhou Bay; LS, the Laoshan coast; AR, the Amphioxus Reserve area.

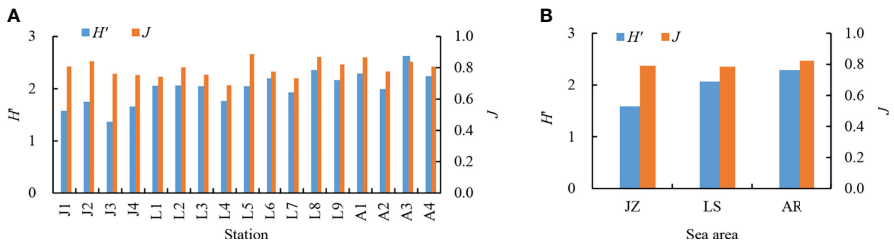

FIGURE 3 | Shannon–Wiener diversity index (*H'*) and Pielou's evenness index (*J*) of dinocysts in the seventeen samples **(A)** and the three sea areas **(B)**. JZ, the inner Jiaozhou Bay; LS, the Laoshan coast; AR, the Amphioxus Reserve area.

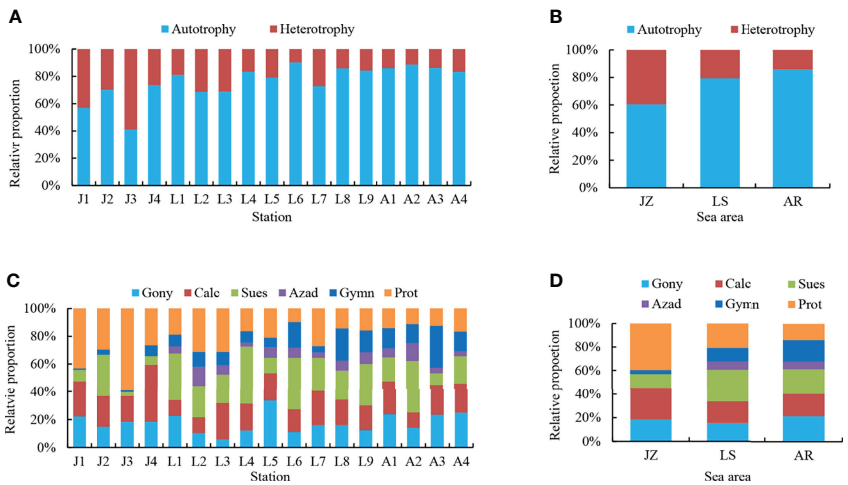

FIGURE 4 | Cyst profile in the seventeen samples **(A, C)** and the three sea areas **(B, D)**. **(A, B)** Percentage proportions of cysts of autotrophic and heterotrophic dinoflagellates. **(C, D)** Percentage proportions of cysts of each dinoflagellate group. Gony, Gonyaulacales; Calc, Calciodinelloideae; Sues, Suessiales; Azad, *Azadinium* (Dinophyceae incertae sedis); Gymn, Gymnodiniales; Prot, Protoperidiniaceae.

in LS varied from 109.4 to 346.5 cysts/g D Wt, with an average of 230.6 cysts/g D Wt. There were few differences in cyst concentrations between samples from AR, ranging from 221.2 to 281.4 cysts/g D Wt, with an average of 249.5 cysts/g D Wt.

Distribution of the 32 dinocyst taxa by dominance is shown in **Figure 6**. Only four cyst types were distributed at all stations, and they were also the top 4 most abundant cyst taxa in this study, including the bloom species *Biecheleria halophila* and *Scrippsiella acuminata*, and the YTX producer *Gonyaulax spinifera*, which ranked first, third, and fourth in cyst abundance, respectively. *Protoperidinium monovelum* was also found at all stations and ranked second in dominance. The average concentrations of the top 4 cyst types ranged between 23.8 and 51.0 cysts/g D Wt. Cysts of the bloom species *Gymnodinium corollarium* were distributed at 14 stations except stations J1–J3 in Jiaozhou Bay with an average of 12.2 cysts/g D Wt. Cysts of *Azadinium trinitatum*, *Alexandrium andersonii*, *Gymnodinium impudicum*, *Gymnodinium microreticulatum*, and *Ensiculifera carinata* occurred in most stations, with average concentrations of 4.5–11.3 cysts/g D Wt, while other cyst types rarely occurred.

Cluster, RDA, and CA Analyses

Cluster analysis of 17 sediment samples showed that four samples in the inner Jiaozhou Bay (JZ1-JZ4) were clustered together with station L5, while other LS and AR samples were clustered together into a large group (**Figure 7**). The results indicated that dinocyst assemblages in the inner Jiaozhou Bay and station L5 were quite different from other samples.

RDA analysis was conducted based on biogenic elements and dinocysts (**Figure 8A**). RDA1 and RDA2 explained 55.21% and 35.18% of the environmental and biological variables, respectively. The biogenic elements and dinocysts scattered in all of the four quadrants. Cysts in Calciodinelloideae showed a narrow intersection angle with BSi, indicating the significant influence of BSi on the distribution of the Calciodinelloideae cysts. Cysts in other classes scattered in the coordinates far away from the biogenic elements, indicating few effects of biogenic elements on their distribution. The ordination sampling station showed that samples in the three sea areas were separately grouped (**Figure 8B**). Samples in the inner Jiaozhou Bay were clustered along the negative axis of RDA2, which indicated the low BSi content and the high organic matter (TN, OM, and TOC) in this area. Samples in the Amphioxus Reserve area were distributed along the positive axis of RDA2, indicating the low organic matter (TOC, OM, and TN) and high BSi in this area. Meanwhile, the arrows of the biogenic elements were distributed within the group of samples of the Laoshan area, indicating the high content of biogenic elements in this area.

Generally, there were no significant correlations between dinocysts and biogenic elements except for a significant positive correlation between cysts in Calciodinelloideae and BSi (**Table 2**). Species richness showed significant correlations with concentrations of overall cysts and cysts in Gonyaulacales, Calciodinelloideae, and Gymnodiniales ($p < 0.05$ or $p < 0.01$). The concentration of overall cysts was positively correlated with the concentration of most cyst groups except for cysts of Protoperidiniaceae. Cysts of autotrophic dinoflagellates were positively correlated with each other, while cysts of heterotrophic Protoperidiniaceae were negatively correlated with other cyst groups.

DISCUSSION

Resting cyst is a specific dormant stage in the life cycle of many dinoflagellates.

Nearly 10%–20% of modern dinoflagellates form resting cysts (Head, 1996), which constitute the coupling between benthic and pelagic stages, and support bloom development and recurrence (Genovesi-Giunti et al., 2006; Anderson et al., 2014). However, the morphological characteristics of many resting cysts are not clear right now, and the corresponding relationships between some cysts and vegetative cells are still unknown (Gu et al., 2022). Therefore, the diversity and abundance of dinocysts are often underestimated based on the morphological characteristics under microscopic observations. Nevertheless, cyst identification

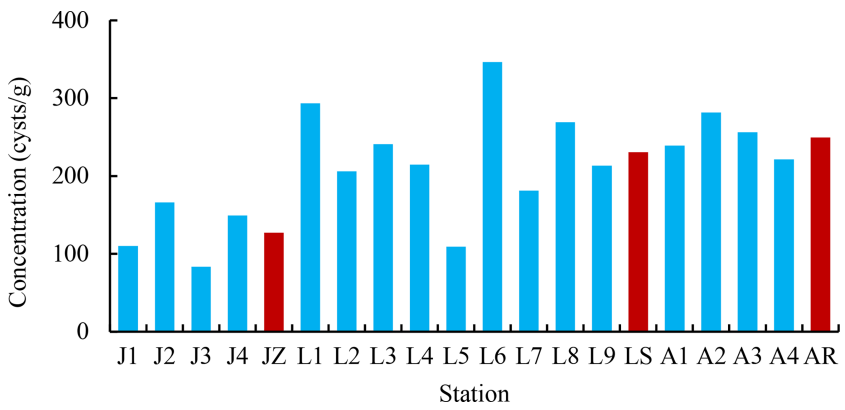

FIGURE 5 | Cyst concentration in the seventeen samples and the three sea areas. The blue bar shows cyst concentration in each sample, and the red bars present averages in the three sea areas.

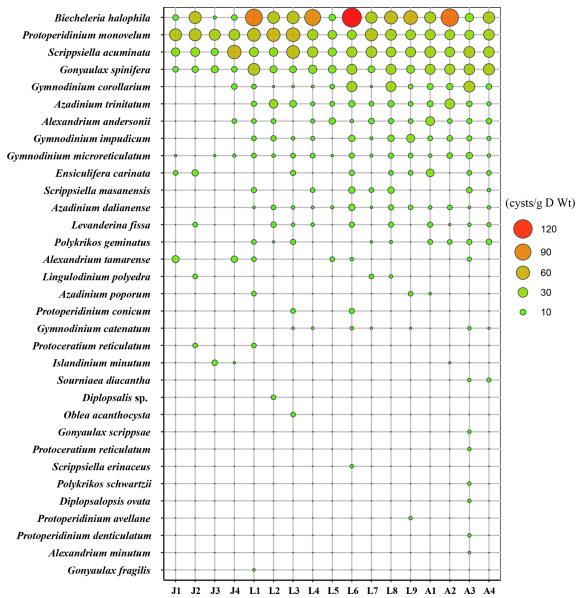

FIGURE 6 | Distribution of dinocysts according to their average abundance.

by traditional morphological classification is the basis for the study of cysts in sediments. In this study, a total of 32 cyst taxa were recorded in 17 surface sediments from the Qingdao coast. The cyst species richness was comparable to those reported in sediments from the other coastal sea areas around the world, which were generally 20–40 taxa recorded (Pospelova et al., 2005; Limoges et al., 2010; Liu et al., 2012; Aydin et al., 2015; Lu et al., 2017).

Although the three sea areas in this study are not far from each other, cyst assemblages differed among sea areas. Only 4 species were shared among all of the 17 stations, and only 34.4% of the species were shared among the three sea areas (**Figure 2**). The inner Jiaozhou Bay had lower cyst diversity and concentration, but a higher proportion of cysts of heterotrophic dinoflagellates. The cluster and RDA analyses showed that samples from Jiaozhou Bay were separately clustered from the other sea areas. Jiaozhou Bay is a semi-enclosed sea area with only a narrow mouth open to the Yellow Sea, which makes it a specific ecosystem and microalgal community, while the Laoshan coast and the Amphioxus Reserve area are connected to the Yellow Sea, which share similar cyst compositions. Eutrophication in Jiaozhou Bay has greatly increased recently, which resulted in frequent algal blooms and decreased phytoplankton biodiversity (Shi et al., 2020). In addition, Jiaozhou Bay is an important sea area for shellfish culturing, and feeding of shellfish also reduces the diversity of phytoplankton to a certain extent (Yu et al., 2019) and thus results in low cyst diversity and abundance. On the other hand, high sedimentation rate (0.19–3.96 cm/a, Li et al., 2011) and low water depth might result in the low abundance of cysts in Jiaozhou Bay. Station L5 showed similar cyst composition to the inner Jiaozhou Bay (**Figure 7**), as it is also a shallow nearshore site close to Qingdao City (**Figure 1**).

Generally, the productivity of heterotrophic dinoflagellates is lower than that of autotrophic ones because heterotrophs need to prey on diatoms or other small planktons. Therefore, the yield of cysts of autotrophic dinoflagellates should be higher than those of heterotrophs. The increased proportion of heterotrophic cysts indicates sufficient food resources for them, which has been regarded as an indicator of eutrophication (Matsuoka, 1999; Kang et al., 2021). Cyst assemblages in the Qingdao coast were dominated by cysts of autotrophic dinoflagellates with an average proportion of 76.48%, suggesting that the water quality in the Qingdao coast has not reached eutrophication level yet. Though nutrient levels had greatly increased in Jiaozhou Bay in recent decades (Shen et al., 2016), nutrient concentrations decreased gradually during 2010–2016, and the water quality had a slightly enriched level based on the national standard of the Marine Water Quality of China (GB3097-1997) (Yuan et al., 2018). Results from pollution assessment of biogenic elements indicated that TOC in the surface sediments from the Qingdao coast belonged to the uncontaminated level, while TN and TP reached moderate pollution levels (Lei et al., 2021). However, cysts of heterotrophic Protoperidiniaceae significantly contributed to cyst assemblages, especially in Jiaozhou Bay with an average proportion of 39.56% (**Figure 4D**). Diatoms generally dominated in phytoplankton community in Jiaozhou

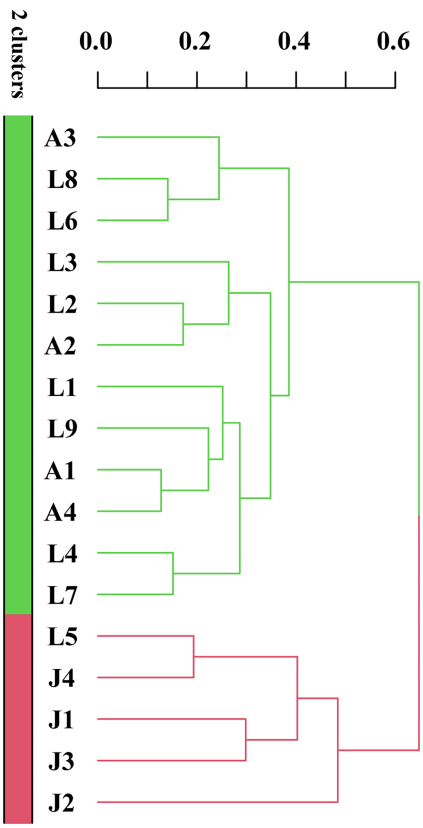

FIGURE 7 | Cluster analysis of seventeen sediment samples from the three sea areas of the Qingdao coast based on Bray–Curtis distance of dinocysts.

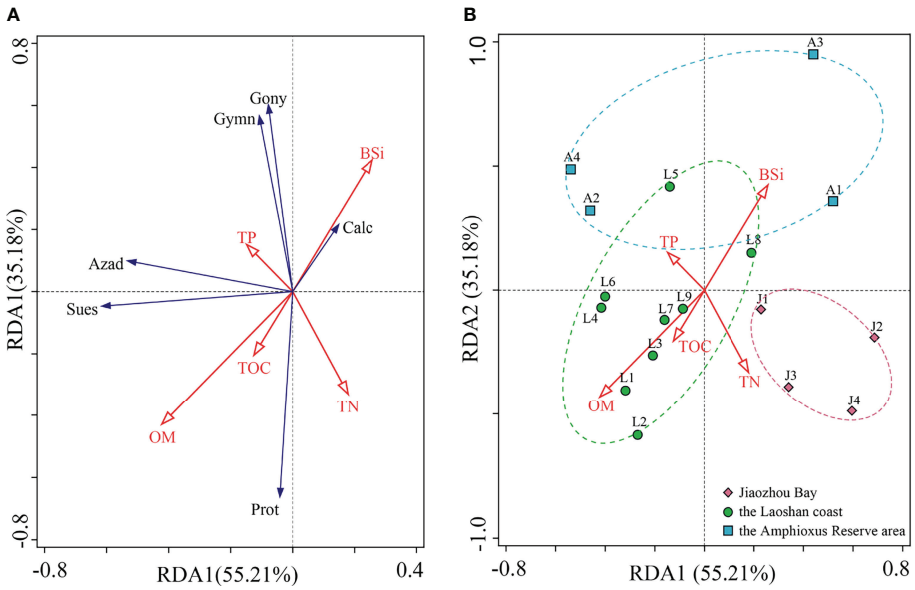

FIGURE 8 | Redundancy analysis (RDA) of biogenic elements and dinocysts in surface sediments from the Qingdao coast, showing cyst distribution and the directions of biogenic elements to the first two RDA axes, RDA1 (55.21%) and RDA2 (35.18%). The length of arrows indicates the importance of biogenic elements in explaining the distribution of cysts. The direction of the arrows shows approximate correlation to the ordination axes. **(A)** Ordination dinocyst groups and **(B)** ordination sampling stations, showing the distribution of the three areas.

Bay, and related blooms have occurred frequently (Yao et al., 2010; Shen et al., 2016). Sufficient food supply (diatoms) promotes the growth of heterotrophic dinoflagellates and thus leads to the increased production of cysts of heterotrophic dinoflagellates.

Seventeen cyst taxa of HAB dinoflagellates were identified in this study, namely, 8 toxin-producing species and 9 bloom species (**Table 1**). Cysts of the potential YTX producer, *Gonyaulax spinifera*, *Lingulodinium polyedra*, and *Protoceratium reticulatum* (Chikwililwa et al., 2019), were detected in this study. Cysts of *G. spinifera* were recorded at all stations and ranked 4th in abundance (**Figure 6**). Coincidentally, large numbers of *G. spinifera* sequences were analyzed in our metabarcoding study using the same sediments (Wang et al., 2022). Blooms of *G. spinifera* occurred in Jiaozhou Bay in 2003 and 2007, respectively (Zhou et al., 2020). As a cyst-forming species, *G. spinifera* can form various types of cysts, mostly belonging to the cyst genus *Spiniferites* with wide morphological variations (Rochon et al., 2009). The wide and abundant occurrence of *G. spinifera* cysts in the Qingdao coast indicated high numbers of its vegetative cells in the water column and the high risk of its blooms.

Species in *Alexandrium* are the major producers of PSP (Lundholm et al., 2009 onwards). *Alexandrium* blooms have occurred frequently in the Chinese coastal waters (Yu et al., 2020), and cysts of *Alexandrium* were widely distributed in sediments of the China coasts (Tang et al., 2021). Meanwhile, PSP toxins have also been detected in phytoplankton and

TABLE 2 | Pearson correlation coefficients between dinoflagellate cysts and biogenic elements.

	TN	TP	BSi	TOC	Species richness	Overall cysts	Gony	Calc	Sues	Azad	Gymn	Prot
TN	1	**0.759****	0.379	**0.866****	0.037	−0.059	−0.019	0.218	−0.076	−0.257	−0.279	0.361
TP	**0.759****	1	**0.512***	**0.636****	0.387	0.193	0.245	0.244	0.095	0.053	0.059	0.069
BSi	0.379	.512*	1	0.327	**0.534***	0.146	0.301	0.403	−0.18	−0.035	0.265	0.043
TOC	**0.866****	**0.636****	0.327	1	0.206	0.093	0.119	0.216	0.113	−0.16	−0.198	0.277
Species richness	0.037	0.387	**0.534***	0.206	1	**0.783****	**0.632****	**0.544***	0.419	0.468	**0.838****	−0.124
Overall cysts	−0.059	0.193	0.146	0.093	**0.783****	1	**0.532***	**0.517***	**0.826****	**0.712****	**0.792****	−0.05
Gony	−0.019	0.245	0.301	0.119	**0.632****	**0.532***	1	0.247	0.248	0.195	**0.564***	−0.426
Calc	0.218	0.244	0.403	0.216	**0.544***	**0.517***	0.247	1	0.173	0.039	**0.513***	−0.015
Sues	−0.076	0.095	−0.18	0.113	0.419	**0.826****	0.248	0.173	1	**0.649****	0.428	−0.065
Azad	−0.257	0.053	−0.035	−0.16	0.468	**0.712****	0.195	0.039	**0.649****	1	**0.547***	0.004
Gymn	−0.279	0.059	0.265	−0.198	**0.838****	**0.792****	**0.564***	**0.513***	0.428	**0.547***	1	−0.331
Prot	0.361	0.069	0.043	0.277	−0.124	−0.05	−0.426	−0.015	−0.065	0.004	−0.331	1

**p < 0.05, **p < 0.01. Gony, Gonyaulacales; Calc, Calciodinelloideae; Sues, Suessiales; Azad, Azadinium (Dinophyceae incertae sedis); Gymn, Gymnodiniales; Prot, Protoperidiniaceae. Correlation coefficients with significance were marked in bold.*

shellfish samples (Zou et al., 2014; Liu et al., 2017). Four cyst types of the PSP producers were detected in this study, i.e., *Alexandrium andersonii*, *A. minutum*, *A. tamarense*, and *Gymnodinium catenatum*, in which *A. Andersonii* was widely distributed with high concentrations, indicating a potential risk of *Alexandrium* blooms and PSP events in the Qingdao coast.

The potential AZP producer, *Azadinium poporum*, occurred in all stations except for those in the inner Jiaozhou Bay, and ranked the sixth most abundant cyst type (**Figure 6**). *A. poporum* was reported to distribute widely in surface sediments from the Chinese coasts (Gu et al., 2013; Liu et al., 2020; Tang et al., 2021), and 13 out of 16 strains of *A. poporum* from different geographic locations along the Chinese coastline contained AZPs (Krock et al., 2014). However, species in *Azadinium* has been seldom reported in the phytoplankton survey, which might be ignored due to their small sizes.

Biecheleria halophila was the most abundant cyst type in sediments from the Qingdao coast in our study. However, this species was rarely observed in the previous routine phytoplankton surveys due to the small size and frangible thin wall. *Biecheleria* has become more frequently detected in the phytoplankton communities as the development of molecular biological techniques (Sundstrom et al., 2010). Taxa in *Biecheleria* generally form resting cysts (Moestrup et al., 2009), which made them common dominant eukaryotes in sediments based on metabarcoding analysis (Dzhembekova et al., 2018; Liu et al., 2020; Rhodes et al., 2020). *B. halophila* was reported to form a co-occurring bloom with *Scrippsiella hangoei* in the Baltic Sea (Kremp et al., 2005). The wide and abundant occurrence of cysts of *B. halophila* in the Qingdao coast suggests that it is a common dominant dinoflagellate species in this sea area, but might be ignored during the microscopic observation because of their fragility and small size.

Cysts of *Scrippsiella acuminata* occurred in all stations and ranked second in abundance (**Figure 6**). *S. acuminata* is a common bloom species in coastal waters (Wang et al., 2007; Zinssmeister et al., 2011), which is easy to form cysts, making its cysts dominant in sediments from worldwide coasts (Tang et al., 2021). In China, the recurrent blooms of *S. acuminata* have occurred in Daya Bay, South China Sea since the end of the 1990s (Wang et al., 2007). *Pseudocochlodinium profundisulcus* and *Levanderina fissa* are common bloom species in the Pearl River Estuary of the South China Sea, and their blooms have frequently occurred in the recent two decades (Wang et al., 2001; Shen et al., 2012; Dong et al., 2020). Their cysts were detected in most stations in this study, and ranked the 13th and 14th most abundant cyst taxa (**Figure 6**). Shang et al. (2022) detected cysts of *P. profundisulcus* in the ballast tank of an international ship arriving at the Jiangyin Port (China), and successfully germinated cysts into the vegetative cells, and thus suggested the feasibility of the bio-invasion risk *via* the transport of live resting cysts by ship's ballast tanks. Although these algal blooms have not occurred in the coastal waters of Qingdao, cysts of the toxic and harmful dinoflagellates were distributed widely and abundantly in surface sediments, indicating the potential risk of these algal blooms in the Qingdao coast to some extent.

CONCLUSION

This study provides an overview of dinocyst assemblages (including those of HAB species) from three different sea areas in the Qingdao coast, the Yellow Sea, China. Our results suggested the quite different cyst assemblages in the inner Jiaozhou Bay, which is a shallow enclosed embayment with intensive human activities, reflected by lower cyst diversity and concentration, and higher proportion of cysts of heterotrophic dinoflagellates. Notably, 17 HAB dinocysts were identified in this study, including cysts of the PSP producers *Alexandrium andersonii*, *A. minutum*, *A. tamarense*, and *Gymnodinium catenatum*; the YTX producers *Gonyaulax spinifera*, *Lingulodinium polyedra*, and *Protoceratium reticulatum*; the AZP producer *Azadinium poporum*; and the ichthyotoxic species *Pseudocochlodinium profundisulcus*. Cysts of the toxic and harmful dinoflagellates were distributed widely and abundantly in surface sediments, indicating the potential risk of HABs in the Qingdao coast to some extent.

DATA AVAILABILITY STATEMENT

The original contributions presented in the study are included in the article/supplementary material. Further inquiries can be directed to the corresponding authors.

AUTHOR CONTRIBUTIONS

ZW, YT, and RH designed the experiment and prepared the manuscript. YZ, ML, and SJ completed the experiment. JC and HZ conducted statistical analyses. All authors contributed to the article and approved the submitted version.

FUNDING

This work was supported by the Science and Technology Basic Resources Investigation Program of China (No. 2018FY100200) and the National Natural Science Foundation of China (No. 42076141), and Key Program of Marine Economy Development (Six Marine Industries) Special Foundation of Department of Natural Resources of Guangdong Province (No. GDNRC [2021]37).

ACKNOWLEDGMENTS

We thank Prof. Tao Jiang for collecting sediment samples. We also thank the funding program from the National Natural Science Foundation of China and Science and Technology Basic Resources Investigation Program of China.

REFERENCES

Anderson, D. M., Keafer, B. A., Kleindinst, J. L., McGillicuddy, D. J.Jr., Martin, J. L., Norton, K., et al. (2014). *Alexandrium Fundyense* Cysts in the Gulf of Maine: Long-Term Time Series of Abundance and Distribution, and Linkages to Past and Future Blooms. *Deep-Sea Res. PT II.* 103, 6–26. doi: 10.1016/j.dsr2.2013.10.002

Aydin, H., Yurur, E. E., Uzar, S., and Kucuksezgin, F. (2015). Impact of Industrial Pollution on Recent Dinoflagellate Cysts in Izmir Bay (Eastern Aegean). *Mar. pollut. Bull.* 94, 144–152. doi: 10.1016/j.marpolbul.2015.02.038

Balkis, N., Atabay, H., Türetgen, I., Albayrak, S., Balkis, H., and Tüfekçi, V. (2011). Role of Single-Celled Organisms in Mucilage Formation on the Shores of Büyükada Island (the Marmara Sea). *J. Mar. Biol. Assoc. UK* 91, 771–781. doi: 10.1017/S0025315410000081

Bravo, I., and Figueroa, R. I. (2014). Towards an Ecological Understanding of Dinoflagellate Cyst Functions. *Microorganisms* 2, 11–32. doi: 10.3390/microorganisms2010011

Castaneda-Quezada, R., García-Mendoza, E., Ramírez-Mendoza, R., Helenes, J., Rivas, D., Romo-Curiel, A., et al. (2021). Distribution of *Gymnodinium Catenatum* Graham Cysts and its Relation to Harmful Algae Blooms in the Northern Gulf of California. *J. Mar. Biol. Assoc. UK* 101, 895–909. doi: 10.1017/S0025315421000795

Chikwililwa, C., McCarron, P., Waniek, J. J., and Schulz-Bull, D. E. (2019). Phylogenetic Analysis and Yessotoxin Profiles of *Gonyaulax Spinifera* Cultures From the Benguela Current Upwelling System. *Harmful Algae* 85, 101626. doi: 10.1016/j.hal.2019.101626

Dong, Y., Cui, L., Cao, R., Cen, J., Zou, J., Zhou, X., et al. (2020). Ecological Characteristics and Teratogenic Retinal Determination of *Cochlodinium Geminatum* Blooms in Pearl River Estuary, South China. *Ecotoxicol. Environ. Safe.* 191, 110226. doi: 10.1016/j.ecoenv.2020.110226

Dzhembekova, N., Moncheva, S., Ivanova, P., Slabakova, N., and Nagai, S. (2018). Biodiversity of Phytoplankton Cyst Assemblages in Surface Sediments of the Black Sea Based on Metabarcoding. *Biotechnol. Biotechnol. Equip.* 32, 1507–1513. doi: 10.1080/13102818.2018.1532816

Ellegaard, M., and Ribeiro, S. (2018). The Long-Term Persistence of Phytoplankton Resting Stages in Aquatic 'Seed Banks'. *Biol. Rev. Camb. Philos. Soc* 93, 166–183. doi: 10.1111/brv.12338

Genovesi-Giunti, B., Laabir, M., and Vaquer, A. (2006). The Benthic Resting Cyst: A Key Actor in Harmful Dinoflagellate Blooms-Areview. *Vie Milieu / Life Environ.* 56, 327–337. doi: 10.1016/j.tree.2006.09.005

Gomez, F. (2012). A Quantitative Review of the Lifestyle, Habitat and Trophic Diversity of Dinoflagellates (Dinoflagellata, Alveolata). *System. Biodivers* 10, 267–275. doi: 10.1080/14772000.2012.721021

Gu, H., Luo, Z., Krock, B., Witt, M., and Tillmann, U. (2013). Morphology, Phylogeny and Azaspiracid Profile of *Azadinium Poporum* (Dinophyceae) From the China Sea. *Harmful Algae* 21-22, 64–75. doi: 10.1016/j.hal.2012.11.009

Gu, H., Mertens, K. D., Amelie, D., Gwenael, B., Zhen, L., Philipp, H., et al. (2022). Unravelling the *Gonyaulax Baltica* Species Complex: Cyst-Theca Relationship of *Impagidinium Variaseptum*, Spiniferites Pseudodelicatus Sp. Nov. And S. Ristingensis (Gonyaulacaceae, Dinophyceae), With Descriptions of *Gonyaulax Bohaiensis* Sp. Nov, G. *Amoyensis* Sp. Nov. And G. *Portimonensis* Sp. Nov. *J. Phycol.* doi: 10.1111/jpy.13245

Hallegraeff, G. M. (1993). A Review of Harmful Algal Blooms and Their Apparent Global Increase. *Phycologia* 32, 79–99. doi: 10.2216/i0031-8884-32-2-79.1

Hallegraeff, G. M., Anderson, D. M., and Cembella, A. D. (2003). *Manual on Harmful Marine Microalgae* (Paris: UNESCO Publishing).

Head, M. J. (1996). ""Modern Dinoflagellate Cysts and Their Biological Affinities"," in *The Palynology: Principles and Applications*. Eds. J. Jansonius and D. C. McGregor (U.S.A: AASP), 1197–1248.

Hu, Z., Xu, N., Gu, H., Chai, Z., Takahashi, K., Li, Z., et al. (2021). Morphomolecular Description of a New HAB Species, *Pseudocochlodinium Profundisulcus* Gen. Et Sp. Nov., and its LSU rRNA Gene Based Genetic Diversity and Geographical Distribution. *Harmful algae* 108, 102098. doi: 10.1016/j.hal.2021.102098

Joyce, L. B., Pitcher, G. C., Randt, A. D., and Monteiro, P. M. S. (2015). Dinoflagellate Cysts From Surface Sediments of Saldanha Bay, South Africa: An Indication of the Potential Risk of Harmful Algal Blooms. *Harmful Algae* 5, 309–318. doi: 10.1016/j.hal.2004.08.001

Kang, Y., Kim, H. J., and Moon, C. H. (2021). Eutrophication Driven by Aquaculture Fish Farms Controls Phytoplankton and Dinoflagellate Cyst Abundance in the Southern Coastal Waters of Korea. *J. Mar. Sci. Eng.* 9, 362. doi: 10.3390/jmse9040362

Kremp, A., Elbrachter, M., Schweikert, M., Wolny, J. L., and Gottschling, M. (2005). *Woloszynskia Halophila* (Biecheler) Comb. Nov.: A Bloom-Forming Cold-Water Dinoflagellate Co-Occurring With *Scrippsiella Hangoei* (Dinophyceae) in the Baltic Sea. *J. Phycol* 41, 629–642. doi: 10.1111/j.1529-8817.2005.00070.x

Krock, B., Tillmann, U., Voss, D., Koch, B. P., Salas, R., Witt, M., et al. (2012). New Azaspiracids in Amphidomataceae (Dinophyceae). *Toxicon* 60, 830–839. doi: 10.1016/j.toxicon.2012.05.007

Krock, B., Tillmann, U., Witt, M., and Gu, H. (2014). Azaspiracid Variability of *Azadinium Poporum* (Dinophyceae) From the China Sea. *Harmful Algae* 36, 22–28. doi: 10.1016/j.hal.2014.04.012

Lee, S. Y., Jeong, H. J., Kim, S. J., Lee, K. H., and Jang, S. H. (2019). *Scrippsiella Masanensis* Sp. Nov. (Thoracosphaerales, Dinophyceae), a Phototrophic Dinoflagellate From the Coastal Waters of Southern Korea. *Phycologia* 58, 287–299. doi: 10.1080/00318884.2019.1568794

Lei, M., Wang, Z., and Jiang, T. (2021). Distribution and Pollution Assessment of Biogenic Elements in Surface Sediments From Qingdao Coastal Area. *Mar. Environ. Sci.* 40, 93–100. doi: 10.13634/j.cnki.mes.2021.01.013

Li, F., Li, X., Qi, J., and Song, J. (2011). Accumulation of Heavy Metals in the Core Sediments From the Jiaozhouwan Bay During Last Hundred Years and its Environmental Significance. *J. Mar. Sci.* 29, 35–45. doi: 10.3969/j.issn.1001-909X.2011.02.004

Limoges, A., Kielt, J. F., Radi, T., Ruiz-Fernandez, A. C., and Vernal, A. D. (2010). Dinoflagellate Cyst Distribution in Surface Sediments Along the South-Western Mexican Coast (14.76 Degrees N to 24.75 Degrees N). *Mar. Micropaleontol* 76, 104–123. doi: 10.1016/j.marmicro.2010.06.003

Li, Y., Tang, Y., Shen, P., Gu, H., and Tan, Y. (2017). Distribution of Dinoflagellate Resting Cysts in Surface Sediment of Jiaozhou Bay, China. *Oceanol. Limnol. Sin.* 48, 760–766. doi: 10.11693/hyhz20161200283

Liu, S., and Chen, N. (2021). Advances in Biodiversity Analysis of Phytoplankton and Harmful Algal Bloom Species in the Jiaozhou Bay. *Mar. Sci.* 45, 170–188. doi: 10.11759/hykx20201021003

Liu, D., Shi, Y., Di, B., Sun, Q., Wang, Y., Dong, Z., et al. (2012). The Impact of Different Pollution Sources on Modern Dinoflagellate Cysts in Sishili Bay, Yellow Sea, China. *Mar. Micropaleontol.* 84-85, 1–13. doi: 10.1016/j.marmicro.2011.11.001

Liu, L., Wang, Z., and Lu, S. (2020). Diversity and Geographical Distribution of Resting Stages of Eukaryotic Algae in the Surface Sediments From the Southern Chinese Coastline Based on Metabarcoding Partial 18S rDNA Sequences. *Mar. Ecol.* 41, e12585. doi: 10.1111/maec.12585

Liu, Y., Yu, R., Kong, F., Chen, Z., Dai, L., Gao, Y., et al. (2017). Paralytic Shellfish Toxins in Phytoplankton and Shellfish Samples Collected From the Bohai Sea, China. *Mar. pollut. Bull.* 115, 324–331. doi: 10.1016/j.marpolbul.2016.12.023

N. Lundholm, C. Churro, M. Hoppenrath, M. Iwataki, J. Larsen, K. Mertens, Ø. Moestrup and A. Zingone (2009 onwards) *IOC-UNESCO Taxonomic Reference List of Harmful Micro Algae*. Available at: https://www.marinespecies.org/hab on 2022-03-11.

Lu, X., Wang, Z., Gu, X., Gu, Y., Liang, W., and Liu, L. (2017). Impacts of Metal Contamination and Eutrophication on Dinoflagellate Cyst Assemblages Along the Guangdong Coast of Southern China. *Mar. pollut. Bull.* 120, 239–249. doi: 10.1016/j.marpolbul.2017.05.032

Matsuoka, K. (1999). Eutrophication Process Recorded in Dinoflagellate Cyst Assemblages-a Case of Yokohama Port, Tokyo Bay, Japan. *Sci. Total. Environ.* 231, 17–35. doi: 10.1016/S0048-9697(99)00087-X

Matsuoka, K., and Fukuyo, Y. (2000). *Technical Guide for Modern Dinoflagellate Cyst Study* (Tokyo: Japan Society for the Promotion of Science). WESTPAC-HAB.

Moestrup, O., Lindberg, K., and Daugbjerg, N. (2009). Studies on Woloszynskioid Dinoflagellates IV: The Genus *Biecheleria* Gen. Nov. *Phycol. Res.* 57, 203–220. doi: 10.1111/j.1440-1835.2009.00540.x

Mortlock, R. A., and Froelich, P. N. (1989). A Simple Method for the Rapid Determination of Biogenic Opal in Pelagic Marine Sediments. *Deep-Sea Res. Part I.* 36, 1415–1426. doi: 10.1016/0198-0149(89)90092-7DEEP-SEARESPTI

Pospelova, V., Chmura, G. L., Boothman, W., and Latimer, J. S. (2005). Spatial Distribution of Modern Dinoflagellate Cysts in Polluted Estuarine Sediments

From Buzzards Bay (Massachusetts, USA) Embayments. *Mar. Ecol. Prog. Ser.* 292, 23–40. doi: 10.3354/meps292023

Rhodes, L. L., Smith, K. F., MacKenzie, L., and Moisan, C. (2020). Checklist of the Planktonic Marine Dinoflagellates of New Zealand. *New Zeal. J. Mar. Fresh* 54, 86–101. doi: 10.1080/00288330.2019.1626746

Rochon, A., Lewis, J., Ellegaard, M., and Harding, L. C. (2009). The *Gonyaulax Spinifera* (Dinophyceae) "Complex": Perpetuating the Paradox? *Rev. Palaeobot. Palynol* 155, 52–60. doi: 10.1016/j.revpalbo.2008.12.017

Shang, L., Zhai, X., Tian, W., Liu, Y., Han, Y., Deng, Y., et al. (2022). *Pseudocochlodinium Profundisulcus* Resting Cysts Detected in the Ballast Tank Sediment of Ships Arriving in the Ports of China and North America and the Implications in the Species' Geographic Distribution and Possible Invasion. *Int. J. Environ. Res. Public Health* 19, 299. doi: 10.3390/ijerph19010299

Shen, P., Li, Y., Qi, Y., Zhang, L., Tan, Y., and Huang, L. (2012). Morphology and Bloom Dynamics of *Cochlodinium Geminatum* (Schütt) Schütt in the Pearl River Estuary, South China Sea. *Harmful Algae* 13, 10–19. doi: 10.1016/j.hal.2011.09.009

Shen, Z., Yao, Y., and Wu, Y. (2016). Silica Supply and Diatom Blooms in the Jiaozhou Bay, China. *Acta Oceanol. Sin.* 35, 20–27. doi: 10.1007/s13131-016-0917-7

Shi, J., Leng, Q., Zhu, J., Gao, H., Guo, X., and Mao, X. (2020). Influences of Nutrient Sources on the Alternation of Nutrient Limitations and Phytoplankton Community in Jiaozhou Bay, Southern Yellow Sea of China. *Sustainability* 12, 2224. doi: 10.3390/su12062224

Sidabutar, T., and Srimariana, E. S. (2021). Dinoflagellate Cyst Assemblages in Surface Sediment From Jakarta Bay. *IOP Conf. Ser.: Earth Environ. Sci.* 718, 12091. doi: 10.1088/1755-1315/718/1/012091

Smayda, T. (1997). Harmful Algal Blooms: Their Ecophysiology and General Relevance to Phytoplankton Blooms in the Sea. *Limnol. Oceanogr* 42, 1137–1153. doi: 10.4319/lo.1997.42.5_part_2.1137

Sundström, A. M., Kremp, A., Daugbjerg, N., Moestrup, Ø., Ellegaard, M., Hansen, R., et al. (2009). *Gymnodinium Corollarium* Sp. Nov. (Dinophyceae)- a New Cold-Water Dinoflagellate Responsible for Cyst Sedimentation Events in the Baltic Sea. *J. Phycol.* 45, 938–952. doi: 10.1111/j.1529-8817.2009.00712.x

Sundstrom, A. M., Kremp, A., Tammilehto, A., Tuimala, J., and Larsson, U. (2010). Detection of the Bloom-Forming Cold-Water Dinoflagellate *Biecheleria Baltica* in the Baltic Sea Using LSU rRNA Probes. *Aquat. Microb. Ecol.* 61, 129–140. doi: 10.3354/ame01442

Tang, Y., Gu, H., Wang, Z., Liu, D., Wang, Y., Lu, D., et al. (2021). Exploration of Resting Cysts (Stages) and Their Relevance for Possibly HABs-Causing Species in China. *Harmful Algae* 107, 102050. doi: 10.1016/j.hal.2021.102050

Taylor, F. J. R., Fukuyo, Y., and Hallegraeff, G. M. (2003). "Taxonomy of Harmful Dinoflagellates," in *Manual on Harmful Marine Microalgae*. Eds. G. M. Hallegraeff, D. M. Anderson and A. D. Cembella (Paris; UNESCO), 389–432.

Thien, S. J., and Myers, R. (1992). Determination of Bioavailable Phosphorus in Soil. *Soil Sci. Soc Am. J.* 56, 814–818. doi: 10.2136/sssaj1992.03615995005600030023x

Wang, Z., Lei, M., Ji, S., Xie, C., Chen, J., Li, W., et al. (2022). Comparison in Diversity of Eukaryotic Algae in Surface Sediments From Different Functional Sea Areas of Qingdao Coast, the Yellow Sea, China: A Metabarcoding Approach. *J. Oceanol. Limnol.* doi: 10.1007/s00343-021-1200-0

Wang, Z., Qi, Y., and Yang, Y. (2007). Cyst Formation: An Important Mechanism for the Termination of *Scrippsiella Trochoidea* (Dinophyceae) Bloom. *J. Plankton Res.* 29, 209–218. doi: 10.1093/plankt/fbm008

Wang, Z., Qi, Y., Yin, Y., Jiang, T., and Xie, L. (2001). Studies on the Cause and the Occurrence Reasons of a *Gyrodinium Instriatum* Red Tides in Shenzhen Bay in Spring of 1998. *Mar. Sci.* 25, 47–49. doi: 10.3969/j.issn.1000-3096.2001.05.015

Yao, P., Yu, Z., Deng, C., Liu, S., and Zhen, Y. (2010). Spatial-Temporal Distribution of Phytoplankton Pigments in Relation to Nutrient Status in Jiaozhou Bay, China. *Estuar. Coast. Shelf. Sci.* 89, 234–244. doi: 10.1016/j.ecss.2010.07.003

Yuan, H., Song, J., Xing, J., Li, X., Li, N., and Duan, L. (2018). Spatial and Seasonal Variations, Partitioning and Fluxes of Dissolved and Particulate Nutrients in Jiaozhou Bay. *Cont. Shelf Res.* 171, 140–149. doi: 10.1016/j.csr.2018.11.004

Yu, R., Lu, S., and Qi, Y. (2020). Progress and Perspectives of Harmful Algal Bloom Studies in China. *Oceanol. Limnol. Sin.* 51, 768–788. doi: 10.11693/hyhz20200400127

Yu, L., Wu, X., Zheng, X., Zheng, T., Xin, J., and Walther, M. (2019). An Index System Constructed for Ecological Stress Assessment of the Coastal Zone: A Case Study of Shandong, China. *J. Environ. Manage.* 232, 499–504. doi: 10.1016/j.jenvman.2018.11.084

Zhou, J., Wang, W., Wu, Z., Wang, Q., Wang, Y., and Gao, X. (2020). The Basic Characteristics and Prevention Countermeasures of Red Tide in Shandong Coast Waters. *Chin. J. Mar. Environ. Sci.* 39, 537–543. doi: 10.13634/j.cnki.mes.2020.04.006

Zingone, A., and Enevoldsen, H. O. (2000). The Diversity of Harmful Algal Blooms: A Challenge for Science and Management. *Ocean Coast. Manag* 43, 725–748. doi: 10.1016/S0964-5691(00)00056-9

Zinssmeister, C., Soehner, S., Facher, E., Kirsch, M., Meier, K. S. J., and Gottschling, M. (2011). Catch Me If You can: The Taxonomic Identity of *Scrippsiella Trochoidea* (F. Stein) AR Loebl. (Thoracosphaeraceae, Dinophyceae). *Syst. Biodivers.* 9, 145–157. doi: 10.1080/14772000.2011.586071

Zonneveld, K. A. F., and Pospelova, V. (2015). A Determination Key for Modern Dinoflagellate Cysts. *Palynology* 39, 387–409. doi: 10.1080/01916122.2014.990115

Zou, C., Ye, R., Zheng, J., Luo, Z., Gu, H., Yang, W., et al. (2014). Molecular Phylogeny and PSP Toxin Profile of the *Alexandrium Tamarense* Species Complex Along the Coast of China. *Mar. pollut. Bull.* 89, 209–219. doi: 10.1016/j.marpolbul.2014.09.056

Conflict of Interest: The handling Editor AL declared a past co-authorship with the author ZW. The authors declare that the research was conducted in the absence of any commercial or financial relationships that could be construed as a potential conflict of interest.

Publisher's Note: All claims expressed in this article are solely those of the authors and do not necessarily represent those of their affiliated organizations, or those of the publisher, the editors and the reviewers. Any product that may be evaluated in this article, or claim that may be made by its manufacturer, is not guaranteed or endorsed by the publisher.

frontiers | Frontiers in Marine Science

ORIGINAL RESEARCH
published: 22 July 2022
doi: 10.3389/fmars.2022.889840

A Decade of Time Series Sampling Reveals Thermal Variation and Shifts in *Pseudo-nitzschia* Species Composition That Contribute to Harmful Algal Blooms in an Eastern US Estuary

Katherine M. Roche[1], *Alexa R. Sterling*[2], *Tatiana A. Rynearson*[1], *Matthew J. Bertin*[3] *and Bethany D. Jenkins*[1,2]*

[1] Graduate School of Oceanography, University of Rhode Island, Narragansett, RI, United States, [2] Department of Cell and Molecular Biology, University of Rhode Island, Kingston, RI, United States, [3] Department of Biomedical and Pharmaceutical Sciences, College of Pharmacy, University of Rhode Island, Kingston, RI, United States

OPEN ACCESS

Edited by:
Margaret R. Mulholland, Old Dominion University, United States

Reviewed by:
Savvas Genitsaris, National and Kapodistrian University of Athens, Greece
Diana Sarno, Research Infrastructures for Marine Biological Resources Department Zoological Station Anton Dohrn, Italy

***Correspondence:**
Bethany D. Jenkins
bdjenkins@uri.edu

Specialty section:
This article was submitted to Aquatic Microbiology, a section of the journal Frontiers in Marine Science

Received: *04 March 2022*
Accepted: *03 June 2022*
Published: *22 July 2022*

Citation:
Roche KM, Sterling AR, Rynearson TA, Bertin MJ and Jenkins BD (2022) A Decade of Time Series Sampling Reveals Thermal Variation and Shifts in Pseudo-nitzschia Species Composition That Contribute to Harmful Algal Blooms in an Eastern US Estuary. Front. Mar. Sci. 9:889840. doi: 10.3389/fmars.2022.889840

In 2016-17, shellfish harvesting closed for the first time in Narragansett Bay, Rhode Island, USA, from domoic acid (DA), a neurotoxin produced by diatoms of the *Pseudo-nitzschia* genus. *Pseudo-nitzschia* have occurred frequently for over 60 years in Narragansett Bay's Long-Term Plankton Time Series (NBPTS), therefore it is surprising that the first closure only recently occurred. *Pseudo-nitzschia* species are known to vary in their toxin production, thus species identification is critical for understanding the underlying ecological causes of these harmful algal blooms (HABs). DNA in plankton biomass can be preserved for many years, so molecular barcoding of archived samples is useful for delineation of taxa over time. This study used amplification of the *Pseudo-nitzschia*-specific 18S-5.8S rDNA internal transcribed spacer region 1 (ITS1) in plankton samples and high throughput sequencing to characterize *Pseudo-nitzschia* species composition over a decade in Narragansett Bay, including eight years before the 2016-17 closures and two years following. This metabarcoding method can discriminate nearly all known *Pseudo-nitzschia* species. Several species recur as year-round residents in Narragansett Bay (*P. pungens* var. *pungens, P. americana, P. multiseries*, and *P. calliantha*). Various other species increased in frequency after 2015, and some appeared for the first time during the closure period. Notably, *P. australis*, a species prevalent in US West Coast HABs and known for high DA production, was not observed in Narragansett Bay until the 2017 closure but has been present in several years after the closures. Annual differences in *Pseudo-nitzschia* composition were correlated with physical and chemical conditions, predominantly water temperature. The long-term composition trends of *Pseudo-nitzschia* in Narragansett Bay serve as a baseline for identifying the introduction of new species, understanding shifting assemblages that contributed to the 2016-17 closures, and monitoring species that may be cause for future concern.

Keywords: *Pseudo-nitzschia*, DNA metabarcoding, Narragansett Bay, harmful algal blooms (HAB), long-term trends

INTRODUCTION

Pseudo-nitzschia, a cosmopolitan genus of diatom, causes harmful algal blooms (HABs) through the production of the neurotoxin domoic acid (DA), which bioaccumulates in primary and secondary consumers and causes the potentially fatal illness Amnesic Shellfish Poisoning in humans (Bates et al., 1989). *Pseudo-nitzschia* HABs are frequent on the US Gulf and Pacific coasts (Del Rio et al., 2010; McCabe et al., 2016), though the Northeast US had not experienced levels of DA high enough to prompt shellfish harvest closures until 2016, followed by additional closures in 2017 (Clark et al., 2019; Sterling et al., in press). This included Narragansett Bay, Rhode Island, where for the first time a closure in RI was triggered by DA in shellfish meat exceeding National Shellfish Sanitation Program limits (reviewed in Bates et al., 2018; NSSP, 2019; Sterling et al., in press). This recent emergence of blooms was unexpected, as the RI Department of Environmental Management (RI DEM) has monitored *Pseudo-nitzschia* HABs in Narragansett Bay since the 1990s without a closure incident (Pers. comm. David Borkman, RI DEM), and *Pseudo-nitzschia* have been recorded for over 60 years at the site of the Narragansett Bay Long-Term Plankton Time Series (NBPTS) (Smayda, 1959-1997; https://web.uri.edu/gso/research/plankton/, 1999-2022).

Only half of the known *Pseudo-nitzschia* species are confirmed toxin producers, which makes identification of species important for monitoring toxic events (reviewed in Bates et al., 2018). Additionally, many *Pseudo-nitzschia* species are morphologically cryptic under light microscopy (Amato & Montresor, 2008; Lundholm et al., 2012). High throughput sequencing techniques and genus-specific amplicon metabarcoding have made it possible to accurately and cost-effectively identify species at high taxonomic resolutions (Canesi & Rynearson, 2016; Lopes dos Santos et al., 2022). Furthermore, this method can be applied to previously archived biomass samples, including those of the NBPTS. Thus, amplicon sequencing is an effective way to analyze the role of species composition in the development of HABs over long periods of time (Lopes dos Santos et al., 2022). For example, a previous study that used *Pseudo-nitzschia*-specific metabarcoding to distinguish species in Narragansett Bay found that the high toxin-producing species *P. australis* likely contributed to the 2017 shellfish harvest closure and several *Pseudo-nitzschia* species more commonly observed at the NBPTS contributed to the precautionary closure in 2016 (Sterling et al., in press). From 2017 – 2019 in Narragansett Bay, low levels of plankton-associated DA were observed with fall and summer maxima, indicating that toxic species of *Pseudo-nitzschia* remained present in seasonally distinct species assemblages (Sterling et al., in press).

Similar to *Pseudo-nitzschia* HABs recently appearing in new locations like Narragansett Bay, they are also increasing in frequency and intensity in many regions of the ocean as climate change increases sea surface temperatures and impacts the phenology of biogeochemical cycling (reviewed in Wells et al., 2015; Bates et al., 2018; Testa et al., 2018). One example of this was in 2015 on the US West Coast, when a large bloom of *P. australis* led to record levels of DA, and an anomalously warm water mass was implicated in bloom formation (McCabe et al., 2016). Narragansett Bay has also been impacted by climate change, with surface water temperatures that increased by 0.23± 0.1°C per decade from 1984 – 2020 and more pronounced winter warming than other seasons (Fulweiler et al., 2015; Benoit and Fox-Kemper, 2021). Additionally, this location has experienced climate-driven nutrient cycle changes as well as a reduction in nutrient inputs due to recent management changes of sewage treatment (Oviatt et al., 2017). Examining whether the long-term patterns in *Pseudo-nitzschia* species composition correlate with these shifting environmental conditions is necessary for understanding the emergent DA events in Narragansett Bay and predicting future HABs.

In this study, we investigated the following questions: (1) Have particular species of *Pseudo-nitzschia* increased in prevalence during the closures and subsequent years? (2) Is *P. australis* a new species in Narragansett Bay? and (3) How have changing environmental conditions influenced *Pseudo-nitzschia* species composition? To address these questions, we examined more than a decade of archived phytoplankton biomass samples collected weekly since 2008 by the NBPTS for DNA analysis, with corresponding chemical and physical measurements. We used metabarcoding of the ITS1 region to identify nearly all known *Pseudo-nitzschia* species during the timeframe prior to closures (2008 - 2015), the years in which closures occurred (2016 and 2017), and the subsequent years (2018 - 2019). Characterizing these long-term patterns in species assemblages and environmental conditions provides a baseline for understanding the changes in closure years and following, informing how future *Pseudo-nitzschia* HABs will be monitored in Narragansett Bay.

METHODS

Phytoplankton Biomass and Field Sampling

Narragansett Bay, a temperate estuary on the northeast continental shelf of the United States, receives riverine freshwater inputs from the north and saline tidal flow from the Atlantic Ocean in the south (Raposa, 2009). Weekly surface water samples from December 2008 to November 2019 were collected at the NBPTS (**Figure 1**), a mid-bay site located in the West Passage (41° 34.2' N, 71° 23.4' W). In this study, two sample sets were combined to analyze over a decade of data: (1) December 2008 - August 2017 samples collected by the NBPTS and (2) September 2017 - November 2019 samples collected at the same location and processed by Sterling et al., in press. The data from Sterling et al., in press are publicly available online through the National Science Foundation Biological and Chemical Oceanography and Data Management Office (BCO-DMO; Jenkins & Bertin, 2021a; Jenkins & Bertin, 2021b). For a comparison of sample set metadata and methods, refer to **Table S2**.

Biomass from the seawater samples collected by the NBPTS was filtered onto 25 mm 0.22 μm pore size ExpressPlus filters (MilliporeSigma, Burlington, MA, USA) and stored at -80°C until DNA extraction. The volume filtered for biomass capture varied and was based on the observed Secchi depth to normalize

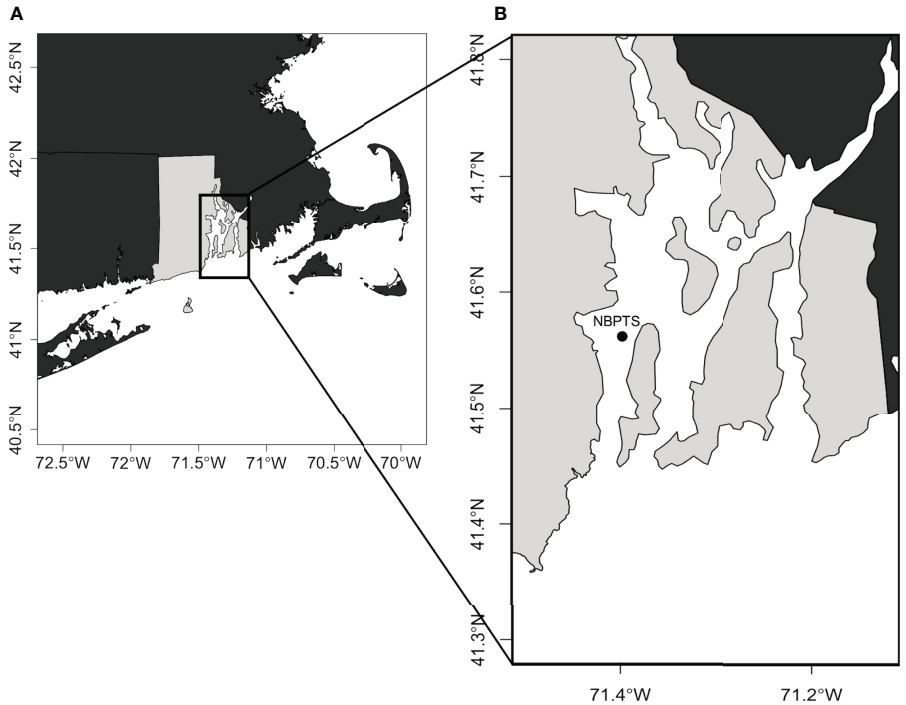

FIGURE 1 | Map of sampling location in Narragansett Bay, Rhode Island, USA. **(A)** Location of Narragansett Bay in Rhode Island (light grey) within the US northeast coast. **(B)** The Narragansett Bay Long Term Plankton Time Series (NBPTS) site is located mid-bay in the West Passage.

biomass collected, with 100 mL of seawater filtered per 1 m of Secchi depth. The volume filtered for NBPTS samples averaged 300 mL and ranged 100 – 600 mL. The Sterling et al., in press biomass samples were passed over 25 mm 5.0 µm pore size polyester membrane filters (Sterlitech, Kent, WA, USA), with an average of 240 mL and range of 75 – 430 mL filtered. Filters were then flash frozen in liquid nitrogen and stored at -80°C until DNA extraction. To ensure the comparability of sample sets using different pore sizes, we performed a comparison of species richness captured on each pore size that is outlined in the supplemental materials **Figure S1**. Sea surface temperature, sea surface salinity, chlorophyll *a* concentrations, *Pseudo-nitzschia* spp. cell counts, and nutrient measurements (nitrate, nitrite, phosphate) were obtained from the NBPTS prior to August 2017 and from the BCO-DMO dataset after September 2017 (NBPTS; Jenkins and Bertin, 2021a; Sterling et al., in press).

Sample Selection, DNA Extraction and Sequencing

DNA from 65 previously extracted NBPTS samples from December 2008 to April 2017 was used in this study (Canesi & Rynearson, 2016; Rynearson et al., 2020; Sterling et al., in press). An additional 76 NBPTS biomass samples from March 2009 to August 2017 were extracted. NBPTS samples with the highest corresponding *Pseudo-nitzschia* spp. cell counts under light microscopy for each month were selected. If all cell counts during a month were zero, samples were selected at random. The following frequency of samples was chosen when available: one sample per month from winter (December - February) and spring (March-May), and two samples per month from summer (June-August) and fall (September-November) due to the more frequent occurrence of high *Pseudo-nitzschia* abundance during these months (Sterling et al., in press). Additionally, 70 publicly available sequenced samples collected at the NBPTS site from September 2017 - November 2019 were used (Jenkins and Bertin, 2021b; Sterling et al., in press). Because only a partial time series exists for 2012, samples from that year were not analyzed as part of this study. In total, the dataset contained 211 samples from the NBPTS site during December 2008 - November 2019.

For all NBPTS samples, including those extracted prior to this study, DNA was extracted from biomass filters using a modified version of the DNeasy Blood & Tissue DNA extraction kit (Qiagen, Germantown, MD, USA) with the addition of 4 µL RNase, a 1 min bead beating step (0.1 mm and 0.5 mm Zirconia/Silica beads, BioSpec Products, Bartlesville, OK, USA), and elution into a total volume of 100 µL Buffer AE. DNA was amplified using a eukaryotic ITS1 forward primer 5' TCCGTAGGTGAACCTGCGG 3' (White et al., 1990) and 5.8S reverse primer 5' CATCCACCGCTGAAAGTTGTAA 3' (Sterling et al., in press), with MiSeq adapters added to the 5' ends of each primer for high throughput sequencing: 5' TCGTCGGCAGCGTCAGATGTGTATAAGAGACAG - forward primer; 5' GTCTCGTGGGCTCGGAGATGTGTATAAGAGAC AG - reverse primer. This reverse primer was designed by Sterling et al., in press using a curated database of *Pseudo-nitzschia* sequences representing 41 species, thus the primer

set can discriminate nearly all known *Pseudo-nitzschia* species with high specificity, though it is also expected to amplify some other diatom and dinoflagellate genera. The ITS region (both ITS1 and ITS2) have been used to distinguish *Pseudo-nitzschia* species in several studies (Lundholm et al., 2003; Amato et al., 2007; Casteleyn et al., 2008; Kaczmarska et al., 2008). The ITS1 region alone has been demonstrated as an effective marker to distinguish intra- and interspecific variation of *Pseudo-nitzschia* species (Hubbard et al., 2008; Hubbard et al., 2014). In *Pseudo-nitzschia*, the ITS1 locus is naturally variable in length, so the expected PCR product length ranged from 235 to 370 base pairs (White et al., 1990; Sterling et al., in press).

For PCR amplification, the following reagents were used in 25 µL reactions: Phusion Hot Start High-Fidelity Master Mix (Thermo Fisher Scientific Inc., Waltham, MA, USA), HPLC-purified forward and reverse primers at 0.5 µM concentration (Integrated DNA Technologies, Coralville, IA, USA), and 2 µL of DNA template. A stepwise thermocycle protocol was used to amplify samples: 30 s denaturation at 98°C, 15 cycles of 98°C (10 s), 64.1°C (30 s), 72°C (30 s), 15 cycles of 98°C (10 s), 72°C (30 s), 72°C (30 s), and 10 min final extension at 72°C (Sterling et al., in press). Positive and negative sequencing controls were used as reported in Sterling et al., in press. PCR products were submitted to the RI Genomics and Sequencing Center (Kingston, RI, USA) for sequencing library preparation and high throughput sequencing. There, ITS1 PCR products were cleaned with KAPA pure beads (KAPA Biosystems, Woburn, MA, USA), sequencing indices and adapters were attached using PCR (50 ng template DNA, 8 cycles) and the Illumina Nextera XT Index Kit (Illumina, San Diego, CA, USA) with Phusion High Fidelity Master Mix (Thermo Fisher Scientific Inc., Waltham, MA, USA), and PCR products were cleaned again with KAPA pure beads before being visualized by agarose gel electrophoresis. Selected samples were run on a Bioanalyzer DNA1000 chip (Agilent, Santa Clara, CA, USA). All samples were quantified using a Qubit fluorometer (Invitrogen, Carlsbad, CA, USA) prior to pooling, and the final pooled library was quantified with qPCR in a LightCycler480 (Roche, Pleasanton, CA, USA) with the KAPA Biosystems Illumina Kit (KAPA Biosystems, Woburn, MA, USA). Samples were analyzed using v3 chemistry, 600 cycles, and 2x250 bp paired-end sequencing on an Illumina MiSeq (Illumina, Inc., San Diego, CA, USA). These sequencing methods were exactly the same as those in Sterling et al., in press.

Sequence Processing and Taxonomic Assignment

Illumina Miseq adapters and primers were trimmed using Cutadapt (v3.2; Martin, 2011) and sequences were quality checked before and after trimming using MultiQC (v1.9; Ewels et al., 2016). Amplicon sequence variants (ASVs) were delineated in DADA2 in R (v1.18.0; Callahan et al., 2016). One sample contained no reads following analysis with DADA2 and was removed. All ASVs, including those sequenced for this study and those from Sterling et al., in press, were assigned taxonomy using the scikit-learn naïve Bayes machine learning classifier in QIIME2 with the default confidence threshold of 0.7 (v2021.4.0; Bolyen et al., 2019). For taxonomic assignment, the curated reference database used in Sterling et al., in press was updated with an additional 170 unique *Pseudo-nitzschia* National Center for Biotechnology Information (NCBI) GenBank sequences, for a total of 302 sequences representing 51 species (retrieved June 1, 2021) (**Table S1**). To maximize the number of ASVs classified to the species level, additional ASVs were assigned by manual inspection of a megablast search that reported the top hit of each ASV from the BLAST nt database (retrieved June 24, 2021). Additional ASVs classified using the megablast search required >98% identity and >98% query cover to an NCBI *Pseudo-nitzschia* species, otherwise classifications were discarded. From this additional classification, we recovered only species already represented in our custom database from the pool of ASVs. All ASVs of the same species were agglomerated in R for downstream analyses.

Analysis of Species Composition and Environmental Conditions

Data were analyzed and visualized in R (v4.0.2; R Core Team, 2017) within RStudio (v1.3.1056; RStudio Team, 2020) using the following packages: phyloseq (v1.34.0; McMurdie & Holmes, 2013) for ASV dataset manipulation and transformations; ggplot2 (v3.3.3; Wickham, 2016) for scatterplot, heatmap, bar plot, and sample frequency plots; vegan (v2.5.7; Dixon, 2003) for dispersion tests and ANOSIM; indicspecies (v1.7.9; De Cáceres & Legendre, 2009) for indicator species analysis; raster (v3.5.15; Hijmans et al., 2015) for the sampling site map; and viridis (v0.6.2; Garnier et al., 2021) for colorblind-friendly figure color palettes. Relative abundances were calculated as the proportion of a species out of the total *Pseudo-nitzschia* sequencing reads for each sample, and these were only used in one visualization (**Figure 3**). Presence-absence Jaccard distances of composition data generated in phyloseq were used in all statistical analyses to avoid distorted relative abundance metrics that may arise from eukaryotic gene copy number variation (reviewed in Canesi & Rynearson, 2016; Gloor et al., 2017). This is a better approach for metabarcoding data than using relative or absolute abundance of sequencing reads (Zaiko et al., 2015; Canesi & Rynearson, 2016; Rynearson et al., 2020).

Similarities between temporal groupings of species composition were characterized using an analysis of similarity (ANOSIM) on a Jaccard distance matrix. An assumption of ANOSIM is relatively equal variances, or lack of dispersion, between groups being compared. Prior to ANOSIM, dispersion of groups was determined using betadisper() and permutest() (R: vegan) with 999 permutations and a significance level of 0.05. Only groups that did not have significant dispersion were used in ANOSIM, which included year and timeframe, the latter defined as two time periods: before closures (2009 - 2015) and during/after closure years (2016 - 2019). The groupings of samples by both month and season exhibited significant dispersion of groups and thus did not meet the assumptions to test for similarity in ANOSIM (p=0.023; p=0.014). ANOSIM was performed using anosim() (R: vegan) with 999 permutations and a significance level of 0.05. To determine which species preferentially

occurred before and during/after closures, an indicator species analysis (ISA) was performed on a Jaccard distance matrix using multipatt() (R: indicspecies), 9999 permutations, and a significance level of 0.05 on p-values adjusted for multiple testing.

A Best Subset of Environmental Variables (BIOENV) multivariate analysis was performed using bioenv() (R: vegan) to correlate environmental conditions with species composition. Environmental variables, including sea surface temperature, sea surface salinity, dissolved inorganic nitrogen (DIN), dissolved inorganic phosphorus (DIP), and chlorophyll *a* concentration were standardized using log-transformation prior to comparison with a Jaccard distance matrix. The BIOENV analysis was performed for all samples with complete physical and chemical data (n=178), as well as for each timeframe (before: n=81, during/after: n=97).

RESULTS

Sequencing and Taxonomic Assignment

Within the 141 samples from December 2008 – August 2017 that were sequenced for this study, there were a total of 12.3 x 10^6 read pairs. Initial reads per sample ranged from 4,821 to 115,087, with an average of 70,104 reads per sample. After DADA2 sequencing error inference, there was an average of 39,673 reads per sample, with a range of 1,335 to 66,903 reads. This is comparable to the average of 35,550 reads per sample reported in the Sterling et al., in press dataset. In total, 5,117 ASVs were recovered in the newly sequenced samples. Taxonomic assignment yielded 57 ASVs at the *Pseudo-nitzschia* species level (46 QIIME2, 11 megablast). When re-classifying the ASVs from Sterling et al., in press with the updated database, 27 ASVs were assigned to the species level (20 QIIME2, 7 megablast). The number of ASVs per sample ranged from 1 to 15 and an average of 5,773 sequencing reads per sample were assigned to *Pseudo-nitzschia* spp. Each species was represented by a minimum of 2 and maximum of 17 ASVs, and after aggregating ASVs by species, 17 *Pseudo-nitzschia* species were characterized in the samples.

Pseudo-nitzschia Species Composition During Periods of High Cell Abundance

During the study period, December 2008 – November 2019, *Pseudo-nitzschia* species were observed by light microscopy each year, excluding the gap in 2012 (**Figure 2**). Cell counts at the genus level surpassed the RI DEM HAB abundance threshold of 20,000 cells per liter each year for which there was abundance data except 2015 (**Figure 2**) (RI DEM, 2021). Specifically, weekly samples surpassed the cell abundance threshold 69 times across all seasons, though more frequently during spring (n=20) and summer (n=33) months (**Figure 2**). The closure years in 2016 and 2017 alone comprised 38% of these high cell abundance samples: 2016 (n=11) and 2017 (n=17). A subset of our total sequenced samples (n=55) have corresponding cells counts that surpassed the RI DEM HAB threshold and were used to analyze *Pseudo-nitzschia* species composition during high abundance periods. *P. pungens* var. *pungens* occurred most frequently on dates of high cell counts, followed by *P. multiseries* and *P. americana* (**Figure 3**). Only one sample contained just one species (*P. pungens* var. *pungens*; Aug 07, 2017), while all other samples contained between 2 and 7 species (**Figure 3**).

Long-Term Patterns of *Pseudo-nitzschia* Species Composition

The 17 species of *Pseudo-nitzschia* identified in the total dataset exhibited varying annual patterns of occurrence (**Figure 4**). Four species were observed most frequently in over 40% of samples - P. *pungens* var. *pungens* (66%), *P. americana* (66%), *P. multiseries* (55%), and *P. calliantha* (44%) - and were found in samples from each year of the dataset (**Figure 4A**). Several species appeared for the first time or increased in prevalence during closure and subsequent years. Most notably, *P. australis*, a well characterized toxin producer, was not present in any of the sequenced samples prior to 2017 and appeared for the first time on February 6, 2017, several weeks before the closure (**Figure 4B**). But from 2017 – 2019, *P. australis* continued to be observed, appearing in 23% of sequenced samples. Similarly, the toxin-capable species

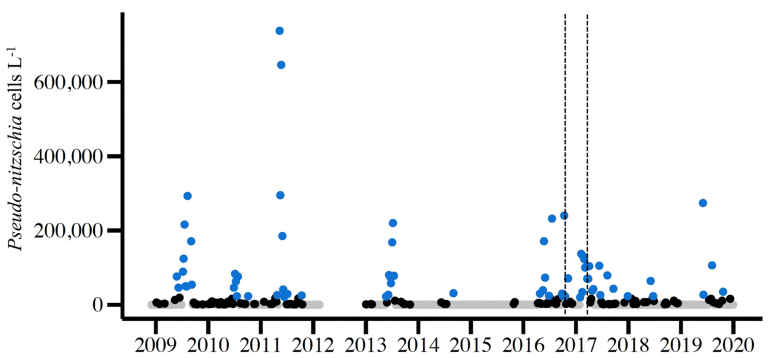

FIGURE 2 | Abundance of live *Pseudo-nitzschia* spp. cells from light microscopy counts of weekly NBPTS surface seawater samples spanning Dec 2008 – Dec 2019 (n=523). The NBPTS paused during Mar 2012 – Dec 2012, so no cell counts were collected. Blue points represent *Pseudo-nitzschia* abundance that surpassed the RI Department of Environmental Management (DEM) HAB abundance threshold of 20,000 cells per liter, while black points are non-zero abundances below the threshold and gray points are zero counts. Dotted lines denote the 2016 precautionary shellfish closure (Oct 7–30) and 2017 closure (Mar 1–24).

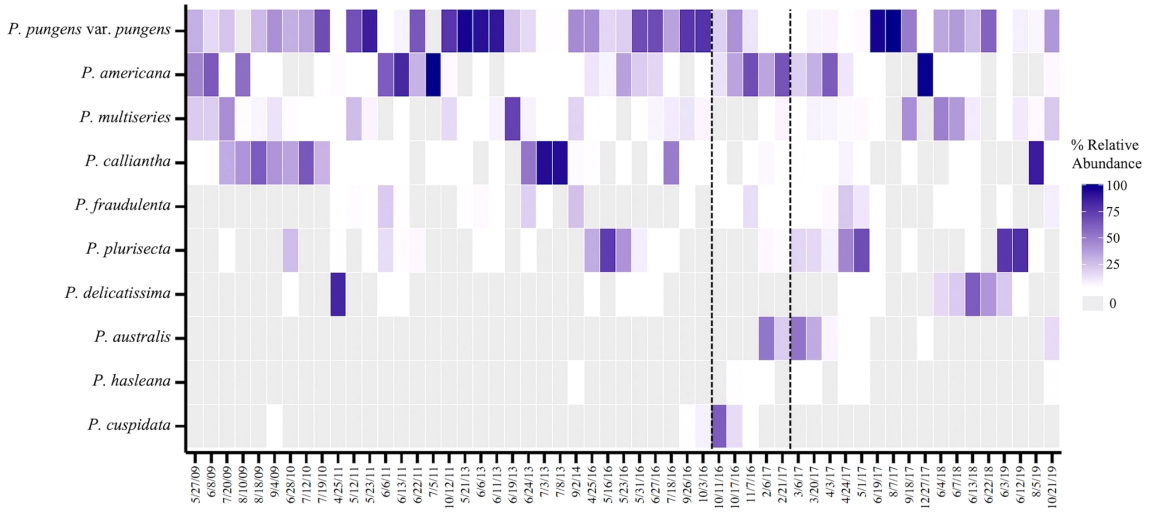

FIGURE 3 | Relative abundance of the top ten species in samples that surpass the RI DEM threshold of 20,000 cells L^{-1} from Dec 2008 - Nov 2019 (n=55). Dotted lines denote the 2016 precautionary shellfish closure and 2017 closure. Gray boxes represent species that were absent in samples.

P. hasleana and *P. subpacifica* appeared relatively infrequently in the years prior to the shellfish closures, however, each became more prevalent in frequency and were found in nearly each year from 2015-2019 (**Figure 4B**). Two additional toxin-capable species *P. fraudulenta* and *P. plurisecta* were present in low proportions of samples (0 - 32%) in the years prior to closures, but both were observed in higher proportions of samples (25 - 74%) from 2016-2019 (**Figure 4B**). Several rare *Pseudo-nitzschia* species that occurred in less than 10% of samples from the entire dataset were more prevalent during the closure years than any other timeframe, including *P. hasleana* in 2016 and 2017 and *P. cuspidata* in 2016 (**Figure 4B**).

To determine if species assemblages differed temporally, ANOSIM was used on the Jaccard distance matrix of *Pseudo-nitzschia* species composition. Two groupings were determined to be viable for ANOSIM based on dispersion of group tests (n=199): year (p=0.286), and timeframe (p=0.658), the latter of which was defined as before closures (2009 - 2015) and during/after closures

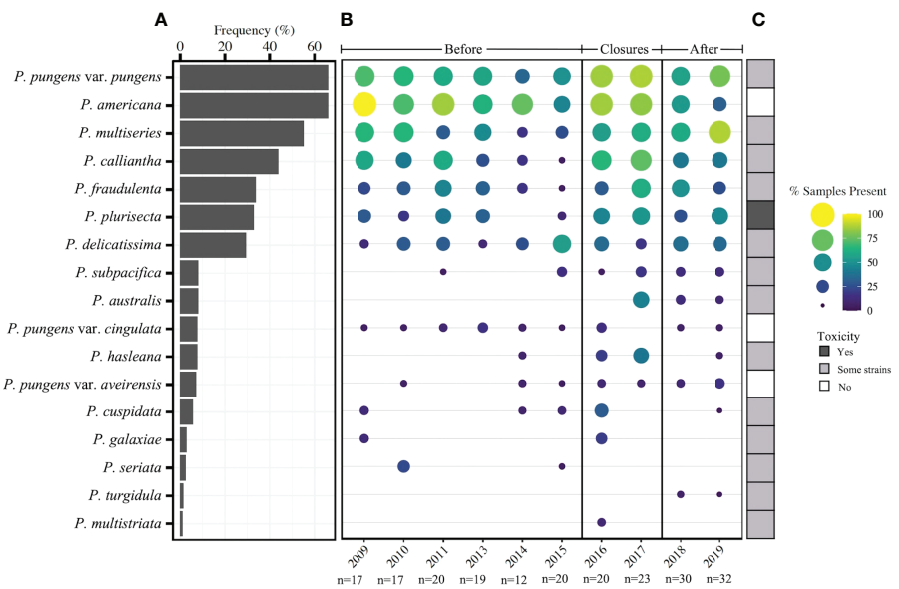

FIGURE 4 | (A) Frequency of occurrence of 17 species of *Pseudo-nitzschia* from 2008 – 2019 (n=214). **(B)** Presence of *Pseudo-nitzschia* species by year for three timeframes: prior to closures, during closure years, and following closures. The size and color of each circle represents the percent of samples in a given year in which *Pseudo-nitzschia* species occurred based on a presence/absence matrix. **(C)** Observed toxicity of each species as reviewed in Bates et al., 2018, with "some strains" meaning that some have been reported to produce toxin while others have not.

(2016 - 2019). ANOSIM revealed significant differences between species assemblages in each temporal grouping (p=0.001, ANOSIM statistic 0.1082 and 0.0625 respectively) (**Figure S2**). On average, species richness by year increased over time (**Figure S3**). An ISA was also performed on a Jaccard matrix to determine which species preferentially occurred in the timeframes before and during/after closures, since the species assemblages between these two timeframes were significantly different (ANOSIM, **Figure S2**). This analysis revealed that the strongest indicator species of the timeframe prior to closures were *P. americana* (p=0.003) and *P. seriata* (p=0.025). Eight species were significant indicators of the timeframe during and after closures, including *P. australis* (p=0.0001), *P. hasleana* (p=0.0002), *P. multiseries* (p=0.0027), *P. plurisecta* (p=0.017), *P. pungens* var. *aveirensis* (p=0.031), *P. pungens* var. *pungens* (p=0.033), *P. subpacifica* (p=0.045), and *P. calliantha* (p=0.046). All other species included in the analysis did not preferentially occur in either of these two timeframes.

Environmental Correlates of Species Composition

A multivariate correlation analysis (BIOENV) showed that *Pseudo-nitzschia* species composition correlated with various environmental conditions. The parameters that best correlated with species composition (0.1545) were surface temperature and DIP (**Table 1**). When the same multivariate correlation analysis was performed on each timeframe (before and during/after closures), the highest correlates prior to closures were temperature and DIP (0.678), while the during/after closure timeframe was most correlated with temperature, DIP, and DIN (0.2725) (**Table 1**).

Pseudo-nitzschia species were found at a wide variety of temperatures in Narragansett Bay (**Figure 5**). During the study period, temperatures ranged from -1.31 – 26.47°C, and *Pseudo-nitzschia* were present in sequenced samples through nearly this entire range, from -1.31 – 25.51°C. The seven most frequently observed species- *P. pungens* var. *pungens, P. americana, P. multiseries, P. calliantha, P. fraudulenta, P. plurisecta*, and *P. delicatissima*- were present over wide temperature ranges that did not differ greatly in the before closure (2008 - 2015) timeframe and during/after closure (2016 - 2019) timeframe. Several less prevalent species had smaller and more distinct temperature ranges. *P. subpacifica* (7.6 – 23.3°C), *P. pungens* var. *cingulata* (4.48 – 22.18°C), *P. pungens* var. *aveirensis* (15.4 – 22.18°C), and *P. cuspidata* (9.97 – 22.4°C) were observed during relatively higher temperatures, while *P. australis* (1.6 – 15.4°C) and *P. hasleana* (2.24 – 22.18°C) tended to occur at relatively lower temperatures (**Figure 5**).

DISCUSSION

Multiple Species Responsible for High Cell Abundance Blooms

Multiple species were present during *Pseudo-nitzschia* blooms in Narragansett Bay, defined here as periods where *Pseudo-nitzschia* cells surpass the RI DEM cell abundance threshold of 20,000 cells per liter (**Figure 2**) (RI DEM, 2021). Exceeding this threshold prompts DA Scotia testing of phytoplankton tow net samples followed by DA screening of shellfish meat, which can trigger shellfish harvest closures (RI DEM, 2021). More weekly light microscopy samples surpassed the cell abundance threshold in 2016 and 2017 than any other year of the study period (**Figure 2**). From 2016 - 2017, *P. pungens* var. *pungens. P. fraudulenta*, and *P. americana* were present in each of the bloom samples, with the first appearance of *P. australis* occurring in 2017 (**Figure 3**). Though *P. calliantha* was the fourth-most prevalent species across the entire study period, it occurred in less than half of the bloom samples (**Figures 3**, **4A**). Most samples that surpassed the abundance threshold contained diverse multi-species assemblages containing as many as seven of the top ten most abundant *Pseudo-nitzschia* species, with the exception of one bloom sample in which just *P. pungens* var. *pungens* occurred (**Figure 3**).

Resident and Indicator Species of Narragansett Bay

From 2008 – 2019, 17 species of *Pseudo-nitzschia* were detected in Narragansett Bay (**Figure 4**). All species were previously observed except *P. seriata*, which was recorded annually from 2012 to 2016 in the nearby Gulf of Maine and has only ever been observed in the North Atlantic (Hasle, 2002; Clark et al., 2019; Sterling et al., in press). Some patterns in species composition differ in the years prior to shellfish harvest closures, while others remain consistent. The four resident species (*P. pungens* var. *pungens, P. americana, P. multiseries*, and *P. calliantha*) that occurred in each year of the dataset followed similar patterns of prevalence before, during, and after the closure periods (**Figure 4**). Furthermore, these resident species occurred across the widest ranges of temperatures and were present through nearly the entire temperature range of Narragansett Bay (**Figure 5**). This prevalence across temperature ranges indicates a plasticity of these species to a range of environmental conditions. Consistent with our observations, *P. pungens* var. *pungens* and *P. multiseries* have been previously characterized as cosmopolitan, occurring in both equatorial and cold-water regions (Hasle,

TABLE 1 | BIOENV results of the three models with the highest Spearman rank correlation coefficient (ρ) for three timeframes: 2008 – 2019; 2008 – 2015; 2016 – 2019.

Entire dataset (n=178) 2008 – 2019		Before closures (n=81) 2008 – 2015		During/after closures (n=97) 2016 – 2019	
Parameters	ρ	Parameters	ρ	Parameters	ρ
Temp + DIP	0.1545	Temp + DIP	0.0678	Temp + DIP + DIN	0.2725
Temp + DIP + DIN	0.1474	Temp + DIP + Chla	0.0410	Temp + DIP	0.2695
Temp + DIP + DIN + Chla	0.1337	Temp + DIP + DIN + Chla	0.0255	Temp	0.2397

The environmental variables that appear in the strongest models are sea surface temperature (Temp), dissolved inorganic phosphorus (DIP), dissolved inorganic nitrogen (DIN), and chlorophyll a of the phytoplankton community (Chla).

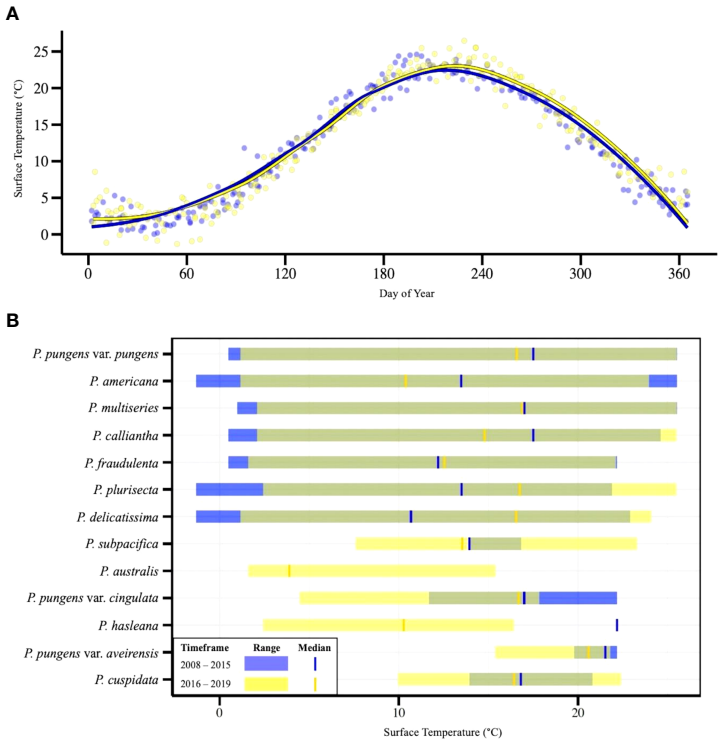

FIGURE 5 | (A) Sea surface temperature at the NBPTS site over an annual cycle with two loess smoother lines representing the timeframes before (2008-2015; blue) and during/after closures (2016-2019; yellow). **(B)** Thermal ranges of *Pseudo-nitzschia* species that were found in >5% of samples. Ranges are based on sea surface temperature of presence/absence occurrence during two timeframes. Samples from 2008-2015 are shown in blue; 2016-2019 are shown in yellow. Temperatures for which the temporal thermal ranges overlap appear in green. The median temperature at which species are observed prior to 2015 are represented by vertical blue bars and after 2016 by vertical yellow bars.

2002). Additionally, *P. americana* has been observed in a wide range of environments, including the Gulf of Maine, Malaysia, Mexico, and Namibia (reviewed in Bates et al., 2018). *P. calliantha*, is also a confirmed cosmopolite with occurrences in warm and cold environments (Stonik et al., 2011).

Species assemblages varied significantly between years and timeframes (before and during/after closures) (**Figure S2**). Though prior work in Narragansett Bay observed distinct species assemblages by season (Sterling et al., in press), the seasonal groupings in this dataset were unable to be tested for similarity because the monthly and seasonal groups displayed significant dispersion. Additionally, distinct species groupings by year and timeframe suggest that composition patterns have shifted over time in Narragansett Bay. The indicator species from each of these timeframes explains some of the temporal shifts. Before the closure periods, *P. americana*, which is a non-toxigenic year-round resident of Narragansett Bay, was the strongest indicator species. This timeframe was characterized by lower species richness and lower prevalence of toxigenic species (**Figure 4**; **Figure S3**). *P. multiseries* and *P. plurisecta* were two of the strongest indicator species for the during closure/after timeframe, and both toxigenic species increased in prevalence 2014 – 2019 (**Figure 4B**). Several other important indicator species of the during closure/after timeframe were *P. hasleana, P. subpacifica*, and *P. pungens* var. *aveirensis*, all of which were present in very few samples prior to closures but persisted in nearly each year of the closures and following (**Figure 4B**).

Temperature was the only consistent environmental driver that appeared in each of the top three multivariate models for the entire species composition dataset, the timeframe prior to closures, and the timeframe encompassing closures and subsequent years (**Table 1**). This is supported by previous work in Narragansett Bay that showed temperature also correlated with both *Thalassiosira* spp. and *Skeletonema* spp. assemblage composition from 2008 - 2014 (Canesi & Rynearson, 2016; Rynearson et al., 2020). The importance of sea surface temperature to phytoplankton community composition may be partially attributed to the wide range of temperatures that Narragansett Bay experiences throughout the year (**Figure 5**). As sea surface temperatures in Narragansett Bay continue to increase over time due to climate change (Fulweiler et al., 2015; Benoit & Fox-Kemper, 2021), this driver of *Pseudo-nitzschia* assemblage composition may lead to further shifts in the prevalence of certain species. This could include continued increases in the frequency of *P. australis, P. hasleana, P. galaxiae*, and *P. subpacifica*, all of which became more prevalent in Narragansett Bay in closure and subsequent years.

Additionally, availability of nutrients, including both DIP and DIN, impacted *Pseudo-nitzschia* species composition. DIP was a driver of species composition in all but one of the top multivariate models (**Table 1**). Phosphorus is a required

macronutrient for phytoplankton growth, though its relationship to *Pseudo-nitzschia* HAB formation is complex because high DIP increases *Pseudo-nitzschia* growth rate but low DIP correlates with increased DA toxin production (Pan et al., 1998; Sun et al., 2011; Brunson et al., 2018). Furthermore, DIN appears in the multivariate model with the highest correlation in the during closures/after timeframe (**Table 1**). The importance of DIN concentration to both *Pseudo-nitzschia* assemblage composition and toxin production in Narragansett Bay is supported by Sterling et al., in press, who found that nitrate and DIN : DIP correlated with species composition and low DIN correlated with elevated particulate DA. The recently reduced DIN in Narragansett Bay following wastewater treatment changes may play a role in impacting the composition and physiology of these *Pseudo-nitzschia* assemblages (Oviatt et al., 2017).

P. australis Introduction and Persistence in Narragansett Bay

P. australis was not observed in Narragansett Bay prior to 2017 (**Figure 4**) and was the strongest indicator species in the during closure/after timeframe as compared to samples prior to the 2016 – 2017 HABs. It appears to be recently introduced to the North Atlantic coasts of the US and Canada during the record HABs of 2016 (Clark et al., 2019, reviewed in Bates et al., 2018). Notably, it was absent during the RI precautionary closure of 2016 in which DA below the NSSP threshold was observed in shellfish meat (**Figure 3**; reviewed in Bates et al., 2018; Sterling et al., in press), meaning there were other species responsible for this event. Toxigenic species present during the 2016 closure included *P. pungen* var. *pungens* and *P. cuspidata*. *P. australis* continued to persist in Narragansett Bay in about one-fifth of the samples from 2017 – 2019, suggesting it remained in the region and may be a cause for concern in future toxic events. However, it was not the only toxic species in Narragansett Bay during the 2016 – 2017 closures, so continued monitoring of *Pseudo-nitzschia* at the species level is important for understanding which species contribute to producing closure levels of DA.

P. australis has been connected to a large 2015 HAB event on the US west coast where increases in both *Pseudo-nitzschia* abundance and DA were attributed to anomalously warm water temperatures and nutrient-rich upwelling (McCabe et al., 2016). Sea surface temperatures in the North Pacific were 2.5°C higher than long term means, ranging about 12 – 18°C during the closure period from May – November 2015 (McCabe et al., 2016). Increased DA production in West Coast *P. australis* strains was also associated with warmer temperatures (Zhu et al., 2017). In contrast to this, we found that *P. australis* occurred at a lower relative thermal range than any other species and was only observed in Narragansett Bay between 1.6 – 15.4°C, with a median temperature of 3.9°C. During the closure in February – March of 2017, the temperatures at which *P. australis* was observed ranged 2.44 – 3.26°C, so this particular toxic event was not initiated by a warm water mass. Increased toxin concentration in shellfish meat has been linked to higher growth potential of *P. australis* (McCabe et al., 2016). Clark et al. (2021) reports that the optimal growth temperature for a strain of *P. australis* isolated from the nearby Gulf of Maine was about 15°C, while studies with US West Coast isolates have found optimal growth temperatures of 17 – 18°C (Monterey Bay, California 2015 isolate; McCabe et al., 2016) and 23 – 26°C (Southern California isolate; Zhu et al., 2017). The presence of *P. australis* at much lower temperatures in Narragansett Bay suggests there may be other factors influencing its growth and toxin production, such as nutrient availability, bacterial associations, or zooplankton grazing (Maldonado et al., 2002; reviewed in Lelong et al, 2012; Lundholm et al., 2018).

CONCLUSION

In this study, we used a DNA metabarcoding approach on more than a decade of plankton samples from Narragansett Bay, RI to characterize *Pseudo-nitzschia* species diversity before, during, and after two shellfish harvest closures. We found that periods of high *Pseudo-nitzschia* cell abundances correspond to a wide diversity of species present, supporting the complexity of bloom-forming assemblages. We characterized several species as residents of Narragansett Bay, which occurred in samples in nearly each year of the study period. *P. australis*, a high toxin producing species, was not present in any of the samples until 2017, and thus is likely to be a newly introduced species. Additionally, species composition was most strongly influenced by water temperature. As water temperatures continue to rise in Narragansett Bay and toxigenic species become more prevalent, it is imperative to continue monitoring *Pseudo-nitzschia* species composition for increased frequency and potential introduction of toxigenic species.

DATA AVAILABILITY STATEMENT

The datasets presented in this study can be found in online repositories. The names of the repository/repositories and accession number(s) can be found below:
https://www.ncbi.nlm.nih.gov/genbank/, OM672116 - OM672173.
https://www.ncbi.nlm.nih.gov/, SAMN25894732 - SAMN25894875.

AUTHOR CONTRIBUTIONS

Conception and design, KR, BJ. Sample collection, TR. Methodology, KR, AS, TR. Formal analysis, KR. Investigation, KR. Resources, BJ. Data curation, KR. Writing—original draft preparation, KR, BJ. Writing—review and editing, all authors. Visualization, KR. Supervision, BJ. Project administration, BJ, TR. Funding acquisition, BJ, MB, TR. All authors contributed to the article and approved the submitted version.

FUNDING

This research was supported by the following awards: MJ and BJ (NA18OAR4170094), TR (NSF1638834), and NSF RI C-AIM EPSCoR Cooperative Agreement (OIA-1655221, OIA-1004057). Sequencing was performed at the Rhode Island RI

NSF EPSCoR research facility, the Genomics and Sequencing Center (OIA-1655221). The Narragansett Bay Long-Term Plankton Time Series is supported by the University of Rhode Island and the Rhode Island Department of Environmental Management.

ACKNOWLEDGMENTS

We acknowledge the Plankton Assistants for collecting NBPTS samples and enumerating cell abundances. We thank Z. Pimentel for help with taxonomic assignment, D. Fontaine for helpful suggestions regarding data analysis, and E. Borbee for help with map design. Thank you to G. Armin, S. Song, and V. Sonnet for helpful discussions on clarity of writing.

SUPPLEMENTARY MATERIAL

The Supplementary Material for this article can be found online at: https://www.frontiersin.org/articles/10.3389/fmars.2022.889840/full#supplementary-material

REFERENCES

Amato, A., Kooistra, W. H. C. F., Levialdi Ghiron, J. H., Mann, D. G., Pröschold, T. and Montresor, M. (2007). Reproductive Isolation Among Sympatric Cryptic Species in Marine Diatoms. *Protist.* 158, 193–207. doi: 10.1016/j.protis.2006.10.001

Amato, A. and Montresor, M. (2008). Morphology, Phylogeny, and Sexual Cycle of *Pseudo-Nitzschia Mannii* Sp. Nov. (Bacillariophyceae): A Pseudo-Cryptic Species Within the *P. Pseudodelicatissima* Complex. *Phycologia.* 47 (5), 487–497. doi: 10.2216/07-92.1

Bates, S. S., Bird, C. J., de Freitas, A. S. W., Foxall, R., Gilgan, M., Hanic, L. A., et al. (1989). Pennate Diatom *Nitzschia Pungens* as the Primary Source of Domoic Acid, a Toxin in Shellfish From Eastern Prince Edward Island, Canada. *Can. J. Fisheries. Aquat. Sci.* 46 (7), 1203–1215. doi: 10.1139/f89-156

Bates, S. S., Hubbard, K. A., Lundholm, N., Montresor, M. and Leaw, C. P. (2018). *Pseudo-Nitzschia, Nitzschia*, and Domoic Acid: New Research Since 2011. *Harmful. Algae.* 79, 3–43. doi: 10.1016/j.hal.2018.06.001

Benoit, J. and Fox-Kemper, B. (2021). Contextualizing Thermal Effluent Impacts in Narragansett Bay Using Landsat-Derived Surface Temperature. *Front. Mar. Sci.* 8, 1247. doi: 10.3389/fmars.2021.705204

Bolyen, E., Rideout, J. R., Dillon, M. R., Bokulich, N. A., Abnet, C. C., Al-Ghalith, G. A., et al. (2019). Reproducible, Interactive, Scalable and Extensible Microbiome Data Science Using QIIME 2. *Nat. Biotechnol.* 37 (8), 852–857. doi: 10.1038/s41587-019-0209-9

Brunson, J. K., McKinnie, S. M., Chekan, J. R., McCrow, J. P., Miles, Z. D., Bertrand, E. M., et al. (2018). Biosynthesis of the Neurotoxin Domoic Acid in a Bloom-Forming Diatom. *Science.* 361 (6409), 1356–1358. doi: 10.1126/science.aau0382

Callahan, B. J., McMurdie, P. J., Rosen, M. J., Han, A. W., Johnson, A. J. A. and Holmes, S. P. (2016). DADA2: High-Resolution Sample Inference From Illumina Amplicon Data. *Nat. Methods* 13 (7), 581–583. doi: 10.1038/nmeth.3869

Canesi, K. L. and Rynearson, T. A. (2016). Temporal Variation of *Skeletonema* Community Composition From a Long-Term Time Series in Narragansett Bay Identified Using High-Throughput DNA Sequencing. *Mar. Ecol. Prog. Ser.* 556, 1–16. doi: 10.3354/meps11843

Casteleyn, G., Chepurnov, V. A. and Leliaert, F.others (2008). *Pseudo-Nitzschia Pungens* (Bacillariophyceae): A Cosmopolitan Diatom Species? *Harmful. Algae.* 7, 241–257. doi: 10.1016/j.hal.2007.08.004

Clark, S., Hubbard, K. A., Anderson, D. M., McGillicuddy, D. J., Jr., Ralston, D. K. and Townsend, D. W. (2019). *Pseudo-Nitzschia* Bloom Dynamics in the Gulf of Maine: 2012-2016. *Harmful. Algae.* 88, 101656. doi: 10.1016/j.hal.2019.101656

Clark, S., Hubbard, K. A., McGillicuddy, D. J., Ralston, D. K. and Shankar, S. (2021). Investigating *Pseudo-Nitzschia Australis* Introduction to the Gulf of Maine With Observations and Models. *Continental. Shelf. Res.* 228, 104493. doi: 10.1016/j.csr.2021.104493

De Cáceres, M. and Legendre, P. (2009). Associations Between Species and Groups of Sites: Indices and Statistical Inference. *Ecology* 90, 3566–3574. doi: 10.1890/08-1823.1

Del Rio, R., Bargu, S., Baltz, D., Fire, S., Peterson, G. and Wang, Z. (2010). Gulf Menhaden (*Brevoortia Patronus*): A Potential Vector of Domoic Acid in Coastal Louisiana Food Webs. *Harmful. Algae.* 10 (1), 19–29. doi: 10.1016/j.hal.2010.05.006

Dixon, P. (2003). VEGAN, a Package of R Functions for Community Ecology. *J. Veg. Sci.* 14 (6), 927-930 doi: 10.1111/j.1654-1103.2003.tb02228.x

Ewels, P., Magnusson, M., Lundin, S. and Käller, M. (2016). MultiQC: Summarize Analysis Results for Multiple Tools and Samples in a Single Report. *Bioinformatics* 32 (19), 3047–3048. doi: 10.1093/bioinformatics/btw354

Fulweiler, R. W., Oczkowski, A. J., Miller, K. M., Oviatt, C. A. and Pilson, M. E. Q. (2015). Whole Truths vs. Half Truths – And a Search for Clarity in Long-Term Water Temperature Records. *Estuarine. Coast. Shelf. Sci.* 157, A1–A6. doi: 10.1016/j.ecss.2015.01.021

Garnier, S., Ross, N., Rudis, R., Camargo, P. A., Sciaini, M. and Scherer, C. (2021). *Viridis—Colorblind-Friendly Color Maps for R. R Package Version 0.6, 2.*

Gloor, G. B., Macklaim, J. M., Pawlowsky-Glahn, V. and Egozcue, J. J. (2017). Microbiome Datasets Are Compositional: And This Is Not Optional. *Front. Microbiol.* 8. doi: 10.3389/fmicb.2017.02224

Hasle, G. R. (2002). Are Most of the Domoic Acid-Producing Species of the Diatom Genus *Pseudo-Nitzschia Cosmopolites*? *Harmful. Algae.* 1 (2), 137–146. doi: 10.1016/S1568-9883(02)00014-8

Hijmans, R. J., Van Etten, J., Cheng, J., Mattiuzzi, M., Sumner, M., Greenberg, J. A., et al. (2015). *Package 'Raster'. R Package*. 734.

Hubbard, K. A., Olson, C. E. and Armbrust, E. V. (2014). Molecular Characterization of *Pseudo-Nitzschia* Community Structure and Species Ecology in a Hydrographically Complex Estuarine System (Puget Sound, Washington, USA). *Mar. Ecol. Prog. Ser.* 507, 39–55. doi: 10.3354/meps10820

Hubbard, K. A., Rocap, G. and Armbrust, E. V. (2008). Inter- and Intraspecific Community Structure Within the Diatom Genus *Pseudo-Nitzschia* (Bacillariophyceae). *J. Phycol.* 44, 637–649. doi: 10.1111/j.1529-8817.2008.00518.x

Jenkins, B. D. and Bertin, M. J. (2021a). "Amplicon Sequence Variants (ASVs) Recovered From Samples and Their Related Identification as Pseudo-Nitzschia Taxa and the Methods Used," in *Biological and Chemical Oceanography Data Management Office* (BCO-DMO). *(Version 1) Version Date 2021-04-05 [Subset to NBPTS Samples]*. doi: 10.26008/1912/bco-dmo.847469.1

Jenkins, B. D. and Bertin, M. J. (2021b). "Pseudo-Nitzschia Spp. Cell Counts, Nutrients Water Temperature and Salinity, and Concentrations of the Toxin Domoic Acid From Weekly Samples and Offshore Cruises With the Northeast U.S. Shelf (NES) Long-Term Ecological Research (LTER)," in *Biological and Chemical Oceanography Data Management Office* (BCO-DMO). *(Version 1) Version Date 2021-04-05 [Subset to NBPTS Samples]*. doi: 10.26008/1912/bco-dmo.847448.1

Kaczmarska, I., Reid, C., Martin, J. L. and Moniz, M. B. J. (2008). Morphological, Biological, and Molecular Characteristics of the Diatom *Pseudo-Nitzschia Delicatissima* From the Canadian Maritimes. *Botany* 86, 763–772. doi: 10.1139/B08-046

Lelong, A., Hégaret, H., Soudant, P. and Bates, S. S. (2012). *Pseudo-Nitzschia* (*Bacillariophyceae*) Species, Domoic Acid and Amnesic Shellfish Poisoning: Revisiting Previous Paradigms. *Phycologia* 51 (2), 168–216. doi: 10.2216/11-37.1

Lopes dos Santos, A., Gérikas Ribeiro, C., Ong, D., Garczarek, L., Shi, X. L., Nodder, S. D., et al. (2022). "Chapter 11 - Phytoplankton Diversity and Ecology Through the Lens of High Throughput Sequencing Technologies," in *Advances in Phytoplankton Ecology*. Eds. Clementson, L. A., Eriksen, R. S. and Willis, A. (Elsevier) Amsterdam, Netherlands, 353–413. doi: 10.1016/B978-0-12-822861-6.00020-0

Lundholm, N., Bates, S. S., Baugh, K. A., Bill, B. D., Connell, L. B., Léger, C., et al. (2012). Cryptic and Pseudo-Cryptic Diversity in Diatoms—With Descriptions of *Pseudo-Nitzschia Hasleana* Sp. Nov. And *P. Fryxelliana* Sp. Nov. 1. *J. Phycol.* 48 (2), 436–454. doi: 10.1111/j.1529-8817.2012.01132.x

Lundholm, N., Krock, B., John, U., Skov, J., Cheng, J., Pančić, M., et al. (2018). Induction of Domoic Acid Production in Diatoms—Types of Grazers and Diatoms are Important. *Harmful. Algae.* 79, 64–73. doi: 10.1016/j.hal.2018.06.005

Lundholm, N., Moestrup, Ø., Hasle, G. R. and Hoef-Emden, K. (2003). A Study of the *Pseudo-Nitzschia Pseudodelicatissima*/Cuspidata Complex (Bacillariophyceae): What is *P. Pseudodelicatissima*? *J. Phycol.* 39, 797–813. doi: 10.1046/j.1529-8817.2003.02031.x

Maldonado, M. T., Hughes, M. P., Rue, E. L. and Wells, M. L. (2002). The Effect of Fe and Cu on Growth and Domoic Acid Production by *Pseudo-Nitzschia Multiseries* and *Pseudo-Nitzschia Australis*. *Limnol. Oceanography.* 47 (2), 515–526. doi: 10.4319/lo.2002.47.2.0515

Martin, M. (2011). Cutadapt Removes Adapter Sequences From High-Throughput Sequencing Reads. *EMBnet. J.* 17 (1), 10–12. doi: 10.14806/ej.17.1.200

McCabe, R. M., Hickey, B. M., Kudela, R. M., Lefebvre, K. A., Adams, N. G., Bill, B. D., et al. (2016). An Unprecedented Coastwide Toxic Algal Bloom Linked to Anomalous Ocean Conditions. *Geophysical. Res. Lett.* 43 (19), 10366–10376. doi: 10.1002/2016GL070023

McMurdie, P. J. and Holmes, S. (2013). Phyloseq: An R Package for Reproducible Interactive Analysis and Graphics of Microbiome Census Data. *PLoS One*. 8 (4) e61217. doi: 10.1371/journal.pone.0061217

NSSP (2019) *National Shellfish Sanitation Program (NSSP) Guide for the Control of Molluscan Shellfish*. Available at: https://www.issc.org/nssp-guide.

Oviatt, C., Smith, L., Krumholz, J., Coupland, C., Stoffel, H., Keller, A., et al. (2017). Managed Nutrient Reduction Impacts on Nutrient Concentrations, Water Clarity, Primary Production, and Hypoxia in a North Temperate Estuary. *Estuarine. Coast. Shelf. Sci.* 199, 25–34. doi: 10.1016/j.ecss.2017.09.026

Pan, Y., Bates, S. S. and Cembella, A. D. (1998). Environmental Stress and Domoic Acid Production by *Pseudo-Nitzschia*: A Physiological Perspective. *Natural Toxins.* 6, 127–135. doi: 10.1002/(SICI)1522-7189(199805/08)6:3/4<127::AID-NT9>3.0.CO;2-2

Raposa, K. B. (2009). "Ch 7: Ecological Geography of Narragansett Bay," in *An Ecological Profile of the Narragansett Bay National Estuarine Research Reserve*. K.B. Raposa and M.L. Schwartz (eds.), Rhode Island Sea Grant, Narragansett, R.I. 176pp.

R Core Team. (2017). *R: A Language and Environment for Statistical Computing* (R Foundation for Statistical Computing). Available at: https://www.R-project.org.

RI DEM (2021). "Rhode Island Department of Environmental Management (RI DEM) and Rhode Island Department of Health (RI DOH)," in *Harmful Algal Bloom and Shellfish Biotoxin Monitoring and Contingency Plan*. Available at: http://www.dem.ri.gov/programs/benviron/water/shellfsh/pdf/habplan.pdf.

RStudio Team (2020). *RStudio: Integrated Development for R* (RStudio, PBC). Available at: http://www.rstudio.com.

Rynearson, T. A., Flickinger, S. A. and Fontaine, D. N. (2020). Metabarcoding Reveals Temporal Patterns of Community Composition and Realized Thermal Niches of *Thalassiosira* Spp. (Bacillariophyceae) From the Narragansett Bay Long-Term Plankton Time Series. *Biology* 9 (1), 19. doi: 10.3390/biology9010019

Smayda, T. J. (1959-1997). *Narragansett Bay Plankton Time Series*.

Sterling, A. R., Kirk, R. D., Bertin, M. J., Rynearson, T. A., Borkman, D. G., Caponi, M. C., et al. (in press). Emerging Harmful Algal Blooms Caused by Distinct Seasonal Assemblages of The Toxic Diatom Pseudo-nitzschia. *Limnol. Oceanography*.

Stonik, I. V., Orlova, T. Y. and Lundholm, N. (2011). Diversity of *Pseudo-Nitzschia* H. Peragallo From the Western North Pacific. *Diatom. Res.* 26 (1), 121–134. doi: 10.1080/0269249X.2011.573706

Sun, J., Hutchins, D. A., Feng, Y., Seubert, E. L., Caron, D. A. and Fu, F.-X. (2011). Effects of Changing Pco_2 and Phosphate Availability on Domoic Acid Production and Physiology of the Marine Harmful Bloom Diatom *Pseudo-Nitzschia Multiseries*. *Limnol. Oceanography.* 56 (3), 829–840. doi: 10.4319/lo.2011.56.3.0829

Testa, J. M., Murphy, R. R., Brady, D. C. and Kemp, W. M. (2018). Nutrient- and Climate-Induced Shifts in the Phenology of Linked Biogeochemical Cycles in a Temperate Estuary. *Front. Mar. Sci.* 5. doi: 10.3389/fmars.2018.00114

Wells, M. L., Trainer, V. L., Smayda, T. J., Karlson, B. S., Trick, C. G., Kudela, R. M., et al. (2015). Harmful Algal Blooms and Climate Change: Learning From the Past and Present to Forecast the Future. *Harmful. Algae.* 49, 68–93. doi: 10.1016/j.hal.2015.07.009

White, T. J., Bruns, T., Lee, S. and Taylor, J. (1990). "Amplification and Direct Sequencing of Fungal Ribosomal RNA Genes for Phylogenetics," in *PCR Protocols: A Guide to Methods and Applications*. Academic Press, Inc., New York, vol. 18. , 315–322.

Wickham, H. (2016). Ggplot2. *Wiley. Interdiscip. Reviews.: Comput. Stat* 3 (2), 180–185. doi: 10.1002/wics.147

Zaiko, A., Samuiloviene, A., Ardura, A. and Garcia-Vazquez, E. (2015). Metabarcoding Approach for Nonindigenous Species Surveillance in Marine Coastal Waters. *Mar. pollut. Bull.* 100 (1), 53–59. doi: 10.1016/j.marpolbul.2015.09.030

Zhu, Z., Qu, P., Fu, F., Tennenbaum, N., Tatters, A. O. and Hutchins, D. A. (2017). Understanding the Blob Bloom: Warming Increases Toxicity and Abundance of the Harmful Bloom Diatom *Pseudo-Nitzschia* in California Coastal Waters. *Harmful. Algae.* 67, 36–43. doi: 10.1016/j.hal.2017.06.004

Conflict of Interest: The authors declare that the research was conducted in the absence of any commercial or financial relationships that could be construed as a potential conflict of interest.

frontiers | Frontiers in Marine Science

TYPE Original Research
PUBLISHED 19 August 2022
DOI 10.3389/fmars.2022.941205

OPEN ACCESS

EDITED BY
Aifeng Li,
Ocean University of China, China

REVIEWED BY
Leila Basti,
Tokyo University of Marine Science and Technology, Japan
Yixiao Xu,
Nanning Normal University, China

*CORRESPONDENCE
Christopher J. Gobler
christopher.gobler@stonybrook.edu
Ying Zhong Tang
yingzhong.tang@qdio.ac.cn

SPECIALTY SECTION
This article was submitted to Aquatic Microbiology, a section of the journal Frontiers in Marine Science

RECEIVED 11 May 2022
ACCEPTED 01 August 2022
PUBLISHED 19 August 2022

CITATION
Yang H, Gobler CJ and Tang YZ (2022) Consistency between the ichthyotoxicity and allelopathy among strains and ribotypes of *Margalefidinium polykrikoides* suggests that its toxins are allelochemicals.
Front. Mar. Sci. 9:941205.
doi: 10.3389/fmars.2022.941205

Consistency between the ichthyotoxicity and allelopathy among strains and ribotypes of *Margalefidinium polykrikoides* suggests that its toxins are allelochemicals

Huijiao Yang[1,2,3], Christopher J. Gobler[4]* and Ying Zhong Tang[1,2,3]*

[1]Chinese Academy of Sciences (CAS) Key Laboratory of Marine Ecology and Environmental Sciences, Institute of Oceanology, Chinese Academy of Sciences, Qingdao, China, [2]Laboratory for Marine Ecology and Environmental Science, Qingdao National Laboratory for Marine Science and Technology, Qingdao, China, [3]Centre for Ocean Mega-Science, Chinese Academy of Sciences, Qingdao, China, [4]School of Marine and Atmospheric Sciences, Stony Brook University, Stony Brook, NY, United States

Harmful algal blooms (HABs) of the ichthytoxic dinoflagellate *Margalefidinium polykrikoides* have caused mass mortality of marine life around the world. While its toxic effects can impact fish, bivalves, coral, zooplankton, and even other phytoplankton, the toxin(s) and allelochemical(s) eliciting these impacts have yet to be definitely identified, leaving open the question as to whether its toxicity and allelopathic effects are caused by the same chemical agents. In this study, we investigated the ability of 10 strains of *M. polykrikoides* with different geographic origins and ribotypes to cause mortality in two strains of the dinoflagellate, *Akashiwo sanguinea* (allelopathy), and the sheepshead minnow, *Cyprinodon variegatus* (toxicity). Results showed that the potency of allelopathy against both strains of *A. sanguinea* and toxicity to the fish were significantly correlated across strains of *M. polykrikoides* ($p < 0.001$ for all). These results strongly support the notion that the major allelochemicals and toxins of *M. polykrikoides* are identical chemicals, an ecological strategy that may be more energetically efficient than the separate synthesis of toxins and allelochemicals as has been reported in other HABs. Our results also highlight the vital significance of the definitive identification of allelochemicals and toxins of *M. polykrikoides* and of the quantitative characterization of these compounds in the field where HABs of *M. polykrikoides* occur during blooms.

KEYWORDS

***Margalefidinium polykrikoides*, ichthyotoxicity, allelopathy, strain variation, toxins, allelochemicals**

Introduction

Margalefidinium (= *Cochlodinium*) *polykrikoides* is a harmful algal bloom (HAB) species that has been responsible for mass mortalities of aquatic organisms worldwide (Dorantes-Aranda et al., 2009b; Jiang et al., 2009; Jose Dorantes-Aranda et al., 2010; Kudela and Gobler, 2012; Cui et al., 2020; Basti et al., 2021). As an ichthyotoxic and HAB-causing species, *M. polykrikoides* not only has caused fish kills across North America and Asia, but also has been known to cause rapid mortality in bivalves, zooplankton, and corals (Kim et al., 1999; Dorantes-Aranda et al., 2009b; Jiang et al., 2009; Tang and Gobler, 2009b; Tang and Gobler, 2009a; Bauman et al., 2010; Tang and Gobler, 2010; Griffith et al., 2019). Beyond being toxic to marine animals, *M. polykrikoides* is also strongly allelopathic to other phytoplankton (Kim et al., 1999; Dorantes-Aranda et al., 2009b; Tang and Gobler, 2009b; Tang and Gobler, 2009a; Tang and Gobler, 2010). Still, the traits and interactions of toxicity and allelopathy and how they may facilitate *M. polykrikoides* blooms remain unclear.

Allelochemicals are chemical agents secreted by photosynthetic organisms that affect (mainly negatively) the growth, health, behavior, or population biology of organisms, mainly plants (Whittaker and Feeny, 1971). Smayda (1997) hypothesized that harmful algae form blooms by four major pathways, with two of them pertinent to allelochemically enhanced interspecific competition. Oppositely, the target species of toxicity are animals (Rice, 1979; Smayda, 1997; Legrand et al., 2003; Granéli and Hansen, 2006).

Many harmful algae can be both allelopathic to other algae and toxic to marine animals. In several cases, allelochemicals and toxins seem to be different compounds as have been demonstrated for the karlotoxin-producer *Karlodinium veneficum* (Yang et al., 2019), the paralytic shellfish toxin-producer *Alexandrium* spp. (Tillmann and John, 2002; Tillmann et al., 2007; Tillmann et al., 2008), and the brevetoxin producer *Karenia brevis* (Kubanek et al., 2005). For some algae, however, their toxicity to animals and allelopathic effects on phytoplankton appear to be caused by common mechanisms, for instance, for *Prymnesium parvum* (Singh et al., 2001; Granéli and Hansen, 2006).

The identity and mechanism of toxins and allelochemicals of *M. polykrikoides* have been the subject of debate. The toxins of *M. polykrikoides* cause damage to different cell types, including hemolysis in fish erythrocytes (Kim et al., 1999; Dorantes-Aranda et al., 2009a; Kim and Oda, 2010). The conceivable ichthyotoxic substances produced by *M. polykrikoides* have been hypothesized to include reactive oxygen species (ROS) (Tang and Gobler, 2009a), sterols, fatty acids (Giner et al., 2016), and mucopolysaccharides (Kim et al., 2002; Kim and Oda, 2010). The short-term nature of *M. polykrikoides* toxicity (minutes in the absence of live cells) and the ability of anti-oxidation compounds to mitigate its toxicity have suggested that ROS are a likely source of this HABs toxicity (Tang and Gobler, 2009b; Jiang et al., 2009). Further studies have also suggested that the existence of a synergistic action of ROS and polyunsaturated fatty acids, docosahexaenoic and eicosapentanoic, that are produced by *M. polykrikoides* may contribute to lipid peroxidation (Dorantes-Aranda et al., 2009a; Dorantes-Aranda et al., 2009b), which is associated with an increase in the solute permeability in the membrane cells, causing swelling and lysis of the vacuoles of the membrane liposomes (Girotti, 1990) and severe damage in fish gill liposomes (Kim et al., 1999). In addition, polysaccharides can exert a damaging effect on branchial cells (Dorantes-Aranda et al., 2009a; Dorantes-Aranda et al., 2009b; Kim and Oda, 2010), which may also contribute to the ichthyotoxic effects of *M. polykrikoides*. As for the allelochemicals of *M. polykrikoides*, they have been reported to affect the growth and survival of many planktonic species (Gobler et al., 2008; Mulholland et al., 2009; Tang and Gobler, 2009b; Tang and Gobler, 2009a; Richlen et al., 2010; Koch et al., 2014; Pérez-Morales et al., 2017; Hattenrath-Lehmann et al., 2019). However, the exact allelopathic mechanisms remain controversial and largely unknown. Prior investigations of *M. polykrikoides* (Kim et al., 1999; Tang and Gobler, 2010) and other allelopathy-causing species (Oda et al., 1992; Marshall et al., 2005; van Rijssel et al., 2008) have suggested that various compounds including ROS, PUFA (polyunsaturated fatty acid), and unidentified toxic metabolites may act as allelochemicals.

The goal of this study was to compare the toxic effects of *M. polykrikoides* on fish to its allelopathic effects on other phytoplankton in terms of characterizing the chemical nature of the toxin(s) and allelochemical(s) produced by the species. Given that prior research has established significant variation in the strength of allelopathy and toxicity among clonal isolates of *M. polykrikoides* (Tang and Gobler, 2010; Wang et al., 2020), we compared the ability of 10 clones isolated from the Atlantic and Pacific Oceans and representing two major ribotypes. Results demonstrated a high degree of similarity between allelochemical potency and ichthyotoxicity across the clones studied.

Materials and methods

Cultures and culturing conditions

Ten strains of *M. polykrikoides* were isolated from coastal areas of the United States, Mexico, and Japan (Table 1). The identity of all strains was confirmed with large subunit (LSU) rDNA sequencing. Two strains of *Akashiwo sanguinea* (ASNP6 and AS2) isolated from the Northport Bay, New York, USA in 19 August 2011 (Tang and Gobler, 2015) were used as the target species of allelopathic tests. All cultures were maintained in exponential phase growth in sterile GSe medium with a salinity of 31–32 made with an autoclave and 0.2 μm filtered seawater,

TABLE 1 Strains of *Margalefidinium polykrikoides* used in this study.

Strain name	Isolated area	Ribotype	Isolated time
CP1	Flanders Bay, NY	American/Malaysian	31 August 2006
CPCB10	Cotuit Bay, MA, USA, MA	American/Malaysian	September 2001
CPPV1	Bahía de La Paz, Mexico	American/Malaysian	Unknown
CPSB-1B	Shinnecock Bay, NY	American/Malaysian	5 August 2010
CPSB-1G	Shinnecock Bay, NY	American/Malaysian	5 August 2010
CPSB-2A	Shinnecock Bay, NY	American/Malaysian	5 August 2010
CPINS129	Japan	East Asian	Unknown
CPNB-3	Noyak Bay, NY	American/Malaysian	16 August 2011
CPNB-6	Noyak Bay, NY	American/Malaysian	16 August 2011
CPGSB-1	Great South Bay, NY	American/Malaysian	17 August 2011

and maintained at 21°C in an incubator with a 12-h light:12-h dark cycle providing ~100 µmol quanta m^{-2} s^{-1}. Cultures were grown with a mixture of penicillin and streptomycin (2% v/v dilution of stock with 200 U·ml^{-1} penicillin and 0.2 mg·ml^{-1} streptomycin) to discourage the growth of bacteria.

Testing the allelopathy of *M. polykrikoides*

Cultures of CPSB-1B, CPSB-1G, CP1, CPNB-3, CPNB-6, CPSB-2A, CPGSB-1, and ASNP-6 were maintained in exponential growth phase in 500-ml conical flasks in GSe medium with 2% antibiotics mixture. For experiments, 10 ml of *M. polykrikoides* and 1 ml of ASNP-6 (both at ~10^3 cells ml^{-1}) were added to one well of a six-well culture plate. One milliliter of ASNP-6 was added into 10 ml of GSe medium as control. Each treatment and control were established in triplicate. After 48 h, all samples (11 ml) were preserved with 2% Lugol's solution (final) and quantified under a light microscope. Cultures of CPSB-2A, CP1, CPSB-1B, and CPSB-1G were also co-cultured with *A. sanguinea* (ASNP-6) for 72 h to test the allelopathic effects using the same methods described above for the 48-h assay, the only difference being that six replicates were set in each group of the latter experiment (n = 6).

Other strains of *M. polykrikoides*, CPINS129, CPCB10, CPPV1, and CP1, were tested with *A. sanguinea* strain AS2 as target species. All strains of *M. polykrikoides* were diluted to different cell densities (650–4,000 cells ml^{-1} for CP1, 2,300–4,300 cells ml^{-1} for CPINS129, 500–1,700 cells ml^{-1} for CPCB10, and 5,300–9,900 cells ml^{-1} for CPPV1) and then co-cultured with AS2 in a six-well culture plate with 9 ml of *M. polykrikoides* and 1 ml of *A. sanguinea* culture in one well, respectively. One milliliter of AS2 with the same cell density as treatments was added to 9 ml of GSe medium as control. All the treatments and controls were in triplicate. Samples were preserved after 24 h with Lugol's solution (2% final) for subsequent cell density quantification.

To quantify and compare the allelopathic effects of *M. polykrikoides* among strains with different cell densities, a parameter, "Relative Mortality compared with control of *A. sanguinea*", was defined as: Relative Mortality (AS) = [(Mean cell density of mono-cultured *A. sanguinea* – mean cell density of *A. sanguinea* co-cultured with *M. polykrikoides*)/mean cell density of mono-cultured *A. sanguinea*] × 100%, but is called "Mortality (AS)" below for simplicity.

Testing the toxicity of *M. polykrikoides*

We used 14-day-old (0.4–0.5 cm in length) *Cyprinodon variegatus* (sheepshead minnows) for toxicity experiments. All 10 strains of *M. polykrikoides* (CP1, CPINS129, CPCB10, CPPV1, CPSB-1B, CPSB-1G, CPSB-2A, CPNB-3, CPNB-6, and CPGSB-1) were maintained in exponential growth phase and diluted to several cell densities (350–4,700 cells ml^{-1} for CP1, 1,200–4,800 cells ml^{-1} for CPINS129, 300–700 cells ml^{-1} for CPCB10, 1,500–3,000 cells ml^{-1} for CPPV1, 1,200–4,000 cells ml^{-1} for CPSB-1B, 1,800 cells ml^{-1} for CPSB-1G, 2,700–5,500 cells ml^{-1} for CPSB-2A, 450–1,700 cells ml^{-1} for CPNB-3, 1,400 cells ml^{-1} for CPNB-6, and 1,400 cells ml^{-1} for CPGSB-1) before the experiment. Fish bioassays were performed in six-well plates with 10 ml of culture and one fish in each well, and one fish was added to 10 ml of GSe medium as control. All the treatments and controls were in replicates of six (n = 6) and were maintained at room temperature without aeration. The survival of fishes was recorded at 24 h. Some treatments (CP1, CPSB-1B, CPSB-1G, CPSB-2A, CPNB-3, CPNB-6, and CPGSB-1) lasted for 6 days to compare the mean death time of fishes in different cultures. A probit regression analysis of cell densities of CP1, CPINS129, and CPSB-2A, and mortality of sheepshead minnows was used to determine the median lethal dose (LD_{50})

and compare the toxicity of different strains of *M. polykrikoides* when the cell densities were unequal across experiments.

Statistics

One-way ANOVAs and multiple comparison tests were used to compare the cell densities of *M. polykrikoides*, mortalities of *A. sanguinea* compared with control, and death time of sheepshead minnows among treatments using SPSS. For the toxicity experiments, G-tests were performed to assess the significance of toxic effects (Woolf, 1957). Spearman correlation coefficients were calculated to examine the correlation between the rank of allelopathy and toxicity of different *M. polykrikoides*. In all cases, the significance level was set at $p < 0.05$.

Results

Comparing allelopathic intensity of different strains of *M. polykrikoides*

During 48-h experiments with *A. sanguinea* strain ASNP-6, cell densities of seven strains of *M. polykrikoides* were similar with the exception of CPSB-1B (H), which was higher than CPSB-1G (H) (Figure 1, Table S1-2, $p = 0.001$), but this made no difference in Mortality (AS) (Table S1-1, $p = 0.55$), indicating that CPSB-1G was allelopathically stronger than CPSB-1B. CPSB-1B was more allelopathic than CPNB-6 given that CPSB-1B (L) had higher Mortality (AS) (Figure 1, Table S1-1, $p = 0.001$) but had equal cell density (Table S1-2, $p = 0.08$). CPNB-6 had a lower cell density than CP1 (Figure 1, Table S1-2, $p = 0.01$) but induced equal Mortality (AS) as CP1 (Figure 1, Table S1-1, $p = 0.68$), indicating that CPNB-6 was more allelopathic than CP1. As for CPNB-6 and CPGSB-1, the two strains exhibited no difference in cell density (Table S1-2, $p = 0.69$) but the former strain was more allelopathic (Figure 1, Table S1-1, $p = 0.01$). Similarly, CP1 and CPSB-2A exhibited no difference in cell density (Figure 1, Table S1-2, $p = 0.66$), but the former strain induced higher Mortality (AS) (Figure 1, Table S1-1, $p = 0.01$). Moreover, CPNB-3 (H), CPSB-2A, and CPGSB-1 led to roughly equal inhibition to ASNP-6 (Table S1, $p > 0.05$ for each pairwise comparison of the three strains) but decreased in order in cell density (Figure 1, Table S1, $p < 0.05$ in each pair of the three strains), indicating that the allelopathic strength was CPGSB-1 > CPSB-2A > CPNB-3. Although we cannot discern the difference in allelopathic strength of CP1 and CPGSB-1, the two strains were weaker than CPNB-6 but stronger than CPSB-2A, meaning the overall rank order of strength was CPSB-1G > CPSB-1B > CPNB-6 > CP1 ≈ CPGSB-1 > CPSB-2A > CPNB-3.

In the experiment of ASNP-6 co-cultured with CPSB-2A, CP1, CPSB-1G, and CPSB-1B for 72 h, CPSB-2A had the highest cell density and the lowest Mortality (AS) (Figure 2, $p < 0.05$, one-way ANOVA) and thus was the least allelopathic strain. CP1 had a higher cell density than CPSB-1G (Figure 2, $p = 0.001$) but showed no difference in inducing Mortality (AS) (Figure 2, $p = 0.13$). Additionally, CP1 showed no difference in cell density with CPSB-1B (Figure 2, $p = 0.09$) but induced lower Mortality (AS) (Figure 2, $p = 0.001$). Thus, CP1 ranked after CPSB-1B and CPSB-1G in allelopathic intensity. Concluding from the above results, the allelopathic intensity in decreasing order was CPSB-1G > CPSB-1B > CPNB-6 > CP1 ≈ CPGSB-1 > CPSB-2A > CPNB-3.

In the allelopathic experiment using AS2 as the target species, four *M. polykrikoides* clones, namely, CP1, CPINS129,

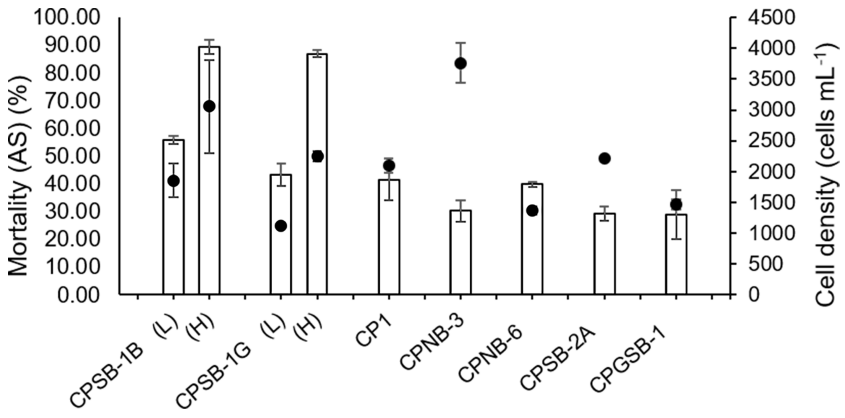

FIGURE 1
Allelopathic effects of *M. polykrikoides* on ASNP-6 in 48 h expressed as Mortality compared with control of *A. sanguinea* [Mortality (AS)]. The dots represent the cell density of different strains of *M. polykrikoides*. Each data point is the mean of triplicates ($n = 3$). Error bars indicate ±1 SD of $n = 3$.

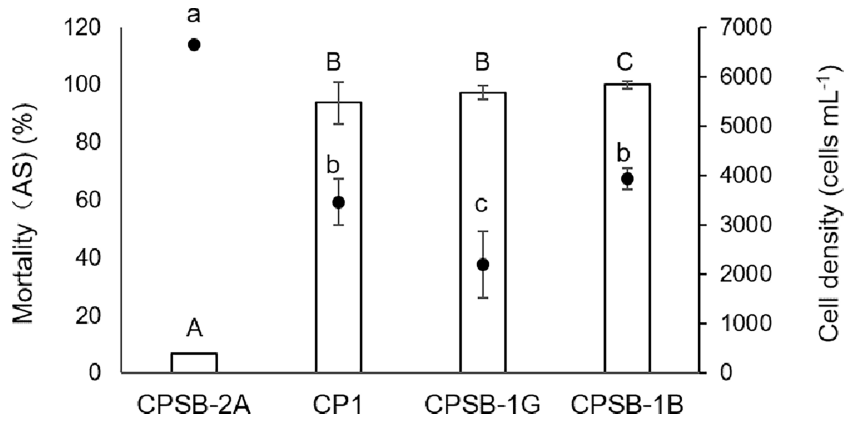

FIGURE 2
Allelopathic effects of *M. polykrikoides* on ASNP-6 in 72 h expressed as Mortality compared with control of *A. sanguinea* [Mortality (AS)]. The dots represent the cell density of different strains of *M. polykrikoides*. Each data point is the mean of sextuplicate (n = 6). Error bars indicate ±1 SD of n = 6. Different letters in uppercase indicate significant differences ($p < 0.05$) among mortalities, and different letters in lowercase indicate significant differences ($p < 0.05$) among cell densities.

CPCB10, and CPPV1, were tested (Figure 3). As shown in Mortality (AS), CPCB10 at 500 cells ml^{-1} was more potent than CP1 at 650 cells ml^{-1} (Figure 3, Table S2-1, p = 0.001) despite similar cell densities (Table S2-2, p = 0.05). Compared with CPINS129 at a cell density of 2,300 cells ml^{-1}, CP1 of 1,900 cells ml^{-1} had a lower cell density (Figure 3, Table S2-2, p = 0.001) but had a higher Mortality (AS) (Figure 3, Table S2-1, p = 0.00). In addition, CCPV1 of 8,300 cells ml^{-1} and CPINS129 of 4,300 cells ml^{-1} led to similar Mortality (AS) (Figure 3, Table S2-1, p = 0.09); however, the former had a higher cell density (Figure 3, Table S2-2, p = 0.00). As a result, the allelopathic intensity in decreasing order of the four strains was CPCB10 > CP1 > CPINS129 > CPPV1.

Comparing ichthyotoxicity among *M. polykrikoides* strains

Ten strains of *M. polykrikoides* at different cell densities were co-cultured with 14-day-old sheepshead minnows to test their toxicity (Figure 4). Four groups of *M. polykrikoides* (CPCB10 in 700 cells ml^{-1}, CPSB-1B in 1,200 cells ml^{-1}, CPNB-6 in 1,400 cells ml^{-1}, and CPSB-1G in 1,800 cells ml^{-1}) all caused 100% mortality of sheepshead minnows within 24 h (Figure 4, Table S3, $p < 0.05$ for pairwise comparisons), and the mean death time of sheepshead minnows was 1.9 h, 4.5 h, 5.4 h, and 13.1 h, respectively, suggesting that their toxic intensity decreased in the order CPCB10 > CPSB-1B > CPNB-6 > CPSB-1G.

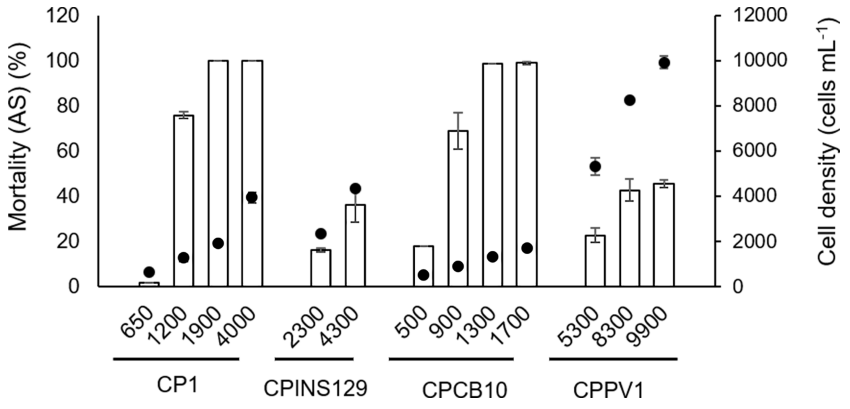

FIGURE 3
Allelopathic effects of *M. polykrikoides* on AS2 in 24 h expressed as Mortality compared with control of *A. sanguinea* [Mortality (AS)]. The dots represent the cell density of different strains of *M. polykrikoides*. Each data point is the mean of triplicates (n = 3). Error bars indicate ±1 SD of n = 3.

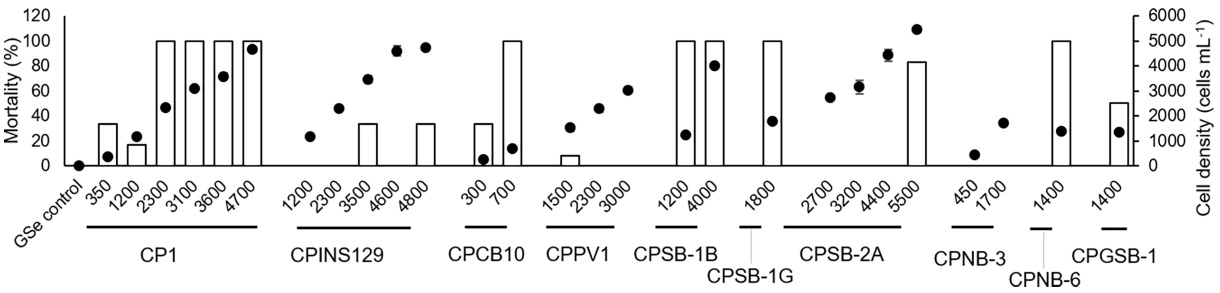

FIGURE 4
Toxic effects of *M. polykrikoides* on sheepshead minnows *Cyprinodon variegatus* in 24 h expressed as mortality (%) of sheepshead minnows (bars). The corresponding cell density of different strains of *M. polykrikoides* was also shown as dots for comparison. Error bars indicate ±1 SD of n = 6.

According to the results of regression analysis, CP1 caused 80% mortality of sheepshead minnows at a cell density of 1,874 cells ml^{-1} (Figure S1), which was lower than 100% mortality of sheepshead minnows co-cultured with 1,800 cells ml^{-1} of CPSB-1G (Figure 4). CP1 caused 60% mortality of sheepshead minnows at a cell density of 1,400 cells ml^{-1} (Figure S1), which was higher than the mortality of sheepshead minnows caused by CPGSB-1 (50%) at the same cell density (Figure 4). The LD_{50} dose of CPINS129 and CPSB-2A was 6,611 cells ml^{-1} and 5,170 cells ml^{-1}, respectively (Figure S1), indicating that CPSB-2A was more ichthyotoxic than CPINS129. Moreover, CPPV1 and CPNB-3 caused the lowest mortality of sheepshead minnows among the 10 strains (Figure 4). Conclusively, the decreasing order of toxic intensity of the 10 strains was CPCB10 > CPSB-1B > CPNB-6 > CPSB-1G > CP1> CPGSB-1 > CPSB-2A> CPINS129 > CPPV1 ≈ CPNB-3.

The death time of sheepshead minnows was also recorded in some groups (Figure 5). In groups of CPSB-2A (5,500 cells ml^{-1}), CP1 (3,100 cells ml^{-1}), CPSB-1G (1,800 cells ml^{-1}), CPNB-6 (1,400 cells ml^{-1}), and CPSB-1B (1,200 cells ml^{-1}), the death time of sheepshead minnows was less than 20 h and did not differ among the strains (Figure 5, Table S4-2, $p > 0.05$ for pairwise comparisons), and cell densities of these groups decreased in order [Figure 5, Table S4-1, $p < 0.05$ for pairwise comparisons excluding groups CPNB-6 in 1,400 cells ml^{-1} vs. CPSB-1B in 1,200 cells ml^{-1} ($p = 0.13$)], indicating that the order of ichthyotoxicity of the five strains was CPSB-1B, CPNB-6 > CPSB-1G > CP1 > CPSB-2A. The death time of sheepshead minnows in groups of CPSB-2A and CPGSB-1 showed no significant difference (Figure 5, Table S4-2, $p = 0.23$), but CPGSB-1 had a lower cell density (Figure 5, Table S4-1, $p = 0.001$), indicating that the toxicity of CPGSB-1 was greater than CPSB-2A. The death time of sheepshead minnows in groups of CPNB-3 was significantly longer than in other groups as most fishes survived the duration of the experiment (Table S4-2, $p = 0.001$), indicating that the toxicity of CPNB-3 was the weakest among the seven strains.

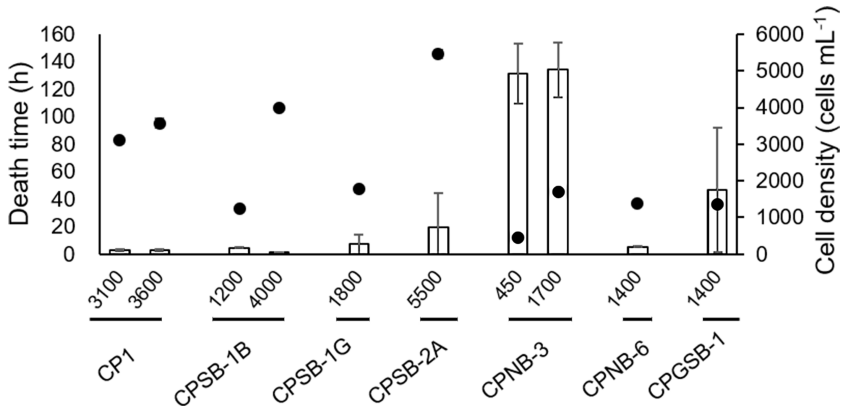

FIGURE 5
Toxic effects of *M. polykrikoides* on sheepshead minnows *Cyprinodon variegatus* expressed as death time. The dots represent the cell density of different strains of *M. polykrikoides*. Error bars indicate ±1 SD of n = 6.

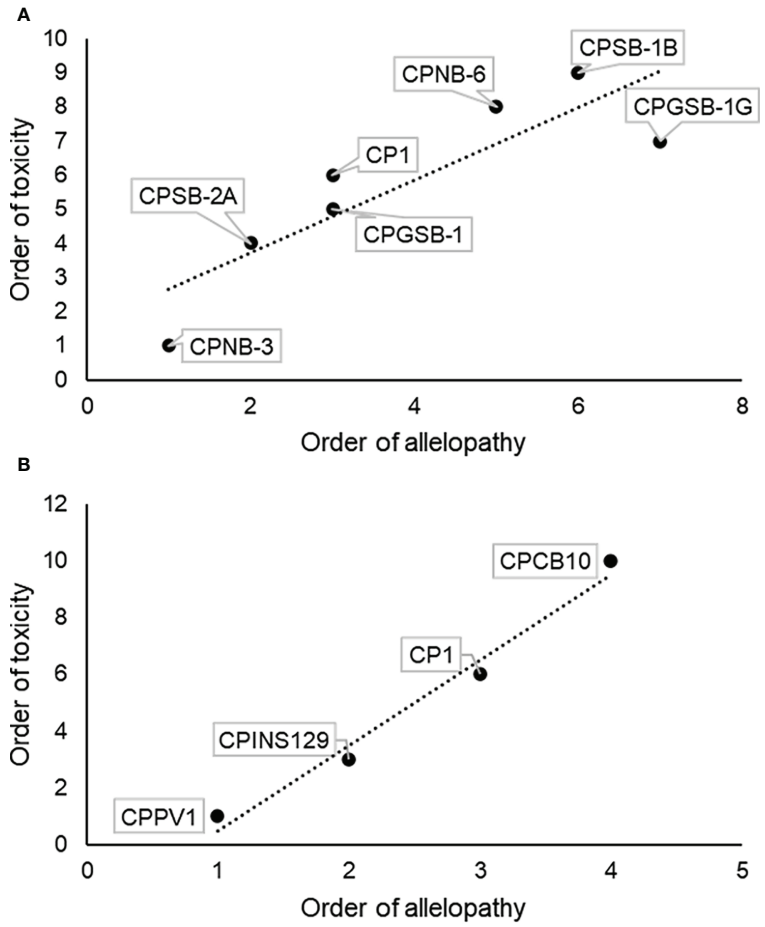

FIGURE 6
Correlation analysis of allelopathic intensity and toxic intensity of different strains of *M. polykrikoides*. **(A)** Order of allelopathic effects of *M. polykrikoides* on ASNP-6 and toxic effects of *M. polykrikoides* on sheepshead minnows. **(B)** Order of allelopathic effects of *M. polykrikoides* on AS2 and toxic effects of *M. polykrikoides* on sheepshead minnows.

Correlation of allelopathy and toxicity of *M. polykrikoides*

The allelopathic and toxic strengths of each strain were ranked according to the orders of allelopathy, which were CPSB-1G > CPSB-1B > CPNB-6 > CP1 ≈ CPGSB-1 > CPSB-2A > CPNB-3, and CPCB10 > CP1 > CPINS129 > CPPV1, and the order of toxicity, which was CPCB10 > CPSB-1B > CPNB-6 > CPSB-1G > CP1> CPGSB-1 > CPSB-2A > CPINS129 > CPPV1 ≈ CPNB-3 (Table S5), upon which the allelopathy and ichthyotoxicity of the strains were compared and found to be linearly correlated (Figure 6). Spearman's rank correlation analysis showed that the allelopathic effects and ichthyotoxicity were significantly positively correlated (Spearman's correlation coefficient = 0.88, $p = 0.01$, $n = 7$ for toxicity to sheepshead minnows and allelopathy to ASNP-6; Spearman's correlation coefficient = 1.0, $p < 0.0001$, $n = 4$ for toxicity to sheepshead minnows and allelopathy to AS2; Figure 6), illustrating consistency between the allelopathy and ichthyotoxicity of the *M. polykrikoides* strains.

Discussion

The consistency between allelopathy and toxicity among strains of *M. polykrikoides*

Margalefidinium polykrikoides strains exhibit variations in both toxicity and allelopathy (Tang and Gobler, 2010; Wang et al., 2020). By phylogenetic analysis of LSU rDNA of *M. polykrikoides* strains, at least four ribotypes have been identified globally (Iwataki et al., 2008; Reñé et al., 2013). Prior research has shown that different ribotypes of *M. polykrikoides* differ in toxicity (Wang et al., 2020), making this trait useful for providing perspective to investigate the relationships and chemical nature of allelopathy and toxicity of *M. polykrikoides*.

Here, 10 strains were studied that varied in different geographic origins, ribotypes, and isolation seasons (Table 1) but were cultured under uniform conditions and maintained in exponential growth. While differences in growth rates and maximum cell concentrations sometimes caused differences in experimental cell densities used, a gradient in cell densities was typically made for comparable treatment densities across strains. Fortunately, we obtained enough data to compare the allelopathy and toxicity between two strains, which yielded similar results and a similar order of strain potency.

Even though the intensity of allelopathy and toxicity of *M. polykrikoides* varied in different strains, especially strains of different ribotypes (Wang et al., 2020), the potencies in toxicity and allelopathy for the different strains of *M. polykrikoides* were consistent, as strains displaying potent toxicity also exhibited strong allelopathy. This consistency provides potent evidence for the hypothesis that chemical agents that are responsible for inhibitory and lethal effects on phytoplankton and marine animals, i.e., allelochemicals and toxins, were the same compounds.

Possible ecological implications of the consistency between allelopathy and toxicity

Plant secondary metabolism is a term for pathways and small-molecule products of metabolism (i.e., secondary metabolites) that are non-essential for the survival of the organism (Kossel, 1891). However, a wide variety and high diversity of secondary metabolites produced by plants are an important part of plant defense system against pathogenic attacks and environmental stresses, including toxins and allelochemicals (Yang et al., 2018). Producing secondary metabolites is thought to have a minor energetic cost (Waterman, 1992). Many harmful algae (e.g., *Alexandrium* spp., *K. brevis*, and *K. veneficum*) produce toxins and allelochemicals that are different compounds (Tillmann and John, 2002; Kubanek et al., 2005; Tillmann et al., 2007; Tillmann et al., 2008; Yang et al., 2019). In contrast, the findings of this study suggest that *M. polykrikoides* produces a singular class of compounds that inhibit competitors and potential predators (e.g., zooplankton and planktivorous fish), representing a potential energetic cost-saving for this HAB-causing species.

Expectations in identifying toxins and allelochemicals of *M. polykrikoides*

While prior studies have identified several kinds of compounds that may be the toxins made by *M. polykrikoides*, more evidence is needed to verify the actual toxicity of these substances. It has been suggested that the toxins of *M. polykrikoides* may be ROS (Kim et al., 1999; Tang and Gobler, 2009a). ROS-scavenging enzymes (peroxidase and catalase) have been shown to mitigate the toxicity and allelopathy of *M. polykrikoides* and multiple attributes of the toxicity are consistent with ROS being the toxic principle. For example, the rapidly diminished toxicity (in minutes) observed in *M. polykrikoides* cells that were freshly killed (Tang and Gobler, 2009a) was consistent with the short half-life of ROS compounds. Furthermore, *M. polykrikoides* exhibited the highest toxicity during the exponential growth phase of cultures, which aligns with reports of ROS production by actively growing, rather than stationary phase, cells of the species (Tang and Gobler, 2009a). While one study found that the O_2^- and H_2O_2 in a toxic strain of *M. polykrikoides* were at trace levels (Kim and Oda, 2010), other ROS compounds were not measured in that study. Mucopolysaccharides produced by *M. polykrikoides* may be attributed to the smothering of fishes (Kim and Oda, 2010), but no study has affirmed this finding and there were no visual signs of polysaccharides on fish during our study. Giner et al. (2016) extracted lipids of *M. polykrikoides* cells and analyzed the compositions of fatty acid and sterol in crude lipids, which consisted of a high proportion of PUFAs (47% of total fatty acids), dinosterol (40% of total sterols), and dihydrodinosterol (32% of total sterols). The identified fatty acids and sterols may contribute to long-term deleterious effects on invertebrates but were unlikely to be effective substances responsible for the acute toxicity to fish (Giner et al., 2016). In addition, according to the definition of allelopathy, allelochemicals *sensu stricto* refer to the substances that are excreted from the producing cells. Thus, the crude lipids extracted with organic solvents from cells may include many more substances than extracellular secretions. While some fatty acids with hemolytic property have also been identified in *M. polykrikoides* (Dorantes-Aranda et al., 2009a), bioassays of these substances have not been implemented and thus their toxic effects remain unknown. In addition, it has been proved that direct physical contact between test animals and algal cells is not necessary for *M. polykrikoides* to cause mortality, which means the toxins of *M. polykrikoides* could be easily released to the extracellular milieu (Tang and Gobler, 2009a).

Our finding strongly suggests that the allelochemicals and toxins of *M. polykrikoides* are the same chemical agents, which could be a cost-saving or energy-saving and thus ecologically advantageous strategy, especially so if the toxin(s) and allelochemical(s) are synthesized *via* a simple pathway. In this regard, the multiple chemical agents proposed to be responsible for the toxicity and allelopathy of the species as reviewed above (e.g., ROS, mucopolysaccharides, fatty acids, and sterols) are certainly not to be all true. It is, therefore, important to fully identify the toxins and allelochemicals of *M. polykrikoides* for the sake of both understanding the bloom ecology and mitigating the harmful effects of the species in the field.

Conclusion

We confirmed that the ichthyotoxicity and allelopathy of *M. polykrikoides* are strain specific and vary with different geographic origins and ribotypes. We further found that the order of ichthyotoxicity and allelopathy from strong to weak of

the 10 strains of *M. polykrikoides* was positively correlated. These results strongly suggest that major allelochemicals and toxins of *M. polykrikoides* are identical chemicals, which could be an energy-saving and thus ecologically advantageous strategy.

Data availability statement

The original contributions presented in the study are included in the article/Supplementary Material. Further inquiries can be directed to the corresponding authors.

Author contributions

HY analyzed the data, searched the literature, and wrote the manuscript. CG supervised the research, edited the manuscript, and acquired the funding. YT designed and performed the experiments, edited the manuscript, and acquired the funding. All authors read and approved the final version of the manuscript.

Funding

This work was financially supported by the National Natural Science Foundation of China (No. 41976134), the Science and Technology Basic Resources Investigation Program of China (2018FY100204), and the Chicago Community Trust.

Conflict of interest

The authors declare that the research was conducted in the absence of any commercial or financial relationships that could be construed as a potential conflict of interest.

Publisher's note

Supplementary material

The Supplementary Material for this article can be found online at: https://www.frontiersin.org/articles/10.3389/fmars.2022.941205/full#supplementary-material

SUPPLEMENTARY FIGURE 1
Regression curves about cell density of *M. polykrikoides* strains (CP1, CPINS129 and CPSB-2A) and mortality of sheepshead minnows by probit regression analysis.

SUPPLEMENTARY TABLE 1
Multiple comparison test of allelopathic effects of *M. polykrikoides* on ASNP-6 in 48 h.

SUPPLEMENTARY TABLE 2
Multiple comparison test of allelopathic effects of *M. polykrikoides* on AS2 in 24 h.

SUPPLEMENTARY TABLE 3
Multiple comparison test of cell densities of *M. polykrikoides* in toxic experiment co-cultured with sheepshead minnows in 24 h.

SUPPLEMENTARY TABLE 4
Multiple comparison test of 6-day toxic effects of *M. polykrikoides* on sheepshead minnows.

SUPPLEMENTARY TABLE 5
Ranks of allelopathic and toxic intensities of different *M. polykrikoides* strains.

References

Basti, L., Go, J., Okano, S., Higuchi, K., Nagai, S., and Nagai, K. (2021). Sublethal and antioxidant effects of six ichthyotoxic algae on early-life stages of the Japanese pearl oyster. *Harmful Algae* 103, 102013. doi: 10.1016/j.hal.2021.102013

Bauman, A. G., Burt, J. A., Feary, D. A., Marquis, E., and Usseglio, P. (2010). Tropical harmful algal blooms: An emerging threat to coral reef communities? *Mar. Pollut. Bull.* 60 (11), 2117–2122. doi: 10.1016/j.marpolbul.2010.08.015

Cui, Y., Chun, S.-J., Baek, S.-S., Baek, S. H., Kim, P.-J., Son, M., et al. (2020). Unique microbial module regulates the harmful algal bloom (*Cochlodinium polykrikoides*) and shifts the microbial community along the southern coast of Korea. *Sci. Total Environ.* 721, 137725. doi: 10.1016/j.scitotenv.2020.137725

Dorantes-Aranda, J. J., Garcia-de la Parra, L. M., Alonso-Rodríguez, R., and Morquecho, L. (2009a). Hemolytic activity and fatty acids composition in the ichthyotoxic dinoflagellate *Cochlodinium polykrikoides* isolated from bahía de la paz, gulf of California. *Mar. Pollut. Bull.* 58 (9), 1401–1405. doi: 10.1016/j.marpolbul.2009.06.007

Dorantes-Aranda, J. J., Garcia-de la Parra, L. M., Alonso-Rodríguez, R., Morquecho, L., and Voltolina, D. (2009b). Toxic effect of the harmful dinoflagellate *Cochlodinium polykrikoides* on the spotted rose snapper *Lutjanus guttatus*. environ. *Toxicol* 25 (4), 319–326. doi: 10.1002/TOX.20507

Giner, J.-L., Ceballos, H., Tang, Y.-Z., and Gobler, C. J. (2016). Sterols and fatty acids of the harmful dinoflagellate *Cochlodinium polykrikoides*. *Chem. Biodiversity* 13 (2), 249–252. doi: 10.1002/cbdv.201500215

Girotti, A. W. (1990). Photodynamic lipid peroxidation in biological systems. *Photochem. Photobiol.* 51 (4), 497–509. doi: 10.1111/J.1751-1097.1990.TB01744.X

Gobler, C. J., Berry, D. L., Anderson, O. R., Burson, A., Koch, F., Rodgers, B. S., et al. (2008). Characterization, dynamics, and ecological impacts of harmful *Cochlodinium polykrikoides* blooms on eastern long island, NY, USA. *Harmful Algae* 7 (3), 293–307. doi: 10.1016/j.hal.2007.12.006

Granéli, E., and Hansen, P. J. (2006). "Allelopathy in harmful algae: A mechanism to compete for resources?," in *Ecology of harmful algae*. Eds. E. Granéli and J. T. Turner (Berlin, Heidelberg: Springer Publishers), 189–201.

Griffith, A. W., Shumway, S. E., and Gobler, C. J. (2019). Differential mortality of north Atlantic bivalve molluscs during harmful algal blooms caused by the dinoflagellate, *Cochlodinium* (a.k.a. *Margalefidinium*) *polykrikoides*. *Estuaries Coasts* 42 (1), 190–203. doi: 10.1007/s12237-018-0445-0

Hattenrath-Lehmann, T. K., Jankowiak, J., Koch, F., and Gobler, C. J. (2019). Prokaryotic and eukaryotic microbiomes associated with blooms of the ichthyotoxic dinoflagellate *Cochlodinium* (*Margalefidinium*) *polykrikoides* in new

York, USA, estuaries. *PloS One* 14 (11), e0223067. doi: 10.1371/journal.pone.0223067

Iwataki, M., Kawami, H., Mizushima, K., Mikulski, C. M., Doucette, G. J., Relox, J. R., et al. (2008). Phylogenetic relationships in the harmful dinoflagellate *Cochlodinium polykrikoides* (Gymnodiniales, dinophyceae) inferred from LSU rDNA sequences. *Harmful Algae* 7 (3), 271–277. doi: 10.1016/j.hal.2007.12.003

Jiang, X., Tang, Y., Lonsdale, D. J., and Gobler, C. J. (2009). Deleterious consequences of a red tide dinoflagellate *Cochlodinium polykrikoides* for the calanoid copepod *Acartia tonsa*. mar. *Ecol. Prog. Ser.* 390, 105–116. doi: 10.3354/meps08159

Jose Dorantes-Aranda, J., Maria Garcia-de la Parra, L., Alonso-Rodriguez, R., Morquecho, L., and Voltolina, D. (2010). Toxic effect of the harmful dinoflagellate *Cochlodinium polykrikoides* on the spotted rose snapper *Lutjanus guttatus*. environ. *Toxicol* 25 (4), 319–326. doi: 10.1002/tox.20507

Kim, C. S., Lee, S. G., Lee, C. K., Kim, H. G., and Jung, J. (1999). Reactive oxygen species as causative agents in the ichthyotoxicity of the red tide dinoflagellate *Cochlodinium polykrikoides*. J. *Plankton Res.* 21 (11), 2105–2115. doi: 10.1093/plankt/21.11.2105

Kim, D., and Oda, T. (2010). "Possible factors responsible for the fish-killing mechanisms of the red tide phytoplankton, Chattonella marina and Cochlodinium polykrikoides," in *Coastal Environmental and Ecosystem Issues of the East China Sea*, eds A. Ishimatsu and H.-J. Lie. (Tokyo: TERRAPUB and Nagasaki University), 245–268.

Kim, D., Oda, T., Muramatsu, T., Kim, D., Matsuyama, Y., and Honjo, T. (2002). Possible factors responsible for the toxicity of *Cochlodinium polykrikoides*, a red tide phytoplankton. *Comp. Biochem. Physiol. C-Toxicol. Pharmacol.* 132 (4), 415–423. doi: 10.1016/S1532-0456(02)00093-5

Koch, F., Burson, A., Tang, Y. Z., Collier, J. L., Fisher, N. S., Sañudo-Wilhelmy, S., et al. (2014). Alteration of plankton communities and biogeochemical cycles by harmful *Cochlodinium polykrikoides* (Dinophyceae) blooms. *Harmful Algae* 33, 41–54. doi: 10.1016/j.hal.2014.01.003

Kossel, A. (1891). Ueber die chemische zusammensetzung der zelle. *Arch. Physiol.* V1, 181–186.

Kubanek, J., Hicks, M. K., Naar, J., and Villareal, T. A. (2005). Does the red tide dinoflagellate *Karenia brevis* use allelopathy to outcompete other phytoplankton? *Limnol. Oceanogr.* 50 (3), 883–895. doi: 10.4319/lo.2005.50.3.0883

Kudela, R. M., and Gobler, C. J. (2012). Harmful dinoflagellate blooms caused by cochlodinium sp.: Global expansion and ecological strategies facilitating bloom formation. *Harmful Algae* 14, 71–86. doi: 10.1016/j.hal.2011.10.015

Legrand, C., Rengefors, K., Fistarol, G. O., and Granéli, E. (2003). Allelopathy in phytoplankton - biochemical, ecological and evolutionary aspects. *Phycologia* 42 (4), 406–419. doi: 10.2216/i0031-8884-42-4-406.1

Marshall, J.-A., Ross, T., Pyecroft, S., and Hallegraeff, G. (2005). Superoxide production by marine microalgae: II. towards understanding ecological consequences and possible functions. *Mar. Biol.* 147 (2), 541–549. doi: 10.1007/S00227-005-1597-6

Mulholland, M. R., Morse, R. E., Boneillo, G. E., Bernhardt, P. W., Filippino, K. C., Procise, L. A., et al. (2009). Understanding causes and impacts of the dinoflagellate, *Cochlodinium polykrikoides*, blooms in the Chesapeake bay. *Estuaries Coasts* 32 (4), 734–747. doi: 10.1007/s12237-009-9169-5

Oda, T., Akaike, T., Sato, K., Ishimatsu, A., Takeshita, S., Muramatsu, T., et al. (1992). Hydroxyl radical generation by red tide algae. *Arch. Biochem. Biophys.* 294 (1), 38–43. doi: 10.1016/0003-9861(92)90133-H

Pérez-Morales, A., Band-Schmidt, C. J., and Martínez-Díaz, S. F. (2017). Mortality on zoea stage of the pacific white shrimp *Litopenaeus vannamei* caused by *Cochlodinium polykrikoides* (Dinophyceae) and chattonella spp. (Raphidophyceae). *Mar. Biol.* 164 (3), 57. doi: 10.1007/s00227-017-3083-3

Reñé, A., Garcés, E., and Camp, J. (2013). Phylogenetic relationships of *Cochlodinium polykrikoides* margalef (Gymnodiniales, dinophyceae) from the Mediterranean Sea and the implications of its global biogeography. *Harmful Algae* 25, 39–46. doi: 10.1016/j.hal.2013.02.004

Rice, E. L. (1979). Allelopathy - update. *Bot. Rev.* 45 (1), 15–109. doi: 10.1007/bf02869951

Richlen, M. L., Morton, S. L., Jamali, E. A., Rajan, A., and Anderson, D. M. (2010). The catastrophic 2008-2009 red tide in the Arabian gulf region, with observations on the identification and phylogeny of the fish-killing dinoflagellate *Cochlodinium polykrikoides*. *Harmful Algae* 9 (2), 163–172. doi: 10.1016/j.hal.2009.08.013

Singh, D. P., Tyagi, M., Kumar, A., Thakur, J., and Kumar, A. (2001). Antialgal activity of a hepatotoxin-producing cyanobacterium, *Microcystis aeruginosa*. *World J. Microbiol. Biotechnol.* 17 (1), 15–22. doi: 10.1023/A:1016622414140

Smayda, T. J. (1997). Harmful algal blooms: Their ecophysiology and general relevance to phytoplankton blooms in the sea. *Limnol. Oceanogr.* 42 (5), 1137–1153. doi: 10.4319/lo.1997.42.5_part_2.1137

Tang, Y. Z., and Gobler, C. J. (2009a). Characterization of the toxicity of *Cochlodinium polykrikoides* isolates from northeast US estuaries to finfish and shellfish. *Harmful Algae* 8 (3), 454–462. doi: 10.1016/j.hal.2008.10.001

Tang, Y. Z., and Gobler, C. J. (2009b). *Cochlodinium polykrikoides* blooms and clonal isolates from the northwest Atlantic coast cause rapid mortality in larvae of multiple bivalve species. *Mar. Biol.* 156 (12), 2601–2611. doi: 10.1007/s00227-009-1285-z

Tang, Y. Z., and Gobler, C. J. (2010). Allelopathic effects of *Cochlodinium polykrikoides* isolates and blooms from the estuaries of long island, new York, on co-occurring phytoplankton. *Mar. Ecol. Prog. Ser.* 406, 19–31. doi: 10.3354/meps08537

Tang, Y. Z., and Gobler, C. J. (2015). Sexual resting cyst production by the dinoflagellate *Akashiwo sanguinea*: A potential mechanism contributing to the ubiquitous distribution of a harmful alga. *J. Phycol.* 51 (2), 298–309. doi: 10.1111/jpy.12274

Tillmann, U., Alpermann, T., John, U., and Cembella, A. (2008). Allelochemical interactions and short-term effects of the dinoflagellate *Alexandrium* on selected photoautotrophic and heterotrophic protists. *Harmful Algae* 7 (1), 52–64. doi: 10.1016/j.hal.2007.05.009

Tillmann, U., and John, U. (2002). Toxic effects of alexandrium spp. on heterotrophic dinoflagellates: an allelochemical defence mechanism independent of PSP-toxin content. *Mar. Ecol. Prog. Ser.* 230, 47–58. doi: 10.3354/meps230047

Tillmann, U., John, U., and Cembella, A. (2007). On the allelochemical potency of the marine dinoflagellate *Alexandrium ostenfeldii* against heterotrophic and autotrophic protists. *J. Plankton Res.* 29 (6), 527–543. doi: 10.1093/plankt/fbm034

van Rijssel, M., de Boer, M. K., Tyl, M. R., and Gieskes, W. W. C. (2008). Evidence for inhibition of bacterial luminescence by allelochemicals from *Fibrocapsa japonica* (Raphidophyceae), and the role of light and microalgal growth rate. *Hydrobiologia* 596 (1), 289–299. doi: 10.1007/s10750-007-9104-3

Wang, H., Hu, Z., Shang, L., Leaw, C. P., Lim, P. T., and Tang, Y. Z. (2020). Toxicity comparison among four strains of *Margalefidinium polykrikoides* from China, Malaysia, and USA (belonging to two ribotypes) and possible implications. *J. Exp. Mar. Biol. Ecol.* 524, 151293. doi: 10.1016/j.jembe.2019.151293

Waterman, P. G. (1992). Roles for secondary metabolites in plants. *Ciba Found. Symp.* 171, 255–269; discussion 269–275.

Whittaker, R. H., and Feeny, P. P. (1971). Allelochemics: Chemical interactions between species. *Science* 171 (3973), 757–770. doi: 10.1126/SCIENCE.171.3973.757

Woolf, B. (1957). The log likelihood ratio test (the G-test) - methods and tables for tests of heterogeneity in contingency tables. *Ann. Hum. Genet.* 21 (4), 397–409. doi: 10.1111/j.1469-1809.1972.tb00293.x

Yang, H., Hu, Z., Xu, N., and Tang, Y. Z. (2019). A comparative study on the allelopathy and toxicity of four strains of *Karlodinium veneficum* with different culturing histories. *J. Plankton Res.* 41 (1), 17–29. doi: 10.1093/plankt/fby047

Yang, L., Wen, K.-S., Ruan, X., Zhao, Y. X., Wei, F., and Wang, Q. (2018). Response of plant secondary metabolites to environmental factors. *Molecules* 23 (4), 762. doi: 10.3390/MOLECULES23040762

frontiers | Frontiers in Marine Science

TYPE Original Research
PUBLISHED 23 August 2022
DOI 10.3389/fmars.2022.976353

OPEN ACCESS

EDITED BY
Zhangxi Hu,
Guangdong Ocean University, China

REVIEWED BY
Dajun Qiu,
South China Sea Institute of Oceanology, Chinese Academy of Sciences, China
Andreas Seger,
University of Tasmania, Australia

*CORRESPONDENCE
Zhiming Yu
zyu@qdio.ac.cn

SPECIALTY SECTION
This article was submitted to Aquatic Microbiology, a section of the journal Frontiers in Marine Science

RECEIVED 23 June 2022
ACCEPTED 04 August 2022
PUBLISHED 23 August 2022

CITATION
Chi L, Ding Y, He L, Wu Z, Yuan Y, Cao X, Song X and Yu Z (2022) Application of modified clay in intensive mariculture pond: Impacts on nutrients and phytoplankton. *Front. Mar. Sci.* 9:976353. doi: 10.3389/fmars.2022.976353

Application of modified clay in intensive mariculture pond: Impacts on nutrients and phytoplankton

Lianbao Chi[1,2,3], Yu Ding[1,2,3,4], Liyan He[1,2,3], Zaixing Wu[1,2,3], Yongquan Yuan[1,2,3], Xihua Cao[1,2,3], Xiuxian Song[1,2,3,4] and Zhiming Yu[1,2,3,4]*

[1]CAS Key Laboratory of Marine Ecology and Environmental Sciences, Institute of Oceanology, Chinese Academy of Sciences, Qingdao, China, [2]Laboratory for Marine Ecology and Environmental Science, Qingdao National Laboratory for Marine Science and Technology, Qingdao, China, [3]Center for Ocean Mega-Science, Chinese Academy of Sciences, Qingdao, China, [4]University of Chinese Academy of Sciences, Beijing, China

Nutrients and phytoplankton associated with mariculture development are important concerns globally, as they can significantly impact water quality and aquaculture yield. Currently, there is still insufficient information regarding the variations in nutrients and phytoplankton community of intensive mariculture systems, and effective treatment is lacking. Here, based on consecutive daily monitoring of two *Litopenaeus vannamei* ponds from July to October, the dynamic variations in nutrients and phytoplankton were elucidated. In addition, modified clay (MC) method was adopted to regulate the nutrients and phytoplankton community. The temporal variations in organic and inorganic nutrients presented fluctuating upward trends. Notably, organic nutrients were the dominant species, with average proportions of TON/P in TN/P were as high as 75.29% and 87.36%, respectively. Furthermore, a marked increase in the ratios of dinoflagellates to diatoms abundance were also observed in the control pond, concurrently with dominant organic nutrients, ascending N/P ratio and decreasing Si/N and Si/P ratios. In the MC-regulated pond, MC reduced the contents of both organic and inorganic nutrients. Furthermore, a distinct change pattern of dominant phytoplankton community occurred, with green algae becoming the most abundant phytoplankton in the MC-regulated pond. This study can provide new insights into an effective treatment for managing water quality and maintaining sustainable mariculture development.

KEYWORDS

mariculture, dynamic variations, nutrient composition and structure, phytoplankton, modified clay

Highlights

- Organic N and P were the dominant species of nutrients in mariculture shrimp ponds.Higher N/Si and N/P ratios were prominent over the production cycle.
- Variations in nutrients favored the potential predominance of dinoflagellates.
- Modified Clay effectively reduced nutrient contents and regulated the phytoplankton community.

Introduction

Mariculture is one of the fastest-expanding sectors worldwide (Campbell and Pauly, 2013; Froehlich et al., 2018; Meng and Feagin, 2019), with global production reaching 87.5 million tons in 2020 (FAO(Food and Agriculture Organization of the United Nations), 2022). Notably, China has played a major role in this growth (Li et al., 2017). In China, pond farming is a dominant aquaculture farming system. For instance, the total production of pond farming continued to increase in 2019, contributing approximately 50% of national aquaculture production (Ministry of Agriculture and Rural Affairs of the People's Republic of China, 2020). However, the rapid development of mariculture has been accompanied by environmental pollution, such as nutrient and organic matter overload, harmful algal blooms, and drug residues, which pose threats to mariculture development (Briggs and Funge-Smith, 1994; Couch, 1998; Bouwman et al., 2013; Han et al., 2021). Currently, mariculture has become a significant and expanding cause of coastal nutrient enrichment and has influenced marine ecosystems of the receiving coastal waters (Bouwman et al., 2013; Li et al., 2017; Yang et al., 2017).

As is the case with all intensive farming systems, large quantities of excess feed and faeces increase the nutrient loading to water bodies, which cause the deterioration of water quality and restrict the sustainable mariculture (Alonso-Rodrıguez and Páez-Osuna, 2003; Casé et al., 2008; Yang et al., 2017; Díaz et al., 2019). Notably, the accumulation of ammonia and nitrite will exert toxic effects on aquaculture organisms and cause disease proliferation in culture ponds (Casé et al., 2008; Glibert, 2016). Moreover, the excessive accumulation and unbalanced proportion of nutrients will influence the phytoplankton community and can cause the occurrence of 'harmful algal blooms (HABs)' (Glibert, 2016; Díaz et al., 2019). Increasing occurrences of HABs, such as *Karenia* spp, *dinoflagellates*, and *Aureococcus anophagefferens*, are leading to growing deleterious impacts including the poisoning, asphyxiation and even the death of mariculture organisms and human poisoning (Davidson et al., 2009; Gobler et al., 2011; Anderson, 2012; Brown et al., 2020). On the other hand, the unbalanced proportion of nutrients can cause a significantly higher toxicity activity of phytoplankton (Johansson and Granéli, 1999; Hagström and Granéli, 2005). Furthermore, the discharge of mariculture effluents generates diverse effects on coastal waters (Bouwman et al., 2013). For instance, over 26% of the excess nitrogen in China's waters is likely a result of shrimp production alone (Meng and Feagin, 2019).

Modified clay (MC), produced from natural clays *via* the surface modification by inorganic or organic compounds, can effectively control HABs (Yu et al., 2017; Song et al., 2021). Currently, MC technology has been included as a national standard method to control HABs and is widely employed in China (Yu et al., 2017). Previous studies found that MC can not only remove algal cells but also reduce nutrients and organic matter contents, improve water quality and reduce the degree of eutrophication (Gao et al., 2007; Lu et al., 2017; Yu et al., 2017; Song et al., 2021). In addition, MC has no adverse effects on the survival and growth of typical economically marine organisms when used at appropriate dosages (Zhang et al., 2019; Song et al., 2021). Furthermore, in mitigating the blooms of toxin-producing dinoflagellates, MC can quickly reduce algal toxins in water (Hagström and Granéli, 2005; Lu et al., 2017; Li et al., 2019).

The variations in nutrients and phytoplankton associated with mariculture development are important concerns globally, as they can have a variety of potential impacts on the mariculture yield and the environment of receiving water. Currently, there is still insufficient information on the dynamic variations in nutrients and phytoplankton, and effective regulation treatment is lacking. In the present study, based on daily monitoring of nutrients and phytoplankton of intensive mariculture shrimp ponds in Laizhou Bay, the specific objectives were to: (i) elucidate the dynamic variations in nutrients and explore the potential responses of phytoplankton community to the variations in content, composition and stochiometric ratio of nutrients, (ii) compare the variations in nutrients and phytoplankton community between an MC-regulated and control ponds and assess the regulation effects of MC. The results of this study are crucial for the comprehensive understanding of the variation patterns of nutrients and phytoplankton in the mariculture systems, and provide new insights into an effective regulation treatment for managing water quality and maintaining sustainable mariculture development.

Materials and methods

Study area

Intensive rearing *Litopenaeus vannamei* ponds were located in Dongying, Laizhou bay, China (118°55'E, 37°27'N), and two shrimp ponds were selected as the control pond and the MC-regulated pond, respectively (Figure 1). Each pond covered an

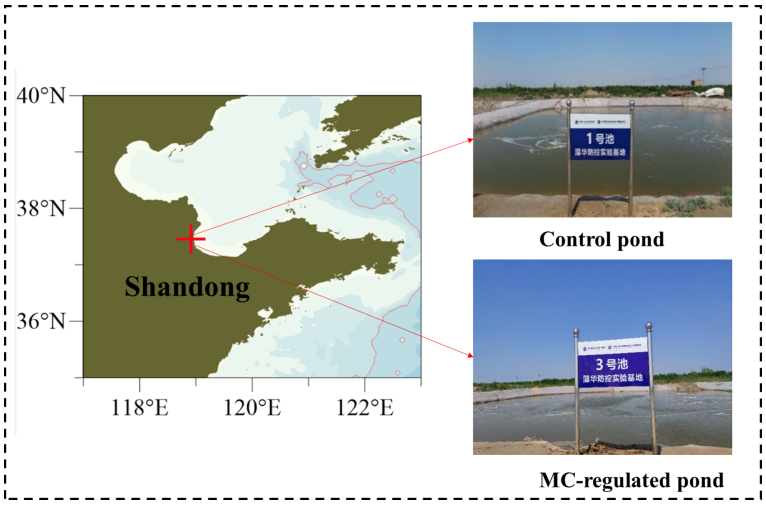

FIGURE 1
The locations of mariculture shrimp ponds in the Laizhou bay.

area of approximately 1000 m^2, with an average water depth of 1.5 m (shrimp stocking density: 5×10^4 shrimp per pond, the average body length of shrimp: 1.6 cm). There were no water changes during the culture process and each pond was equipped with an aerator to ensure a suitable dissolved oxygen concentration. The control pond adopted the traditional culture method for breeding, while the MC-regulated pond adopted MC to regulate water quality and phytoplankton community. The elemental composition and content of the MC were determined by XRF, as shown in Table S1. The MC is prepared into a suspension with seawater and then sprayed on the pond in a boat with spraying equipment. And the spraying of the MC were determined according to the variations in water quality and phytoplankton community (Table S2).

Sampling and analysis

Hydrographic parameters, including temperature and salinity, were measured by a YSI multiparameter water quality meter (YSI Ltd., USA). The water samples analyzed for nutrients, Chl *a* and 18S rDNA were collected at a depth of 0.5 m below the surface from multiple points (four corners and the center) in the pond every two days. In addition, parallel samples were collected every week. Samples for measuring total nitrogen (TN) and total phosphorus (TP) were collected and stored at -20°C in a sulfuric acid solution (50% v/v) with a final concentration of 0.2%. Water samples for the determination of dissolved inorganic nutrients were filtered under dim light through Whatman GF/F filter membranes (pore size: 0.68 μm). The filtrate was poured into 60 mL polyethylene bottles added to approximately 0.1 mL of chloroform and stored at -20°C. For the Chl *a* measurement, 100 mL of water sample was filtered using What man GF/F filters after initial filtration through a 200 μm nylon sieve, and the filter membrane was wrapped in stored in a dark environment at -20°C. Water samples for 18S rDNA were filtered through a 200 μm nylon sieve to eliminate the interference of zooplankton. Following filtration, the samples were passed through a 0.22 μm cellulose acetate membrane filter. The filters were collected in a centrifuge tube and stored in liquid nitrogen at -196°C.

In the laboratory, the concentrations of TN, TP, and dissolved inorganic nitrogen [DIN, including nitrate (NO_3^-), nitrite (NO_2^-), TAN (non-ionic ammonia (NH_3) and ammonium ion (NH_4^+))], dissolved inorganic phosphorous (DIP) and dissolved silicate (DSi) were measured with a SKALAR Flow Analyser (Skalar Ltd., Netherlands). The TON and TOP contents were calculated by the differential subtraction method, i.e. TON=TN-DIN, TOP=TN-DIP. Chl *a* was extracted in acetone, and its concentrations were determined by using a Trilogy fluorometer (Turner Design Ltd., USA).

DNA extraction, PCR, and gene sequencing

DNA was extracted using the HiPure Soil DNA Kits (Magen, Guangzhou, China) according to the manufacturer's protocol. For 18S rDNA genes, universal primers 528F (5'-GCGGTAATTCCAGCTCCAA-3') and 706R (5'-AATCCRA GAATTTCACCTCT-3') targeting the V4 regions were used for PCR (95°C for 2 min, followed by 35 cycles at 95°C for 30 s, 60°C for 45 s, 72°C for 90 s, and a final extension at 72°C for 10 min). Ampicons were extracted using 2% agarose gels and purified using

the AxyPrep DNA Gel Extraction Kit (Axygen Biosciences, Union City, CA, USA) according to the manufacturer's instructions. Purified amplicons were pooled in equimolar amounts and paired-end sequenced (PE250) on an Illumina platform according to the standard protocols.

Data processing and analysis

The raw reads were further filtered using FASTP to obtain high-quality clean reads. Paired-end clean reads were merged as raw tags using FLASH, with a minimum overlap of 10 bp and a mismatch error rate of 2%. The clean tags subjected to specific filtering conditions were clustered into operational taxonomic units (OTUs) of ≥ 97% similarity using the UPARSE pipeline. All chimeric tags were removed using the UCHIME algorithm; finally, effective tags were obtained for further analysis. The tag sequence with the highest abundance was selected as the representative sequence within each cluster. The representative OTU sequences were classified into organisms by a naïve Bayesian model using the RDP classifier based on the SILVA database, with a confidence threshold value of 0.8. To further elucidate the abundance and richness of eukaryotic phytoplankton from the 18S rDNA results, the nonalgal OTUs, including Metazoa, Fungi, Apicomplexa, Intramicronucleata, Streptopyta, Postciliodesmatophora, Opalozoa, and unclassified data were removed. In addition, the relative abundance of each taxon was calculated by dividing the sequence number of OTUs of this group by the total sequence number of algae.

The ranking analysis of phytoplankton and environmental factors was performed using CANOCO for Windows 5.0 software package. To satisfy the assumptions of normality and homogeneity of variance, all species data and environmental data were subjected to log (x + 1) transformation prior to multivariate analysis (Lepš and Šmilauer, 2003). According to the results of detrended correspondence analysis (DCA), redundancy analysis (RDA) was selected to determine the relationship between phytoplankton and environmental factors. The significance of the RDA ranking model was verified by the Monte Carlo permutation test.

Results

Temporal variations in nutrients

The TN and TP concentrations in the control and MC-regulated ponds varied in the ranges of 95.10-588.76 μmol/L, 100.86-557.41μmol/L and 1.73-22.47 μmol/L, 2.24-19.32 μmol/L, respectively. Notably, the contents of TN (Figure 2A) and TP (Figure 2B) in both ponds exhibited a rapid and fluctuating upward trend over time. Overall, during the main culture period, the TN and TP concentration of the MC-regulated pond were lower than those of the control pond. As for TON and TOP, the ranges in the control and MC-regulated ponds were 88.66-478.81 μmol/L, 43.81-387.82 μmol/L, and 0.81-21.42 μmol/L, 1.85-18.60 μmol/L, respectively. The mean concentrations of TON (Figure 2C) and TOP (Figure 2D) were significantly higher than those of DIN and DIP, which indicated that organic nutrients were the predominant species of nutrients in the water column of shrimp ponds. Similarly, significant temporal variations in TON and TOP concentrations were observed over the study period, which showed an increasing trend over time. Overall, in the late stage, the TOP concentration of the MC-regulated pond was lower than that of the control pond. The concentrations of DIN and DIP in the control and MC-regulated ponds varied in the ranges of 0.91-281.82 μmol/L, 0.79-248.37 μmol/L, and 0.22-5.62 μmol/L, 0.19-3.75 μmol/L, respectively. Significant temporal variations in the DIN (Figure 2E) and DIP (Figure 2F) were observed, with a fluctuating upward trend observed in the middle and late stages. Comparatively, the concentrations of DIN, especially DIP, in the MC-regulated pond were lower than those in the control pond during the study period. The DSi concentrations remained relatively stable during the study period (Figure 2G), and DSi concentrations in the control and MC-regulated ponds varied in the ranges of 1.55-8.96 μmol/L and 1.81-8.86 μmol/L.

The concentrations of TAN, NO_2^- and NO_3^- ranged as follows: 0.78-301.93 μmol/L, 0.01-9.41 μmol/L and 0.00-8.63 μmol/L, respectively, in the control pond; while 0.70-239.71 μmol/L, 0.00-6.23μmol/L, and 0.00-9.21 μmol/L, respectively, in the MC-regulated pond. Notably, TAN was the predominant species of DIN, with significantly higher concentrations than those of NO_2^- and NO_3^-, and its average content accounted for 86.72% and 88.30% of the DIN concentration in the control and MC-regulated ponds, respectively (Figure 3A). Temporal variations in the TAN (Figure 3B) and NO_2^- (Figure 3C) concentrations of both ponds were observed, which exhibited an overall increasing trend during the study period. In addition, the TAN and NO_2^- concentrations were lower in the MC-regulated pond than in the control pond during the main study period. Differently, the concentrations of NO_3^- exhibited a different temporal variation (Figure 3D), decreasing in the early stage and then increasing in volatility during the middle and late stages.

Temporal variations in Chl *a* concentrations and phytoplankton community

The Chl *a* concentrations ranged between 12.57-635.40 μg/L and 12.25-489.93 μg/L in the control and MC-regulated ponds, respectively. There were significant temporal variations in Chl *a* concentrations in the two ponds, with considerably lower concentrations observed during the initial stage than the other

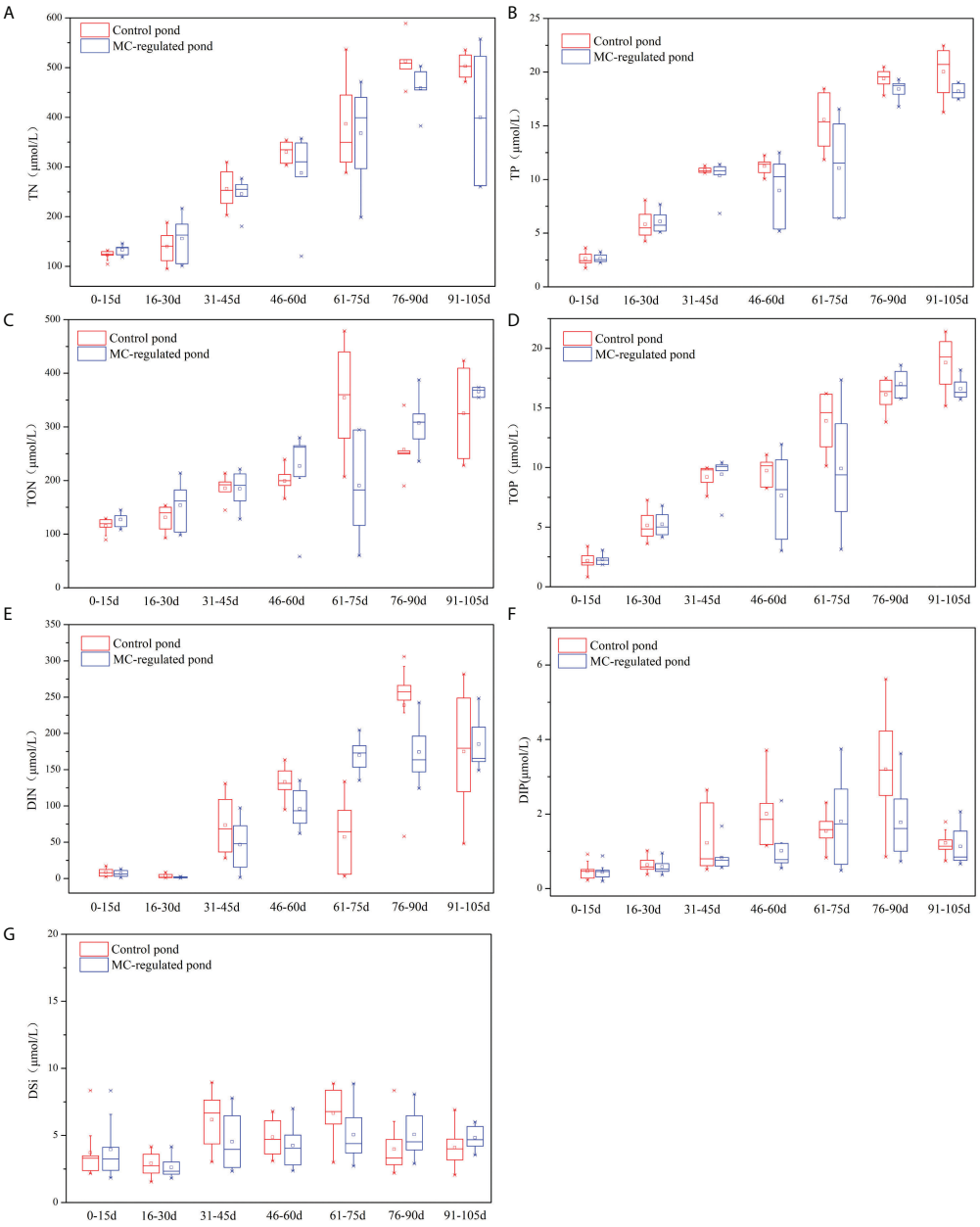

FIGURE 2
Temporal variations in **(A)** TN, **(B)** TP, **(C)** DON, **(D)** DOP, **(E)** DIN, **(F)** DIP and **(G)** DSi concentrations in the water column.

two stages (Figure 4A). Comparatively, the variation of Chl *a* in the control pond exhibited greater fluctuations than that in the MC-regulated pond. As for phytoplankton community, a total of 2,728,684 effective tags by 18S rDNA gene sequencing were obtained, after quality screening, with an average N50 of 343 bp. After clustering based on a 97% similarity threshold and removing non-algal OTUs, 212 and 222 algal OTUs were obtained from the control and the MC-regulated ponds, respectively. Overall, six phyla, 16 classes, 22 orders, 29 families, 33 genera and 38 species were identified after annotation. Among them, the top ten algae with the highest abundance at the family level were defined as the dominant phytoplankton genera, and the abundance of families in the two ponds is shown in Figures 4B, C. In the initial stage, the phytoplankton community in both the control and the MC-regulated ponds were similar and dominated by diatoms, mainly including Stephanodiscaceae at the family level. Thereafter, the phytoplankton composition exhibited temporal variations, with

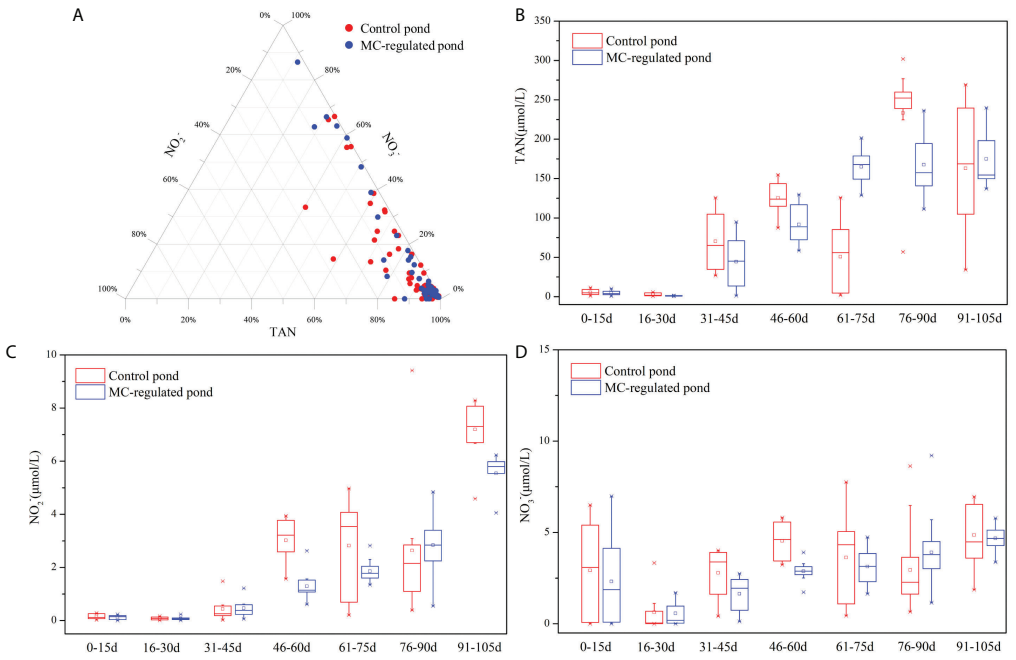

FIGURE 3
(A) The composition of DIN and temporal variations in each component (**(B)** TAN, **(C)** NO_2^-, **(D)** NO_3^-) of DIN.

a decreasing ratio of diatoms was observed. Moreover, the dominant phytoplankton species exhibited different variation pattern between the two ponds. Notably, the dominant phytoplankton species in the control pond changed to dinoflagellates, mainly including Gymnodiniaceae at the family level. And the proportion of dinoflagellates (30.02%) in the control pond was higher than that of the MC-regulated pond (25.37%) (Welch's t-test, $P > 0.05$). In addition, the Chattonellaceae (*Heterosigma* at the genus level), one of the HABs species, was another dominant family in the control pond, and had a much higher proportion in the control pond (13.09%) than the MC-regulated pond (0.92%). In contrast, the dominant phytoplankton species in the MC-regulated pond became green algae, mainly including Chlorellaceae at the family level and *Nannochloris* at the genus level, which had the highest proportion. In addition, the mean relative abundance (29.9%) of Chlorellaceae was significantly higher than that in the control pond (6.41%) (Welch's t-test, $P < 0.05$).

RDA ranking analysis between the abundance of major phytoplankton species and environmental variables

Overall, the phytoplankton richness, indicated by Chl *a* concentration, was negatively correlated with salinity and temperature, and positively correlated with nutrients in both organic and inorganic forms (Figure 5), resulting in gradually higher phytoplankton biomass as the nutrient accumulated during the study period. As for the phytoplankton communities, the RDA results indicated that the phytoplankton patterns were largely grouped by nutrient regimes. In addition, there were temporal variations in the relationship between phytoplankton communities and environmental variables. In the initial stage, the clustering characteristics of the samples from the control and MC-regulated ponds were basically the same. During this period, the phytoplankton composition was dominated by diatoms, mainly including Stephanodiscaceae, whose abundance was positively correlated with DSi. Thereafter, the clustering characteristics of the samples from the two shrimp ponds differed, indicating that the environmental influences on the distribution of the samples from the two ponds became inconsistent. In the control pond, the dominant phytoplankton species have become harmful dinoflagellates, mainly including Gymnodiniaceae and Thoracosphaeraceae. And their abundance responded strongly to TON and TOP, as indicated by their positive correlations. In contrast, the dominant species of phytoplankton in the MC-regulated pond was Chlorellaceae, a kind of green algae, and its abundance exhibited a significant positive correlation with TOP and DIP and a significant negative correlation with DSi.

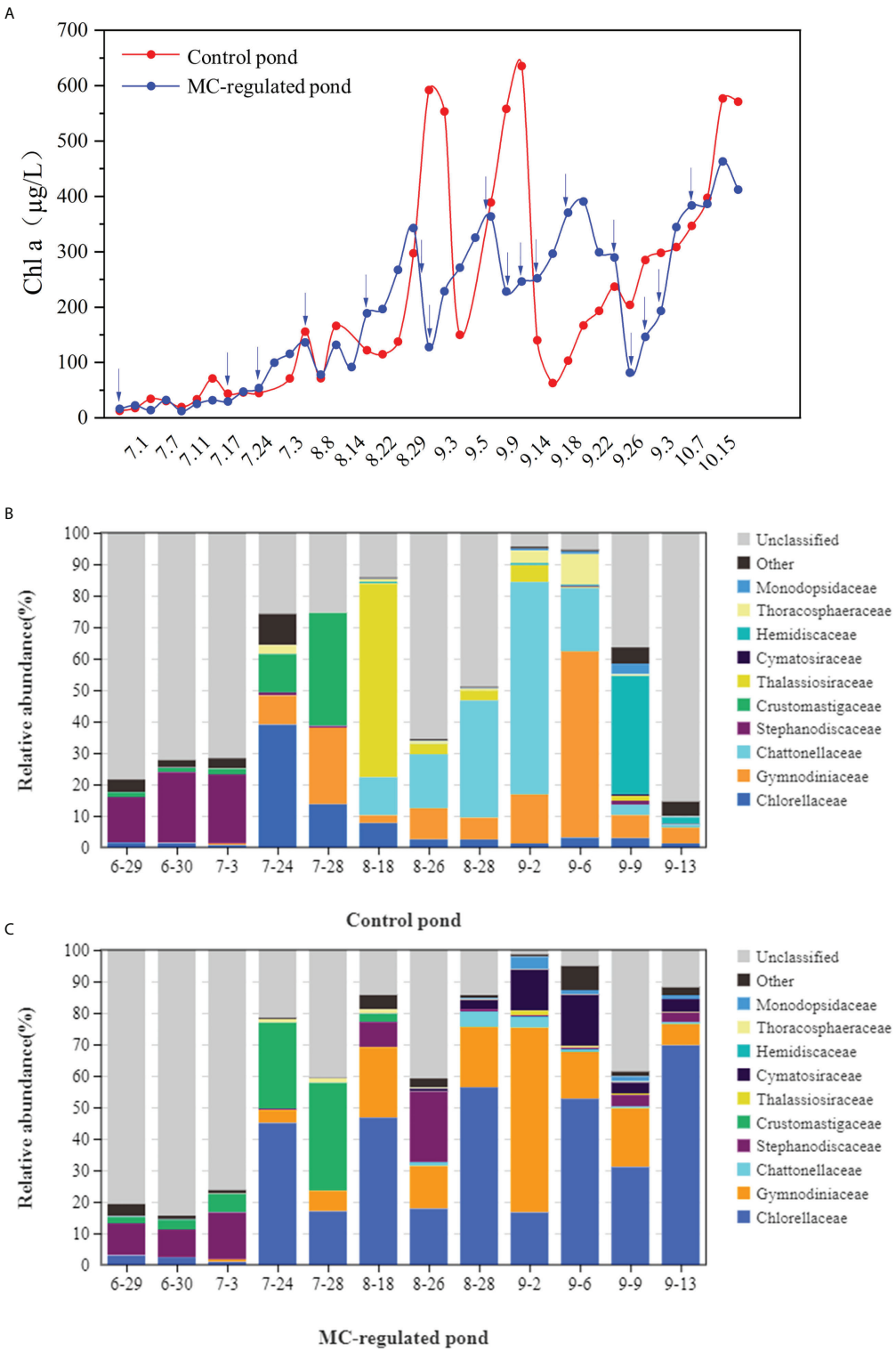

FIGURE 4
Temporal variations in the **(A)** Chl *a* concentrations and relative abundance of major taxa of phytoplankton in **(B)** the control pond and **(C)** MC-regulated pond at the family level. The blue arrows indicates the date when MC was applied.

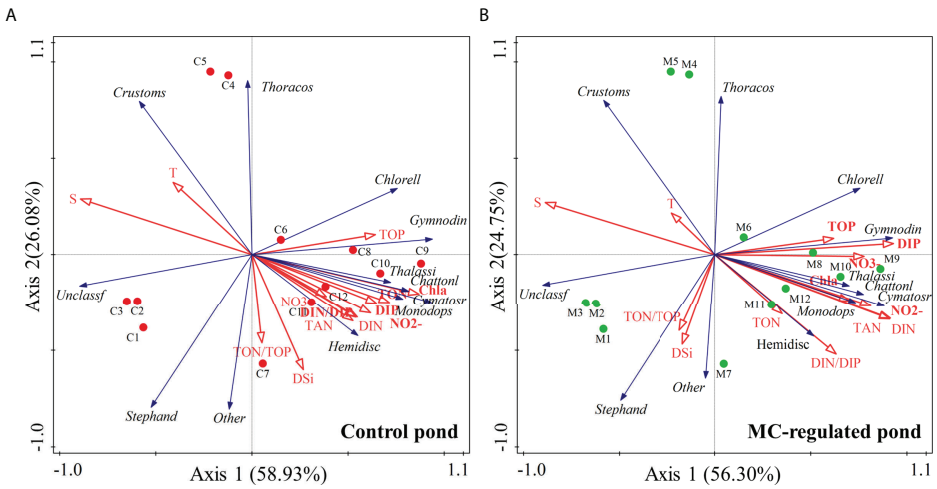

FIGURE 5
RDA ranking of samples and phytoplankton families with environmental variables in **(A)** the control pond and **(B)** the MC-regulated pond.

Discussion

Nutrient variation characteristics in mariculture ponds and their impacts on water quality of receiving coastal waters

In the intensive mariculture pond systems, the variation and accumulation of nutrients could cause the deterioration of water quality and pose threat to the organisms (Alonso-Rodrıguez and Páez-Osuna, 2003; Casé et al., 2008; Ray et al., 2011; Yang et al., 2017; Díaz et al., 2019). In addition, the export of mariculture pond effluents is an important anthropogenic source of nutrients pollution in coastal waters (Cao et al., 2017; Li et al., 2017; Yang et al., 2017), which has significantly increased the nutrients concentrations (Paerl, 2006; Danielsson et al., 2008; Glibert and Burford, 2017), and altered the nutrients composition and structure (Glibert et al., 2012; Peñuelas et al., 2012; Sutton et al., 2013). In the present study, the nutrients of the mariculture shrimp ponds exhibited unique characteristics compared with typical coastal regions. The concentrations of TON/P and DIN/P in the shrimp ponds were significantly higher, while DSi concentrations were lower than those in typical coastal waters. Notably, organic forms of nitrogen and phosphate were dominant (Figure 6), which could be attributed to continuous input and lower utilization efficiency of feeds (Bouwman et al., 2013). In general, more than 63% of nitrogen and 83% of phosphorus from feed have been discharged into the water column and sediment (Bouwman et al., 2013). Moreover, a large supply of organic nutrients stimulates microbial decomposition in the water column and sediment, as indicated by the increasing trend of DIN concentrations and DIN/TN ratios in this study. Notably, TAN was the predominant species of DIN, and it could be oxidized to NO_2^- and NO_3^-. Yang et al., 2017 found that the sediment fluxes in the shrimp ponds were

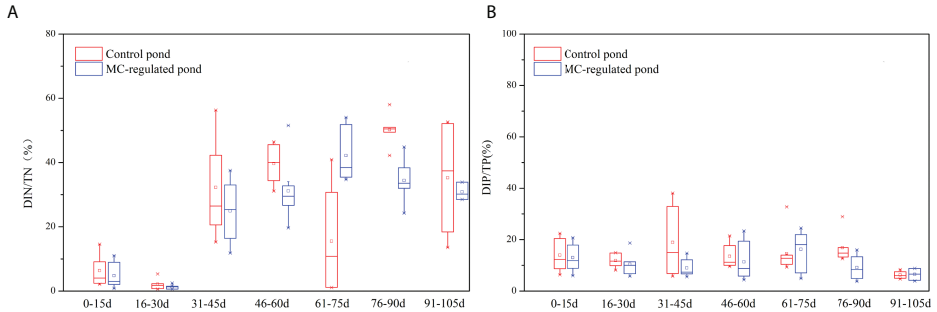

FIGURE 6
Temporal variations in **(A)** DIN/TN and **(B)** DIP/TP ratios.

significantly higher than the range of 0.01-31.25 mg N/(m^2 h). As the most common toxicant in mariculture (Santacruz-Reyes and Chien, 2010), the general safe concentrations for TAN and NO_2^- in mariculture systems are under 200 μg/L and 10 μg/L, respectively (Lai, 2014), although the specific toxicity is species-dependent. In this study, the concentrations of TAN and NO_2^- were higher than the safe concentrations, and this result was consistent with the study by Yang et al. (2017), which could potentially restrict the development of shrimp farming.

Moreover, as an important anthropogenic source of nutrient pollution in coastal waters (Table 1). (Lacerda et al., 2008) estimated that more than 827 t N/yr and 69.2 t P/yr were exported from shrimp ponds of northeastern Brazil. In the Gulf of California, the estimated nutrients loads from shrimp aquaculture were 9044 t N/yr and 3078 t P/yr (Páez-Osuna et al., 1997; Páez-Osuna et al., 2013; Páez-Osuna et al., 2017). In the present study, we further estimated the potential impacts of effluent discharge on water quality of receiving coastal waters. Assuming that our average data during the study period are representative of the aquaculture ponds across China, with a total area of 2.57×10^{10} m^2 and a mean water depth of 1.4 m (Yang et al., 2017), approximately 1.05×10^5 t TON (in terms of N), 1.08×10^4 t TOP (in terms of P), 4.80×10^4 t DIN and 1.69×10^3 t DIP accumulated in the pond system and could be discharged into coastal waters. This value represents approximately 16% of the total nutrient fluxes from the main rivers of China into the sea, whose contribution was smaller than other anthropogenic nutrient sources (SOA (State Oceanic Administration), 2017). Our results were basically consistent with the estimation of Meng and Feagin, 2019, which proposed that more than 26% of the excess nitrogen in China's waters likely originates from shrimp production alone (Meng and Feagin, 2019). With the rapid development of marine aquaculture in China, its potential impact on water pollution will be more prominent in the future. In addition, the nutrients characteristics of the shrimp ponds could also significantly alter the composition and structure of phytoplankton community and cause the occurrence of HABs, which could also limit healthy mariculture development.

The impacts of nutrient variations on the phytoplankton community and potential occurrences of HABs

A healthy and stable phytoplankton community structure is crucial for the stability and balance of mariculture ecosystems (Alonso-Rodrıguez and Páez-Osuna, 2003; Casé et al., 2008). Previous studies have documented the negative effect of algal blooms, especially dinoflagellate blooms, on shrimp development (Shumway et al., 1990; Alonso-Rodrıguez and Páez-Osuna, 2003; Matsuyama and Shumway, 2009; Lou and Hu, 2014). Generally, the structure and variation of phytoplankton communities are controlled by the complex interactions between environmental drivers and biotic interactions (Griffiths et al., 2016). Among them, the concentration, composition, and structure of nutrients are crucial for the growth and community succession of phytoplankton and the potential occurrence of HABs. Generally, both the inorganic (Altman and Paerl, 2012; Kamp et al., 2015) and organic nutrients are available for phytoplankton (McCarthy, 1972; Lønborg and Álvarez-Salgado, 2012). This could also be verified by the positive correlations between the Ch l *a* concentration with both the TON/P and DIN/P concentrations in the present study. Generally, most phytoplankton preferentially assimilate NH_4^+ due to the lower energy consumption requirements than those (Kamp et al., 2015). In addition, different species of phytoplankton differ in their preferences and responses to different forms of nutrients, previous studies indicated that NO_3^- is preferred by diatoms (Goldman and Glibert, 1983; Lomas and Glibert, 1999; Lomas et al., 2002; Berg et al., 2003), while organic nitrogen is preferred by dinoflagellates (Glibert

TABLE 1 Main negative impacts caused by intensive mariculture systems in the Laizhou bay compared with other coastal areas.

Location of the mariculture systems	Main cultivated organism species	Main negative impacts	Reference
Laizhou bay, China	Shrimp	Increase in DIN/P, TON/P and Chl *a* concentrations, dinoflagellates bloom	This study
Weihai coastal area, China	Kelp, shellfish, and fish	Increase in DIN and DON concentrations	Li et al., 2017
Jiangsu coastal area, China	Seaweed, crab, and shellfish	Increase in DIN and DON concentrations, harmful macroalgal bloom	Liu et al., 2013
Hainan coastal area, China	Shrimp and fish	Increase in DIN and DON, dissolved organic carbon, and Chl *a* concentrations	Herbeck et al., 2013
Urias coastal lagoon, USA	Shrimp	Increase in nitrite and decrease in dissolved oxygen concentrations	Cardoso-Mohedano et al., 2016
Güllük Bay (Turkey)	Fish	Increase in inorganic N and P concentrations	Demirak et al., 2006
Coastal areas of the Gulf of California, USA	Shrimp	Contribution of 10.1% N and 3.3% P to total nutrient loading	Miranda et al., 2009

and Terlizzi, 1999; Dyhrman and Anderson, 2003; Fan et al., 2003). For instance, dinoflagellates could absorb DON and easily replace other algae as the dominant species when DON is the nitrogen source (Collos et al., 2014). In the present study, DON/P were the predominant species, although an increasing trend in the ratio of DIN was observed in the late stages, with an average proportion of 78.92% and 88.18% in TN and TP, respectively. Furthermore, the predominant TAN in DIN were observed in this study, with a significantly higher proportion than those of the NO_2^- and NO_3^-. This was consistent with previous studies, which could be attributed to the continuous decomposition of protein-rich feeds (Yang et al., 2017). Consequently, as the main forms of nutrient reservoirs, the nutrient pattern, dominated by TON and TAN, could contribute to the potential dominance of dinoflagellates, as verified by the 18S rDNA results.

In addition, the fluctuation in nutrient structure can induce a shift in dominant species of phytoplankton, and researchers have proposed that the variation of N/P ratios might stimulate HABs worldwide (Alonso-Rodrıguez and Páez-Osuna, 2003; Davidson et al., 2012; Li et al., 2014). Generally, the pattern of "more N, less P and Si" may lead to a shift in the dominant species from diatoms to dinoflagellates (Li et al., 2014; Wang et al., 2015). For instance, excessive DIN and persistently elevated N/P have led to the dominant species shifting from diatoms to dinoflagellates in the Changjiang estuary (Wang and Cao, 2012). Likewise, Justić et al., (1995) suggested that the increase in N and P and the relative stabilization of Si in coastal waters, increased the possibility of Si limitation, leading to a shift in dominant phytoplankton species from diatom to non-diatom species. By comparing the differences in phosphorus requirements and uptake and utilization strategies of different algal species, the previous study has indicated that diatoms have the lowest mean optimum nitrogen to phosphorus ratio, followed by dinoflagellates, and green algae have the highest mean optimum nitrogen to phosphorus ratio (Hillebrand et al., 2013). In this study, there were no absolute concentration limitations of N, P, and Si in mariculture pond systems. However, the nutrient structure in terms of N/P and N/Si ratios exhibited significant temporal variations during the culture process. Relatively stable ratios of TON/TOP (with an average value of 27) but fluctuating increasing ratios of DIN/DIP (with an average value of 66) were found, which could be attributed to the higher mineralization and accumulation rate of N than P. In addition, increased DIN/DSi and decreased DSi/DIP ratios, indicating potential Si limitation, were observed especially in the middle and late stages. The variations in the nutrient stoichiometric ratios favored the shift in the dominant species that changed from diatoms to dinoflagellates. In addition, a gradually increasing proportion of dinoflagellates and decreasing proportion of diatoms corresponded well with the variations in N/P and N/Si ratios.

Regulation effects of MC on nutrients and the phytoplankton community

The intensive mariculture systems are under the threat of excessive organic loading and nutrient accumulation, which cause water quality problems and subsequent diseases (Hargreaves and Tucker, 2004; Santacruz-Reyes and Chien, 2010; Castillo-Soriano et al., 2013; Hu et al., 2014). Notably, the TAN threat can become pronounced in intensive culture systems when TAN is rapidly accumulated to concentrations beyond the safe level (Santacruz-Reyes and Chien, 2010). More importantly, it can trigger outbreaks of HABs and pose a serious threat to the aquaculture ecosystem (Huang et al., 2016; Brown et al., 2020). In this study, the initiative MC technology was adopted to regulate the nutrients and phytoplankton in the typical mariculture pond system. We observed that the nutrient contents of both organic and inorganic forms in the water column effectively decreased in most instances 24 h after the spray of MC (Figure 7). The TON and TOP contents could be reduced by up to 57% and 65%, respectively. While the TAN, NO_2^- and PO_4^{3-} concentrations could be reduced by up 32%, 45%, and 64%, respectively, in the MC-regulated pond. In contrast, both organic and inorganic forms in the water column of the control pond increased in most instances. Overall, the contents of these nutrients in the MC-regulated pond were lower than those in the control pond. It has been suggested that MC can reduce inorganic nutrients, especially phosphate, and organic nutrients through adsorption flocculation and chelation (Lu et al., 2015; Yu et al., 2017). In addition, MC could cause algal cells to flocculate and settle to the bottom layer, and the interaction of clay minerals with organic matter provides physical protection for organic matter (Hemingway et al., 2019). This protection could delay the microbial (Pinck and Allison, 1951) and oxidative (Eusterhues et al., 2003) decomposition processes of organic matter and reduce the mineralized regeneration of nutrients.

Furthermore, MC exerted a moderating effect on the phytoplankton biomass and community in the shrimp pond. In this study, the phytoplankton biomass was significantly higher and exhibited greater volatility in the control pond. In addition, HABs have occurred twice in the control pond, including an *H. akashiwo* bloom on September 2 with a density of 1.26×10^5 cells/mL (He et al., unpublished data). In contrast, the phytoplankton community in the MC-regulated pond was relatively stable in change and no HABs occurred during the study period. Based on the mean Bray-Curtis distances and molecular ecological network analysis of the community, (Ding et al. 2021) proposed that MC could enhance the resistance of phytoplankton ecological communities in cultured waters to environmental disturbance. Moreover, under the traditional condition, a high propensity for dinoflagellate blooms existed, influenced by the variation in the

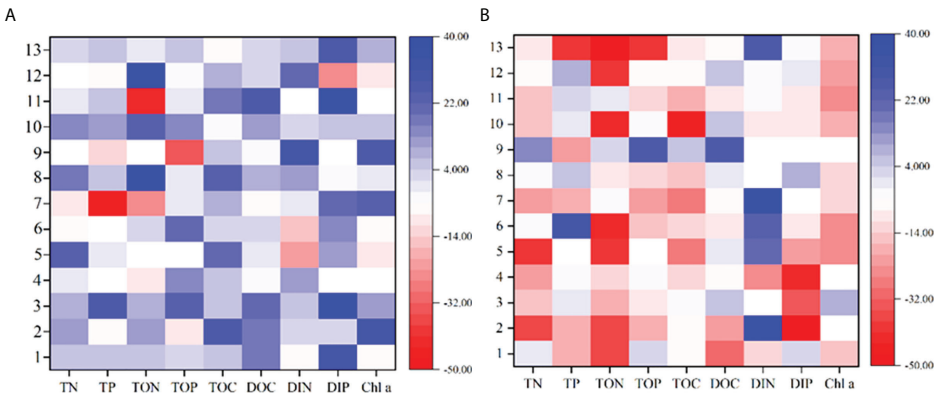

FIGURE 7
Changes in nutrients and Chl *a* in **(A)** the MC-regulated pond before and after spraying of MC and the comparison with **(B)** the control pond.

composition and structure of nutrients, and posed a potential risk to the growth of shrimp. This result could be verified by the variation in the dominant species of phytoplankton that changed from diatoms to dinoflagellates in the control pond. Compared with the control pond, the percentage of dinoflagellates in the MC-regulated pond was maintained at a lower level, and the percentage of green algae was higher, with *Nannochloris* being the dominant species. As an aquatic bait algae species, *Nannochloris* can improve the survival and production rate of fish and shrimp to some extent, which is important to maintain the stability of the ecosystem (Alonso-Rodrıguez and Páez-Osuna, 2003; Davidson et al., 2009). MC can directly dispose of HAB organisms through flocculation; additionally, they can induce the programmed mortality of red tide organisms through oxidative stress and other effects, thus controlling HABs (Yu et al., 2017). On the one hand, the *Nannochloris* could occupy a favorable ecological niche and became dominant after the removal of targeted dinoflagellates in the MC-regulated pond. On the other hand, the MC increased the N/P ratio and favored the *Nannochloris*, which has a higher average optimal nitrogen to phosphorus ratio than dinoflagellates (Hillebrand et al., 2013).

Conclusion

This research studied the dynamic variations in nutrients and phytoplankton of intensive mariculture systems and explored the effects of MC. The intensive culture of *Litopenaeus vannamei* caused a temporal significant increase in nutrients, especially in the organic forms. In addition, concurrently with ascending N/P ratio and decreasing Si/N and Si/P ratios, a marked increase in the biomass and ratios of dinoflagellates to diatoms abundance were also observed, which pose a potential threat to the mariculture organism. The MC reduced the contents of nutrients in both organic and inorganic forms, and improved the water quality. Moreover, MC effectively removed the dinoflagellates and contribute to the dominance of *Nannochloris*, which improved the stability of the phytoplankton community. This study provide new insights into an effective regulation treatment for managing water quality and maintaining sustainable mariculture development.

Data availability statement

The original contributions presented in the study are included in the article/Supplementary Material. Further inquiries can be directed to the corresponding author.

Author contributions

LC: writing – original draft and investigation. YD: writing – review & editing and formal analysis. LH: writing – review & editing and data curation. ZW: writing – review & editing and data curation. YY: writing – review & editing and investigation. XC: writing – review & editing and formal analysis. XS: writing – review & editing. ZY: writing – review & editing and supervision. All authors contributed to the article and approved the submitted version.

Acknowledgments

We would like to thank the research group for their assistance with data acquisition during the experiments. Additionally, we are grateful to the reviewers for their constructive comments and suggestions. This study was supported by the “Strategic Priority Research Program” of the Chinese Academy of Sciences (Grants No. XDA19060203), the “Key Research Program of the Center for Ocean Mega-Science, Chinese Academy of Sciences (Grants No. COMS2020J02)”, and the National Natural Science Foundation of China (Grants No. 42006119).

Conflict of interest

The authors declare that the research was conducted in the absence of any commercial or financial relationships that could be construed as a potential conflict of interest.

Publisher's note

All claims expressed in this article are solely those of the authors and do not necessarily represent those of their affiliated organizations, or those of the publisher, the editors and the reviewers. Any product that may be evaluated in this article, or claim that may be made by its manufacturer, is not guaranteed or endorsed by the publisher.

Supplementary material

The Supplementary Material for this article can be found online at: https://www.frontiersin.org/articles/10.3389/fmars.2022.976353/full#supplementary-material

References

Alonso-Rodrıguez, R., and Páez-Osuna, F. (2003). Nutrients, phytoplankton and harmful algal blooms in shrimp ponds: a review with special reference to the situation in the gulf of California. *Aquaculture.* 219 (1-4), 317–336. doi: 10.1016/S0044-8486(02)00509-4

Altman, J. C., and Paerl, H. W. (2012). Composition of inorganic and organic nutrient sources influences phytoplankton community structure in the new river estuary, north Carolina. *Aquat. Ecol.* 46 (3), 269–282. doi: 10.1007/s10452-012-9398-8

Anderson, D. M. (2012). HABs in a changing world: a perspective on harmful algal blooms, their impacts, and research and management in a dynamic era of climactic and environmental change. *Harmful Algae.* 2012 (3), 17.

Berg, G. M., Balode, M., Purina, I., Bekere, S., Béchemin, C., and Maestrini, S. Y. (2003). Plankton community composition in relation to availability and uptake of oxidized and reduced nitrogen. *Aquat. Microb. Ecol.* 30 (3), 263–274. doi: 10.3354/ame030263

Bouwman, L., Beusen, A., Glibert, P. M., Overbeek, C., Pawlowski, M., and Herrera, J. (2013). Mariculture: significant and expanding cause of coastal nutrient enrichment. *Environ. Res. Lett.* 8 (4), 044026. doi: 10.1088/1748-9326/8/4/044026

Briggs, R. M., and Funge-Smith, S. J. (1994). A nutrient budget of some intensive marine shrimp ponds in Thailand. *Aquac. Reaearch.* 25 (8), 789–811. doi: 10.1111/j.1365-2109.1994.tb00744.x

Brown, A. R., Lilley, M., Shutler, J., Lowe, C., Artioli, Y., Torres, R., et al. (2020). Assessing risks and mitigating impacts of harmful algal blooms on mariculture and marine fisheries. *Rev. Aquac.* 12 (3), 1663–1688. doi: 10.1111/raq.12403

Campbell, B., and Pauly, D. (2013). Mariculture: A global analysis of production trends since 1950. *Mar. Pol.* 39, 94–100. doi: 10.1016/j.marpol.2012.10.009

Cao, L., Wang, W. M., Yang, Y., Yang, C. T., Yuan, Z. H., Xiong, S. B., et al. (2017). Environmental impact of aquaculture and countermeasures to aquaculture pollution in China. *Environ. Sci. pollut. Res. Int.* 14 (7), 452–462.

Cardoso-Mohedano, J. G., Páez-Osuna, F., Amezcua-Martínez, F., Ruiz-Fernández, A. C., Ramírez-Reséndiz, G., and Sanchez-Cabeza, J. A. (2016). Combined environmental stress from shrimp farm and dredging releases in a subtropical coastal lagoon (SE gulf of California). *Mar. pollut. Bull.* 104 (1-2), 83–91. doi: 10.1016/j.marpolbul.2016.02.008

Casé, M., Leça, E. E., Leitao, S. N., Sant, E. E., Schwamborn, R., and de Moraes Junior, A. T. (2008). Plankton community as an indicator of water quality in tropical shrimp culture ponds. *Mar. pollut. Bull.* 56 (7), 1343–1352. doi: 10.1016/j.marpolbul.2008.02.008

Castillo-Soriano, F. A., Ibarra-Junquera, V., Escalante-Minakata, P., Mendoza-Cano, O., Ornelas-Paz, J. C., Almanza-Ramírez, J. C., et al. (2013). Nitrogen dynamics model in zero water exchange, low salinity intensive ponds of white shrimp, litopenaeus vannamei, at colima, Mexico. *Lat. Am. J. Aquat. Res.* 41 (1), 68–79. doi: 10.3856/vol41-issue1-fulltext-5

Collos, Y., Jauzein, C., Ratmaya, W., Souchu, P., Abadie, E., and Vaquer, A. (2014). Comparing diatom and alexandrium catenella/tamarense blooms in thau lagoon: Importance of dissolved organic nitrogen in seasonally n-limited systems. *Harmful Algae.* 37, 84–91. doi: 10.1016/j.hal.2014.05.008

Couch, J. A. (1998). *Characterization of water quality and a partial nutrient budget for experimental shrimp ponds in Alabama* (Alabama, United States: Auburn University).

Danielsson, Å., Papush, L., and Rahm, L. (2008). Alterations in nutrient limitations — scenarios of a changing Baltic Sea. *J. Mar. Syst.* 73 (3-4), 263–283. doi: 10.1016/j.jmarsys.2007.10.015

Davidson, K., Gowen, R. J., Tett, P., Bresnan, E., Harrison, P. J., McKinney., A., et al. (2012). Harmful algal blooms: how strong is the evidence that nutrient ratios and forms influence their occurrence? *Estua. Coast. Shelf. Sci.* 115, 399–413. doi: 10.1016/j.ecss.2012.09.019

Davidson, K., Miller, P., Wilding, T. A., Shutler, J., Bresnan, E., Kennington, K., et al. (2009). And prolonged bloom of karenia mikimotoi in Scottish waters in 2006. *Harmful algae.* 8 (2), 349–361. doi: 10.1016/j.hal.2008.07.007

Demirak, A., Balci, A., and Tüfekci, M. (2006). Environmental impact of the marine aquiculture in güllük bay, Turkey. *Environ. Monit. Assess.* 123 (1), 1–12.

Díaz, P. A., Álvarez, G., Varela, D., Pérez-Santos, I., Díaz, M., Molinet, C., et al. (2019). Impacts of harmful algal blooms on the aquaculture industry: Chile as a case study. *Perspect. Phycol.* 6 (1-2), 39–50. doi: 10.1127/pip/2019/0081

Ding, Y., Song, X., Cao, X., He, L., Liu, S., and Yu, Z. (2021). Healthier communities of phytoplankton and bacteria achieved via the application of modified clay in shrimp aquaculture ponds. *Int. J. Environ. Res. Public Health.* 18 (21), 11569. doi: 10.3390/ijerph182111569

Dyhrman, S. T., and Anderson, D. M. (2003). Urease activity in cultures and field populations of the toxic dinoflagellate alexandrium. *Limnol. Oceanogr.* 48 (2), 647–655. doi: 10.4319/lo.2003.48.2.0647

Eusterhues, K., Rumpel, C., Kleber, M., and Kögel-Knabner, I. (2003). Stabilisation of soil organic matter by interactions with minerals as revealed by mineral dissolution and oxidative degradation. *Org. Geochem.* 34 (12), 1591–1600. doi: 10.1016/j.orggeochem.2003.08.007

Fan, C., Glibert, P. M., and Burkholder, J. M. (2003). Characterization of the affinity for nitrogen, uptake kinetics, and environmental relationships for prorocentrum minimum in natural blooms and laboratory cultures. *Harmful Algae.* 2 (4), 283–299. doi: 10.1016/S1568-9883(03)00047-7

FAO and (Food and Agriculture Organization of the United Nations) (2022). *The state of world fisheries and aquiculture (SOFIA).* Rome, Italy.

Froehlich, H. E., Gentry, R. R., and Halpern, B. S. (2018). Global change in marine aquaculture production potential under climate change. *Nat. Ecol. Evol.* 2 (11), 1745–1750. doi: 10.1038/s41559-018-0669-1

Gao, Y. H., Yu, Z. M., Song, X. X., and Cao, X. H. (2007). Impact of modified clays on the infant oyster (Crassostrea gigas). *Mar. Sci. Bull.* 26 (3), 53–60. doi: 10.1002/cem.1038

Glibert, P. M. (2016). Margalef revisited: A new phytoplankton mandala incorporating twelve dimensions, including nutritional physiology. *Harmful Algae.* 55, 25–30. doi: 10.1016/j.hal.2016.01.008

Glibert, P. M., and Burford, M. A. (2017). Globally changing nutrient loads and harmful algal blooms: recent advances, new paradigms, and continuing challenges. *Oceanography.* 30 (1), 58–69. doi: 10.5670/oceanog.2017.110

Glibert, P. M., Burkholder, J. M., and Kana, T. M. (2012). Recent insights about relationships between nutrient availability, forms, and stoichiometry, and the distribution, ecophysiology, and food web effects of pelagic and benthic prorocentrum species. *Harmful Algae.* 14, 231–259. doi: 10.1016/j.hal.2011.10.023

Glibert, P. M., and Terlizzi, D. E. (1999). Cooccurrence of elevated urea levels and dinoflagellate blooms in temperate estuarine aquaculture ponds. *Appl. Environ. Microbiol.* 65 (12), 5594–5596. doi: 10.1128/AEM.65.12.5594-5596.1999

Gobler, C. J., Berry, D. L., Dyhrman, S. T., Wilhelm, S. W., Salamov, A., Lobanov, A. V., et al. (2011). Niche of harmful alga aureococcus anophagefferens revealed through ecogenomics. *Proc. Natl. Acad. Sci. U.S.A.* 108 (11), 4352–4357. doi: 10.1073/pnas.1016106108

Goldman, J. C., and Glibert, P. M. (1983). Kinetics of inorganic nitrogen uptake by phytoplankton. *Nitrogen Mar. Environ*, 233–274. doi: 10.1016/B978-0-12-160280-2.50015-8

Griffiths, J. R., Hajdu, S., Downing, A. S., Hjerne, O., Larsson, U., and Winder, M. (2016). Phytoplankton community interactions and environmental sensitivity in coastal and offshore habitats. *Oikos* 125 (8), 1134–1143. doi: 10.1111/oik.02405

Hagström, J. A., and Granéli, E. (2005). Removal of prymnesium parvum (Haptophyceae) cells under different nutrient conditions by clay. *Harmful algae.* 4 (2), 249–260. doi: 10.1016/j.hal.2004.03.004

Han, Q. F., Song, C., Sun, X., Zhao, S., and Wang, S. G. (2021). Spatiotemporal distribution, source apportionment and combined pollution of antibiotics in natural waters adjacent to mariculture areas in the laizhou bay, bohai Sea. *Chemosphere.* 279, 130381. doi: 10.1016/j.chemosphere.2021.130381

Hargreaves, J. A., and Tucker, C. S. (2004). *Managing ammonia in fish ponds* Vol. 4603 (South Carolina, USA: Southern Regional Aquaculture Center Stoneville).

Hemingway, J. D., Rothman, D. H., Grant, K. E., Rosengard, S. Z., and Galy, V. V. (2019). Mineral protection regulates long-term global preservation of natural organic carbon. *Nature.* 570 (7760), 228–231. doi: 10.1038/s41586-019-1280-6

Herbeck, L. S., Unger, D., Wu, Y., and Jennerjahn, T. C. (2013). Effluent, nutrient and organic matter export from shrimp and fish ponds causing eutrophication in coastal and backreef waters of NE hainan, tropical China. *Cont. Shelf Res.* 57, 92–104. doi: 10.1016/j.csr.2012.05.006

Hillebrand, H., Steinert, G., Boersma, M., Malzahn, A., Meunier, C. L., Plum, C., et al. (2013). Goldman Revisited: Faster-growing phytoplankton has lower n: P and lower stoichiometric flexibility. *Limnol. Oceanogr.* 58 (6), 2076–2088. doi: 10.4319/lo.2013.58.6.2076

Huang, S. L., Wu, M., Zang, C. J., Du, S. L., Domagalski, J., Gajewska, M., et al. (2016). Dynamics of algae growth and nutrients in experimental enclosures culturing bighead carp and common carp: Phosphorus dynamics. *Int. J. Sediment Res.* 31 (2), 173–180. doi: 10.1016/j.ijsrc.2016.01.003

Hu, Z., Lee, J. W., Chandran, K., Kim, S., Sharma, K., and Khanal, S. K. (2014). Influence of carbohydrate addition on nitrogen transformations and greenhouse gas emissions of intensive aquaculture system. *Sci. Total Environ.* 470, 193–200. doi: 10.1016/j.scitotenv.2013.09.050

Johansson, N., and Granéli, E. (1999). Influence of different nutrient conditions on cell density, chemical composition and toxicity of prymnesium parvum (Haptophyta) in semi-continuous cultures. *J. Exp. Mar. Biol. Ecol.* 239 (2), 243–258. doi: 10.1016/S0022-0981(99)00048-9

Justić, D., Rabalais, N. N., Turner, R. E., and Dortch, Q. (1995). Changes in nutrient structure of river-dominated coastal waters: stoichiometric nutrient balance and its consequences. *Estuarine Coastal Shelf Sci.* 40 (3), 339–356.

Kamp, A., Hogslund, S., Risgaard-Petersen, N., and Stief, P. (2015). Nitrate storage and dissimilatory nitrate reduction by eukaryotic microbes. *Front. Microbiol.* 6, 1492. doi: 10.3389/fmicb.2015.01492

Lønborg, C., and Álvarez-Salgado, X. A. (2012). Recycling versus export of bioavailable dissolved organic matter in the coastal ocean and efficiency of the continental shelf pump. *Glob. Biogeochem. Cycle* 26 (3), 1–12 doi: 10.1029/2012gb004353

Lacerda, L. D., Molisani, M. M., Sena, D., and Maia, L. P. (2008). Estimating the importance of natural and anthropogenic sources on n and p emission to estuaries along the ceará state coast NE Brazil. *Environ. Monit. Assess.* 141 (1), 149–164. doi: 10.1007/s10661-007-9884-y

Lai, S. Y. (2014). *The ecological aquaculture technique of prawn* (Beijing (in Chinese with English abstract: China Agriculture Press).

Lepš, J., and Šmilauer, P. (2003). *Multivariate analysis of ecological data using CANOCO* (Cambridge, England: Cambridge University Press).

Li, H. M., Li, X. M., Li, Q., Liu, Y., Song, J. D., and Zhang, Y. Y. (2017). Environmental response to long-term mariculture activities in the weihai coastal area, China. *Sci. Total Environ.* 601, 22–31. doi: 10.1016/j.scitotenv.2017.05.167

Li, J., Song, X. X., Zhang, Y., Xu, X. X., and Yu, Z. M. (2019). Effect of modified clay on the transition of paralytic shellfish toxins within the bay scallop argopecten irradians and sediments in laboratory trials. *Aquaculture.* 505, 112–117. doi: 10.1016/j.aquaculture.2019.02.038

Li, H. M., Tang, H. J., Shi, X. Y., Zhang, C. S., and Wang, X. L. (2014). Increased nutrient loads from the changjiang (Yangtze) river have led to increased harmful algal blooms. *Harmful Algae.* 39, 92–101. doi: 10.1016/j.hal.2014.07.002

Liu, D., Keesing, J. K., He, P. M., Wang, Z. L., Shi, Y. J., Wang, Y. J., et al. (2013). The world's largest macroalgal bloom in the yellow Sea, China: formation and implications. *Estuar* 129, 2–10 doi: 10.1016/j.ecss.2013.05.021

Lomas, M. W., and Glibert, P. M. (1999). Temperature regulation of nitrate uptake: A novel hypothesis about nitrate uptake and reduction in cool-water diatoms. *Limnol. Oceanogr.* 44 (3), 556–572. doi: 10.4319/lo.1999.44.3.0556

Lomas, M. W., Trice., T., Glibert, P. M., Bronk, D. A., and McCarthy, J. J. (2002). Temporal and spatial dynamics of urea uptake and regeneration rates and concentrations in Chesapeake bay. *Estuaries.* 25 (3), 469–482. doi: 10.1007/BF02695988

Lou, X., and Hu, C. (2014). Diurnal changes of a harmful algal bloom in the East China Sea: Observations from GOCI. *Remote Sens. Environ.* 140, 562–572. doi: 10.1016/j.rse.2013.09.031

Lu, G. Y., Song, X. X., Yu, Z. M., and Cao, X. H. (2017). Application of PAC-modified kaolin to mitigate prorocentrum donghaiense: effects on cell removal and phosphorus cycling in a laboratory setting. *J. Appl. Phycol.* 29 (2), 917–928. doi: 10.1007/s10811-016-0992-3

Lu, G. Y., Song, X. X., Yu, Z. M., Cao, X. H., and Yuan, Y. Q. (2015). Effects of modified clay flocculation on major nutrients and diatom aggregation during skeletonema costatum blooms in the laboratory. *Chin. J. Oceanol. Limnol.* 33 (4), 1007–1019. doi: 10.1007/s00343-015-4162-2

Matsuyama, Y., and Shumway, S. (2009). Impacts of harmful algal blooms on shellfisheries aquaculture. *New Technol. Aquac. Elsevier* 2009, 580–609. doi: 10.1533/9781845696474.3.580

McCarthy, J. J. (1972). The uptake of urea by natural populations of marine phytoplankton. *Limnol. Oceanogr.* 17 (5), 738–748. doi: 10.4319/lo.1972.17.5.0738

Meng, W., and Feagin, R. A. (2019). Mariculture is a double-edged sword in China. *Estua. Coast. Shelf. Sci.* 222, 147–150. doi: 10.1016/j.ecss.2019.04.018

Ministry of Agriculture and Rural Affairs of the People's Republic of China. (2020). *The China fishery statistical yearbook of 2019.* Beijing,China.

Miranda, A., Voltolina, D., Frías-Espericueta, M. G., Izaguirre-Fierro, G., and Rivas-Vega, M. E. (2009). Budget and discharges of nutrients to the gulf of California of a semiintensive shrimp farm (NW Mexico). *Hidrobiológica* 19 (1), 43–48.

Paerl, H. W. (2006). Assessing and managing nutrient-enhanced eutrophication in estuarine and coastal waters: Interactive effects of human and climatic perturbations. *Ecol. Eng.* 26 (1), 40–54. doi: 10.1016/j.ecoleng.2005.09.006

Páez-Osuna, F., Álvarez-Borrego, S., Ruiz-Fernández, A. C., García-Hernández, J., Jara-Marini, M. E., Bergés-Tiznado, M. E., et al. (2017). Environmental status of the gulf of California: a pollution review. *Earth-Sci. Rev.* 166, 181–205. doi: 10.1016/j.earscirev.2017.01.014

Páez-Osuna, F., Guerrero-Galván, S., Ruiz-Fernández, A., and Espinoza-Angulo, R. (1997). Fluxes and mass balances of nutrients in a semi-intensive shrimp farm in north-western Mexico. *Mar. pollut. Bull.* 34 (5), 290–297. doi: 10.1016/S0025-326X(96)00133-6

Páez-Osuna, F., Piñón-Gimate, A., Ochoa-Izaguirre, M., Ruiz-Fernández, A., Ramírez-Reséndiz, G., and Alonso-Rodríguez, R. (2013). Dominance patterns in macroalgal and phytoplankton biomass under different nutrient loads in subtropical coastal lagoons of the SE gulf of California. *Mar. pollut. Bull.* 77 (1-2), 274–281. doi: 10.1016/j.marpolbul.2013.09.048

Peñuelas, J., Sardans, J., Rivas-ubach, A., and Janssens, I. A. (2012). The human-induced imbalance between c, n and p in earth's life system. *Glob. Change Biol.* 18 (1), 3–6 doi: 10.1111/j.1365-2486.2011.02568.x

Pinck, L., and Allison, F. (1951). Resistance of a protein-montmorillonite complex to decomposition by soil microorganisms. *Science.* 114 (2953), 130–131 doi: 10.1126/science.114.2953.130

Ray, A. J., Dillon, K. S., and Lotz, J. M. (2011). Water quality dynamics and shrimp (Litopenaeus vannamei) production in intensive, mesohaline culture systems with two levels of biofloc management. *Aquac. Eng.* 45 (3), 127–136. doi: 10.1016/j.aquaeng.2011.09.001

Santacruz-Reyes, R. A., and Chien, Y. H. (2010). Yucca schidigera extract–a bioresource for the reduction of ammonia from mariculture. *Bioresour. Technol.* 101 (14), 5652–5657. doi: 10.1016/j.biortech.2010.01.127

Shumway, S. E., Barter, J., and Sherman-Caswell, S. (1990). Auditing the impact of toxic algal blooms on oysters. *Environ. Auditor.* 2 (1), 41–56.

SOA (State Oceanic Administration). (2017). *Bulletin of China marine environment status in 2016.* Beijing China

Song, X. X., Zhang, Y., and Yu, Z. M. (2021). An eco-environmental assessment of harmful algal bloom mitigation using modified clay. *Harmful Algae.* 107, 102067. doi: 10.1016/j.hal.2021.102067

Sutton, M. A., Bleeker, A., Howard, C., Erisman, J., Abrol, Y., Bekunda, M., et al (2013). Our nutrient world. the challenge to produce more food & energy with less pollution. *Centre Ecol. Hydrology.*

Wang, J., and Cao, J. (2012). Variation and effect of nutrient on phytoplankton community in changjiang estuary during last 50 years. *Mar. Environ. science.* 31 (6), 310–315. doi: 10.1007/s11783-011-0280-z

Wang, J. N., Yan, W. J., Chen, N. W., Li, X. Y., and Liu, L. S. (2015). Modeled long-term changes of DIN: DIP ratio in the changjiang river in relation to chl-α and DO concentrations in adjacent estuary. *Estuar. Coast. Shelf Sci.* 166, 153–160. doi: 10.1016/j.ecss.2014.11.028

Yang, P., Lai, D. Y., Jin, B., Bastviken, D., Tan, L. S., and Tong, C. (2017). Dynamics of dissolved nutrients in the aquaculture shrimp ponds of the Min river estuary, China: Concentrations, fluxes and environmental loads. *Sci. Total Environ.* 603, 256–267. doi: 10.1016/j.scitotenv.2017.06.074

Yu, Z. M., Song, X. X., Cao, X., and Liu, Y. (2017). Mitigation of harmful algal blooms using modified clays: Theory, mechanisms, and applications. *Harmful Algae.* 69, 48–64. doi: 10.1016/j.hal.2017.09.004

Zhang, Y., Song, X. X., Yu, Z. M., Zhang, P. P., Cao, X. H., and Yuan, Y. Q. (2019). Impact assessment of modified clay on embryo-larval stages of turbot scophthalmus maximus. *L. J. Oceanol. Limnol.* 37, 1051–1061. doi: 10.1007/s00343-019-8043-y

frontiers | Frontiers in Microbiology

TYPE Original Research
PUBLISHED 26 August 2022
DOI 10.3389/fmicb.2022.942205

OPEN ACCESS

EDITED BY
Zhangxi Hu,
Guangdong Ocean University, China

REVIEWED BY
Renhui Li,
Wenzhou University, China
Chandramali Jayawardana,
Sabaragamuwa University, Sri Lanka

*CORRESPONDENCE
Xinxin Lu
luxinxinchina@163.com
Yawen Fan
fanyaw_hrbnu@163.com

†These authors have contributed equally to this work

SPECIALTY SECTION
This article was submitted to Aquatic Microbiology, a section of the journal Frontiers in Microbiology

RECEIVED 12 May 2022
ACCEPTED 08 August 2022
PUBLISHED 26 August 2022

CITATION
Li Z, Ma C, Sun Y, Lu X and Fan Y (2022) Ecological health evaluation of rivers based on phytoplankton biological integrity index and water quality index on the impact of anthropogenic pollution: A case of Ashi River Basin. *Front. Microbiol.* 13:942205. doi: 10.3389/fmicb.2022.942205

Ecological health evaluation of rivers based on phytoplankton biological integrity index and water quality index on the impact of anthropogenic pollution: A case of Ashi River Basin

Zhenxiang Li[1†], Chao Ma[1†], Yinan Sun[1], Xinxin Lu[1,2*] and Yawen Fan[1,2*]

[1]College of Life Science and Technology, Harbin Normal University, Harbin, China, [2]Key Laboratory of Biodiversity of Aquatic Organisms, Harbin Normal University, Harbin, China

Based on the phytoplankton community matrices in the Ashi River Basin (ASRB), Harbin city, we developed an evaluation method using the phytoplankton index of biotic integrity (P-IBI) to evaluate ecological health while investigating the response of P-IBI to anthropogenic activities. We compared the effectiveness of P-IBI with that of the water quality index (WQI) in assessing ecological health. Between April and October 2019, phytoplankton and water samples were collected at 17 sampling sites in the ASRB on a seasonal basis. Our results showed that seven phyla were identified, comprising 137 phytoplankton species. From a pool of 35 candidate indices, five critical ecological indices (Shannon–Wiener index, total biomass, percentage of motile diatoms, percentage of stipitate diatom, and diatom quotient) were selected to evaluate the biological integrity of phytoplankton in the ASRB. The ecological status of the ASRB as measured by the P-IBI and WQI exhibited a similar spatial pattern. It showed a spatial decline in ecological status in accordance with the flow of the river. These results highlighted that P-IBI was a reliable tool to indicate the interaction between habitat conditions and environmental factors in the ASRB. Our findings contribute to the ecological monitoring and protection of rivers impacted by anthropogenic pollution.

KEYWORDS

phytoplankton biological integrity index, water quality index, Ashi River Basin, anthropogenic activity, water pollution

Introduction

In recent years, the water pollution caused by anthropogenic sewage discharges, agricultural runoff, and industrial wastewater discharges has adversely impacted the health of aquatic ecosystems in numerous rivers and lakes (Griffiths et al., 2018; Xu et al., 2018). The current methods for assessing the health of the aquatic ecosystem are mainly based on water quality indicators and aquatic organisms. These include the water quality index (WQI; De La Mora-Orozco et al., 2017), biological integrity index (IBI; Wu et al., 2019), and species diversity index (SDI; Meng et al., 2020). A healthy aquatic ecosystem must have high-quality biological integrity before it can be sustainably used and developed (Scanlon et al., 2007).

Biological integrity refers to the ability of a biotic community to maintain structural equilibrium and adapt to environmental changes (Souza and Vianna, 2020). Karr (1981) assessed the ecological conditions of aquatic groups based on 12 attributes linked to the species composition and ecological structure of fish communities. This was the initial approach for assessing biological integrity, and it has been expanded and modified on an ongoing basis (Cui et al., 2018). Assessing biological integrity is a crucial method for assessing the status of ecosystems, and biological integrity indices (IBIs) play a key role in global water resource management (Zhu et al., 2019). Current research on IBIs mainly focuses on fish (Cooper et al., 2018), macroinvertebrates (Wahl et al., 2019), plankton (Zhang et al., 2019), and bacteria (Li et al., 2017, 2018). These aquatic biological community structures are important markers of water pollution and eutrophication; therefore, they are often used to evaluate the damage to and health of aquatic ecosystems (Pereira et al., 2018). Phytoplankton rapidly respond to environmental changes, and their community structure accurately reflects the short-term effects of anthropogenic and natural disturbances on aquatic ecosystems (Busseni et al., 2019). The composition, abundance, biomass, and community stability of phytoplankton are widely used as important indicators of environmental change (Marvaetal et al., 2014). The discharge of pollutants decreases phytoplankton diversity and community structure stability in rivers. In addition, it substantially impacts the biological integrity of phytoplankton and the ecological service functions of river ecosystems (Inyang and Wang, 2020; Hu et al., 2022). Phytoplankton, functioning as producers in the biological chain, are the most sensitive to changes in the river environment; therefore, they are widely used to evaluate changes in aquatic ecology (Amorim and Moura, 2021). The phytoplankton biological integrity index (P-IBI) has received less attention than other IBIs based on fish and macroinvertebrates. Although it has been used to assess river ecosystems in recent years, few studies have focused on its application to assess the impact of anthropogenic activities on river ecosystems (Lin et al., 2021; Wan et al., 2021). Therefore, it is necessary to conduct further research on the potential of phytoplankton to assess the impact of anthropogenic activities on the biological integrity of river ecosystems.

In recent years, rivers in Heilongjiang Province have been polluted to varying degrees owing to the acceleration of industrialization and urbanization, with the Songhua River Basin being heavily polluted. The Ashi River is the main tributary to the southern bank of the Songhua River. The reserve water supply for Harbin is sourced from the Xiquanyan Reservoir upstream of the Ashi River. In recent years, water pollution in the basin has become an increasingly serious concern in light of the steady expansion of the regional economy and grain production. During the wet season, a large quantity of pesticides and fertilizer residues enters the Ashi river combined with surface runoff from the extensive farmland in the middle reaches of the Ashi River Basin (ASRB) (Chen et al., 2022). The region downstream of the ASRB is densely populated, with land use dominated by cities and towns that are severely impacted by anthropogenic activities. There are several small and medium-sized enterprises in the area, and industrial effluent discharge is typically the primary source of pollution (Zhao et al., 2020b). The water quality of the Songhua River, the critical control river of the Harbin region, is gravely threatened by the deterioration of the water quality of the Ashi River, which has destroyed the ecological balance.

In this study, we established a P-IBI method to assess the health status of the ASRB aquatic ecosystem. The main purposes of this study were as follows: (1) to establish the P-IBI of the ASRB under the influence of anthropogenic activities and (2) to effectively explain the water quality and temporal and spatial distribution patterns of the ASRB. In addition, to evaluate the performance of P-IBI, we compared P-IBI evaluation results with those of a water quality index (WQI). We hypothesize that the P-IBI assessment standard can effectively represent the water quality status of the ASRB and is consistent with the performance of the WQI assessment standard. Therefore, we also aim (3) to reveal the relationship between P-IBI and environmental factors. Our research is beneficial to local water resource management, including the formulation of associated control policies, and it makes specific contributions to the development of P-IBIs.

Materials and methods

Study sites

The Ashi River is a primary tributary to the Songhua River on its right bank. It is situated only 80 km from Harbin city. The study area was located between 126°43′ and 127°36′ E longitude and 45°08′ and 45°50′ N latitude (a total distance of 213 km) (**Figure 1** and **Supplementary Table 1**).

The Xiquanyan Reservoir is a connected reservoir upstream of the main ASRB. The climate is characterized by a temperate continental monsoon, with subfreezing temperatures from November to April. The annual precipitation in the basin is 580–600 mm, and the annual average temperature is 3.6°C. In this study, 17 sampling sites were selected along the main channel of the river. Samples were collected every 3 months from April to October 2019 to represent the spring, summer, and autumn seasons. We were unable to collect all samples at certain sites owing to heavy precipitation in the spring and summer.

Water sampling and processing

At each sampling site, surface water samples (0–0.5 m) were collected and subjected to phytoplankton and physicochemical analyses in triplicate. Phytoplankton samples were collected in glass bottles (1 L), immediately fixed with 3% acid-Lugol's solution, and stored in a dark room at 20°C until further processing. Water temperature (WT), dissolved oxygen (DO), conductivity (Cond.), pH, and turbidity (Tur.) were recorded using a multi-parameter water quality analyser (YSI ProPlus, YSI, United States). Total phosphorus (TP, GB/T11893-89), total nitrogen (TN, HJ 636-2012), chemical oxygen demand (COD_{Mn}, GB/T11892-89), and biochemical oxygen demand (BOD_5, HJ 50-2009) were the environmental factors analyzed in the laboratory.

Plankton identification

Phytoplankton were examined at ×400 magnification (× 10 eyepiece and × 40 objective) using an Olympus microscope (Optec B302, Chongqing, China) with a 0.1 mL plankton counting chamber (Yuan et al., 2018). Most phytoplankton samples were identified at the species level, and their abundance was expressed as ind. L^{-1}. The publication "Freshwater algae in China: systems, classification and ecology" (Hu and Wei, 2006) was used to identify phytoplankton.

Establishing the phytoplankton index of biotic integrity assessment system

In accordance with previous studies (Lacouture et al., 2006), the steps to establish an IBI system are as follows:

Determination of reference and impaired points

In this study, the WQI was used in conjunction with the results of an *in situ* investigation, and sampling sites were divided into two groups, namely, reference and impaired points. The points were evaluated using the WQI method (Pesce and Wunderlin, 2000; Kannel et al., 2007; Koçer and Sevgili, 2014; Sun et al., 2016). The equation used for calculating WQI was as follows:

$$WQI = \frac{\sum_{i=1}^{n} C_i P_i}{\sum_{i=1}^{n} P_i} \quad (1)$$

where n is the total number of parameters included in the study, C_i is the normalized value of parameter i, and P_i is the weight of parameter i. The minimum value of P_i was 1, and the maximum weight assigned to parameters that affect water quality was 4; these values have been verified in previous publications (**Supplementary Table 2**; Pesce and Wunderlin, 2000; Kannel et al., 2007; Koçer and Sevgili, 2014; Sun et al., 2016). The WQI ranged from 0 to 100, with high values indicating good water quality. Based on the WQI scores, water quality was categorized into five grades as follows: excellent (91–100), good (71–90), moderate (51–70), low (26–50), and bad (0–25) (Wu et al., 2019). The seasonal WQI values of each sampling site were averaged to determine the final WQI value.

Since there are numerous villages and agricultural land along the ASRB and many factories in its middle and lower reaches, it is difficult to obtain a clean water reference point for the development of a P-IBI unaffected by anthropogenic activities (Stoddard et al., 2006). Such a point should adhere to four conditions: (1) a good or excellent annual average WQI index evaluation grade; (2) high vegetation coverage, no overdevelopment of the shoreline, no sand fields, no wharf, and no random reclamation on the bank slopes; (3) no garbage stacking on the bank slope, no garbage floating on the water surface, no peculiar odor, and a relatively clear water body; and (4) a good phytoplankton diversity and phytoplankton abundance at less than 2×10^6 ind./L (Li et al., 2014, 2020).

Biological indicators screening

The biological indicators for establishing IBI need to be followed by the distribution range, discriminant ability, and correlation tests, and the remaining indicators were used to construct the IBI assessment system (Lacouture et al., 2006). To perform the distribution range test, it was necessary to calculate the values of candidate biological indicators based on the data at the reference and impaired points. Then, the responses of the candidate biological indicators to anthropogenic disturbances were analyzed to identify those that increased or decreased unidirectionally. The discrimination ability test initially screened strong ability indicators by evaluating the extent of boxplot overlap between the reference and impaired points. In cases where the correlation coefficients between a pair of indicators in Spearman's correlation analysis show $|r| > 0.75$, one of the indicators should be omitted to avoid redundancy (Maxted et al., 2006).

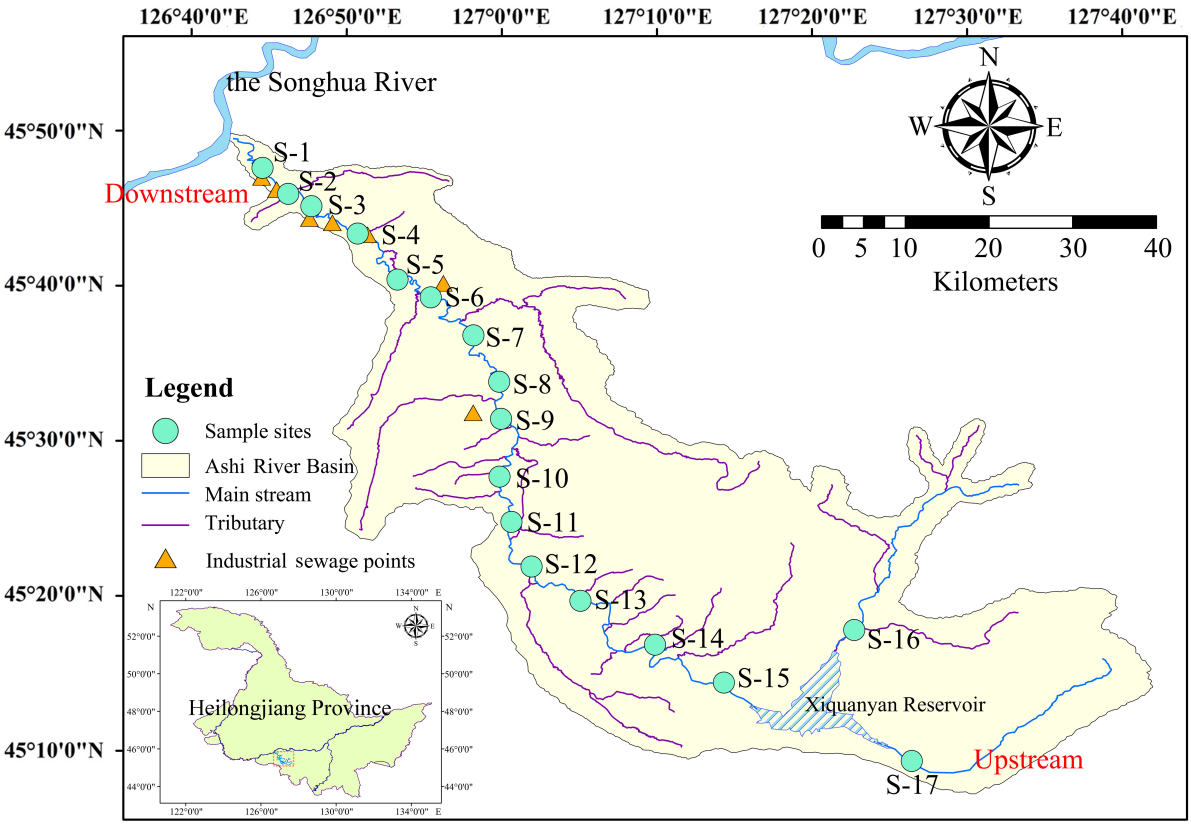

FIGURE 1
Map of the Ashi River Basin (ASRB) illustrating the sampling sites for this study.

Index of biotic integrity calculation and assessment grading standards

The ratio method was applied to unify the indicator dimensions (Zhang et al., 2019). The scores for the ratio method were calculated in different ways. For indicators where the values decreased as anthropogenic intervention increased, we used:

$$S = (P - P_{min})/(P_{95\%} - P_{min}) \quad (2)$$

where P refers to the indicator value and $P_{95\%}$ is the 95% percentile of this indicator for all points. P_{min} is the minimum value of a specified indicator. For indicators where the values increased as anthropogenic intervention increased, we used:

$$S = (P_{max} - P)/(P_{max} - P_{5\%}) \quad (3)$$

where P_{max} was the maximum value of a specified indicator and $P_{5\%}$ was the 5% quantile for all points. The P-IBI of each sampling site equaled the average of S for all the selected indicators at that point, which was given as follows:

$$P - IBI = \frac{1}{t}\sum_{j=1}^{n} S_j \quad (4)$$

where S_j was the S value of the j_{th} point and t was the number of samples collected at each site. Finally, the 95% quantiles of P-IBI for all sampling sites were used as the lower limit for delineating the excellent level. If the P-IBI of the sampling sites was greater than this value, the sampling point was healthier and less impacted by anthropogenic disturbances. The IBI range that was less than the lower limit for delineating the 'excellent' grade was divided into four categories: "good," "fair," "poor," and "extremely poor."

Statistical analyses and tools

Microsoft Excel 2016 was used for data processing, partial biological index calculations, and box plots. Shannon–Wiener, Margalef, and Pielou index calculations were performed using R 3.6.3, and inverse distance weighting interpolation within the study area was performed using ArcGIS 10.2. An independent-samples t-test was conducted to evaluate differences in environmental data and was performed using SPSS 20.0 for Windows (SPSS Inc., Chicago, IL, United States).

Prior to performing a multiple regression analysis, the collinearity among the independent variables should be

diagnosed according to the eigenvalues, condition index (CI), variance proportion, tolerance, and variance inflation factor (VIF) (Liu et al., 2010). P-IBI was used as the dependent variable in an MLR (with forwarding selection) where partial regression coefficients for the independent variables were selected using a *t*-test at a significance level of 0.05 using SPSS 20.0 software (SPSS Inc., Chicago, IL, United States).

Results

Species and abundance of phytoplankton

In this study, 137 species of phytoplankton belonging to 7 phyla, 10 classes, 15 orders, 26 families, and 62 genera were identified throughout the spring, summer, and autumn of 2019. Phytoplankton species were mainly composed of Bacillariophyta (65 species, 47.45%) and Chlorophyta (40 species, 29.20%), followed by Cyanobacteria (14 species, 10.22%) and Euglenophyta (11 species, 8.03%), whereas the proportions of Cryptophyta, Dinophyta, and Chrysophyta were lower than those of the aforementioned phyla. Overall, the number of phytoplankton species in autumn (97) was much higher than that observed in spring (74) and summer (76). The abundance and relative abundance of phytoplankton at various sampling sites during the three seasons are shown in **Figure 2**. The temporal and spatial distributions of phytoplankton abundance in the ASRB exhibited distinct differences. In terms of time, the abundance of phytoplankton in spring (4.48×10^6 ind./L) was much greater than that in summer (3.60×10^5 ind./L) and autumn (1.29×10^6 ind./L), with the abundance of phytoplankton declining from spring to summer and increasing from summer to autumn. Except for S7, S8, and S12 in the summer, diatoms were the predominant organisms at each sampling site during the study period. In a spatial context, upstream phytoplankton abundance was determined to be the lowest, whereas downstream phytoplankton abundance was determined to be the highest. Simultaneously, during summer and autumn, the dominant position of diatoms from upstream to downstream gradually declined.

Environmental factors of Ashi River Basin

Except for TN, other environmental factors exhibited statistically significant seasonal differences ($P < 0.05$) (**Table 1**). The WT ranged from 3.7 to 26.0°C, reaching its highest value in summer. The pH values of the water ranged from 7.16 to 9.14, making it alkaline. Conductivity values ranged from 78.3 μS/cm (S15 in autumn) to 649 μS/cm (S2 in spring). TN values were similar in spring and summer, and the highest TN concentrations were recorded at S2 (2.33 mg/L). The highest TP concentrations were recorded in summer, ranging from 0.01 to 1.08 mg/L. COD_{Mn} concentrations ranged from 3.88 to 12.86 mg/L, with the highest value recorded at S2 in summer, and the lowest value recorded at S17 in spring. DO values ranged between 1.40 and 16.44 mg/L. The highest BOD_5 value was recorded at S4 (10.10 mg/L) in spring, and the lowest values were recorded at S10 and S11 (0.30 mg/L) in spring. The Tur. ranged from 7.5 NTU (S14 in autumn) to 155.5 NTU (S9 in summer).

Water quality assessments based on water quality index

During the study period, the WQI had distinct patterns of temporal and spatial changes (**Figure 3**). From a seasonal perspective, the WQI was highest in autumn (77), followed by spring (64) and summer (61). Compared with spring and summer, the WQI of autumn showed a significant change ($P < 0.01$), indicating that the water quality in autumn (good) was significantly better than that in spring and summer (moderate). From a spatial perspective, the WQI of the sampling sites surrounding the reservoir upstream of the river had the highest value during each season. Simultaneously, the changes in the WQI manifested as a gradual upstream-to-downstream decline in the river. Similar WQI spatial patterns were observed among seasons, indicating that the water quality of the ASRB was best upstream and gradually deteriorated downstream. According to the WQI classification standard, 12 sampling sites (S1–S12) in the ASRB were classified as "moderate," and 5 sampling sites (S13–S17) were classified as "good."

Phytoplankton index of biotic integrity calculations and health assessment of river ecosystems

The primary sources of water pollution in the ASRB were industrial effluent and agricultural runoff, and single-factor evaluation methods could not accurately determine the relative severity of water pollution. We used the WQI to determine the water quality at each sampling point. The higher the WQI value, the better the water quality; conversely, the lower the WQI value, the worse the water quality. For rivers, it is more practical to determine reference and impaired points via comprehensive analyses of on-site investigation results and water quality. In conjunction with the field survey and WQI values, sampling sites S13-S17, which were less disturbed by anthropogenic activities near the reservoir, were used as the reference points in this study. The remaining sampling sites (S1–S12) were used as impaired points in the subsequent analysis.

First, we selected 35 candidate indicators that represented the diversity, abundance, biomass, and evenness of communities

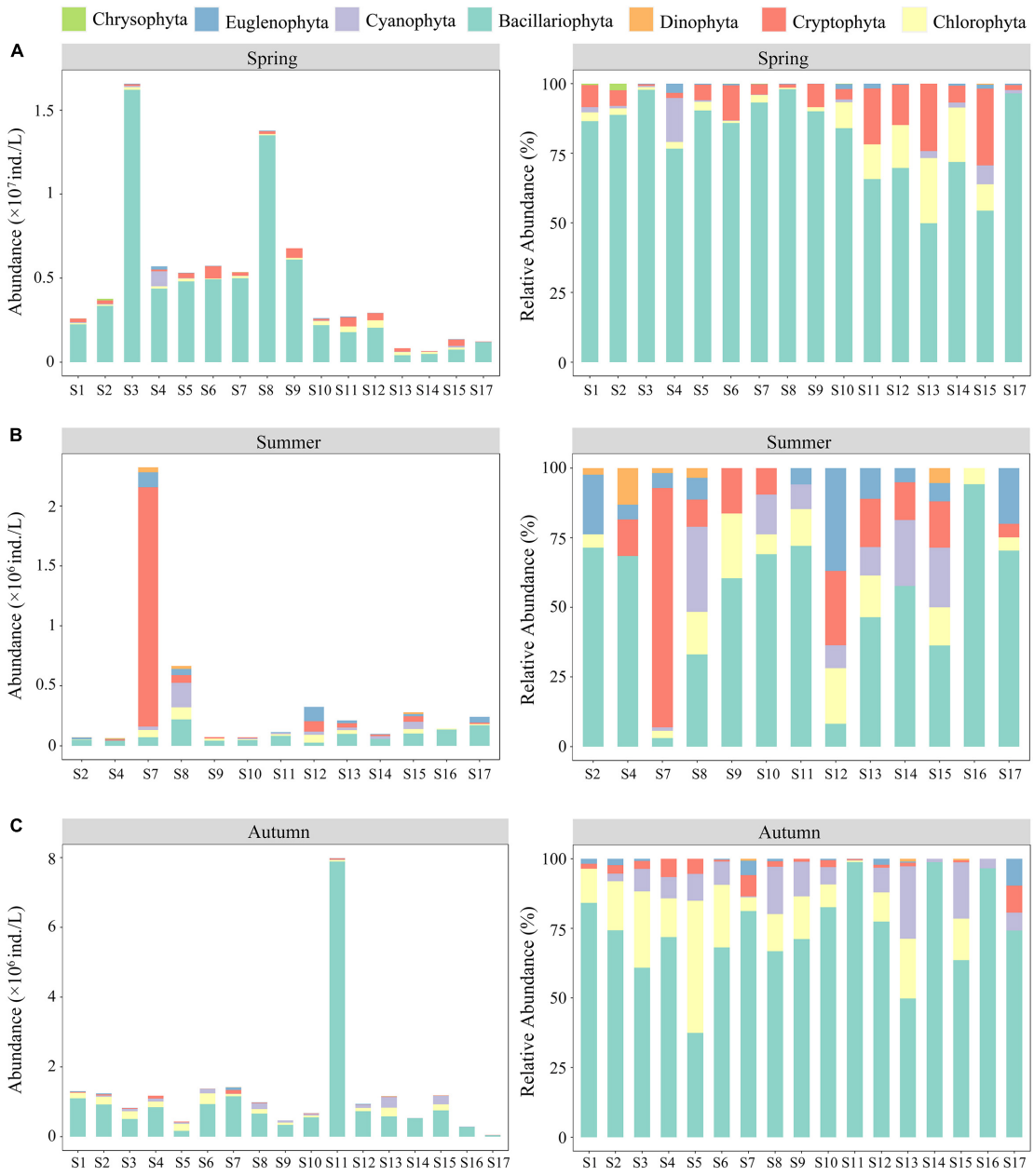

FIGURE 2
Abundance and relative abundance of phytoplankton at various sampling sites: **(A)** spring; **(B)** summer; and **(C)** autumn.

to establish the P-IBI evaluation system (Table 2). Second, indicators with little cabinet overlap were admissible to the subsequent screening stage; the metrics with the strongest separation power between the reference and impaired groups (the degree that the interquartile ranges overlapped between boxes, IQ < 2) were eliminated (Zhang et al., 2020). The 11 indicators with clear discrepancies between the impaired and reference points were selected for further analysis (Figure 4). Finally, using the Spearman correlation test (Supplementary Table 3), five non-redundant indicators were selected to calculate the P-IBI evaluation system: Shannon–Wiener index (M1), total biomass (M22), percentage of motile diatoms (M32), percentage of stipitate diatom (M33), and diatom quotient (M35).

The ratio method was used to calculate the P-IBI values at each site. Since the selected indicators M1, M32, and M33 all decreased as anthropogenic influence and interference increased, M22 and M35 had opposite response trends. The specific calculation methods according to the calculation formula are presented in Table 3. The P-IBI values were

TABLE 1 Maximum, minimum, and mean values of envorinment factors in the ASRB.

		Season			T-text	
		Spring	Summer	Autumn	Spring-Summer	Summer-Autumn
WT	Max	17.9	26	13.6	$P < 0.05$	$P < 0.05$
	Min	10	18.7	3.7		
	Mean	15.56	22.72	9.34		
pH	Max	9.14	7.08	8.15	$P < 0.05$	$P < 0.05$
	Min	7.16	6.66	7.31		
	Mean	8.4	6.91	7.81		
Cond.	Max	694	136	338.7	$P < 0.05$	$P < 0.05$
	Min	121.6	78.3	96.6		
	Mean	366.49	107.61	209.22		
TN	Max	2.33	0.9	0.83	$P > 0.05$	$P < 0.05$
	Min	0.12	0.14	0.41		
	Mean	0.95	0.78	0.59		
TP	Max	0.76	1.08	0.56	$P < 0.05$	$P < 0.05$
	Min	0.01	0.06	0.01		
	Mean	0.21	0.44	0.14		
COD_{Mn}	Max	10.9	12.86	12.84	$P < 0.05$	$P < 0.05$
	Min	3.88	5.65	4.75		
	Mean	6.48	10.7	8.39		
DO	Max	15.1	10.1	16.44	$P < 0.05$	$P < 0.05$
	Min	12.3	1.4	9.6		
	Mean	13.36	8.05	12.81		
BOD_5	Max	10.1	9.8	1.9	$P < 0.05$	$P < 0.05$
	Min	6.1	0.9	0.3		
	Mean	7.59	3.3	0.98		
Tur.	Max	89.2	155.5	31.3	$P < 0.05$	$P < 0.05$
	Min	16.8	18.8	7.5		
	Mean	48.35	81.25	14.72		

calculated using the aforementioned biological indicators, and the classification standard for the state of the aquatic environment was generated using the P-IBI. The 95% percentile (4.73) of the P-IBI for all sampling sites was the lower limit of Class I (excellent). P-IBI scores less than 4.73 were divided into four levels: "good" (II), "fair" (III), "poor" (IV), and "extremely poor" (V). Table 4 lists the classification criteria for ecosystem health.

Ecosystem health assessments based on phytoplankton index of biotic integrity

The health statuses of aquatic ecosystems at 17 sampling sites corresponding to the different seasons were classified according to the calculated P-IBI values and the classification standard in Table 4. From the perspective of seasonal change, the P-IBI values and health statuses in different seasons can be ranked as follows: summer (good) > autumn (fair) > spring (poor). Only the difference in the P-IBI values between spring and summer was significant ($P < 0.01$). Figure 5 illustrates that the health status of aquatic ecosystems had distinct spatial differences. In the present study, there was a difference of more than four evaluation levels from upstream to downstream of the river. The evaluation ranges for the mean P-IBI during the study period were "good" (4.65) to "poor" (1.85). The three sites of S10, S14, and S16-S17 were evaluated as "good"; S11-S13 and S15 were evaluated as "fair"; and the nine sites of S1-S9 were evaluated as "poor."

Multiple linear regression analysis between phytoplankton index of biotic integrity and environmental factors

On the basis of the significant correlations between the environmental factors and P-IBI, three environmental factors

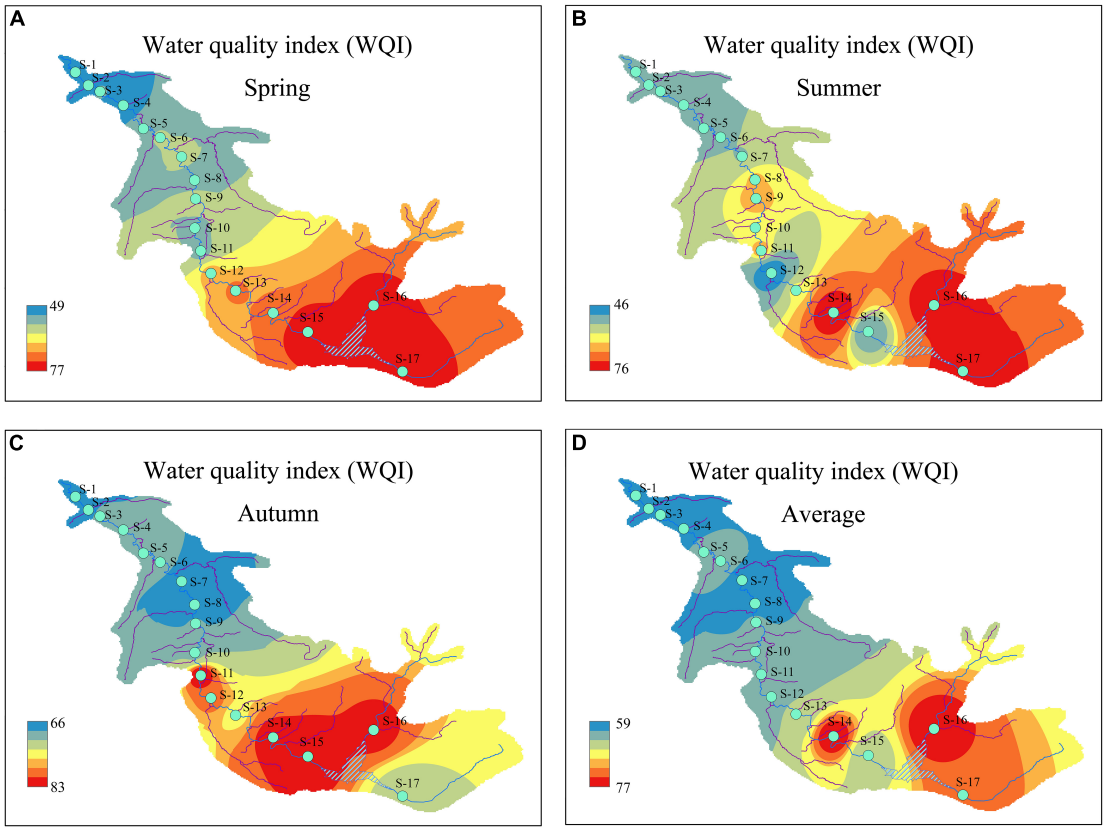

FIGURE 3
Temporal and spatial distributions of water quality index (WQI) during the study period: **(A)** spring; **(B)** summer; **(C)** autumn; and **(D)** average.

(Cond., pH, and DO) were screened to develop an MLR model. The eigenvalues, CI, variance proportion, tolerance, and VIF, which are characteristic parameters of the collinearity diagnostics, are listed in **Table 5** and **Supplementary Table 5**. Multiple linear regression analysis showed that the regression equation was significant, $F = 19.548$, $P < 0.001$. Conductivity (B = -0.003, β = -0.441, P = 0.001), pH (B = -0.918, β = -0.656, $P < 0.001$), and DO (B = 0.151, β = 0.430, $P = 0.005$) significantly negatively and positively predicted P-IBI, respectively. Collectively, these variables explained 55.30% of the variation in P-IBI (**Table 5**), and the MLR model was as follows:

$$\mathrm{P-IBI} = 8.887 - 0.003\mathrm{Cond.} - 0.918\mathrm{pH} + 0.151\mathrm{DO} \quad (5)$$

Discussion

The IBI is a measurement method proposed by Karr (1981) that has evolved into the most widely used biological indicator. Many countries and regions have developed numerous IBI-based assessment methods for different levels of damage to aquatic ecosystems (Bae et al., 2010; Zalack et al., 2010; Wu et al., 2019). Phytoplankton comprise small individuals of a diverse range of species that occur in large quantities. They are extensively distributed in natural waters and constitute an essential component of river biodiversity; at the same time, they provide an important foundation for primary productivity in river ecosystems (Hötzel and Croome, 1999). Phytoplankton communities are the first response assemblage of organisms directly affected by environmental changes in aquatic lotic and lentic systems (Halsey and Jones, 2015). As rivers are dynamic and have expansive watersheds, the natural environment and socioeconomic conditions of the areas intersected by river flows are diverse (Acreman et al., 2014). The community structure of phytoplankton in rivers (lotic systems) is less stable than that of the phytoplankton in lakes and reservoirs (lentic systems), and both their seasonal changes are apparent (Tang et al., 2018; Minaudo et al., 2021). In addition, the biomass and species composition of phytoplankton in rivers are influenced by the combined effects of river morphology, hydrology, light, and reproduction rate, and they exhibit a clear spatial heterogeneity (Yang et al., 2019a). In recent years, the community structure of river phytoplankton has been influenced not only by the natural habitats of rivers but also by human activities and the upstream

TABLE 2 35 candidate metrics.

Type of Metric	No.	Metrics
Diversity of community	M1	Shannon-Wiener index
	M2	Margalef index
	M3	Simpson index
	M4	Pielou index
	M5	Menhinick index
	M6	Odum index
	M7	Total number of taxa
	M8	Number of taxa of Bacillariophyta
	M9	Percentage of Bacillariophyta taxa
	M10	Number of taxa in Cyanophyta
	M11	Percentage of Cyanophyta taxa
	M12	Number of taxa in Chlorophyta
	M13	Percentage of Chlorophyta taxa
	M14	Number of non-diatom taxa
Abundance of community	M15	Abundance of Bacillariophyta
	M16	Abundance of Cyanophyta
	M17	Abundance of Chlorophyta
	M18	Mean Taxon Abundance
	M19	Total abundance
	M20	Abundance of top3 dominant species
	M21	Abundance of dominant species
Biomass of community	M22	Total biomass
	M23	Biomass of Bacillariophyta
	M24	Biomass of Cyanophyta
	M25	Biomass of Chlorophyta
Evenness of community	M26	Percentage of abundance of Bacillariophyta
	M27	Percentage of abundance of Cyanophyta
	M28	Percentage of abundance of Chlorophyta
	M29	Percentage of abundance of Chlorophyta and Bacillariophyta
	M30	Percentage of abundance of top3 dominant species
	M31	Percentage of abundance of dominant species
	M32	Percentage of motile diatoms
	M33	Percentage of stipitate diatom
	M34	Percentage of *Nitzschia*
	M35	Diatom quotient

and downstream relationships of rivers (Zhao et al., 2020a). Human activities have gradually changed the types of land use in river basins, mainly through changes in nutrient enrichment, hydrological regimes, riparian habitat quality, and other ecological processes, resulting in a series of adverse effects on river ecosystems (Chen et al., 2022). With the escalation in anthropogenic stress, the loss of natural land, and the increase in pollutants discharged into rivers, the number of pollution-sensitive phytoplankton species in rivers decreased, and pollution-resistant species became the dominant group (Moghadam, 1975; Montoya-Moreno and Aguirre-Ramírez, 2013). The advantages of using phytoplankton as an IBI over other taxa (benthic diatoms, invertebrates, and fish) include simple collection, wide distribution, sensitivity to changes in aquatic conditions, short community renewal time, rapid response to changes in river water chemistry and habitat quality, and greater predictability of community trends (Zhou et al., 2019). Before and after a disturbance, the community structure of phytoplankton typically shifts dramatically, whereas the community structures of macroinvertebrates and fish are different (Wu et al., 2019; Feng et al., 2021). Therefore, phytoplankton can be used to assess the biological integrity of aquatic ecosystems, reflect the temporal and spatial changes in the condition of aquatic ecosystems in river basins, and serve as a crucial supplementary indicator for the evaluation of water quality.

Similar to the already adopted IBI based on fish and macroinvertebrates, our research has developed a standardized P-IBI system (Wu et al., 2019; Feng et al., 2021) to evaluate the ecosystem health status in the ASRB. The results showed that the aquatic ecosystem health status in the ASRB was "fair." The evaluation based on P-IBI showed that the ASRB exhibited clear seasonal changes. According to Wu et al. (2012, 2019), the typical performance of the P-IBI evaluation system showed seasonal characteristics. According to the P-IBI results, the health of the aquatic ecosystem in the ASRB during summer was better than that during autumn and spring. This may be due to the fact that in temperate rivers, suitable temperatures, light, and nutrient conditions promote phytoplankton growth during summer (Wu and Zhang, 2013), thereby sustaining a high P-IBI value. From the perspective of the WQI, the seasonal change was autumn > spring > summer, indicating that the water quality was good in autumn and poor in summer during the study. According to the WQI classification, water quality in summer was the worst. This may be a result of exceptionally heavy rainfall in the area during the 2019 summer period, which resulted in domestic garbage entering the river via surface water runoff. Seasonal changes in nutrient concentrations are also important factors affecting P-IBIs and WQIs (Paerl et al., 2011; Song et al., 2017). Spring had substantially higher TN contents than those recorded in summer and autumn. The P-IBI indicated that the biological health of the phytoplankton community was at its worst in spring, while the WQI was higher than that in summer but remained at a "medium" level. Compared to other seasons, it was more common for a single phytoplankton species to dominate in spring. For example, *Cyclotella meneghiniana* Kützing had a higher degree of dominance at various sampling sites in spring. In addition, we found that the succession of dominant phytoplankton species exhibited substantial seasonal changes. In essence, diatoms bloomed in spring, Cryptophyta had a higher dominance in summer, and Chlorophyta and Cyanophyta dominated in autumn. Therefore, the P-IBI should be evaluated comprehensively in different seasons to eliminate evaluation errors caused by seasonal changes, which represents

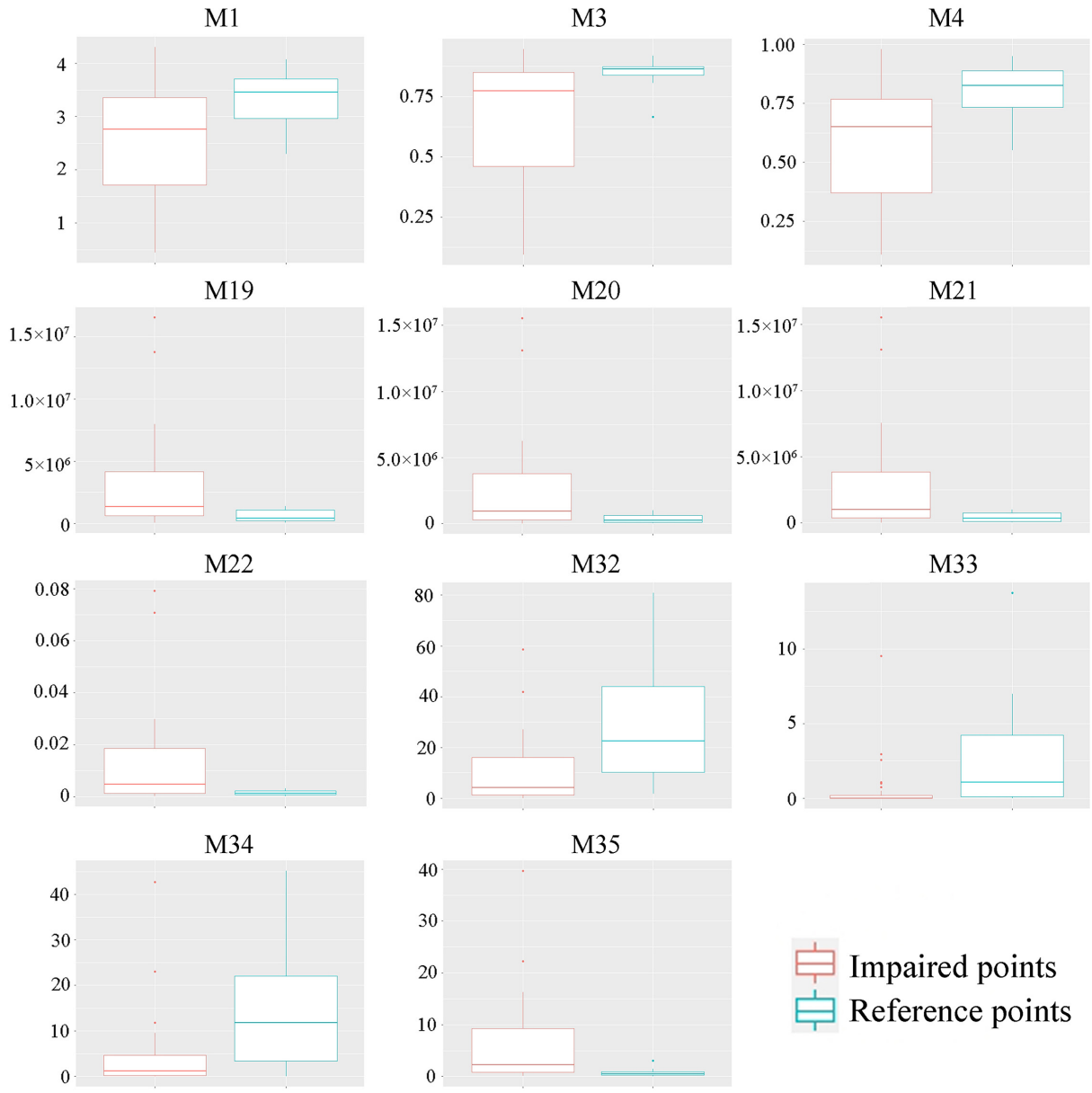

FIGURE 4
Boxplot of the selected indicators. The indicators are listed in Table 2.

a more scientific approach for evaluating watershed health over a wide variety of time scales.

In this study, all reference points were rated as "good" or "fair" according to the P-IBI evaluation standard, whereas 16.7% of impaired points were rated as "fair" and 83.3% were rated as "poor." These results indicated that P-IBI could acutely respond to environmental changes in the ASRB and accurately reflect the biological integrity at each sampling point (Supplementary Figure 1). Among them, the sampling points of "good" and "fair" were located in the upper reaches of the river, at the inlet and outlet of the Xiquanyan Reservoir, with high forest cover, shallow water, and high transparency, whereas the upstream current was swift, the phytoplankton abundance was low, and the area was less impacted by human activities. Sampling sites rated as "poor" were located downstream of the river in a dense urban area, with many sewage outfalls on both banks, slow flow, and turbid waters, and the area is strongly impacted by human activities. The P-IBI uses the ecological adaptability of different phytoplankton species to evaluate the health of river ecosystems. For example, the dominant phytoplankton species in the "fair" and "good" sampling

TABLE 3 The ratio method's calculation standard of 5 selected metrics.

No.	Selected indicators	Response to degradation	S
M1	Shannon-Wiener index	Decrease	(M1-0.45)/3.52
M22	Total biomass	Increase	(0.087-M22)/0.087
M32	Percentage of motile diatoms	Decrease	M32/54.84
M33	Percentage of stipitate diatom	Decrease	M33/6.69
M35	Diatom quotient	Increase	(39.68-M35)/39.54

sites included *Encyonema minutum* (Hilse) Mann, *Amphora ovalis* (Kützing) Kützing, *Gomphonema parvulum* (Kützing) Kützing, and *Navicula radiosa* Kützing. These dominant species are the most sensitive, and they have poor pollution tolerance; they cannot survive in heavily polluted waters. Therefore, their presence typically indicates a lightly polluted or non-polluted environment (Moghadam, 1975; Montoya-Moreno and Aguirre-Ramírez, 2013). The dominant species at the sampling sites with "poor" evaluation results mainly included *C. meneghiniana*, *Ulnaria ulna* (Kützing) Aboal, *Ankistrodesmus falcatus* (A. Braun) Korschikoff, and *Limnothrix redekei* Van Goor, which are common pollution-resistant taxa (Singh et al., 2013; Dwivedi and Srivastava, 2017). In addition, Zhang et al. (2019) determined from the P-IBI of the Bali River that pollution downstream of the river is the source of the lowest biological integrity in an estuary. The results of this study were consistent with our previous evaluation of the nutritional status in the ASRB using the benthic diatom index (Zhao et al., 2020b). In other words, rivers with obvious spatial changes in the ASRB were shown to be impacted by anthropogenic activities and nutritional conditions. This may be because there were more industrial activities in the

TABLE 4 Based on the phytoplankton index of biotic integrity (P-IBI's) grading standards of each ecosystem health status.

Grading	I	II	III	IV	V
Status	Excellent	Good	Fair	Poor	Extremely poor
Range	>4.73	[3.21, 4.73)	[2.76, 3.21)	[1.33, 2.76)	<1.33

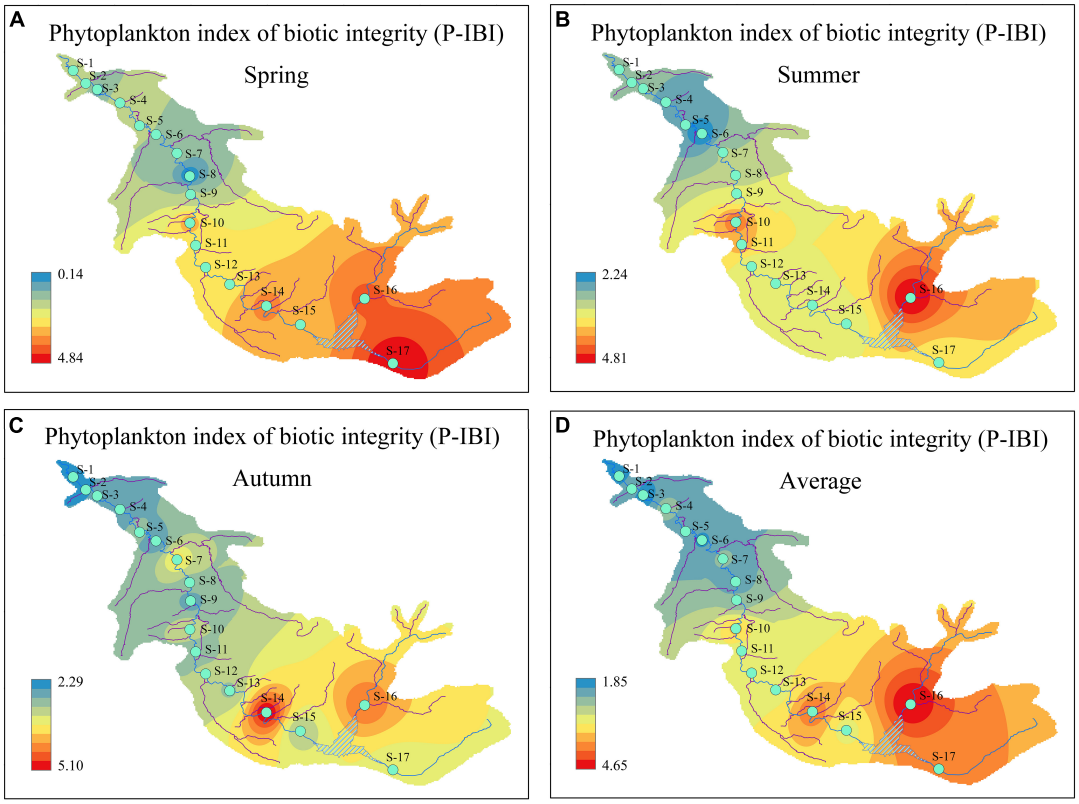

FIGURE 5
Temporal and spatial distribution of phytoplankton index of biotic integrity (P-IBI) during the study period. **(A)** spring; **(B)** summer; **(C)** autumn; and **(D)** average.

TABLE 5 The multiple linear regression of phytoplankton index of biotic integrity (P-IBI) and environment factors.

Variable	Unstandardized Coefficients		Standardized Coefficients			Collinearity Statistics		Overall model		
	B	Standard Error	β	*t*-test	*P*	Tolerance	VIF	*F*	$R_{adj.}^2$	Durbin-Watson
Constant	8.887	1.362		6.527	0			19.548***	0.553	2.085
Cond.	−0.003	0.001	−0.441	−3.639	0.001	0.678	1.475			
pH	−0.918	0.229	−0.656	−4.008	0	0.37	2.7			
DO	0.151	0.051	0.43	2.949	0.005	0.467	2.141			

VIF: variance inflation factor, ***$P \leq 0.001$.

middle and lower reaches of the ASRB, and the increase in sewage discharge caused by industrialization has caused a significant deterioration in downstream water quality (Li et al., 2018; Feng et al., 2019). Ultimately, this phenomenon affected the diversity and abundance of phytoplankton, thereby reducing the biological integrity index of phytoplankton in the lower reaches of the river. Consequently, the P-IBI could effectively reflect the health of the river ecosystem within the ASRB.

During the study, the P-IBI and WQI exhibited clear spatial changes during each season. Both indices showed a gradual decline, as anthropogenic activities increased from upstream to downstream of the ASRB. Wu et al. (2019) studied the Taihu Lake Basin and found that the value of the P-IBI gradually decreased as the degree of anthropogenic interference increased; concurrently, there was a positive correlation between the P-IBI and WQI (**Supplementary Figure 2**). This suggested that P-IBI and WQI were negatively correlated with anthropogenic interference, which was consistent with the results of this study. Comparing the evaluation results of the WQI and P-IBI, we found that both methods could distinguish the ecosystem health status of impaired and reference points, but that there were substantial variations in the evaluation results at the same sampling sites. At the same time, P-IBI and WQI exhibited seasonal characteristics. In previous studies, a single factor or indicator was typically used to evaluate water quality, and different results were obtained when different research methods were used. The WQI is weighted by the values of physical and chemical parameters, and the evaluation process is straightforward, quick, and simple to grasp; however, it lacks indicators related to the composition and structure of biological communities (De La Mora-Orozco et al., 2017; Nong et al., 2020). The P-IBI evaluation system lacked indicators for water quality, habitat, and hydrological conditions, and the evaluation process was relatively complicated. However, the P-IBI used phytoplankton as a biological indicator, and its community structure rapidly responded to habitat, hydrological conditions, and anthropogenic interference, and it integrated various indicators, such as community structure, biomass, and pollution tolerance. Therefore, P-IBI was a comprehensive tool that could accurately depict the health of river ecosystems. It compensated for the shortcomings of WQI when evaluating the health of rivers at the biological level. In this study, the P-IBI was constructed using a standardized method to effectively screen out indicators that are sensitive to anthropogenic disturbances. Furthermore, the current state of the aquatic ecosystem in the region could be derived through a comprehensive analysis of multiple indicators, which was a necessary complement to the water quality evaluation using WQI.

This study used environmental factors, such as WT, Cond., pH, DO, TP, COD_{Mn}, TN, BOD_5, and Tur. to perform

multiple linear regression analyses with P-IBI. The results indicated that Cond. and pH values significantly negatively predicted P-IBI, whereas DO positively predicted P-IBI. Cond. was an effective indicator of the inorganic ion content in water. Studies have shown that the higher the water purity, the lower the Cond. value (Flores and Barone, 1998; Trebitz et al., 2019). In the waters of the ASRB, Cond. gradually increased from the upper to the lower reaches of the river. This might be due to the large amounts of industrial wastewater discharged into the middle and lower reaches of the river, increasing the inorganic ion content of the downstream water and making it less suitable for the growth and reproduction of phytoplankton. This phenomenon was consistent with the gradual decrease in P-IBI values from upstream to downstream. As an important ecological factor, pH was closely associated with phytoplankton growth. The pH of the water is primarily controlled by CO_2 content; therefore, when the abundance of phytoplankton increases to a certain level, their biological activities have a certain impact on the CO_2 content in the water, which in turn changes the pH of the water (Zhang et al., 2019). The P-IBI decreased as the pH increased in the ASRB. DO is a key factor influencing phytoplankton reproduction and metabolism. The decrease in DO concentrations has a negative impact on the growth of phytoplankton and its biomass (Xu et al., 2010). In this study, the DO concentration in spring was higher than that in autumn and summer. In terms of spatial changes, DO and P-IBI gradually decreased as anthropogenic activity increased. In addition, nitrogen is an essential nutrient in water, and it is a limiting factor in the growth of phytoplankton. An increase in TN can promote the reproduction of dominant phytoplankton species to a certain extent (Shetye et al., 2019), thereby changing the phytoplankton population structure. For example, the N/P mass ratios of sampling sites S3 and S8 in spring were close to the optimal N/P ratio for phytoplankton growth (7:1), (Hu, 2009), and the appropriate nutrient concentration promoted the propagation of a large number of the dominant species of *C. meneghiniana* (1.5×10^7 ind./L and 1.3×10^7 ind./L, respectively), resulting in the P-IBI values at these sites reaching their lowest values during the study period.

In this study, we developed a P-IBI system composed of various indices based on the multimetric indices concept. From a pool of 35 candidate ecological indices, the Shannon–Wiener index, total biomass, percentage of motile diatoms, percentage of stipitate diatom, and diatom quotient were selected based on their correlations and environmental factors. Wu et al. (2019) screened three indicators, phytoplankton density, chlorophyll a (Chl a), and Menhinick's richness index, to create a P-IBI system to evaluate the ecological health of the Taihu Basin. Feng et al. (2021) suggested that the P-IBI be constructed based on the percentage of Cyanophyta genera, the number of total species, percentage of Cyanophyta abundance, Shannon–Wiener index, and Pielou index to evaluate the impact of anthropogenic activities (i.e., industrial activities, dam construction, and mining) on biological integrity. In addition, other studies have also considered the development and creation of indicators, such as the density of inedible algae, water-bloom-forming algal species biomass, and density of toxic phytoplankton (Yang et al., 2019b; Zuo et al., 2019). The IBI assessment system lacks comparability owing to a large number of candidate indicators, and the relationship between different indicators and the complexity of the health of different watersheds can be filtered. Studies evaluating the ecological health of rivers in northeast China based on P-IBI are sparse, and the results of this study provided crucial information on the biological integrity of the region.

Even though P-IBI was able to assess the ecosystem health of the ASRB, there were still some uncertainties in the development process. First, to develop the P-IBI, it was impossible to locate pristine water bodies that were completely unaffected by anthropogenic activities as reference points. Second, because P-IBI exhibited certain seasonal change characteristics, the sampling frequency should have been increased, and the river ecosystem health should have been assessed regularly. Third, the P-IBI should have been continuously verified using large quantities of data and adjusted accordingly to anticipate the future impact of anthropogenic activities on river ecosystem health. Future research should focus on these existing problems and should be conducted with more depth.

Conclusion

The IBI is a potential tool for monitoring the ecological health of rivers, as it can reflect temporal and spatial changes in river ecological health. This study used the WQI and P-IBI to evaluate the impacts of anthropogenic activities on the ASRB. The seasonal characteristics of P-IBI were as follows: summer (good) > autumn (fair) > spring (poor). Based on the WQI evaluation, the water quality of the ASRB was best in autumn, followed by spring and summer. The overall health of ASRB was 'fair', and anthropogenic activities have severely damaged the biological integrity of the aquatic ecosystem in this region. Although the P-IBI and WQI established in this study showed similar spatial patterns and shared certain seasonal characteristics, the environmental state varied during different seasons. The development of P-IBI in ASRB enabled effective identification of the health status of reference and impaired points while compensating for the shortcomings of the WQI. Our findings have important implications for the ecological monitoring and protection of rivers impacted by anthropogenic activities.

Data availability statement

The original contributions presented in this study are included in the article/**Supplementary material**, further inquiries can be directed to the corresponding authors.

Author contributions

ZL was a major contributor to writing the manuscript, analyzing the data, and preparing figures and tables. XL and YF conceived and designed the experiments. ZL and CM performed the experiments. CM and YS contributed reagents and materials. All authors reviewed the manuscript.

Funding

This work received financial aid extended by the National Natural Science Foundation of China (31870187) and the Natural Science Foundation of Heilongjiang, China (LH2020C067), the Innovative talent training programme of Heilongjiang (UNPYSCT-2020133), and Science and Technology Innovation Climbing Program of Harbin Normal University (No. XPPY202207).

Conflict of interest

The authors declare that the research was conducted in the absence of any commercial or financial relationships that could be construed as a potential conflict of interest.

Publisher's note

All claims expressed in this article are solely those of the authors and do not necessarily represent those of their affiliated organizations, or those of the publisher, the editors and the reviewers. Any product that may be evaluated in this article, or claim that may be made by its manufacturer, is not guaranteed or endorsed by the publisher.

Supplementary material

The Supplementary Material for this article can be found online at: https://www.frontiersin.org/articles/10.3389/fmicb.2022.942205/full#supplementary-material

References

Acreman, M., Arthington, A. H., Colloff, M. J., Couch, C., Crossman, N. D., Dyer, F., et al. (2014). Environmental flows for natural, hybrid, and novel riverine ecosystems in a changing world. *Front. Ecol. Environ.* 12, 466–473. doi: 10.1890/130134

Amorim, C. A., and Moura, A. D. N. (2021). Ecological impacts of freshwater algal blooms on water quality, plankton biodiversity, structure, and ecosystem functioning. *Sci. Total Environ.* 758:143605. doi: 10.1016/j.scitotenv.2020.143605

Bae, D. Y., Kumar, H. K., Han, J. H., Kim, J. Y., Kim, K. W., Kwon, Y. H., et al. (2010). Integrative ecological health assessments of an acid mine stream and in situ pilot tests for wastewater treatments. *Ecol. Eng.* 36, 653–663. doi: 10.1016/j.ecoleng.2009.11.027

Busseni, G., Vieira, F. R. J., Amato, A., Pelletier, E., Pierella Karlusich, J. J., Ferrante, M. I., et al. (2019). Meta-omics reveals genetic flexibility of diatom nitrogen transporters in response to environmental changes. *Mol. Biol. Evol.* 36, 2522–2535. doi: 10.1093/molbev/msz157

Chen, J., Du, C., Nie, T., Han, X., and Tang, S. (2022). Study of non-point pollution in the ashe river basin based on SWAT Model with different land use water. *Water* 14:2177.

Cooper, M. J., Lamberti, G. A., Moerke, A. H., Ruetz, C. R. III, Wilcox, D. A., Brady, V. J., et al. (2018). An expanded fish-based index of biotic integrity for Great Lakes coastal wetlands. *Environ. Monit. Assess.* 190, 580. doi: 10.1007/s10661-018-6950-6

Cui, W. Y., Guo, S. Y., Meng, X. Z., and Kong, F. Q. (2018). Application of adapted Benthic Index of Biotic Integrity (B-IBI) for river ecosystem health assessment in Zhanghe River Watershed, China. *Pol. J. Ecol.* 66, 407–415. doi: 10.3161/15052249pje2018.66.4.008

De La Mora-Orozco, C., Flores-Lopez, H., Rubio-Arias, H., Chavez-Duran, A., and Ochoa-Rivero, J. (2017). Developing a Water Quality Index (WQI) for an irrigation dam. *Int. J. Environ. Res. Public Health* 14:439. doi: 10.3390/ijerph14050439

Dwivedi, B. K., and Srivastava, A. K. (2017). Diatoms as indicator of pollution gradients of the River Ganga, Allahabad, India. *Intl. J. Curr. Microbiol. Appl. Sci.* 6, 4323–4334. doi: 10.20546/ijcmas.2017.607.450

Feng, B., Wang, C., Wu, X., Tian, C., Zhang, M., Tian, Y., et al. (2019). Spatiotemporal dynamics of cell abundance, colony size and intracellular toxin concentrations of pelagic and benthic Microcystis in Lake Caohai. China. *J. Environ. Sci (China)* 84, 184–196. doi: 10.1016/j.jes.2019.05.010

Feng, B., Zhang, M., Chen, J., Xu, J., Xiao, B., Zhou, M., et al. (2021). Reduction in the phytoplankton index of biotic integrity in riverine ecosystems driven by industrial activities, dam construction and mining: A case study in the Ganjiang River. *China. Ecol. Indic.* 120:106907. doi: 10.1016/j.ecolind.2020.106907

Flores, L. N., and Barone, R. (1998). Phytoplankton dynamics in two reservoirs with different trophic state (Lake Rosamarina and Lake Arancio, Sicily, Italy). *Hydrobiologia* 36, 163–178. doi: 10.1007/978-94-017-2668-9_15

Griffiths, K., Thienpont, J. R., Jeziorski, A., and Smol, J. P. (2018). The impact of Ca-rich diamond mining effluent on downstream cladoceran communities in softwater lakes of the Northwest Territories. Canada. *Can. J. Fish. Aquat. Sci.* 75, 2221–2232. doi: 10.1139/cjfas-2017-0469

Halsey, K. H., and Jones, B. M. (2015). Phytoplankton strategies for photosynthetic energy allocation. *Ann. Rev. Mar. Sci.* 7, 265–297. doi: 10.1146/annurev-marine-010814-015813

Hötzel, G., and Croome, R. Dr (1999). *A phytoplankton methods manual for Australian freshwaters*. Canberra: Land and Water Resources Research and Development Corporation.

Hu, H., and Wei, Y. (2006). *Freshwater algae in China: Systems, classification and ecology*. Beijing: Science Press.

Hu, X. (2009). Summing up the research on eutrophication mechanisms of lakes and reservoirs. *Water Resour. Prot.* 25, 44–47.

Hu, X., Hu, M., Zhu, Y., Wang, G., Xue, B., and Shrestha, S. (2022). Phytoplankton community variation and ecological health assessment for impounded lakes along the eastern route of China's South-to-North Water Diversion Project. *J. Environ. Manag.* 318:115561. doi: 10.1016/j.jenvman.2022.115561

Inyang, A. I., and Wang, Y. S. (2020). Phytoplankton diversity and community responses to physicochemical variables in mangrove zones of Guangzhou Province. *China. Ecotoxicol.* 29, 650–668. doi: 10.1007/s10646-020-02209-0

Kannel, P. R., Lee, S., Lee, Y. S., Kanel, S. R., and Khan, S. P. (2007). Application of water quality indices and dissolved oxygen as indicators for river water classification and urban impact assessment. *Environ. Monitor. Assess.* 132, 93–110. doi: 10.1007/s10661-006-9505-1

Karr, J. R. (1981). Assessment of Biotic Integrity Using Fish Communities. *Fisheries* 6, 21–27.

Koçer, M. A. T., and Sevgili, H. (2014). Parameters selection for water quality index in the assessment of the environmental impacts of land-based trout farms. *Ecol. Indic.* 36, 672–681. doi: 10.1016/j.ecolind.2013.09.034

Lacouture, R. V., Johnson, J. M., and Marshall, B. H. G. (2006). Phytoplankton index of biotic integrity for Chesapeake Bay and its tidal tributaries. *Estuaries Coast* 29, 598–616. doi: 10.1007/bf02784285

Li, B., Liu, L., Zhu, Y., and Chen, X. (2020). Assessment of river health by using phytoplanktonic index of biotic integrity. *Yelloe River* 42, 73–78.

Li, J., Li, Y., Qian, B., Niu, L., Zhang, W., Cai, W., et al. (2017). Development and validation of a bacteria-based index of biotic integrity for assessing the ecological status of urban rivers: A case study of Qinhuai River basin in Nanjing. *China. J. Environ. Manag.* 196, 161–167. doi: 10.1016/j.jenvman.2017.03.003

Li, Y., Shi, Z., Zhang, Y., Zhao, Q., Li, A., Jin, Y., et al. (2014). Evaluation method and application on cyanobacteria bloom degree classification with algal density. *Environ. Sustain. Dev.* 39, 67–68.

Li, Y., Yang, N., Qian, B., Yang, Z., Liu, D., Niu, L., et al. (2018). Development of a bacteria-based index of biotic integrity (Ba-IBI) for assessing ecological health of the three gorges reservoir in different operation periods. *Sci. Total Environ.* 64, 255–263. doi: 10.1016/j.scitotenv.2018.05.291

Lin, L., Wang, F., Chen, H., Fang, H., Zhang, T., and Cao, W. (2021). Ecological health assessments of rivers with multiple dams based on the biological integrity of phytoplankton: A case study of North Creek of Jiulong River. *Ecol. Indic.* 121:106998. doi: 10.1016/j.ecolind.2020.106998

Liu, Y., Guo, H., and Yang, P. (2010). Exploring the influence of lake water chemistry on chlorophyll a: A multivariate statistical model analysis. *Ecol. Model.* 221, 681–688. doi: 10.1016/j.ecolmodel.2009.03.010

Marvaetal, F., Garcia-Balboa, C., Baselga-Cervera, B., and Costas, E. (2014). Rapid adaptation of some phytoplankton species to osmium as a result of spontaneous mutations. *Ecotoxicology* 23, 213–220. doi: 10.1007/s10646-013-1164-8

Maxted, J., Barbour, M., Gerritsen, J., and Poretti, V. (2006). Assessment Framework for Mid-Atlantic Coastal Plain Streams Using Benthic Macroinvertebrates. *J. North Am. Benthol. Soc.* 19, 128–144. doi: 10.2307/1468286

Meng, F., Li, Z., Li, L., Lu, F., Liu, Y., Lu, X., et al. (2020). Phytoplankton alpha diversity indices response the trophic state variation in hydrologically connected aquatic habitats in the Harbin Section of the Songhua River. *Sci. Rep.* 10:21337. doi: 10.1038/s41598-020-78300-7

Minaudo, C., Abonyi, A., Leitao, M., Lancon, A. M., Floury, M., Descy, J. P., et al. (2021). Long-term impacts of nutrient control, climate change, and invasive clams on phytoplankton and cyanobacteria biomass in a large temperate river. *Sci. Total Environ.* 756, 144074. doi: 10.1016/j.scitotenv.2020.144074

Moghadam, F. (1975). Diatoms as Indicator of Pollution Zayandeh River, Iran. *Proc. Acad. Nat. Sci. Phila.* 127, 281–297.

Montoya-Moreno, Y., and Aguirre-Ramírez, N. (2013). Knowledge to Ecological Preferences in a Tropical Epiphytic Algae to Use with Eutrophication Indicators. *J. Environ. Prot.* 4, 27–35. doi: 10.4236/jep.2013.411A1004

Nong, X., Shao, D., Zhong, H., and Liang, J. (2020). Evaluation of water quality in the South-to-North Water Diversion Project of China using the water quality index (WQI) method. *Water Res.* 178, 115781. doi: 10.1016/j.watres.2020.115781

Paerl, H. W., Hall, N. S., and Calandrino, E. S. (2011). Controlling harmful cyanobacterial blooms in a world experiencing anthropogenic and climatic-induced change. *Sci. Total Environ.* 409, 1739–1745. doi: 10.1016/j.scitotenv.2011.02.001

Pereira, A., Dâmaso-Rodrigues, M., Amorim, A., Daam, M., and Cerejeira, M. (2018). Aquatic community structure in Mediterranean edge-of-field waterbodies as explained by environmental factors and the presence of pesticide mixtures. *Ecotoxicology* 27, 661–671. doi: 10.1007/s10646-018-1944-2

Pesce, S. F., and Wunderlin, D. A. (2000). Use of water quality indices to verify the impact of Córdoba City (Argentina) on Suquıa River. *Water Res.* 34, 2915–2926. doi: 10.1016/s0043-1354(00)00036-1

Scanlon, B. R., Jolly, I., Sophocleous, M., and Zhang, L. (2007). Global impacts of conversions from natural to agricultural ecosystems on water resources: Quantity versus quality. *Water Resour. Res.* 43, 215–222. doi: 10.1029/2006wr005486

Shetye, S. S., Kurian, S., Naik, H., Gauns, M., Chndrasekhararao, A. V., Kumar, A., et al. (2019). Variability of organic nitrogen and its role in regulating phytoplankton in the eastern Arabian Sea. *Mar. Pollut. Bull.* 141, 550–560. doi: 10.1016/j.marpolbul.2019.02.036

Singh, U. B., Ahluwalia, A. S., Sharma, C., Jindal, R., and Thakur, R. (2013). Planktonic indicators: A promising tool for monitoring water quality (early-warning signals). *Ecol. Environ. Conserv.* 3, 793–800.

Song, H., Xu, J., Lavoie, M., Fan, X., Liu, G., Sun, L., et al. (2017). Biological and chemical factors driving the temporal distribution of cyanobacteria and heterotrophic bacteria in a eutrophic lake (West Lake, China). *Appl. Microbiol. Biotechnol.* 101, 1685–1696. doi: 10.1007/s00253-016-7968-8

Souza, G. B. G., and Vianna, M. (2020). Fish-based indices for assessing ecological quality and biotic integrity in transitional waters: A systematic review. *Ecol. Indic.* 109:105665. doi: 10.1016/j.ecolind.2019.105665

Stoddard, J. L., Larsen, D. P., Hawkins, C. P., Johnson, R. K., and Norris, R. H. (2006). Setting expectations for the ecological condition of streams: The concept of reference condition. *Ecol. Appl.* 16, 1267–1276. doi: 10.1890/1051-0761(2006)016[1267:seftec]2.0.co;2

Sun, W., Xia, C., Xu, M., Guo, J., and Sun, G. (2016). Application of modified water quality indices as indicators to assess the spatial and temporal trends of water quality in the Dongjiang River. *Ecol. Indic.* 66, 306–312. doi: 10.1016/j.ecolind.2016.01.054

Tang, D., Liu, X., Wang, X., and Yin, K. (2018). relationship between the main communities and environments of an urban river and reservoir: Considering integrated structural and functional assessments of ecosystems. *Int. J Environ. Res. Public Health* 15:2302. doi: 10.3390/ijerph15102302

Trebitz, A. S., Nestlerode, J. A., and Herlihy, A. T. (2019). USA-scale patterns in wetland water quality as determined from the 2011 national wetland condition assessment. *Environ. Monitor. Assess.* 191:266. doi: 10.1007/s10661-019-7321-7

Wahl, D. H., Effert-Fanta, E. L., and Fischer, R. U. (2019). Effects of riparian forest buffers and agricultural land use on macroinvertebrate and fish community structure. *Hydrobiologia* 841, 45–64. doi: 10.1007/s10750-019-04006-1

Wan, X., Yang, T., Zhang, Q., Wang, W., and Wang, Y. (2021). Joint effects of habitat indexes and physic-chemical factors for freshwater basin of semi-arid area on plankton integrity – A case study of the Wei River Basin. China. *Ecol. Indic.* 120:106909. doi: 10.1016/j.ecolind.2020.106909

Wu, N., Schmalz, B., and Fohrer, N. (2012). Development and testing of a phytoplankton index of biotic integrity (P-IBI) for a German lowland river. *Ecol. Indic.* 13, 158–167. doi: 10.1016/j.ecolind.2011.05.022

Wu, Z., and Zhang, Y. (2013). Temporal and spatial variability of phytoplankton in Lake Poyang: The largest freshwater lake in China. *J. Great Lakes Res.* 39, 476–483. doi: 10.1016/j.jglr.2013.06.008

Wu, Z., Kong, M., Cai, Y., Wang, X., and Li, K. (2019). Index of biotic integrity based on phytoplankton and water quality index: Do they have a similar pattern on water quality assessment? A study of rivers in Lake Taihu Basin, China. *Sci. Total Environ.* 658, 395–404. doi: 10.1016/j.scitotenv.2018.12.216

Xu, F., Cao, F. Q., Kong, Q., Zhou, L. L., Yuan, Q., Zhu, Y. J., et al. (2018). Electricity production and evolution of microbial community in the constructed wetland-microbial fuel cell. *Chem. Eng. J.* 339, 479–486. doi: 10.1016/j.cej.2018.02.003

Xu, J., Yin, K., Lee, J. H. W., Liu, H., Ho, A. Y. T., Yuan, X., et al. (2010). Long-Term and Seasonal Changes in Nutrients, Phytoplankton Biomass, and Dissolved Oxygen in Deep Bay, Hong Kong. *Estuaries Coast* 33, 399–416. doi: 10.1007/s12237-009-9213-5

Yang, J., Wang, F., Lv, J., Liu, Q., Nan, F., Liu, X., et al. (2019a). Interactive effects of temperature and nutrients on the phytoplankton community in an urban river in China. *Environ. Monit. Assess.* 191:688. doi: 10.1007/s10661-019-7847-8

Yang, Y., Shen, Q., Hu, J., and Wang, W. (2019b). Plankton Community Structure and Water Ecology Assessment in Shitouhe Reservoir. Shanxi Province. *J. Hydroecol.* 40, 24–29.

Yuan, Y. X., Jiang, M., Liu, X. T., Otte, M. L., Ma, C. X., and Her, Y. G. (2018). Environmental variables influencing phytoplankton communities in hydrologically connected aquatic habitats in the Lake Xingkai basin. *Ecol. Indic.* 91, 1–12. doi: 10.1016/j.ecolind.2018.03.085

Zalack, J. T., Smucker, N. J., and Vis, M. L. (2010). Development of a diatom index of biotic integrity for acid mine drainage impacted streams. *Ecol. Indic.* 10, 287–295. doi: 10.1016/j.ecolind.2009.06.003

Zhang, H., Duan, Z., Wang, Z., Zhong, M., Tian, W., Wang, H., et al. (2019). Freshwater lake ecosystem health assessment and its response to pollution stresses based on planktonic index of biotic integrity. *Environ. Sci. Pollut. Res. Int.* 26, 35240–35252. doi: 10.1007/s11356-019-06655-0

Zhang, Y., Ban, X., Li, E., Wang, Z., and Xiao, F. (2020). Evaluating ecological health in the middle-lower reaches of the Hanjiang River with cascade reservoirs using the Planktonic index of biotic integrity (P-IBI). *Ecol. Indic.* 114:106282.

Zhao, Y., Lu, X., Ma, Y., Li, Z., Liu, Y., and Fan, Y. (2020b). Benthic diatoms community characteristics in AShi River Basin and aquatic environmental health assessment. *Oceanologia et Limnologia Sinica* 51, 307–317.

Zhao, G., Pan, B., Li, Y., Zheng, X., Zhu, P., Zhang, L., et al. (2020a). Phytoplankton in the heavy sediment-laden Weihe River and its tributaries from the northern foot of the Qinling Mountains: Community structure and environmental drivers. *Environ. Sci. Pollut. Res. Int.* 27, 8359–8370. doi: 10.1007/s11356-019-07346-6

Zhou, Y., Zhang, Y., Liang, T., and Wang, L. (2019). Shifting of phytoplankton assemblages in a regulated Chinese river basin after streamflow and water quality changes. *Sci. Total Environ.* 654, 948–959. doi: 10.1016/j.scitotenv.2018.10.348

Zhu, W., Liu, Y., Wang, S., Yu, M., and Qian, W. (2019). Development of microbial community–based index of biotic integrity to evaluate the wetland ecosystem health in Suzhou. China. *Environ. Monitor. Assess.* 191:377. doi: 10.1007/s10661-019-7512-2

Zuo, X., Cheng, S., Peng, H., Xu, H., and Lv, P. (2019). Evaluation of ecological health degree of Daning River based on Phytoplankton Index of Biotic Integrity. *Yangtze River* 50, 44–49+155.

frontiers | Frontiers in Marine Science

TYPE Original Research
PUBLISHED 20 September 2022
DOI 10.3389/fmars.2022.1013471

OPEN ACCESS

EDITED BY
Zhangxi Hu,
Guangdong Ocean University, China

REVIEWED BY
Linjian Ou,
Jinan University, China
Xudong Ye,
Memorial University of Newfoundland, Canada

*CORRESPONDENCE
Zhiming Yu
zyu@qdio.ac.cn

SPECIALTY SECTION
This article was submitted to Aquatic Microbiology, a section of the journal Frontiers in Marine Science

RECEIVED 07 August 2022
ACCEPTED 01 September 2022
PUBLISHED 20 September 2022

CITATION
Liu Z, Yu Z, Cao X, Jiang W, Yuan Y and Song X (2022) An environmentally friendly material for red tide algae removal: Performance and mechanism.
Front. Mar. Sci. 9:1013471.
doi: 10.3389/fmars.2022.1013471

An environmentally friendly material for red tide algae removal: Performance and mechanism

Zhengyu Liu[1,2,3,4], Zhiming Yu[1,2,3,4]*, Xihua Cao[1,2,3,4], Wenbin Jiang[1,2,3,4], Yongquan Yuan[1,2,3,4] and Xiuxian Song[1,2,3,4]

[1]Chinese Academy of Science (CAS) Key Laboratory of Marine Ecology and Environmental Sciences, Institute of Oceanology, Chinese Academy of Sciences, Qingdao, China, [2]Laboratory of Marine Ecology and Environmental Science, Qingdao National Laboratory for Marine Science and Technology, Qingdao, China, [3]University of Chinese Academy of Sciences, Beijing, China, [4]Center for Ocean Mega-Science, Chinese Academy of Sciences, Qingdao, China

Red tide is a kind of marine disaster caused by the accumulation or proliferation of microalgae and other organisms in a short period of time, and utilizing modified clay to control and inhibit red tide is the preferred method. Among them, the application potential of organic-modified clay is high; unlike inorganic and microbial modifications, it has a broad-spectrum removal capacity on red tide algae at extremely low dosages. However, it has some disadvantages such as severe toxicity and high residual turbidity, leading to several limitations in its practical application. Therefore, it has become urgent to select organic-modified reagents with higher efficiency, weaker toxicity and lower residual turbidity. In this study, the typical red tide alga——*Prorocentrum donghaiense* was selected to detect the removal capacity of Polydimethyl diallyl ammonium chloride (PDMDAAC) modified clay (MP) by comparing with the Hexadecyl trimethyl ammonium bromide (HDTMA) modified clay (MH). Not only the physiological stress and flocculation effects of two modified clays on microalgae had been discussed, but also the properties of the modified clays had been characterized in this study. The results showed that the low degree of oxidative stress and less damage to the cell membrane make MP more environmentally friendly, PDMDAAC can remove microalgae at a low dose (2 mg/L) and quickly clarify the water by significantly enhancing the flocculation capacity of clay. In addition to discussing the removal mechanism of two modified clays on microalgae, schematic diagrams of the pathways were drafted. This study will provide support for the development of organic-modified clay.

KEYWORDS

poly dimethyl diallyl ammonium chloride, modified clay, flocculation performance, physiological stress, removal mechanism

1 Introduction

Red tide is mainly caused by the proliferation of microalgae and other organisms within a short period of time, which can inhibit marine organisms, endanger ecosystems and compromise human security (Anderson, 2009; Lee et al., 2013; NOAA, 2016). Therefore, the effective prevention and emergency control of red tide has become a hotspot. Currently, utilizing clay minerals to control and inhibit red tide is a common measure. Multinational scholars from China (Cao et al., 2006; Liu et al., 2016; Yu et al., 2017; Wu et al., 2020), Japan (Shirota, 1989), South Korea (Na et al., 1996; Seger et al., 2017), the United States (Sengco and Anderson, 2004; Sengco et al., 2005), Saudi Arabia (Alshahri et al., 2021) and other countries have promoted the development of this method. However, due to the disadvantages of poor sol properties and low removal efficiency of clay minerals, in practical applications, due to the large amount of clay, the amount of sludge is high (Na et al., 1996). Therefore, scholars have developed inorganic or organic reagents, such as polyaluminum chloride (PAC), Aluminum sulfate, hexadecyl trimethyl ammonium bromide (HDTMA), and ferrate, to modifyclay, which greatly improved the removal efficiency of microalgae (Sengco et al., 2005; Cao et al., 2006; Liu et al., 2016; Yu et al., 2017; Alshahri et al., 2021).

Through the above studies, we found that inorganic modification can significantly improve the flocculation capacity of clay, while organically modified reagents tend to sterilize algae (Cao et al., 2006; Yu et al., 2017). Organically modified reagents are widely used in the control of red tides, and they always have a broad-spectrum removal capacity on microalgae at extremely low dosages (Cao et al., 2006; Zhang, 2016; Wu et al., 2020). Generally, due to its severe sterilization, organic-modified reagents always have a high toxicity, and the 48 h-LC_{50} of HDTMA on *Penaeus japonicus* was 1.482 mg/L (Cao et al., 2006), so there are several limitations in practical applications. Scholars have paid increasing attention to the sterilization effect of organic reagents, but have ignored the flocculation efficiency. Therefore, most organic-modified clays have defects such as slow floc sedimentation and high turbidity. Therefore, it has become an urgent demand to select organic-modified reagents with environmental friendliness and well promoted flocculation capacity. Polydimethyl diallyl ammonium chloride (PDMDAAC) is a cationic surfactant, that is widely used in water treatment (Li et al., 2018; Xin et al., 2015; Zhang et al., 2019). In the previous experiments of this study, it was found that PDMDAAC has a relatively high synergistic effect on clay, which can effectively remove *Prorocentrum donghaiense* in modified clay with a low dose (≤2 mg/L), and can rapidly flocculate and sediment microalgae, which can clarify the solution in 3 h. Different from that of the organic-modified reagents utilized in previous researches, the 96h-LC_{50} of PDMDAAC on juveniles of *Penaeus vannamei* is as high as 364 mg/L, which means PDMDAAC is an environmentally friendly algaecide.

This study speculates that the mechanism by which PDMDAAC inhibits algae is different from that of algaecides in previous researches. Therefore, this study utilized PDMDAAC to modify kaolin, explored the removal performance and mechanism of PDMDAAC modified clay, by observing the physiological indicators of microalgae, flocculation parameters and the property characterization of modified clay. This study will provide support for the development of organic-modified clay.

2 Materials and methods

2.1 Preparation of experimental reagents and modified clay

The clay used in the experiment was kaolin, produced in Indonesia. PDMDAAC was obtained from Aladdin, and the relative molecular mass was 100, 000, in a 35% aqueous solution. HDTMA was obtained from Aladdin, and was analytically pure. In the experiment, the PDMDAAC-modified clay was recorded as MP, HDTMA-modified clay was recorded as MH. Two kinds of modified clays were manufactured according to the mass ratio of clay: PDMDAAC or HDTMA of 200: 1, 2 or 5, recorded as MP1 or MH1, MP2 or MH2, and MP5 or MH5, respectively. The dose of modified clay was set to 0.2 g/L and the samples were prepared as aqueous solutions before use.

2.2 Modified material safety assessment

In this study, *P. vannamei* (approximately 11.91 mm in length and 26.28 mg in weight) was chosen as the test organism, and a 96-h acute toxicity test was conducted to evaluate the safety of PDMDAAC. PDMDAAC concentration gradients were set to 0, 20, 40, 80, 120, 200, 400, 800 mg/L. After domestication and cultivation, 20 P. *vannamei* were randomly selected and placed in a 5 L beaker containing sterilized seawater. PDMDAAC was added according to the dose above. Three parallels experimental groups were conducted, and dead individuals were counted and removed every 24 h, continuous experiment for 96h. After plotting the viability table, 96h-LC_{50} was calculated by linear interpolation.

2.3 Microalgal culture and treatment system

P. donghaiense was isolated from the Changjiang Estuary, which was kindly provided by Key Laboratory of Marine Ecology

and Environmental Sciences, Institute of Oceanology, Chinese Academy of Sciences. The natural seawater used in this experiment was taken from the coastal waters of Qingdao, filtered through a 0.45 μm cellulose acetate membrane (Shanghai, Xinya) before the experiment, and used after sterilization. The salinity and pH of seawater were 31 ± 1 and 8.00 ± 0.05 respectively. Inoculated an appropriate amount of *P. donghaiense* into a 5 L conical flask containing L1 cultural medium (Guillard and Hargraves, 1993), the initial density was 1×10^4 cells/mL, the culture temperature was 20 ± 1°C, the light intensity was 65 μmol photons m^{-2} s^{-1}, and the light-dark cycle was 12 h: 12 h. Experiments were performed when cultured to the later stage of exponential growth.

1) The microalgae removal experiment was carried out in 50 mL colorimetric tubes. After adding the modifier or modified clay according to the corresponding amount, the tubes were inverted and mixed three times, until sampling after 3 h. Three parallel experimental groups were conducted, and a blank control group was used. A chlorophyll *in vivo* fluorescence detector (Trilogy, Turner Designs, US) was used to measure viable microalgae density after treatment and calculate the removal rate of microalgae according to the following formula:

$$Microalgae\ removal\ rate(\%) = (1 - Experimental\ data/Blank\ control\ data) \times 100$$

2) The determination of the reactive oxygen species (ROS) was carried out in a 1 L beaker. The modified clay was added to the algae solution according to the corresponding amount, mixed well and sampled after 3 h. Three parallels experimental groups were conducted, and a blank control group was set. The microalgae in supernatant were collected by filtration through a GF/D membrane. Then, a cell disruptor was used to crush the cells (5.5 m/s, 30 s, 2 times) in an ice-bath environment, and the supernatant was extracted by centrifugation (5000 rpm, 10 min), which was the crude enzyme solution. Then use the crude enzyme solution obtained by the above method to measure the indicators including the protein content (BCA method), superoxide dismutase (SOD, WST-1 method) activity, catalase (CAT, ammonium molybdate method) activity, peroxidase (POD, colorimetry method) activity and malondialdehyde (MDA) content, which were determined with the assay kits purchase from Jiancheng (Nanjing) by a microplate reader (EnSight, Perkinelmer, US). Three parallel experimental groups were conducted, and a blank control group was used.

3) Trypan blue ($C_{34}H_{24}N_6Na_4O_{14}S_4$) is a kind of nucleic acid stain, that can be applied to detect the integrity of cell membranes. In this part of experiment, the proportion of modified clay reduced to clay: modified reagent of 200: 0.2, 0.5, 0.8 or 1 (mass ratio), the naming method of each group was similar as section 2.1, due to the low density of residual microalgae. The membrane stability test of microalgae was carried out in a 50mL colorimetric tube. After adding the modified clay according to the corresponding amount, the tube was inverted and mixed for three times. Three parallel experimental groups were conducted, and a blank control group was used. The supernatant was sampled at 3 h and stained and unstained cells were counted under an inverted microscope. The ratio of unstained cells was defined as cell activity in this study.

2.4 Modified clay flocculation experiment

2.4.1 Static flocculation experiment

The flocculation process of *P. donghaiense* by the modified clay under static conditions was observed by Particle Image Velocimetry (PIV, Flow Master, LaVision, Germany) The laser was used to illuminate a particular layer of flocs in the quartz tank, and a high-resolution image was obtained with a high-speed charge-coupled device (CCD) camera. The image was analyzed by using Davis 8.40 software (LaVision, Germany) to obtain the particle size and number of flocs. Experiments were carried out in 50ml quartz tanks, modified clay were added into algae according to the dose of 0.2 g/mL and mixed well. The samples were photographed with a specific time gradient until 180 min. The main indicators were floc particle size (D_{50}) and the particle density. The surface morphology of the flocs was carefully observed by scanning electron microscopy.

2.4.2 Coagulated flocculation experiments

The flocculation process of *P. donghaiense* with the modified clays and the self- flocculation process of the modified clays under coagulation conditions were observed by PIV. The measurement protocol is described in Section 2.4.1. Experiments were carried out in 100 ml quartz dishes; modified clay were added into algae according to the dose and mixed well. By adjusting the stirring speed, divide the experimental process into the growth phase (50 rpm, 15 min) - breakage phase (150 rpm, 10 min) - regrowth phase (50 rpm, 20 min). The main indicators (Wu et al., 2020): ①the floc particle size (D_{50}); ②particle density; ③fractal dimension; ④ flocculation speed (sg): $sg = dt1/tg$; ⑤ floc recovery factor (R_f): $Rf = 100\% \times (dt3 - dt2) / (dt2 - dt1)$; ⑤ floc strength ($M$): $M = 100 \times dt2 / dt1$. The M indicates the ability of flocs to resist rupture by a certain velocity gradient and the capacity of flocs to regrow is evaluated by the R_f (Jarvis et al., 2005; Zhao et al., 2011).

2.5 Characterization of modified clay

The zeta potentials of the samples were measured by a Malvern nanoparticle potentiometer (Zetasizer, Malvern, UK). The apparatus used for FTIR spectroscopy was a Nicolet FTIR-740 spectrometer. The mineral sample ground to −5 μm was put into a beaker with a certain amount of polymer agents according

to the experimental conditions and the suspension was stirred for 20 min. After washing and filtration, the filter cake was dried at 50°C in a vacuum drying oven. Finally, the infrared spectra of the mineral samples and these reagents were determined by this spectrometer. Scanning electron microscopy (SEM) images were taken by using a Japan Hitachi S-3400N. The powdered samples were first affixed onto adhesive tapes supported on metallic disks and then covered with a thin, electrically conductive gold film. Images were recorded at different magnifications (200–7000×) at an operating voltage of 5.0 kV. ①The flocs for SEM was collected in the bottom of the vessel in microalgae removal experiment, and freeze-dried for 48 h, the samples were obtained; ② The modified clay samples were dried at 60°C for 12 h, and ground into powder prior to SEM analysis.

2.6 Data statistics and analysis

Origin 2018 (OriginPro 2018C, Origin Lab, US) and Microsoft Excel (Microsoft® Excel® 2019MSO, Microsoft, US) were used to generate graphs, and data are expressed as the mean ± standard deviation (mean ± SD); Statistical analysis of the data was performed using one-way ANOVA and the independent samples T test in SPSS 19.0 (IBM SPSS Statistics 19, IBM, US), $P<0.05$ indicated that the difference was significant, and $P<0.01$ indicated that the difference was extremely significant.

3 Results

3.1 Modified material safety assessment

A 96h-acute toxicity experiment of PDMDAAC on juveniles of *P. vannamei* was carried out to evaluate its ecological safety (Table 1). The 96 h-LC_{50} can be calculated by the linear interpolation method to be approximately 364.96 mg/L. The safe concentration of PDMDAAC was determined to be 36.45 mg/L and subsequent experimental concentrations were based on the above results.

3.2 Removal performance of modified clay on microalgae

The removal ability of *P. donghaiense* by kaolin was weak, and the removal rate was only approximately 20% when the dose was 0.2 g/L (Figure 1). PDMDAA had a significant synergistic effect on kaolin ($P<0.05$). MP can significantly reduce the algal density rapidly (3 h), even the removal rate of the lowest concentration group (MP1) reached approximately 50%, and gradually surpassing 95% removal, the removal effect can be maintained up to 24 h. The treatments of microalgae by HDTMA modified clay had a similar trend to the MP group, and the removal rate of each group was slightly improved at 24 h.

3.3 Physiological stress of microalgae

After adding the two modified clays, the activities of the two antioxidant enzymes (SOD and CAT) in microalgae were significantly promoted ($P<0.05$), indicating that these two modified clays could inhibit the microalgae by producing ROS stress (Figure 2A). The activities of the three antioxidant enzymes in the MH group were higher than those in the MP group, and the enzyme activities showed a more significant gradient growth. PDMDAAC had a weak induction of POD, and only the highest concentration group (MP5) significantly increased ($P<0.05$). The MDA content had a positive correlation with the degree of lipid peroxidation, and both modified clays can increase the MDA content of the microalgae (Figure 2B). However, microalgae in the MH group experienced higher lipid peroxidation than those in the control group, and the MDA content in MP5 was only 68.8% of that in

TABLE 1 96h acute toxicity test results of Poly dimethyl diallyl ammonium chloride (PDMDAAC) on juveniles of *P. vannamei*.

PDMDAAC (mg/L)	Death rate (%)			
	24 h	48 h	72 h	96 h
0	0.00 ± 0.00	0.00 ± 0.00	0.00 ± 0.00	0.00 ± 0.00
20	0.00 ± 0.00	0.00 ± 0.00	0.00 ± 0.00	0.00 ± 0.00
40	0.00 ± 0.00	3.33 ± 4.71	6.67 ± 4.71	6.67 ± 4.71
80	0.00 ± 0.00	0.00 ± 0.00	10.00 ± 0.00	16.67 ± 4.71
120	6.67 ± 4.71	6.67 ± 4.71	20.00 ± 0.00	26.67 ± 4.71
200	0.00 ± 0.00	10.00 ± 8.16	26.67 ± 4.71	36.67 ± 4.71
400	6.67 ± 4.71	23.33 ± 4.71	43.33 ± 4.71	63.33 ± 4.71
600	3.33 ± 4.71	23.33 ± 4.71	63.33 ± 4.71	83.33 ± 4.71
800	10.00 ± 0.00	43.33 ± 9.42	80.00 ± 0.00	100.00 ± 0.00

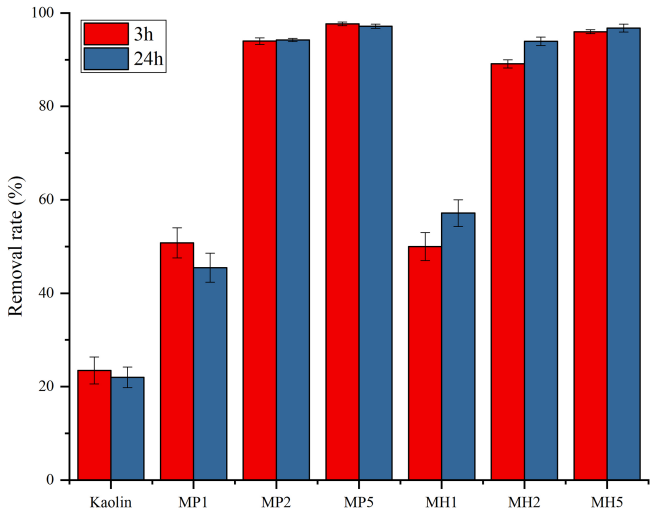

FIGURE 1
Removal effects of two modified clays on *P. Donghaiense*.

MH2 (Figure 2B). In conclusion, MH led to severe peroxidative stress of *P. donghaiense* and induce a higher degree of lipid peroxidation than MP.

The removal ability of *P. donghaiense* by kaolin was slightly increased after modification with a lower dose of PDMDAAC and HDTMA (Figure 2C). The microalgae of the MP group were almost unstained, and 94% of the MP5 cells were healthy. The cell membranes of the MH group lacked integrity, and the cell activity gradually decreased from 99% to 17%. The above results indicated that MH caused a more severe damage to the microalgal membrane, which was consistent with the change in MDA content.

3.4 Discrepancies in the flocculation of modified clays

3.4.1 Flocculation performance under static conditions

The addition of modified clay resulted in a blurred view, and evenly distributed microalgae could still be observed. It could be observed that the microalgae in the MP group began to aggregate at 15 min, and flocs were continuously generated in the following 10 min; the D_{50} and particle density began to decrease after 25 min (Figure 3), which indicated that the flocs could sediment quickly. Until 90 min, the visual field was dominated by small flocs. There was no significant change of D_{50} in the MH group among the whole experimental process (Figure 3), and the particles were evenly distributed in the view. The tendency of the particle density in the MH group was similar to that in the MP group, but caused a higher residual turbidity because of the slower sedimentation speed of flocs. In conclusion, MP had a higher flocculation capacity on *P. donghaiense*, and the flocs hada higher D_{50} and faster sedimentation speed.

3.4.2 The surface morphology of the floc surface

To further explore the differences in flocculation, we photographed the surface images of flocs in section 3.4.1. The kaolin group was dominated by small flocs, and there were many clustered structures attached to the surface of flocs (Figures 4A, B). MP could flocculate microalgae well, even though the lowest concentration group (MP1) mainly consisted of medium-sized flocs (≥200 μm) (Figure 4C). The surface of the flocs was dominated by square-shaped protrusions with rounded edges (Figures 4D–F). These protrusions were arranged in an irregular superimposed manner, causing the flocs to present a relatively three-dimensional spatial structure. With the increase in PDMDAAC addition, the density of such protrusions gradually increased, and microalgae embedded in flocs were observed in each group. The flocculation capacity of MH was weaker, and MH5 was dominated by small flocs with particle sizes between 100-200 μm (Figure 4G). After adjusted the magnification to 7000×, the morphology of the flocs was coated with clustered structures similar in the kaolin group and a small amount of square protrusions; only in the two relatively high concentration groups (MH2&MH5) could embedded microalgae be observed (Figures 4H–J).

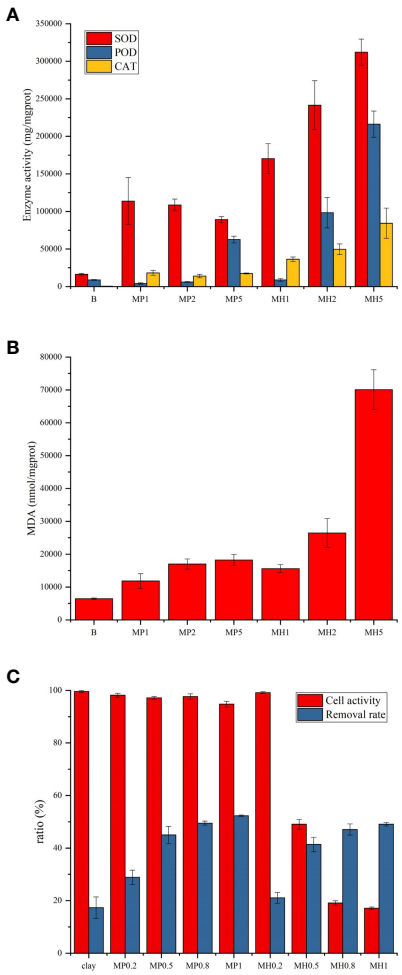

FIGURE 2
Effects of two modified clays on antioxidant enzyme activity, MDA and cell activity in *P. donghaiense* **(A–C)**.

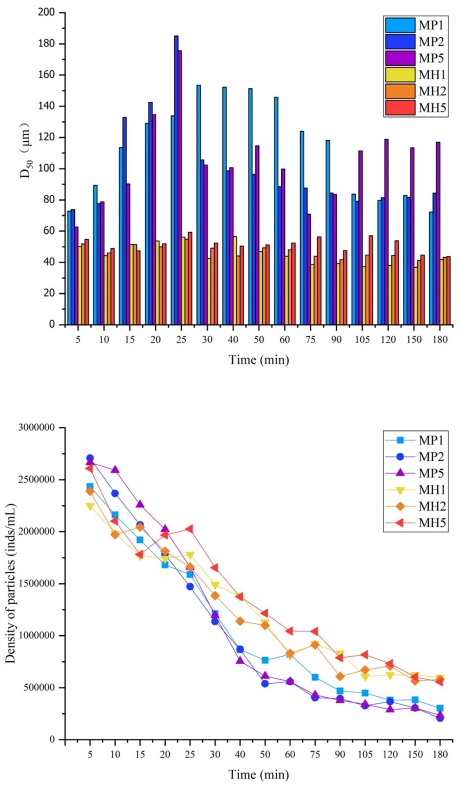

FIGURE 3
Changes in D_{50} and particle density during the process of flocculating microalgae with modified clay under static conditions.

3.4.3 Flocculation process under coagulation conditions

Similar to the static flocculation experiment, the vision clarity gradually recovered after the addition of the modified clay, and this process was significantly accelerated under coagulated conditions. This phenomenon caused the particle density of each group to first increase and then decrease from 0 to 15 min (Figure 5). Both modified clays showed a strong flocculation effect, and the MP group clarified faster and had a higher s_g than the MH group (Table 2). The higher stirring rate (150 rpm) in the breakage phase greatly improved the growth of flocs, leading to a nearly double increase in D_{50}. Afterwards, due to the rapid sedimentation of large flocs from 25 to 27 min, the particle density and D_{50} of each group were maintained at a low degree (Figure 5). The M and R_f of the two modified clays were high (Table 2), which indicated that the coagulation system could significantly improve the flocculation capability.

The self-flocculation experiment showed that, the D_{50} and fractal dimension of the MH group were higher than those of the MP group (Figure 6), which indicated that HDTMA could combine with clay to generate large and compact flocs. The flocs produced by self-flocculation had a low strength (Table 3), which was reflected in the significant changes in the floc size and particle density when the stirring speed increased to 150 rpm. After 35 min, the D_{50} and fractal dimension of the MH group decreased significantly, which might be caused by floc sedimentation. The self-flocculation capability of MP was slightly weaker, and MP was greatly affected by high-speed stirring, causing the wild fluctuations of the three parameters in Figure 6. However, the flocs formed by MP had higher recovery rates between 100-181 (Table 3), which helped the floc size to improve quickly.

3.5 Characterization of modified materials

3.5.1 Zeta potential of modified clay in different media

The results showed that Indonesian kaolin exhibited strong electronegativity (-10 mV) in pure water (Figure 7). Both

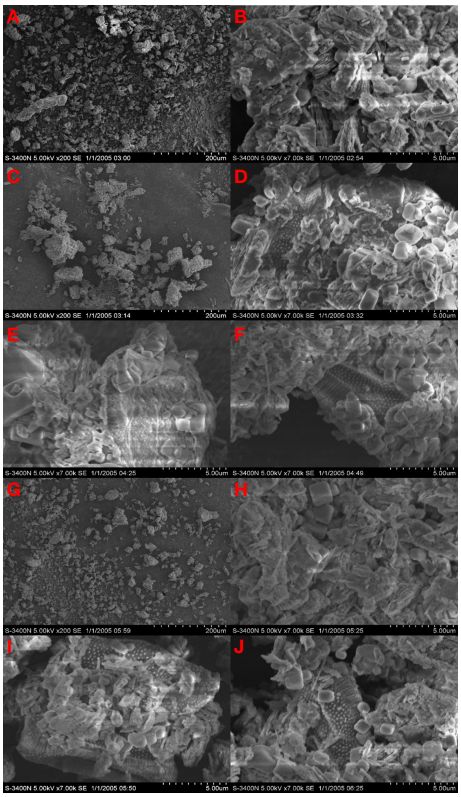

FIGURE 4
SEM images of flocs in the kaolin, MP and MH group under static conditions **(A–J)**.

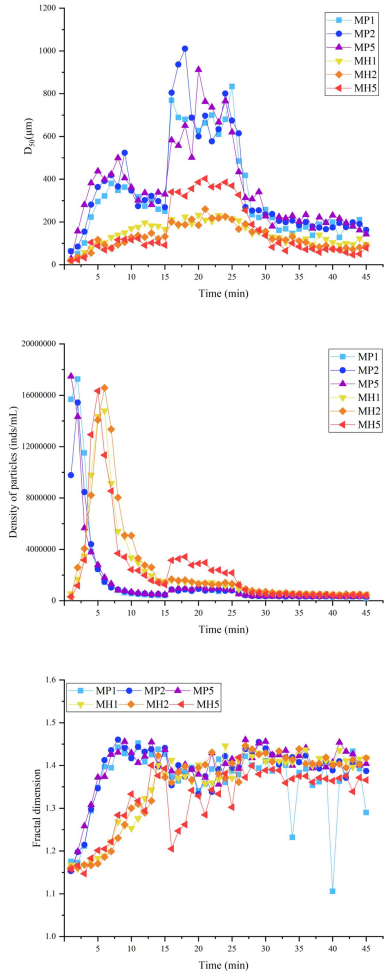

FIGURE 5
Changes in the D_{50}, particle density and fractal dimension during flocculation of microalgae with modified clay under coagulation conditions.

modification methods significantly increased the zeta potential of kaolin, MP was more positive than MH, and the zeta potential of the three concentration groups reached 26.30, 37.00, and 44.80 mV (Figure 7). The zeta potential elevating effect of MH was weak, and the zeta potential of each concentration was lower than that of the former samples.

Zeta potential can be applied to evaluate the physical stability of the particle dispersion system. The lower the absolute value of the zeta potential, the weaker the electrostatic repulsion is between particles and the easier the aggregation or agglomeration. The addition of kaolin to the microalgae would reduce the potential to approximately -16.00 mV (Figure 7). The repulsion between particles was strong under these conditions, which proved the weak flocculation ability of kaolin to microalgae. The PDMDAAC modified clay had a strong positive charge, which could significantly increase the zeta potential. The improvements in zeta potential of the MH group were weak, and MH5 had no significant difference from *P. donghaiense*, which could be one of the reasons for the observed weaker flocculation of MH than of MP outlined in Section 3.4.1. Aiming at self-flocculation, this study investigated the zeta potential of two modified clays in seawater, and kaolin could further reduce the zeta potential of seawater to -14.50 mV (Figure 7). The potential of the two modified clays increased in steps, and MP could turn the entire solution positively charged. While HDTMA failed to change the electronegativity, however, the absolute value of its zeta potential was low. which could promote particle agglomeration.

3.5.2 The surface morphology of clay

As shown in the SEM images, a dense laminated structure could be observed in Figure 8A, and the surface of the layered structure was mostly covered with a large number of clustered structures (Figure 8B).

Solid PDMDAAC was white and translucent crystalline particles. We observed several holes and fragments attached to the compound surface (Figure 8C). The protuberances were distributed on the surface of the particles in a scale-like pattern,

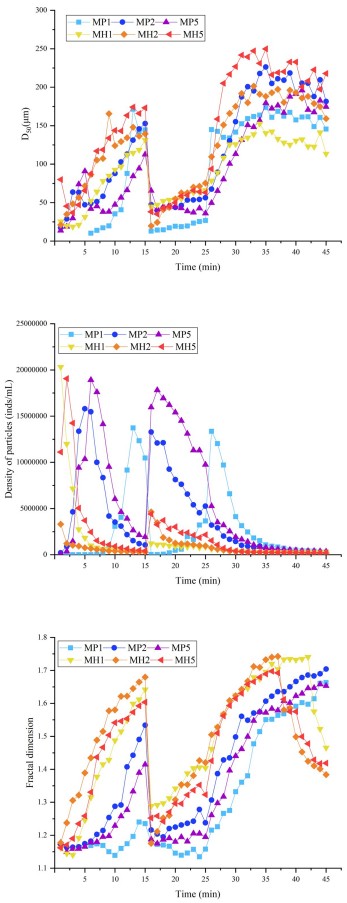

FIGURE 6
Changes in the D50, particle density and fractal dimension during self-flocculation of modified clay under coagulation conditions.

presenting a three-dimensional spatial network structure, and there were rounded protrusions attached to the surface (Figure 8D). PDMDAAC could significantly reduce the clustered structures on the clay surface, and replace them with rounded protrusions. Similar to PDMDAAC, the surface of MP became compact (Figures 8E, F). The above phenomenon showed that PDMDAAC had been successfully loaded on the clay, and the density of such a flaky distribution gradually increased, indicating that the loading of the modified reagents increased gradually.

The surface of HDTMA particles was free of voids and depressions, and the structure was entirely compact and smooth (Figure 8G). It could be observed (Figure 8H) that a large number of sheet-like structures with smooth edges were distributed on the surface of material. HDTMA modification has a certain ability to modify the surface structure of clay. Two high concentration groups (MH2&MH5) were accompanied by a small number of sheet-like protrusions and a higher proportion of clustered structures (Figures 8I, J).

3.5.3 Characterization of the surface functional groups of clay and modified reagents

The surface functional groups of clay and modified reagents were observed by FT-IR spectroscopy (Figure 9). As an inorganic mineral, the characteristic peaks of kaolin are mainly distributed in the far-infrared region (400-33 cm^{-1}). Two weak absorption peaks could be observed above 3000 cm^{-1}, O-H at 3688.62 cm^{-1} and =C-H at 3619.09 cm^{-1}. The absorption peaks below were all located in the fingerprint region (1300-400 cm^{-1}), 1050 ± 50 cm^{-1} was generally the stretching vibration peak of -C-O, 910.54 cm^{-1} was the bending vibration of -OH, and 660 ± 20 cm^{-1} was the rocking vibration peak of -OH.

The infrared spectrum of PDMDAAC was investigated, and we observed a strong N-H absorption peak at 3361.88 cm^{-1} and a weaker stretching vibration absorption peak of unsaturated C (sp^2)-H at 3010.40 cm^{-1}. The asymmetric stretching vibration peak of $-CH_2$ appeared at 2934.25 cm^{-1}. Corresponding to the two absorption peaks above 3000 cm^{-1}, the bending vibration peak of N-H appeared at 1630.20 $cm^{-1}$and the out-of-plane twist vibration peak of $=CH_2$ appeared at 988.84 cm^{-1}.

The infrared spectrum of HDTMA is shown in Figure 9. We found that 3016.90 cm^{-1} is the weak stretching vibration peak of C-H, 2915.52 cm^{-1} is the asymmetric stretching vibration peak of $-CH_2$, and 2848.09 cm^{-1} is the symmetric stretching vibration peak of $-CH_2$. The absorption peaks in the interval of 1500-1400 cm^{-1} were mostly the bending vibration region of the group, such as the scissor vibration peak of $-CH_2$ at 1462.05 cm^{-1}, the bending vibration peak of C-N at 1430.74 cm^{-1}, and the symmetric bending vibration peak of CH_3 at 1382.50 cm^{-1}. In the fingerprint region, 1000-650 cm^{-1} was the out-of-plane bending vibration region of unsaturated C-H, 910.97 and 829.75 cm^{-1} represented the C-N absorption peaks, and the peak at 720 ± 10 cm^{-1} should be the rocking vibration of $-CH_2$.

TABLE 2 Changes in parameters during flocculation of microalgae with modified clay under coagulation conditions.

Group	MP1	MP2	MP5	MH1	MH2	MH5
s_g (μm/min)	16.69	17.93	21.98	11.11	8.77	6.11
M	332.83	250.76	187.84	129.27	160.64	403.28
R_f (%)	117.44	126.20	164.64	245.49	152.01	104.90

(s_g, flocculation speed; R_f, floc recovery factor; M, floc strength).

TABLE 3 Changes in parameters during self-flocculation of modified clay under coagulation conditions.

Group	MP1	MP2	MP5	MH1	MH2	MH5
s_g (μm/min)	9.64	10.19	7.507	8.77	9.29	11.55
M	18.46	36.91	32.06	50.27	54.02	36.37
R_f (%)	100.85	129.77	181.06	72.48	130.89	140.47

(s_g, flocculation speed; R_f, floc recovery factor; M, floc strength).

4 Discussion

Through microalgae removal experiments, this study found that PDMDAAC has a significantly synergistic effect on kaolin and can quickly remove *P. donghaiense* at a relatively low dose. Considering the practical application, this study conducted toxicological experiments and found that PDMDAAC is environmentally friendly, which is contrary to the high toxicity of the organic-modified reagents used in previous researches. Therefore, this study hypothesized and explored the removal mechanism of PDMDAAC, with the physiological indicators, flocculation parameters and modified clay characterization.

4.1 The flocculation mechanism of modified clay on microalgae

The sterilization ability of Indonesian kaolin clay against *P. donghaiense* was weak, and the removal rate was approximately 20% when the dosage was 0.2 g/L, and no microalgae were observed on flocs. The addition of clay reduced the zeta potential of the microalgal solution from -12.7 mV to approximately -16.0 mV. The repulsion between particles was intensive under this condition, indicating that particles do not easily to agglomerate. This should be one of the reasons why it is difficult for kaolin to flocculate microalgae. The synergistic ability of PDMDAAC to clay was remarkable, and the removal rate of microalgae in the MP2 group reached 90% with a lower residual turbidity after treatment. The flocculation experiment could intuitively explain the above phenomenon. The MP could significantly reduce the absolute value of the zeta potential in solution; that is, adding MP to the algae liquid could provide a suitable environment for particle aggregation and agglomeration, and promote flocculation. The electron microscopic images showed that PDMDAAC can be loaded on the surface of kaolin. The flocs of the MP group also retained more sheet-like protrusions similar to MP, which enabled the flocs to electrostatically tract the microalgae, and the spatial net structure helped the flocs to further sweep and capture microalgae. This prompted the microalgae to aggregate and form flocs quickly, which manifested as a rapid decrease in particle density and an increase in D_{50} in the experimental parameters. The higher agglomeration and sedimentation capacity of flocs jointly accelerated the clarification of the solution.

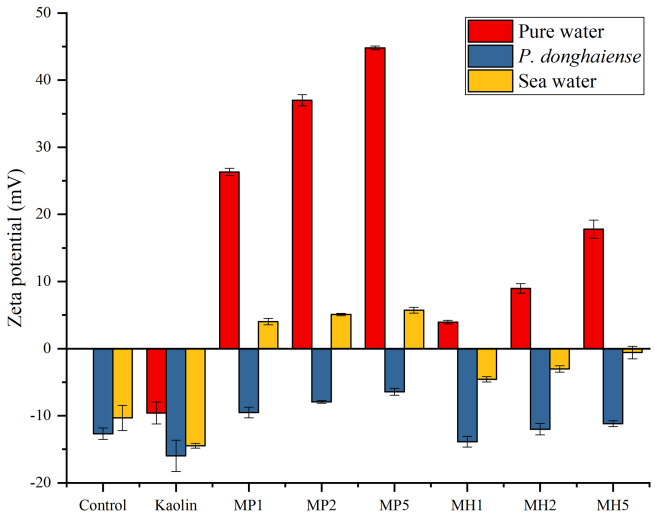

FIGURE 7
Effects of two modified clays on the zeta potential of pure water, *P. donghaiense* and natural seawater.

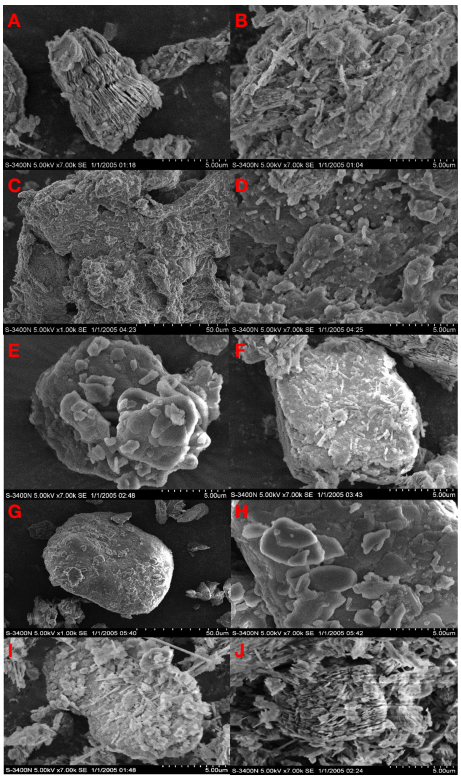

FIGURE 8
Surface structure of kaolin, modified reagents, MP and MH under SEM **(A–J)**.

Among the MH group, the average distribution of microalgae and small flocs could be observed during the whole experiment. Due to the low sedimentation speed, the solution turbidity was still high until 180 min. This phenomenon could be due to the inappropriate zeta potential of the solution, and the intense repulsion between particles obstructs MH flocculation of microalgae. Through SEM images, we found that HDTMA did not modify the clay surface as much as PDMDAAC, which weakened the electrostatic traction effect of modified clay. The floc particle size of MH5 was approximately 50 μm, which was consistent with the PIV observation (180 min-D_{50} = 43.8 μm). The surface of the floc had no kaolin, and no attached modified structure, which may be one of the reasons for its weak floc growth, and only a small number of microalgae can be observed in the two high concentration groups.

Red tides often break out in coastal areas, estuaries, etc. Wind, ocean currents and thermal cycles maintain the environmental dynamics, and these disturbances will inevitably affect the flocculation. Appropriate physical disturbance can increase the collision frequency of particles in the dispersion system, thereby improving the flocculation efficiency, making it obvious to identify differences in flocculation characteristics. Therefore, the flocculation ability of modified clay under coagulation conditions was observed in this study. The flocculation efficiency of MP on microalgae increased with increasing stirring speed, and D_{50} increased significantly at 150 rpm. The coagulation conditions improved the flocculation effect of MH on microalgae, and the flocs could also resist the shear force caused by a high stirring speed, but the flocculation parameters such as D_{50} and particle density reduction rate were lower than those of MP. The binding force between MP and microalgae was tough, and this force should be related to the PDMDAAC loaded on the modified clay.

In addition to the flocculation of microalgae, there is also an interaction between modified clay particles, called self-flocculation. Studies have shown that powerful self-flocculation impacts the algae removal efficiency of modified clays (Jiang et al., 2021). In seawater under coagulation conditions, the D_{50}

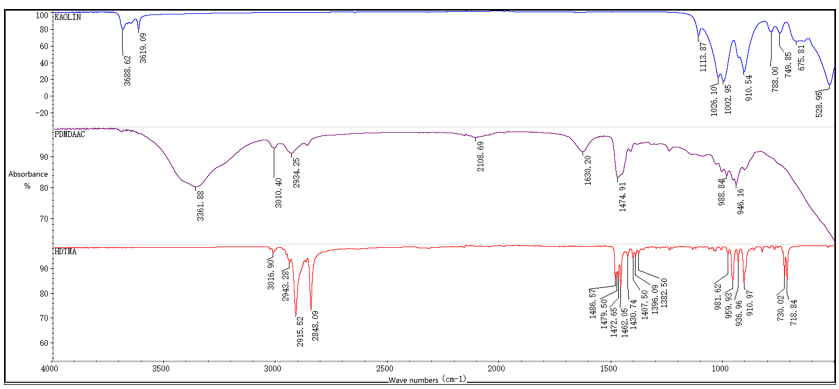

FIGURE 9
FT-IR spectra of kaolin, PDMDAAC and HDTMA.

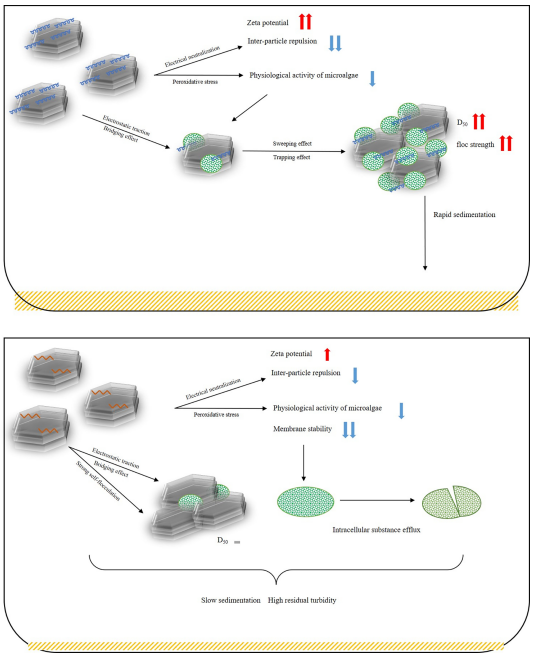

FIGURE 10
Schematic diagram of the algae removal pathway of two modified clays (MP and MH).

and fractal dimension of the MH group were both higher, which indicated that there was a powerful binding force between HDTMA and clay. Additionally, this study found that the zeta potential of kaolin in seawater was -14.5 mV, and MH had an appropriate prompt effect on the zeta potential, which could significantly reduce the repulsion between particles in the solution. The strong self-flocculation ability of MH should be due to the moderate stirring rate and the zeta potential, the former can significantly improve the collision efficiency of particles, and the latter may reduce the repulsion between particles.

4.2 Environmental friendliness mechanism of PDMDAAC modified clay

Quaternary ammonium salts (QACs) are a kind of sterilant, that are widely used in water disinfection, biofilm inhibition and other fields (Andrzej et al., 2017; Pang et al., 2020; Zhang et al., 2021), Some kinds of QACs can notably promote the disinfectant properties of clay (Cao et al., 2006; Zhang, 2016; Wu et al., 2020). It is well known that the sterilization mechanisms of QACs include the following: ①The positively charged nitrogen atom in the QAC molecule has a severe electrostatic interaction with the negatively charged cell membrane, and the long-chain alkyl group binds to the cell membrane, destroying the hydrophobic surface, resulting in irreversible damage, which will force the cell contents to flow out, killing cells by lysis (Huang and Kim, 2013; Wessels and Ingmer, 2013; Gerba, 2015; Seo et al., 2016); ②inducing the production of excess reactive oxygen species, including single oxygen ($1O^{2-}$), hydroxyl radicals (OH·), superoxide anion radicals (O^{2}·) and hydrogen peroxides (H_2O_2) could cause oxidative stress and lead to cell injury (Mittler et al., 2011; Fu et al., 2014); ③positively charged nitrogen atoms in QAC molecules tend to replace Ca^{2+} on the cell membrane, which can reduce the stability of the cell membrane and interfere with the ion exchange between cells and outside (Chen and Cooper, 2002; Jellali et al., 2013; Das et al., 2014); and ④QACs can reduce the chlorophyll content, weaken photochemical quenching, break the chloroplast membrane structure, and inhibit the photoreaction process (Cao et al., 2006; Pérez et al., 2009; Sukenik et al., 2017). Based on the above mechanisms, this study explored the stress effects of MP and MH on the antioxidant defenced system and cell membrane of microalgae. The results showed that both modified clays could induce microalgae cells to produce excess reactive oxygen species, resulting in peroxidative stress. MDA is an essential indicator of peroxidative damage in addition to the antioxidant enzyme system, and its content is positively correlated with the degree of lipid peroxidation. The MDA content of the microalgae in the MH group was higher than that in the MP group, which may indicate that the cell membrane of the microalgae in the MH group was more damaged. The results of trypan blue staining showed that the microalgae in the MP group were almost unstained, while the microalgae in the MH group suffered strong damage to the cell membrane, and the cell viability gradually decreased with increasing modifier concentration, which was similar to lipid peroxidation.

Through the above process, this study found that the ability of QACs to sterilize microalgae mainly originates from there quaternary amino (C-N) functional groups. By exploring the molecular configurations of the two organic agents, this study found that the content of quaternary amino groups of PDMDAAC should be 2.25 times that of HTDMA of the same quality. According to the mechanism of action of QAC, compounds with more C-N should be more toxic. However, PDMDAAC is significantly safer than HDTMA, which is contrary to the observed results. Through FT-IR, this study found that a strong N-H absorption peak can be observed on PDMDAAC, which might be due to the high level of polymerization of this molecule. The stacking of long carbon chains exposed the conjugated electrons on the quaternary ammonium group and bound to H. The N-H bond might weaken the sterilization effect of PDMDAAC by inhibiting the activity of the quaternary ammonium group, thereby making PDMDAAC environmentally friendly.

4.3 Overview of modified clay removal pathways

In summary, the removal pathway of MP to microalgae was shown in a schematic diagram (Figure 10): PDMDAAC can exert an electric neutralization effect to increase the zeta potential of the solution, reduce the repulsion between particles, and promote agglomeration. The PDMDAAC attached to the surface of MP and flocs can assist the clay in capturing and sweeping the microalgae through electrostatic traction and bridging, thereby promoting floc aggregation and sedimentation, to achieve rapid water clarification. MP can also reduce microalgal activity by inducing peroxidative stress, making it easier to remove.

As shown in Figure 10, the inferior flocculation capacity of MH on microalgae should be consistent with the following points: Weak electric neutralization of MH made it difficult for the particles in the solution to agglomerate. HDTMA had a weak modification effect on the surface of clay, which undermined the binding force between MH and microalgae, and the strong self-flocculation ability jointly obstructed the flocculation of microalgae. However, MH could induce microalgae to produce excess reactive oxygen species, resulting in significant peroxidative stress, forcing high degree of lipid peroxidation and destroying the structure of microalgal membranes. The intense cytotoxicity of HDTMA compensated for the lack of flocculation, thereby sterilizing microalgae effectively.

5 Conclusions

1. The extremely low dose of PDMDAAC had a significantly synergistic effect on kaolin, and the MP could remove *P. donghaiense* effectively.
2. The flocculation effect of MH on microalgae was negligible, which should be caused by its strong self-flocculation ability, weak positive charge, and short carbon chain. MH could increase the degree of peroxidative stress and lipid peroxidation, and destroy the structure of the cell membrane, thereby sterilizing microalgae.
3. The low degree of oxidative stress and less damage to the cell membrane made MP more environmentally friendly, and the microalgae removal effect was mainly due to flocculation. PDMDAAC could exert an electrical neutralization effect to increase the zeta potential of algal liquid and reduce the repulsion between particles in the solution, and the PDMDAAC attached to the surface of modified clay and flocs assisted clay in capturing and sweeping microalgal cells through electrostatic traction and bridging.

Data availability statement

The original contributions presented in the study are included in the article/Supplementary Material. Further inquiries can be directed to the corresponding author.

Author contributions

ZL, conceptualization, writing – original draft, investigation, resources, and methodology. ZY, conceptualization, formal analysis, writing – review and editing, project administration, and funding acquisition. XC, conceptualization, writing – review and editing, funding acquisition. WJ, resources and investigation. YY, writing – review and editing, investigation. XS, writing – review and editing, funding acquisition. All authors contributed to the article and approved the submitted version.

Funding

This research was financially supported by the Marine S&T Fund of Shandong Province for Pilot National Laboratory for Marine Science and Technology (Qingdao) (No. 2021QNLM040001), National Natural Science Foundation of China (41976145), and the Taishan Scholars Climbing Program of Shandong Province of 2019.

Conflict of interest

The authors declare that the research was conducted in the absence of any commercial or financial relationships that could be construed as a potential conflict of interest.

Publisher's note

Supplementary material

The Supplementary Material for this article can be foundonline at: https://www.frontiersin.org/articles/10.3389/fmars.2022.1013471/full#supplementary-material

References

Alshahri, A. H., Fortunato, L., Ghaffour, N., and Leiknes, T. O. (2021). Controlling harmful algal blooms (HABs) by coagulation-Flocculation-Sedimentation using liquid ferrate and clay. *Chemosphere* 274 (68), 129676. doi: 10.1016/j.chemosphere.2021.129676

Anderson, D. M. (2009). Approaches to monitoring, control and management of harmful aalgal blooms (habs). *Ocean Coast. Manage.* 52 (7), 342. doi: 10.1016/j.ocecoaman.2009.04.006

Andrzej, B., Pawe, K., Grzegorz, C., Jolanta, C., Tomasz, C., Anna, M. F., et al. (2017). Interaction of quaternary ammonium ionic liquids with bacterial membranes – studies with escherichia coli R1–R4-type lipopolysaccharides - ScienceDirect. *J. Mol. Liquids* 246, 282–289. doi: 10.1016/j.molliq.2017.09.074

Cao, X., Song, X., Yu, Z., and Wang, K. (2006). Study on the mechanism of removing red tide organisms by organically modified clay. *Environ. Sci.* 27 (8), 1522–1530. doi: 10.3321/j.issn:0250-3301.2006.08.009

Chen, C. Z., and Cooper, S. L. (2002). Interactions between dendrimer biocides and bacterial membranes. *Biomaterials* 23 (16), 3359–3368. doi: 10.1016/S0142-9612(02)00036-4

Das, T., Sehar, S., Koop, L., Wong, Y. K., Ahmed, S., Siddiqui, K. S., et al. (2014). Influence of calcium in extracellular DNA mediated bacterial aggregation and biofilm formation. *PloS One* 9 (3), e91935. doi: 10.1371/journal.pone.0091935

Fu, P., Xia, Q., Hwang, H., Ray, P. C., and Yu, H. (2014). Mechanisms of nanotoxicity: Generation of reactive oxygen species. *J. Food Drug Anal.* 22 (1), 64–75. doi: 10.1016/j.jfda.2014.01.005

Gerba, C. P. (2015). Quaternary ammonium biocides: Efficacy in application. *Appl. Environ. Microbiol.* 81 (2), 464–469. doi: 10.1128/AEM.02633-14

Guillard, R., and Hargraves, P. E. (1993). Stichochrysis immobilis is a diatom, not a chrysophyte. *Phycologia* 32 (3), 234–236. doi: 10.2216/i0031-8884-32-3-234.1

Huang, W. C., and Kim, J. D. (2013). Cationic surfactant-based method for simultaneous harvesting and cell disruption of a microalgal biomass. *Bioresource Technol.* 149 (Complete), 579–581. doi: 10.1016/j.biortech.2013.09.095

Jarvis, P., Jefferson, B., Gregory, J., and Parsons, S. A. (2005). A review of floc strength and breakage. *Water Res.* 39 (14), 3121–3137. doi: 10.1016/j.watres.2005.05.022

Jellali, R., Kromkamp, J. C., Campistron, I., Laguerre, A., Lefebvre, S., Perkins, R. G., et al. (2013). Antifouling action of polyisoprene-based coatings by inhibition of photosynthesis in microalgae. *Environ. Sci. Technol.* 47 (12), 6573–6581. doi: 10.1021/es400161t

Jiang, W., Yu, Z., Cao, X., Jiang, K., Yuan, Y., Anderson, D. M., et al. (2021). Effects of soluble organics on the settling rate of modified clay and development of improved clay formulations for harmful algal bloom control. *Environ. pollut.* (2021) 289, 117964. doi: 10.1016/j.envpol.2021.117964

Lee, C. K., Park, T. G., Park, Y. T., and Lim, W. A. (2013). Monitoring and trends in harmful algal blooms and red tides in Korean coastal waters, with emphasis on *Cochlodinium polykrikoides*. *Harmful Algae* 30 (dec.suppl.1), S3–S14. doi: 10.1016/j.hal.2013.10.002

Liu, Y., Cao, X., Yu, Z., Song, X., and Qiu, L. (2016). Controlling harmful algae blooms using aluminum-modified clay. *Mar. Pollut. Bull.* 103 (1/2), 211–219. doi: 10.1016/j.marpolbul.2015.12.017

Li, N., Yue, Q., Gao, B., Xu, X., Kan, Y., and Zhao, P. (2018). Magnetic graphene oxide functionalized by polydimethyldiallylammonium chloride for efficient removal of cr(vi). *J. Taiwan Inst Chem. Engineers* 91, S187610701830302X. doi: 10.1016/j.jtice.2018.05.028

Mittler, R., Vanderauwera, S., Suzuki, N., Miller, G., Tognetti, V. B., Vandepoele, K., et al. (2011). Ros signaling: the new wave? *Trends Plant Sci.* 16 (6), 300–309. doi: 10.1016/j.tplants.2011.03.007

Na, G. H., Choi, W. J., and Chun, Y. Y. (1996). A study on red tide control with loess suspension. *J. Aquacult* 9.3, 239–245.

NOAA (2016). Available at: http://www.noaa.gov/what-is-harmful-algal-bloom.

Pang, X., Chen, L., and Yuk, H. G. (2020). Stress response and survival of salmonella enteritidis in single and dual species biofilms with pseudomonas fluorescens following repeated exposure to quaternary ammonium compounds - sciencedirect. *Int. J. Food Microbiol.* 325, 108643. doi: 10.1016/j.ijfoodmicro.2020.108643

Perez, P., Fernandez, E., and Beiras, R. (2009). Toxicity of Benzalkonium Chloride on Monoalgal Cultures and Natural Assemblages of Marine Phytoplankton. *Water Air & Soil Pollution* 201 (1–4), 319–330. doi: 10.1007/s11270-008-9947-x

Seger, A., Park, T. G., and Hallegraeff, G. (2017). Assessment of the efficacy of clay flocculation in Korean fish farm waters: Cochlodinium cell removal and mitigation of ichthyotoxicity. *Harmful Algae* 61, 46–55. doi: 10.1016/j.hal.2016.11.014

Sengco, M. R., and Anderson, D. M. (2004). Controlling harmful algal blooms through clay Flocculation1. *J. Eukaryotic Microbiol.* 51 (2), 169–172. doi: 10.1111/j.1550-7408.2004.tb00541.x

Sengco, M. R., Hagstroem, J. A., and E Granéli Anderson, D. M. (2005). Removal of prymnesium parvum (haptophyceae) and its toxins using clay minerals. *Harmful Algae* 4 (2), 261–274. doi: 10.1016/j.hal.2004.05.001

Seo, J. Y., Praveenkumar, R., Kim, B., Seo, J. C., and Oh, Y. K. (2016). Downstream integration of microalgae harvesting and cell disruption by means of cationic surfactant-decorated Fe_3O_4 nanoparticles. *Green Chem.* 18 (14), 3981–3989. doi: 10.1039/C6GC00904B

Shirota, A. (1989). Red tide problem and countermeasures (2). *Int.j.fish.technol.* 1, 195–293.

Sukenik, A., Viner-Mozzini, Y., Tavassi, M., and Nir, S. (2005). Removal of cyanobacteria and cyanotoxins from lake water by composites of bentonite with micelles of the cation octadecyltrimethyl ammonium (ODTMA). *Water Research* 120 (Sept. 1), 165. doi: 10.1016/j.watres.2017.04.075

Wessels, S., and Ingmer, H. (2013). Modes of action of three disinfectant active substances: a review. *Regul. Toxicol. Pharmacol.* 67 (3), 456–467. doi: 10.1016/j.yrtph.2013.09.006

Wu, T., Cao, X., Yu, Z., Song, X., Jiang, W., Yuan, Y., et al. (2020). Study on the flocculation behavior of DPQAC-PAC-MC composite modified clay in different media. *Oceanol Limnol Sin.* 52 (1), 106–113. doi: 10.11693/hyhz20200400118

Xin, H., Gao, B., Rong, H., Yue, Q., Zhang, Y., and Teng, P. (2015). Effect of using poly dimethyl diallyl ammonium chloride as coagulation aid on polytitanium salt coagulation performance, floc properties and sludge reuse. *Separation Purification Technol.* 143, 64–71. doi: 10.1016/j.seppur.2015.01.024

Yu, Z., Song, X., Cao, X., and Liu, Y. (2017). Mitigation of harmful algal blooms using modified clays: Theory, mechanisms, and applications. *Harmful Algae* 69 (nov.), 48–64. doi: 10.1016/j.hal.2017.09.004

Yu, Z., Zou, J., Ma, X., and Li, Q. (1993). Chemical methods for red tide control. *Oceanol Limnol Sin.* 24 (3), 314–318. doi: CNKI:SUN:HYFZ.0.1993-03-012

Zhang, Z. (2016). *Preparation of quaternized organoclay minerals and their algae-removing properties* (Engineering University of Xian), Degree thesis. (in Chinese).

Zhang, J., Tan, W., Li, Q., Liu, X., and Guo, Z. (2021). Preparation of cross-linked chitosan quaternary ammonium salt hydrogel films loading drug of gentamicin sulfate for antibacterial wound Dressing. *Mar. Drugs* 19 (9), 479. doi: 10.3390/md19090479

Zhang, S., Zheng, H., Tang, X., Zhao, C., and Gao, B. (2019). Sterilization by flocculants in drinking water treatment. *Chem. Eng. J.* 382, 122961. doi: 10.1016/j.cej.2019.122961

Zhao, Y. X., Gao, B. Y., Rong, H. Y., Shon, H. K., Kim, J. H., Yue, Q. Y., et al. (2011). The impacts of coagulant aid-polydimethyldiallylammonium chloride on coagulation performances and floc characteristics in humic acid–kaolin synthetic water treatment with titanium tetrachloride. *Chem. Eng. J.* 173 (2), 376–384. doi: 10.1016/j.cej.2011.07.071

frontiers | Frontiers in Microbiology

TYPE Original Research
PUBLISHED 17 October 2022
DOI 10.3389/fmicb.2022.993914

OPEN ACCESS

EDITED BY
Zhangxi Hu,
Guangdong Ocean University,
China

REVIEWED BY
Yida Gao,
Florida Fish and Wildlife Research Institute,
United States
Ahmed Moustafa,
American University in Cairo, Egypt
Ruoyu Guo,
Second Institute of Oceanography, Ministry of Natural Resources, China

*CORRESPONDENCE
Caiwen Li
cwli@qdio.ac.cn

SPECIALTY SECTION
This article was submitted to Aquatic Microbiology, a section of the journal Frontiers in Microbiology

RECEIVED 14 July 2022
ACCEPTED 20 September 2022
PUBLISHED 17 October 2022

CITATION
Chen T, Liu Y, Song S, Bai J and Li C (2022) Full-length transcriptome analysis of the bloom-forming dinoflagellate *Akashiwo sanguinea* by single-molecule real-time sequencing.
Front. Microbiol. 13:993914.
doi: 10.3389/fmicb.2022.993914

Full-length transcriptome analysis of the bloom-forming dinoflagellate *Akashiwo sanguinea* by single-molecule real-time sequencing

Tiantian Chen[1,2], Yun Liu[3,4], Shuqun Song[3,4], Jie Bai[1,2] and Caiwen Li[3,4]*

[1]College of Environmental Science and Engineering, Ocean University of China, Qingdao, China, [2]Key Laboratory of Marine Environment and Ecology, Ocean University of China, Qingdao, China, [3]CAS Key Laboratory of Marine Ecology and Environmental Sciences, Institute of Oceanology, Chinese Academy of Sciences, Qingdao, China, [4]Laboratory of Marine Ecology and Environmental Science, Qingdao National Laboratory for Marine Science and Technology, Qingdao, China

The dinoflagellate *Akashiwo sanguinea* is a harmful algal species and commonly observed in estuarine and coastal waters around the world. Harmful algal blooms (HABs) caused by this species lead to serious environmental impacts in the coastal waters of China since 1998 followed by huge economic losses. However, the full-length transcriptome information of *A. sanguinea* is still not fully explored, which hampers basic genetic and functional studies. Herein, single-molecule real-time (SMRT) sequencing technology was performed to characterize the full-length transcript in *A. sanguinea*. Totally, 83.03Gb SMRT sequencing clean reads were generated, 983,960 circular consensus sequences (CCS) with average lengths of 3,061bp were obtained, and 81.71% (804,016) of CCS were full-length non-chimeric reads (FLNC). Furthermore, 26,461 contigs were obtained after being corrected with Illumina library sequencing, with 20,037 (75.72%) successfully annotated in the five public databases. A total of 13,441 long non-coding RNA (lncRNA) transcripts, 3,137 alternative splicing (AS) events, 514 putative transcription factors (TFs) members from 23 TF families, and 4,397 simple sequence repeats (SSRs) were predicted, respectively. Our findings provided a sizable insights into gene sequence characteristics of *A. sanguinea*, which can be used as a reference sequence resource for *A. sanguinea* draft genome annotation, and will contribute to further molecular biology research on this harmful bloom algae.

KEYWORDS

***Akashiwo sanguinea*, harmful algal blooms, full-length transcript, single molecule real-time sequencing, reference resource**

Introduction

Harmful algal blooms (HABs) have occurred intensively and frequently during the last two decades, and turned into the major marine ecological disaster in coastal waters around the world (Hallegraeff, 1993; Du et al., 2011; Anderson et al., 2012; Chen et al., 2015; Glibert and Burford, 2017). *Akashiwo sanguinea*, a harmful and conspicuous species, is a bloom-forming dinoflagellate capable of discoloring seawater with cells densities exceeding 10^5 cells L^{-1} (Lu and Hodgkiss, 2004; Kudela et al., 2005; Chen et al., 2019). Annual blooms of *A. sanguinea* have been observed along the coastal waters of China since 1998, resulting in huge economic losses to aquaculture and tourism (Wu et al., 2001; Hao et al., 2011; Chen et al., 2019). Although *A. sanguinea* is not toxigenic, large scale blooms of this species still have a severe impact on the marine ecosystem, which could form surfactant foams under the interaction of wind mixing and surfaction, and cause mass stranding and subsequent mortality of fishes, scallops and birds (Horner et al., 1997; Jessup et al., 2009).

Previous studies mainly focus on the growth, diversity, life cycle, stress responses, physiological and biochemical characteristics of *A. sanguinea* (Matsubara et al., 2007; Chen et al., 2015; Deng et al., 2015; Liu et al., 2015, 2019; Tang and Gobler, 2015; Luo et al., 2017). Furthermore, more efforts have been made to explore the eco-physiology of *A. sanguinea* at the molecular level. For instance, Deng et al. (2015) and Liu et al. (2020) characterized the Hsp 70 gene and the photosynthesis-related genes in *A. sanguinea* during the formation of resting cysts, respectively. The abundance of transcriptome data can facilitate the investigation of biochemical and physiological processes, while only hundreds of Expressed Sequence Tag (EST) sequences and several second-generation transcriptome sequencing data are obtained in NCBI database for *A. sanguinea*, and no full-length transcriptome is openly available, which limited the basic genetic and functional studies in *A. sanguinea*. To date, it is difficult to obtain the reference genome of *A. Sanguinea* through assembly and annotation due to its enormous genome, and transcript sequencing has proved to be one of the most effective technologies for obtaining reliable gene sequences (Erdner and Anderson, 2006; Wisecaver and Hackett, 2010).

The next-generation high-throughput sequencing, also known as second generation sequencing, has been employed to analyze gene expression levels for several marine dinoflagellates, largely increasing the transcript information of these dinoflagellates (Bender et al., 2014; Krueger et al., 2015; Shikata et al., 2019; Li et al., 2021). However, the inherent limitation for the next-generation sequencing is short-read RNA sequencing, which cannot provide a full-length transcript (Wang et al., 2022). Recently, the single-molecule real-time (SMRT) sequencing technology from Pacific Biosciences (PacBio), also called the third generation sequencing, has been proved to be an efficient approach to capture full length sequencing gradually (Wisecaver and Hackett, 2010; Haile et al., 2021; Yang et al., 2021). The full-length cDNA sequences can be generated without assembly *via* PacBio's SMRT sequencing, dramatically increasing accuracy of alternative splice detection and genes discovery. Even though it is higher error rate (up to 15%) and relevant lower throughput may miss some rare transcript isoforms, these shortcomings can be corrected with high-accurate and high-throughput short reads and/or self-correct *via* circular-consensus reads (Au et al., 2013; Li et al., 2014).

Herein, the marine dinoflagellate *A. sanguinea* was collected and isolated from Jiaozhou Bay, China, and successfully established as continuous culture in June 2020. A full-length transcriptomic analysis of *A. sanguinea* under different nutrition conditions was performed using SMRT sequencing. Based on the obtained transcriptome data, transcript functional annotation, simple sequence repeat analysis, and coding sequence prediction were analyzed. Our findings provided the full-length sequences of *A. sanguinea*, which will be benefit for the further research on the bloom-forming dinoflagellate.

Materials and methods

Algal isolation and maintenance

Akashiwo sanguinea was obtained and isolated from Jiaozhou Bay, China (36°24′N, 120°11′E) in June 2020. The clonal culture of *A. sanguinea* was established by pipetting single cells under an inverted microscope (Olympus IX71, Japan) to 24-well polystyrene cell culture plates containing sterile f/2-Si medium in natural seawater base (salinity of 30 ± 0.1; Guillard and Ryther, 1962; Kim et al., 2004). Cultures were grown and maintained in an incubator (20 ± 1°C; 12 h:12 h light: dark cycle), with cool white fluorescent light providing 78.14 μE m^{-2} s^{-1}. To inhibit the growth of fungus and bacteria, an antibiotic-antimycotic solution, with final concentrations of 0.05 μg ml^{-1} amphotericin B, 100 μg ml^{-1} streptomycin, and 100 I. U. penicillin (Solarbio Inc., Beijing, China), was added to the medium prior to inoculation. This antibiotic mixture had no negative effects on the growth and survival of *A. sanguinea*, as determined in preliminary experiments (Chen et al., 2015; Liu et al., 2020). The stock culture was maintained in the exponential growth phase by transferring into fresh f/2-Si medium bi-weekly.

Sample processing, RNA isolation, quantification, and qualification

For experiments, stock *A. sanguinea* in exponential growth was inoculated into various types of nutrients: f/2-Si, f/2-Si-N, f/2-Si-P, f/2-Si-NP, natural seawater (as detailed in Table 1). All treatments were conducted in 1 l Pyrex culture flasks containing 800 ml f/2-Si medium (salinity of 30 ± 0.1), with an initial cell density of $2 \pm 0.1 \times 10^3$ cells ml^{-1}. To monitor growth of *A. sanguinea*, algal cell counts were performed by light microscopy every day as described in Chen et al. (2015). For the f/2-Si

TABLE 1 Laboratory setting of different nutritional conditions for growth of *Akashiwo sanguinea*.

Medium type	NO_3^- addition (μM)	PO_4^{3-} addition (μM)
f/2-Si	883	36.3
f/2-Si-N	–	36.3
f/2-Si-P	883	–
f/2-Si-NP	–	–
Natural seawater	–	–

treatment, 200 ml were concentrated by centrifugation (800 *g*, 5 min) and frozen in liquid nitrogen during the three different developmental stages (exponential growth phase, stationary phase, and decline phase). Other stressed cultures were incubated for 5 days (exponential growth phase) before cells were collected as described above.

Total RNA from each culture was extracted using the RNeasy Plus Mini Kit (Qiagen, Valencia, CA, United States), and further treated with RNase-free DNase I (TakaRa, Japan) to remove contaminated genomic DNA. Agilent 2100 Bioanalyzer (Agilent Technologies, Palo Alto, CA, United States) and agarose gel electrophoresis were used to determine the RNA integrity. The purity and concentration of RNA samples were ascertained with the Nanodrop microspectrophotometer (Thermo Fisher Scientific, United States) and Qubit 2.0 fluorometer (Life Technologies, Carlsbad, CA, United States), respectively. Then, RNA samples with a 260/280 ratio of ≥1.8, 260/230 ≥ 1.8 and RIN ≥ 7 were used to construct the Pacbio sequencing library. Finally, equal amounts of RNA samples from different culture conditions were pooled for the following library construction and sequencing.

Library construction and single-molecule real-time sequencing

A total of 5 μg of total RNA (equally mixed with all RNAs) was used to prepare SMRT libraries. Then, mRNA was reverse-transcribed into cDNA using the Clontech SMARTer PCR cDNA Synthesis Kit (Clontech, CA, United States) according to the Isoform Sequencing protocol. The PCR reactions were optimized to determine the optimal number of amplification cycles for the downstream large-scale PCR procedures. The large-scale double-strand cDNA was produced with the determined number of cycles using Phusion DNA polymerase (NEM, Beverly, MA, United States). The cDNA molecules >5 kb in length were selected using a Blue Pippin™ Size-Selection System (Sage Science, Beverly, MA, United States) and mixed equally with non-size-selected cDNA. Then, another large-scale PCR was preformed, and the amplified and size selected cDNA products were made into SMRTbelll Template libraries. The quality of the libraries was evaluated using the Agilent Bioanalyzer 2100 system. Finally, sequencing reactions were conducted on a PacBio Bioscience Sequel platform (Novogene Bioinformatics Technology Co., Ltd., Beijing, China).

Data processing

The raw sequencing data of the cDNA libraries was initially processed following the SMRT Link (v 9.0.0) pipeline with parameters: minReadScore = 0.75, minlength = 200. First, high-quality circular consensus sequences (CCSs, HiFi reads) were generated from subread BAM files using the CCS function with parameter settings as: min length = 200, min passes = 1, max drop fraction = 0.8, min zscore = −9,999, no polish = TRUE, max length = 15,000, and min predicted accuracy = 0.8. To obtain the full-length nonchimeric (FLNC) reads, the primers, barcodes, polyA tails, and concatemers of full passes were removed. Then, consensus isoforms were identified using the algorithm of ICE (Iterative Clustering for Error Correction) from FLNC and were further polished with non-full length reads to obtain high-quality isoforms with post-correction accuracy above 99% using Quiver (parameters: bin by primer = false, hq quiver min accuracy = 0.99, qv trim 3p = 30, qv trim 5p = 100, and bin size kb = 1). The Cluster Database at High Identity with Tolerance (CD-HIT) program (v 4.6.7) was used to further correct the consensus sequences with the following parameters: −c = 0.99, −G = 0, −T = 6, −AL = 100, −aL = 0.90, −AS = 30, and −aS = 0.99, and the BUSCO (v3.0.2) was used to benchmark transcriptome completeness (Waterhouse et al., 2018). All the raw sequence data have been uploaded to NCBI with the Sequence Read Archive (SRA) number PRJNA827604.

Functional annotation

Corrected isoforms were searched against Nr (non-redundant protein sequences), Nt (non-redundant nucleotide sequences), Swiss-Prot (a manually annotated and reviewed protein sequence database), KOG/COG (Cluster of Orthologous Groups of proteins), and KEGG (Kyoto Encyclopedia of Genes and Genomes) with BLAST software (v 2.2.26) under a threshold *E*-value ≤ 10^{-5}. KEGG pathway analyses were determined using the KEGG Automatic Annotation Server (KAAS1) and HMMER software (Eddy, 1998) was used to search Pfam database (Protein family http://pfam.xfam.org/). Gene Ontology (GO) annotations were performed based on the best BLASTX hit from the NR database using the Blast2GO software (v 2.3.5, -value ≤10^{-5}).

Gene structure prediction

The unigenes were blastx searched against the databases with the *E*-value ≤ 10^{-5} to retrieve a protein sequence for each unigene from either of the four databases in the order of NR, Swiss-Prot,

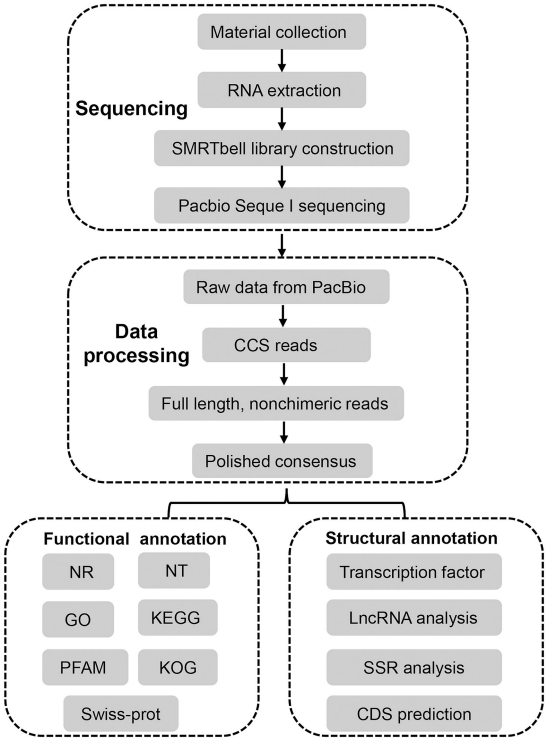

FIGURE 1
Overall experimental workflow and transcriptome bioinformatics analysis pipeline in this study.

KEGG and KOG, which then located the CDS of the unigene. The unigenes, failing to retrieve a protein sequence, were subjected to ANGEL for CDS prediction (Shimizu et al., 2006). Four tools, including coding potential calculator (CPC), coding-non-coding index (CNCI), coding potential assessment tool (CPAT), and predictor of long non-coding RNAs and messenger RNAs based on an improved *k*-mer scheme (PLEK), were combined to identify LncRNA candidates from putative protein coding RNAs. LncRNAs with >200 nucleotides were selected. Then, the transcripts with encoding ORFs longer than 100 amino acids predicted by these tools were filtered out, and those without coding potential were selected as candidates of lncRNAs. BLASTN was used to get rid of the previously discovered lncRNAs under a criteria of e-value ≤ 1e−10, min-identity = 90% and min-coverage = 85%. Hmmscan against the Plant TFdb database was used to perform TF analysis (Tian et al., 2020). The alternative splicing (AS) events of the transcript isoforms were identified using the Coding GENome reconstruction Tool (Cogent, v 3.3) with the default parameters to divide the transcripts into gene families based on *k*-mer similarity and to reconstruct each family into a coding reference genome based on a De Bruijn graph (Alamancos et al., 2015; Li et al., 2017). The AS events were detected using SUPPA with references. The microsatellite identification tool (MISA) was used to identify simple sequence repeats (SSRs) within the FL transcriptome according to the criteria blow: length-minimum number of repetitions = 2–6 or 3–5 or 4–4 or 5–4 or 6–4 and interruptions of 100 bp (Beier et al., 2017). To characterize full-length transcripts in *A. sanguinea*, an experimental workflow and analysis pipeline was followed as illustrated in Figure 1.

TABLE 2 Summary of the *A. sanguinea* transcriptome statistics.

Statistical data	*Akashiwo sanguinea*	
Raw reads	Subread number	29,370,228
	Average length (bp)	2,827
	N50 length (bp)	2,003
CCSs	Number of reads	983,960
	Number of CCS bases	3,011,901,560
	CCS read average length (bp)	3,061
	Average number of passes	8
Clustered reads	Number of polished isoforms	110,200
	Polished isoform average length (bp)	2,764
	Polished isoform N50 length (bp)	2,936
Unigenes	Total number	26,461
	Total length (bp)	72,946,143
	Maximum length (bp)	11,908
	Minimum length (bp)	283
	Average length (bp)	2,757
	N50 length (bp)	2,926

Results

Data summary

Based on the PacBio SMRT Sequencing technology, a total of 85.19 Gb of nucleotide data with the average read length of 77,216 bp was obtained. After removing shorter reads (<50 bp in length) and adaptors, a total of 29,370,228 reads (83.03 Gb of nucleotides) were obtained, with an average length and N50 of 2,827 and 3,051 bp, respectively. After merging transcripts with at least two full passes, 983,960 circular consensus sequences (CCSs) with an average length of 3,061 bp were retained. The full-length non-chimeric (FLNC) sequences of the CCSs were further clustered and polished, and 110,200 high-quality (HQ) isoforms were produced, with an average length and N50 of 2,764 and 2,936 bp, respectively. The HQ isoforms were clustered to 26,461 unigenes after removing the sequence redundancy (Table 2).

Gene annotations and taxonomy

To analyze the function of the 26,461 unigenes, five databases, including the non-redundant protein (Nr) database and the NCBI

non-redundant nucleotide (Nt) database, the Kyoto Encyclopedia of Genes, and Genomes (KEGG) database, Gene Ontology (GO) database, and Clusters of eukaryotic Ortholog Groups (KOG) database, were used to perform functional annotations. Totally, 20,037 unigenes (75.72%) were annotated prediction and functional annotation of the coded transcripts showed that 13,198 (49.88%), 10,458 (39.52%), 12,933 (48.88%), 12,208 (46.14%), and 17,202 (65.01%) were annotated in the Nr, KOG, KEGG, Nt, and GO database, respectively (Figure 2).

With regard to Nr annotation, the top 10 species classifications were *Symbiodinium microadriaticum* (a symbiotic dinoflagellate, 13,725, 51.87%), *Vitrella brassicaformis* (a photosynthetic alveolates, 1,362, 5.15%), *Perkinsus marinus* (a protozoan parasite, 487, 1.84%), *Emiliania huxleyi* (a coccolithophore, 276, 1.04%), *Chrysochromulina* sp. (230, 0.87%), *Aureococcus anophagefferens* (a heterokont alga, 180, 0.68%), *Guillardia theta* (a cryptophyte alga, 175, 0.66%), *Ectocarpus siliculosus* (a filamentous brown alga, 124, 0.47%), *Plasmodiophora brassicae* (a fungus, 82, 0.31%), *Thalassiosira oceanica* (a marine diatom, 66, 0.25%; Figure 3).

A total of 10,458 transcripts (39.52%) were annotated in the KOG database, which can be assigned to 26 subcategories (Figure 4). The highest percentage of subcategory was the signal transduction mechanisms subcategory, reaching 2,095. The rest were general function prediction only (1,628), posttranslational modification, protein turnover, chaperones (1,252), and cytoskeleton (669).

Regarding functional annotations, 17,202 (65.01%) transcripts were annotated to three major categories of "biological process," "cellular component," and "molecular function" in the GO database. The most enriched terms in the biological process category (44.76%) were the "cellular process" (9.43%), "metabolic process" (9.20%), "single-organism process" (6.32%), and "localization" (4.77%) terms. Within the cellular component category (25.33%), the genes involved in "cell" (4.14%), "cell par" (4.14%), "organelle" (2.97%), and "membrane" (2.88%) accounted for the largest proportion. In terms of molecular function (29.91%), "binding" (14.59%), "catalytic activity" (10.18%), "transporter activity" (2.89%), and "molecular transducer activity" (0.62%) covered the most abundant genes (Figure 5).

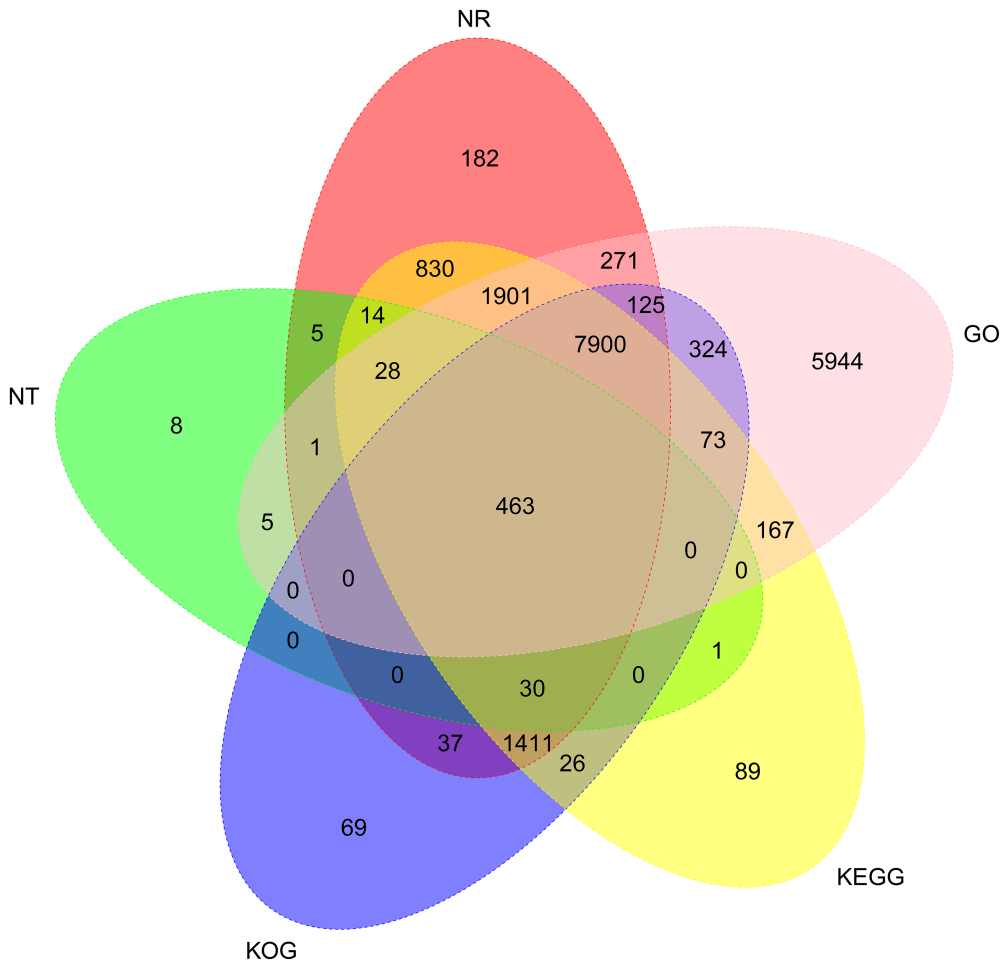

FIGURE 2
Venn diagram of NR, NT, GO, KOG, and KEGG annotation of the *Akashiwo sanguinea* full-length transcriptome.

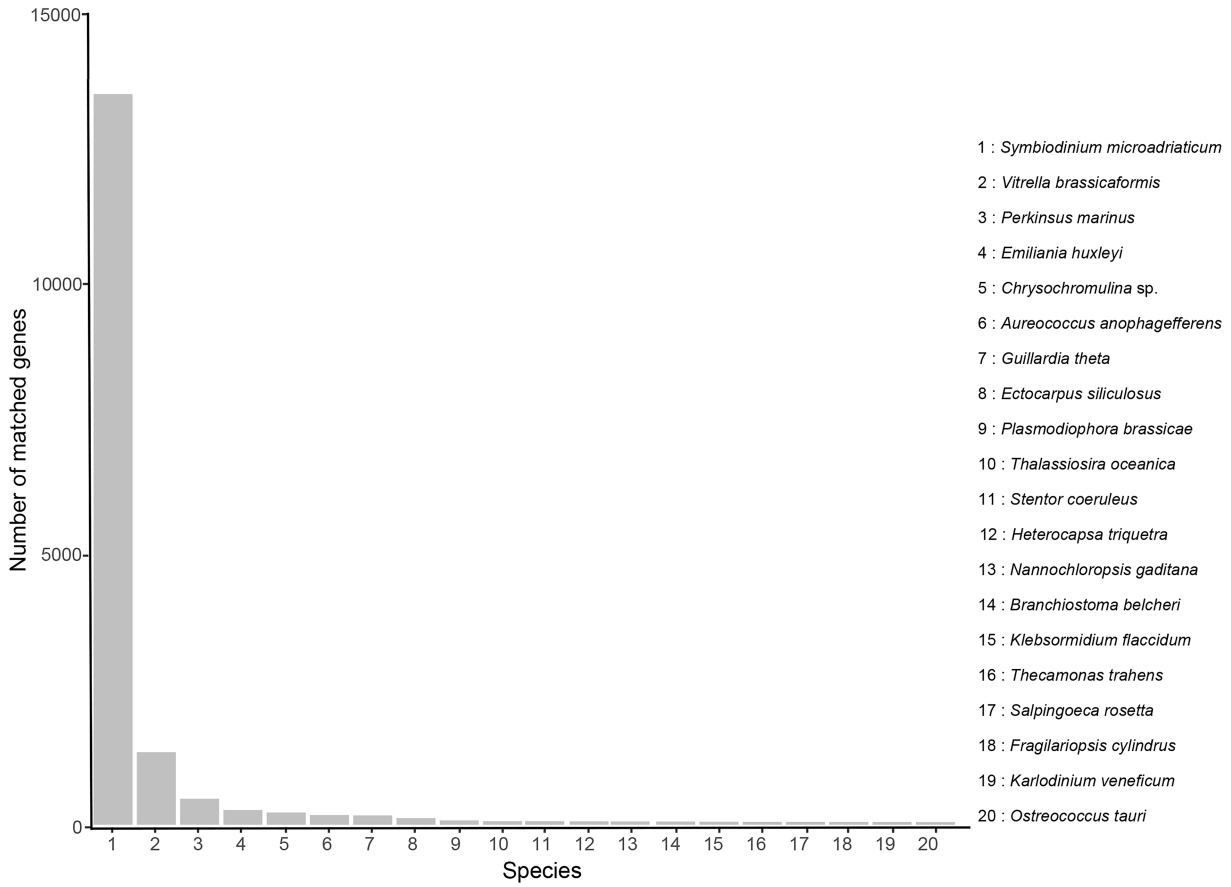

FIGURE 3
Nr classification of high-quality transcripts of the *A. sanguinea* full-length transcriptome.

Totally, 13,699 transcripts were classified into the KEGG database, belonging to KEGG's six primary metabolic pathway (Lev 1) branches, namely, "cellular processes," "environmental information processing," "genetic information processing," "human diseases," "metabolism" and "organismal systems," and the most prominent subcategory was "metabolism." These transcripts were also annotated to 45 secondary pathways (Lev 2) of the six primary metabolic pathway (Lev 1). On the Lev 2 pathway, the genes involved in "signal transduction," "global and overview maps," "carbohydrate metabolism" and "folding, sorting and degradation" accounted for the majority (Figure 6).

Analyses of coding sequence, long non-coding RNAs, and transcription factor

In 26,461 transcripts with an average length of 2,757 bp, 20,037 (75.72%) CDSs were predicted. Totally, 13,441 lncRNAs (50.80%) were identified using CPC, CNCI, Pfam, and PLEK approaches. The number of putative lncRNAS by CPC, CNCI, Pfam, and PLEK databases were 340, 72, 11,478, and 4,230, respectively. Only 5 common lncRNAs transcripts were predicted in *A. sanguinea* by the four methods (Figure 7A). BLASTN was used to get rid of the previously discovered 11 lncRNAs downloaded from ensemble website, and most of lncRNA were identified as novel lncRNAs (Figure 7B). A total number of 514 putative TF members were obtained and categorized into 23 families. The top 10 TFs were ranked according to the number of sequences that were aligned to the transcripts, which were C3H (137), SNF2 (72), SET (63), CSD (63), Others (41), TRAF (31), C2H2 (28), Jumonji (16), HMG (13), and GNAT (12) (Figure 7C).

Analyses of alternative splicing and simple sequence repeats

The alternative splicing (AS) event provides eukaryotes with peculiarly versatile means of genetic regulation. In total, 3,137 AS events were identified, with the genes containing two isoforms (2,523) ranked the highest, followed by three and four isoforms (Figure 8A). Only 57 events were classified into five AS types, and the major AS types were retained intron (23) and alternative 3′ splice sites (17) (Figure 8B). In the *A. sanguinea* full-length

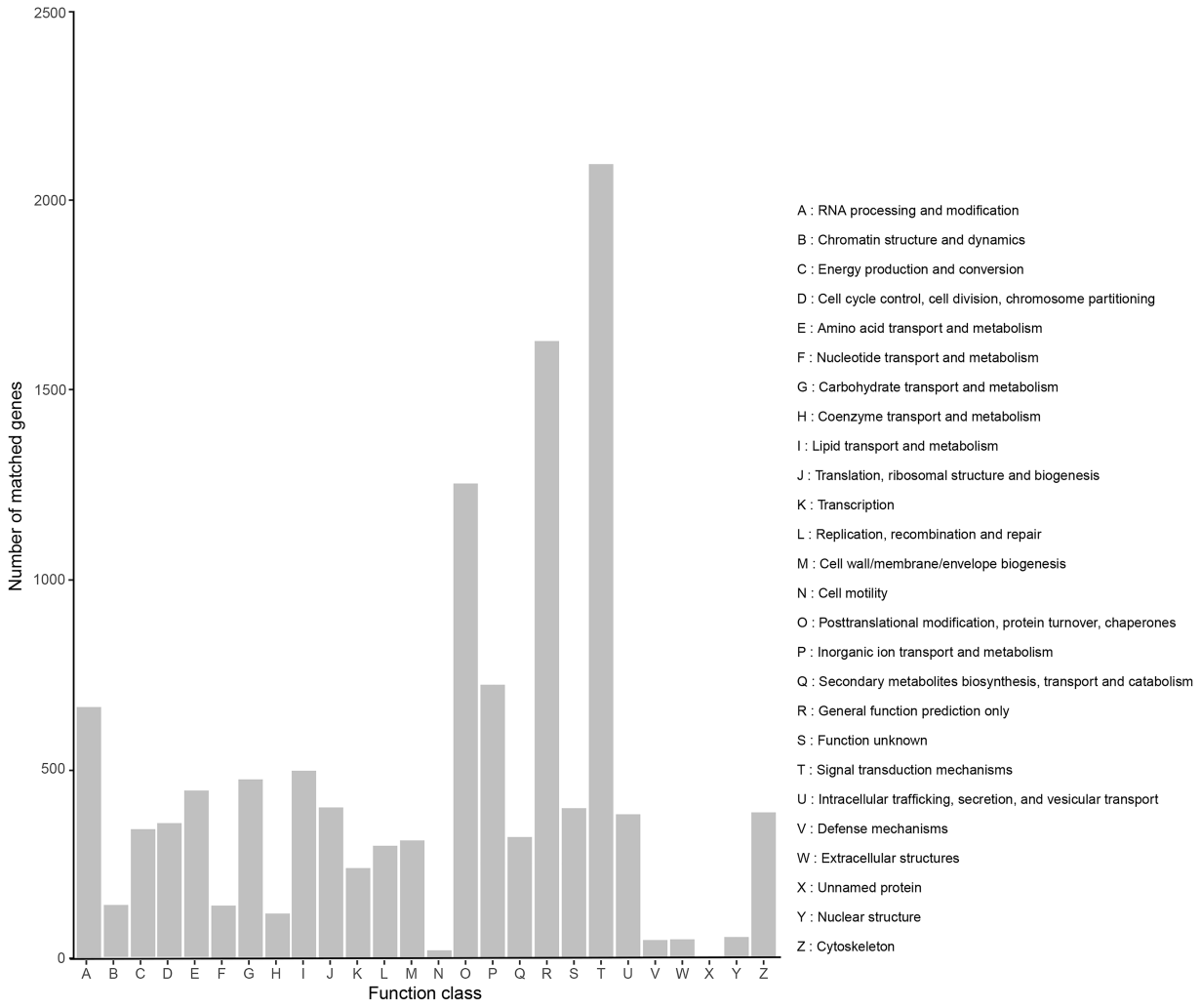

FIGURE 4
KOG classification of high-quality transcripts of the *Akashiwo sanguinea* full-length transcriptome.

transcriptome, exonskipping, mutually exclusive exons and alternative first exon AS events were not detected.

An simple sequence repeats (SSRs) is a repetitive DNA sequence where certain motifs are repeated. In total, 4,397 SSRs were identified, and these were containing in 32,563 sequences (Figure 8C). The SSR lengths ranged from 10 to 1,354 bp, with a mean of 41.49 bp, and the number of repeat SSR motifs ranged from 5 to 67. Of these SSRs, 2,160 (49.12%) were trinucleotide repeats, most of which consisted of 5–8 repeated sequences; 527 (11.99%) were mononucleotide repeats with 9–12 repeats. In addition, 321 (7.30%) were hexanucleotide repeats with 5–8 repeats (Figure 8D).

Discussion

Akashiwo sanguinea is a commonly observed bloom-forming dinoflagellate distributed worldwide (Trainer et al., 2010; White et al., 2014). Information on partial transcripts of *A. sanguinea* have been obtained by Illumina sequencing in previous studies (NCBI accession: SRR1294461–SRR1294464). While the inherent limitations of Illumina sequencing, including short read length and amplification biases, still limit its application in acquiring a full-length transcript (Abdel-Ghany et al., 2016). Until now, the full-length nucleotide sequence information is still deficient in *A. sanguinea*, which has impeded basic genetic research in this species. With the development of sequencing technologies, PacBio sequencing is widely used in obtaining full-length transcript sequences of microorganisms without assembly (Cheng et al., 2021). Herein, the first high-quality collection of transcripts in *A. sanguinea* was generated by single-molecule long-read PacBio sequencing, and 83.03 Gb clean data were obtained including 983,960 circular consensus sequences (CCSs) and 110,200 high-quality (HQ) isoforms. Long non-coding RNAs (lncRNAs), alternative splicing (AS), simple sequence repeats (SSRs), and transcription factors (TFs) were further revealed in the present

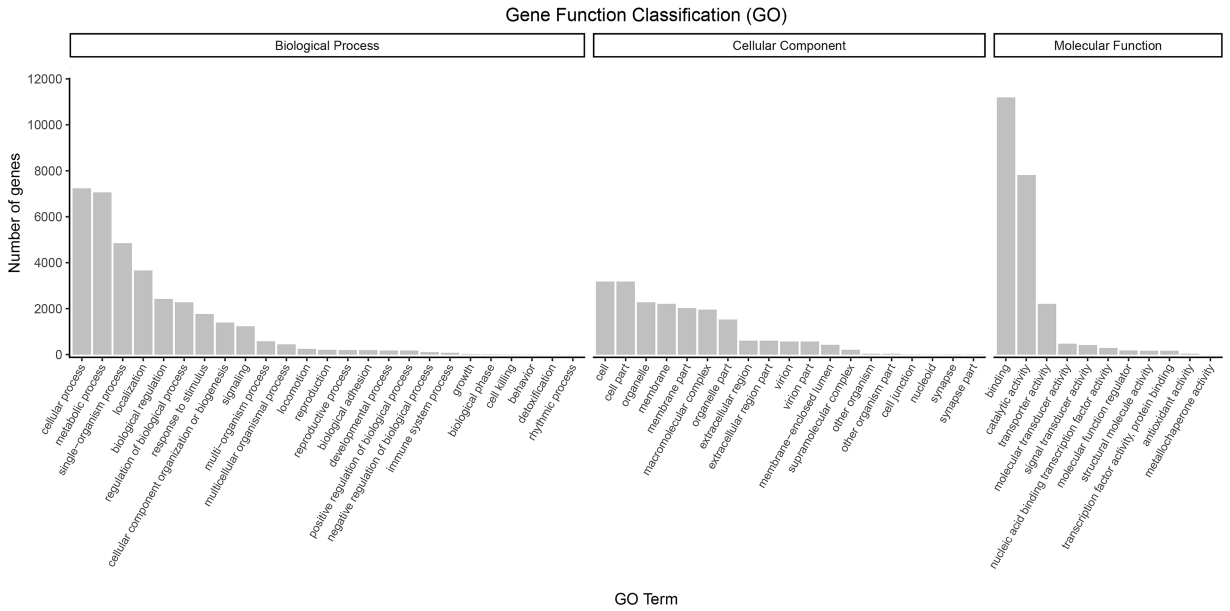

FIGURE 5
GO classification of high-quality transcripts of the *A. sanguinea* full-length transcriptome.

study. Our findings provided more accurate annotated unigene information in *A. sanguinea*, which will be useful for the future basic genetic and gene functional studies in this bloom-forming dinoflagellate.

In order to obtain transcripts with very low or no expression in the collected samples, the strategy of pooling of developmental stages and various nutritional conditions has been adopted to capture more complete transcript information (Hoang et al., 2017). The cDNA library was pooled from three developmental stages and five nutritional conditions in the present study. The integrity and reliability of our transcriptome were further confirmed by BUSCO analysis. Higher number of reads was always produced in the Illumina sequencing than that in the PacBio's SMRT sequencing, however, nearly half of the short contigs generated in former were multiple alignments (Wang et al., 2022). SMRT sequencing provided new insights into capturing long transcript sequences; under normal circumstances, a single read was considered a complete transcript (Sharon et al., 2013; Chao et al., 2018). 97.64% of the generated contigs were >1,000 bp in length in the contigs length distribution of the full-length transcriptome of *A. sanguinea*. Our results demonstrated that SMRT sequencing is an effective and powerful technology for obtaining reliable full-length transcriptome in *A. sanguinea*.

Totally, 20,037 unigenes were annotated in the five public databases, and 6,424 unigenes with unpredicted functions might likely to be species-specific or unknown genes in *A. sanguinea*. With regard to GO annotation, transcripts assigned to categories such as "binding," "catalytic activity," "cellular process," "metabolic process" and "single-organism" were significantly enriched. A total of 10,458 transcripts were assigned to "signal transduction mechanisms subcategory," "general function prediction only," and "posttranslational modification, protein turnover, chaperones" according to the KOG annotation analysis. A large of transcripts were involved in specific KEGG pathways, including "signal transduction," "global and overview maps" and "carbohydrate metabolism." Additionally, numerous transcripts showed participated in diverse biological pathways and multiple molecular functions. Our results provided a large amount of genetic information for functional investigation in *A. sanguinea*. However, the isoform expression levels was not analyzed in current project, and expression analysis of isoforms derived from one gene in *A. sanguinea* should be analyzed in detail in the future.

LncRNAs emerged as key regulatory molecules in important biological process, including transcription, translation, cellular structure integrity, and sex regulation and aging (Perry and Ulitsky, 2016; Jia et al., 2018). LncRNAs played crucial roles in the nucleus, where they regulate the target genes expression by controlling nuclear architecture and transcription (Wang et al., 2022). LncRNAs also regulated translation, modulated mRNA stability and post-translational modifications in the cytoplasm (Yao et al., 2019). In the current study, 13,441 lncRNAs with a mean length of 2,757 bp were identified. By comparison, the identified lncRNA were much longer than that of known lncRNA (the mean length of 93.09 bp), which showed that SMRT has a better capacity in capturing transcript sequences, especially long transcript sequences.

TFs play a vital role in regulating gene transcription by recognizing and binding specific nucleotide sequences (Fulton et al., 2009). A total number of 514 TFs were obtained and categorized into 23 families, with C3H (137) ranked the highest, followed by SNF2 (72), SET (63), CSD (63), and Others (41). Since all eukaryotic TF families were historically identified and

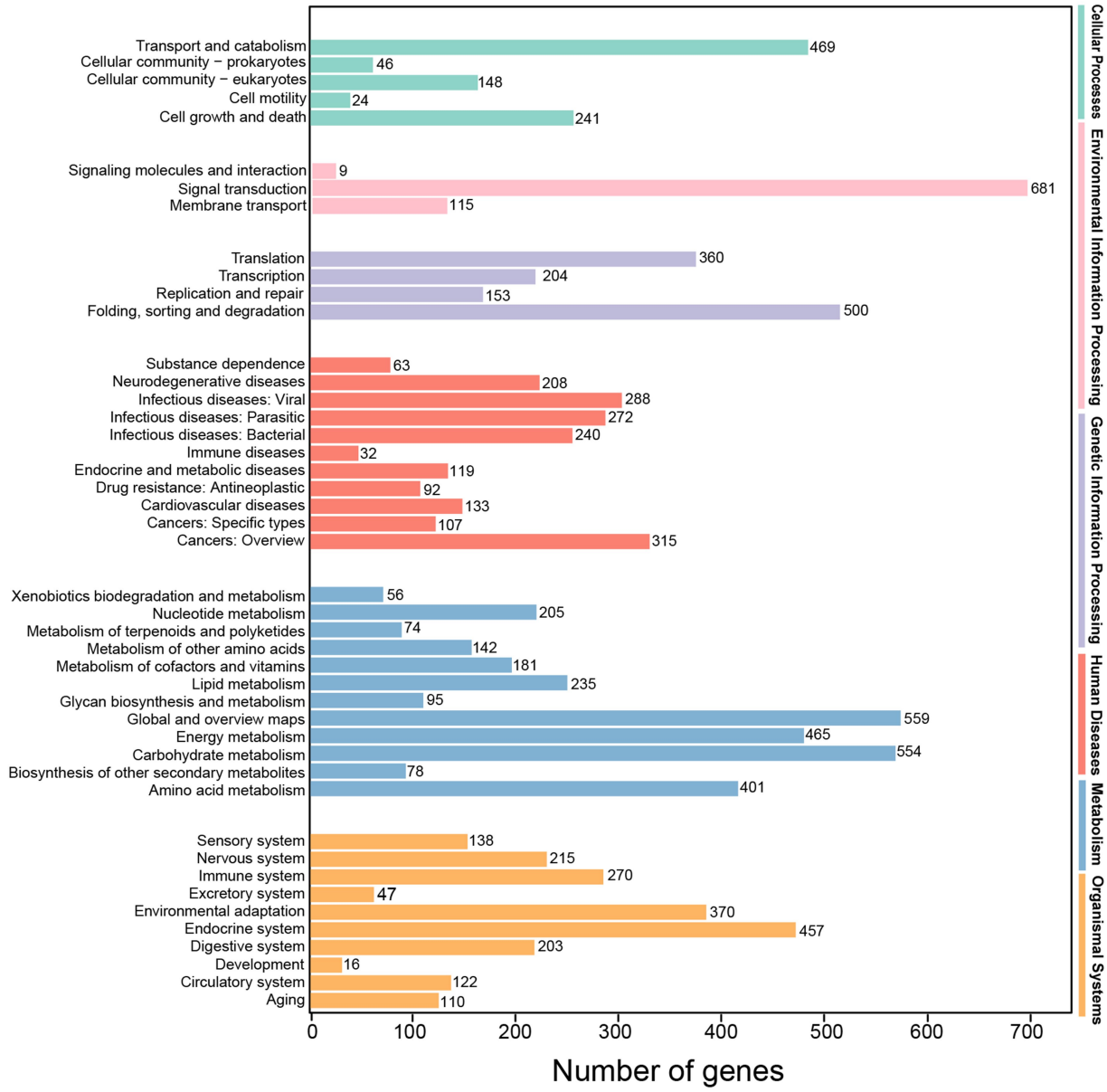

FIGURE 6
KEGG classification of high-quality transcripts of the *A. sanguinea* full-length transcriptome.

characterized in plants, fungi or animals, these numbers were likely to be underestimated (Rayko et al., 2010). The SNF2 and C3H families were involved in biological processes, such as processing of DNA damage, maintenance of chromosome stability, and RNA processing (Eisen et al., 1995; Delaney et al., 2006), which were commonly present in all the organisms or eukaryote. While the heat shock transcription factor (HSF) family was the two most abundant TF family encoded in diatoms (Rayko et al., 2010). For example, the number of HSF were 187 (51.5%), 70 (33.0%), and 94 (36.4%) in *Thalassiosira weissflogii*, *Phaeodactylum tricornutum*, and *Thalassiosira pseudonana*, respectively (Rayko et al., 2010; Cheng et al., 2021). Besides, Myb and C2H2-type zinc finger TFs were overamplified and constituted the most abundant class of TFs in stramenopile (Rayko et al., 2010).

SSR polymorphic genetic markers, also known as microsatellites, show significant species-specific differences and have been widely used for genetic map construction, functional gene mining, genetic diversity analyses, and molecular marker-related studies (Shen et al., 2014; Feng et al., 2021). A total of 4,397 SSRs identified in *A. sanguinea*, exceeding the SSRs detected in *T. weissflogii* (3,295 SSRs) and *P. tricornutum* (1,390 SSRs) on numbers (Rastogi et al., 2018; Cheng et al., 2021). Herein, the mono-nucleotide (A/T) and tri-nucleotide (GCA/CAG) were the most abundant loci in *A. sanguinea*, and most of SSRs were identified within or around CDS regions and associated with

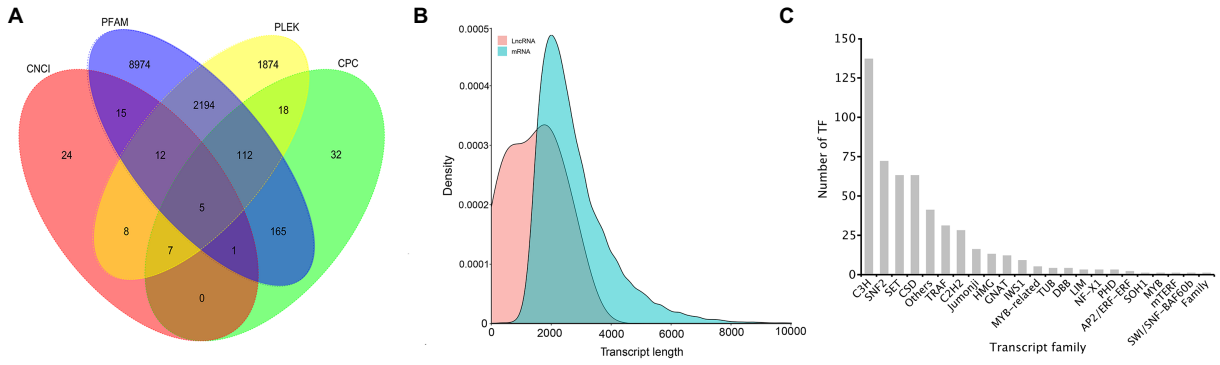

FIGURE 7
The identification of lncRNAs and the transcript family of the *A. sanguinea* transcriptome. **(A)** The venn diagram of the number of lncRNAs predicted by CPC2, CPAT, PLEK, and CNCI. **(B)** Density and length distributions of mRNAs and lncRNA in *A. sanguinea*. **(C)** Transcript families in the *A. sanguinea* full-length transcriptome.

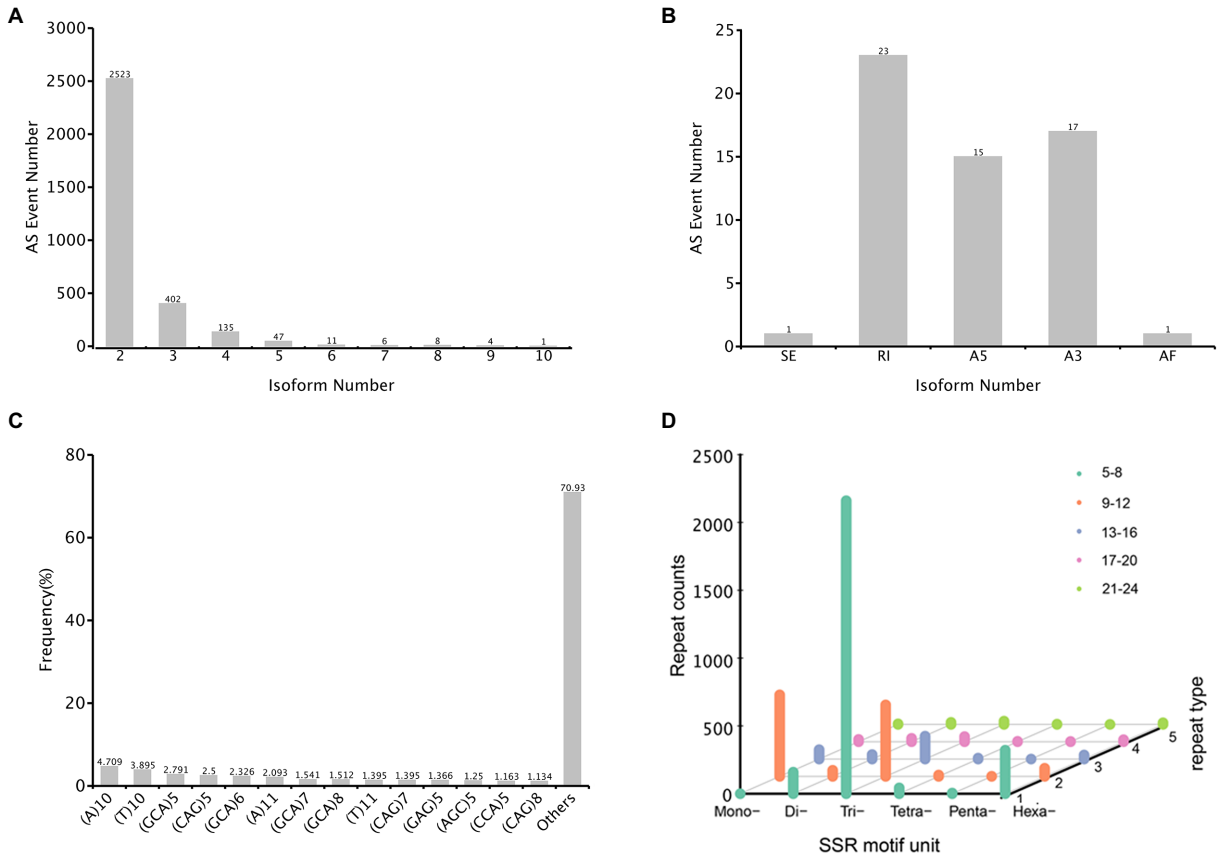

FIGURE 8
Characterization of structural annotation. **(A)** Distribution of alternative splicing (AS) in each isoform. **(B)** Count of five types of AS. **(C)** The distribution of simple sequence repeats (SSR) type counts. **(D)** SSR motif unit distribution, *x*-axis represented the type of motif unit, *y*-axis represented the count number and *z*-axis represented different repeat number.

functional genes. The SSRs found here will be of convenience for phylogenetic studies of *A. sanguinea*, and experimental validation should be performed before further using.

Recently, omics analyses have the potential to expand our understanding of the physiological, the initiation and dissipation of algal blooms, and underlying molecular processes of

A. sanguinea. In the present study, a high-quality and more complete transcriptome analysis of *A. sanguinea* was conducted by the SMRT sequencing, which enabled the generation of full-length transcripts and related analysis, such as efficient gene annotation, lncRNAs, TFs, AS events, and SSRs. Our findings provided a valuable foundation for improving the genome assembly and annotation of *A. sanguinea* by adding accurate genes and structures, which will be helpful to analyze the eco-physiological features of this harmful algae at the molecular level.

Data availability statement

The data presented in the study are deposited in the NCBI with the Sequence Read Archive (SRA) repository, accession number PRJNA827604.

Author contributions

TC: conceptualization, investigation, and writing–original draft. YL and SS: methodology, validation, and project administration. SS and JB: methodology and software. CL: supervision, funding acquisition, writing–review and editing, and writing–original draft. All authors contributed to the article and approved the submitted version.

Funding

This study was financially supported by National Natural Science Foundation of China (grant number 41906122, 41876120, and 41606128), the Key Deployment Project of Centre for Ocean Mega-Science, Chinese Academy of Sciences (grant number COMS2020Q06), and the Marine S & T Fund of Shandong Province for Pilot National Laboratory for Marine Science and Technology (Qingdao) (grant number 2021QNLM040001).

Acknowledgments

We are grateful to Novogene Bioinformatics for the technical assistance in PacBio sequencing and data analyses. We also thank Meng Li for his assistance in the preparations of samples and data analyses.

Conflict of interest

The authors declare that the research was conducted in the absence of any commercial or financial relationships that could be construed as a potential conflict of interest.

The handling editor ZH declared a past collaboration with the author TC.

Publisher's note

All claims expressed in this article are solely those of the authors and do not necessarily represent those of their affiliated organizations, or those of the publisher, the editors and the reviewers. Any product that may be evaluated in this article, or claim that may be made by its manufacturer, is not guaranteed or endorsed by the publisher.

Supplementary material

The Supplementary material for this article can be found online at: https://www.frontiersin.org/articles/10.3389/fmicb.2022.993914/full#supplementary-material

References

Abdel-Ghany, S. E., Hamilton, M., Jacobi, J. L., Ngam, P., Devitt, N., Schilkey, F., et al. (2016). A survey of the sorghum transcriptome using single-molecule long reads. *Nat. Commun.* 7:11706. doi: 10.1038/ncomms11706

Alamancos, G. P., Pagès, A., Trincado, J. L., Bellora, N., and Eyras, E. (2015). Leveraging transcript quantification for fast computation of alternative splicing profiles. *RNA* 21, 1521–1531. doi: 10.1261/rna.051557.115

Anderson, D. M., Cembella, A. D., and Hallegraeff, G. M. (2012). Progress in understanding harmful algal blooms: paradigm shifts and new technologies for research, monitoring, and management. *Annu. Rev. Mar. Sci.* 4, 143–176. doi: 10.1146/annurev-marine-120308-081121

Au, K. F., Sebastiano, V., Afshar, P. T., Durruthy, J. D., Lee, L., Williams, B. A., et al. (2013). Characterization of the human ESC transcriptome by hybrid sequencing. *Proc. Natl. Acad. Sci. U. S. A.* 110, E4821–E4830. doi: 10.1073/pnas.1320101110

Beier, S., Thiel, T., Münch, T., Scholz, U., and Mascher, M. (2017). MISA-web: a web server for microsatellite prediction. *Bioinformatics* 33, 2583–2585. doi: 10.1093/bioinformatics/btx198

Bender, S. J., Durkin, C. A., Berthiaume, C. T., Morales, R. L., and Armbrust, E. V. (2014). Transcriptional responses of three model diatoms to nitrate limitation of growth. *Front. Mar. Sci.* 1:3. doi: 10.3389/fmars.2014.00003

Chao, Y., Yuan, J., Li, S., Jia, S., Han, L., and Xu, L. (2018). Analysis of transcripts and splice isoforms in red clover (*Trifolium pratense* L.) by single-molecule long-read sequencing. *BMC Plant Biol.* 18:300. doi: 10.1186/s12870-018-1534-8

Chen, B., Kang, W., and Hui, L. (2019). *Akashiwo sanguinea* blooms in Chinese waters in 1998-2017. *Mar. Pollut. Bull.* 149:110652. doi: 10.1016/j.marpolbul.2019.110652

Chen, T., Liu, Y., Song, S., Li, C., Tang, Y. Z., and Yu, Z. (2015). The effects of major environmental factors and nutrient limitation on growth and encystment of planktonic dinoflagellate *Akashiwo sanguinea*. *Harmful Algae* 46, 62–70. doi: 10.1016/j.hal.2015.05.006

Cheng, H., Bowler, C., Xing, X., Bulone, V., Shao, Z., and Duan, D. (2021). Full-length transcriptome of *Thalassiosira weissflogii* as a reference resource and mining of chitin-related genes. *Mar. Drugs* 19:392. doi: 10.3390/md19070392

Delaney, K. J., Xu, R., Zhang, J., Li, Q. Q., Yun, K. Y., Falcone, D. L., et al. (2006). Calmodulin interacts with and regulates the RNA-binding activity of an Arabidopsis polyadenylation factor subunit. *Plant Physiol.* 140, 1507–1521. doi: 10.1104/pp.105.070672

Deng, Y., Hu, Z., Zhan, Z., Ma, Z., and Tang, Y. Z. (2015). Differential expressions of an Hsp70 gene in the dinoflagellate *Akashiwo sanguinea* in response to

temperature stress and transition of life cycle and its implication. *Harmful Algae* 50, 57–64. doi: 10.1016/j.hal.2015.10.007

Du, X., Peterson, W., McCulloch, A., and Liu, G. (2011). An unusual bloom of the dinoflagellate *Akashiwo sanguinea* off the Central Oregon, USA, coast in autumn 2009. *Harmful Algae* 10, 784–793. doi: 10.1016/j.hal.2011.06.011

Eddy, S. R. (1998). Profile hidden markov models. *Bioinformatics* 14, 755–763. doi: 10.1093/bioinformatics/14.9.755

Eisen, J. A., Sweder, K. S., and Hanawalt, P. C. (1995). Evolution of the SNF2 family of proteins: subfamilies with distinct sequences and functions. *Nucleic Acids Res.* 23, 2715–2723. doi: 10.1093/nar/23.14.2715

Erdner, D. L., and Anderson, D. M. (2006). Global transcriptional profiling of the toxic dinoflagellate *Alexandrium fundyense* using massively parallel signature sequencing. *BMC Genomics* 7:88. doi: 10.1186/1471-2164-7-88

Feng, Y., Zhao, Y., Zhang, J., Wang, B., Yang, C., Zhou, H., et al. (2021). Full-length SMRT transcriptome sequencing and microsatellite characterization in *Paulownia catalpifolia*. *Sci. Rep.* 11:8734. doi: 10.1038/s41598-021-87538-8

Fulton, D. L., Sundararajan, S., Badis, G., Hughes, T. R., Wasserman, W. W., Roach, J. C., et al. (2009). TFCat: the curated catalog of mouse and human transcription factors. *Genome Biol.* 10:R29. doi: 10.1186/gb-2009-10-3-r29

Glibert, P. M., and Burford, M. A. (2017). Globally changing nutrient loads and harmful algal blooms: recent advances, new paradigms, and continuing challenges. *Oceanography* 30, 58–69. doi: 10.5670/oceanog.2017.110

Guillard, R. R. L., and Ryther, J. H. (1962). Studies of marine planktonic diatoms: I. Cyclotella nana Hustedt, and Detonula confervacea (Cleve) gran. *Can. J. Microbiol.* 8, 229–239. doi: 10.1139/m62-029

Haile, S., Corbett, R. D., LeBlanc, V. G., Wei, L., Pleasance, S., Bilobram, S., et al. (2021). A scalable strand-specific protocol enabling full-length total RNA sequencing from single cells. *Front. Genet.* 12:665888. doi: 10.3389/fgene.2021.665888

Hallegraeff, G. M. (1993). A review of harmful algal blooms and their apparent global increase. *Phycologia* 32, 79–99. doi: 10.2216/i0031-8884-32-2-79.1

Hao, Y., Tang, D., Yu, L., and Xing, Q. (2011). Nutrient and chlorophyll a anomaly in red-tide periods of 2003-2008 in Sishili Bay, China. *Chin. J. Oceanol. Limnol.* 29, 664–673. doi: 10.1007/s00343-011-0179-3

Hoang, N. V., Furtado, A., Mason, P. J., Marquardt, A., Kasirajan, L., Thirugnanasambandam, P. P., et al. (2017). A survey of the complex transcriptome from the highly polyploidy sugarcane genome using full-length isoform sequencing and de novo assembly from short read sequencing. *BMC Genomics* 18:395. doi: 10.1186/s12864-017-3757-8

Horner, R. A., Garrison, D. L., and Plumley, F. G. (1997). Harmful algal blooms and red tide problems on the US west coast. *Limnol. Oceanogr.* 42, 1076–1088. doi: 10.4319/lo.1997.42.5_part_2.1076

Jessup, D. A., Miller, M. A., Ryan, J. P., Nevins, H. M., Kerkering, H. A., Mekebri, A., et al. (2009). Mass stranding of marine birds caused by a surfactant-producing red tide. *PLoS One* 4:e4550. doi: 10.1371/journal.pone.0004550

Jia, D., Wang, Y., Liu, Y., Hu, J., Guo, Y., Gao, L., et al. (2018). SMRT sequencing of full-length transcriptome of flea beetle *Agasicles hygrophila* (Selman and Vogt). *Sci. Rep.* 8:2197. doi: 10.1038/s41598-018-20181-y

Kim, S., Park, M. G., Yih, W., and Coats, D. W. (2004). Infection of the bloom-forming thecate dinoflagellates *Alexandrium affine* and *Gonyaulax spinifera* by two strains of *Amoebophrya* (Dinophyta). *J. Phycol.* 40, 815–822. doi: 10.1111/j.1529-8817.2004.04002.x

Krueger, T., Fisher, P. L., Becker, S., Pontasch, S., Dove, S., Hoegh-Guldberg, O., et al. (2015). Transcriptomic characterization of the enzymatic antioxidants FeSOD, MnSOD, APX and KatG in the dinoflagellate genus *Symbiodinium*. *BMC Evol. Biol.* 15:48. doi: 10.1186/s12862-015-0326-0

Kudela, R., Pitcher, G., Probyn, T., Figueiras, F., Moita, T., and Trainer, V. (2005). Harmful algal blooms in coastal upwelling systems. *Oceanography* 18, 184–197. doi: 10.5670/oceanog.2005.53

Li, T., Chen, X., and Lin, S. (2021). Physiological and transcriptomic responses to N-deficiency and ammonium: nitrate shift in *Fugacium kawagutii* (Symbiodiniaceae). *Sci. Total Environ.* 753:141906. doi: 10.1016/j.scitotenv.2020.141906

Li, J., Harata-Lee, Y., Denton, M. D., Feng, Q., Rathjen, J. R., Qu, Z., et al. (2017). Long read reference genome-free reconstruction of a full-length transcriptome from *Astragalus membranaceus* reveals transcript variants involved in bioactive compound biosynthesis. *Cell Discov.* 3:17031. doi: 10.1038/celldisc.2017.31

Li, Q., Li, Y., Song, J., Xu, H., Xu, J., Zhu, Y., et al. (2014). High-accuracy de novo assembly and SNP detection of chloroplast genomes using a SMRT circular consensus sequencing strategy. *New Phytol.* 204, 1041–1049. doi: 10.1111/nph.12966

Liu, Y., Chen, T., Song, S., and Li, C. (2015). Effects of nitrogenous nutrition on growth and nitrogen assimilation enzymes of dinoflagellates *Akashiwo sanguinea*. *Harmful Algae* 50, 99–106. doi: 10.1016/j.hal.2015.10.005

Liu, Y., Chen, T., Song, S., and Li, C. (2019). Variation in biochemical composition during encystment of the planktonic dinoflagellate *Akashiwo sanguinea* in N-limited cultures. *Mar. Biol.* 166:120. doi: 10.1007/s00227-019-3569-2

Liu, Y., Chen, T., Wang, X., Song, S., and Li, C. (2020). Variation in the photosynthetic activities of the dinoflagellate *Akashiwo sanguinea* during formation of resting cysts. *Mar. Biol.* 167:158. doi: 10.1007/s00227-020-03774-y

Lu, S., and Hodgkiss, I. J. (2004). Harmful algal bloom causative collected from Hong Kong waters. *Hydrobiologia* 512, 231–238. doi: 10.1023/B:HYDR.0000020331.75003.18

Luo, Z., Yang, W., Leaw, C. P., Pospelova, V., Bilien, G., Liow, G. R., et al. (2017). Cryptic diversity within the harmful dinoflagellate *Akashiwo sanguinea* in coastal Chinese waters is related to differentiated ecological niches. *Harmful Algae* 66, 88–96. doi: 10.1016/j.hal.2017.05.008

Matsubara, T., Nagasoe, S., Yamasaki, Y., Shikata, T., Shimasaki, Y., Oshima, Y., et al. (2007). Effects of temperature, salinity, and irradiance on the growth of the dinoflagellate *Akashiwo sanguinea*. *J. Exp. Mar. Bio. Ecol.* 342, 226–230. doi: 10.1016/j.jembe.2006.09.013

Perry, R. B., and Ulitsky, I. (2016). The functions of long noncoding RNAs in development and stem cells. *Development* 143, 3882–3894. doi: 10.1242/dev.140962

Rastogi, A., Maheswari, U., Dorrell, R. G., Vieira, F. R. J., Maumus, F., Kustka, A., et al. (2018). Integrative analysis of large scale transcriptome data draws a comprehensive landscape of *Phaeodactylum tricornutum* genome and evolutionary origin of diatoms. *Sci. Rep.* 8:4834. doi: 10.1038/s41598-018-23106-x

Rayko, E., Maumus, F., Maheswari, U., Jabbari, K., and Bowler, C. (2010). Transcription factor families inferred from genome sequences of photosynthetic stramenopiles. *New Phytol.* 188, 52–66. doi: 10.1111/j.1469-8137.2010.03371.x

Sharon, D., Tilgner, H., Grubert, F., and Snyder, M. (2013). A single-molecule long-read survey of the human transcriptome. *Nat. Biotechnol.* 31, 1009–1014. doi: 10.1038/nbt.2705

Shen, X., Kwan, H. Y., Thevasagayam, N. M., Prakki, S. R. S., Kuznetsova, I. S., Ngoh, S. Y., et al. (2014). The first transcriptome and genetic linkage map of *Asian arowana*. *Mol. Ecol. Resour.* 14, 622–635. doi: 10.1111/1755-0998.12212

Shikata, T., Takahashi, F., Nishide, H., Shigenobu, S., Kamei, Y., Sakamoto, S., et al. (2019). RNA-Seq analysis reveals genes related to photoreception, nutrient uptake, and toxicity in a noxious red-tide raphidophyte *Chattonella antiqua*. *Front. Microbiol.* 10:1764. doi: 10.3389/fmicb.2019.01764

Shimizu, K., Adachi, J., and Muraoka, Y. (2006). Angle: a sequencing errors resistant program for predicting protein coding regions in unfinished cDNA. *J. Bioinf. Comput. Biol.* 4, 649–664. doi: 10.1142/S0219720006002260

Tang, Y. Z., and Gobler, C. J. (2015). Sexual resting cyst production by the dinoflagellate Akashiwo sanguinea: a potential mechanism contributing to the ubiquitous distribution of a harmful alga. *J. phycol.* 51, 298–309. doi: 10.1111/jpy.12274

Tian, F., Yang, D., Meng, Y. Q., Jin, J., and Gao, G. (2020). PlantRegMap: charting functional regulatory maps in plants. *Nucleic Acids Res.* 48, D1104–D1113. doi: 10.1093/nar/gkz1020

Trainer, V. L., Pitcher, G. C., Reguera, B., and Smayda, T. J. (2010). The distribution and impacts of harmful algal bloom species in eastern boundary upwelling systems. *Prog. Oceanogr.* 85, 33–52. doi: 10.1016/j.pocean.2010.02.003

Wang, L., Zhu, P., Mo, Q., Luo, W., Du, Z., Jiang, J., et al. (2022). Comprehensive analysis of full-length transcriptomes of *Schizothorax prenanti* by single-molecule long-read sequencing. *Genomics* 114, 456–464. doi: 10.1016/j.ygeno.2021.01.009

Waterhouse, R. M., Seppey, M., Simão, F. A., Manni, M., Ioannidis, P., Klioutchnikov, G., et al. (2018). BUSCO applications from quality assessments to gene prediction and phylogenomics. *Mol. Biol. Evol.* 35, 543–548. doi: 10.1093/molbev/msx319

White, A. E., Watkins-Brandt, K. S., Mckibben, S. M., Wood, A. M., Hunter, M., Forster, Z., et al. (2014). Large-scale bloom of *Akashiwo sanguinea* in the northern California current system in 2009. *Harmful Algae* 37, 38–46. doi: 10.1016/j.hal.2015.02.005

Wisecaver, J. H., and Hackett, J. D. (2010). Transcriptome analysis reveals nuclear-encoded proteins for the maintenance of temporary plastids in the dinoflagellate *Dinophysis acuminate*. *BMC Genomics* 11:366. doi: 10.1186/1471-2164-11-366

Wu, Y., Zhou, C., Zhang, Y., Pu, X., and Li, W. (2001). Evolution and causes of formation of *Gymnodinium sanguinea* bloom in Yantai Sishili Bay. *Oceanologia Et Limnologia Sinica* 32, 159–167. (in Chinese, with English abstract). doi: 10.3321/j.issn:0029-814X.2001.02.007

Yang, M., Shang, X., Zhou, Y., Wang, C., Wei, G., Tang, J., et al. (2021). Full-length transcriptome analysis of *plasmodium falciparum* by single-molecule long-read sequencing. *Front. Cell. Infect. Microbiol.* 11:631545. doi: 10.3389/fcimb.2021.631545

Yao, R., Wang, Y., and Chen, L. (2019). Cellular functions of long noncoding RNAs. *Nat. Cell Biol.* 21, 542–551. doi: 10.1038/s41556-019-0311-8

frontiers | Frontiers in Marine Science

TYPE Original Research
PUBLISHED 21 December 2022
DOI 10.3389/fmars.2022.1033851

OPEN ACCESS

EDITED BY
Simon Mitrovic,
University of Technology Sydney, Australia

REVIEWED BY
Haiyan Wu,
Yellow Sea Fisheries Research Institute, Chinese Academy of Fishery Sciences (CAFS), China
Junhui Chen,
First Institute of Oceanography, China

*CORRESPONDENCE
Aifeng Li
lafouc@ouc.edu.cn

SPECIALTY SECTION
This article was submitted to Aquatic Microbiology, a section of the journal Frontiers in Marine Science

RECEIVED 01 September 2022
ACCEPTED 06 December 2022
PUBLISHED 21 December 2022

CITATION
Fu Y, Li A, Qiu J, Yan W, Yan C, Zhang L and Li M (2022) Effects of the neurotoxin *β*-*N*-methylamino-*L*-alanine (BMAA) on the early embryonic development of marine shellfish and fish. *Front. Mar. Sci.* 9:1033851. doi: 10.3389/fmars.2022.1033851

Effects of the neurotoxin *β*-*N*-methylamino-*L*-alanine (BMAA) on the early embryonic development of marine shellfish and fish

Yilei Fu[1], Aifeng Li[1,2]*, Jiangbing Qiu[1,2], Wenhui Yan[1], Chen Yan[1], Lei Zhang[1] and Min Li[1]

[1]College of Environmental Science and Engineering, Ocean University of China, Qingdao, China, [2]Key Laboratory of Marine Environment and Ecology, Ocean University of China, Ministry of Education, Qingdao, China

The neurotoxin *β*-*N*-methylamino-*L*-alanine (BMAA) produced by cyanobacteria and diatoms can accumulate in diverse aquatic organisms through the food web. In the present study, embryos of mussel *Mytilus galloprovincialis* (Lamarck, 1819), oyster *Magallana gigas* (Thunberg, 1793), and marine medaka *Oryzias melastigma* (McClelland, 1839) were exposed to BMAA dissolved in seawater and monitored for early developmental effects. Results demonstrated that the embryonic development of mussels and oysters were significantly inhibited when BMAA concentrations were above 100 μg BMAA·HCl/L (0.65 μM) and 800 μg BMAA·HCl/L (5.18 μM), respectively. The shell growth of mussel embryos was also markedly inhibited by BMAA ≥ 100 μg BMAA·HCl/L (0.65 μM). Based on the dose-response curves related to the modified malformation rate of embryos, the median effective concentration (EC_{50}) values of mussel (48 h) and oyster (24 h) embryos were 196 μg BMAA·HCl/L (1.27 μM) and 1660 μg BMAA·HCl/L (10.7 μM), respectively. A sustained and dose-dependent decrease in heart rate was apparent in marine medaka embryos at 9-days post fertilization following BMAA exposure. However, no obvious effect on ATP concentration was noted in these marine medaka embryos. The current study contributes to our understanding of the sublethal effects of BMAA on the early embryonic development of marine bivalves and medaka. Further research examining the long-term effects of BMAA on the early development of marine organisms is necessary to determine seawater quality criteria for protection.

KEYWORDS

β-*N*-methylamino-*L*-alanine (BMAA), embryonic development, *Mytilus galloprovincialis*, *Magallana gigas*, *Oryzias melastigma*

Highlights

- Effect of BMAA on embryonic development of marine shellfish and fish were eplored.
- The 48 h-EC_{50} for the inhibition of embryonic development of mussels was 1.27 μM.
- The 24 h-EC_{50} for the inhibition of embryonic development of oysters was 10.7 μM.
- Heart rate of medaka embryos was dose-dependent and reduced by BMAA at 9 DPF.
- No obvious effect on the ATP content was found due to BMAA in marine medaka embryos.

1 Introduction

The non-protein amino acid *β-N*-methylamino-*L*-alanine (BMAA) is linked to the high incidence of Amyotrophic Lateral Sclerosis/Parkinsonism Dementia Complex (ALS/PDC) in Guam (Cox et al., 2016), and the adverse effects and toxicological mechanisms of BMAA have been considered (Delcourt et al., 2018; Dunlop et al., 2021). The establishment of animal models to evaluate the neurotoxicity of BMAA has been fundamental to our understanding of human risk. Various *in vivo* studies on non-human primates, chicks, rats, and mice document neurodegenerative symptoms including ataxia and convulsions, as well as the formation of neurofibrillary tangles, *β*-amyloid plaques, ALS-related proteinopathy, and microglia activation as a result of BMAA exposure (Chiu et al., 2011; Cox et al., 2016; Davis et al., 2020). Furthermore, *in vitro* studies suggest that BMAA can selectively damage motor neurons through multiple mechanisms including excitotoxicity mediated by the carbamate adduct (Rao et al., 2006; Lopicic et al., 2009). In recent years, multiple studies have examined the adverse effects of BMAA on different aquatic organisms. For example, BMAA inhibited the oxidative stress defense and biotransformation enzymes of *Daphnia magna* (Straus, 1820) (Esterhuizen-Londt et al., 2015), altered phototaxis in brine shrimp *Artemia salina* (Linnaeus, 1758) (Purdie et al., 2009a), and caused abnormal spinal axis formation and some degree short-term learning and memory deficit in zebrafish *Danio rerio* (Hamilton, 1822) (Purdie et al., 2009b; Wang et al., 2020a). The combined evidence of these animal studies suggests that BMAA causes disease consistent with ALS/PDC.

Multiple toxicological mechanisms for BMAA neurotoxicity have been proposed. The role of BMAA as a glutamate receptor agonist has been deemed a key toxicological mechanism affecting motor neurons. In humans, an over-stimulation of glutamate and glutamatergic pathways may contribute to the development of various neurodegenerative diseases such as Alzheimer's disease, Parkinson's disease, and Huntington's disease (Salińska et al., 2005). BMAA has been shown to react with bicarbonate (HCO_3^-) to produce a *β*-carbamate that, in turn, acts as an agonist due to its structural homology to glutamate (Weiss and Choi, 1988). Most glutamate receptors including NMDA, AMPA/kainate, and metabotropic receptors are sensitive to the *β*-carbamate of BMAA (Rao et al., 2006; Lopicic et al., 2009; Chiu et al., 2012). Subsequently, an increase in intracellular Ca^{2+} further damages the mitochondria of neurons, promotes endoplasmic reticulum stress, and induces cell apoptosis (Delcourt et al., 2018). In addition, the competition of BMAA with cystine at the cystine/glutamate antiporter (system Xc^-) could also lead to glutathione depletion and aggravate oxidative stress (Albano and Lobner, 2018). In a rat model, neonatal exposure to BMAA increased protein ubiquitination in the cornus ammonis 1 region of the adult hippocampus indicating that BMAA may induce protein aggregation (Hanrieder et al., 2014).

The ubiquity of BMAA in marine seafood products increases the potential for human exposure to this neurotoxin (Lance et al., 2018; Li et al., 2018; Wang et al., 2021). Further, the health risk of BMAA to marine fauna is poorly documented. The embryonic development and early life stages (ELS) of mollusks and fish may be influenced by environmental BMAA released through diatom metabolism or from the broken cells of BMAA producers. It is important to assess the risk of BMAA exposure to marine animals in order to understand the risk to aquatic ecosystems.

The early life stages of marine bivalves have been used to develop toxicity bioassay models and assess the ecological effects of marine pollutants due to the transparency of embryo and larva, fast development, high-throughput screening format, and their sensitivity to contaminants (Capela et al., 2020). Mussels and oysters are commonly used as model organisms in marine/brackish ecotoxicology due to their economic and ecological significance for the near-shore ecosystem. In addition, the ELS of fish, such as marine medaka *Oryzias melastigma*, have been used as biologically significant endpoints to evaluate the effects of pollutants on aquatic teleosts (Wang et al., 2020b).

In this study, embryos of mussel (*Mytilus galloprovincialis*), Pacific oyster (*Magallana gigas*), and marine medaka (*O. melastigma*) were used to assess the ecotoxicological effects of the neurotoxin BMAA through exposure to dissolved toxin in seawater. The rate of development, malformation ratio, and heart rate were recorded along with morphological observations to evaluate the toxicological mechanisms of BMAA.

2 Materials and methods

2.1 Chemicals

Standard reference material of L-BMAA hydrochloride (B107, 50 mg) was obtained from Sigma-Aldrich (Oakville,

ON, Canada). Hydrochloric acid (HCl) was obtained from Sinopharm Chemical Reagent. The BMAA·HCl was dissolved in 2 mM HCl at 5 g/L to create a stock solution. The assay kit for ATP concentration was obtained from Solarbio (Beijing, China). The water used in these experiments was purified by a Milli-Q ultrapure water system (Millipore SAS, Molsheim, France) to 18.2 MΩ cm.

2.2 Animal gametes and fertilization

Sexually mature mussels (*M. galloprovincialis*) obtained from a local breeding farm in Qingdao, Shandong Province, China, between March and May 2020, were transferred to the laboratory and acclimatized in tanks containing natural seawater for 48 h. The collection of mussel gametes was carried out within a 2-day window during the period of spontaneous spawning. Each spawning individual was placed in a 250 mL beaker containing 200 mL of aerated 0.45 μm filtered seawater (FSW) until complete gamete release. The sperm and eggs of mussels were sieved through 50 μm and 90 μm meshes, respectively, to remove impurities after spawning. Egg quality (shape, size) and sperm motility were checked using an inverted microscope. Eggs were fertilized by adding sperm (1:10 ratio) in 6-well plates (NEST, Naisi Life Technology Co., Ltd., Wuxi, China). After 30 min, successful fertilization (n. fertilized eggs/n. total eggs × 100) was checked by microscopic observation (>85%) (Balbi et al., 2018).

Sexually mature Pacific oysters (*M. gigas*) were collected from a local breeding farm in Qingdao, Shandong Province, China, between May and August 2020, and transferred to the laboratory and acclimatized using the same method descried above. The oyster gametes were collected by dissection within a 7-day period. Gametes were transferred from the oyster gonads to 0.45 μm FSW using a pipette. The washing and fertilization procedure for these gametes used the same method described above.

Five-month-old male and female marine medaka were quartered in 10-L glass aquaria with 6-L natural seawater at 28 ± 1°C, with a 14:10 h light-dark cycle. Marine medaka were fed with Artemia nauplii three times a day, and the excreta was removed daily. The males and females of medaka were paired with equal individuals in a breeding aquarium before spawning. Spawned eggs were collected the next morning (8:00-9:00 am), rinsed with FSW, and examined under a stereomicroscope (Zhongheng Instrument Ltd., Shanghai, China) to ensure fertilization.

2.3 BMAA exposure experiments for bivalve embryos

Mussel embryos exposed to BMAA were observed for 48 h in 48-well microwell plates containing 1 mL of liquid per well. A total of 25 embryos were exposed in each well with a range of different concentrations of BMAA including a zero blank control (FSW only), solvent control (2 mM HCl in FSW), 50 (0.32 μM), 100 (0.65 μM), 200 (1.29 μM), 400 (2.59 μM) and 800 (5.18 μM) μg BMAA·HCl/L in FSW. Each treatment was prepared in triplicate. Microplates were maintained at 16 ± 1°C for 48 h, with a 16 h: 8 h cycle of light: dark.

The bioassay for oyster embryos was carried out using the same method described above, except using higher concentrations of BMAA: 800 (5.18 μM), 1200 (7.77 μM), 1600 (10.36 μM), 2000 (12.94 μM) and 2400 (15.53 μM) μg BMAA·HCl/L. Each treatment was prepared in triplicate and the microplates were incubated at 24 ± 1°C for 24 h in the dark.

At the end of the incubation period, samples were fixed with a buffered formalin (4%) solution. All larvae in each well were examined using an inverted microscope (Olympus, Milano, Italy). A larva was considered normal when its shell was D-shaped (straight hinge) and the mantle did not protrude out of the shell. Meanwhile, a malformed embryo was defined as not reaching the normal 48 hours post fertilization (HPF) stage for mussels and not reaching the 24 HPF for oysters (trochophore or earlier stages) or considered malformed if other developmental defects were observed (concave, malformed or damaged shell, protruding mantle). The recorded endpoint was the percentage of normal D-larvae (D-veligers) in each well relative to the total number, including malformed larvae and pre-D stages. The blank control with only seawater and solvent control with HCl were run in parallel, and no obvious effects of HCl solvent on the embryo development were observed even at the highest concentration of HCl added in seawater.

To calculate the EC_{50} values of BMAA for mussel and oyster embryos, the percent of biological response was modified by the solvent control following the equation:

$$P = (P_o - P_c) \times 100/(100 - P_c)$$

where P is the modified response (%), P_o is the observed initial response (%) and P_c is the control response (%) (His et al., 1999).

In addition, the length (the anterior-posterior dimension of the shell parallel to the hinge line) and height (the dorsal-ventral dimension perpendicular to the hinge) of mussel D-veligers at 48 HPF in different experimental groups were also measured under an inverted microscope (Kurihara et al., 2008).

2.4 BMAA exposure experiments for marine medaka embryos

To evaluate the effects of BMAA on the embryonic development of fish, 15 embryos (3-5 HPF) of medaka were selected and exposed to FSW (blank control), FSW with 2 mM HCl (solvent control), and 20 (0.13 μM), 200 (1.29 μM), 2000 (12.9 μM), 20000 (129 μM) μg BMAA·HCl/L in each treatment until hatching. Embryonic development was examined every day under an inverted microscope (Olympus, Milano, Italy) equipped with a

color CCD camera. Several sublethal endpoints were observed during the exposure period, including developmental rate (occurrence/percentage of head bud at 24 HPF and eye pigmentation at 48 HPF), heart beat at 6 days post fertilization (DPF) and 9 DPF, hatching time-course and hatching success rate, cumulative mortality and mortality ratio at four developmental periods, morphological abnormality, malformed characteristic (Wang et al., 2020b). Embryos were judged as dead if they turned opaque and/or white in early developmental stages and if a heart beat could not be observed in the later stages. Dead embryos were counted and removed daily. The solutions were renewed once after three days. A hatching failure was recorded if the embryo did not hatch within 18 days.

2.5 Effect of BMAA on the ATP concentration of marine medaka embryos

The ATP concentration of medaka embryos was determined using an ATP assay kit (Solarbio, Beijing, China). Embryos (3-5 HPF) were exposed to FSW (blank control), FSW with 2 mM HCl (solvent control), and 20000 μg BMAA·HCl/L. Based on previous experiments (tested in section 2.4), embryos started to hatch at 10 DPF. Thus, embryos were collected at 9 DPF, i.e. one day before hatching, to test for ATP. Embryos and ATP extract solvent were mixed at a ratio of 1:10 (embryo weight: ATP extraction volume, m/v) and were homogenized within an ice bath. The homogenates were centrifuged at 8000 ×*g*, 4°C for 10 min. Supernatants were collected and chloroform was added. The mixed liquid was centrifuged at 10000 ×*g*, 4°C for 3 min. Supernatants were collected and 20 μL were transferred to a 96-well plate. The ATP reaction solution was added to these samples in each well. The ATP concentration was analyzed at 340 nm using a Synergy MX microplate reader after gently shaking the mixture.

2.6 Statistical analysis

All data were expressed as means ± standard deviations (SDs). The EC_{50} values for BMAA were calculated by probability unit conversion and analysis (Giannuzzi et al., 2021). Statistical analysis was performed using the IMB SPSS Statistics V25.0 software (IBM Corporation, New York, USA). Results were initially tested for normality and equality of variance (Levene's test, 5% risk). Percentage data were arcsine transformed to achieve normality and equality of variance criteria. If assumptions of homogeneity of variances were satisfied, one-way analysis of variance (ANOVA) followed by LSD's test was used. A p-value< 0.05 indicated a statistically significant result.

3 Results

3.1 Survival

The embryo mortality of mussel and oysters were less than 20% and 10%, respectively, in all experimental groups (Figure S1). No acute lethal effect of BMAA on either bivalve was observed in this study. Accumulative mortality of marine medaka did not significantly differ between the solvent controls and BMAA exposure treatments (Figure S2). The LC_{50} value of marine medaka embryo was higher than 20000 μg BMAA·HCl/L.

3.2 Effects of BMAA on the development of bivalve embryos

The effects of BMAA exposure on the embryonic development of mussel and oysters are summarized in Figure 1. The percentage of normal D-veligers in the mussel embryo bioassay decreased with rising concentrations of BMAA (Figure 1A), and no normal D-veligers were found in the BMAA exposure treatments at 400 and 800 μg BMAA·HCl/L. The percentage of mussel trochophores gradually increased with the concentration of BMAA in the exposure groups, and all embryos were blocked at the trochophore stage in the 400 and 800 μg BMAA·HCl/L treatments. Furthermore, the percentage of malformed D-veligers also positively increased as the BMAA increased from 0 to 200 μg BMAA·HCl/L.

Within the oyster embryo bioassay (Figure 1B), the percent variation of normal D-veligers and trochophores of oysters demonstrated similar trends as those seen with the mussel embryos from 0 to 2400 μg BMAA·HCl/L treatments. However, the percentage of malformed oyster D-veligers was less than 10% and did not significantly change between different BMAA treatments.

The modified responses of mussel and oyster embryos demonstrated that the mussel embryos were more sensitive to BMAA exposure than oyster embryos (Figure S3). The dose-response curves for mussel and oyster embryos exposed to BMAA were shown in Figure 2. Finally, the 48 h-EC_{50} for mussel embryos was 196 μg BMAA·HCl/L (1.27 μM), and the 24 h-EC_{50} for oyster embryos was 1660 μg BMAA·HCl/L (10.7 μM) (Table 1).

To assess the impact of BMAA on the growth and development of mussel embryos, the shell length and height of normal D-veligers at 48 HPF were calculated (Figure 3). The mussel shell size significantly reduced when the embryos were exposed to BMAA at 100 and 200 μg BMAA·HCl/L.

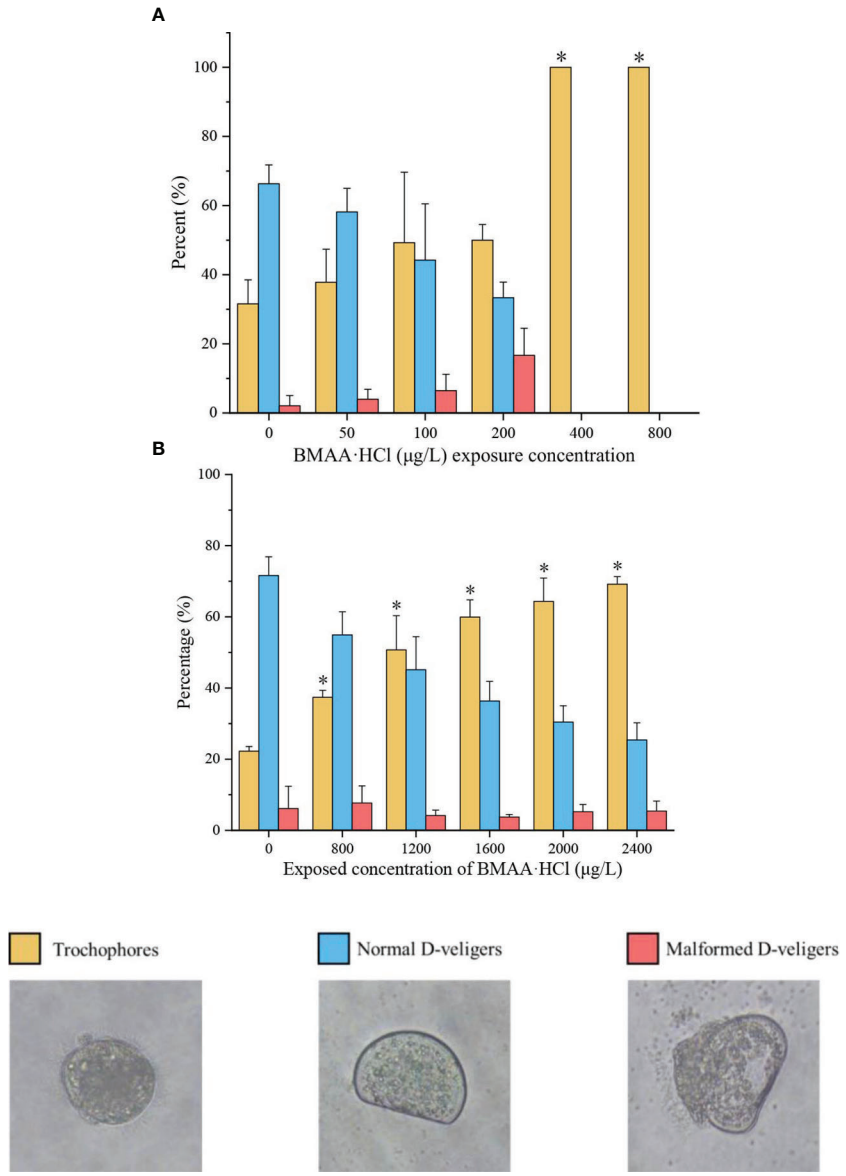

FIGURE 1
Percentage of trochophores, normal D-veligers, and malformed D-veligers of mussel (*Mytilus galloprovincialis*) at 48 hours post fertilization (HPF) **(A)** and oyster (*Magallana gigas*) at 24 HPF **(B)** in the BMAA exposure experiments. Note: An equivalent volume of 2 mM HCl used in the highest BMAA exposure treatments was added into the culture wells as a solvent control, which was labeled as a zero concentration of BMAA. Only the percentage of trochophores between control group and BMAA exposure treatments were statistically analyzed. An asterisk indicates the results were significantly difference at $p < 0.05$.

3.3 Effects of BMAA on development and ATP concentration within marine medaka embryos

The development of head bud (1 DPF) and eye pigmentation (2 DPF) were above 90% in all treatments (Figure S4). No significant difference between the developmental rates of medaka embryos occurred in the solvent control and BMAA treatments. The heart rate of embryos recorded at 6 DPF indicated no differences between treatment groups (Figure 4). However, the heart rate of embryos at 9 DPF were reduced in a dose-dependent manner when exposed to BMAA at 200, 2000 and 20000 μg BMAA·HCl/L.

The hatching rates of marine medaka embryos slightly increased with rising BMAA concentrations but no statistical difference between solvent control and exposure treatments were

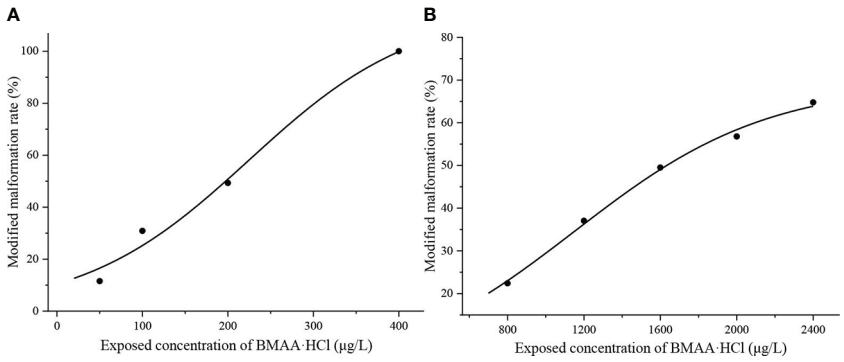

FIGURE 2
Modified malformation ratios of mussel (*Mytilus galloprovincialis*) embryos at 48 hours post fertilization (HPF) **(A)** and oyster (*Magallana gigas*) embryos at 24 HPF **(B)** during the BMAA exposure experiments.

found (Figure S5A). We note that the error bars between replicates showed that variation in the hatching rate in BMAA exposure treatments were higher than that in the solvent control group. The hatching time-course of medaka embryos was not obviously affected by BMAA exposure in this study (Figure S5B). In addition, no observed changes for the development of eye melanin in medaka embryos were found in the BMAA exposure treatments.

No significant differences were found in the ATP concentrations between blank controls and solvent controls used with the medaka embryos, which demonstrated that the additional low concentration of HCl did not affect the ATP concentration of medaka embryos. Although the result was not statistically significant, the ATP concentration of medaka embryos exposed to 20000 μg BMAA·HCl/L decreased and expressed relatively large variation within the replicated groups (Figure 5).

4 Discussion

BMAA is hydrophilic and can be accumulated by shellfish and marine opossum shrimp (*Neomysis awatschensis*) through water filtration (Baptista et al., 2015; Wang et al., 2020a). Prior research has demonstrated that soluble BMAA was directly transferred to marine organisms from a seawater medium (Baptista et al., 2015; Wang et al., 2020a). Exogenous BMAA has been shown to disrupt the antioxidant system and cause significant DNA damage in the hemocytes of freshwater bivalves (Contardo-Jara et al., 2014; Lepoutre et al., 2018).

To further explore the toxicological effects of BMAA dissolved in seawater environments on marine bivalves and fish, we examined the external fertilization and early development of bivalve and fish embryos exposed to exogenous BMAA. We did not find a lethal effect on mussel and oyster embryos exposed to BMAA at the experimental dose used here, but demonstrated that embryo development was markedly inhibited (Figure 1). The development of all mussel embryos was delayed at the trochophore stage (48-hours post fertilization, HPF) by exposure to BMAA concentrations of 400 and 800 μg BMAA·HCl/L (Figure 1A). Comparatively, the oyster embryos were not sensitive to BMAA exposure as 25% of the embryos entered the D-veliger stage from the trochophore stage at 24 HPF while exposed to 2400 μg BMAA·HCl/L (Figure 1B). This discrepancy suggests that sensitivity to BMAA exposure during embryogenesis was interspecific in bivalves. Due to the delayed development process, the malformation rate of bivalve embryos was modified and used to calculate the EC_{50} values for mussel (48 h) and oyster (24 h) embryos at 1.27 and 10.7 μM BMAA, respectively (Table 1). In our previous study, the fertilization and development of sea urchin embryos were also significantly inhibited by BMAA above 300 μg/L (2.54 μM), and EC_{50} value calculated by the percent of active swimming larvae was 1.4 μM BMAA (Li et al., 2020). Therefore, the EC_{50} values for mussel and sea urchin embryos were similar, which was

TABLE 1 The EC_{50} values calculated by the malformation ratios of different embryos exposed to BMAA.

Species	Exposure time	EC_{50} (μg BMAA·HCl/L)	Formula	R^2
mussel (*Mytilus galloprovincialis*)	48 h	196	y = 1.9608x+0.5066	0.9889
oyster (*Magallana gigas*)	24 h	1660	y = 2.3705x-2.6331	0.9986
marine medaka (*Oryzias melastigma*)	9 d	>20000	/	/

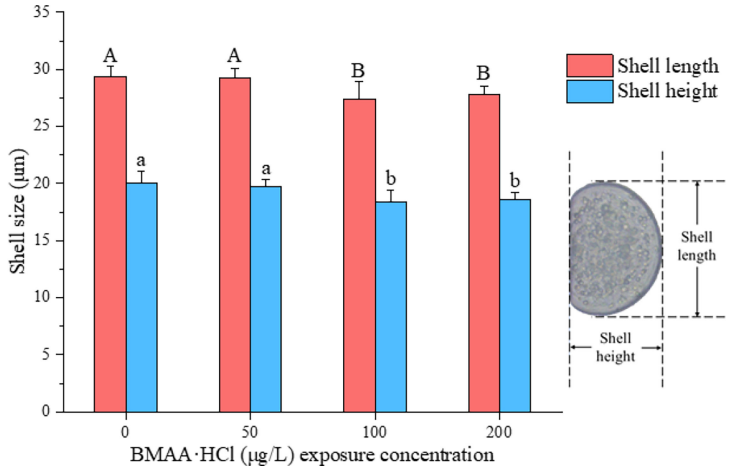

FIGURE 3
Shell size of normal D-veligers at 48 HPF in the mussel (*Mytilus galloprovincialis*) embryos following exposure to BMAA. Note: An equivalent volume of 2 mmol/L HCl used in the highest BMAA exposure treatments was added into the culture wells as a solvent control group and labeled as a zero concentration of BMAA. The different letters indicate a significantly different result between treatments ($p < 0.05$).

significantly lower than that for oyster embryos. Similar sensitivities during embryogenesis were noted among sea urchins, mussels, and copepods exposed to aromatic hydrocarbons found in heavy fuel oil (Saco-Álvarez et al., 2008). The sensitivity discrepancy we noted in bivalve embryos exposed to BMAA suggests that oysters have a relatively high resistivity to environmental contaminants. In this current study, we did not observe significant changes in the fertilization efficiency of oyster sperm exposed to a high concentration of BMAA 3200 μg BMAA·HCl/L (20.7 μM) (Figure S6). This is in contrast to our previous observations of the fertilization ability of sea urchin sperm which were significantly reduced after exposure to 500 μg BMAA/L (4.24 μM) for 10 min (Li et al., 2020). This difference further supports the conclusion that both gametes and embryos of oysters were more resistant to BMAA than those of sea urchins.

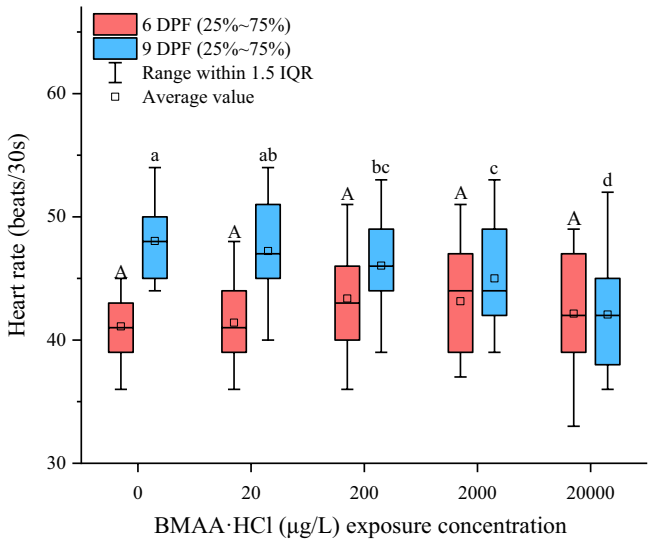

FIGURE 4
Heart rates measured at 6 days post fertilization (DPF) and 9 DPF in marine medaka (*Oryzias melastigma*) embryos exposed to BMAA. Note: An equivalent volume of 2 mM HCl used in the highest BMAA exposure treatments was added into the culture wells as solvent control group and labeled as a zero concentration of BMAA. The different letters indicate a significantly different result between treatments ($p < 0.05$).

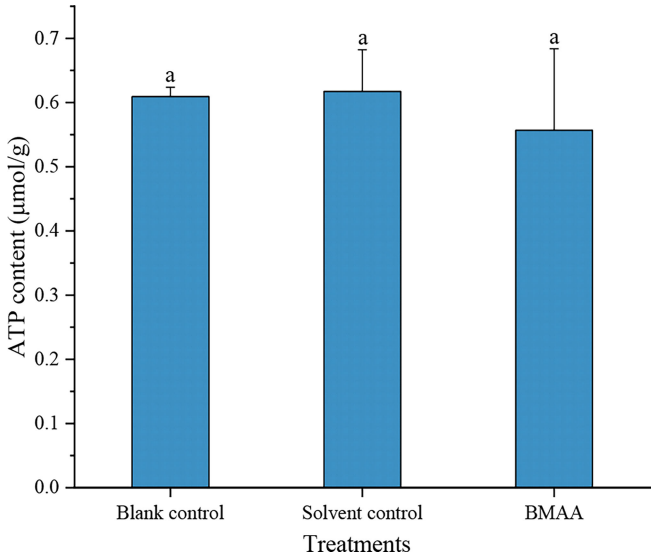

FIGURE 5
The ATP concentrations in marine medaka (*Oryzias melastigma*) embryos at 9 days post fertilization (DPF) in different treatments. An equivalent volume of 2 mM HCl was added into the culture well as a solvent control group.

In addition to the delayed bivalve embryogenesis, as discussed above, the shell size of normal D-veliger also decreased with increasing BMAA concentrations. In recent studies, the larval shell formation of oysters was shown to be modulated by monoamine neurotransmitters, 5-HT and dopamine (DA), through the TGF-β smad pathway, triggering the expression of tyrosinase to form the initial shell which further inhibited the expression of chitinase at the trochophore stage (Liu et al., 2018; Liu et al., 2020). Interestingly, DA levels were altered in the central nervous system of adult rats and reduced in the substantia nigra of the rat brain due to the loss of tyrosine hydroxylase (TH)-positive dopaminergic neurons following BMAA exposure (Santiago et al., 2006; Scott and Downing, 2019). For aquatic animals, the expression of dopamine D4 receptor (DRD4) and monoamine oxidase A (MAOA) were also differentially down-regulated in the brain of mangrove rivulus fish (*Kryptolebias marmoratus*) exposed to BMAA at 15 mg/L (Carion et al., 2020). The inhibition of DA and serotonin biosynthesis were hypothesized to explain the destruction of swimming ability of sea urchin larva (Li et al., 2020). We here hypothesize that disruption or inhibition of 5-HT and/or DA biosynthesis were possibly responsible for the inhibitory effects of BMAA on shell formation and growth of shellfish embryos in this current study.

The heart development is a key process for successful embryogenesis of fish. The delivery of nutrients necessary for growth would be reduced if cardiac function was impaired by either heart malformations or a reduced heartbeat. The heart rate of marine medaka larvae was significantly reduced in a dose-dependent manner at 9 DPF, in this study (Figure 4). This same effect has been noted in previous studies using the freshwater zebrafish larvae model exposed to BMAA (Purdie et al., 2009b; Wang, 2015). The embryonic heartbeat of zebrafish was linked to several ionic currents including sodium, T-type and L-type calcium and several potassium currents (Rottbauer et al., 2001). Increased Ca^{2+} in the sarcoplasmic reticulum caused delayed post depolarization and arrhythmia in this model (Zhang et al., 2016). Likewise, the β-carbamate adduct of BMAA could act on glutamate receptors to activate Ca^{2+} influx into cells through NMDA receptors and result in the accumulation of intracellular Ca^{2+} (Salińska et al., 2005). Recently, it has been confirmed that the endoplasmic reticulum releases Ca^{2+} in rat primary motor neurons (Petrozziello et al., 2022). Glutamate receptors exist not only in the CNS, but also in other non-neuronal tissues such as the heart, pancreas and skin (Skerry and Genever, 2001; Mueller et al., 2003). In the current study, the decreased embryonic heart rate of medaka was possibly caused by the abnormal activation of glutamate receptors resulting in an increase of intracellular Ca^{2+} in embryonic cardiomyocytes as a direct consequence of BMAA exposure.

Mitochondrial dysfunction could lead to cardiac developmental defects because the cardiac contraction and relaxation processes relies on ATP biosynthesis by the mitochondria. Our results demonstrated that the average content of ATP in medaka embryos treated with BMAA at 9 DPF was slightly lower than that of the control group but with greater variation (Figure 5). However, an increase of intracellular ATP levels occurred in a fish immune cell line (CLC) exposed to 1.5 mM BMAA without dose-

dependence, which indicated that the BMAA exposure could alter ATP biosynthesis (Sieroslawska and Rymuszka, 2019). It is possible that BMAA could affect mitochondrial function *via* multiple mechanisms in different species (Chiu et al., 2012).

The indexes of eye, heart and hatching rate are commonly used to assess the embryogenesis development of fish in toxicological tests. The eyes of medaka embryos begin to develop at about 28 HPF, and the optic choroidea darken because of melanin pigmentation at about 50 HPF (González-Doncel et al., 2005). In the present study, the development of eye melanin in medaka embryos was not significantly affected by BMAA. Reportedly, BMAA binds to melanin and neuromelanin cells in animals, which may lead to changes in the structure and characteristics of melanin and neuromelanin. Long term exposure to BMAA possibly caused the disintegration of melanin polymers in cells containing melanin and neuromelanin (Karlsson et al., 2009). Although no obvious effect of BMAA on melanin synthesis in medaka embryos was found, its possible impact on the later life development of medaka embryos could not be excluded.

The hatching rate of medaka embryos was not affected by BMAA. The majority of embryos in all treatments hatched in the time interval from 10 to 14 DPF. No effect of BMAA on the incubation time of zebrafish embryos was observed in previous studies using even higher concentrations of BMAA (50 and 100 mg/L) (Purdie et al., 2009b; Wang, 2015). The BMAA exposure did not cause abnormal death of medaka embryos in this study, which is similar to a previous study on freshwater fish (Wang, 2015). We observed a reduction in the heart rate of medaka embryos at 9 DPF, which could have an effect on the later developmental stages of medaka embryos. In prior *in vivo* experiments, almost no acute lethal effect was recorded and abnormal biological behaviors were observed only following the injection of BMAA at even higher concentrations (Chiu et al., 2011; Delcourt et al., 2018; Wang et al., 2020a). Long-term observations of aquatic organisms exposed to BMAA are needed to assess its full ecological impact.

5 Conclusions

The adverse effects of BMAA on the early embryo development of marine bivalves and marine medaka were explored and discussed in this study. We documented the sublethal effects of BMAA on the embryogenesis and growth of bivalve and fish embryos. The embryonic development and growth of mussel and oyster larvae, as well as the shell formation and growth of mussel larvae, were inhibited by BMAA exposure. Comparatively, mussel embryos were more sensitive to BMAA than oyster embryos. Arrhythmias and a slight reduction of average ATP concentration occurred in marine medaka embryos exposed to BMAA. Long-term effects of BMAA on the production and development of aquatic organisms should be explored in future research.

Data availability statement

The original contributions presented in the study are included in the article/Supplementary Material. Further inquiries can be directed to the corresponding author.

Author contributions

YF: Experimental design, Data acquisition and processing, Manuscript draft. AL: Experimental design, Supervisor, Funding acceptance, Manuscript review and editing. JQ: Project supervision, Manuscript review and editing. WY: Experimental animal maintenance. CY: Experimental animal maintenance. LZ: Experimental design. ML: Experimental design. All authors contributed to the article and approved the submitted version.

Acknowledgments

This work was funded by the National Natural Science Foundation of China (U2106205, 41676093). We appreciate Dr. Sandra Banack at the Brain Chemistry Laboratories, Institute for Ethnomedicine, USA editing this manuscript before resubmission.

Conflict of interest

The authors declare that the research was conducted in the absence of any commercial or financial relationships that could be construed as a potential conflict of interest.

Publisher's note

Supplementary material

The Supplementary Material for this article can be found online at: https://www.frontiersin.org/articles/10.3389/fmars.2022.1033851/full#supplementary-material

References

Albano, R., and Lobner, D. (2018). Transport of BMAA into neurons and astrocytes by system xc⁻. *Neurotox. Res.* 33, 1–5. doi: 10.1007/s12640-017-9739-4

Balbi, T., Montagna, M., Fabbri, R., Carbone, C., Franzellitti, S., Fabbri, E., et al. (2018). Diclofenac affects early embryo development in the marine bivalve *Mytilus galloprovincialis*. *Sci. Total Environ.* 642, 601–609. doi: 10.1016/j.scitotenv.2018.06.125

Baptista, M. S., Vasconcelos, R. G., Ferreira, P. C., Almeida, C. M., and Vasconcelos, V. M. (2015). Assessment of the non-protein amino acid BMAA in Mediterranean mussel *Mytilus galloprovincialis* after feeding with estuarine cyanobacteria. *Environ. Sci. Pollut. Res.* 22, 12501–12510. doi: 10.1007/s11356-015-4516-5

Capela, R., Garric, J., Castro, L. F. C., and Santos, M. M. (2020). Embryo bioassays with aquatic animals for toxicity testing and hazard assessment of emerging pollutants: A review. *Sci. Total Environ.* 705, 135740. doi: 10.1016/j.scitotenv.2019.135740

Carion, A., Markey, A., Hetru, J., Carpentier, C., Suarez-Ulloa, V., Denoel, M., et al. (2020). Behavior and gene expression in the brain of adult self-fertilizing mangrove rivulus fish (*Kryptolebias marmoratus*) after early life exposure to the neurotoxin β-N-methylamino-L-alanine (BMAA). *Neurotoxicol* 79, 110–121. doi: 10.1016/j.neuro.2020.04.007

Chiu, A. S., Gehringer, M. M., Braidy, N., Guillemin, G. J., Welch, J. H., and Neilan, B. A. (2012). Excitotoxic potential of the cyanotoxin β-methyl-amino-L-alanine (BMAA) in primary human neurons. *Toxicon* 60, 1159–1165. doi: 10.1016/j.toxicon.2012.07.169

Chiu, A. S., Gehringer, M. M., Welch, J. H., and Neilan, B. A. (2011). Does α-amino-β-methylaminopropionic acid (BMAA) play a role in neurodegeneration? *Int. J. Environ. Res. Public Health* 8, 3728–3746. doi: 10.3390/ijerph8093728

Contardo-Jara, V., Otterstein, S. K. B., Downing, S., Downing, T. G., and Pflugmacher, S. (2014). Response of antioxidant and biotransformation systems of selected freshwater mussels (*Dreissena polymorpha*, anadonta cygnea, unio tumidus, and *Corbicula javanicus*) to the cyanobacterial neurotoxin β-N-methylamino-L-alanine. *Toxicol. Environ. Chem.* 96, 451–465. doi: 10.1080/02772248.2014.945452

Cox, P. A., Davis, D. A., Mash, D. C., Metcalf, J. S., and Banack, S. A. (2016). Dietary exposure to an environmental toxin triggers neurofibrillary tangles and amyloid deposits in the brain. *Proc. Biol. Sci.* 283, 20152397.. doi: 10.1098/rspb.2015.2397

Davis, D. A., Cox, P. A., Banack, S. A., Lecusay, P. D., Garamszegi, S. P., Hagan, M., et al. (2020). L-serine reduces spinal cord pathology in a vervet model of preclinical ALS/MND. *J. Neuropathol. Exp. Neurol.* 79, 393–406. doi: 10.1093/jnen/nlaa002

Delcourt, N., Claudepierre, T., Maignien, T., Arnich, N., and Mattei, C. (2018). Cellular and molecular aspects of the β-N-methylamino-L-alanine (BMAA) mode of action within the neurodegenerative pathway: Facts and controversy. *Toxins* 10, 6. doi: 10.3390/toxins10010006

Dunlop, R. A., Banack, S. A., Bishop, S. L., Metcalf, J. S., Murch, S. J., Davis, D. A., et al. (2021). Is exposure to BMAA a risk factor for neurodegenerative diseases? a response to a critical review of the BMAA hypothesis. *Neurotox. Res.* 39, 81–106. doi: 10.1007/s12640-020-00302-0

Esterhuizen-Londt, M., Wiegand, C., and Downing, T. G. (2015). β-N-methylamino-L-alanine (BMAA) uptake by the animal model, *Daphnia magna* and subsequent oxidative stress. *Toxicon* 100, 20–26. doi: 10.1016/j.toxicon.2015.03.021

Giannuzzi, L., Lombardo, T., Juárez, I., Aguilera, A., and Blanco, G. (2021). A stochastic characterization of hydrogen peroxide-induced regulated cell death in *Microcystis aeruginosa*. *Front. Microbiol.* 12, 636157. doi: 10.3389/fmicb.2021.636157

González-Doncel, M., Okihiro, M. S., Villalobos, S. A., Hinton, D. E., and Tarazona, J. V. (2005). A quick reference guide to the normal development of *Oryzias latipes* (Teleostei, adrianichthyidae). *J. Appl. Ichthyol.* 21, 39–52. doi: 10.1111/j.1439-0426.2004.00615.x

Hanrieder, J., Gerber, L., Sandelius, Å. P., Brittebo, E. B., Ewing, A. G., and Karlsson, A. (2014). High resolution metabolite imaging in the hippocampus following neonatal exposure to the environmental toxin BMAA using ToF-SIMS. *Neurosci* 5, 568–575. doi: 10.1021/cn500039b

His, E., Beiras, R., and Seaman, M. N. L. (1999). The assessment of marine pollution - bioassays with bivalve embryos and larvae. *Adv. Mar. Biol* 37, 1–178.. doi: 10.1016/S0065-2881(08)60428-9

Karlsson, O., Berg, C., Brittebo, E. B., and Lindquist, N. G. (2009). Retention of the cyanobacterial neurotoxin β-N-methylamino-L-alanine in melanin and neuromelanin-containing cells - a possible link between Parkinson-dementia complex and pigmentary retinopathy. *Pigment Cell Melanoma Res.* 22, 120–130. doi: 10.1111/j.1755-148X.2008.00508.x

Kurihara, H., Asai, T., Kato, S., and Ishimatsu, A. (2008). Effects of elevated pCO_2 on early development in the mussel *Mytilus galloprovincialis*. *Aquat. Biol.* 4, 225–233. doi: 10.3354/ab00109

Lance, E., Arnich, N., Maignien, T., and Bire, R. (2018). Occurrence of β-N-methylamino-L-alanine (BMAA) and isomers in aquatic environments and aquatic food sources for humans. *Toxins* 10, 83. doi: 10.3390/toxins10020083

Lepoutre, A., Milliote, N., Bonnard, M., Palos-Ladeiro, M., Rioult, D., Bonnard, I., et al. (2018). Genotoxic and cytotoxic effects on the immune cells of the freshwater bivalve *Dreissena polymorpha* exposed to the environmental neurotoxin BMAA. *Toxins* 10, 106. doi: 10.3390/toxins10030106

Li, A., Espinoza, J., and Hamdoun, A. (2020). Inhibitory effects of neurotoxin β-N-methylamino-L-alanine on fertilization and early development of the Sea urchin *Lytechinus pictus*. *Aquat. Toxicol.* 221, 105425. doi: 10.1016/j.aquatox.2020.105425

Li, A., Hu, Y., Song, J., Wang, S., and Deng, L. (2018). Ubiquity of the neurotoxin β-N-methylamino-L-alanine and its isomers confirmed by two different mass spectrometric methods in diverse marine mollusks. *Toxicon* 151, 129–136. doi: 10.1016/j.toxicon.2018.07.004

Liu, Z. Q., Wang, L. L., Yan, Y. C., Zheng, Y., Ge, W. J., Li, M. J., et al. (2018). D1 dopamine receptor is involved in shell formation in larvae of pacific oyster *Crassostrea gigas*. *Dev. Comp. Immunol.* 84, 337–342. doi: 10.1016/j.dci.2018.03.009

Liu, Z., Zhou, Z., Zhang, Y., Wang, L., Song, X., Wang, W., et al. (2020). Ocean acidification inhibits initial shell formation of oyster larvae by suppressing the biosynthesis of serotonin and dopamine. *Sci. Total Environ.* 735, 139469. doi: 10.1016/j.scitotenv.2020.139469

Lopicic, S., Nedeljkov, V., and Cemerikic, D. (2009). Augmentation and ionic mechanism of effect of β-N-methylamino-L-alanine in presence of bicarbonate on membrane potential of retzius nerve cells of the leech *Haemopis sanguisuga*. *Comp. Biochem. Physiol. A. Mol. Integr. Physiol.* 153, 284–292. doi: 10.1016/j.cbpa.2009.02.038

Mueller, R. W., Gill, S. S., and Pulido, O. M. (2003). The monkey (*Macaca fascicularis*) heart neural structures and conducting system: An immunochemical study of selected neural biomarkers and glutamate receptors. *Toxicol. Pathol.* 31, 227–234. doi: 10.1080/01926230390183724

Petrozziello, T., Boscia, F., Tedeschi, V., Pannaccione, A., de Rosa, V., Corvino, A., et al. (2022). Na^+/Ca^{2+} exchanger isoform 1 takes part to the Ca^{2+}-related prosurvival pathway of SOD1 in primary motor neurons exposed to beta-methylamino-L-alanine. *Cell Commun. Signal.* 20, 8. doi: 10.1186/s12964-021-00813-z

Purdie, E. L., Metcalf, J. S., Kashmiri, S., and Codd, G. A. (2009a). Toxicity of the cyanobacterial neurotoxin β-N-methylamino-L-alanine to three aquatic animal species. *Amyotroph. Lateral Scler.* 2, 67–70. doi: 10.3109/17482960903273551

Purdie, E. L., Samsudin, S., Eddy, F. B., and Codd, G. A. (2009b). Effects of the cyanobacterial neurotoxin β-N-methylamino-L-alanine on the early-life stage development of zebrafish (*Danio rerio*). *Aquat. Toxicol.* 95, 279–284. doi: 10.1016/j.aquatox.2009.02.009

Rao, S. D., Banack, S. A., Cox, P. A., and Weiss, J. H. (2006). BMAA selectively injures motor neurons *via* AMPA/Kainate receptor activation. *Exp. Neurol.* 201, 244–252. doi: 10.1016/j.expneurol.2006.04.017

Rottbauer, W., Baker, K., Wo, Z. G., Mohideen, M. P. K., Cantiello, H. F., and Fishman, M. C. (2001). Growth and function of the embryonic heart depend upon the cardiac-specific l-type calcium channel α1 subunit. *Dev. Cell* 1, 265–275. doi: 10.1016/s1534-5807(01)00023-5

Saco-Álvarez, L., Bellas, J., Nieto, Ó., Bayona, J. M., Albaigés, J., and Beiras, R. (2008). Toxicity and phototoxicity of water-accommodated fraction obtained from *Prestige* fuel oil and marine fuel oil evaluated by marine bioassays. *Sci. Total Environ.* 394, 275–282. doi: 10.1016/j.ecoenv.2015.09.002

Salińska, E., Danysz, W., and Łazarewicz, J. W. (2005). The role of excitotoxicity in neurodegeneration. *Folia Neuropathol.* 43, 322–339. doi: 10.1016/s0163-7258(98)00042-4

Santiago, M., Matarredona, E. R., Machado, A., and Cano, J. (2006). Acute perfusion of BMAA in the rat's striatum by in vivo microdialysis. *Toxicol. Lett.* 167, 34–39. doi: 10.1016/j.toxlet.2006.08.005

Scott, L., and Downing, T. (2019). Dose-dependent adult neurodegeneration in a rat model after neonatal exposure to β-N-methylamino-L-alanine. *Neurotox. Res.* 35, 711–723. doi: 10.1007/s12640-019-9996-5

Sieroslawska, A., and Rymuszka, A. (2019). Assessment of the cytotoxic impact of cyanotoxin beta-N-methylamino-L-alanine on a fish immune cell line. *Aquat. Toxicol.* 212, 214–221. doi: 10.1016/j.aquatox.2019.05.012

Skerry, T. M., and Genever, P. G. (2001). Glutamate signalling in non-neuronal tissues. *Trends Pharmacol. Sci.* 22, 174–181. doi: 10.1016/S0165-6147(00)01642-4

Wang, J. (2015). *Acute toxicity of β-N-methylamino-L-alanine (BMAA) to fathead minnow (Pimephales promelas) and zebrafish (Danio rerio). (Master dissertation, Digital Commons, University of Nebraska, Lincoln, Nebraska, USA.).*

Wang, S., Qiu, J., Zhao, M., Li, F., Yu, R., and Li, A. (2020a). Accumulation and distribution of neurotoxin BMAA in aquatic animals and effect on the behavior of zebrafish in a T-maze test. *Toxicon* 173, 39–47. doi: 10.1016/j.toxicon.2019.11.005

Wang, C., Yan, C., Qiu, J., Liu, C., Yan, Y., Ji, Y., et al. (2021). Food web biomagnification of the neurotoxin β-N-methylamino-L-alanine in a diatom-dominated marine ecosystem in China. *J. Hazard. Mater.* 404, 124217. doi: 10.1016/j.jhazmat.2020.124217

Wang, R. F., Zhu, L. M., Zhang, J., An, X. P., Yang, Y. P., Song, M., et al. (2020b). Developmental toxicity of copper in marine medaka (*Oryzias melastigma*) embryos and larvae. *Chemosphere* 247, 125923. doi: 10.1016/j.chemosphere.2020.125923

Weiss, J. H., and Choi, D. W. (1988). Beta-N-methylamino-L-alanine neurotoxicity: Requirement for bicarbonate as a cofactor. *Sci* 241, 973–975. doi: 10.1126/science.3136549

Zhang, X., Ai, X., Nakayama, H., Chen, B., Harris, D. M., Tang, M., et al. (2016). Persistent increases in Ca^{2+} influx through Cav1.2 shortens action potential and causes Ca^{2+} overload-induced after depolarizations and arrhythmias. *Basic Res. Cardiol.* 111, 4. doi: 10.1007/s00395-015-0523-4

frontiers | Frontiers in Microbiology

TYPE Original Research
PUBLISHED 22 December 2022
DOI 10.3389/fmicb.2022.1091561

OPEN ACCESS

EDITED BY
Zhangxi Hu,
Guangdong Ocean University, China

REVIEWED BY
Kathryn Coyne,
University of Delaware, United States
Hui Wang,
Shantou University, China

*CORRESPONDENCE
Nanjing Ji
✉ jinanjing@126.com
Xin Shen
✉ shenthin@163.com

SPECIALTY SECTION
This article was submitted to Aquatic Microbiology, a section of the journal Frontiers in Microbiology

RECEIVED 07 November 2022
ACCEPTED 05 December 2022
PUBLISHED 22 December 2022

CITATION
Wang J, Yin X, Xu M, Chen Y, Ji N, Gu H, Cai Y and Shen X (2022) Isolation and characterization of a high-efficiency algicidal bacterium *Pseudoalteromonas* sp. LD-B6 against the harmful dinoflagellate *Noctiluca scintillans*. *Front. Microbiol.* 13:1091561. doi: 10.3389/fmicb.2022.1091561

Isolation and characterization of a high-efficiency algicidal bacterium *Pseudoalteromonas* sp. LD-B6 against the harmful dinoflagellate *Noctiluca scintillans*

Junyue Wang[1,2], Xueyao Yin[1,2], Mingyang Xu[1,2], Yifan Chen[1,2], Nanjing Ji[1,2]*, Haifeng Gu[3], Yuefeng Cai[1,2] and Xin Shen[1,2]*

[1]Jiangsu Key Laboratory of Marine Bioresources and Environment, Jiangsu Key Laboratory of Marine Biotechnology, Jiangsu Ocean University, Lianyungang, China, [2]Co-Innovation Center of Jiangsu Marine Bio-Industry Technology, Jiangsu Ocean University, Lianyungang, China, [3]Third Institute of Oceanography, Ministry of Natural Resources, Xiamen, China

The dinoflagellate *Noctiluca scintillans* is a harmful algal species that is globally distributed and poses a certain threat to marine ecosystems. Recent research has shown that the application of algicidal bacteria is a promising method to prevent and control such harmful algal blooms (HABs), given its advantages of safety and efficiency. In this study, a strain of algicidal bacterium LD-B6 with high efficiency against *N. scintillans* was isolated from the coastal waters of Lianyungang, China. 16S rDNA sequence analysis showed that the strain LD-B6 belongs to the genus *Pseudoalteromonas*. Furthermore, the algicidal effect of LD-B6 on *N. scintillans* was investigated. The results showed that strain LD-B6 exerted strong algicidal activity against *N. scintillans*. After 12 h of bacterial culture addition to algal cultures at a 2% final volume rate, the algicidal activity reached 90.5%, and the algicidal activity of LD-B6 was influenced by the density of *N. scintillans*. In addition, the algicidal bacterium LD-B6 was found to indirectly lyse algal cells by secreting extracellular compounds. These algicidal compounds were stable, indicating that they are not proteins. Importantly, strain LD-B6 was broadly general, showing varying degrees of lysing effects against five of the six algal species tested. On the basis of the described studies above, the algicidal powder was also initially developed. In summary, the isolated bacterial strain LD-B6 shows the potent algicidal capability to serve as a candidate algicidal bacterium against *N. scintillans* blooms.

KEYWORDS

Noctiluca scintillans*, harmful algal bloom, algicidal bacteria, algicidal activity, *Pseudoalteromonas

Introduction

Blooms usually refer to the phenomenon documented when some microalgae, protozoa, or bacteria over-proliferate or accumulate in aquatic environments, causing water discoloration. The international scientific community collectively refers to harmful algal blooms (HABs) as for those harmful or toxic blooms (Anderson et al., 2002; Grattan et al., 2016). In recent years, there has been a significant increase in the scale and frequency of HABs with the intensification of water eutrophication, global warming, ocean acidification, and other phenomena (Griffith and Gobler, 2020; Karlson et al., 2021; Sha et al., 2021).

The dinoflagellate *Noctiluca scintillans* is a harmful algal species with a global distribution that has caused severe HABs in many coastal waters around the world, posing a significant threat to fishery resources and marine ecosystems (Qi et al., 2019; Piontkovski et al., 2021). According to the differences in nutritional requirements, there are two forms of *N. scintillans*: Red and green (Harrison et al., 2011). Red *N. scintillans* is a heterotrophic plankton. In contrast, green *N. scintillans* is a mixoplankton that contains a photosynthetic symbiont, *Pedinomonas noctilucae* (a prasinophyte). Although *N. scintillans* does not produce phytotoxins or other toxins, its bloom secretes a large amount of mucus that adheres to fish gills and causes suffocation (Tan et al., 2002). Most importantly, it may cause hypoxia in the surrounding environment and release a high concentration of ammonia when the bloom declines, which not only impact aquaculture but also have a detrimental effect on aquatic environments (Montani et al., 1998; Miyaguchi et al., 2008; Zhang et al., 2017). In addition, the food vacuoles of *N. scintillans* have been found to contain toxigenic microalgae, suggesting that *N. scintillans* may act as a vector of phycotoxins to higher trophic levels (Escalera et al., 2007). Due to such harmful attributes of *N. scintillans* blooms, it is particularly important and urgent to carry out related research on its prevention and control.

In this regard, physical, chemical, and biological methods have been proposed for controlling the HABs (Anderson, 2009). The use of modified clay is one of the most common physical methods (Liu et al., 2016; Yu et al., 2017). The chemical approach refers to the use of foreign additives such as chemical reagents (Geciova et al., 2002; Maršálek et al., 2020). However, the implementation of chemical and physical methods for the management of HABs is still limited due to the disadvantages of high cost, poor specificity, and secondary pollution (Yu et al., 2017). Biological methods such as the use of algicidal bacteria have been widely studied in the control of HABs because of their advantages of safety and efficiency (Wang et al., 2020; Coyne et al., 2022). Studies have shown that about 50% of the algicidal bacteria belong to the Cytophaga/Flavobacterium/Bacteroidetes (CFB) group, and about 45% belong to Gammaproteobacteria. The remaining bacteria are from the Gram-positive genera *Micrococcus*, *Bacillus*, and *Planomicrobium* (Roth et al., 2008). Algicidal bacteria generally attack the target algae through two strategies: directly by being in contact with algal cells and indirectly by competition or secretion of extracellular active compounds by the bacteria (Azam, 1998). The mechanisms associated with algicidal bacteria mainly include a few pathways, like the destruction of cell structure, the change in enzyme activity, and the influence of algal photosynthesis or respiration (Zhang et al., 2020a; Chen et al., 2022). A large number of highly efficient algicidal bacteria have been recently isolated from various eutrophic regions (Lu et al., 2016; Zheng et al., 2018; Li et al., 2022). However, few studies have isolated algicidal bacteria against *N. scintillans* despite the potential impacts discussed above. At present, only *Marinobacteria salsuginis* BS2 (Gammaproteobacteria) has been documented to show algicidal activity against *N. scintillans* (Keawtawee et al., 2011).

In this study, the isolation of an efficient *N. scintillans* algicidal bacterium from the coastal waters of Lianyungang, China, is reported. The strain was identified by 16S rDNA sequence analysis. Its algicidal effects against red *N. scintillans* were also explored. We have also developed a preliminary algicidal powder based on the nascent research for future *N. scintillans* algal bloom management.

Materials and methods

Noctiluca scintillans cultures

The red *N. scintillans* strain was originally isolated from the coastal waters of Lianyungang, China (October 2020). Briefly, *N. scintillans* single cell was isolated with a large-diameter pipette based on the morphology and maintained in sterilized seawater (salinity of 30‰), which was prepared by filtration (0.22 μm filter) and autoclaving of *in situ* seawater. The culture was incubated at 20°C under light (100 μE m^{-2} s^{-1}, 14: 10 h light–dark cycle) and with *Tetraselmis subcordiformis* as the prey (Wu et al., 1994; Luo et al., 2022).

To inhibit the growth of excess bacteria in the algae, *N. scintillans* cultures of 100 mL were pretreated with an antibiotic mixture of 100 μL ampicillin (200 mg/mL), kanamycin (100 mg/mL), and streptomycin (100 mg/mL) before the experiment. In preliminary experiments, this antibiotic mixture did not adversely affect the growth of *N. scintillans*.

Isolation, screening, and identification of algicidal bacteria

We collected surface seawater from a phytoplankton bloom in the coastal waters of Lianyungang, China (34°46'57"N, 119°27'8"E) (Zhang et al., 2022). The water samples were serially

diluted 10-fold with sterilized seawater, and 0.2 mL of each 10-fold serially diluted dilution was spread onto 2216E (10 g L^{-1} of tryptone, 2 g L^{-1} of yeast extract, 0.2 g L^{-1} of ferrous sulfate, and 1.0 L seawater) agar plates and incubated at 28°C for 48 h. The single colonies with significant differences in morphology were selected to obtain pure strains.

In order to screen the strains with algicidal activity against *N. scintillans*, we conducted pre-experiments in 24-well plates. All the purified strains were inoculated in 100 mL 2216E medium and cultured at 28°C, 180 rpm to their exponential growth period (OD_{600}: 0.6–0.8). The bacterial culture was inoculated into 1 mL (10 cells mL^{-1}) of algae cultures at 2 and 5% volume ratio, and an equal volume of sterilized 2216E medium and natural seawater was added to the algal cultures as control and blank groups, respectively. Bioassays were performed in triplicate, and all experiments were conducted during the light phase of the light cycle (20°C). The algal cells were counted at 4, 8, and 12 h to calculate the algicidal activity as follows:

$$\text{Algicidal activity (\%)} = (\text{Nc} - \text{Nt})/\text{Nc} \times 100$$

where Nc and Nt represent the cell concentrations of *N. scintillans* measured in the control and experimental groups, respectively.

The cell density of *N. scintillans* was counted using a macroscopic observation because the cells are large enough (~200–2,000 μm in diameter) to be seen by the naked eye (Zhang et al., 2020b). Gently shake the algal culture and collect 1 mL of culture for cell counting. Counting was performed three times in triplicate.

The morphological changes of algae cells were also examined and recorded under an inverted microscope to confirm the algicidal effect. The most effective and stable algicidal strain was selected for follow-up experiments.

Individual colonies of the screened algicidal bacterium were picked in 50 μL ddH_2O (double distilled water), incubated at 100°C for 10 min, and then quickly transferred to ice. The bacterial lysate was taken as a template, and its 16S rDNA was amplified by PCR using the universal primers 16S-27F (5′-AGAGTTTGATCMTGGCTCAG-3′) and 16S-1492R (5′-TACGGYTACCTTGTTACGACTT-3′) for bacterial identification (DeLong, 1992). PCR amplification was performed in a 25 μL amplification volume, which contained 1 μL of each primer (10 μM), 2 μL of template, 12.5 μL of 2 × *Accurate Taq* Master Mix (Accurate Biology, China), and 8.5 μL ddH_2O. An initial denaturation period of 95°C for 5 min, followed by 30 cycles of 94°C for 1 min, 55°C for 1 min, 72°C for 2 min, and the final extension at 72°C. Then the amplicons were sent to MAP (MAP Biotech, Shanghai, China) for sequencing. The obtained sequences were compared with those from the database for homology analysis using BLAST from the National Center for Biotechnology Information (Altschul et al., 1990). Multiple 16S rDNA sequences were aligned using ClustalW (Thompson et al., 2003). After removing the variable regions at both ends, 1,216 nucleotides positions were selected for phylogenetic analysis using the maximum-likelihood method with the Tamura-Nei model (1,000 bootstrap replications) in the MEGA 7.0 program (Kumar et al., 2016).

Algicidal activity of LD-B6

Among 45 isolates, strain LD-B6 was chosen for further analysis. The LD-B6 strain was inoculated in 100 mL 2216E medium and cultured at 28°C, 180 rpm to their exponential growth period to obtain the LD-B6 cultures (**Supplementary Figure 1**). In order to assess the algicidal activity of different final concentrations of LD-B6 against *N. scintillans*, LD-B6 cultures were added to the pretreated (antibiotic-treated) algal cultures with different volume ratios (0.5, 1, 2, and 5%). To elaborate, 0.25, 0.5, 1, and 2.5 mL of bacterial cultures were added to 50 mL (10 cells mL^{-1}) of the pretreated algal cultures. The same volume of sterilized seawater and 2216E medium was added to 50 mL of *N. scintillans* cultures as blank and control, respectively. All treatments were performed in triplicate and conducted during the light phase of the light cycle (20°C). The algal cells were counted after 4, 8, and 12 h of treatment, and the algicidal activity was calculated as described above.

To investigate the algicidal effect of LD-B6 on different densities of algal cultures, a 2% volume of cell-free supernatant of LD-B6 was added to 50 mL of the pretreated *N. scintillans* algal cultures with initial densities of 10, 30, and 50 cells mL^{-1}, respectively. Also, a 2% volume of sterilized 2216E medium was used as a control. All experiments were performed in triplicate and conducted during the light phase of the light cycle (20°C). The algal cell concentration was counted at 12 h, and the algicidal activity was calculated as described above.

Analysis of the algicidal mechanisms of LD-B6

To study the algicidal mode of LD-B6 against *N. scintillans*, the bacterial culture was treated in different ways: first, strain LD-B6 was inoculated in 100 mL of sterilized 2216E medium and cultured at 28°C, 180 rpm to their exponential growth phase to obtain the bacterial cultures, and then 10 mL bacterial cultures were collected and centrifuged at 12,000 rpm for 10 min. The collected supernatant was filtered with a 0.22-μm membrane to obtain the cell-free supernatant. The remaining cells were washed thrice with sterilized seawater and resuspended in 10 mL of sterilized seawater to obtain bacterial cells. The bacterial culture, cell-free supernatant, and bacterial cells were added to 50 mL (10 cells mL^{-1}) of the pretreated algal cultures at the optimum concentration of 2% (*v/v*) to investigate the algicidal activity of these fractions. In addition,

the same amounts of sterilized 2216E medium were added to the algal culture as the experimental control. All experiments were performed in triplicate and conducted during the light phase of the light cycle (20°C). The algal cells were counted after 4, 8, and 12 h of treatment, and the algicidal activity was calculated as described earlier.

Stability of the LD-B6 cell-free supernatant

To examine the stability of the cell-free supernatant of strain LD-B6, the effect of different treatments on algicidal activity was investigated. The LD-B6 cell-free supernatant was incubated at different temperatures of −80, −20, 0, 15, 30, 60, and 100°C for 2 h, and then thawed or cooled to room temperature. The LD-B6 cell-free supernatant was adjusted to pH 3, 8, and 12 using NaOH or HCl and then adjusted back to the initial pH of 8 after 2 h. The supernatants treated in these two ways were inoculated into 50 mL (10 cells mL^{-1}) of the pretreated algal cultures at 2% (*v/v*). All treatments were performed in triplicate and conducted during the light phase of the light cycle (20°C). The algicidal activity was calculated at 12 h to test the heat and acid-base tolerance of the cell-free supernatant. The algal cell count and the algicidal activity were computed as described above.

LD-B6 cell-free supernatant tubes were then put in liquid nitrogen for 5 min. They were taken it out and thawed in a thermostat water bath at 65°C, and this freeze-thaw step was repeated three times. The supernatant was cooled to room temperature and inoculated into 50 mL (10 cells mL^{-1}) of the pretreated algal cultures at 2% (*v/v*). All experiments were performed in triplicate and conducted during the light phase of the light cycle (20°C). The algal cells were counted at 4, 8, and 12 h to calculate the algicidal activity. The algal cell counting and algicidal activity computations were as described above.

Algicidal activity of LD-B6 on several HABs species

The algicidal efficiency of strain LD-B6 against typical HAB species was tested, including dinoflagellates (*N. scintillans* CCMA-LYG006, *Prorocentrum micans* CCMA-NT010, *Gymnodinium impudicum* CCMA-LYG009, and *Heterocapsa steinii* CCMA-LYG002), raphidophytes (*Heterosigma akashiwo* CCMA-LYG001), and diatoms (*Skeletonema costatum* CCMA277). Among them, *P. micans* was isolated from Nantong, China. *S. costatum* was provided by the Center for Collection of Marine Algae at Xiamen University. The rest strains were isolated from Lianyungang, China. Among them, *S. costatum* was cultured in the F/2 medium, and the other algae were cultured in the F/2-Si medium (Guillard, 1975). All algal cultures were incubated at 20°C under a 14: 10 h light–dark cycle with a photon flux of 100 μE m^{-2} s^{-1}.

Flasks containing 50 mL of each species in an exponential growth period were inoculated with LD-B6 cultures at a final volume ratio of 2% (*v/v*). The same amounts of sterilized 2216E medium were used as controls. All treatments were performed in triplicate and incubated at 20°C. Algal cell concentrations were counted after 24 h. The cell concentration of *N. scintillans* was determined using macroscopic observations, and the algal cell density of other cultures was counted using a Sedgwick-Rafter chamber under a microscope.

Algicidal powder production and application

Here, sawdust was selected as a carrier for LD-B6 immobilization. Briefly, sawdust was sterilized twice, dried, and used as the carrier. The carrier was added to the bacterial culture in the stable growth phase of LD-B6 at a mass fraction of 15% and then placed at 28°C and 180 rpm for co-incubation for 6 h to facilitate the sufficient adsorption of the sawdust. The un-adsorbed bacterial culture was removed by a screen mesh, and the adsorbed sawdust was placed on a glass petri dish and freeze-dried for 24 h. The lyophilized powder was stored at 4°C.

To assess the effectiveness of algicidal powder, 0.1 g of powder was added to 50 mL (10 cells mL^{-1}) of the pretreated algal cultures, and the same volume of sterilized sawdust was added to 50 mL of *N. scintillans* cultures as control. All treatments were performed in triplicate and conducted during the light phase of the light cycle (20°C). The algal cells were counted at 12 h, and the algicidal activity was calculated as described above.

Statistical analyses

All experiments were performed in triplicate, and data were presented as mean ± standard deviations. Statistical analyses were performed using SPSS16.0 software, and the significant

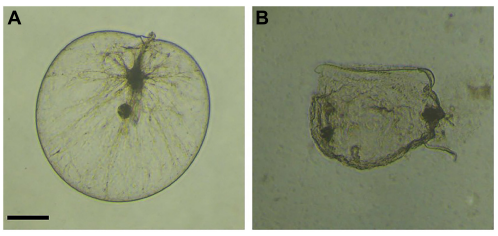

FIGURE 1
Microscope images of *Noctiluca scintillans* when co-incubated with strain LD-B6 at **(A)** 0 h, **(B)** 12 h. Scale bars = 100 μm.

differences among treatments in this study were analyzed by one-way ANOVA ($p < 0.05$).

Results

Screening and identification of algicidal bacteria

After isolation and purification, a total of 45 strains were initially obtained. Among them, 11 strains showed algicidal activity against *N. scintillans*, and the LD-B6 strain had the strongest algicidal activity in the experiments with 2 and 5% volumes (**Supplementary Figure 2**). At the same time, microscopic imaging confirmed the effective algicidal activity of strain LD-B6. As shown in **Figure 1** and **Supplementary Video 1**, the cell wall of *N. scintillans* began to break (6 h), and the contents flowed out after a period of co-culture of the bacterial culture and the algal culture, and then the rupture expanded continuously. Thus, the strain LD-B6 was selected for further study.

The 16S rDNA gene of LD-B6 was amplified and sequenced (GenBank accession number: OP010006.1). The 16S rDNA sequence of this strain showed the highest similarity (100%) to that of *Pseudoalteromonas* sp. CF1 (accession number KX570621). Meanwhile, in phylogenetic analysis, strain LD-B6 formed a monophyletic group with *Pseudoalteromonas* sp., corresponding to the Gammaproteobacteria subclass (**Figure 2**). This result indicated that strain LD-B6 belonged to *Pseudoalteromonas* sp., and it was designated as *Pseudoalteromonas* sp. LD-B6.

Algicidal effects of LD-B6 on *Noctiluca scintillans*

The algicidal activity of LD-B6 against *N. scintillans* at different concentrations was examined to determine the optimum final volume of the bacterial culture for further experiments. As shown in **Figure 3B**, LD-B6 at 1, 2, and 5% final volume activity have a certain algicidal effect against *N. scintillans*, and its algicidal activity increased in a concentration- and time-dependent manner, reaching 37.9 ± 1.8, 90.5 ± 3.2, and 100% at 12 h, respectively. However, the 0.5% treatment group only inhibited the growth of *N. scintillans* and did not kill algal cells (**Figure 3A**). Thus, the algicidal effect of strain LD-B6 against *N. scintillans* was concentration-dependent. As the algicidal activity in the 2% treatment group was higher than 90% at 12 h, this dose was chosen for further studies.

The cell-free supernatant of LD-B6 was added to *N. scintillans* cultures at different initial densities to examine its algicidal activity. As shown in **Figure 4**, the algicidal effect of the cell-free supernatant was the highest when the initial density

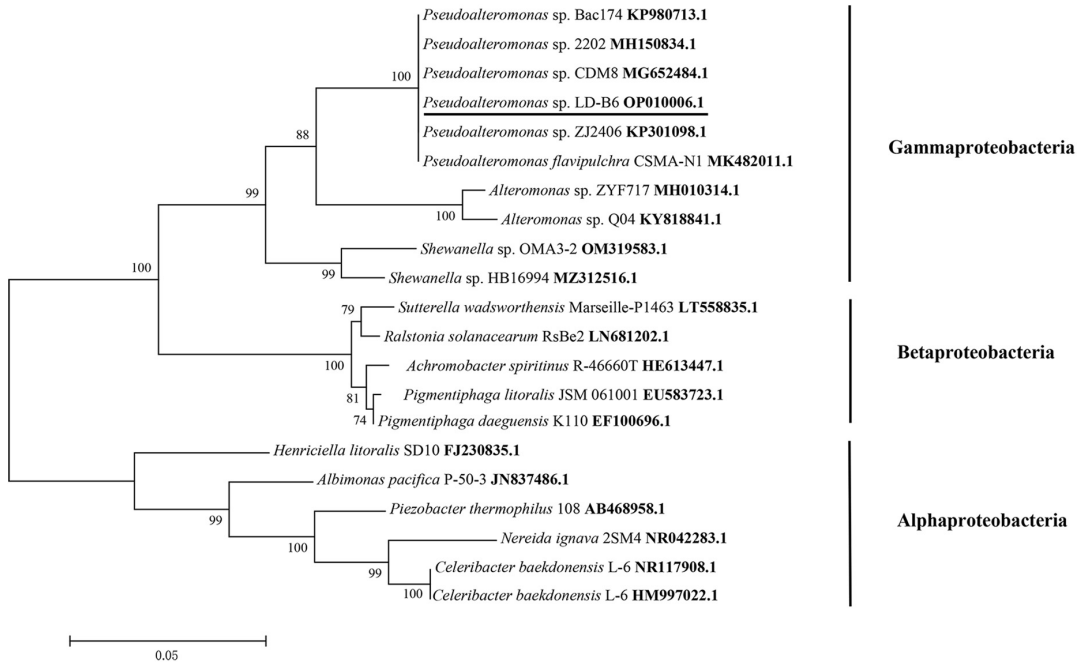

FIGURE 2
Phylogenetic tree of algicidal bacterial strain LD-B6 based on 16S rDNA sequence. Support of nodes > 50% is shown. Bar 0.05 means a nucleotide substitution rate of 0.05.

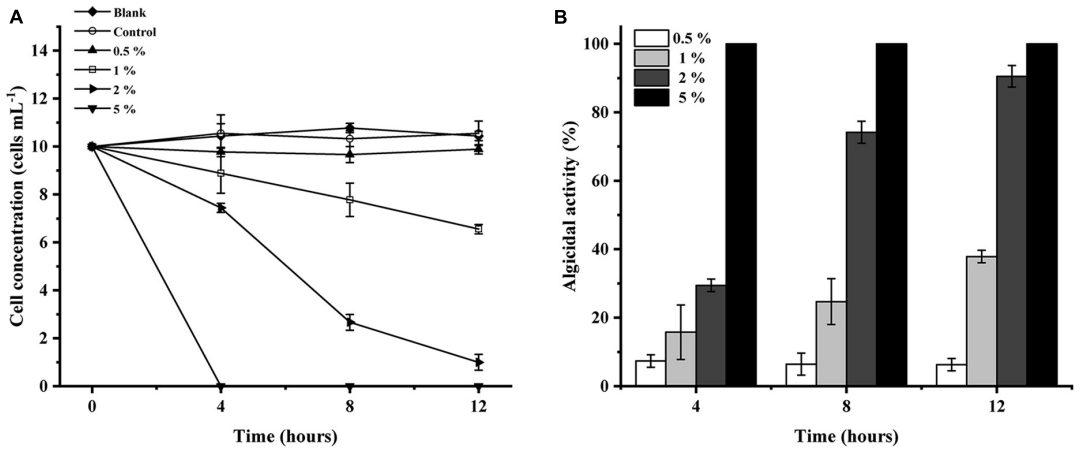

FIGURE 3
Algicidal activities of different concentrations of LD-B6 culture on *Noctiluca scintillans* based on **(A)** algal cell concentration and **(B)** algicidal activity. The error bars represent standard deviations (n = 3).

was 10 cells mL^{-1}, followed by 30 and 50 cells mL^{-1}at algicidal activity of 93.8 ± 3.1, 78.2 ± 1.7, and 61.9 ± 1.7%, respectively. Generally, the algicidal activity of LD-B6 against *N. scintillans* decreased with the initial density of the algal culture increasing.

Algicidal mechanisms of LD-B6 on *Noctiluca scintillans*

To initially investigate the algicidal mechanisms of strain LD-B6, we added different fractions of bacterial cultures to *N. scintillans* cultures. The strain culture and cell-free supernatant showed an algicidal activity of 89.5 ± 1.8 and 89.5 ± 4.8%, respectively, after treatment for 12 h, while the algicidal effect of the bacterial cells was only 14.7 ± 3.2% and not obvious (Figure 5). The algicidal effect of the supernatant was significantly better than that of the bacterial cells themselves. It is presumed that strain LD-B6 lyses algal cells by secreting active compounds into the cell-free supernatant, and therefore strain LD-B6 lysed *N. scintillans* indirectly.

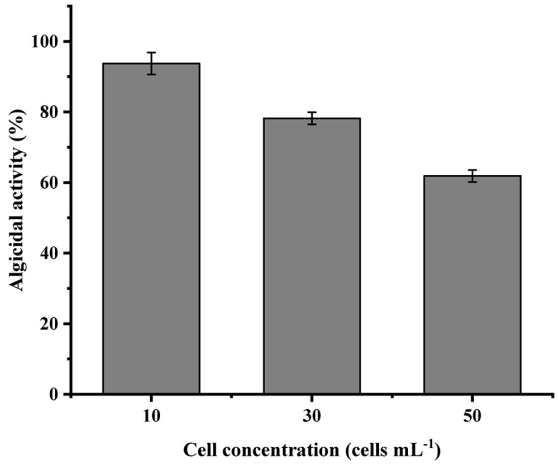

FIGURE 4
Algicidal effect of strain LD-B6 at different *Noctiluca scintillans* initial cell densities. The error bars represent standard deviations (n = 3).

Stability of the LD-B6 filtrate

Under different temperature treatment conditions, the algicidal effect of strain LD-B6 compounds on *N. scintillans* is shown in Figure 6A. Although the algicidal activity was slightly different among treatments, there was no significant difference. It shows that the algicidal compounds of strain LD-B6 have definite thermal stability. Incubation at different pH values for 2 h had an effect on the algicidal activity of the cell-free supernatant of strain LD-B6. The algicidal compounds of strain LD-B6 were sensitive to acid, and their algicidal activities were significantly decreased under acidic conditions. In contrast, the algicidal effect of the cell-free supernatant was stable under alkaline conditions (Figure 6B). Repeated freezing and thawing had almost no effect on the algicidal activity of the LD-B6 cell-free supernatant, and there was no significant difference in the algicidal effect between the control and the experiments (Figure 6C).

Algicidal activity of LD-B6 on several HABs species

The algicidal activity of LD-B6 culture against six different HABs species is shown in Figure 7. Within 24 h of incubation,

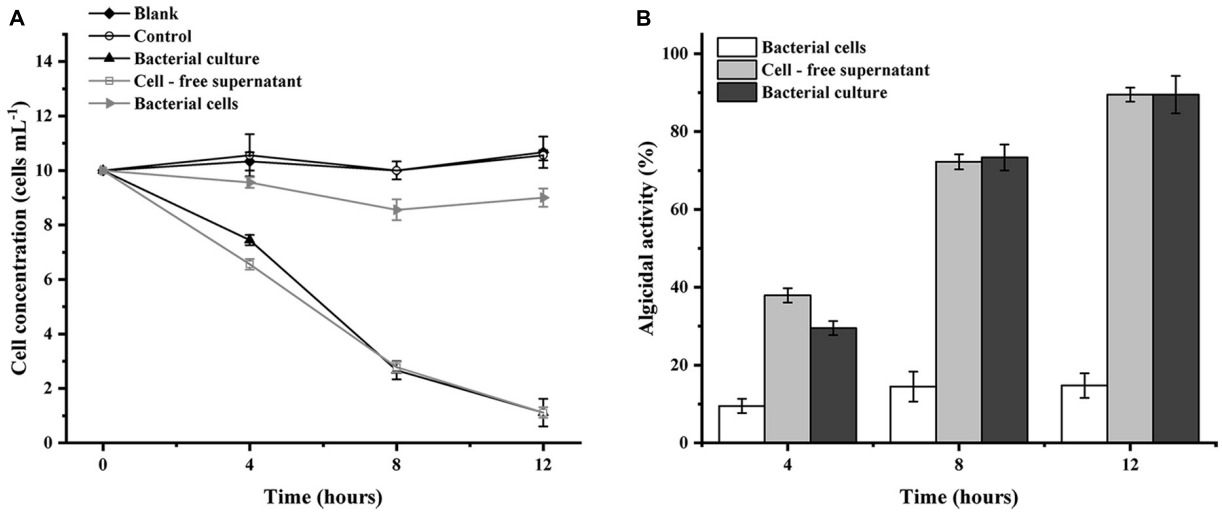

FIGURE 5
Algicidal activities of different fractions of LD-B6 culture on *Noctiluca scintillans* based on **(A)** algal cell concentration and **(B)** algicidal activity. The error bars represent standard deviations (n = 3).

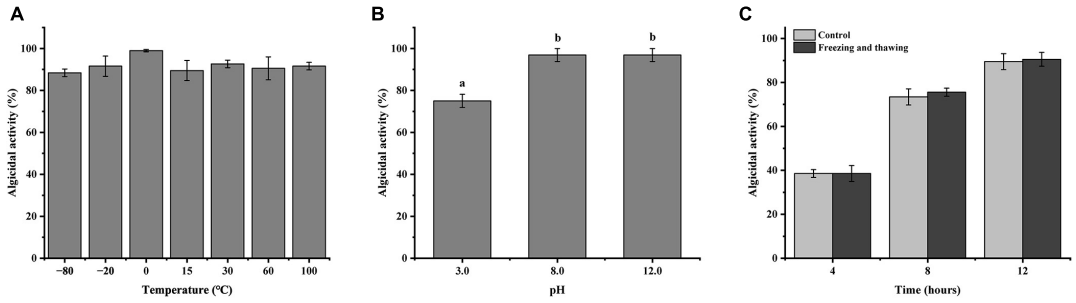

FIGURE 6
Algicidal effect of strain LD-B6 cell-free supernatant at different temperatures **(A)**, pH **(B)** conditions, and repeated freeze-thaw **(C)** treatment against *Noctiluca scintillans*. The error bars represent standard deviations (n = 3). Different letters a, b represent significant differences between groups ($p < 0.05$).

the LD-B6 culture showed the strongest algicidal effect on *N. scintillans* and *H. akashiwo*, and the algicidal activity reached 100%. It also had a strong algicidal activity on *H. steinii* and *G. impudicum*, with the algicidal activity of 73.3 ± 1.3 and 63.7 ± 9.2%, respectively. A weak effect on *P. micans* (26.7 ± 0.68%) was observed. In contrast, the growth of *S. costatum* was slightly promoted by strain LD-B6.

Algicidal powder production and application

Algicidal powder product status is shown in **Supplementary Figure 3**. The algicidal powder of LD-B6 was added to *N. scintillans* cultures to assess its algicidal effect. As shown in **Supplementary Figure 4**, the algicidal activity of 100% at 12 h with 0.2% final volume of algicidal powder. This result indicated that the developed algicidal powder has a strong algicidal effect and that the production method is feasible.

Discussion

During algal bloom formation and decline, the populations and dominance of marine bacteria change significantly, especially in the period of extinction (Yang et al., 2015). More importantly, some marine bacteria play an important role at the end of the HABs (Li et al., 2018). Therefore, the research on the relationship between bacteria and algae in controlling algal blooms has become a hot topic. However, the interactions between bacteria and the alga *N. scintillans* have received limited attention. In this work, a bacterial strain LD-B6 with algicidal activity against *N. scintillans* was isolated. This strain was identified by 16S rDNA sequencing to

belong to *Pseudoalteromonas* in the class Gammaproteobacteria (**Figure 2**). Several investigations have documented that Gammaproteobacteria is the dominant bacteria during HABs, and the dominant population of marine bacteria exhibit a succession from Alphaproteobacteria to Gammaproteobacteria during the late-blooming phase, indicating that they may influence algal bloom dynamics (Teeling et al., 2012; Zhang et al., 2016; Li et al., 2018). *Pseudoalteromonas* sp. is one of the most frequently reported and abundant algicidal bacterial species in the ocean. It has been documented that bacteria of this genus show algicidal effects against phytoplankton, including Dinophyceae, Raphidophyceae, and Bacillariophyceae (Lovejoy et al., 1998; Lee et al., 2000; Zhang et al., 2022). Therefore, this isolate may be involved in the regulation of algal blooms.

Strain LD-B6 had a strong algicidal effect on *N. scintillans*. The normal cells of *N. scintillans* are nearly spherical, with a full and smooth surface. Twelve hours after LD-B6 bacterial cultures were added, the cells showed obvious folds and atrophy under the microscope (**Figure 1**). In addition, the algicidal activity of LD-B6 on *N. scintillans* was also recorded by an inverted microscope (**Supplementary Video 1**), which indicates that the cell wall of *N. scintillans* was the main target of LD-B6. At present, a number of algicidal bacteria have been proven to lyse algal cells by degrading cell wall polysaccharides (Kim et al., 2009; Wang et al., 2010; Li et al., 2022). Hydrolytic enzymes such as amylase, cellulase, and xylanase are the causes of such polysaccharide degradation (Li et al., 2022). These results enrich the understanding of the mechanism of algal cell lysis by LD-B6.

It has been reported that the algicidal activity of bacteria depends on bacterial concentration and algal cell density (Tian et al., 2012; Kong et al., 2020; Al-Hakimi et al., 2020). For instance, Shao et al. (2015) found that *Bacillus* sp. B50 showed an algicidal activity when the bacterial concentration reached 1.9×10^6 CFU/mL, while the algicidal activity was lost at a cell concentration below 1.9×10^5 CFU/mL. Yang et al. (2020) indicated that the higher the initial concentration of algal cells, the poorer the algicidal activity of the *Ponticoccus* sp. CBA02. Similar to these previous reports, the algicidal effect of LD-B6 against *N. scintillans* also reflects these patterns. When a low concentration of bacterial culture was inoculated into the algal culture, it only inhibited the growth of *N. scintillans*, while the high concentration of bacteria cultures showed a strong algicidal effect (**Figure 3**). In addition, we also found that the algicidal effect of LD-B6 decreased with the increase in the initial density of algal cultures (**Figure 4**). These observations can be explained as that with the increase in the bacterial concentration, there are more algicidal compounds per unit volume, and the contact probability between algae cells and algicidal compounds is further increased, thus enhancing the algicidal effect. On the contrary, a high concentration of algal cells may reduce the concentration of algicidal compounds exposed to individual algal cells, thereby affecting the algicidal activity. Therefore, the control of HABs can entail the inoculation of a certain concentration of algicidal bacteria at the initial stage of bloom, or the concentration of algicidal bacteria can be adjusted according to the development stage of an algal bloom.

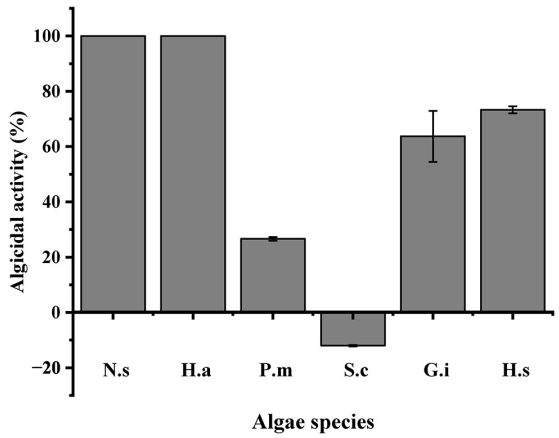

FIGURE 7
Algicidal activity of bacterial strain LD-B6 on representative HABs species. N.s, *Noctiluca scintillans*; H.a, *Heterosigma akashiwo*; P.m, *Prorocentrum micans*; S.c, *Skeletonema costatum*; G.i, *Gymnodinium impudicum*; H.s, *Heterocapsa steinii*. The error bars represent standard deviations (n = 3).

Algicidal bacteria generally exert two main strategies for lysing algae: direct and indirect modes (Azam, 1998). In this study, the cell-free supernatant of strain LD-B6 showed a strong algicidal effect against *N. scintillans*, indicating an indirect manner of targeting. This is on the same lines as algicidal bacteria belonging to *Pseudoalteromonas* spp. previously reported (Wang et al., 2020), which lyse target algae by releasing extracellular substances. The characteristics of algicidal compounds are influenced by various factors such as temperature and pH (Fu et al., 2011; Zhang et al., 2022). Bai et al. (2011) reported that the compounds of *Brevibacterium* sp. BS01 were heat tolerant and stable in acidic or alkali conditions, indicating these compounds are not proteins. In addition, the algicidal compounds of *Pseudoalteromonas* sp. SP48 are tolerant to heat but unstable under acidic conditions (Su et al., 2007). Our findings showed that the algicidal compounds of LD-B6 had freeze-thaw stability, were heat tolerant, and were stable under alkaline conditions, while acidic conditions had a significant effect on the algicidal activity (**Figure 6**). As described in reviews, algicidal bacteria can produce several kinds of algicidal substances, including ectoenzymes (e.g., serine protease and extracellular agarase), pigments (e.g., isatin and prodigiosin) (Meyer et al., 2017; Wang et al., 2020; Coyne et al., 2022). Based on the thermal stability of algicidal compounds secreted by strain LD-B6, it is unlikely that this compound is a protein. Alternatively, it is possible that algicidal compounds of LD-B6 are a pigment. Examples include an algicidal substance of *Pseudomonas* sp. C55a-2 was identified as a pigment (Sakata et al., 2011).

Further, the properties, types, and extraction of algicidal compounds still need to be studied.

Different strains of algicidal bacteria likely show different degrees of specificity. Some bacteria are species-specific, lysing only specific algae. Shi et al. (2020) isolated a strain FDHY-CJ8, which had algicidal activity only on *S. costatum*, but almost no algicidal effect on other algae. Pokrzywinski et al. (2012) found that the algicidal bacterium *Shewanella* sp. IRI-160 showed selectivity toward dinoflagellates. Some strains have broad specificity and are able to lyse a wide range of algal species. For example, the bacterium YX04 has an algicidal effect on the taxa of Bacillariophyceae, Pyrrophyta, and Chrysophyta (Zhu et al., 2022). Highly species-specific or broadly specific algicidal bacteria are related to their type and secreted compounds (Meyer et al., 2017). Most bacteria in the free-living form are highly species-specific, and the bacteria in the particle-associated form are mostly broadly specific (Park et al., 2010). Strain LD-B6 showed varying degrees of algicidal effects against five of the six typical harmful algal species tested, including dinoflagellates and a raphidophyte (**Figure 7**), indicating its broad-spectrum algicidal ability. This potential of LD-B6 to control HABs, combined with the stability of the algicidal compounds as previously described, makes it potentially useful as a promising agent against HABs.

In recent years, more and more algicidal agents have been developed to control algal blooms. The use of carrier immobilization to improve the colonization activity of algicidal agents is an effective way to ensure the sustainability of the algicidal effect; sawdust is regarded as an ideal carrier because of its outstanding adsorption ability (Ye et al., 2022). In this study, strain LD-B6 was also immobilized, and sterile sawdust was used as a carrier to prepare an algicidal powder (**Supplementary Figure 3**). The results showed that the algicidal activity of the prepared powder was 100% (12 h), which was 9.5% higher than that of the bacterial culture at a final concentration of 2%. It may be that the immobilization by the carrier effectively improves the biomass of microbial agents, their resistance to water flow, and their tolerance to toxic compounds (Chen et al., 2003).

Conclusion

The algicidal bacterium LD-B6, with strong algicidal activity against *N. scintillans*, was isolated from the coastal waters of Lianyungang, China. This bacterium lysed algae indirectly by secreting extracellular compounds, and these algicidal compounds are stable, indicating that they are not proteins. In addition, strain LD-B6 was broadly specific, and the preliminary development of an algicidal powder is also presented. These results documented the ability of strain LD-B6 and its algicidal compounds to control *N. scintillans* blooms and provide a foundation for their practical applications. In the future, it would be necessary to extract and analyze algicidal compounds and control them in a targeted manner according to the characteristics of the applied environment, such as solving the adaptation problems of salinity, temperature, pH, etc., to develop more efficient algicidal agents to control HABs.

Data availability statement

The datasets presented in this study can be found in online repositories. The names of the repository/repositories and accession number (s) can be found in the article/ **Supplementary material**.

Author contributions

JW and NJ conceived the study, performed the experiment, and prepared the manuscript. XY, MX, and YCh completed the experiment. HG, YCa, and XS prepared the manuscript. All authors have read and agreed to the published version of the manuscript.

Funding

This work was supported by the National Key R&D Program of China (#2020YFD0900203), the Natural Science Foundation of China (#42006135), the Environmental Protection Science and Technology Plan Project of Fujian Provincial Department of Ecological Environment (2022R005), Jiangsu Agriculture Science and Technology Innovation Fund (JASTIF) [CX(22)2032], the Young Talents Elevating Project for Jiangsu Association for Science and Technology, and the Project Funded by the Priority Academic Program Development of Jiangsu Higher Education Institutions (PAPD).

Conflict of interest

The authors declare that the research was conducted in the absence of any commercial or financial relationships that could be construed as a potential conflict of interest.

The handling editor declared a past collaboration with the author HG.

Publisher's note

Supplementary material

The Supplementary Material for this article can be found online at: https://www.frontiersin.org/articles/10.3389/fmicb.2022.1091561/full#supplementary-material

SUPPLEMENTARY FIGURE 1
Growth curve of strain LD-B6.

SUPPLEMENTARY FIGURE 2
The algicidal effects of different strains and concentrations on *Noctiluca scintillans*.

SUPPLEMENTARY FIGURE 3
Algicidal powder product status.

SUPPLEMENTARY FIGURE 4
Algicidal activity of algicidal powder of LD-B6 on *Noctiluca scintillans*.

SUPPLEMENTARY VIDEO 1
Algicidal activity of LD-B6 on *Noctiluca scintillans*.

References

Al-Hakimi, A., Alminderej, F., and Noman, E. (2020). Optimizing of *Microcystis aeruginosa* inactivation in freshwater using algicidal *Bacillus subtilis* by central composite design. *Desalin. Water Treat.* 181, 228–238. doi: 10.5004/dwt.2020.25117

Altschul, S. F., Gish, W., Miller, W., Myers, E. W., and Lipman, D. J. (1990). Basic local alignment search tool. *J. Mol. Biol.* 215, 403–410. doi: 10.1016/S0022-2836(05)80360-2

Anderson, D. M. (2009). Approaches to monitoring, control and management of harmful algal blooms (HABs). *Ocean Coast. Manag.* 52, 342–347. doi: 10.1016/j.ocecoaman.2009.04.006

Anderson, D. M., Glibert, P. M., and Burkholder, J. M. (2002). Harmful algal blooms and eutrophication: Nutrient sources, composition, and consequences. *Estuar. Coast.* 25, 704–726. doi: 10.1007/BF02804901

Azam, F. (1998). Microbial control of oceanic carbon flux: The plot thickens. *Science* 280, 694–696. doi: 10.1126/science.280.5364.694

Bai, S. J., Huang, L. P., Su, J. Q., Tian, Y., and Zheng, T. L. (2011). Algicidal effects of a novel marine actinomycete on the toxic *dinoflagellate Alexandrium tamarense*. *Curr. Microbiol.* 62, 1774–1781. doi: 10.1007/s00284-011-9927-z

Chen, F. Z., Cui, M. C., Fu, J. M., Sheng, G. Y., Sun, G. P., and Xu, M. Y. (2003). Biodegradation of quinoline by freely suspended and immobilized cells of *Comamonas* sp. strain Q10. *J. Gen. Appl. Microbiol.* 49, 123–128. doi: 10.2323/jgam.49.123

Chen, X., Wang, D. Y., Wang, Y. Q., Sun, P. F., Ma, S. H., and Chen, T. T. (2022). Algicidal effects of a high-efficiency algicidal bacterium *Shewanella* Y1 on the toxic bloom-causing *dinoflagellate Alexandrium pacificum*. *Mar. Drugs* 20, 239. doi: 10.3390/md20040239

Coyne, K. J., Wang, Y., and Johnson, G. (2022). Algicidal bacteria: A review of current knowledge and applications to control harmful algal blooms. *Front. Microbiol.* 13:871177. doi: 10.3389/fmicb.2022.871177

DeLong, E. F. (1992). Archaea in coastal marine environments. *Proc. Natl. Acad. Sci. U.S.A.* 89, 5685–5689. doi: 10.1073/pnas.89.12.5685

Escalera, L., Pazos, Y., Moroño, Á, and Reguera, B. (2007). *Noctiluca scintillans* may act as a vector of toxigenic microalgae. *Harmful Algae* 6, 317–320. doi: 10.1016/j.hal.2006.04.006

Fu, L. J., An, X. L., Li, D., Zhou, L. J., Tian, Y., and Zheng, T. L. (2011). Isolation and alga-inhibiting characterization of *Vibrio* sp. BS02 against *Alexandrium tamarense*. *World J. Microb. Biot.* 27, 2949–2956. doi: 10.1007/s11274-011-0778-3

Geciova, J., Bury, D., and Jelen, P. (2002). Methods for disruption of microbial cells for potential use in the dairy industry—a review. *Int. Dairy. J.* 12, 541–553. doi: 10.1016/S0958-6946(02)00038-9

Grattan, L. M., Holobaugh, S., and Morris, J. G. (2016). Harmful algal blooms and public health. *Harmful Algae* 57, 2–8. doi: 10.1016/j.hal.2016.05.003

Griffith, A. W., and Gobler, C. J. (2020). Harmful algal blooms: A climate change co-stressor in marine and freshwater ecosystems. *Harmful Algae* 91:101590. doi: 10.1016/j.hal.2019.03.008

Guillard, R. R. L. (1975). "Culture of phytoplankton for feeding marine invertebrates," in *Culture of marine invertebrate animals*, eds W. L. Smitha and M. H. Chanley (New York, NY: Plenum Press), 26–60.

Harrison, P. J., Furuya, K., Glibert, P. M., Xu, J., Liu, H. B., Yin, K., et al. (2011). Geographical distribution of red and green *Noctiluca scintillans*. *Chin. J. Oceanol. Limn.* 29, 807–831. doi: 10.1007/s00343-011-0510-z

Karlson, B., Andersen, P., Arneborg, L., Cembella, A., Eikrem, W., John, U., et al. (2021). Harmful algal blooms and their effects in coastal seas of Northern Europe. *Harmful Algae* 102:101989. doi: 10.1016/j.hal.2021.101989

Keawtawee, T., Fukami, K., Songsangjinda, P., and Muangyao, P. (2011). Isolation and characterization of *Noctiluca*-killing bacteria from a shrimp aquaculture pond in Thailand. *Fish Sci.* 77, 657–664. doi: 10.1007/s12562-011-0373-4

Kim, J.-D., Kim, J.-Y., Park, J.-K., and Lee, C.-G. (2009). Selective control of the *Prorocentrum minimum* harmful algal blooms by a novel algal-lytic bacterium *Pseudoalteromonas haloplanktis* AFMB-008041. *Mar. Biotechnol.* 11, 463–472. doi: 10.1007/s10126-008-9167-9

Kong, Y., Wang, Q., Chen, Y. J., Xu, X. Y., Zhu, L., Yao, H. M., et al. (2020). Anticyanobacterial process and action mechanism of *Streptomyces* sp. HJC-D1 on *Microcystis aeruginosa*. *Environ. Prog. Sustain.* 39:e13392. doi: 10.1002/ep.13392

Kumar, S., Stecher, G., and Tamura, K. (2016). MEGA7: Molecular evolutionary genetics analysis version 7.0 for bigger datasets. *Mol. Biol. Evol.* 33, 1870–1874. doi: 10.1093/molbev/msw054

Lee, S. O., Kato, J., Takiguchi, N., Kuroda, A., Ikeda, T., Mitsutani, A., et al. (2000). Involvement of an extracellular protease in algicidal activity of the marine bacterium *Pseudoalteromonas* sp. strain A28. *Appl. Environ. Microb.* 66, 4334–4339. doi: 10.1128/AEM.66.10.4334-4339.2000

Li, D. X., Zhang, H., Chen, X. H., Xie, Z. X., Zhang, Y., Zhang, S. F., et al. (2018). Metaproteomics reveals major microbial players and their metabolic activities during the blooming period of a marine *dinoflagellate Prorocentrum donghaiense*. *Environ. Microbiol.* 20, 632–644. doi: 10.1111/1462-2920.13986

Li, S. F., Shilin, W., Xie, L. S., Liu, Y., Chen, H. R., Feng, J., et al. (2022). Identification and optimization of the algicidal activity of a novel marine bacterium against *Akashiwo sanguinea*. *Front. Mar. Sci.* 380:798544. doi: 10.3389/fmars.2022.798544

Liu, Y., Cao, X. H., Yu, Z. M., Song, X. X., and Qiu, L. X. (2016). Controlling harmful algae blooms using aluminum-modified clay. *Mar. Pollut. Bull.* 103, 211–219. doi: 10.1016/j.marpolbul.2015.12.017

Lovejoy, C., Bowman John, P., and Hallegraeff Gustaaf, M. (1998). Algicidal effects of a novel marine *Pseudoalteromonas* isolate (class *Proteobacteria*, gamma subdivision) on harmful algal bloom species of the genera *Chattonella*, *Gymnodinium*, and *Heterosigma*. *Appl. Environ. Microb.* 64, 2806–2813. doi: 10.1128/AEM.64.8.2806-2813.1998

Lu, X. H., Zhou, B., Xu, L. L., Liu, L., Wang, G. Y., Liu, X. D., et al. (2016). A marine algicidal *Thalassospira* and its active substance against the harmful algal bloom species *Karenia mikimotoi*. *Appl. Microbiol. Biot.* 100, 5131–5139. doi: 10.1007/s00253-016-7352-8

Luo, H., Wang, J. T., Goes, J. I., Gomes, H. D. R., Al-Hashmi, K., Tobias, C., et al. (2022). A grazing-driven positive nutrient feedback loop and active sexual reproduction underpin widespread *Noctiluca* green tides. *ISME Commun.* 2, 1–10. doi: 10.1038/s43705-022-00187-4

Maršálek, B., Zezulka, Š, Maršálková, E., Pochylý, F., and Rudolf, P. (2020). Synergistic effects of trace concentrations of hydrogen peroxide used in a novel hydrodynamic cavitation device allows for selective removal of *cyanobacteria*. *Chem. Eng. J.* 382:22383. doi: 10.1016/j.cej.2019.122383

Meyer, N., Bigalke, A., Kaulfuß, A., and Pohnert, G. (2017). Strategies and ecological roles of algicidal bacteria. *FEMS Microbiol. Rev.* 41, 880–899. doi: 10.1093/femsre/fux029

Miyaguchi, H., Kurosawa, N., and Toda, T. (2008). Real-time polymerase chain reaction assays for rapid detection and quantification of *Noctiluca scintillans* zoospore. *Mar. Biotechnol.* 10, 133–140. doi: 10.1007/s10126-007-9031-3

Montani, S., Pithakpol, S., and Tada, K. (1998). Nutrient regeneration in coastal seas by *Noctiluca scintillans*, a red tide-causing *dinoflagellate*. *J. Mar. Biotechnol.* 6, 224–228.

Park, J. H., Yoshinaga, I., Nishikawa, T., and Imai, I. (2010). Algicidal bacteria in particle-associated form and in free-living form during a diatom bloom in the Seto Inland Sea. Japan. *Aquat. Microb. Ecol.* 60, 151–161. doi: 10.3354/ame01416

Piontkovski, S. A., Serikova, I. M., Evstigneev, V. P., Prusova, I. Y., Zagorodnaya, Y. A., Al-Hashmi, K. A., et al. (2021). Seasonal blooms of the *dinoflagellate* algae *Noctiluca scintillans*: Regional and global scale aspects. *Reg. Stud. Mar. Sci.* 44:101771. doi: 10.1016/j.rsma.2021.101771

Pokrzywinski, K. L., Place, A. R., Warner, M. E., and Coyne, K. J. (2012). Investigation of the algicidal exudate produced by *Shewanella* sp. IRI-160 and its effect on *dinoflagellates*. *Harmful Algae* 19, 23–29. doi: 10.1016/j.hal.2012.05.002

Qi, L., Tsai, S.-F., Chen, Y. L., Le, C. F., and Hu, C. M. (2019). In search of red *Noctiluca scintillans* blooms in the East China sea. *Geophys. Res. Lett.* 46, 5997–6004. doi: 10.1029/2019GL082667

Roth, P. B., Twiner, M. J., Mikulski, C. M., Barnhorst, A. B., and Doucette, G. J. (2008). Comparative analysis of two algicidal bacteria active against the red tide *dinoflagellate Karenia brevis*. *Harmful Algae* 7, 682–691. doi: 10.1016/j.hal.2008.02.002

Sakata, T., Yoshikawa, T., and Nishitarumizu, S. (2011). Algicidal activity and identification of an algicidal substance produced by marine *Pseudomonas* sp. C55a-2. *Fish. Sci.* 77, 397–402. doi: 10.1007/s12562-011-0345-8

Sha, J., Xiong, H. Y., Li, C. J., Lu, Z. Y., Zhang, J. C., Zhong, H., et al. (2021). Harmful algal blooms and their eco-environmental indication. *Chemosphere* 274:129912. doi: 10.1016/j.chemosphere.2021.129912

Shao, J. H., He, Y. X., Chen, A. W., Peng, L., Luo, S., Wu, G. Y., et al. (2015). Interactive effects of algicidal efficiency of *Bacillus* sp. B50 and bacterial community on susceptibility of *Microcystis aeruginosa* with different growth Rates. *Int. Biodeter. Biodegr.* 97, 1–6. doi: 10.1016/j.ibiod.2014.10.013

Shi, X. G., Li, Y., Zheng, W. H., Xiao, Y. C., Liu, L. M., and Chen, J. F. (2020). Isolation and algicidal characteristics of a specific algicidal bacterium on *Skeletonema costatum*. *Microbiol. China* 47, 3527–3538. doi: 10.13344/j.microbiol.china.190991

Su, J. Q., Yang, X. R., Zheng, T. L., Tian, Y., Jiao, N. Z., Cai, L. Z., et al. (2007). Isolation and characterization of a marine algicidal bacterium against the toxic *dinoflagellate Alexandrium tamarense*. *Harmful Algae* 6, 799–810. doi: 10.1016/j.hal.2007.04.004

Tan, Z. J., Yan, T., and Zhou, M. J. (2002). Current status of studies on the effects of harmful algae on fish. *J. Fish. China* 6, 561–568.

Teeling, H., Fuchs, B. M., Becher, D., Klockow, C., Gardebrecht, A., Bennke, C. M., et al. (2012). Substrate-controlled succession of marine bacterioplankton populations induced by a phytoplankton bloom. *Science* 336, 608–611. doi: 10.1126/science.1218344

Thompson, J. D., Gibson, T. J., and Higgins, D. G. (2003). Multiple sequence alignment using ClustalW and ClustalX. *Curr. Protoc. Bioinformatics* 2:2.3. doi: 10.1002/0471250953.bi0203s00

Tian, C., Liu, X. L., Tan, J., Lin, S. Q., Li, D. T., and Yang, H. (2012). Isolation, identification and characterization of an algicidal bacterium from Lake Taihu and preliminary studies on its algicidal compounds. *J. Environ. Sci.* 24, 1823–1831. doi: 10.1016/S1001-0742(11)60983-2

Wang, M., Chen, S. B., Zhou, W. G., Yuan, W. Q., and Wang, D. (2020). Algal cell lysis by bacteria: A review and comparison to conventional methods. *Algal Res.* 46:101794. doi: 10.1016/j.algal.2020.101794

Wang, X., Li, Z. J., Su, J. Q., Tian, Y., Ning, X. R., Hong, H. S., et al. (2010). Lysis of a red-tide causing alga, *Alexandrium tamarense*, caused by bacteria from its phycosphere. *Biol. Control.* 52, 123–130. doi: 10.1016/j.biocontrol.2009.10.004

Wu, Y. L., Zhou, C. X., and Zhang, Y. S. (1994). Laboratory culture of *Noctiluca scintillans* (Macartney). *Oceanol. Limnol. Sin.* 25, 165–167. doi: 10.3321/j.issn:0029-814X.1994.02.009

Yang, B. J., Xiang, W. Z., Jin, X. J., Chen, Z. S., Wang, L., and Wu, H. B. (2020). Isolation and identification of an algicidal bacterium CBA02 and its algae-lysing characteristics. *Biotechnol. Bul.* 36, 55–62. doi: 10.13560/j.cnki.biotech.bull.1985.2020-0394

Yang, C. Y., Li, Y., Zhou, B., Zhou, Y. Y., Zheng, W., Tian, Y., et al. (2015). Illumina sequencing-based analysis of free-living bacterial community dynamics during an *Akashiwo sanguine* bloom in Xiamen sea. China. *Sci. Rep.* 5:8476. doi: 10.1038/srep08476

Ye, Y. H., Yang, X. N., Hu, W. Z., Yu, M. Y., and Chen, L. T. (2022). Advances in functional diversity and application of algicidal bacteria. *Acta. Microbiol. Sin.* 62, 1171–1189. doi: 10.13343/j.cnki.wsxb.20210417

Yu, Z. M., Song, X. X., Cao, X. H., and Liu, Y. (2017). Mitigation of harmful algal blooms using modified clays: Theory, mechanisms, and applications. *Harmful Algae* 69, 48–64. doi: 10.1016/j.hal.2017.09.004

Zhang, H. J., Peng, Y., Zhang, S., Cai, G. J., Li, Y., Yang, X. J., et al. (2016). Algicidal effects of prodigiosin on the harmful algae *Phaeocystis globosa*. *Front. Microbiol.* 7:602. doi: 10.3389/fmicb.2016.00602

Zhang, S. W., Harrison, P. J., Song, S. Q., Chen, M. R., Kung, H. S., Lau, W. K., et al. (2017). Population dynamics of *Noctiluca scintillans* during a bloom in a semi-enclosed bay in Hong Kong. *Mar. Pollut. Bull.* 121, 238–248. doi: 10.1016/j.marpolbul.2017.06.025

Zhang, S., Zheng, W., and Wang, H. (2020a). Physiological response and morphological changes of *Heterosigma akashiwo* to an algicidal compound prodigiosin. *J. Hazard. Mater.* 385, 121530. doi: 10.1016/j.jhazmat.2019.121530

Zhang, S. W., Li, C., Cheung, S. Y., Sun, M. M., Song, S. Q., Guo, W., et al. (2020b). Snapshot of peptidomics of the red tide forming species *Noctiluca scintillans*. *Front. Mar. Sci.* 7:569807. doi: 10.3389/fmars.2020.569807

Zhang, Z. Z., Wang, J. Y., Hu, G. W., Huang, J. W., Chen, L., Yin, Y., et al. (2022). Isolation and characterization of an algicidal bacterium against the bloom-forming algae *raphidophyte Heterosigma akashiwo*. *Environ. Technol.* [Epub ahead of print]. doi: 10.1080/09593330.2022.2036250

Zheng, N. N., Ding, N., Gao, P. K., Han, M., Liu, X., Wang, J. G., et al. (2018). Diverse algicidal bacteria associated with harmful bloom-forming *Karenia mikimotoi* in estuarine soil and seawater. *Sci. Total Environ.* 631, 1415–1420. doi: 10.1016/j.scitotenv.2018.03.035

Zhu, X. Y., Chen, S. S., Luo, G. Y., Zheng, W., Tian, Y., Lei, X. Q., et al. (2022). A novel algicidal bacterium, *Microbulbifer* sp. YX04, triggered oxidative damage and autophagic cell death in *Phaeocystis globosa*, which causes harmful algal blooms. *Microbiol. Spectr.* 10:e934–e921. doi: 10.1128/spectrum.00934-21

frontiers | Frontiers in Marine Science

TYPE Original Research
PUBLISHED 26 January 2023
DOI 10.3389/fmars.2023.1116050

OPEN ACCESS

EDITED BY
Zhangxi Hu,
Guangdong Ocean University, China

REVIEWED BY
Yang Li,
South China Normal University, China
Anglu Shen,
Shanghai Ocean University, China

*CORRESPONDENCE
Jufa Chen
chenjf@ysfri.ac.cn
Tao Jiang
jiangtaojnu@163.com

†These authors have contributed equally to this work and share first authorship

SPECIALTY SECTION
This article was submitted to Aquatic Microbiology, a section of the journal Frontiers in Marine Science

RECEIVED 05 December 2022
ACCEPTED 09 January 2023
PUBLISHED 26 January 2023

CITATION
Xin Q, Qin X, Wu G, Ding X, Wang X, Hu Q, Mu C, Wei Y, Chen J and Jiang T (2023) Phytoplankton community structure in the Western Subarctic Gyre of the Pacific Ocean during summer determined by a combined approach of HPLC-pigment CHEMTAX and metabarcoding sequencing. *Front. Mar. Sci.* 10:1116050. doi: 10.3389/fmars.2023.1116050

Phytoplankton community structure in the Western Subarctic Gyre of the Pacific Ocean during summer determined by a combined approach of HPLC-pigment CHEMTAX and metabarcoding sequencing

Quandong Xin[1,2,3†], Xiaohan Qin[1†], Guannan Wu[1], Xiaokun Ding[1], Xinliang Wang[3], Qingjing Hu[3], Changkao Mu[2], Yuqiu Wei[3], Jufa Chen[3*] and Tao Jiang[1*]

[1]School of Ocean, Yantai University, Yantai, China, [2]School of Marine Sciences, Ningbo University, Ningbo, China, [3]Key Laboratory of Sustainable Development of Marine Fisheries, Ministry of Agriculture, Yellow Sea Fisheries Research Institute, Chinese Academy of Fishery Sciences, Qingdao, China

The Western Subarctic Gyre (WSG) is a cyclonic upwelling gyre in the northwest subarctic Pacific, which is a region with a high concentration of nutrients but low chlorophyll. We investigated the community structure and spatial distribution of phytoplankton in this area by using HPLC-pigment CHEMTAX (a chemotaxonomy program) and metabarcoding sequencing during the summer of 2021. The phytoplankton community showed significant differences between the two methods. The CHEMTAX analyses identified eight major marine phytoplankton assemblages. Cryptophytes were the major contributors (24.96%) to the total Chl *a*, followed by pelagophytes, prymnesiophytes, diatoms, and chlorophytes. The eukaryotic phytoplankton OTUs obtained by metabarcoding were categorized into 149 species in 96 genera of 6 major groups (diatoms, prymnesiophytes, pelagophytes, chlorophytes, cryptophytes, and dinoflagellates). Dinoflagellates were the most abundant group, accounting for 44.74% of the total OTUs obtained, followed by cryptophytes and pelagophytes. Sixteen out of the 97 identified species were annotated as harmful algal species, and *Heterocapsa rotundata*, *Karlodinium veneficum*, and *Aureococcus anophagefferens* were assigned to the abundant group (i.e., at least 0.1% of the total reads). Nutrients were more important in shaping the phytoplankton community than temperature and salinity. The 24 stations were divided into southern and northern regions along 44°N according to the *k*-means method, with the former being dominated by high

Chl *a* and low nutrients. Although different phytoplankton assemblages analyzed by the two methods showed various relationships with environmental factors, a common feature was that the dinoflagellate proportion showed a significantly negative correlation with low nutrients and a positive correlation with Chl *a*.

KEYWORDS

metabarcoding analysis, pigments, phytoplankton, Western Subarctic Gyre metabarcoding analysis, Western Subarctic Gyre

1 Introduction

Marine phytoplankton form the basis of the marine food web and play an essential role in biogeochemical processes and the mitigation of global climate change (Sunagawa et al., 2015). The geographic patterns of phytoplankton assemblages are governed by spatial and environmental factors, especially temperature, on a global scale (Villar et al., 2015). For regional areas, the distribution of phytoplankton community compositions is also shaped by different processes, such as ocean currents, water column depths and environmental stresses (e.g., nutrient and light limitation) (Paerl et al., 2018; Wu et al., 2020; Liu et al., 2022). Considering phytoplankton's ability to rapidly adapt to environmental changes, these can be used as indicators of marine environmental changes (Paerl et al., 2018).

Accurate identification of phytoplankton population structure is difficult, especially for small-sized (e.g., picoplankton) or fragile cells. This is a hindrance in studying the spatial and temporal dynamics of phytoplankton assemblages in the natural environment (Hattori et al., 2004; Wang et al., 2022). Traditionally, information on phytoplankton assemblages is determined through the use of taxonomic methods (i.e., microscopic observation and HPLC-pigment analyses) (e.g., Hattori et al., 2004; Fujiki et al., 2009; Kwak et al., 2014; Waga et al., 2022). Only large phytoplankton (> 10 μm, such as diatoms and dinoflagellates) were identified and counted by light microscopy in most previous studies due to the lack of distinguishing characteristics of small phytoplankton and the limitation of microscope resolution (Hattori et al., 2004; Komuro et al., 2005; Fujiki et al., 2009). Many phytoplankton species are fragile and often damaged during the fixation process by Lugol's solution or formalin. Moreover, taxonomic identification is extremely time-consuming and requires well-trained specialists (Wang et al., 2022). By comparison, HPLC-pigment CHEMTAX analyses are highly efficient in measuring the biomass of different phytoplankton assemblages, including picoplankton and fragile cells (e.g., cryptophytes), in batches. Consequently, HPLC-pigment analyses have been widely used for qualitative and quantitative analyses of phytoplankton groups in various sea areas (e.g., Obayashi et al., 2001; Fujiki et al., 2009; Kwak et al., 2014; Waga et al., 2022). Nevertheless, the main problem with HPLC-pigment CHEMTAX is that the phytoplankton population classification is at the phylum level, not at the species level or even the class level.

Our ability to assess the biodiversity of phytoplankton and identify their ecological significance in the marine environment has been enhanced due to the development of molecular biology-based methods (Bik et al., 2012). Based on these modern molecular approaches, phytoplankton assemblages showed much greater diversity across different aquatic environments than was detectable by traditional methods, such as microscopy and HPLC-pigment analyses (Gong et al., 2020; Wang et al., 2022). In particular, DNA metabarcoding methods based on molecular marker amplification and high-throughput sequencing approaches have been rapidly developed in recent years (Gong et al., 2020). In numerous studies, the metabarcoding method has been applied widely to investigate phytoplankton communities in various seas, such as the northwestern Pacific Ocean (Wu et al., 2020), South China Sea (Wang et al., 2022), Neuse River Estuary (Gong et al., 2020), and Jiaozhou Bay (Liu et al., 2022). Those studies showed that environmental factors (i.e., environmental selection) and geographical distance (i.e., dispersal limitation) are important factors that shape the phytoplankton community in the ocean, even on a small scale (Wu et al., 2020; Li et al., 2022; Zhang et al., 2022). In particular, metabarcoding has an extraordinary advantage in distinguishing harmful and/or toxic algal species, some of which are easily missed by microscopic methods (Liu et al., 2022; Wang et al., 2022). Consequently, the metabarcoding approach has expanded our understanding of the relationship between environmental factors and phytoplankton population diversity in the marine environment.

The Western Subarctic Gyre (WSG) is situated in the subarctic North Pacific, which is characterized by high nutrient and low chlorophyll (HNLC) concentrations and contains distinctive differences in oceanographic and biogeochemical processes. Fe deficiency and grazing pressure are the main reasons for the low Chl *a* concentration in this area (Harrison et al., 2004). Nevertheless, seasonal phytoplankton blooms with high Chl *a* concentrations (1–12 μg/L) occurred frequently during late spring in the WSG (Obayashi et al., 2001; Imai et al., 2002), which suggests that the environmental factors affecting the spatial and temporal distribution of phytoplankton populations are complex. Consequently, the phytoplankton community structure and the correlation between phytoplankton assemblages and environmental factors in this area have been extensively studied. Nevertheless, phytoplankton community structure was investigated by microscopy and HPLC-pigment methods in previous studies (e.g., Suzuki et al., 2002;

Harrison et al., 2004; Fujiki et al., 2009; Kwak et al., 2014; Waga et al., 2022). Information on the molecular composition of phytoplankton is very limited in the WSG, which suggests a significant knowledge gap in understanding the spatial and temporal distribution of the algal community.

In the present study, we combined HPLC-pigment CHEMTAX and metabarcoding of the V4 region of the 18S rDNA sequence (1) to investigate the diversity and spatial distribution of phytoplankton assemblages in WSG during summer, (2) to investigate how environmental factors affect the spatial distribution of phytoplankton communities, and (3) to determine the agreement between CHEMTAX and metabarcoding and discuss their advantages and disadvantages. To the best of our knowledge, this study presents the first combined metabarcoding and HPLC-pigment analyses of the phytoplankton community in open oceans.

2 Materials and methods

2.1 Sampling strategy

From 23 May to 17 July 2021, a field investigation was conducted in the WSG of the Northwest Pacific Ocean (40°25'12"-48°4'48"N, 163°25'12"-171°26'24"E) by the saury fishing vessel "Minghualun" (Figure 1). A total of 24 stations (St. M1–M24, listed in chronological order) were randomly set up depending on the navigation track of the fishing vessel, in south to north order. Temperature and salinity were measured using a SBE-37 MicroCAT recorder (Seabird Electronics, Inc., Washington, USA).

Triplicate water samples were taken from the surface layer (5 m) of each site by using a Niskin water sampler (5 L). For phytopigment analyses, 2.5 L seawater was filtered by GF/F membranes (0.7 µm pore size, Whatman, Britain), which were quickly stored in liquid nitrogen in the laboratory for HPLC analyses. The filtered seawater (300 mL) was stored at -20°C for later nutrient analyses. For molecular analyses, the phytoplankton cells were collected through 0.22 µm polycarbonate membranes (0.22 µm, Whatman, Britain) from 3 L seawater for three parallel samples, which were stored in liquid nitrogen.

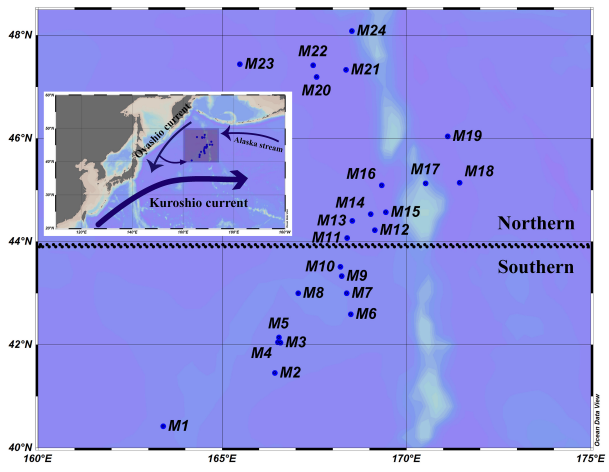

FIGURE 1
Sampling sites and schematic illustration of the Kuroshio and Oyashio currents. Southern area: M1–M10; northern area: M11–M24.

2.2 Nutrient analyses

Nutrients, including nitrate (NO_3^-), nitrite (NO_2^-), ammonium (NH_4^+), dissolved reactive phosphorous (DIP), and dissolved silicate (DSi), were determined by a QuAAtro continuous flow analyzer (SEAL, Germany), as described by Strickland and Parsons (Strickland and Parsons, 1972). Concentrations of DIN were the sum of NO_3^-, NO_2^-, and NH_4^+.

2.3 Phytoplankton pigment analyses

The frozen filters were cut into small pieces and transferred into a 15 mL polypropylene centrifuge tube, to which 3 mL 95% HPLC-grade acetone was added. The mixture was sonicated for 5 min in an ice bath under low light conditions. Pigment determination was performed according to the method of Zapata et al. (2004). The HPLC instrument (Agilent 1200, USA) was equipped with an autosampler and diode array detector (Model G1315C). The pigments extracted were separated by a C8 column (150 mm, 4.6 mm, Waters Symmetry) at 25°C.

The following 20 authentic pigment standards were purchased from DHI Inc. (Denmark): Chl *a*, Chl *b*, Chl *c*2, Chl *c*3, pheophythin *a* (Phe *a*), pheophorbide *a* (Pheide *a*), Mg-2,4-divinylpheoporphyrin (MgDVP), alloxanthin (Allo), 19'-but-fucoxanthin (But-Fuco), β-carotene (β-Car), diadinoxanthin (Diadino), diatoxanthin (Diato), fucoxanthin (Fuco), 19'-hex-fucoxanthin (Hex), lutein (Lut), neoxanthin (Neo), Peridinin (Peri), prasinoxanthin (Pras), violaxanthin (Viola), and zeaxanthin (Zea).

2.4 CHEMTAX

We calculated the relative contribution of the different phytoplankton groups to the total Chl *a* from pigment concentration data by using version 1.95 of the CHEMTAX software (Mackey et al., 1996; Wright et al., 2009). The program uses factor analyses and the steepest descent algorithm to find the best fit to the data based on an initial guess of the pigment ratios for the algal group to be determined (Mackey et al., 1996; Suzuki et al., 2002). To select the best input ratios for the pigment data set, we generated a series of 60 derivative pigment ratio matrixes by multiplying each cell of the initial input ratio by a random function to optimize the matrix. We considered the best 10% of the results as the optimized results. We presented the output data as absolute concentrations of Chl *a* (µg/L) attributed to each algal group (Table 1; Figure 2).

2.5 DNA extraction, PCR amplification, and high-throughput sequencing

Total genomic DNA of each sample was extracted by using a DNeasy Power Water Kit (QIAGEN, USA) according to the

10.3389/fmars.2023.1116050

TABLE 1 Average values of environmental factors and phytoplankton pigments in the WSG.

Parameters	Southern area [a,b]	Northern area [a,b]	Sig [c]
Physical and chemical variables			
Temperature (°C)	10.05 ± 1.64	9.18 ± 1.93	
Salinity	34.11 ± 0.46	33.78 ± 0.36	
DIN (μmol/L)	3.79 ± 1.52	6.15 ± 0.55	**
DIP (μmol/L)	0.347 ± 0.18	0.664 ± 0.04	**
Dsi (μmol/L)	17.06 ± 6.40	31.31 ± 3.82	**
Phytoplankton pigments			
Chl *a* (μg/L)	0.535 ± 0.289	0.248 ± 0.217	*
Fucoxanthin (μg/L)	0.117 ± 0.084	0.069 ± 0.049	
19'-Hex- Fucoxanthin (μg/L)	0.132 ± 0.073	0.068 ± 0.079	*
19'-But- Fucoxanthin (μg/L)	0.047 ± 0.026	0.020 ± 0.019	**
Alloxanthin (μg/L)	0.023 ± 0.011	0.008 ± 0.004	**
Zeaxanthin (μg/L)	0.010 ± 0.006	0.010 ± 0.017	
Prasinoxanthin (μg/L)	0.011 ± 0.008	0.001 ± 0.004	**
Phytoplankton composition by CHEMTAX			
Diatoms (%)	8.72 ± 0.036	17.71 ± 0.06	**
Prymnesiophytes (%)	14.88 ± 0.026	15.08 ± 0.07	
Pelagophytes (%)	18.53 ± 0.051	17.26 ± 0.059	
Chlorophytes (%)	10.52 ± 0.062	12.60 ± 0.13	
Prasinophytes (%)	5.209 ± 0.026	1.499 ± 0.021	**
Cryptophytes (%)	31.59 ± 0.087	28.79 ± 0.18	
Dinoflagellates (%)	5.10 ± 0.032	1.18 ± 0.026	**
Cyanobacteria (%)	5.46 ± 0.053	5.88 ± 0.068	
Phytoplankton composition by metabarcoding			
Diatoms (%)	8.33 ± 0.061	8.94 ± 0.062	
Prymnesiophytes (%)	0.26 ± 0.003	0.52 ± 0.002	**
Pelagophytes (%)	4.39 ± 0.033	17.41 ± 0.089	**
Chlorophytes (%)	20.10 ± 0.097	10.91 ± 0.082	*
Cryptophytes (%)	11.46 ± 0.11	20.79 ± 0.084	
Dinoflagellates (%)	53.28 ± 0.091	38.64 ± 0.13	**
Others (%)	2.30 ± 0.014	2.72 ± 0.01	

[a]The values mean average value ± std.
[b]Southern area and northern area include the stations W1-W10 and W11-W24, respectively. Please see Figure 1.
[c]Asterisks indicate a significant difference between the southern and northern areas (wilcoxon test; * $p < 0.05$; ** $p < 0.01$).

manufacturer's protocols, and the qualified DNA samples were stored at -80°C for subsequent analyses. The V4 variable region of the 18S rDNA gene was amplified using universal primers (TAReuk454FWD1F: 5'- CCAGCA(G/C)C(C/T)GCGGTAATTCC-3' and TAReukREV3R: 5'- ACTTTCGTTCTTGAT(C/T)(A/G)A-3') (Stoeck et al., 2010) by an ABI GeneAmp® 9700 PCR thermocycler (ABI, CA, USA). The PCR mixture contained 5 × Trans Start Fast Pfu buffer 4 μL, 2.5 mM dNTPs 2 μL, forward primer (5 μM) 0.8 μL, reverse primer (5 μM) 0.8 μL, Trans Start Fast Pfu DNA Polymerase 0.4 μL, template DNA 10 ng, and ddH_2O up to 20 μL. PCRs were performed in triplicate. The PCR conditions were as follows: first, the initial denaturation at 95°C for 3 min; then, 35 cycles of 95°C for 30 s, 55°C for 30 s, 72°C for 45 s; and finally, the extension at 72°C for 10 min. Degradation and contamination of PCR products were monitored on 2% agarose gels and purified with the AxyPrep DNA Gel Extraction Kit (Axygen Biosciences, Union City, CA, USA). The

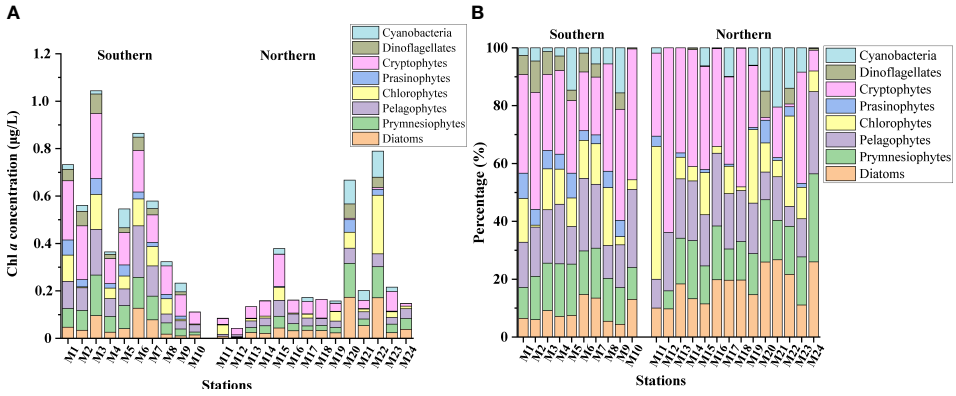

FIGURE 2
Absolute **(A)** and relative **(B)** CHEMTAX-derived Chl *a* concentrations of phytoplankton groups in the summer in the Northwest Pacific Ocean.

purified amplicons were pooled in equimolar amounts, and then paired-end sequencing was performed on an Illumina NovaSeq PE250 platform (Illumina, San Diego, USA) using the standard protocols of Majorbio Bio-Pharm Technology Co., Ltd. (Shanghai, China). All raw reads were deposited in the NCBI Sequence Read Archive (SRA) database (Accession Number: SRP392983).

2.6 Data processing, clustering, annotation, and statistical analyses

Raw sequencing reads were denoised, trimmed, and filtered using Fastq version 0.20.0 (Chen et al., 2018) and merged by FLASH version 1.2.7 (Magoč and Salzberg, 2011). OTUs were generated on the basis of 97% similarity after the removal of singletons and doubletons (Edgar, 2013). The taxonomy of each OTU representative sequence was analyzed by RDP Classifier version 2.2 (Wang et al., 2007) against the SILVA 18S rRNA database (release138, www.arb-silva.de) for phytoplankton and zooplankton groups using a confidence threshold of 0.7. The raw sequencing data were equalized using the "gclus" package in R based on random subsampling of the least sequence number per sample (10757 sequence reads here) to standardize sampling efforts and bring the data from different samples onto a common scale. We identified eukaryotic algae OTUs by using the taxonomic information of AlgaeBase (https://www.algaebase.org/). The species was annotated as a harmful algal bloom (HAB) species if it was categorized as harmful microalgae in the IOC-UNESCO Taxonomic Reference List of Harmful Micro Algae (http://www.marinespecies.org/hab/) or had been reported as an HAB species in previous studies.

Analyses of sites were clustered using the "stats" package by *the k*-means method. ODV (Ocean Data View) was used to draw the station map and spatial distribution contour map of temperature, salinity, nutrients and abundant HAB species. Alpha-diversity analyses were calculated by the "vegan" package in R (v. 4.1.3), including richness (OTUs) and Shannon diversity. The rarefaction curves were plotted with richness using the R package "vegan" for all samples. For beta-diversity analyses, nonmetric multidimensional scaling (NMDS) analyses were performed in R based on Bray–Curtis similarity by the "vegan" package. The Wilcoxon signed-rank test was used to analyze the differences in the environmental parameters, alpha diversity indices, and relative abundance of specific taxa across all samples. The analyses of ADONIS were used to statistically test for significant differences in microeukaryotic communities in the two regions. Bar and bubble charts were plotted using the R package ggplot2 (Wickham, 2016). Mantel tests of the environmental factors with phytoplankton were carried out by using the R package ggcor, and the figures were drawn by the R package ggplot2. After the prediction of detrended correspondence analysis (DCA) using the R package vegan, Redundancy analyses (RDA) were performed with CANOCO 5 software to explore the relationships between environmental and phytoplankton variables. The agreement between the CHEMTAX and metabarcoding results was evaluated by regression analyses using Origin 2017 software. Correlations between phytoplankton and zooplankton from phyla to OTU levels were analyzed using the Spearman method using the R package psych and visualized using the R package circlize (Gu et al., 2014) and cytoscape. The interactions were filtered with Spearman's coefficient < 0.6 and $p > 0.05$ clustered into phylum levels for visualization.

3 Result

3.1 Environmental characteristics

Clustering was performed according to the *k*-means method, and the 24 stations were divided into southern (M1–M10) and northern (M11–M24) regions along 44°N (Figure 1). The environmental parameters in the surface layer have been described in detail by Figure S1 and Table 1. The temperature and salinity ranged from 6.96°C to 13.71°C and from 33.22 to 34.92 with average values of 9.54°C and 33.92, respectively. No significant differences were found between the southern and northern regions (Wilcoxon test, $p > 0.05$). Nevertheless, the nutrient concentrations of DIN (1.63–7.38 μmol/L), DIP (0.10–0.94 μmol/L), and DSi (7.51–39.01 μmol/L) in the northern area were significantly higher than those in the southern area (Wilcoxon test, $p < 0.01$).

3.2 Phytoplankton assemblages identified by the HPLC–pigment CHEMTAX approach

A total of 20 pigments were identified in this survey by high-performance liquid chromatography (HPLC), and the average Chl *a* concentration was 0.37μg/L and ranged from 0.042μg/L (M12) to 1.04μg/L (M3) (Figure 2A) and showed a significant decline from the southern to northern area ($p < 0.05$; Table 1). Similarly, the concentrations of 19'-hex-fucoxanthin, 19'-but-fucoxanthin, alloxanthin, lutein and prasinoxanthin in the southern area were significantly higher than those in the northern area. The CHEMTAX analyses identified eight major marine phytoplankton assemblages (Figure 2B). Cryptophytes were the major contributors (24.96%) to the total Chl *a*, followed by pelagophytes (16.86%), prymnesiophytes (15.85%), diatoms (13.27%) and chlorophytes (13.17%) in the whole study area (Figure 3A). The proportion of diatoms to total Chl *a* in the southern area was significantly lower than in the northern area, whereas prasinophytes and dinoflagellates showed the reverse trend ($p < 0.05$; Table 1).

3.3 Phytoplankton community based on metabarcoding analyses

After quality control, chimeric filtering, singleton deletion, and screening, 3,948,649 high-quality sequences were obtained from 72 samples. Through random sampling according to the lowest read number (10,757), 527 operational taxonomic units (OTUs) were clustered at the 0.03 distance level. The rarefaction curves were roughly saturated for all samples (Figure S2A). In α diversity analyses, the richness index showed no remarkable differences ($p > 0.05$, Wilcoxon's test) across the southern and northern regions. However, the Shannon diversity index of samples in the northern region was significantly higher than in the southern region ($p < 0.01$, Wilcoxon's test) (Figure S2B). In β diversity analyses, the first two principal components of the NMDS plot could explain 58.11% of the total variation among all samples (Figure 4A), and the 24 sites could be clearly clustered into southern and northern groups. Analyses of similarity (ADONIS) also showed that the communities of the two regions were significantly ($p < 0.01$) separated.

The eukaryotic phytoplankton OTUs were categorized into 149 species in 96 genera of 6 major groups (diatoms, prymnesiophytes, pelagophytes, chlorophytes, cryptophytes, and dinoflagellates) (Figure 4A). Dinoflagellates were the most abundant group, accounting for 44.74% of the total obtained OTUs, followed by cryptophytes and pelagophytes, accounting for 16.90% and 11.99%, respectively (Figure 4B). The relative abundances of different phytoplankton groups in the two regions exhibited different patterns (Table 1; Figure S3B). The dinoflagellate and chlorophyte distribution characteristics were obviously higher in the south than in the north ($p < 0.05$), whereas pelagophytes showed the opposite distribution trend ($p < 0.01$). In addition, a difference was found in the average abundance of cryptophytes between the two regions, but it was not significant ($p > 0.05$).

3.4 Comparison of the phytoplankton communities identified by the two methods

The phytoplankton community showed significant differences between the results from CHEMTAX and metabarcoding analyses. Cryptophytes predominated in the phytoplankton community based on CHEMTAX estimates, and dinoflagellates dominated based on metabarcoding analyses (Figure 3A). At the phylum level, metabarcoding annotated more phyla (13 phyla) than CHEMTAX (8 phyla). Six phyla of phytoplankton were identified by both methods. Cyanobacteria were not detected by metabarcoding methods, because we used eukaryotic primers. In addition, metabarcoding analyses detected a small percentage of the phylum (< 2.5%), such as prasinophytes, raphidophytes, and xanthophytes. The linear fitting curve showed that only cryptophytes and dinoflagellates had significantly positive correlations between the two methods ($p < 0.01$) (Figures 3B, C). However, no significant correlation was found for other phytoplankton groups ($p > 0.05$) (Figure S4).

3.5 Identification of HAB species

To further explore the distribution of harmful algal bloom (HAB) causative species in the study area, 16 out of the 97 identified species were annotated as HAB-forming species if they were previously reported to be HAB-forming species (Table 2; Figure 5), including

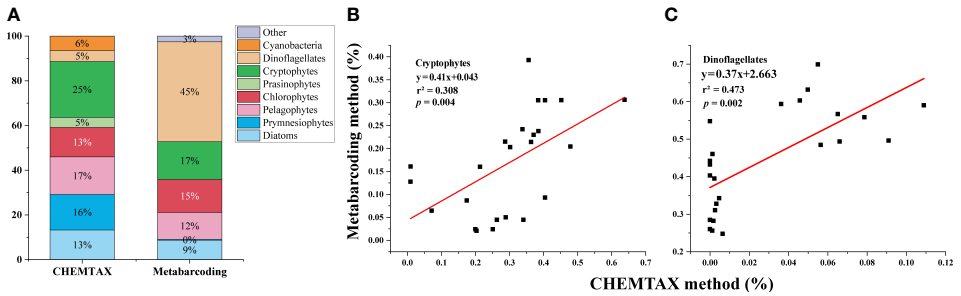

FIGURE 3
Composition of phytoplankton assemblages based on the phylum level by HPLC-pigment CHEMTAX and metabarcoding analyses **(A)**. Pairwise comparison of CHEMTAX and metabarcoding in determining phytoplankton taxonomic composition: Cryptophytes **(B)** and Dinoflagellates **(C)**.

8 diatom species, 6 dinoflagellate species, 1 haptophyte species, and 1 heterokontophyte species. The HAB-forming species were classified into three groups according to their relative abundance (Logares et al., 2014). Nine HAB-forming species were assigned to the rare group (i.e., no more than 0.01% of the total reads), four HAB-forming species were assigned to the intermediate group (i.e., between 0.1% and 0.01% of the total reads), and *Heterocapsa rotundata*, *Karlodinium veneficum*, and *Aureococcus anophagefferens* were assigned to the abundant group (i.e., at least 0.1% of the total reads).

Different HAB-forming species exhibited differential geographical dynamics even for those belonging to the same phylum. The dinoflagellate *H. rotundata* showed preference to the northern region ($p < 0.01$), whereas *K. veneficum* showed the opposite geographical pattern ($p < 0.01$) (Figures S4B and 5). However, the abundance of the pelagophyte *A. anophagefferens* showed no significant difference between the southern and northern areas ($p > 0.05$) (Figure S4C). The HAB-forming species annotated here might be an underestimation of the number of HAB-forming species in the WSG. Some species can only be identified at the genus level, such as *Phaeocystis* spp., *Coscinodiscus* spp., and *Neoceratium* spp.

3.6 Impact of environmental factors on phytoplankton and HAB-forming species by the two methods

We used the Mantel test to determine the impact of environmental factors on shaping the phytoplankton communities. Nutrients, Chl *a*, and geographical location were the main factors affecting phytoplankton communities. According to CHEMTAX analyses (Figure 6A), prasinophytes and dinoflagellates were significantly correlated with nutrients, Chl *a*, and latitude ($p < 0.01$). Based on metabarcoding analyses (Figure 6B), more phytoplankton groups were associated with environmental factors. For example, prasinophytes and dinoflagellates were significantly correlated with most nutrient elements and Chl *a* ($p < 0.01$), and pelagophytes and chlorophytes were correlated with nutrients, latitude, and longitude ($p < 0.01$ or $p < 0.05$). However, we found no correlation between temperature and salinity and phytoplankton populations by using either method. When both methods' results were pooled together, redundancy analyses (RDA) revealed that the sampling stations were separated into two groups along the nutrient gradient and the first axis (Figure 6C), which was consistent with the results of the *k*-means method. Dioflagellates (as found by CHEMTAX and metabrarcoding) were positively associated with Chl *a* and salinity and negatively associated with nutrients. We selected the three abundant HAB-forming species by metabarcoding for RDA analyses. *K. veneficum* was positively correlated with temperature, salinity, and Chl *a* and negatively correlated with nutrients at the first axis, whereas *H. rotundata* showed the opposite pattern. *A. anophagefferens* showed no correlation with these environmental factors (Figure 6C).

The top five most abundant zooplankton groups, such as Arthropoda, Chordata, Ciliophora, Ctenophora, and Picozoa, were selected for correlation analyses with the predominant phytoplankton communities in this area (Figure 6D). A total of 120 OTUs showed 1917 significant correlations between zooplankton and phytoplankton communities by screening, and 68.54% of the total correlations established in the chordal graph were positive. This finding suggested that zooplankton survival selection might play an important role in shaping phytoplankton communities.

4 Discussion

4.1 Comparison of phytoplankton assemblages determined by HPLC-pigment CHEMTAX and metabarcoding approach

HPLC-pigment CHEMTAX is widely used for qualification and quantification of phytoplankton assemblages in the WSG (Suzuki et al., 2002; Fujiki et al., 2009; Fujiki et al., 2014; Gong et al., 2020). Consistent with previous investigations, the present study showed that no single phytoplankton group absolutely dominated the phytoplankton assemblages in this area. Recently, the metabarcoding approach has been widely used in oceans and has become a competitive method for determining the biodiversity of marine phytoplankton communities (Gong and Marchetti, 2019; Liu

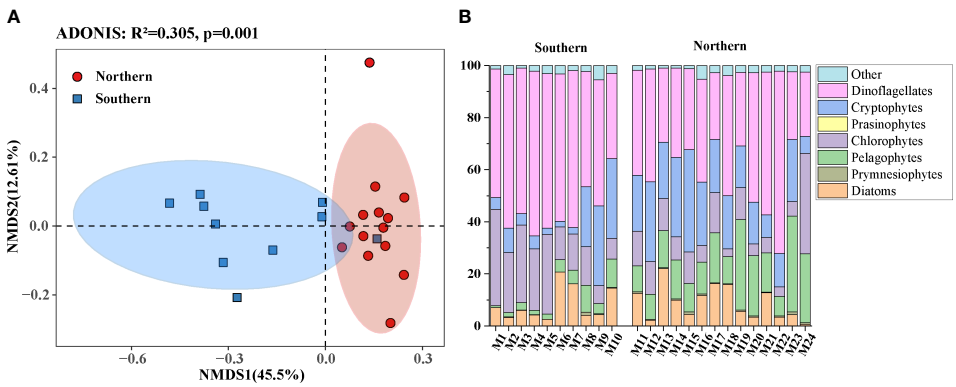

FIGURE 4
NMDS analyses were analyzed between southern and northern seawater to test the differences **(A)**. Relative abundance of major phytoplankton groups of the Northwest Pacific Ocean as determined by metabarcoding in the summer **(B)**.

TABLE 2 HAB species detected in surface water samples from the Northwest Pacific Ocean based on metabarcoding analysis.

Phylum	Class	Species	Level	Referrence
Bacillariophyta	Coscinodiscophyceae	*Chaetoceros atlanticus*	Intermediate	(Lundholm et al., 2009)
		Thalassiosira rotula	Rare	(Huang et al., 2021)
		Thalassiosira tenera	Rare	(Lundholm et al., 2009)
		Rhizosolenia etigera	Intermediate	(Chen et al., 2021)
	Bacillariophyceae	*Pseudo-nitzschia subcurvata*	Rare	(Lundholm et al., 2009)
		Pseudo-nitzschia brasiliana	Rare	(Lundholm et al., 2009)
		Pseudo nitzschia turgidula	Rare	(Lundholm et al., 2009)
	Mediophyceae	*Eucampia cornuta*	Intermediate	(Chen et al., 2021)
Dinophyta	Dinophyceae	*Heterocapsa rotundata*	Abundant (18.18%)	(Huang et al., 2021)
		Karlodinium veneficum	Abundant (15.28%)	(Wang et al., 2022)
		Prorocentrum mexicanum	Intermediate	(Huang et al., 2021)
		Dinophysis acuminata	Rare	(Wang et al., 2022)
		Alexandrium minutum	Rare	(Wang et al., 2022)
		Protoperidinium pellucidum	Rare	(Chen et al., 2021)
Haptophyta	Prymnesiophyceae	*Chrysochromulina leadbeateri*	Rare	(Lundholm et al., 2009)
		Phaeocystis spp.	Intermediate	(Chen et al., 2021)
Heterokontophyta	Pelagophyceae	*Aureococcus anophagefferens*	Abundant (0.597%)	(Chen et al., 2021)

et al., 2022), which was not performed in the WSG. This study used the V4 region of 18 s rDNA, which is among the best choices for metabarcoding the whole eukaryotic algal community in the marine environment (Lear et al., 2017). Although metabarcoding can provide detailed phytoplankton species/genus composition, only the composition at the phylum level can be compared for the results obtained from the two methods. The structure of the phytoplankton community displayed marked differences for some phytoplankton assemblages, according to the two methods. Dinoflagellates were more represented when the metabarcoding approach was used compared with CHEMTAX. This might be ascribed to the fact that (1) some dinoflagellates could not be counted by the CHEMTAX method due to a lack of Peridinin (Mackey et al., 1996) and (2) dinoflagellates contain larger genome sizes and higher 18S gene copy numbers than other phytoplankton assemblages, especially diatoms (Lin, 2011; Gong and Marchetti, 2019; Liu et al., 2022). Similarly, Wang et al. (2022) showed that metabarcoding overestimated the contribution of dinoflagellates to total phytoplankton compared with

FIGURE 5
The distribution and relative abundance of 16 HAB-forming species in the surface seawater of the Northwest Pacific Ocean.

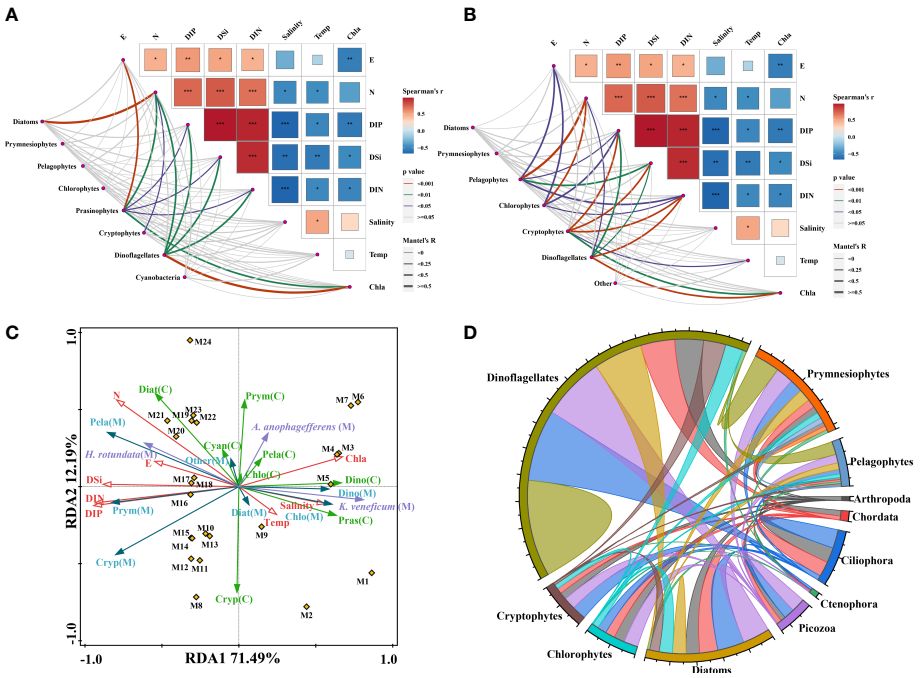

FIGURE 6
Comparisons of environmental factors and the major phytoplankton communities based on CHEMTAX **(A)** and metabarcoding analyses **(B)**. Redundancy analyses (RDA) of environmental factors (red) and phytoplankton communities by CHEMTAX (green), metabarcoding (blue), and abundant HAB-forming species (purple) **(C)**. Interaction networks between major phytoplankton OTUs with phytoplankton and the top five zooplankton **(D)**.

microscopic analyses. It was strange that prymnesiophytes were almost absent from the metabarcoding analyses, whereas they were abundant according to CHEMTAX (Figure 3A). Morphological analyses by SEM confirmed the existence of a large number of haptophyte (i.e., prymnesiophyte) cells in this area, as mentioned in previous studies (Taylor and Waters, 1982; Hattori et al., 2004; Komuro et al., 2005). The results of those studies revealed that *Coccolithus pelagicus* f. *pelagicus* and *Emiliania huxleyi* var. *huxleyi* were the most abundant taxa in the WSG and in the western subarctic Pacific. Our results and those from previous studies (Fujiki et al., 2009; Fujiki et al., 2014) showed that the content of Hex-Fuco (the marker pigment of prymnesiophytes) was the highest among all carotenoids. Furthermore, the results of *rbcL* gene analysis in the summer of 2020 showed that haptophytes were the most abundant phylum, accounting for approximately 30.80% of the total chromophytic phytoplankton in the same area (Jiang et al., 2022). In addition, prasinophytes accounted for 5% of phytoplankton by CHEMTAX, whereas those were not identified by metabarcoding. Similar to our results, prasinophytes made up an important component of phytoplankton biomass (7.5%–30.9%) by CHEMTAX in previous studies (Liu et al., 2004; Fujiki et al., 2009; Fujiki et al., 2014). Furthermore, the results of microscopic observations also showed that prasinophyte species, such as *Micromonas pusilla*, were abundant in the WSG (Taylor and Waters, 1982; Fujiki et al., 2009). Consequently, our results combined with those of previous studies (e.g., Taylor and Waters, 1982; Hattori et al., 2004; Liu et al., 2004; Komuro et al., 2005; Jiang et al., 2022) indicate that metabarcoding might underestimate the contribution of prymnesiophytes and prasinophytes to the total phytoplankton.

The comparison between metabarcoding and CHEMTAX was rarely reported; one study that performed this comparison was conducted by Gong et al. (2020), who revealed that 18S rRNA gene sequencing and CHEMTAX displayed similar compositions of phytoplankton communities in the Neuse River Estuary. The results of Gong et al. (2020) are strikingly different from those of this study, which might be ascribed to the difference in the phytoplankton communities between the two investigation areas. The eight phytoplankton assemblages derived from CHEMTAX accounted for 5%–25% of the total phytoplankton with no absolutely dominant groups in our results. Comparatively, the investigation area of Gong et al. (2020) was a eutrophic estuary, where chlorophytes (i.e., Trebouxiophyceae) were the dominant phytoplankton group based on CHEMTAX and 18S sequencing. The absolute dominance of Trebouxiophyceae could cause a good linear relationship between both methods, according to Gong et al. (2020). Nevertheless, a significant positive correlation of cryptophytes between the metabarcoding analyses and CHEMTAX was also observed in the present study (Figures 6A, B), and such correlation deserves further study.

In summary, some limitations and uncertainties of CHEMTAX and metabarcoding should be considered, because these could further help elucidate the discrepancy of the results from both methods. The factors affecting CHEMTAX calculation mainly included the following aspects. (1) The marker pigment/Chl *a* ratios of the local phytoplankton assemblages were largely unknown in the study area, which might greatly affect the results obtained, as the choice of the initial pigment ratio matrix is very important (Mackey et al., 1996). (2) It was not clear whether some dinoflagellate species contain Peridinin (the marker pigment of dinoflagellates) in this area. (3)

Several algal assemblages contained the same marker pigments. For example, fucoxanthin can be produced by diatoms, prymnesiophytes, and pelagophytes (Fujiki et al., 2014). Nevertheless, the HPLC-pigment CHEMTAX method still has broad application prospects because of its high efficiency, low cost, and strong comparability between different research results. For metabarcoding, some limitations cannot be ignored. The real biomass of different phytoplankton species or assemblages cannot be effectively quantified based on the absolute sequence abundance (Pochon et al., 2015). Variation in DNA copy number among algal species can lead to differential amplification in PCR and result in sequence read abundances that do not match species abundances. For example, experiments that used mock communities showed that the relative abundance obtained using high-throughput DNA sequencing differed significantly from that counted by microscopic analyses even in the same phytoplankton genus, such as *Skeletonema* (Canesi and Rynearson, 2016). Although metabarcoding analyses may misjudge the composition of different phytoplankton assemblages, it is effective for identifying the algal species composition (especially small-sized, rare, and cryptic species) in the phytoplankton community, as discussed in the following sections. Furthermore, this study strongly suggested that microscopic counting of phytoplankton abundance should be included in the future study. As the classical and most common technique, light microscopy can quantify and qualify phytoplankton communities, involving identification, cells counting, and size measurement (Pan et al., 2020), which is significant to verify the accuracy of phytoplankton species identification by molecular methods (Gong et al., 2020; Wang et al., 2022). However, microscopic still has many deficiencies in many aspects. For example, large phytoplankton (> 10 μm) can be identified and counted easily by light microscopy, which omits some small-sized phytoplankton assemblages (e.g., pico-phytoplankton and fragile cells) and cause an overestimation of diatom and dinoflagellate proportions to total phytoplankton (Pan et al., 2020; Wang et al., 2022). Each method has its own shortcomings, which requires the combination of various methods as far as possible to analyze the composition characteristics of phytoplankton in more detail.

4.2 Phytoplankton population structure with an emphasis on harmful algal bloom species based on metabarcoding sequencing

Dinoflagellates were the dominant phytoplankton assemblages in the study area, according to metabarcoding. Their abundance was comparable with those reported in temperate areas of the northwestern Pacific (Huang et al., 2020; Wu et al., 2020; Liu et al., 2022) and much lower than those in tropical regions, such as the South China Sea (Wang et al., 2022) and the Western Pacific seamount regions (Xu et al., 2021). By comparison, haptophytes were the minor component (0.53% of phytoplankton) in the WSG, but they occupied a relatively high proportion of phytoplankton in the South China Sea (Wang et al., 2022) and the temperate regions of the northwest Pacific controlled by the Kuroshio current (Wu et al., 2020). A high proportion of pelagophytes and cryptophytes was an important characteristic of the WSG when compared with previous studies (Huang et al., 2020; Wu et al., 2020; Xu et al., 2021). Environmental selection and dispersal limitation might be important factors that shape the phytoplankton communities in the subarctic area of this study, which was characterized by high macronutrients (i.e., N, P, and Si) and Fe deficiency (Suzuki et al., 2002; Harrison et al., 2004).

Our analyses identified 97 phytoplankton species, many of which were newly recorded in the WSG. For example, *K. veneficum*, *H. rotundata*, and *A. anophagefferens* were first reported and showed high contributions to total phytoplankton in this area. Those species were HAB-forming species. The other 13 HAB-forming species were rare but were also identified by metabarcoding analyses, which demonstrated the advantage of identifying HAB-forming species in the phytoplankton community.

Karlodinium is a mixotrophic dinoflagellate genus with several fish killing members. Mixotrophic characters make this genus grow relying on photosynthesis and/or by feeding on various tiny marine organisms, e.g., diatoms, dinoflagellates, and even zooplanktons (Place et al., 2012). This species is common in coastal sea areas but is easily overlooked or misidentified in microscopic analyses due to its small cell size (< 8–12 μm) and lack of obvious morphological characteristics (Huang et al., 2019; Huang et al., 2020). It is frequently present with relatively low cell abundance but can form intense blooms that are often associated with fish kills. Numerous mortality events of wild and cultured fish were found to be associated with *K. veneficum* blooms around the world (Huang et al., 2019; Karlson et al., 2021). The WSG and its adjacent waters are important fishing grounds for Pacific saury in the world. Consequently, more effort should be made to study the temporal and spatial distributions of the genus *Karlodinium* and its impact on marine animals in the WSG, which has shown a saury biomass decline in recent decades (Kulik et al., 2022).

H. rotundata is ubiquitously distributed in various marine environments and occasionally forms large blooms, e.g., in Manim Bay (Shahi et al., 2015), the Baltic Sea (Jaschinski et al., 2015), and Chesapeake Bay (Millette et al., 2015). It is nontoxic, although several *Heterocapsa* species, such as *H. circularisquama*, are toxic to marine animals (Sato et al., 2002). *H. rotundata* is mixotrophic and can ingest picoplankton, including bacteria (Millette et al., 2016); thus, it can outcompete other phytoplankton species in the WSG that suffer from Fe deficiency (Suzuki et al., 2002; Harrison et al., 2004).

Among the 16 HAB-forming species, *Alexandrium minutum*, *Dinophysis acuminata*, *Pseudonitzschia brasiliana*, and *P. turgidula* produce paralytic shellfish poisoning toxins (PSTs), diarrhetic shellfish poisoning toxins (DSTs), and domoic acid (DA), respectively (Lundholm et al., 2009; Lian et al., 2022). These toxins are known to accumulate in shellfish and fish and lead to human intoxication (Lian et al., 2022). The accurate identification of *Pseudonitzschia* species is difficult under light microscopy (Mochizuki et al., 2002; Jiang et al., 2017), but this can be resolved easily by metabarcoding (Wang et al., 2022). Three *Pseudonitzschia* species, including *P. brasiliana*, *P. turgidula*, and *P. subcurvata*, were identified in our results, among which the former two species can produce DA (Lundholm et al., 2009). The above toxic algal species show a wide distribution in the coastal waters of the world (Lundholm et al., 2009; Jiang et al., 2017; Wang et al., 2022) but are rarely observed in the WSG and subarctic Pacific in previous studies (e.g., Taylor and Waters, 1982; Mochizuki et al., 2002; Komuro et al., 2005).

Although the four species make up a small proportion of the total phytoplankton, the rare taxa could also act as seeds for seasonal succession or sporadic blooms (Logares et al., 2014). For example, toxic *A. tamarense* blooms were found in the Chukchi Sea of the Arctic Ocean. Increased temperatures might be an important factor in promoting the cell growth and cyst germination of toxic algal taxa, such as *Alexandrium* (Natsuike et al., 2017). With the intensification of global climate change (e.g., global warming and ocean acidification), these toxic algal species deserve attention because of their potential role in inducing blooms in subarctic sea areas (Lian et al., 2022).

4.3 Influence of environmental factors on the spatial distribution of phytoplankton assemblages

The investigation stations were divided into southern and northern regions along 44°N. Similarly, Favorite et al. (1976) defined that the Pacific Subarctic Gyres Province (PSAG) and the Transition Zone are divided by the temperature 4°C at 100 m depth. Combined with the temperature of 100m depth in 2021 (unpublished), this result is consistent with our classification. In the southern area, the physical and chemical parameters showed patchy distributions, suggesting the mixing process of the subarctic current and Kuroshio current. By comparison, environmental parameters presented a relatively uniform distribution in the northern area. Wu et al. (2020) showed that protistan composition fluctuated obviously among different sites in the mixed water region between the Kuroshio and Oyashio currents. Similarly, the phytoplankton composition of our results also varied among different stations and showed a significant difference between the southern and northern regions, suggesting that the mixing process of the Kuroshio and subarctic currents in the surface seawater played an important role in controlling the distribution of phytoplankton.

In this study, nutrients played an important role in shaping the distribution of phytoplankton assemblages, as shown by the Mantel test and RDA analyses (Figure 6C). Different algal species adapt to their optimal growth concentrations in the marine environment (Follows and Dutkiewicz, 2011; Pei et al., 2019). However, the relationship between phytoplankton assemblages, according to metabarcoding and CHEMTAX, and nutrients is different, mostly due to the discrepancy in phytoplankton composition by the two methods. Nevertheless, dinoflagellates determined by the two methods grouped together in the RDA analyses and showed a significantly negative correlation with nutrients (Figure 6C), which indicated that they could outcompete other algal assemblages in the southern region with low nutrient concentrations, presumably due to their mixotrophic characteristic. In contrast, pelagophytes, and cryptophytes, a significant correlation with nutrients was demonstrated by metabarcoding, whereas this trend was not observed by CHEMTAX. Although the two methods can analyze the composition characteristics of phytoplankton in detail, they easily lead to confusion in the analyses of the relationship between phytoplankton and environmental factors.

Numerous studies have shown that temperature and salinity have important impacts on community composition and diversity in the marine environment (Li et al., 2018; Wang et al., 2018; Wu et al., 2020). In this study, temperature and salinity were not significantly correlated with the phytoplankton assemblages, as analyzed by the Mantel test. Eddies at various scales (shown by the patchy distribution of temperature and salinity) in the transition domain caused by the mixing process of subarctic and subtropical waters lead to a heterogeneous phytoplankton distribution (Mochizuki et al., 2002), which might be the reason for the lack of a significant correlation between the two physical factors and phytoplankton. Notably, the two dominant species, *H. rotundata* and *K. veneficum*, showed significantly negative and positive correlations with temperature and salinity, respectively ($P < 0.05$; Figures 6A, B), indicating that they are in different ecological niches. Place et al. (2012) suggest that *K. veneficum* blooms are caused by eutrophic environments and/or co-occurrence of cryptophytes and *K. veneficum*, which were not observed in this study.

Some complex chemical and biological factors also influence the distribution of various phytoplankton assemblages, such as the input of Fe from atmospheric deposition in Fe-deficient areas (Boyd and Ellwood, 2010) and top-down control of zooplankton (Liu et al., 2022). Atmospheric deposition has been suggested as an important source of Fe to these regions (Boyd and Ellwood, 2010). Episode supplies of aeolian dust containing Fe from central Asia were possible reasons for the sporadic phytoplankton blooms in the WSG (Liu et al., 2004). The dust storms in central Asia in the spring of 2021 are the strongest in the past 10 years. For example, between 6 and 24 May (during the early stage of this investigation), three dust storms in Central Asia seriously affected the eastern coastal provinces of China, although no data are available in the sea (China Meteorological Administration, 2022). Tang et al. (2022) showed that the center of the spring dust storm reached the northwest Pacific at latitudes between 30° and 40°, which was south of our study area. The atmospheric deposition of nutrients, especially Fe, might be the main factor for the high phytoplankton biomass (i.e., Chl *a*) in the southern region of the study area (Figure S1). Moreover, most phytoplankton and zooplankton groups had more correlations than connections within phytoplankton groups (Figure 6D), suggesting that zooplankton assemblages had an important impact on the distribution of phytoplankton assemblages. Overall, the relationship between phytoplankton and environmental factors seems to be cloaked by the above uncertainties and the relatively small span of latitude and longitude in our study area. More research is needed to investigate the relationship among phytoplankton, zooplankton, and physical and chemical factors in such complex marine ecosystems.

5 Conclusion

The structure of phytoplankton communities determined by HPLC-pigment CHEMTAX and metabarcoding analyses displayed marked differences for some phytoplankton assemblages in the study area. Determining which method gives more accurate results is difficult, because each method has led to some uncertainties. Although CHEMTAX can only give the composition of phytoplankton groups, we strongly suggest that this method be

applied widely in WSG to investigate the long-term succession of phytoplankton community structure, as it has been used for this purpose for several decades. By comparison, metabarcoding provides a more informative assessment of phytoplankton species and better elucidates their responses to environmental conditions than the CHEMTAX method. For example, some toxic and HAB-forming species that have not been reported in previous studies were identified in the WSG. This study highlights the benefits of the combination of CHEMTAX and metabarcoding analyses in determining the phytoplankton communities in a marine environment, especially in open seas such as the subarctic North Pacific.

Data availability statement

The datasets presented in this study can be found in online repositories. The names of the repository/repositories and accession number(s) can be found in the article/Supplementary Material.

Author contributions

QX: Conceptualization, Methodology, Software, Writing – original draft. GW: Software, Writing, Data curation. XQ: Methodology, Software, Investigation, Writing – original draft. XD: Methodology, Resources, Writing – review & editing, Data curation. XW: Validation, Formal analysis, Visualiza- tion. QH: Software, Investigation, Writing – review & editing. CM: Methodology, Resources, Writing – review & editing, Data curation. YW: Methodology, Resources. JC: Methodology, Writing – review & editing. All authors contributed to the article and approved the submitted version.

Funding

This study was funded by the National Key Research and Development Program of China (2019YFD0901401), Natural Science Foundation of Shandong Province (ZR2021MD071).

Conflict of interest

The authors declare that the research was conducted in the absence of any commercial or financial relationships that could be construed as a potential conflict of interest.

Publisher's note

All claims expressed in this article are solely those of the authors and do not necessarily represent those of their affiliated organizations, or those of the publisher, the editors and the reviewers. Any product that may be evaluated in this article, or claim that may be made by its manufacturer, is not guaranteed or endorsed by the publisher.

Supplementary material

The Supplementary Material for this article can be found online at: https://www.frontiersin.org/articles/10.3389/fmars.2023.1116050/full#supplementary-material

References

Bik, H. M., Porazinska, D. L., Creer, S., Caporaso, J. G., Knight, R., and Thomas, W. K. (2012). Sequencing our way towards understanding global eukaryotic biodiversity. *Trends Ecol. Evol.* 27, 233–243. doi: 10.1016/j.tree.2011.11.010

Boyd, P., and Ellwood, M. (2010). The biogeochemical cycle of iron in the ocean. *Nat. Geosci.* 3, 675–682. doi: 10.1038/ngeo964

Canesi, K., and Rynearson, T. (2016). Temporal variation of skeletonema community composition from a long-term time series in Narragansett bay identified using high-throughput sequencing. *Mar. Ecol. Prog. Ser.* 556, 1–16. doi: 10.3354/meps11843

Chen, S., Zhou, Y., Chen, Y., and Gu, J. (2018). Fastp: an ultra-fast all-in-one FASTQ preprocessor. *Bioinformatics* 34, i884–i890. doi: 10.1093/bioinformatics/bty560

China Meteorological Administration. (2022). *China Meteorological Administration China Climate Bulletin in 2021*. Meteorological Press, Beijing.

Edgar, R. C. (2013). UPARSE: highly accurate OTU sequences from microbial amplicon reads. *Nat. Methods* 10, 996–998. doi: 10.1038/nmeth.2604

Favorite, F., Dodimead, A., and Nasu, K. (1976). Oceanography of the subarctic pacific region 1960–1971. *Bull. Int. North Pac. Fish. Comm.* 33, 1–187.

Follows, M., and Dutkiewicz, S. (2011). Modeling diverse communities of marine microbes. *Annu. Rev. Mar. Sci.* 3, 427–451. doi: 10.1146/annurev-marine-120709-142848

Fujiki, T., Matsumoto, K., Honda, M. C., Kawakami, H., and Watanabe, S. (2009). Phytoplankton composition in the subarctic north pacific during autumn 2005. *J. Plankton Res.* 31, 179–191. doi: 10.1093/plankt/fbn108

Fujiki, T., Matsumoto, K., Mino, Y., Sasaoka, K., Wakita, M., Kawakami, H., et al. (2014). Seasonal cycle of phytoplankton community structure and photophysiological state in the western subarctic gyre of the north pacific. *Limnol. Oceanogr.* 59, 887–900. doi: 10.4319/lo.2014.59.3.0887

Gong, W., Hall, N., Paerl, H., and Marchetti, A. (2020). Phytoplankton composition in a eutrophic estuary: Comparison of multiple taxonomic approaches and influence of environmental factors. *Environ. Microbiol.* 22, 4718–4731. doi: 10.1111/1462-2920.15221

Gong, W., and Marchetti, A. (2019). Estimation of 18S gene copy number in marine eukaryotic plankton using a next-generation sequencing approach. *Front. Mar. Sci.* 6. doi: 10.3389/fmars.2019.00219

Gu, Z., Gu, L., Eils, R., Schlesner, M., and Brors, B. (2014). Circlize implements and enhances circular visualization in r. *Bioinformatics* 30, 2811–2812. doi: 10.1093/bioinformatics/btu393

Harrison, P., Whitney, F., Tsuda, A., Saito, H., and Tadokoro, K. (2004). Nutrient and plankton dynamics in the NE and NW gyres of the subarctic pacific ocean. *J. Oceanogr.* 60, 93–117. doi: 10.1023/B:JOCE.0000038321.57391.2a

Hattori, H., Koike, M., Tachikawa, K., Saito, H., and Nagasawa, K. (2004). Spatial variability of living coccolithophore distribution in the Western subarctic pacific and Western Bering Sea. *J. Oceanogr.* 60, 505–515. doi: 10.1023/B:JOCE.0000038063.81738.ab

Huang, B., Liang, Y., Pan, H., Xie, L., Jiang, T., and Jiang, T. (2020). Hemolytic and cytotoxic activity from cultures of aureococcus anophagefferens–a causative species of brown tides in the north-western bohai Sea, China. *Chemosphere* 247, 125819. doi: 10.1016/j.chemosphere.2020.125819

Huang, H.-L., Shao, Q.-W., Zhu, X.-J., Luo, J., Meng, R., Zhou, C.-X., et al. (2019). Distribution of karlodinium veneficum in the coastal region of xiangshan bay in the East China Sea, as detected by a real-time quantitative PCR assay of ribosomal ITS sequence. *Harmful Algae* 81, 65–76. doi: 10.1016/j.hal.2018.12.001

Imai, K., Nojiri, Y., Tsurushima, N., and Saino, T. (2002). Time series of seasonal variation of primary productivity at station KNOT (44°N, 155°E) in the sub-arctic western north pacific. *Deep Sea Res. Part II: Topic. Stud. Oceanogr.* 49, 5395–5408. doi: 10.1016/S0967-0645(02)00198-4

Jaschinski, S., Flöder, S., Petenati, T., and Göbel, J. (2015). Effects of nitrogen concentration on the taxonomic and functional structure of phytoplankton communities in the Western Baltic Sea and implications for the European water framework directive. *Hydrobiologia* 745, 201–210. doi: 10.1007/s10750-014-2109-9

Jiang, T., Liu, L., Li, Y., Zhang, J., Tan, Z., Wu, H., et al. (2017). Occurrence of marine algal toxins in oyster and phytoplankton samples in daya bay, south China Sea. *Chemosphere* 183, 80–88. doi: 10.1016/j.chemosphere.2017.05.067

Jiang, T., Qin, X., Wu, G., Zhao, H., Yu, X., Xiao, X., et al. (2022) Distribution of chromophytic phytoplankton in the Western subarctic gyre of pacific ocean revealed by morphological observation and rbcL gene sequences. *J. Oceanol. Limnol.* doi: 10.1007/s00343-022-2197-8

Karlson, B., Andersen, P., Arneborg, L., Cembella, A., Eikrem, W., John, U., et al. (2021). Harmful algal blooms and their effects in coastal seas of northern Europe. *Harmful Algae* 102, 101989. doi: 10.1016/j.hal.2021.101989

Komuro, C., Narita, H., Imai, K., Nojiri, Y., and Jordan, R. W. (2005). Microplankton assemblages at station KNOT in the subarctic western pacific 1999–2000. *Deep Sea Res. Part II: Topic. Stud. Oceanogr.* 52, 2206–2217. doi: 10.1016/j.dsr2.2005.08.006

Kulik, V. V., Prants, S. V., Uleysky, M., Uleysky, M. Y., and Budyansky, M. V. (2022). Lagrangian Characteristics in the western north pacific help to explain variability in pacific saury fishery. *Fish. Res.* 252, 106361. doi: 10.1016/j.fishres.2022.106361

Kwak, J. H., Lee, S. H., Hwang, J., Suh, Y.-S., Je Park, H., Chang, K.-I., et al. (2014). Summer primary productivity and phytoplankton community composition driven by different hydrographic structures in the East/Japan Sea and the Western subarctic pacific. *J. Geophys. Res.: Oceans* 119, 4505–4519. doi: 10.1002/2014JC009874

Lear, G., Dickie, I., Banks, J. C., Boyer, S., Buckley, H. L., Buckley, T. R., et al. (2018) Methods for the extraction, storage, amplification and sequencing of DNA from environmental samples. *New Z. J. Ecol.* 42, 10–50A. doi: 10.20417/nzjecol.42.9

Lian, Z., Li, F., He, X., Chen, J., and Yu, R.-C. (2022). Rising CO2 will increase toxicity of marine dinoflagellate alexandrium minutum. *J. Hazard. Mater.* 431, 128627. doi: 10.1016/j.jhazmat.2022.128627

Li, Y.-Y., Chen, X.-H., Xie, Z.-X., Li, D.-X., Wu, P.-F., Kong, L.-F., et al. (2018). Bacterial diversity and nitrogen utilization strategies in the upper layer of the northwestern pacific ocean. *Front. Microbiol.* 9. doi: 10.3389/fmicb.2018.00797

Li, C., Liu, J., Chen, X., Ren, H., Su, B., Ma, K., et al. (2022). Determinism governs the succession of disturbed bacterioplankton communities in a coastal maricultural ecosystem. *Sci. Total Environ.* 828, 154457. doi: 10.1016/j.scitotenv.2022.154457

Lin, S. (2011). Genomic understanding of dinoflagellates. *Res. Microbiol.* 162, 551–569. doi: 10.1016/j.resmic.2011.04.006

Liu, S., Cui, Z., Zhao, Y., and Chen, N. (2022). Composition and spatial-temporal dynamics of phytoplankton community shaped by environmental selection and interactions in the jiaozhou bay. *Water Res.* 218, 118488. doi: 10.1016/j.watres.2022.118488

Liu, H., Suzuki, K., and Saito, H. (2004). Community structure and dynamics of phytoplankton in the Western subarctic pacific ocean: A synthesis. *J. Oceanogr.* 60, 119–137. doi: 10.1023/B:JOCE.0000038322.79644.36

Logares, R., Audic, S., Bass, D., Bittner, L., Boutte, C., Christen, R., et al. (2014). Patterns of rare and abundant marine microbial eukaryotes. *Curr. Biol.* 24, 813–821. doi: 10.1016/j.cub.2014.02.050

Lundholm, N., Churro, C., Fraga, S., Hoppenrath, M., Iwataki, M., Larsen, J., et al. (2009) *IOC-UNESCO taxonomic reference list of harmful micro algae*. Available at: https://www.marinespecies.org/hab.

Mackey, M., Mackey, D., Higgins, H., and Wright, S. (1996). CHEMTAX - a program for estimating class abundances from chemical markers: Application to HPLC measurements of phytoplankton. *Mar. Ecol. - Prog. Ser.* 144, 265–283. doi: 10.3354/meps144265

Magoč, T., and Salzberg, S. L. (2011). FLASH: fast length adjustment of short reads to improve genome assemblies. *Bioinformatics* 27, 2957–2963. doi: 10.1093/bioinformatics/btr507

Millette, N. C., Pierson, J. J., Aceves, A., and Stoecker, D. K. (2016). Mixotrophy in heterocapsa rotundata: A mechanism for dominating the winter phytoplankton: Mixotrophy in heterocapsa rotundata. *Limnol. Oceanogr.* 62, 836–845. doi: 10.1002/lno.10470

Millette, N., Stoecker, D., and Pierson, J. (2015). Top-down control of micro- and mesozooplankton on winter dinoflagellate blooms of heterocapsa rotundata. *Aquat. Microb. Ecol.* 76, 15–25. doi: 10.3354/ame01763

Mochizuki, M., Shiga, N., Saito, M., Imai, K., and Nojiri, Y. (2002). Seasonal changes in nutrients, chlorophyll a and the phytoplankton assemblage of the western subarctic gyre in the pacific ocean. *Deep Sea Res. Part II: Topic. Stud. Oceanogr.* 49, 5421–5439. doi: 10.1016/S0967-0645(02)00209-6

Natsuike, M., Matsuno, K., Hirawake, T., Yamaguchi, A., Nishino, S., and Imai, I. (2017). Possible spreading of toxic alexandrium tamarense blooms on the chukchi Sea shelf with the inflow of pacific summer water due to climatic warming. *Harmful Algae* 61, 80–86. doi: 10.1016/j.hal.2016.11.019

Obayashi, Y., Tanoue, E., Suzuki, K., Handa, N., Nojiri, Y., and Wong, C. (2001). Spatial and temporal variabilities of phytoplankton community structure in the northern north pacific as determined by phytoplankton pigments. *Deep-sea Res. Part I-oceanogr. Res. Pap. - DEEP-SEA Res. PT. I-OCEANOG. Res.* 48, 439–469. doi: 10.1016/S0967-0637(00)00036-4

Paerl, H. W., Crosswell, J. R., Van Dam, B., Hall, N. S., Rossignol, K. L., Osburn, C. L., et al. (2018). Two decades of tropical cyclone impacts on north carolina's estuarine carbon, nutrient and phytoplankton dynamics: implications for biogeochemical cycling and water quality in a stormier world. *Biogeochemistry* 141, 307–332. doi: 10.1007/s10533-018-0438-x

Pan, H., Li, A., Cui, Z., Ding, D., Qu, K., Zheng, Y., et al. (2020). A comparative study of phytoplankton community structure and biomass determined by HPLC-CHEMTAX and microscopic methods during summer and autumn in the central bohai Sea, China. *Mar. pollut. Bull.* 155, 111172. doi: 10.1016/j.marpolbul.2020.111172

Pei, S., Laws, E. A., Zhu, Y., Zhang, H., Ye, S., Yuan, H., et al. (2019). Nutrient dynamics and their interaction with phytoplankton growth during autumn in liaodong bay, China. *Continent. Shelf Res.* 186, 34–47. doi: 10.1016/j.csr.2019.07.012

Place, A. R., Bowers, H. A., Bachvaroff, T. R., Adolf, J. E., Deeds, J. R., and Sheng, J. (2012). Karlodinium veneficum–the little dinoflagellate with a big bite. *Harmful Algae* 14, 179–195. doi: 10.1016/j.hal.2011.10.021

Pochon, X., Wood, S. A., Keeley, N. B., Lejzerowicz, F., Esling, P., Drew, J., et al. (2015). Accurate assessment of the impact of salmon farming on benthic sediment enrichment using foraminiferal metabarcoding. *Mar. pollut. Bull.* 100, 370–382. doi: 10.1016/j.marpolbul.2015.08.022

Sato, Y., Oda, T., Muramatsu, T., Matsuyama, Y., and Honjo, T. (2002). Photosensitizing hemolytic toxin in heterocapsa circularisquama, a newly identified harmful red tide dinoflagellate. *Aquat. Toxicol. (Amsterdam Netherlands)* 56, 191–196. doi: 10.1016/S0166-445X(01)00191-6

Shahi, N., Godhe, A., Mallik, S., Aloisi, K., and Nayak, B. (2015). The relationship between variation of phytoplankton species composition and physico-chemical parameters in northern coastal waters of Mumbai, India. *Indian Journal of Geo-Marine Sciences* 44, 673–684.

Stoeck, T., Bass, D., Nebel, M., Christen, R., Jones, M. D. M., Breiner, H.-W., et al. (2010). Multiple marker parallel tag environmental DNA sequencing reveals a highly complex eukaryotic community in marine anoxic water. *Mol. Ecol.* 19, 21–31. doi: 10.1111/j.1365-294X.2009.04480.x

Strickland, J. D. H., and Parsons, T. R.. (1972). A practical handbook of seawater analysis. *Bulletin*. doi: 10.1086/406210

Sunagawa, S., Coelho, L. P., Chaffron, S., Kultima, J. R., Labadie, K., Salazar, G., et al. (2015). Structure and function of the global ocean microbiome. *Science* 348, 1261359. doi: 10.1126/science.1261359

Suzuki, K., Minami, C., Liu, H., and Saino, T. (2002). Temporal and spatial patterns of chemotaxonomic algal pigments in the subarctic pacific and the Bering Sea during the early summer of 1999. *Deep Sea Res. Part II: Topic. Stud. Oceanogr.* 49, 5685–5704. doi: 10.1016/S0967-0645(02)00218-7

Tang, W., Dai, T., Cheng, Y., Wang, S., and Liu, Y. (2022). A study of a severe spring dust event in 2021 over East Asia with WRF-chem and multiple platforms of observations. *Remote Sens.* 14, 3795. doi: 10.3390/rs14153795

Taylor, F. J. R., and Waters, R. E. (1982). Spring phytoplankton in the subarctic north pacific ocean. *Mar. Biol.* 67, 323–335. doi: 10.1007/BF00397673

Villar, E., Farrant, G. K., Follows, M., Garczarek, L., Speich, S., Audic, S., et al. (2015). Environmental characteristics of agulhas rings affect interocean plankton transport. *Science* 348, 1261447. doi: 10.1126/science.1261447

Waga, H., Fujiwara, A., Hirawake, T., Suzuki, K., Yoshida, K., Abe, H., et al. (2022). Primary productivity and phytoplankton community structure in surface waters of the western subarctic pacific and the Bering Sea during summer with reference to bloom stages. *Prog. Oceanogr.* 201, 102738. doi: 10.1016/j.pocean.2021.102738

Wang, Q., Garrity, G. M., Tiedje, J. M., and Cole, J. R. (2007). Naive Bayesian classifier for rapid assignment of rRNA sequences into the new bacterial taxonomy. *Appl. Environ. Microbiol.* 73, 5261–5267. doi: 10.1128/AEM.00062-07

Wang, Z., Liu, L., Tang, Y., Li, A., Liu, C., Xie, C., et al. (2022). Phytoplankton community and HAB species in the south China Sea detected by morphological and metabarcoding approaches. *Harmful Algae* 118, 102297. doi: 10.1016/j.hal.2022.102297

Wang, F., Xie, Y., Wu, W., Sun, P., Wang, L., and Huang, B. (2018). Picoeukaryotic diversity and activity in the northwestern pacific ocean based on rDNA and rRNA high-throughput sequencing. *Front. Microbiol.* 9. doi: 10.3389/fmicb.2018.03259

Wickham, H. (2016). *ggplot2: Elegant graphics for data analysis* (New York: Springer-Verlag). Available at: https://ggplot2.tidyverse.org.

Wright, S. W., Ishikawa, A., Marchant, H. J., Davidson, A. T., van den Enden, R. L., and Nash, G. V. (2009). Composition and significance of picophytoplankton in Antarctic waters. *Polar Biol.* 32, 797–808. doi: 10.1007/s00300-009-0582-9

Wu, P.-F., Li, D.-X., Kong, L.-F., Li, Y.-Y., Zhang, H., Xie, Z.-X., et al. (2020). The diversity and biogeography of microeukaryotes in the euphotic zone of the northwestern pacific ocean. *Sci. Total Environ.* 698, 134289. doi: 10.1016/j.scitotenv.2019.134289

Xu, Q., Wang, C., Xu, K., and Chen, N. (2021). Metabarcoding analysis of harmful algal bloom species in the Western pacific seamount regions. *Int. J. Environ. Res. Public Health* 18, 11470. doi: 10.3390/ijerph182111470

Zapata, M., Jeffrey, S., Wright, S., Rodríguez, F., Garrido, J., and Clementson, L. (2004). Photosynthetic pigments in 37 species (65 strains) of haptophyta. *Mar. Ecol.-Prog. Ser.* 270, 83–102. doi: 10.3354/meps270083

Zhang, T., Xu, S., Yan, R., Wang, R., Gao, Y., Kong, M., et al. (2022). Similar geographic patterns but distinct assembly processes of abundant and rare bacterioplankton communities in river networks of the taihu basin. *Water Res.* 211, 118057. doi: 10.1016/j.watres.2022.118057

frontiers | Frontiers in Marine Science

TYPE Original Research
PUBLISHED 26 May 2023
DOI 10.3389/fmars.2023.1127871

OPEN ACCESS

EDITED BY
Zhangxi Hu,
Guangdong Ocean University, China

REVIEWED BY
Ning Xu,
Jinan University, China
Allan Douglas Cembella,
Alfred Wegener Institute Helmholtz Centre for Polar and Marine Research (AWI), Germany

*CORRESPONDENCE
Wai Mun Lum
lumwaimun@gmail.com
Mitsunori Iwataki
iwataki@g.ecc.u-tokyo.ac.jp

†PRESENT ADDRESS
Wai Mun Lum,
Fisheries Technology Institute, Japan Fisheries Research and Education Agency, Fukuura, Kanagawa, Japan

RECEIVED 20 December 2022
ACCEPTED 09 May 2023
PUBLISHED 26 May 2023

CITATION
Lum WM, Sakamoto S, Yuasa K, Takahashi K, Kuwata K, Kodama T, Katayama T, Leaw CP, Lim PT, Takahashi K and Iwataki M (2023) Comparative effects of temperature and salinity on growth of four harmful *Chattonella* spp. (Raphidophyceae) from tropical Asian waters.
Front. Mar. Sci. 10:1127871.
doi: 10.3389/fmars.2023.1127871

Comparative effects of temperature and salinity on growth of four harmful *Chattonella* spp. (Raphidophyceae) from tropical Asian waters

Wai Mun Lum[1*†], Setsuko Sakamoto[2], Koki Yuasa[2], Kazuya Takahashi[1], Koyo Kuwata[1], Taketoshi Kodama[1], Tomoyo Katayama[1], Chui Pin Leaw[3], Po Teen Lim[3], Kazutaka Takahashi[1] and Mitsunori Iwataki[1*]

[1]Graduate School of Agricultural and Life Sciences, University of Tokyo, Tokyo, Japan, [2]Fisheries Technology Institute, Japan Fisheries Research and Education Agency, Hatsukaichi, Japan, [3]Bachok Marine Research Station, Institute of Ocean and Earth Sciences, University of Malaya, Bachok, Malaysia

In Asia, four harmful raphidophyte species, *Chattonella malayana*, *C. marina*, *C. subsalsa*, and *C. tenuiplastida*, coexist in the tropical waters but only *C. marina* was detected in temperate waters. This occurrence pattern pointed to a potentially distinct ecophysiological niche occupancy and possible species dispersion. The growth physiology of these species isolated from tropical Southeast Asia was investigated using unialgal cultures in ten temperatures (13.0–35.5°C) and five salinities (15–35) to better understand the factors driving their distribution. The highest maximum specific growth rates were observed in *C. subsalsa* (0.65 ± 0.01 d^{-1}), followed by *C. malayana* (0.47 ± 0.03 d^{-1}), *C. marina* (0.45 ± 0.02 d^{-1}), and *C. tenuiplastida* (0.39 ± 0.01 d^{-1}). Their optimal temperatures were 28.0, 30.5, 25.5, and 30.5°C, respectively, of which *C. marina* preferred colder water. *C. subsalsa* exhibited a wider growth temperature range (20.5–35.5°C), followed by *C. marina* (20.5–30.5°C), *C. tenuiplastida* (23.0–33.0°C), and *C. malayana* (25.5–33.0°C). Optimal salinities were similar between *C. subsalsa* and *C. malayana* (30), and between *C. marina* and *C. tenuiplastida* (25), but *C. subsalsa* and *C. marina* exhibited a similar growth salinity range of 15–35, while *C. malayana* and *C. tenuiplastida* was 20–35. High values of F_v/F_m were observed in *C. subsalsa* and *C. marina* (> 0.5) in all tested conditions, but F_v/F_m of *C. malayana* and *C. tenuiplastida* were significantly lower at 20.5°C. All four species achieved a maximum cell density of > 10^4 cells mL^{-1} in their optimal conditions. Optimal temperatures in *C. subsalsa* and *C. marina* were identical to previous reports. The high adaptability of *C. subsalsa* in various temperatures and salinities suggests its high competitiveness and bloom potential. The high adaptability of *C. marina* in colder waters compared to other species likely contributes to its wide distribution in the temperate Asian

waters. The narrow temperature window of *C. malayana* and *C. tenuiplastida* suggests their endemicity and limited distribution in the tropical waters. This study provides evidence about the occurrences and bloom potential of *Chattonella* spp. in Asia, but the endemicity versus dispersion issue remains unresolved.

KEYWORDS

bloom potential, endemicity, harmful algae, adaptive ecology, algal growth, Fv/Fm, specific growth rate, Southeast Asia (SEA)

1 Introduction

Global warming has been perceived as a factor in the geographical expansion, intensification, and earlier timing of harmful algal blooms (HABs), especially along the coasts of tropical, subtropical, and temperate countries (Hallegraeff, 2010; Fu et al., 2012; Anderson et al., 2021; Sakamoto et al., 2021). In Southeast Asia, harmful algae are commonly found and records of HABs have been increasing (Maclean, 1984; Edvardsen and Imai, 2006; Lim et al., 2012; Azanza et al., 2017; Furuya et al., 2018; Mohammad-Noor et al., 2018; Yñiguez et al., 2021). Some of these HABs species were newly discovered in the region, and likely were introduced by anthropogenic transport or due to the adaptive strategies in the changing environment. The harmful dinoflagellate *Cochlodinium* Schütt (= *Margalefidinium* Gómez, Richlen et Anderson) is a case in point, blooms of the species have been discovered in Indonesia, Malaysia, and Philippines (Iwataki et al., 2007; Anton et al., 2008; Azanza et al., 2008; Iwataki et al., 2008; Iwataki et al., 2015); other example species are harmful raphidophytes *Chattonella* Biecheler and *Heterosigma akashiwo* (Hada) Hada ex Hara et Chihara that have been found in Indonesia, Malaysia, and Thailand (Lirdwitayaprasit et al., 1996; Gin et al., 2006; Ayu-Lana-Nafisyah et al., 2018). It is difficult to trace the origin of these HABs species due to a lack of reliable knowledge of their previous distributions, but studies have shown that they can adapt to various environments, e.g., the raphidophyte *H. akashiwo* was first detected in the USA (Hulburt, 1965), but later has been detected in Japan (Hada, 1967; Hada, 1968; Hara and Chihara, 1987), UK (Leadbeater, 1969), Norway (Throndsen, 1969), Russia and Arctic waters (Konalova, 1995; Ratkova and Wassmann, 2005; Engesmo et al., 2016). The successive adaptation of HAB species could be attributed to favorable environmental conditions such as temperature, salinity, and cyst formation ability (Marshall and Hallegraeff, 1999; Smayda, 2002; Mehnert et al., 2010; Thomas et al., 2012; Boyd et al., 2013).

The raphidophyte *Chattonella* is one of the noxious microalgae that has caused mass mortalities of coastal marine organisms, particularly farmed fish (Imai and Yamaguchi, 2012; Viana et al., 2019; Sakamoto et al., 2021; Lum et al., 2022). Recently, the wide distribution of *Chattonella* and associated fisheries damages have been clarified in the ten countries of Southeast Asia (Edvardsen and Imai, 2006; Lum et al., 2019; Lum et al., 2021; Lum et al., 2022). Moreover, recent phylogeographic studies have revealed the presence of four *Chattonella* species in Southeast Asia, including *C. subsalsa* Biecheler, *C. marina* (as the *C. marina* complex including *C. antiqua* (Hada) Ono, *C. marina*, and *C. ovata* Hara et Chihara), and two newly described species, *C. malayana* W.M. Lum, H.C. Lim, S.T. Teng, K. Takahashi, Leaw, P.T. Lim et Iwataki, and *C. tenuiplastida* W.M. Lum, H.C. Lim, K. Takahashi, S.T. Teng, Benico et Iwataki (Bowers et al., 2006; Ayu-Lana-Nafisyah et al., 2018; Lum et al., 2019; Lum et al., 2021; Lum et al., 2022). As physiological responses can vary among species, strains, and populations, the coexistence and interaction between these four *Chattonella* species arouse scientific interest in their ecophysiological traits because each may have a distinct environmental adaptability and different dispersion background (Marshall and Hallegraeff, 1999; Band-Schmidt et al., 2012; Viana et al., 2019). Furthermore, while the bloom of *C. malayana* had caused wild fish kills in Malaysia in 2016, and the distribution of *C. subsalsa* coincided with the locations where fish kills have been reported, the environmental parameters promoting their blooms have not been identified (Lum et al., 2021; Lum et al., 2022).

In situ population dynamics of HABs species are difficult to be understood without long-term observation data in specific habitats or regions, as such, data from laboratory-based growth experiments are essential to understand the effects of environmental parameters on their occurrence patterns and blooms, including *Chattonella* (Fu et al., 2012; Wells et al., 2015). Due to difficulties in the *in situ* growth rate assessment, the growth characteristics of *Chattonella* have been commonly elucidated by laboratory experiments using single or multiple unialgal culture strains under the effects of temperature, salinity, irradiance, and nutrient concentrations, i.e., *C. subsalsa* from Brazil and USA (Zhang et al., 2006; Viana et al., 2019), and *C. marina* complex (hereinafter referred to as *C. marina*) from Australia (Marshall and Hallegraeff, 1999), Japan (e.g., Nakamura and Watanabe, 1983), Korea (Lim et al., 2020), and Mexico (Band-Schmidt et al., 2012). Among these environmental parameters, temperature and salinity are two major factors in promoting/demoting the growth of *Chattonella* (Nakamura and Watanabe, 1983; Yamaguchi et al., 1991; Noh et al., 2006a; Noh et al., 2006b; Yamatogi et al., 2006; Zhang et al., 2006; Salvitti, 2010). *Chattonella marina* from different localities in Japan grew in a similar temperature range of 15–30°C (optimum 25°C), but with a slightly different salinity range of 15–35 (Yamaguchi et al., 1991;

Khan et al., 1995). On a wider scale, a similar response against temperatures was observed in *C. marina* from Australia, Japan, and Korea, but they had different optimal salinities (Yamaguchi et al., 1991; Kahn et al., 1998; Marshall and Hallegraeff, 1999; Noh et al., 2006a; Noh et al., 2006b). *Chattonella subsalsa* from the USA had a wider temperature range of 10–30°C (optimum 30°C) and salinity range of 5–30 (optimum 25) for growth while the same species from Brazil had an optimal salinity of 30 (Zhang et al., 2006; Viana et al., 2019).

In Southeast Asia, there was limited studies investigating the growth characteristics of *Chattonella*, further, past studies demonstrated inconsistent conclusions (Lee, 2014; Ayu-Lana-Nafisyah et al., 2018). Lee (2014) reported *C. marina* from Sarawak, Malaysia (strain CtSb02, reported as *C. subsalsa* without molecular characterization, see Lum et al., 2022) had an optimal growth at salinity 25, which was similar to those in the temperate waters. However, Ayu-Lana-Nafisyah et al. (2018) revealed that *C. marina* from a mangrove area in Indonesia had a lower optimal salinity of 15. Whether the unique salinity preference of *C. marina* in Indonesia was a strain-specific, species-specific, or ecotypic adaptation in tropical Asian waters remains unclear. The growth characteristics of *C. marina* and other *Chattonella* species in tropical waters, including *C. subsalsa* and the two new *Chattonella* species recently described from Southeast Asia (*C. tenuiplastida* and *C. malayana*), need to be investigated and clarified to further understand the effects of the abiotic factors on their occurrence patterns and bloom dynamics. This study compared the growth responses of single unialgal cultures of the four *Chattonella* species in various temperatures and salinities to achieve the following objectives: (1) to provide baseline growth information of *Chattonella* spp. in tropical waters, (2) to recognize the ecophysiological niches (growth temperature/salinity ranges) of these *Chattonella* species, and (3) to determine their optimal temperature and/or salinity that may contribute to the formation of HABs in this region. The ecophysiological comparison in this study may reveal the bloom potentials of *Chattonella* spp. in each respective temperature and salinity and help to specify the factors promoting their blooms in the natural environment.

2 Materials and methods

2.1 Algal cultures

All *Chattonella* cultures were previously established by Lum et al. (2021; 2022). from Southeast Asia. One representative strain of *C. malayana*, *C. marina*, *C. subsalsa*, and *C. tenuiplastida* was selected (Table 1). They were grown in IMK medium (Wako, Tokyo, Japan), made up of 0.22 µm filter-sterilized, nutrient-depleted aged oceanic seawater pre-adjusted to a salinity of 30. The cultures were maintained at 23.0°C, a light intensity of 70–100 μmol photons m^{-2} s^{-1} of cool, white fluorescent light under a 12:12 h light: dark cycle regime. Note that cultures used in the growth experiments were not axenic, but culture vessels and media were sterilized by autoclaving at 120°C for 15 min, and inoculation was operated aseptically in a laminar flow cabinet.

2.2 Temperature experiment

The temperature experiment was performed in ten temperature treatments, i.e., 13.0, 15.5, 18.0, 20.5, 23.0, 25.5, 28.0, 30.5, 33.0, and 35.5°C (Yamatogi et al., 2006; Sakamoto et al., 2009). Cells of each strain were inoculated into 50 mL culture flasks with filtered caps (Sumitomo Bakelite, Tokyo, Japan) containing IMK medium prepared from aged offshore seawater pre-adjusted to a salinity of 30 by distilled water. The experiment was conducted at a light intensity of 220 μmol photons m^{-2} s^{-1} under a 12:12 h light: dark photocycle. Before the experiment, cells were pre-acclimatized to the targeted temperatures at a rate of ± 2.5°C every two days, starting from 23.0°C. After the acclimatization, an inoculum was transferred to a 50 mL fresh medium to make up for 100 ± 50 cells mL^{-1} initial cell densities for each flask. The experiment was performed in triplicate for each strain at each temperature treatment for a growth cycle of 20 days.

2.3 Salinity experiment

The salinity experiment was performed in five salinity treatments i.e., 15, 20, 25, 30, and 35. Lower salinity IMK media were prepared by pre-dilution with sterile distilled water. The experiment was conducted at 28.0°C under the same light conditions as described above. Prior to the experiment, cells were pre-acclimatized to the targeted salinities by decreasing/increasing the salinity of five every two days, starting from salinity 30. After the acclimatization, an inoculum was transferred to a 50 mL fresh medium to make up for 100 ± 50 cells mL^{-1} initial cell densities for each flask. The experiment was performed in triplicate for each strain at each salinity treatment for a growth cycle of 20 days.

2.4 Cross-factorial temperature and salinity experiment

To further understand the combined effects of temperature and salinity on the two recently described *Chattonella tenuiplastida* and *C. malayana* (Lum et al., 2022), a cross-factorial experiment was conducted with 12 treatments (in triplicate), by crossing temperatures of 25.5, 28.0, 30.5 and 33.0°C with salinities of 25, 30 and 35 in 50 mL culture flasks with non-filtered caps (Sumitomo Bakelite, Tokyo, Japan). Cells in each treatment were pre-acclimatized as described above and subsequently transferred to 50 mL fresh medium to make up for 100 ± 50 cells mL^{-1} initial cell densities for each flask. The experiment was carried out for at least 20 days and monitored until day 40.

2.5 Cell count and growth rate

Two milliliters subsamples were collected from each culture flask every two days until day 20 or day 40, and cells were fixed with HEPES-buffered glutaraldehyde before counting (Katano et al., 2009). Fixed samples were manually counted by a Sedgwick-rafter

TABLE 1 Culture strains of *Chattonella* species used in this study (Lum et al., 2021; Lum et al., 2022).

Species	Strain	Sampling location	Date of collection
C. marina	ChMi02	Miri, Sarawak, Malaysia	2013
C. subsalsa	CtSg02	St John's Island, Singapore	2014
C. malayana	CtBK02	Pantai Melawi, Bachok, Kelantan, Malaysia	20 Apr 2016
C. tenuiplastida	St1409S2	Sematan Beach, Lundu, Sarawak, Malaysia	14 Sept 2017

chamber until ≥ 100 cells. Specific growth rate (μ, d^{-1}) was calculated from the following equation, where N is the number of cells and t is time (Hall et al., 2014).

$$\mu = \frac{\ln(N_t - N_0)}{\Delta t}$$

The maximum specific growth rate (μ_{max}) was calculated from the maximum slope over a five-point window (h = 5), in other words, the highest growth rate in any eight days (Hall et al., 2014) using the package *growthrates* (Petzoldt, 2022) in R (R Core Team, 2022). Growth rates of *Chattonella* were classified into four levels; (1) negative growth where cells died after the experiment had begun and were omitted from graphs, (2) no growth indicating the survival and mortality of *Chattonella* were almost equal, and no observable μ, (3) growth where $\mu > 0.1$ d^{-1}, and (4) optimal growth with the highest μ (μ_{max}). Treatments where *Chattonella* spp. achieved high cell densities (10^4 cells mL^{-1}) were noted.

2.6 F_v/F_m measurement

To determine the effects of temperature and salinity on the *Chattonella* cell conditions, the maximum quantum yield of photosystem II (F_v/F_m) was determined by measuring chlorophyll fluorescence from selected conditions, i.e., temperatures 20.5, 25.5, and 30.5°C, and salinities 25, 30, and 35 (Yuasa et al., 2020a; Yuasa et al., 2020b). Subsamples (2 mL) were collected from each culture flask in 4-day intervals, cells were incubated in the dark for 10–15 min, and F_v/F_m values were measured subsequently by a Water-PAM fluorometer (Walz, Effeltrich, Germany). The value of F_v/F_m was calculated by the following equation:

$$F_v/F_m = \frac{F_m - F_o}{F_m}$$

where F_m and F_o are the maximum and minimum fluorescence, respectively. Measurement was conducted in triplicate.

2.7 Statistical analyses

For the single-factor experiments of the effects of temperature and salinity, the μ and F_v/F_m were analyzed by one-way variance analysis (ANOVA), followed by Tukey's *post hoc* comparison test to determine the statistical significance at $p < 0.01$. For the cross-factorial experiment of temperature and salinity, the μ was analyzed by two-way ANOVA. Tukey's *post hoc* comparison test was performed at a statistical significance of $p < 0.01$ when the result of ANOVA was significant. Statistical analyses were conducted in R ver. 4 (R Core Team, 2022).

3 Results

3.1 Effects of temperature

None of the four *Chattonella* species grew at 13.0°C (Figure 1A). However, the effects of temperature on the growth varied among species when temperature > 13.0°C (Figures 1A, 2A and Tables 2, S1, S2). In general, growth was suppressed at 15.5 and 18.0°C, *C. subsalsa* and *C. marina* showed no growth with almost constant cell densities, while *C. tenuiplastida* and *C. malayana* exhibited negative growth (Figure 1A).

Growth temperature ranges were different among the *Chattonella* species. *Chattonella subsalsa* showed a wide temperature range of 20.5–35.5°C, while *C. malayana* demonstrated a remarkably narrow range (25.5–33.0°C). *Chattonella marina* and *C. tenuiplastida* exhibited moderate temperature ranges of 23.0–30.5°C and 23.0–33.0°C, respectively (Figures 1A, 2A). When comparing the μ_{max} and their respective optimal temperature (Tables 2, S1), *C. subsalsa* had the highest μ_{max} among all four *Chattonella* species (0.65 ± 0.01 d^{-1} at 28.0°C), followed by *C. marina* (0.41 ± 0.07 d^{-1} at 25.5°C), and the μ_{max} were similar for *C. tenuiplastida* (0.38 ± 0.01 d^{-1} at 30.5°C) and *C. malayana* (0.38 ± 0.04 d^{-1} at 30.5°C).

Cells of *C. subsalsa* entered the exponential phase in day 2–8, which demonstrated the shortest lag phase among all *Chattonella* species (Figure 1A). Comparable to *C. subsalsa*, *C. marina* entered the exponential phase in day 4–10. In contrast, *C. tenuiplastida* and *C. malayana* displayed a much longer lag phase and entered the exponential phase after day 8 (Figure 1A).

The culture of *C. subsalsa* showed the highest maximum cell densities, with the maximum cell yield of 7.9 × 10^4 cells mL^{-1} observed at 25.5°C. High cell densities of > 6 × 10^4 cells mL^{-1} were recorded throughout the temperature treatments (25.5–33.0°C) (Figure 1A). The highest maximum cell density of *C. marina* was recorded at 25.5°C (> 6 × 10^4 cells mL^{-1}), however, cell densities were relatively high at 20.5–30.5°C (> 10^3 cells mL^{-1}). High cell densities of *C. tenuiplastida* were recorded at 28.0–30.5°C (> 10^4 cells mL^{-1}), with the maximum cell density of 2.1 × 10^4 cells mL^{-1} observed at 30.5°C. The culture of *C. malayana* exhibited the lowest maximum cell yield among the species examined, with the highest maximum cell density of 1.7 × 10^4 cells mL^{-1} observed at 30.5°C. At 28.0 and 33.0°C, cell densities remained high (10^4 cells mL^{-1}) on day

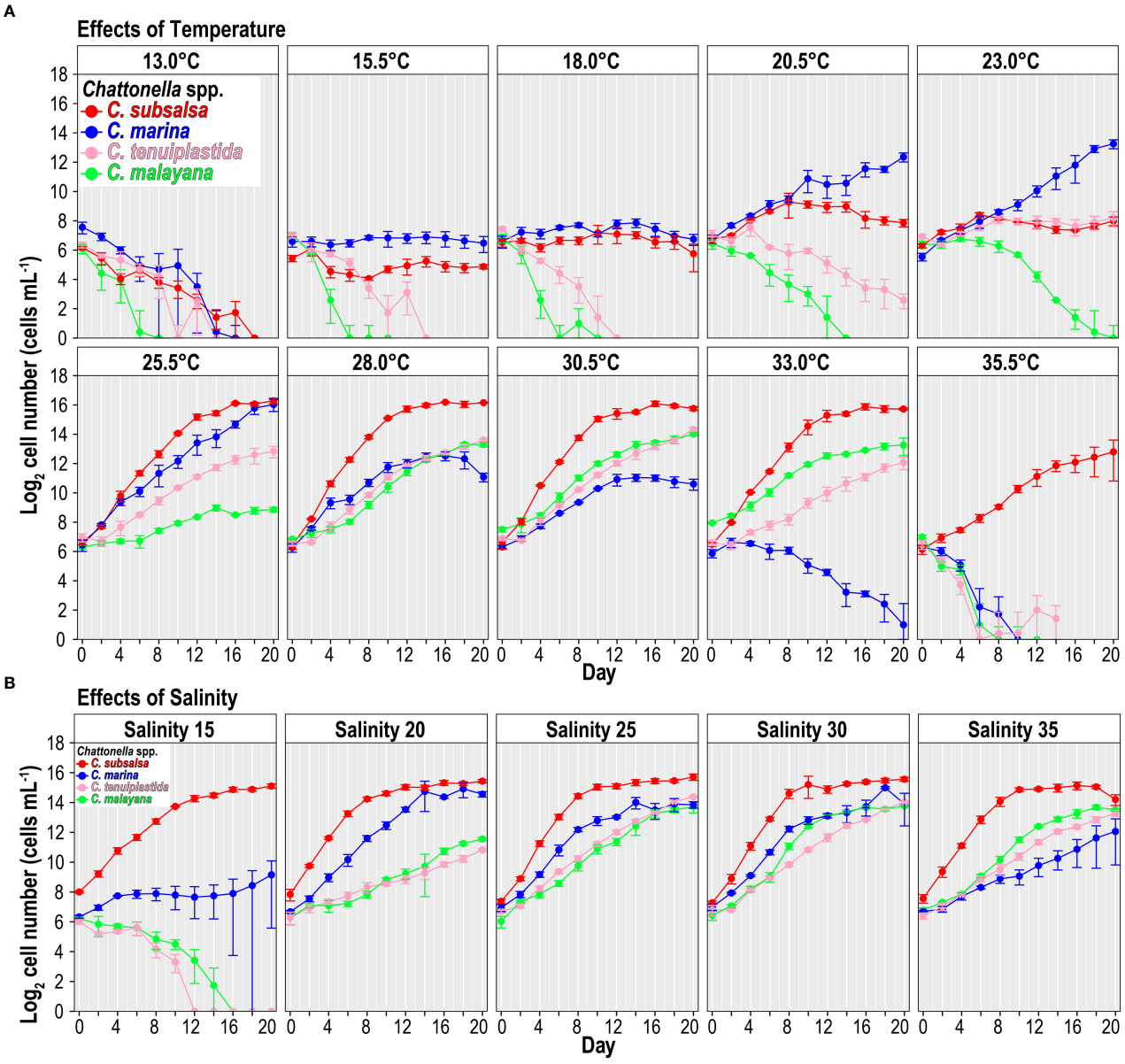

FIGURE 1
Growth of *Chattonella subsalsa*, *C. marina*, *C. tenuiplastida*, and *C. malayana* at different temperature **(A)** and salinity **(B)** treatments. Error bars represent standard deviations (n = 3).

20 but observation of whether the cells continued to grow was not available at the time.

The maximum quantum yield of photosystem II (F_v/F_m), an indicator of photosynthetic potential, has been commonly used to determine whether cells are under stress (Vonshak et al., 1994; Qiu et al., 2013; Katayama et al., 2017; Yuasa et al., 2020b). In this experiment, the F_v/F_m values of four *Chattonella* species were monitored in 20.5, 25.5, and 30.5°C treatments in 4-day intervals. *Chattonella subsalsa* and *C. marina* exhibited relatively high F_v/F_m (≥ 0.5) at all temperatures during the experiment period, indicating their photosynthetic potential was retained over the period (Figure 3A and Tables S5, S6). F_v/F_m of *C. subsalsa* were significantly higher at 25.5°C than that of 20.5°C throughout the experiment period ($p< 0.01$) (Figure 3A and Table S6). F_v/F_m values of *C. marina* were significantly different in all temperature treatments starting from day-8 ($p< 0.01$), the highest F_v/F_m was observed at 30.5°C (Figure 3A and Table S6). The differences of F_v/F_m among treatments were obvious in *C. tenuiplastida* and *C. malayana*. Both species showed negative F_v/F_m values at 20.5°C, implying their growth and photosynthetic potential were negatively affected by lower temperatures (Figure 3A and Table S6). At higher temperature treatments, F_v/F_m of *C. malayana* were significantly different ($p< 0.01$) between 25.5 and 30.5°C treatments after day 12, but those of *C. tenuiplastida* were not significantly different between 25.5 and 30.5°C ($p \geq 0.01$; Table S6), suggesting that *C. malayana* might be less tolerant to temperatures lower than 25.5°C.

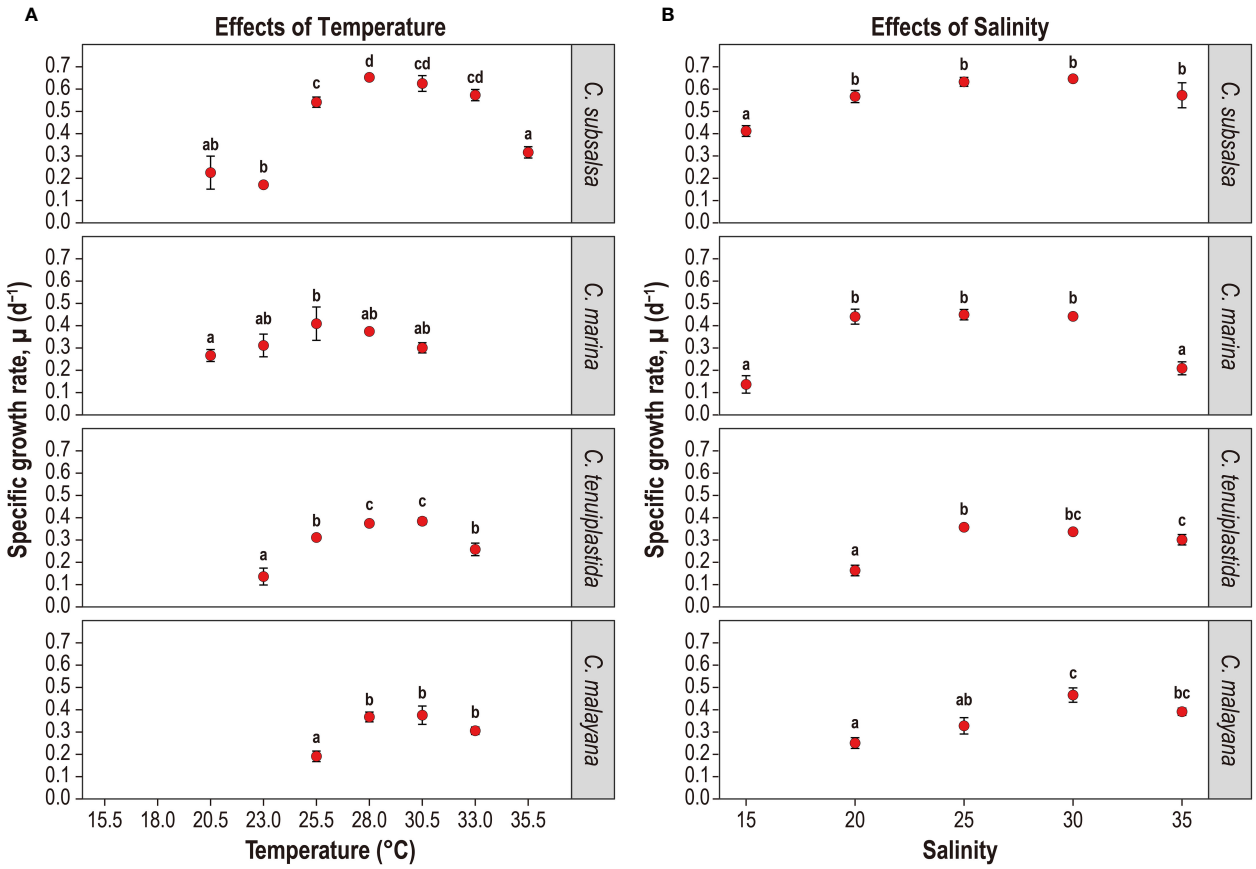

FIGURE 2
Specific growth rate, μ (d^{-1}) of *Chattonella subsalsa*, *C. marina*, *C. tenuiplastida*, and *C. malayana* at different temperature **(A)** and salinity **(B)** treatments. Note that treatments with negative or no growth were not shown, i.e., *C. subsalsa* (≤ 18.0°C), *C. marina* (≤ 18.0°C and ≥ 33.0°C), *C. tenuiplastida* (≤ 20.5°C and 35.5°C), *C. malayana* (≤ 23.0°C and 35.5°C), and *C. tenuiplastida* and *C. malayana* at salinity 15. Alphabets indicate ANOVA significant level of between-treatment comparisons ($p < 0.01$, Tukey's test). Error bars represent standard deviations ($n = 3$).

3.2 Effects of salinity

Overall, all *Chattonella* spp. showed similar growth responses to the salinity treatments (Figures 1B, 2B and Tables 2, S3, S4). Growth of *C. subsalsa* and *C. marina* was observed in the salinity range of 15–35, while *C. tenuiplastida* and *C. malayana* were in the salinity range of 20–35 (Table S3). At salinity 15, the growth of *C. tenuiplastida* and *C. malayana* were suppressed and cells died after day 12–14 (Figure 1B). Growth of *C. subsalsa* was significantly lower at salinity 15 than those at 20–35 ($p < 0.01$) (Figure 2B and Table S4).

Among all species, the highest μ_{max} was observed in *C. subsalsa* (0.65 ± 0.004 d^{-1} at salinity 30, Tables 2, S3), followed by *C. malayana* (0.47 ± 0.03 d^{-1} at salinity 30), *C. marina* (0.45 ± 0.02 d^{-1} at salinity 25), and *C. tenuiplastida* (0.36 ± 0.01 d^{-1} at salinity 25), respectively (Figures 1B, 2B).

For the growth phase, the exponential phase of *C. subsalsa* started on day 4 across all salinity treatments, which was the

TABLE 2 Growth ranges and maximum specific growth rates (μ_{max}) on *Chattonella* spp. in the single-factor experiments.

Species	Growth ranges		μ_{max}, d^{-1} (respective optimal growth condition)	
	Temperature (°C)	Salinity	Temperature (°C)	Salinity
C. subsalsa	20.5–35.5	15–35	0.65 ± 0.01 (28.0)	0.65 ± 0.004 (30)
C. marina	20.5–30.5	15–35	0.41 ± 0.07 (25.5)	0.45 ± 0.02 (25)
C. tenuiplastida	23.0–33.0	20–35	0.38 ± 0.01 (30.5)	0.36 ± 0.01 (25)
C. malayana	25.5–33.0	20–35	0.38 ± 0.04 (30.5)	0.47 ± 0.03 (30)

Salinity of 30 was used in the temperature treatments, whereas temperature of 28.0°C was fixed in the salinity treatments. The definition of growth range is temperature/salinity where cells could grow, and optimal growth is the temperature/salinity where cells achieved the highest μ (μ_{max}).

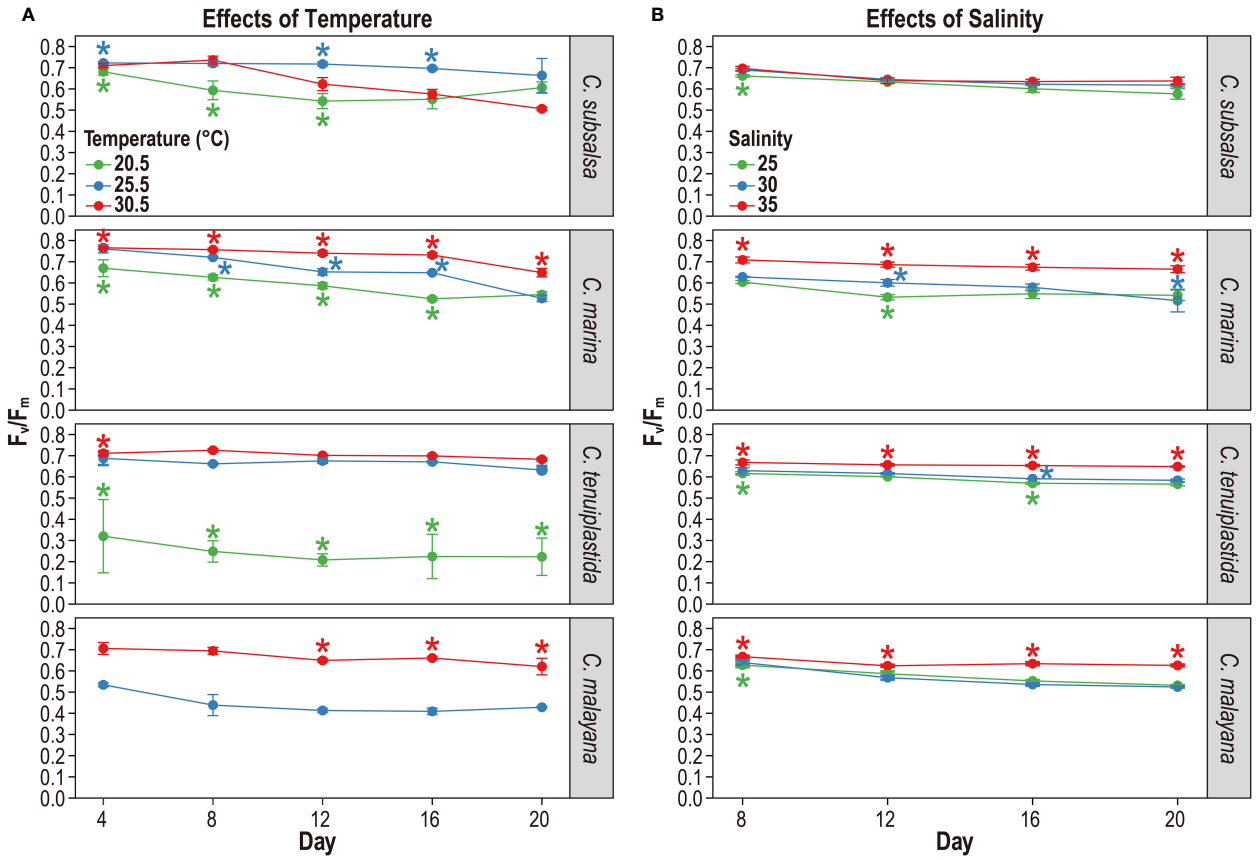

FIGURE 3
The maximum quantum yield of photosystem II (F_v/F_m) of *Chattonella subsalsa*, *C. marina*, *C. tenuiplastida*, and *C. malayana* at temperature treatments of 20.5, 25.5, and 30.5°C **(A)**, and salinity treatments of 25, 30, and 35 **(B)**. Asterisks indicate ANOVA significance differences ($p < 0.01$) between different temperature or salinity treatments on the sampling days. Note that F_v/F_m of *C. malayana* at 20.5°C (< 0.1) was excluded, and no data for day 4 of the salinity experiment due to equipment failure. Error bars represent standard deviations ($n = 3$).

shortest among all species (Figure 1B). *Chattonella marina* entered the exponential phase on day 6 at salinities 20–30, but with a longer lag phase (10 days) at salinities 15 and 35 (Figure 1B). *Chattonella malayana* also started to grow exponentially on day 6, similar to *C. marina*, at salinity 30 (Figure 1B). The culture of *C. tenuiplastida* exhibited the longest lag phase, as its exponential phase only started after day 8 (Figure 1B).

The maximum cell densities of *C. subsalsa* exceeded 3.5×10^4 cells mL^{-1} at all salinity treatments, which was much higher than other species (Figure 1B). The maximum cell densities of *C. marina* exceeding 10^4 cells mL^{-1} were recorded at salinities 20–30 but were lower ($< 5 \times 10^3$ cells mL^{-1}) at salinities 15 and 35. Maximum cell densities of both *C. tenuiplastida* and *C. malayana* were comparable to *C. subsalsa* and *C. marina* ($> 10^4$ cells mL^{-1}) at salinities 25–35.

The maximum quantum yield of photosystem II (F_v/F_m) was observed for salinities 25, 30, and 35 in 4-day intervals, and the results showed that the effects of salinity on the photosynthetic potential of the four *Chattonella* species were minor (Figure 3B and Tables S7, S8). High F_v/F_m (> 0.6) was observed in *C. subsalsa* in all salinity treatments, and they were not significantly different ($p \geq 0.01$; Figure 3B and Table S8). At salinity 35, *C. marina*, *C. tenuiplastida*, and *C. malayana* had lower μ but higher F_v/F_m as compared to those at salinities 30 and 25, suggesting that the three species could tolerate high salinity of 35 (Figures 2B, 3B and Table S8).

3.3 Cross-factorial effects of temperature and salinity

The combined effects of temperature and salinity produced similar results from the single-factor experiments, and no significant differences were observed among treatments, including the interaction effects of temperature and salinity (Figure 4 and Tables 3, 4). The only statistically significant result was detected in temperature ($p = 0.0064$, two-way ANOVA) in *C. tenuiplastida*, but almost all results showed no statistical differences ($p \geq 0.01$), except for 25.5-30.5°C ($p = 0.0055$, Tukey's test) (Tables 4, S9). Cells of *C. tenuiplastida* did not grow at 33.0°C across the salinities 25, 30, and 35, except for one replicate, which grew at salinity 35 ($\mu = 0.12$ d^{-1}). *Chattonella malayana* grew in all tested conditions but μ was extremely low (0.03 ± 0.02 d^{-1}) at 33.0°C and salinity 25. μ_{max} of *C. malayana* (0.40 ± 0.10 d^{-1}) was higher than that of *C. tenuiplastida* (0.39 ± 0.05 d^{-1}), comparable to previous experiments (Table 3).

The optimal growth of *C. malayana* was observed at 28.0°C and salinity 25, with a remarkable μ of 0.51 d^{-1} observed in a replicate

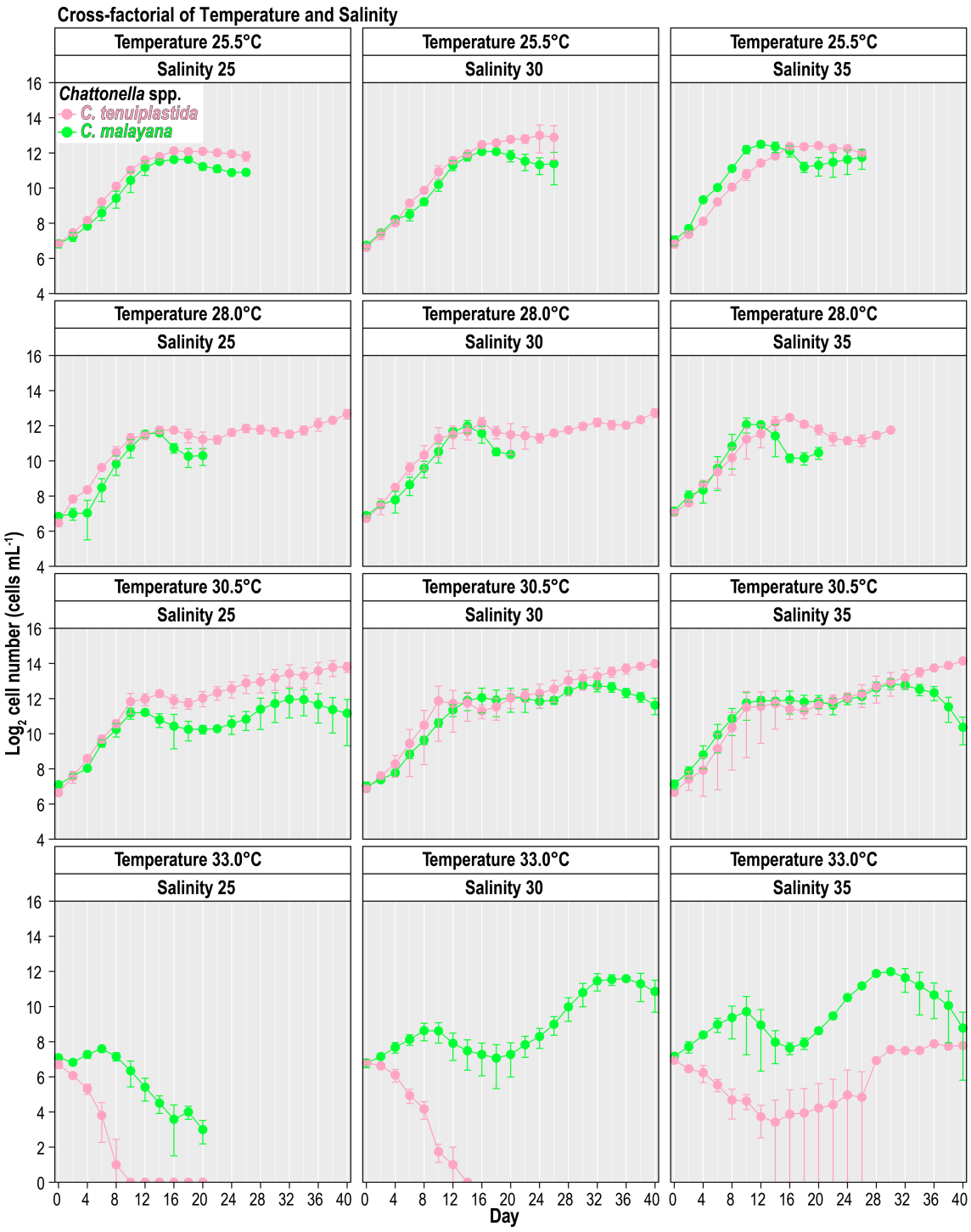

FIGURE 4
Growth of *Chattonella tenuiplastida* and *C. malayana* in the cross-factorial experiment of various temperatures and salinities. Error bars represent standard deviations (n = 3).

(Figure 5A and Table 3). The maximum cell density of 8.3 × 10^3 cells mL^{-1} was observed at 30.5°C and salinity 30, which was lower than those observed in the single-factor experiments (Figure 4). In contrast, the optimal growth of *C. tenuiplastida* was at 30.5°C and salinity 30, with its highest μ_{max} of 0.39 ± 0.05 d^{-1} (Figure 5B and Table 3). In the cross-factorial experiment with temperatures set at 28.0 and 30.5°C, a fluctuating pattern of growth was observed where cell densities declined slightly around day 20 and gradually increased to higher cell densities, resulting in two peaks in the growth curves (Figure 4). This type of growth curve was not observed at 25.5°C, as cells entered the exponential phase from day 4 and then stationary/death phases before day 20. High cell densities (> 10^4 cells mL^{-1}) were recorded at their optimal temperature of 30.5°C across all salinities 25–35.

TABLE 3 Specific growth rate (μ) in the cross-factorial experiments on *Chattonella malayana* and *C. tenuiplastida*, n = 3.

Species	Temperature (°C)	Salinity	Mean μ ± s.d. (d^{-1})	Range of μ (d^{-1})
C. malayana	25.5	25	0.30 ± 0.03	0.27–0.34
	25.5	30	0.30 ± 0.004	0.296–0.305
	25.5	35	0.37 ± 0.004	0.366–0.373
	28.0*	25*	0.40 ± 0.10	0.32–0.51
	28.0	30	0.33 ± 0.04	0.29–0.37
	28.0	35	0.36 ± 0.04	0.32–0.40
	30.5	25	0.32 ± 0.03	0.29–0.35
	30.5	30	0.30 ± 0.02	0.28–0.32
	30.5	35	0.35 ± 0.03	0.32–0.38
	33.0	25	0.03 ± 0.02	0.005–0.05
	33.0	30	0.29 ± 0.06	0.25–0.35
	33.0	35	0.28 ± 0.03	0.26–0.31
C. tenuiplastida	25.5	25	0.30 ± 0.01	0.29–0.31
	25.5	30	0.31 ± 0.05	0.28–0.36
	25.5	35	0.31 ± 0.01	0.30–0.33
	28.0	25	0.34 ± 0.03	0.30–0.36
	28.0	30	0.33 ± 0.09	0.23–0.40
	28.0	35	0.32 ± 0.04	0.29–0.37
	30.5	25	0.37 ± 0.01	0.36–0.38
	30.5*	30*	0.39 ± 0.05	0.33–0.44
	30.5	35	0.38 ± 0.01	0.37–0.40
	33.0	35	0.12	–

Asterisks mark the optimal conditions for each species when the highest μ (μ_{max}) was achieved.

4 Discussion

4.1 *Chattonella* in the tropical and temperate waters

Studies of temperature effects on the growth of *C. subsalsa* and *C. marina* focus mainly on temperate waters (Australia, Japan, Korea, and the USA), only a few reports had investigated the growth characteristics of *Chattonella* in tropical waters (Lee, 2014; Ayu-Lana-Nafisyah et al., 2018; Kok et al., 2019) (Table 5). In this study, we demonstrated that all four species, *C. subsalsa*, *C. malayana*, *C. marina*, and *C. tenuiplastida* from tropical Asian waters exhibited comparable growth (μ_{max}) and maximum quantum yield of photosystem II (F_v/F_m) to those of temperate *C. subsalsa* and *C. marina* (Salvitti, 2010; Qiu et al., 2013; Yuasa et al., 2020b) (Table 5). This study revealed that *C. subsalsa* achieved its μ_{max} at 28.0°C and salinity 30 (single-factor), *C. malayana* at 28.0°C and salinity 30 (single-factor), *C. marina* at 28.0°C and salinity 25 (single-factor), and *C. tenuiplastida* at 30.5°C and salinity 30 (cross-factor).

When comparing the tolerance of two distinct geographical populations of *C. subsalsa*, the tropical Singapore strain from this study showed a narrower temperature range (20.5–35.5°C), in contrast to the temperate USA strain which showed the range of 10–30°C (Zhang et al., 2006; this study; Table 5). As for *C. marina*, past studies have revealed a lower temperature tolerance limit (10–30°C) of the temperate strains, while the tropical *C. marina* strain demonstrated an upper temperature tolerance limit in the range of 20.5–34°C (Yamaguchi et al., 1991; Khan et al., 1995; Ayu-Lana-Nafisyah et al., 2018; this study). In both cases, tropical *C. subsalsa* and *C. marina* have higher growth temperature ranges than the temperate ones, suggesting that they have well adapted to the local environment and intraspecific variability by latitudinal differences is prominent.

Previous studies have reported higher optimal temperatures in *C. subsalsa* (28–30°C) as compared to *C. marina*, which was 25°C (Yamaguchi et al., 1991; Khan et al., 1995; Kahn et al., 1998; Marshall and Hallegraeff, 1999; Noh et al., 2006a; Noh et al., 2006b; Zhang et al., 2006; Wang et al., 2011; this study). This is in agreement with the present study. A study by Band-Schmidt et al.

TABLE 4 Two-way ANOVA for cross-factorial experiments on *Chattonella malayana* and *C. tenuiplastida*, *n* = 3.

	df	Sum of Squares	Mean Square	F	Sig
C. malayana					
Temperature	3	0.0236	0.00785	4.14	0.0181
Salinity	2	0.00818	0.00409	2.16	0.140
Temperature : Salinity	5	0.0121	0.00241	1.27	0.311
Residuals	22	0.0418	0.00190		
C. tenuiplastida					
Temperature	2	0.0243	0.0122	6.78	0.0064*
Salinity	2	0.000160	0.00008	0.045	0.956
Temperature : Salinity	4	0.000550	0.000139	0.077	0.988
Residuals	18	0.0323	0.00179		

df, degree of freedom; F, F-statistic; Sig, significance level.
Only the temperature factor of *C. tenuiplastida* was statistically different ($p < 0.01$), indicated by an asterisk. Note there were no significant differences in the combined effects of temperature and salinity.

(2012) also showed that the Mexican *C. marina* strain grew better in colder water than *C. subsalsa* strain. The adaptability to a broader temperature range of *C. marina* explained its wide latitudinal distribution across the tropical Southeast Asia and temperate East Asia.

On the other hand, the salinity ranges for growth were inconclusive, as intraspecific variation occurred in *Chattonella* species from similar climates (Table 5). For example, the *C. subsalsa* strain from the USA had a broad salinity range of 5–30 but the *C. subsalsa* strain from Brazil was unable to grow at a salinity below 20 (Zhang et al., 2006; Viana et al., 2019). As for *C. marina*, the temperate Korean strains grew in a salinity of 7.5 (Noh et al., 2006a; Noh et al., 2006b), which was the lowest salinity ever reported for *C. marina*, whereas the Japanese and Australian strains grew in higher salinity ranges (Yamaguchi et al., 1991; Khan et al., 1995; Kahn et al., 1998; Marshall and Hallegraeff, 1999) (Table 5). The tropical *C. marina* strains also showed slightly different salinity ranges, i.e., *C. marina* from Malaysia grew at salinity ranges of 10–

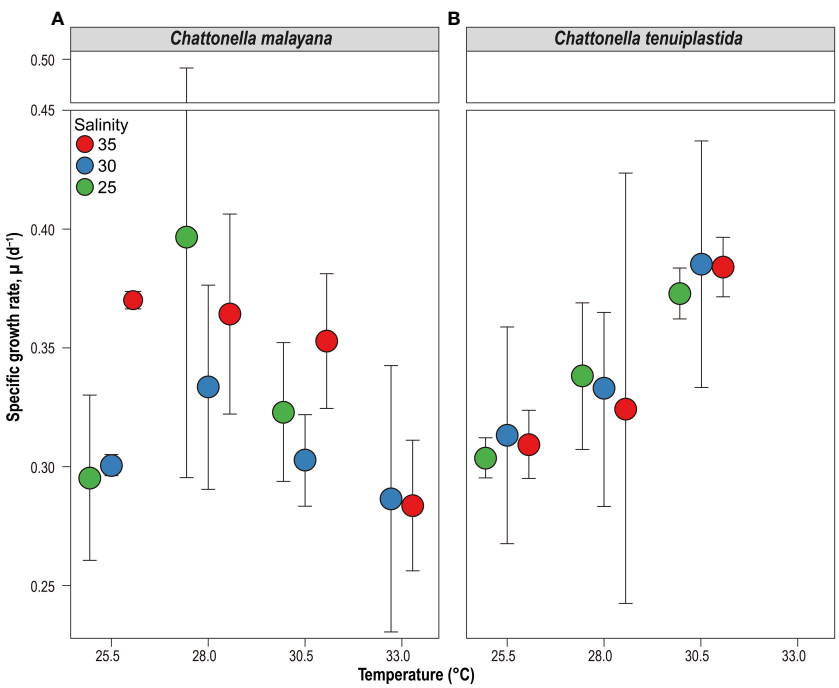

FIGURE 5
Specific growth rate, μ (d^{-1}) of *Chattonella malayana* **(A)** and *C. tenuiplastida* **(B)** and in the cross-factorial experiments of temperatures (x-axis) and salinity (colored circles). Note that *C. tenuiplastida* showed no growth at 33.0°C at salinities of 25 and 30, and only one replicate grew at salinity 35 (μ = 0.12 d^{-1}), which is not included in the plot. Error bars represent standard deviations (n = 3).

TABLE 5 Growth ranges, optimum growth conditions, and maximum specific growth rates (μ_{max}) of *Chattonella* spp.

Species	Growth ranges		Optimal growth		μ_{max} (d^{-1})	Origin
	Temperature (°C)	Salinity	Temperature (°C)	Salinity		
C. subsalsa	20.5–35.5	15–35	28.0[a]	30[a]	0.65	Singapore[†]
	10–30	5–30	30[a]	25[a]	0.60	Delaware, USA[7]
	–	20–30	–	30	0.54	Guanabara Bay, Brazil[10]
C. marina	20.5–30.5	15–35	25.5[a]	25[a]	0.45	Sarawak, Malaysia[†]
C. marina var. *antiqua*	15–30	10–35	25	25	0.67[b]	Seto Inland Sea, Japan[1]
	15–30	15–40	25[a]	35[a]	0.45[b]	Seto Inland Sea, Japan[2]
	15–30	10–40	25[a]	35[a]	0.49[b]	Kagoshima Bay, Japan[2]
C. marina var. *marina*	15–30	10–35	25	20	0.42[b], 0.56[b]	Seto Inland Sea[1] and Yatsushiro Sea, Japan[3]
	10–30	15–45	25[a]	30[a]	0.33[b]	Boston Bay, Australia[4]
	15–30	10–35	25[a]	25[a]	0.64	Gamak Bay, Korea[6]
	–	10–30	–	25[a]	0.28	Sarawak, Malaysia[8]
	25–34	15–33	–	15[a]	0.83	East Java, Indonesia[9]
C. marina var. *ovata*	15–30	7.5–40	25[a]	30[a]	0.47	Jangheung, Korea[5]
C. tenuiplastida	23.0–33.0	20–35	30.5[a]	25[a]	0.39	Sarawak, Malaysia[†]
C. malayana	25.5–33.0	20–35	30.5[a]	30[a]	0.47	Kelantan, Malaysia[†]

[1]Yamaguchi et al. (1991); [2]Khan et al. (1995); [3]Kahn et al. (1998); [4]Marshall and Hallegraeff (1999); [5]Noh et al. (2006a); [6]Noh et al. (2006b); [7]Zhang et al. (2006); [8]Lee (2014); [9]Ayu-Lana-Nafisyah et al. (2018); [10]Viana et al., 2019; [†]Present study.
[a]Optimal temperature/salinity from single-factor experiments.
[b]Data recalculated from the divisions per day reported in the original paper.

30 or 15–35 (both were optimal at 25), but those from Indonesia had a salinity range of 15–33, with an optimum salinity of 15 (Lee, 2014; Ayu-Lana-Nafisyah et al., 2018; this study). The specific growth rates of the tropical and temperate *C. marina* varied at salinity 35, i.e., the tropical strains had lower growth rates (0.2–0.4 d^{-1}) as compared to the Japanese strains (0.4–0.7 d^{-1}) (Nakamura and Watanabe, 1983; Khan et al., 1995; Lee, 2014; Ayu-Lana-Nafisyah et al., 2018; this study). In short, the salinity ranges are not species-specific and could not be explained by the latitudinal differences.

As for *C. tenuiplastida* and *C. malayana*, where their ecophysiology was firstly examined in the present study, relatively narrower growth ranges of temperatures and salinities were observed. The strains exhibited longer lag phases, slightly lower growth rates, and affected F_v/F_m at low temperature (20.5°C) when compared to the tropical *C. subsalsa* and *C. marina* in this study. This suggested that the two species have lower adaptability to colder water and thus restricted their distributions in warm waters. However, their μ_{max} were comparable to those of *C. subsalsa* from Brazil, Malaysia, and Mexico, and *C. marina* from Australia, Japan, and Korea, suggesting competitive growth potentials in the two species (Table 5).

Combined effects of temperature and salinity on the optimal growth have been observed in *Chattonella* (Smayda, 1969; Tomas, 1978; Yamaguchi et al., 1991; Yamatogi et al., 2006). In our single-factor experiments, results showed that *C. tenuiplastida* and *C. malayana* had relatively slower growth (longer lag phase) and relatively lower μ than *C. subsalsa* and *C. marina*, but since *Chattonella* usually could grow very dense (Marshall and Hallegraeff, 1999), the interaction effect of temperature and salinity on these two species had been determined to better understand their growth characteristics. Although our cross-factorial experiments did not show significant differences among all tested conditions (Table 4), the optimal temperature and salinity differed from that observed in the single-factor experiments, i.e., the optimum growth in *C. malayana* had changed from 30.5°C (when salinity was 30) and salinity 30 (when the temperature was 28.0°C) to the combined factors of 28.0°C and salinity 25 (Table 3). The optimal temperature of *C. tenuiplastida* remained the same at 30.5°C but its optimal salinity changed from 25 to 30 in the cross-factorial experiments (Table 3). The changes in the optimal temperature and salinity suggested that other factors not considered in this study might have affected the physiological responses, e.g., the use of non-filtered caps that limited the gaseous exchange. The accumulation of high carbon dioxide (CO_2) concentration resulting in acidic conditions has produced different growth responses in *C. marina* var. *marina* and *C. marina* var. *ovata* (Lim et al., 2020). Increased growth of *H. akashiwo* has also been observed in higher concentrations of CO_2 (Fu et al., 2008).

The μ_{max} of these two species, however, was similar to those of the single-factor experiments, further supported their optimal growths and adaptability. In the cross-factorial experiments, there was no significant difference in the growth response of *C. tenuiplastida* and *C. malayana* in the treatments of salinities 25,

30, and 35, unlike those demonstrated in the single-factor salinity experiments (Figures 2B, 4 and Tables 4, S4). Unfortunately, no constructive conclusion can be drawn from the cross-factorial experiments, except the evidence that the two species exhibited narrow windows of temperature and salinity tolerances. The results from the cross-factorial experiment somewhat agree with those in the single-factor experiments, which suggested the limited distribution of *C. tenuiplastida* and *C. malayana* in the tropical Asian waters.

4.2 Indigenous or alien *Chattonella* spp.?

It is difficult to ascertain the origin and the geographical introduction of these *Chattonella*, but the ability to adapt to a new environment has been suggested as an important driver for the widespread distribution of some phytoplankton especially the bloom-forming raphidophytes and dinoflagellates (Richlen et al., 2010; Zerebecki and Sorte, 2011; Sala-Pérez et al., 2021). They can adapt to warmer temperatures, less saline water, lower nutrient availability, and/or high CO_2 concentration (Cubillos et al., 2007; Hallegraeff, 2010; Thomas et al., 2012; Sala-Pérez et al., 2021). As a case in point, the harmful raphidophyte *H. akashiwo* is widely distributed globally, likely owing to its adaptability to a wide growth temperature and salinity range, where it has high growth in warmer temperatures (Zhang et al., 2006; Fu et al., 2008). Another example is *Margalefidinium polykrikoides* (Margalef) Gómez, Richlen et Anderson, which is a euryhaline and eurythermal bloom-forming dinophyte that could grow in a wide range of temperatures and salinities (Richlen et al., 2010; Kudela and Gobler, 2012). Its widespread global distribution has been well-known, and many newly detected locations have been reported since its first discovery (Richlen et al., 2010; Kudela and Gobler, 2012; Thoha et al., 2019). Similarly, the adaptation of *Gymnodinium aureolum* (Hulburt) Hansen in the Black Sea since its first report in the USA has also been pointed to its euryhaline traits (Sala-Pérez et al., 2021).

The first reports of *Chattonella* in Asia and Southeast Asia were in 1969 and 1983, respectively, which were 30 years later than the first discovery of *C. subsalsa* in France (1933) and 10 years after the discovery of *C. marina* in India (1949), but the understanding on the origin and dispersion of these *Chattonella* was limited (Biecheler, 1936; Subrahmanyan, 1954; Khoo, 1985; Okaichi, 2003). Among the four *Chattonella* species tested in our experiments, we anticipated that *C. subsalsa* and *C. marina* could have been transported in or out of tropical Asian waters and adapted to the new environments as they exhibited high adaptability to broad temperature ranges. Cyst formation in *C. subsalsa* and *C. marina* has also been observed, and these cysts could survive for months in the dark and be transported by ballast water, further suggesting the chance of them being transported (Imai and Itoh, 1988; Imai, 1989; Portune et al., 2009; Jeong et al., 2013; Satta et al., 2017).

In contrast to *C. subsalsa* and *C. marina*, *C. tenuiplastida* and *C. malayana* exhibit narrower temperature and salinity ranges for growth (Lum et al., 2022; this study). In addition, their growths were unparalleled to those observed in *C. subsalsa*, suggesting that these two species may have a weaker ability to spread to other regions. The ability of cyst formation in *C. tenuiplastida* and *C. malayana* has yet to be clarified.

4.3 Potential harmful algal bloom formation

Cell densities of *Chattonella* species ranging from 35×10^3 to 28×10^7 cells L^{-1} have been reported to be associated with fish kill events (Okaichi, 2003; Barraza-Guardado et al., 2004; Cortés-Altamirano et al., 2006; Martínez-López et al., 2006; Jugnu and Kripa, 2009; Satta et al., 2017). In this study, the cell density of all four *Chattonella* species exceeded 10^7 cells L^{-1} in their respective temperatures and salinities, suggesting that they can form high cell biomass when conditions are favorable. The growth rates of the *Chattonella* spp. in this study are comparable to those of *C. marina* estimated from an *in situ* mesocosm experiment (0.1–0.36 d^{-1}) and during a HAB incident in Yatsushiro Sea, Japan (~1 division d^{-1}, Watanabe et al., 1995; Nakashima et al., 2019).

One of the major factors affecting *Chattonella* blooms in their natural habitat is the water temperature (Imai and Yamaguchi, 2012; Satta et al., 2017). Blooms of *C. subsalsa* occurred in tropical Guanabara Bay, Brazil at 21–31°C, and in Santa Giusta Lagoon, Italy at 20–30°C (Satta et al., 2017; Branco et al., 2019; Viana et al., 2019). *Chattonella subsalsa* in our study demonstrated high growth rates in a wide range of temperatures (25.5–33.0°C), which overlaps with the known bloom temperature of this species. *Chattonella tenuiplastida* and *C. malayana* also showed better growth in warmer temperatures, which were ≥ 25.5°C and ≥ 28.0°C, respectively. These three species could possibly achieve high growth and form HABs in Southeast Asia as the coastal water ranges from 27.2–32.5°C fit their preferred temperature (Lau et al., 2017; Hii et al., 2021). Blooms of *C. marina* have been observed in slightly lower temperatures, such as in southwest India (25–27°C, Sanilkumar et al., 2012), and Mexico (17–22.7°C, Cortés-Altamirano et al., 2006; García-Mendoza et al., 2018). Our tropical *C. marina* maintained these growth characteristics, where it preferred colder water and may have a lower chance to form HABs in Southeast Asia. However, its ichthyotoxicity should not be underestimated as it had caused fish kills in low cell densities (Nishikawa et al., 2014).

Another factor, salinity, has seldom been related to the blooms of *Chattonella*, except when there is a nutrient influx from the river discharge (Onitsuka et al., 2011; Aoki et al., 2012). A wide range of salinities has been reported during their blooms, i.e., blooms of *C. subsalsa* at 38.5 (Mexico, Martínez-López et al., 2006), and 50 (Salton Sea, Tiffany et al., 2001), and blooms of *C. marina* at 35.3–36.9 (Australia, Marshall, 2002), 30–32.8 (Japan, Nakamura et al., 1988), 11.6–33.2 (Korea, Jeong et al., 2013), 33–38.9 (Mediterranean Sea, Ismael and Halim, 2001), and 34.5–34.7 (Mexico, Cortés-Altamirano et al., 2006). In Southeast Asia, heavy rainfalls and low salinity conditions in the coastal areas are common (Leong et al., 2015; Lau et al., 2017; Razali et al., 2022). In such cases, salinity adaptability is important for the survival of these HABs species and the chance to bloom (Nakamura, 1985;

Onitsuka et al., 2011; Aoki et al., 2012; Kok et al., 2019; Hii et al., 2021). In the present study, *C. subsalsa* and *C. marina* could grow in lower salinity and the growth ranges were larger than *C. tenuiplastida* and *C. malayana*, suggesting the former two had higher potential to proliferate and form blooms in the tropical Southeast Asian region.

Based on the historical records of *Chattonella* blooms and fisheries damages in Southeast Asia, *C. subsalsa* has been suggested as the responsible species in the region because of its occurrence in the fish-kill locations (Lum et al., 2021). Its higher growth and maximum cell densities in a wider range of temperatures and salinities as in this study, compared to the other three species, have further supported this claim. Aside from *C. subsalsa*, *C. malayana* had been reported to cause a harmful algal bloom resulting in massive wild fish mortality in Malaysia (Lum et al., 2022). It is interesting to note that, however, the cell density of *C. malayana* examined in this study was relatively low as compared to the other three species. This implied that there are other bloom-promoting factors that may affect the species but have yet to be unveiled. García-Mendoza et al. (2018) suggested that changes in the phytoplankton community must also be considered in understanding the bloom dynamics of *Chattonella*. In future studies, other factors such as irradiance, nutrient availability, CO_2 concentration, strain variability, and their interaction effects should be clarified (Yamaguchi et al., 1991; Marshall and Hallegraeff, 1999; Yamaguchi et al., 2008; Salvitti, 2010; Band-Schmidt et al., 2012; Wells et al., 2015; Kok et al., 2019; Viana et al., 2019; Lim et al., 2020; Yuasa et al., 2020a). To truly explain the ichthyotoxicity of these *Chattonella* species, the linkage between bloom potential and the production of reactive oxygen species (ROS) or other allelopathic chemicals should also be explored (Liu et al., 2007; Imai and Yamaguchi, 2012; Qiu et al., 2013; Yuasa et al., 2020a; Yuasa et al., 2020b; Ahumada-Fierro et al., 2021; Shikata et al., 2021; Cho et al., 2022).

Data availability statement

The original contributions presented in the study are included in the article/Supplementary Material. Further inquiries can be directed to the corresponding authors.

Author contributions

WL conducted the experiments, and wrote and finalized the manuscript. SS and KY assisted in data collection. TKo, TKa, and KyT assisted in data analyses. KK, CL and PL provided and maintained cultures. KtT and MI conceptualized, reviewed and finalized the manuscript, and funding acquisition. All authors contributed to the article and approved the submitted version.

Funding

This work was partially supported by JSPS Kakenhi 19H03027 and 19KK0160 to MI.

Acknowledgments

We express our deepest gratitude to the staffs at Japan Fisheries Research and Education Agency for sharing the equipment necessary for the experiments. This international collaborative study was conducted under the Core-to-Core Program (B. Asia-Africa Science Platforms) of JSPS and IOC/WESTPAC-HAB project.

Conflict of interest

The authors declare that the research was conducted in the absence of any commercial or financial relationships that could be construed as a potential conflict of interest.

The handling editor ZH declared a past collaboration with the author MI.

Publisher's note

Supplementary material

The Supplementary Material for this article can be found online at: https://www.frontiersin.org/articles/10.3389/fmars.2023.1127871/full#supplementary-material

References

Ahumada-Fierro, N. V., García-Mendoza, E., Sandoval-Gil, J. M., and Band-Schmidt, C. J. (2021). Photosynthesis and photoprotection characteristics related to ROS production in three *Chattonella* (Raphidophyceae) species. *J. Phycol.* 57, 941–954. doi: 10.1111/jpy.13138

Anderson, D. M., Fensin, E., Gobler, C. J., Hoeglund, A. E., Hubbard, K. A., Kulis, D. M., et al. (2021). Marine harmful algal blooms (HABs) in the United States: history, current status and future trends. *Harmful Algae* 102, 101975. doi: 10.1016/j.hal.2021.101975

Anton, A., Teoh, P. L., Mohd-Shaleh, S. R., and Mohammad-Noor, N. (2008). First occurrence of *Cochlodinium* blooms in Sabah, Malaysia. *Harmful Algae* 7, 331–336. doi: 10.1016/j.hal.2007.12.013

Aoki, K., Onitsuka, G., Shimizu, M., Kuroda, H., Matsuyama, Y., Kimoto, K., et al. (2012). Factors controlling the spatio-temporal distribution of the 2009 *Chattonella antiqua* bloom in the Yatsushiro Sea, Japan. *Estuar. Coast. Shelf. Sci.* 114, 148–155. doi: 10.1016/j.ecss.2012.08.028

Ayu-Lana-Nafisyah,, Endang-Dewi-Masithah,, Matsuoka, K., Mirni-Lamid,, Mochammad-Amin-Alamsjah,, O-hara, S., et al. (2018). Cryptic occurrence of *Chattonella marina* var. *marina* in mangrove sediments in Probolinggo, East Java province, Indonesia. *Fish. Sci.* 84, 877–887. doi: 10.1007/s12562-018-1219-0

Azanza, R., Benico, G., Iwataki, M., and Fukuyo, Y. (2017). *Harmful marine dinoflagellates in the Philippines* (Diliman: The Marine Science Institute, University of the Philippines), 96.

Azanza, R. V., David., L. T., Borja, R. T., Baula, I. U., and Fukuyo, Y. (2008). An extensive *Cochlodinium* bloom along the western coast of Palawan, Philippines. *Harmful Algae* 7, 324–330. doi: 10.1016/j.hal.2007.12.011

Band-Schmidt, C. J., Martínez-López, A., Bustillos-Guzmán, J. J., Carreón-Palau, L., Morquecho, L., Olguín-Monroy, N. O., et al. (2012). Morphology, biochemistry, and growth of raphidophyte strains from the Gulf of California. *Hydrobiologia* 693, 81–97. doi: 10.1007/s10750-012-1088-y

Barraza-Guardado, R., Cortés-Altamirano, R., and Sierra-Beltrán, A. (2004). Marine die-offs from *Chattonella marina* and *Ch.* cf. *ovata* in Kun Kaak Bay, Sonora in the Gulf of California. *Harmful Algae News* 25, 7–8.

Biecheler, B. (1936). Sur une chloromonadine nouvelle d'eau saumatre *Chattonella subsalsa* n. gen., n. sp. *Arch. Zool. Expérimentale. 19énérale.* 78, 79–83.

Bowers, H. A., Tomas, C. R., Tengs, T., Kempton, J. W., Lewitus, A. J., Baruch, B. W., et al. (2006). Raphidophyceae [Chadefaud ex Silva] systematics and rapid identification: sequence analyses and real-time PCR assays. *J. Phycol.* 42, 1333–1348. doi: 10.1111/j.1529-8817.2006.00285.x

Boyd, P. W., Rynearson, T. A., Armstrong, E. A., Fu, F., Hayashi, K., Hu, Z., et al. (2013). Marine phytoplankton temperature versus growth responses from polar to tropical waters – outcome of a scientific community-wide study. *PloS One* 8, e63091. doi: 10.1371/journal.pone.0063091

Branco, S., Almeida, L. L., Alves-de-Souza, C., Oliveira, M. M. M., Proença, L. A. O., and Menezes, M. (2019). Morphological and genetic characterization of bloom-forming raphidophyceae from Brazilian coast. *Phycol. Res.* 67, 279–290. doi: 10.1111/pre.12377

Cho, K., Ueno, M., Liang, Y., Kim, D., and Oda, T. (2022). Generation of reactive oxygen species (ROS) by harmful algal bloom (HAB)-forming phytoplankton and their potential impact on surrounding living organisms. *Antioxidants* 11, 206. doi: 10.3390/antiox11020206

Cortés-Altamirano, R., Alonso-Rodriguez, R., and Sierra-Beltrán, A. (2006). Fish mortality associated with *Chattonella marina* and *C.* cf. *ovata* (Raphidophyceae) blooms in Sinaloa (Mexico). *Harmful Algae News* 31, 7–8.

Cubillos, J. C., Wright, S. W., Nash, G., De Salas, M. F., Griffiths, B., Tilbrook, B., et al. (2007). Calcification morphotypes of the coccolithophorid *Emiliania huxleyi* in the Southern Ocean: changes in 2001 to 2006 compared to historical data. *Mar. Ecol. Prog. Ser.* 348, 47–54. doi: 10.3354/meps07058

Edvardsen, B., and Imai, I. (2006). "The ecology of harmful flagellates within Prymnesiophyceae and Raphidophyceae," in *Ecology of harmful algae*. Eds. E. Granéli and J. T. Turner (Berlin: Springer-Verlag), 67–79.

Engesmo, A., Eikrem, W., Seoane, S., Smith, K., Edvardsen, B., Hofgaard, A., et al. (2016). New insights into the morphology and phylogeny of *Heterosigma akashiwo* (Raphidophyceae), with the description of *Heterosigma minor* sp. nov. *Phycologia* 55, 279–294. doi: 10.2216/15-115.1

Fu, F. X., Tatters, A. O., and Hutchins, D. A. (2012). Global change and the future of harmful algal blooms in the ocean. *Mar. Ecol. Prog. Ser.* 470, 207–233. doi: 10.3354/meps10047

Fu, F. X., Zhang, Y., Warner, M. E., Feng, Y., Sun, J., and Hutchins, D. A. (2008). A comparison of future increased CO_2 and temperature effects on sympatric *Heterosigma akashiwo* and *Prorocentrum minimum*. *Harmful Algae* 7, 76–90. doi: 10.1016/j.hal.2007.05.006

Furuya, K., Iwataki, M., Lim, P. T., Lu, S., Leaw, C.-P., Azanza, R. V., et al. (2018). "Overview of harmful algal blooms in Asia," in *Global ecology and oceanography of harmful algal blooms*. Eds. P. M. Glibert, E. Berdalet, M. A. Burford, G. C. Pitcher and M. Zhou (Berlin: Springer-Verlag), 289–308.

García-Mendoza, E., Cáceres-Martínez, J., Rivas, D., Fimbres-Martinez, M., Sánchez-Bravo, Y., Vásquez-Yeomans, R., et al. (2018). Mass mortality of cultivated northern bluefin tuna *Thunnus thynnus orientalis* associated with *Chattonella* species in Baja California, Mexico. *Front. Mar. Sci.* 5. doi: 10.3389/fmars.2018.00454

Gin, K. Y. H., Holmes, M. J., Zhang, S., and Lin, X. (2006). ""Phytoplankton structure in the tropical port waters of Singapore," in *The environment in Asia pacific harbours*. Ed. E. Wolanski (Netherlands: Springer), 347–375.

Hada, Y. (1967). Protozoan plankton of the Inland Sea, Setonaikai. I. the mastigophora. *Bull. Suzugamine. Women's. Coll. Natural Sci.* 13, 1–26.

Hada, Y. (1968). Protozoan plankton of the Inland Sea, Setonaikai. II. the mastigophora and sarcodina. *Bull. Suzugamine. Women's. Coll. Natural Sci.* 14, 1–28.

Hall, B. G., Acar, H., Nandipati, A., and Barlow, M. (2014). Growth rates made easy. *Mol. Biol. Evol.* 31, 232–238. doi: 10.1093/molbev/mst187

Hallegraeff, G. M. (2010). Ocean climate change, phytoplankton community responses, and harmful algal blooms: a formidable predictive challenge. *J. Phycol.* 46, 220–235. doi: 10.1111/j.1529-8817.2010.00815.x

Hara, Y., and Chihara, M. (1987). Morphology, ultrastructure and taxonomy of the raphidophycean alga *Heterosigma akashiwo*. *Bot. Mag. Tokyo.* 100, 151–163. doi: 10.1007/BF02488320

Hii, K. S., Mohd-Din, M., Luo, Z., Tan, S. N., Lim, Z. F., Lee, L. K., et al. (2021). Diverse harmful microalgal community assemblages in the Johor Strait and the environmental effects on its community dynamics. *Harmful Algae* 107, 102077. doi: 10.1016/j.hal.2021.102077

Hulburt, E. M. (1965). Flagellates from brackish waters in the vicinity of Woods Hole, Massachusetts. *J. Phycol.* 1, 87–94. doi: 10.1111/j.1529-8817.1965.tb04563.x

Imai, I. (1989). Cyst formation of the noxious red tide flagellate *Chattonella marina* (Raphidophyceae) in culture. *Mar. Biol.* 103, 235–239. doi: 10.1007/BF00543353

Imai, I., and Itoh, K. (1988). Cysts of *Chattonella antiqua* and *C. marina* (Raphidophyceae) in sediments of the Inland Sea of Japan. *Bull. Plankton. Soc Japan.* 35, 35–44.

Imai, I., and Yamaguchi, M. (2012). Life cycle, physiology, ecology and red tide occurrences of the fish-killing raphidophyte *Chattonella*. *Harmful Algae* 14, 46–70. doi: 10.1016/j.hal.2011.10.014

Ismael, A., and Halim, Y. (2001). "Occurrence and succession of potentially harmful phytoplankton species in the Eastern harbour of Alexandria, Egypt," in *Harmful algal blooms 2000: proceedings of the ninth international conference on harmful algal blooms*. Eds. G. M. Hallegraeff, S. I. Blackburn, C. J. S. Bolch and R. J. Lewis (Hobart: Intergovernmental Oceanographic Commission of UNESCO), 141–143.

Iwataki, M., Kawami, H., and Matsuoka, K. (2007). *Cochlodinium fulvescens* sp. nov. (Gymnodiniales, dinophyceae), a new chain-forming unarmored dinoflagellate from Asian coasts. *Phycol. Res.* 55, 231–239. doi: 10.1111/j.1440-1835.2007.00466.x

Iwataki, M., Kawami, H., Mizushima, K., Mikulski, C. M., Doucette, G. J., Relox, J. R.Jr, et al. (2008). Phylogenetic relationship in the harmful dinoflagellate *Cochlodinium polykrikoides* (Gymnodiniales, dinophyceae) inferred from LSU rDNA sequences. *Harmful Algae* 7, 271–277. doi: 10.1016/j.hal.2007.12.003

Iwataki, M., Takayama, H., Takahashi, K., and Matsuoka, K. (2015). "Taxonomy and distribution of the unarmored dinoflagellates *Cochlodinium polykrikoides* and *C. fulvescens*," in *Marine protists: diversity and dynamics*. Eds. S. Ohtsuka, T. Suzaki, T. Horiguchi, N. Suzuki and F. Not (Tokyo: Springer), 551–565.

Jeong, H. J., Yoo, Y., Lim, A. S., Kim, T. W., Lee, K., and Kang, C. K. (2013). Raphidophyte red tides in Korean waters. *Harmful Algae* 30, S41–S52. doi: 10.1016/j.hal.2013.10.005

Jugnu, R., and Kripa, V. (2009). Effect of *Chattonella marina* [(Subrahmanyan) Hara et Chihara 1982] bloom on the coastal fishery resources along Kerala coast, India. *Indian J. Mar. Sci.* 38, 77–88.

Kahn, S., Arakawa, O., and Onoue, Y. (1998). Physiological investigations of a neurotoxin-producing phytoflagellate, *Chattonella marina* (Raphidophyceae). *Aquac. Res.* 29, 9–17. doi: 10.1046/j.1365-2109.1998.00928.x

Katano, T., Yoshida, M., Lee, J., Han, M.-S., and Hayami, Y. (2009). Fixation of *Chattonella antiqua* and *C. marina* (Raphidophyceae) using Hepes-buffered paraformaldehyde and glutaraldehyde for flow cytometry and light microscopy. *Phycologia* 48, 473–479. doi: 10.2216/08-102.1

Katayama, T., Makabe, R., Sampei, M., Hattori, H., Sasaki, H., and Taguchi, S. (2017). Photoprotection and recovery of photosystem II in the Southern Ocean phytoplankton. *Polar. Sci.* 12, 5–11. doi: 10.1016/j.polar.2016.12.003

Khan, S., Arakawa, O., and Onoue, Y. (1995). Effects of physiological factors on morphology and motility of *Chattonella antiqua* (Raphidophyceae). *Bot. Mar.* 38, 347–354. doi: 10.1515/botm.1995.38.1-6.347

Khoo, E. W. (1985). Occurrences of "red tide" along Johore Straits, Malaysia, resulted in heavy mortality of shrimp. *World Maricult. Soc News.* 16, 4.

Kok, J. W. K., Yeo, D. C. J., and Leong, S. C. Y. (2019). Growth, pigment, and chromophoric dissolved organic matter responses of tropical *Chattonella subsalsa* (Raphidophyceae) to nitrogen enrichment. *Phycol. Res.* 67, 134–144. doi: 10.1111/pre.12360

Konalova, G. V. (1995). "The dominant and potentially dangerous species of phytoflagellates in the coastal waters of east Kamchatka," in *Harmful marine algal blooms: proceedings of the sixth international conference on toxic marine phytoplankton*. Eds. P. Lassus, G. Arzul, E.E.-L. Denn, P. Gentien and C. Marcaillou-Le Baut (Nantes, France: Lavoisier Publishing), 169–174.

Kudela, R. M., and Gobler, C. J. (2012). Harmful dinoflagellate blooms caused by *Cochlodinium* sp.: global expansion and ecological strategies facilitating bloom formation. *Harmful Algae* 14, 71–86. doi: 10.1016/j.hal.2011.10.015

Lau, W. L. S., Law, I. K., Liow, G. R., Hii, K. S., Usup, G., Lim, P. T., et al. (2017). Life-history stages of natural bloom populations and the bloom dynamics of a tropical Asian ribotype of *Alexandrium minutum*. *Harmful Algae* 70, 52–63. doi: 10.1016/j.hal.2017.10.006

Leadbeater, B. S. C. (1969). A fine structural study of *Olisthodiscus luteus* carter. *Br. Phycol. J.* 4, 3–17. doi: 10.1080/00071616900650021

Lee, S. W. (2014). *Effect of salinity and light intensity on the growth of Chattonella (Raphidophyceae). [Bachelor's thesis]* (Kota Samarahan (Sarawak: University Malaysia Sarawak).

Leong, S. C. Y., Lim, L. P., Chew, S. M., Kok, J. W. K., and Teo, S. L. M. (2015). Three new records of dinoflagellates in Singapore's coastal waters, with observations on environmental conditions associated with microalgal growth in the Johor Straits. *Raffles. Bull. Zool.* 31, 24–36.

Lim, M. H., Lee, C. H., Min, J., Lee, H. G., and Kim, K. Y. (2020). Effect of elevated pCO_2 on thermal performance of *Chattonella marina* and *Chattonella ovata* (Raphidophyceae). *Algae* 35, 375–388. doi: 10.4490/ALGAE.2020.35.12.8

Lim, P. T., Usup, G., and Leaw, C. P. (2012). Harmful algal blooms in Malaysian waters. *Sains. Malaysiana.* 41, 1509–1515.

Lirdwitayaprasit, T., Ochi, T., and Montani, S. (1996). "Changes in cell chemical composition during the growth cycle of *Chattonella* sp. and *Heterosigma* sp. found in the shrimp ponds at Chantaburi, Thailand," in *Harmful and toxic algal blooms*. Eds. T. Yasumoto, Y. Oshima and Y. Fukuyo (Sendai: Intergovernmental Oceanographic Commission of UNESCO), 507–510.

Liu, W., Au, D. W. T., Anderson, D. M., Lam, P. K. S., and Wu, R. S. S. (2007). Effects of nutrients, salinity, pH and light:dark cycle on the production of reactive oxygen species in the alga *Chattonella marina*. *J. Exp. Mar. Bio. Ecol.* 346, 76–86. doi: 10.1016/j.jembe.2007.03.007

Lum, W. M., Benico, G., Azanza, R., Furio, E., Lim, P. T., Lim, H. C., et al. (2019). Morphology and molecular phylogeny of the harmful raphidophyte *Chattonella subsalsa* isolated from Bolinao, Philippines. *Philipp. J. Nat. Sci.* 24, 50–56.

Lum, W. M., Benico, G., Doan-Nhu, H., Furio, E., Leaw, C. P., Leong, S. C. Y., et al. (2021). The harmful raphidophyte *Chattonella* (Raphidophyceae) in Western Pacific: its red tides and associated fisheries damage over the past 50 years (1969–2019). *Harmful Algae* 107, 102070. doi: 10.1016/j.hal.2021.102070

Lum, W. M., Lim, H. C., Lau, W. L. S., Law, I. K., Teng, S. T., Benico, G., et al. (2022). Description of two new species *Chattonella tenuiplastida* sp. nov. and *Chattonella malayana* sp. nov. (Raphidophyceae) from South China Sea, with a report of wild fish mortality. *Harmful Algae* 118, 102322. doi: 10.1016/j.hal.2022.102322

Maclean, J. L. (1984). "Indo-pacific toxic red tide occurrences (1972–1984," in *Toxic red tides and shellfish toxicity in southeast Asia: proceedings of a consultative meeting held in Singapore*. Eds. A. W. White, M. Anraku and K.-K. Hooi (Singapore: Southeast Asian Fisheries Development Center and the International Development Research Centre), 92–104. Available at: http://hdl.handle.net/20.500.12066/4873.

Marshall, J. (2002). *Comparative ecophysiology, chemotaxonomy and ichthyotoxicity of Chattonella marina (Raphidophyceae) from Australia and Japan* (Hobart (TAS: University of Tasmania).

Marshall, J., and Hallegraeff, G. M. (1999). Comparative ecophysiology of the harmful alga *Chattonella marina* (Raphidophyceae) from south Australian and Japanese waters. *J. Plankton. Res.* 21, 1809–1822. doi: 10.1093/plankt/21.10.1809

Martínez-López, A., Band-Schmidt, C. J., Escobedo-Urías, D., and Ulloa-Pérez, A. E. (2006). Bloom of *Chattonella subsalsa* in an impacted coastal lagoon in the Gulf of California. *Harmful Algae News* 31, 1–12.

Mehnert, G., Leunert, F., Cirés, S., Jöhnk, K. D., Rücker, J., Nixdorf, B., et al. (2010). Competitiveness of invasive and native cyanobacteria from temperate freshwaters under various light and temperature conditions. *J. Plankton. Res.* 32, 1009–1021. doi: 10.1093/plankt/fbq033

Mohammad-Noor, N., Moestrup, Ø., Leaw, C. P., Lim, P. T., Chin, G. J. W. L., and Usup, G. (2018). *Harmful algae of Malaysia* (Kuala Lumpur: IIUM Press), 80.

Nakamura, Y. (1985). Kinetics of nitrogen- or phosphorus-limited growth and effects of growth conditions on nutrient uptake in *Chattonella antiqua*. *J. Oceanogr. Soc Japan.* 41, 381–387. doi: 10.1007/BF02109032

Nakamura, Y., Takashima, J., and Watanabe, M. (1988). Chemical environment for red tides due to *Chattonella antiqua* in the Seto Inland Sea, Japan – part 1. growth bioassay of the seawater and dependence of growth rate on nutrient concentrations. *J. Oceanogr. Soc Japan.* 44, 113–124. doi: 10.1007/BF02302618

Nakamura, Y., and Watanabe, M. M. (1983). Growth characteristics of *Chattonella antiqua*. *J. Oceanogr. Soc Japan.* 39, 151–155. doi: 10.1007/BF02070258

Nakashima, H., Murata, K., Yano, K., Nishi, H., Yoshimura, N., Kuroki, Y., et al. (2019). A *Chattonella* bloom in the Yatsushiro Sea, Japan in summer 2016: environmental characteristics during the bloom and mortality of cultured yellowtail *Seriola quinqueradiata*. *Nippon Suisan Gakkaishi* 85, 162–172. doi: 10.2331/suisan.18–00006

Nishikawa, T., Hori, Y., Nagai, S., Miyahara, K., Nakamura, Y., Harada, K., et al. (2014). Long-term (36-year) observations on the dynamics of the fish-killing raphidophyte *Chattonella* in Harima-Nada, eastern Seto Inland Sea, Japan. *J. Oceanogr.* 70, 153–164. doi: 10.1007/s10872-014-0219-7

Noh, I.-H., Yoon, Y.-H., and Kim, D.-I. (2006a). "Effect of water temperature, salinity and light on the growth of the poisonous acicular algae *Chattonella ovata* isolated from Jangheung coastal water in South Sea, Korea," in *Proceedings of the 2006 fall conference of the Korean society of marine and environmental energy* (Busan, Korea: Korean Society of Marine and Environmental Energy), 184–190.

Noh, I.-H., Yoon, Y.-H., Kim, D.-I., and Oh, S.-J. (2006b). Effects of water temperature, salinity and irradiance on the growth of the harmful algae *Chattonella marina* (Subrahmanyan) Hara et Chihara (Raphidophyceae) isolated from Gamak Bay, Korea. *Korean. J. Fish. Aquat. Sci.* 39, 487–494. doi: 10.5657/kfas.2006.39.6.487

Okaichi, T. (2003). *Red tides* (Tokyo: Terra Scientific Publishing Company).

Onitsuka, G., Aoki, K., Shimizu, M., Matsuyama, Y., Kimoto, K., Matsuo, H., et al. (2011). Short-term dynamics of a *Chattonella antiqua* bloom in the Yatsushiro Sea, Japan, in summer 2010: characteristics of its appearance in the southern area. *Bull. Japan. Soc Fish. Oceanogr.* 75, 143–153.

Petzoldt, T. (2022) *Growthrate [Estimate growth rates from experimental data]*. Available at: https://github.com/tpetzoldt/growthrates (Accessed September 4, 2022).

Portune, K. J., Coyne, K. J., Hutchins, D. A., Handy, S. M., and Cary, S. C. (2009). Quantitative real-time PCR for detecting germination of *Heterosigma akashiwo* and *Chattonella subsalsa* cysts from Delaware's Inland Bays, USA. *Aquat. Microb. Ecol.* 55, 229–239. doi: 10.3354/ame01292

Qiu, X., Shimasaki, Y., Tsuyama, M., Yamada, T., Kuwahara, R., Kawaguchi, M., et al. (2013). Growth-phase dependent variation in photosynthetic activity and cellular protein expression profile in the harmful raphidophyte *Chattonella antiqua*. *Biosci. Biotechnol. Biochem.* 77, 46–52. doi: 10.1271/bbb.120543

Ratkova, T. N., and Wassmann, P. (2005). Sea Ice algae in the white and barents seas: composition and origin. *Polar. Res.* 24, 95–110. doi: 10.3402/polar.v24i1.6256

Razali, R. M., Mustapa, N. I., Md. Noordin, W. N., Rahim, M. A., Hii, K. S., Lim, P. T., et al. (2022). Report of a fish kill due to a dinoflagellate bloom in Perak and Penang, Malaysia. *Asian Fish. Sci.* 35, 257–268. doi: 10.33997/j.afs.2022.35.3.004

R Core Team. (2022) *R: a language and environment for statistical computing (R foundation for statistical computing)*. Available at: https://www.R-project.org.

Richlen, M. L., Morton, S. L., Jamali, E. A., Rajan, A., and Anderson, D. M. (2010). The catastrophic 2008–2009 red tide in the Arabian Gulf region, with observations on the identification and phylogeny of the fish-killing dinoflagellate *Cochlodinium polykrikoides*. *Harmful Algae* 9, 163–172. doi: 10.1016/j.hal.2009.08.013

Sakamoto, S., Lim, W. A., Lu, D., Dai, X., Orlova, T., and Iwataki, M. (2021). Harmful algal blooms and associated fisheries damage in East Asia: current status and trends in China, Japan, Korea and Russia. *Harmful Algae* 102, 101787. doi: 10.1016/j.hal.2020.101787

Sakamoto, S., Yamaguchi, M., Yamatogi, T., Kim, D. I., and Honjo, T. (2009). Growth physiology of *Cochlodinium polykrikoides*. *Bull. Plankton. Soc Japan.* 56, 32–36.

Sala-Pérez, M., Lockyer, A. E., Anesio, A., and Leroy, S. A. G. (2021). Effect of temperature and salinity on the growth and cell size of the first cultures of *Gymnodinium aureolum* from the Black Sea. *Bot. Mar.* 64, 201–210. doi: 10.1515/bot-2020-0076

Salvitti, L. (2010). *The effects of temperature, CO_2, and nitrogen source on the growth and physiology of the raphidophytes Heterosigma akashiwo and Chattonella subsalsa* (Newark (DE: University of Delaware).

Sanilkumar, M., Thomas, A. M., Vijayalakshmi, K. C., Mohamed Hatha, A. A., and Saramma, A. V. (2012). *Chattonella marina* bloom in the coastal sea off Mahe, southwest India. *Curr. Sci.* 103, 624–626.

Satta, C. T., Padedda, B. M., Sechi, N., Pulina, S., Loria, A., and Lugliè, A. (2017). Multiannual *Chattonella subsalsa* Biecheler (Raphidophyceae) blooms in a Mediterranean lagoon (Santa giusta lagoon, Sardinia island, Italy). *Harmful Algae* 67, 61–73. doi: 10.1016/j.hal.2017.06.002

Shikata, T., Yuasa, K., Kitatsuji, S., Sakamoto, S., Akita, K. , Fujinami, Y., et al. (2021). Superoxide production by the red tide-producing *Chattonella marina* complex (Raphidophyceae) correlates with toxicity to aquacultured fishes. *Antioxidants* 10, 1635. doi: 10.3390/antiox10101635

Smayda, T. J. (1969). Experimental observations on the influence of temperature, light, and salinity on cell division of the marine diatom, *Detonula confervacea* (Cleve) gran. *J. Phycol.* 5, 150–157. doi: 10.1111/j.1529-8817.1969.tb02596.x

Smayda, T. J. (2002). Adaptive ecology, growth strategies and the global bloom expansion of dinoflagellates. *J. Oceanogr.* 58, 281–294. doi: 10.1023/A:1015861725470

Subrahmanyan, R. (1954). On the life-history and ecology of *Hornellia marina* gen, et sp. nov., (Chloromonadineae), causing green discoloration of the sea and mortality among marine organisms off the Malabar coast. *Indian J. Fish.* 1, 182–203.

Thoha, H., Muawanah,, Bayu Intan, M. D., Rachman, A., Sianturi, O. R., Sidabutar, T., et al. (2019). Resting cyst distribution and molecular identification of the harmful dinoflagellate *Margalefidinium polykrikoides* (Gymnodiniales, Dinophyceae) in Lampung Bay, Sumatra, Indonesia. *Front. Microbiol.* 10. doi: 10.3389/fmicb.2019.00306

Thomas, M. K., Kremer, C. T., Klausmeier, C. A., and Litchman, E. (2012). A global pattern of thermal adaptation in marine phytoplankton. *Science* 338, 1085–1088. doi: 10.1126/science.1224836

Throndsen, J. (1969). Flagellates of Norwegian coastal waters. *Nytt. Magasin. Botanikk.* 16, 161–216.

Tiffany, M. A., Barlow, S. B., Matey, V. E., and Hurlbert, S. H. (2001). *Chattonella marina* (Raphidophyceae), a potentially toxic alga in the Salton Sea, California. *Hydrobiologia* 466, 187–194. doi: 10.1023/A:1014503920898

Tomas, C. R. (1978). *Olisthodiscus luteus* (Chrysophyceae) i. effects of salinity and temperature on growth, motility and survival. *J. Phycol.* 14, 309–313. doi: 10.1111/j.1529-8817.1978.tb00303.x

Viana, T. V., Fistarol, G. O., Amario, M., Menezes, R. B., Carneiro, B. L. R., Chaves, D. M., et al. (2019). Massive blooms of *Chattonella subsalsa* Biecheler (Raphidophyceae) in a hypereutrophic, tropical estuary-Guanabara Bay, Brazil. *Front. Mar. Sci.* 6. doi: 10.3389/fmars.2019.00085

Vonshak, A., Torzillo, G., and Tomaseli, L. (1994). Use of chlorophyll fluorescence to estimate the effect of photoinhibition in outdoor cultures of *Spirulina platensis*. *J. Appl. Phycol.* 6, 31–34. doi: 10.1007/BF02185901

Wang, Z., Yuan, M., Liang, Y., and Lu, S. (2011). Effects of temperature and organic and inorganic nutrients on the growth of *Chattonella marina* (Raphidophyceae) from the Daya Bay, South China Sea. *Acta Oceanol. Sin.* 30, 124–131. doi: 10.1007/s13131-011-0127-2

Watanabe, M., Kohata, K., Kimura, T., Takamatsu, T., Yamaguchi, S., and Ioriya, T. (1995). Generation of a *Chattonella antiqua* bloom by imposing a shallow nutricline in a mesocosm. *Limnol. Oceanogr.* 40, 1447–1460. doi: 10.4319/lo.1995.40.8.1447

Wells, M. L., Trainer, V. L., Smayda, T. J., Karlson, B. S. O., Trick, C. G., Kudela, R. M., et al. (2015). Harmful algal blooms and climate change: learning from the past and present to forecast the future. *Harmful Algae* 49, 68–93. doi: 10.1016/j.hal.2015.07.009

Yamaguchi, M., Imai, I., and Honjo, T. (1991). Effects of temperature, salinity and irradiance on the growth rates of the noxious red tide flagellates *Chattonella antiqua* and *C. marina* (Raphidophyceae). *Nippon Suisan Gakkaishi* 57, 1277–1284. doi: 10.2331/suisan.57.1277

Yamaguchi, H., Sakamoto, S., and Yamaguchi, M. (2008). Nutrition and growth kinetics in nitrogen- and phosphorus-limited cultures of the novel red tide flagellate *Chattonella ovata* (Raphidophyceae). *Harmful Algae* 7, 26–32. doi: 10.1016/j.hal.2007.05.011

Yamatogi, T., Sakaguchi, M., Iwataki, M., and Matsuoka, K. (2006). Effects of temperature and salinity on the growth of four harmful red tide flagellates occurring in Isahaya Bay in Ariake Sound, Japan. *Nippon Suisan Gakkaishi* 72, 160–168. doi: 10.2331/suisan.72.160

Yñiguez, A. T., Lim, P. T., Leaw, C. P., Jipanin, S. J., Iwataki, M., Benico, G., et al. (2021). Over 30 years of HABs in the Philippines and Malaysia: what have we learned? *Harmful Algae* 102, 101776. doi: 10.1016/j.hal.2020.101776

Yuasa, K., Shikata, T., Ichikawa, T., Tamura, Y., and Nishiyama, Y. (2020b). Nutrient deficiency stimulates the production of superoxide in the noxious red-tide-forming raphidophyte *Chattonella antiqua*. *Harmful Algae* 99, 101938. doi: 10.1016/j.hal.2020.101938

Yuasa, K., Shikata, T., Kitatsuji, S., Yamasaki, Y., and Nishiyama, Y. (2020a). Extracellular secretion of superoxide is regulated by photosynthetic electron transport in the noxious red-tide-forming raphidophyte *Chattonella antiqua*. *J. Photochem. Photobiol. B.: Biol.* 205, 111839. doi: 10.1016/j.jphotobiol.2020.111839

Zerebecki, R. A., and Sorte, C. J. B. (2011). Temperature tolerance and stress proteins as mechanisms of invasive species success. *PloS One* 6, e14806. doi: 10.1371/journal.pone.0014806

Zhang, Y., Fu, F. X., Whereat, E., Coyne, K. J., and Hutchins, D. A. (2006). Bottom-up controls on a mixed-species HAB assemblage: a comparison of sympatric *Chattonella subsalsa* and *Heterosigma akashiwo* (Raphidophyceae) isolates from the Delaware Inland bays, USA. *Harmful Algae* 5, 310–320. doi: 10.1016/j.hal.2005.09.001

frontiers | Frontiers in Microbiology

TYPE Original Research
PUBLISHED 05 October 2023
DOI 10.3389/fmicb.2023.1267299

OPEN ACCESS

EDITED BY
Jin Zhou,
Tsinghua University, China

REVIEWED BY
Kui Xu,
Sun Yat-sen University, China
Yan Li,
Fujian University of Technology, China
Fengjiao Liu,
Minnan Normal University, China

*CORRESPONDENCE
Yongcan Jiang
✉ jiangyc6@zju.edu.cn

†These authors have contributed equally to this work and share first authorship

RECEIVED 26 July 2023
ACCEPTED 21 September 2023
PUBLISHED 05 October 2023

CITATION
Jiang Y, Wang Y, Huang Z, Zheng B, Wen Y and Liu G (2023) Investigation of phytoplankton community structure and formation mechanism: a case study of Lake Longhu in Jinjiang.
Front. Microbiol. 14:1267299.
doi: 10.3389/fmicb.2023.1267299

Investigation of phytoplankton community structure and formation mechanism: a case study of Lake Longhu in Jinjiang

Yongcan Jiang[1,2*†], Yi Wang[3†], Zekai Huang[4], Bin Zheng[1], Yu Wen[1] and Guanglong Liu[3]

[1]PowerChina Huadong Engineering Corporation Ltd., Hangzhou, Zhejiang Province, China, [2]College of Environmental and Resource Sciences, Zhejiang University, Hangzhou, Zhejiang, China, [3]College of Resources and Environment, Huazhong Agricultural University, Wuhan, Hubei, China, [4]State Key Laboratory of Environmental Criteria and Risk Assessment, Chinese Research Academy of Environmental Sciences, Beijing, China

In order to explore the species composition, spatial distribution and relationship between the phytoplankton community and environmental factors in Lake Longhu, the phytoplankton community structures and environmental factors were investigated in July 2020. Clustering analysis (CA) and analysis of similarities (ANOSIM) were used to identify differences in phytoplankton community composition. Generalized additive model (GAM) and variance partitioning analysis (VPA) were further analyzed the contribution of spatial distribution and environmental factors in phytoplankton community composition. The critical environmental factors influencing phytoplankton community were identified using redundancy analysis (RDA). The results showed that a total of 68 species of phytoplankton were found in 7 phyla in Lake Longhu. Phytoplankton density ranged from 4.43×10^5 to 2.89×10^6 ind./L, with the average density of 2.56×10^6 ind./L; the biomass ranged from 0.58–71.28 mg/L, with the average biomass of 29.38 mg/L. *Chlorophyta*, *Bacillariophyta* and *Cyanophyta* contributed more to the total density, while *Chlorophyta* and *Cryptophyta* contributed more to the total biomass. The CA and ANOSIM analysis indicated that there were obvious differences in the spatial distribution of phytoplankton communities. The GAM and VPA analysis demonstrated that the phytoplankton community had obvious distance attenuation effect, and environmental factors had spatial autocorrelation phenomenon, which significantly affected the phytoplankton community construction. There were significant distance attenuation effects and spatial autocorrelation of environmental factors that together drove the composition and distribution of phytoplankton community structure. In addition, pH, water temperature, nitrate nitrogen, nitrite nitrogen and chemical oxygen demand were the main environmental factors affecting the composition of phytoplankton species in Lake Longhu.

KEYWORDS

phytoplankton community, structural characteristics, spatial distance, environmental factors, formation mechanism

1. Introduction

Global warming exacerbates the process of lake eutrophication, which further changes the distribution, phenology, abundance, composition, and trophic interactions of phytoplankton (Yan et al., 2017; Ajani et al., 2020). Phytoplankton is the important primary producer of aquatic ecosystems and plays a key role in the process of material circulation and energy flow (Lin, 2023). The complexity of their community structure in terms of temporal and spatial distribution is the premise to maintain the functional integrity of the ecosystem (Rodríguez-Gómez et al., 2022). As one of the essential indicators of aquatic environment, the structure, abundance and seasonal succession of phytoplankton communities are highly susceptible to environmental factors, and its sensitivity to hydrological environment can effectively indicate the health status of aquatic ecosystems and changes in water quality (Dong et al., 2021; Xu Q. S. et al., 2022; Xu Y. P. et al., 2022). Studies have confirmed that abiotic factors such as availability of light, temperature, inorganic nutrients (nitrogen, phosphate, silicates, and iron), hydrological connectivity, and biotic factors (e.g., zooplankton) can affect the growth and community succession of phytoplankton (Zhang et al., 2018; Han et al., 2021). In addition, the decomposition of phytoplankton has been shown to generate greenhouse gases (CO_2, CH_4, N_2O) and release dissolved nutrients that can retroactively favor climate change and eutrophication (Li and Li, 2018). The optical feedback effect of chlorophyll in phytoplankton also leads to a warming of the lake surface, which in turn significantly affects eutrophication (Lewis et al., 1990; Park et al., 2015). Therefore, understanding the structural characteristics of phytoplankton communities and their formation mechanism is essential to strengthen the management of lake aquatic ecological environment.

Previous studies on phytoplankton communities mainly proceeded from the niche theory, connecting species, communities and environmental factors, and believed that environmental processes (environmental filtration) were the most important factors affecting the structure of phytoplankton communities, and environmental heterogeneity caused differences in species composition in different environments (Valencia et al., 2004). Nevertheless, the neutral theory based on species dispersal and stochastic processes emphasizes the impact of spatial processes on biological communities where the existence, absence, and relative abundance of species is controlled by random seeding, dispersal, ecological drift, and extinction processes (Pos et al., 2019; He et al., 2022). Several recent studies indicate that the neutral theory might play an important role in phytoplankton communities (Mutshinda et al., 2016), as it underpins unexplained (random) variation in the relative abundances of species in phytoplankton communities, or on clumpy distributions of species traits such as cell size (Vergnon et al., 2009; Burson et al., 2019). There is also a view that the small phytoplankton floating on surface waters are easily dispersed passively through hydrology (Liu H. et al., 2022; Liu X. et al., 2022). This leads to highly similar algal community compositions at distant locations largely independent of environmental variables (Wu et al., 2023).

At present, numerous studies also have shown that environmental processes and spatial processes (diffusion limitation) play a role in the construction of phytoplankton communities, whereas their relative importance may vary across ecosystems and spatiotemporal scales (Heino et al., 2015; Chang et al., 2023). Compared with the ocean, the phytoplankton community composition of lake systems is more easily affected by spatial processes (Shurin et al., 2009), yet for lake phytoplankton, environmental factors (such as temperature, light, and hydrodynamic conditions) are still the main factors affecting the community structure (Wang et al., 2011; Mucina et al., 2016; Anceschi et al., 2019). Many studies have indeed confirmed that non-biological environmental variables (such as macronutrients and micronutrients), acting as indispensable protein cofactors and nutritional elements, were the main driving factors for abundance and composition of phytoplankton in aquatic ecosystems (Chiellini et al., 2020; Xue et al., 2021). Particularly, changes in nitrogen and phosphorus loads may lead to phytoplankton niche differentiation, and this different response to nutrient availability is mainly attributed to differences in explanatory degrees of niche differentiation and neutral competition (Burson et al., 2019). Consequently, it is of great significance to explore the phytoplankton community structure in lakes and its response mechanism to environmental factors and spatial processes for exploring the status of aquatic ecosystems.

In this study, the phytoplankton of Lake Longhu was the research object. Based on the monitoring of the spatial distribution of phytoplankton and water quality, the spatial differences in the community structure were analyzed. And the principal coordinate analysis of the neighbor matrix was used to identify the spatial structure of phytoplankton community formation, combined with variance decomposition to quantify the role of environmental factors, spatial processes, and their joint actions in the phytoplankton communities of Lake Longhu, and finally use canonical correspondence analysis to influence the phytoplankton community structure. It can identify significant environmental factors and provide basic data support for the water environment management and aquatic ecosystem protection of Lake Longhu.

2. Materials and methods

2.1. Study area

Lake Longhu (24°37′53″-24°39′7″N, 118°36′22″-118°37′7″E) is the largest natural shallow lake in Fujian Province, China, with a surface area of 1.60 km^2, a rainfall catchment area of 11.37 km^2, and an average water depth of 2.00–3.00 m (Figure 1). Lake Longhu is also an important water source for the water supply project of Jinjiang four towns and Jinmen county, undertaking the 4.40 m^3s^{-1} distribution of water in Jinji Gate Reservoir of Jinjiang. The total reservoir capacity of Lake Longhu is 4.05 million m^3, the annual runoff is 5.15 million m^3, and the water exchange cycle of the entire lake area is about 10 days. With a certain capacity for regulation and storage, and self-regulating through the overflow outlet in the lower reaches of the lake. The climate of this area belongs to the subtropical monsoon climate, the average annual rainfall is 911–1,231 mm. The rainfall is mainly concentrated in the typhoon and rainstorm season in July and September, accounting for about 70% of the total rainfall (Wang and Ye, 2009).

2.2. Sample collection and preparation

According to the topography and surrounding environment of the lake, ten sampling sites were set up in Lake Longhu (as shown in

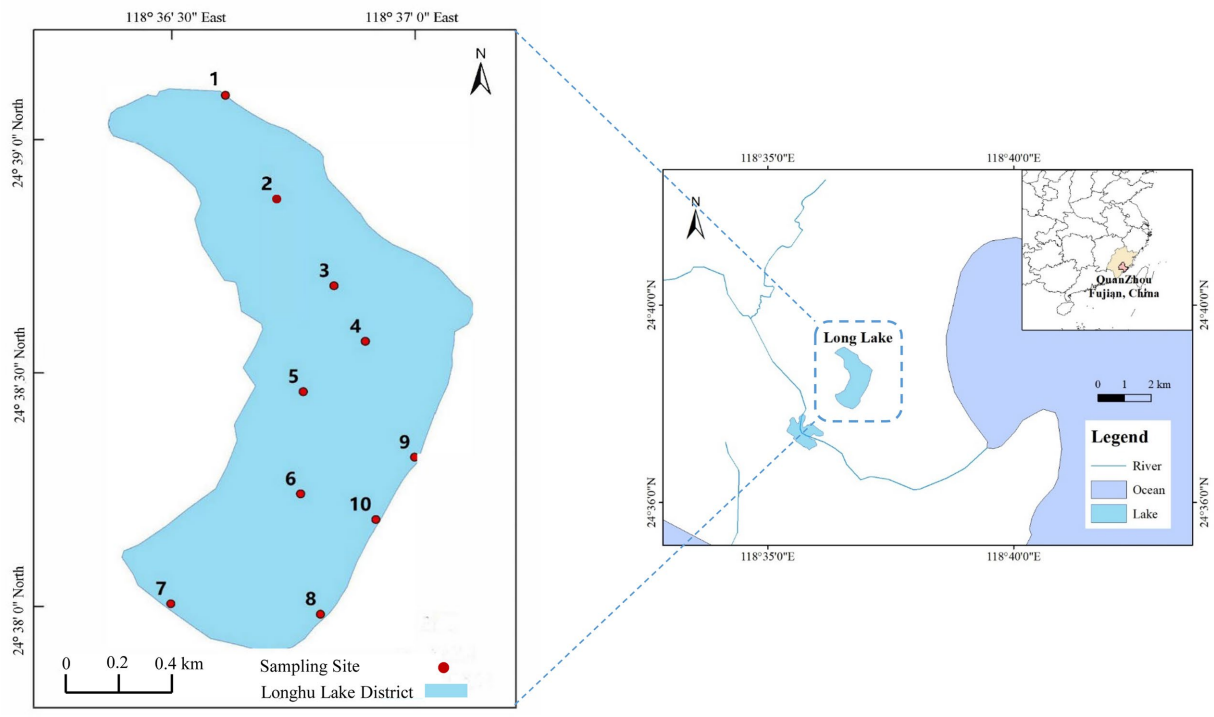

FIGURE 1
Location of Lake Longhu and the distribution of sampling sites.

Figure 1), and the longitude and latitude information of each sampling site was detailed in Supplementary Table S1. Sampling site 1 is in the entrance of Lake Longhu, sampling sites 2–7 are the open water in the lake, and sampling sites 8–10 are a small wetland in the shoreline zone of the lake. A total of 30 samples were collected from June to July in 2020. Water samples from the surface (at 0.5 m below the lake surface), middle layer (at water depth of l.5 m) and bottom layer (0.5 m on the surface of the sediment) were collected with a Patalas water collector, and the three layers of water samples were mixed. The mixed water sample were treated with nitric acid (pH < 2) and filtered with 0.45 μm microporous membrane, and then stored at 4°C for subsequent analysis.

The collection of phytoplankton in the field was divided into qualitative sampling and quantitative sampling. The qualitative samples were fished out of surface water with No. 25 phytoplankton nets, fixed with Lugol's reagent on site and then brought back to the laboratory for identification. Quantitative samples were collected with a water collector of 1.0 L water samples at each sampling site, also fixed with 1.5% Lugol's reagent on site, brought back to the laboratory to stand for 24–36 h, concentrated to 30 mL, and then 0.1 mL of the samples were microscographed with a counting frame to record phytoplankton species and quantities. Phytoplankton species were identified according to Hu and Wei (2006). Cell density was measured with a counting chamber under microscopic magnification of × 200–400. Algal biovolumes were calculated from cell numbers and cell size measurements. Conversion to biomass assumes that 1 mm^3 of volume is equivalent to 1 mg of fresh weight biomass.

2.3. Physicochemical parameters analysis

Water temperature (WT), pH, dissolved oxygen (DO) and conductivity (EC) were determined *in situ* by the multiparameter water quality monitor (EXO, Yellow Springs Instruments, United States). Transparency of the mixed water was measured using a Cypriot disc (SD). The concentrations of total nitrogen (TN), total phosphorus (TP), ammonia nitrogen (NH_4^+-N), nitrate nitrogen (NO_3^--N), and nitrite nitrogen (NO_2^--N) in lake water were measured following standard methods (State Environmental Protection Administration of China, 2002). The chemical oxygen demand (COD_{Mn}) in water sample was analyzed by potassium dichromate. Chlorophyll-a (Chla) was extracted using ethanol at 4°C. The Chla concentration was expressed as the difference in absorbance between 665 nm and 649 nm using ethanol as the control (Shi et al., 2015).

2.4. Statistical analysis

Calculation of Shannon-Wiener diversity index of phytoplankton communities based on species abundance. Clustering analysis was used to identify the spatial distribution of phytoplankton communities, and the Bray–Curtis similarity coefficient between sampling sites was calculated after the phytoplankton density data was converted to the fourth power root and normalized, so as to reduce the influence of excessive density of dominant species, and then hierarchical clustering was carried out by group average. Similarity Profiles (SIMPROF) analysis was used to verify whether the community structure obtained

by clustering is significantly different from the random spatial structure ($p < 0.05$). One-way ANOSIM was used to verify whether there were significant differences in species composition at different sampling sites. And diversity index calculations, cluster analysis, SIMPROF analysis and ANOSIM analysis were all completed by PRIMER 6.0 (Clarke et al., 2006).

The generalized additive model (GAM) was used to fit the relationship between community heterogeneity, geographical distance and environmental distance, respectively. The community phase heterogeneity matrix was based on phytoplankton density data, and the Bray-Curtis phase dissimilarity matrix was calculated by quadruple root transformation. The geographic distance matrix was obtained by calculating the geographic distance of each pair of stations based on the latitude and longitude coordinates of the sampling sites. And the Euclidian distance matrix was calculated from the environmental variables of the sampling sites. The Bray-Curtis heterogeneity matrix and Euclidian distance matrix were completed using the "vegan" package of the R language (4.03); The geographic distance matrix was done using the package "geosphere"; GAM was done using the package "mgcv" (Team, R.C, 2014).

Principal coordinate analysis of neighborhood matrix (PCNM) was used to identify the spatial structure formed by phytoplankton communities. Variance partitioning analysis (VPA) was used to assess the extent to which environmental and spatial variables explained the variation in phytoplankton community. Before the VPA analysis, in order to ensure the simplicity of the model, the significant ($p < 0.05$) environment factors and spatial variables were selected and screened out based on the previous term, and then brought into the model for VPA analysis. The correlation between phytoplankton communities and environmental factors was analyzed by redundancy analysis (RDA). Significant environmental factors were screened out using forward selection, and model significance was detected by Monte Carlo displacement tests (499 times). PCNM vector acquisition, VPA analysis, and RDA analysis were all done using Canoco 5 software (Šmilauer and Lepš, 2003).

3. Results

3.1. Water quality of each sampling site

As shown in Figure 2, the variation of physicochemical indicators of water in Lake Longhu were presented. The range of pH was between 7.50 and 8.25. pH of the sampling site from 1 to 7 was higher than that at the 8–10 sampling sites. The range of DO in water was 6.06 to 8.29 mg/L in Lake Longhu, respectively. DO value was the lowest at the entrance of sampling site, and the value of DO at 2 to 7 sampling sites was higher. SD and DO had the same variation trend (Supplementary Table S2). EC ranged from 143.0–331.0 μS/cm, and the conductivity at site 2 in the north was 159 μS/cm, which was lower than the measured value at the entrance level, indicating that the conductivity brought by the entrance water had little effect (Supplementary Table S2). And the conductivity measured at sampling sites 8–10 was generally higher, which might be mainly due to the slow flow of water. Furthermore, the chlorophyll content of water showed a lower level in general, and the contents of Chla and SD both showed a higher trend in the north than in the south. The highest chlorophyll content was found near site 2, indicating that the water environment near it was suitable for the growth and reproduction of algae. Both Chla and SD were lower in the small wetlands of sites 8 and 10, which may be due to the predominant influence of suspended particulate matter in the lake on transparency, while the influence of algae was more limited.

Judging from the change trend of COD_{Mn} concentration in Lake Longhu, the highest COD_{Mn} concentration was 36.46 mg/L at site 1, and the other sampling sites were between 10.54 and 18.35 mg/L. The content of TP ranged from 0.04 to 0.09 mg/L and TP in open water was generally lower, with the highest content at the entrance, indicating that the content of TP in Lake Longhu was affected by certain entrance water. The overall TN concentration in the water was generally higher, ranging from 1.04 to 2.51 mg/L, and the TN concentration showed a decreasing trend from north to south, in addition, the TN concentration at the entrance site 1 was also substantially higher than the average value in the lake. The concentrations of NH_4^+-N, NO_3^--N and NO_2^--N in the water were between 0.07–0.19 mg/L, 0.81–2.22 mg/L and 0.01–0.06 mg/L, respectively. And the overall trend was similar to that of TP and TN. From the northern lake area to the southern lake area, the N, P levels showed a gradual downward trend, while there was an increase at sampling sites 8 and 10, indicating that the entrance water quality of Lake Longhu was poor and may be the main source of water pollution. In terms of the overall analysis from the north to the south of the lake, the overall water quality of Long Lake was in good condition. Moreover, the ratio of N/P combined with their concentration has great effects on algal growth, physiological response, biochemical compositions, and potentially impacted the function and community structure of aquatic ecosystems (Keck and Lepori, 2012; Huang et al., 2019; Zhao et al., 2019). Generally, the N/P molar ratio required for phytoplankton growth and physiological balance was 16: 1 (Redfield, 1960), and it was changed with phytoplankton species due to their different requirements for N and P (Ho et al., 2003; Wagner et al., 2021). In this study, the N/P molar ratio of all sampling sites was greater than 16, indicating phosphorus limitation. In addition, lower phosphorus content also inhibited organic synthesis of nitrogen (Meunier et al., 2017).

3.2. Phytoplankton community structures

A total of 68 species of phytoplankton were identified at the sampling sites (Supplementary Table S3), *Cyanophyta*, *Chlorophyta*, and *Bacillariophyta* were identified as dominant phyla, with 29 species of *Chlorophyta*, accounting for 42.6% of the total number of species, followed by 21 species of *Bacillariophyta* (30.9%), and 7 species of *Cyanophyta*, accounting for 10.3%. *Cryptophyta*, *Euglenophyta*, *Pyrrophyta*, and *Chrysophyta* were 4, 3, 3 and 1 respectively, accounting for 5.9%, 4.4%, 4.4%, and 1.5% of the total species. The spatial variations of phytoplankton composition percentages was shown in Figure 3, and the spatial change of phytoplankton community characteristics was shown in Figure 4. The number of phytoplankton species varies from 8 to 38 species at different sampling sites, with an average number of 30 species. The least number of phytoplankton species was found at the entrance of Lake Longhu, and the general trend from the south to the north of the lake was a decrease in species.

10.3389/fmicb.2023.1267299

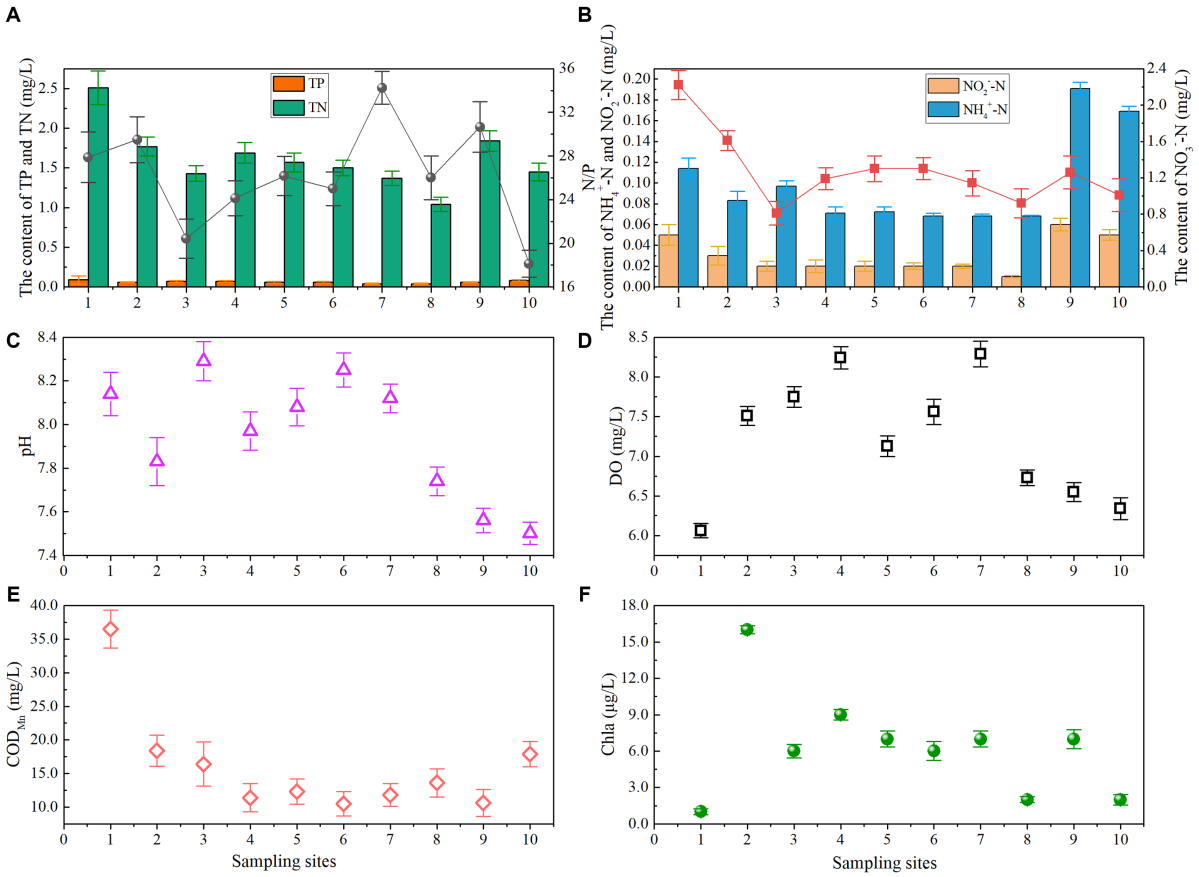

FIGURE 2
Spatial distribution of water quality parameters in Lake Longhu [**(A)** TP, TN, and N/P; **(B)** NH_4^+-N, NO_3^--N, and NO_2^--N; **(C)** pH; **(D)** DO; **(E)** COD_{Mn}; **(F)** Chla].

The total density of phytoplankton was 2.56×10^7 ind./L, and the density variation range was 4.43×10^5–2.89×10^6 ind./L, and the average density was 2.56×10^6 ind./L. The total biomass of phytoplankton was 293.82 mg/L, the biomass variation ranged from 0.58 to 71.28 mg/L, and the average biomass was 29.38 mg/L. In terms of density composition, *Chlorophyta* (8.84×10^6 ind./L), *Cyanophyta* (7.72×10^6 ind./L), *Bacillariophyta* (4.86×10^6 ind./L), and *Cryptophyta* (2.46×10^6 ind./L) became the main phytoplankton of Lake Longhu in this study with abundance ratios of 34.5%, 30.1%, 19.0%, and 9.58%, respectively. With respect to biomass composition, *Chlorophyta* (154.67 mg/L) and *Cryptophyta* (88.66 mg/L) accounted for 47.95% and 31.67% of the total biomass, which were the phytoplankton with the highest proportion of biomass in Lake Longhu, followed by *Bacillariophyta* and *Pyrrophyta*, with a biomass proportion of 8.98% and 6.29%, respectively. From the overall perspective of the lake, the density and biomass of phytoplankton at the entrance were lower, and the density and biomass of phytoplankton in the open waters of the lake showed a consistent trend, while the biomass decreased from north to south, and increased at sampling sites 8, 9, and 10. Judging from the survey results, the phytoplankton in the water of Lake Longhu were mainly *Chlorophyta*, *Cyanophyta*, *Bacillariophyta* and *Cryptophyta* (Xu Y. P. et al., 2022). Further identification of algal species revealed that the dominant species of *Chlorophyta* were *Pandorina morum (Muell.) Bory* and *Chlorella* sp., the dominant species of *Cyanophyta* were *Merismopedia tenuissima Lemm.* and *Aphanizomenon* sp., and the dominant species of *Bacillariophyta* were *Cyclotella meneghiniana Kütz.* and *Melosira* sp.

3.3. Phytoplankton diversity index and similarity analysis

The Shannon-Wiener diversity index of the phytoplankton communities was calculated based on species abundance, and the results showed that the Shannon-Wiener diversity index of phytoplankton at different sampling sites in Lake Longhu varied from 0.47 to 2.62, with an average diversity index of 2.09 (Supplementary Figure S1), indicating that the phytoplankton community parameters at different sampling sites fluctuated widely, and there were spatial differences in the species distribution of phytoplankton. In addition, the results of cluster analysis and SIMPROF analysis also showed that there were significant differences in the spatial distribution of phytoplankton communities among sampling sites (Figure 5). At the 15% similarity level, there was a significant difference between sampling site 1 and other sampling sites ($p = 0.001$); at the 50% similarity level, there was a significant difference between sampling site 10 and other sampling sites ($p = 0.001$); and there was a significant difference between sampling site 2 and other sampling sites at the 60%

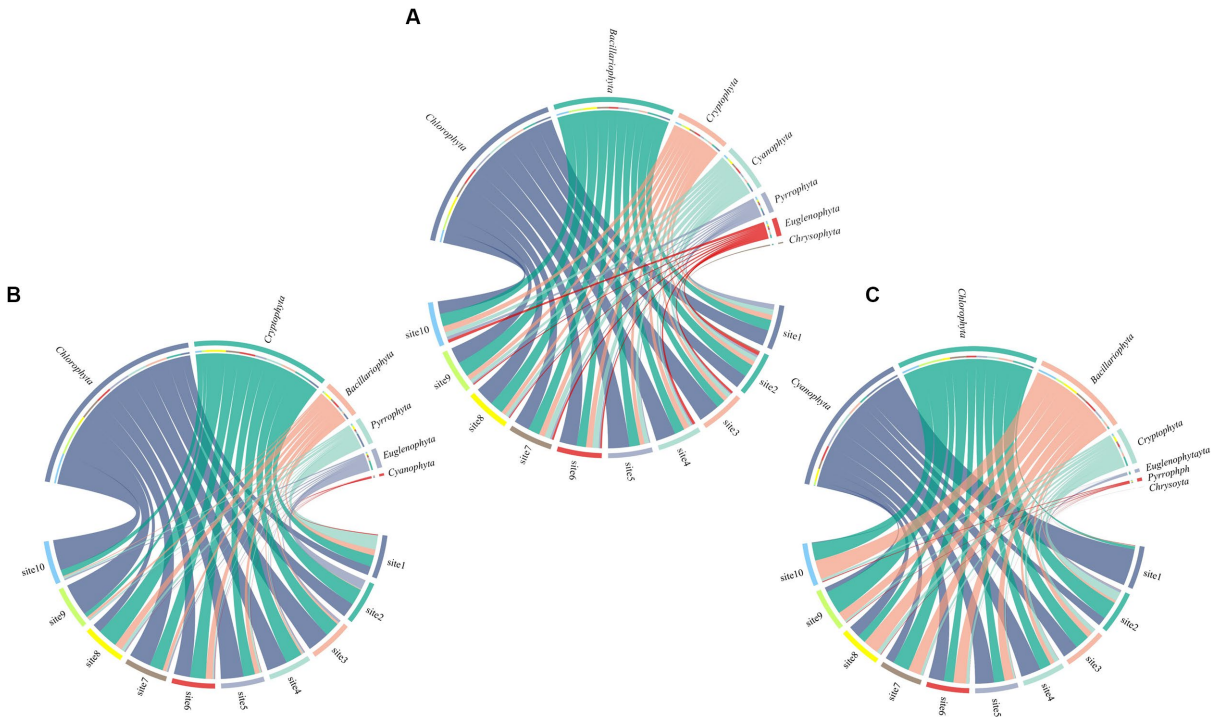

FIGURE 3
Spatial variations of phytoplankton composition percentages [**(A)** species; **(B)** biomass; **(C)** density].

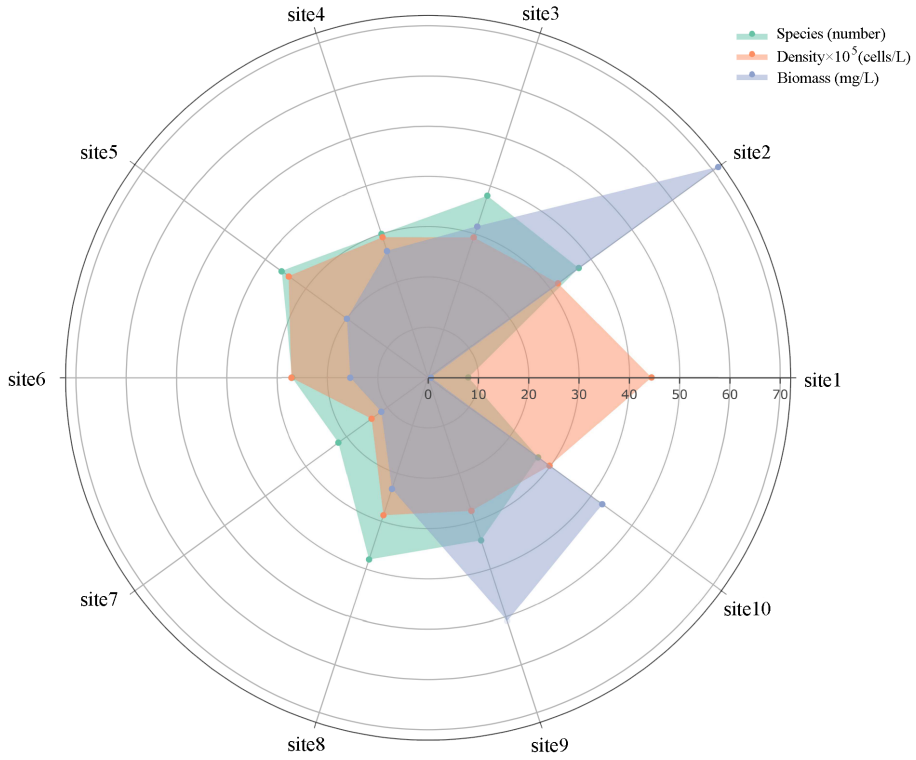

FIGURE 4
Spatial variations of phytoplankton community characteristics.

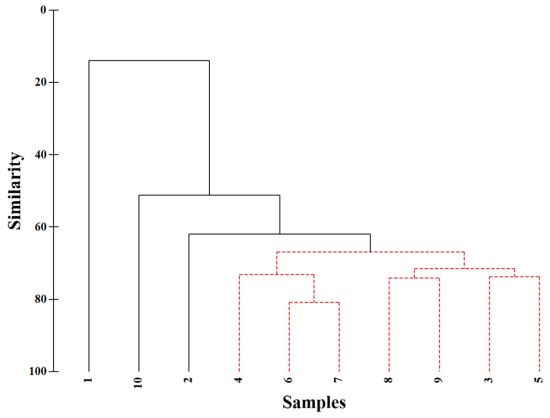

FIGURE 5
Cluster analyses for the phytoplankton community structure in Lake Longhu.

similarity level ($p = 0.005$). The ANOSIM analysis showed that there were significant differences in phytoplankton community structure at different sampling sites ($R^2 = 0.933$, $p = 0.008$), indicating significant spatial variability in phytoplankton community structure.

3.4. Distance attenuation effect of phytoplankton

In order to further investigate the variation of phytoplankton along different geographical distances and environmental factors, a generalized additive model (GAM) was constructed with the relative values of phytoplankton abundance as response values and geographical distance and environmental distance factors as independent variables, and the fitting results of the composition GAM model showed that there was a significant distance attenuation effect in phytoplankton communities, namely the heterogeneity of community composition increased with the increase of geographical distance ($R^2 = 0.332$, $p < 0.001$; Figure 6A). Environmental factors play an important role in phytoplankton community construction, and community heterogeneity increased with increasing environmental distance ($R^2 = 0.852$, $p < 0.001$), while the change in community heterogeneity slowed down when the environmental distance was large enough (Figure 6B). On the other hand, there was spatial autocorrelation in environmental factors, and environmental distance increased with the increase of geographical distance ($R^2 = 0.475$, $p < 0.001$; Figure 6C), which indicated that the environmental distance and water correlation factors of Lake Longhu jointly drove the composition and distribution of phytoplankton community structure.

3.5. Correlation of community composition and water quality parameters

The spatial structure characteristics of phytoplankton community formation were identified based on the principal coordinate analysis of the neighborhood matrix (PCNM), and the results showed that the previous selection screened out five environmental factors (pH, water temperature, NO_2^--N, NO_3^--N and COD_{Mn}) and one spatial factor (PCNM1) had a significant impact on the phytoplankton community structure ($p < 0.05$). In addition, the variance decomposition (VPA) results showed that the environment variable ($p = 0.002$) and the spatial variable ($p = 0.026$) jointly explain 41.6% of the community variation of the phytoplankton community, respectively. The environment variable explained more community variation than the spatial variable, with the two together explaining 7.3% of the community variation (Supplementary Figure S2).

The relationship between the major drivers and phytoplankton community composition was examined based on the RDA models. The RDA explained about 59.26% of the variation in phytoplankton community composition in Lake Longhu. Most of this variation is explained by the first axis (33.12%) with the second axis explaining an additional 26.14% (Figure 7). It was clearly from the figure that pH, temperature, NO_2^--N, NO_3^--N and COD_{Mn} were the main environmental factors affecting the distribution of the phytoplankton community. In addition, a good correlations among NO_2^--N, NO_3^--N, NH_4^+-N, COD_{Mn}, TN and TP was also demonstrated from the smaller pinch angles between environmental factors. From the effects of environmental factors on the abundance of specific phytoplankton, DO and pH mainly affected the growth of *Chlorophyta*, while water temperature, NO_2^--N and NH_4^+-N mainly affected the relative abundance of *Chrysophyta*, *Euglenophyta* and *Bacillariophyta*, and the growth of *Pyrrophyta*, *Cryptophyta*, *Cyanophyta* was mainly related to the amount of NO_2^--N, NO_3^--N, NH_4^+-N, COD_{Mn}, TN and TP.

4. Discussion

4.1. Distribution characteristics of phytoplankton communities and their influencing factors

Overall, the species, density and biomass of phytoplankton showed that the sampling site 1 at the entrance was the smallest, sampling site 2 was the most suitable for algae growth, and phytoplankton trends decreased at sampling sites 2 to 7, while phytoplankton growth at sampling sites 8, 9, and 10 showed a slight increase trend, indicating that the phytoplankton species and biomass at the entrance were the least and the structure was relatively simple, while the water of the vast lake surface was suitable for the growth and reproduction of phytoplankton. However, in general, the composition of the phytoplankton structure in the lake was relatively simple, the stability was good, and the overall water quality was also better. Phytoplankton are extremely sensitive and perceptive to lake water quality. It has been shown that different species of phytoplankton are often found together in water with frequent blooms, dominate in different areas of the water, and show dominant population succession in time series (Zhang et al., 2016). Since realized niches of phytoplankton in various environmental factors are different and also contribute to explaining the succession of phytoplankton community in the complicated environment under the multiple stresses of anthropogenic activities and climate changes. The dominant population composition reflected the pollution status of the lakes and reservoirs to a certain extent, and in terms of community composition, *Chlorophyta*, *Cyanophyta*, *Bacillariophyta* and *Cryptophyta* in Lake Longhu were the dominant populations in phytoplankton in our study. According to the density composition, the proportion of *Cyanophyta* in the entrance was the largest, and *Cyanophyta* were the most typical dominant group of

10.3389/fmicb.2023.1267299

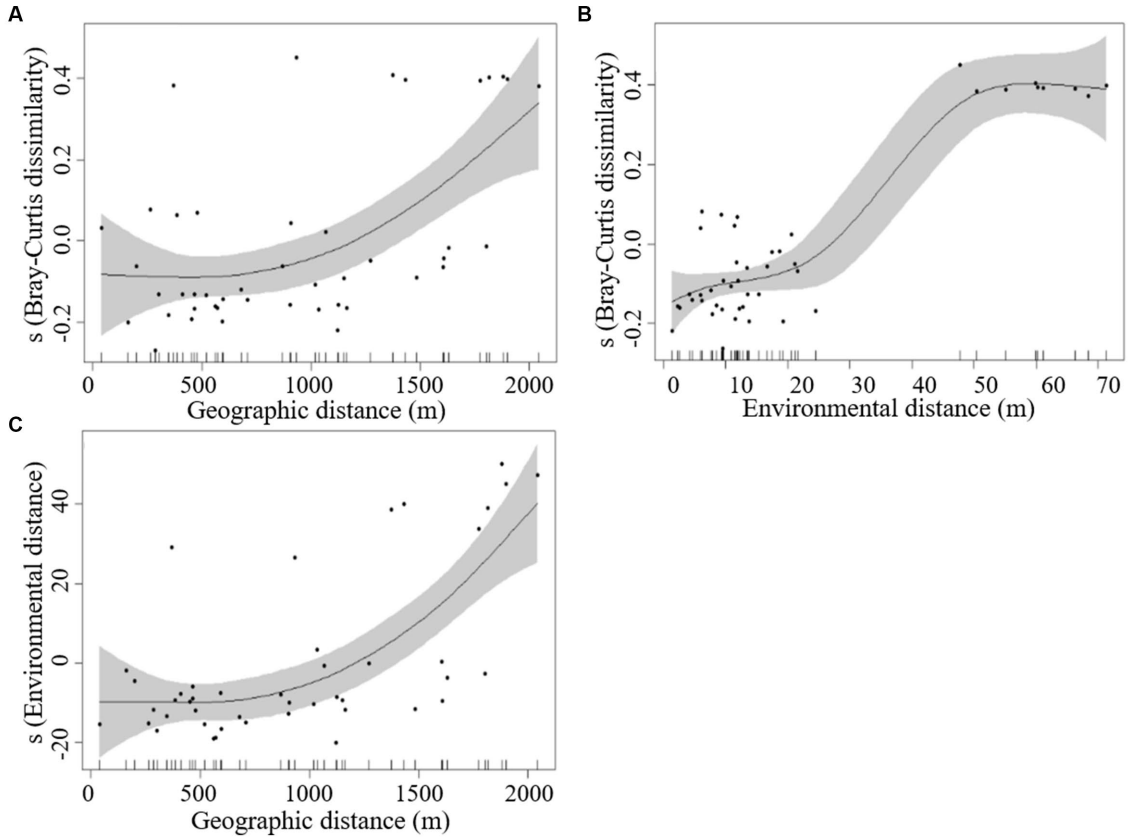

FIGURE 6
The fitted curves between Bray–Curtis dissimilarity of phytoplankton, geographic distance, and environmental distance based on GAM models [**(A)** Bray–Curtis dissimilarity and geographic distance; **(B)** Bray–Curtis dissimilarity and environmental distance; **(C)** environmental distance and geographic distance].

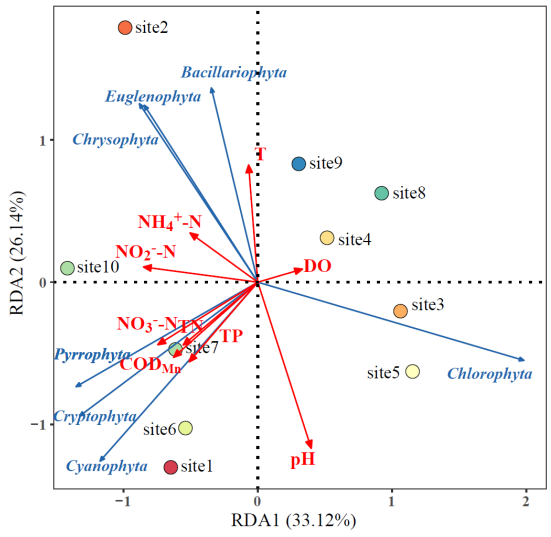

FIGURE 7
Redundancy analysis (RDA) of phytoplankton community species composition and environmental factors.

eutrophic water, which indicated that there was a certain degree of pollution in the entrance water. Hydraulic residence time or flow rate can also affect the occurrence of *Cyanophyta*. Some studies have confirmed that the slower flow rate and longer retention time of lake and reservoir water intercepted higher nutrients, which was conducive to the growth and propagation of *Cyanophyta* (Han et al., 2022). Studies have also demonstrated that *Cyanophyta* as prokaryotes have a significant competitive advantage over other eukaryotic producers (such as *Chlorophyta*, *Bacillariophyta*, etc.) under nutrient-rich conditions (Paerl et al., 2011). Furthermore, temperature as a climatic factor also significantly influenced the growth of *Cyanophyta*, and relatively higher temperature enhanced the competitiveness of *Cyanophyta* with other eukaryotic phytoplankton (Kim et al., 2020). It has been noted that some *Cyanophyta* are recorded to have a dominant position in comparison with diatom above 25°C (Berg and Sutula, 2015).

With the gradual decrease of *Cyanophyta* density from the north to the south of Lake Longhu, the dominant algae population of the water changed to *Chlorophyta*, which also indicated that the probability of eutrophication in the lake gradually decreased. There are many factors that cause this change, the most important of which is nutrient elements. Nitrogen and phosphorus are the main drivers of phytoplankton growth in lakes, and it has been found that *Chlorophyta* have a stronger growth advantage than *Cyanophyta* and grow faster compared to *Cyanophyta* under conditions of sufficient phosphate concentration (Klisarova et al., 2023). In addition, the nitrate nitrogen content in Lake Longhu is higher (Figure 2), and some researchers have found that *Cyanophyta* are less competitive in this environment (Chen et al., 2017), which is consistent with the results of this study.

In addition, *Chlorophyta*, as important primary producers in aquatic and terrestrial ecosystems, exhibit great diversity in morphological and ultrastructural characteristics, which leads to their better viability and wider ecological niche compared to other phytoplankton (Fields et al., 2021). Interestingly, *Cryptophyta* were more sensitive to temperature than nutrients (Rao et al., 2021). Furthermore, *Cryptophyta* have a unique auxiliary pigment for photosynthesis and a competitive advantage in lake with their own advantages as a dominant taxon in July when light is stronger and water temperature is higher, so *Cryptophyta* has higher biomass in the vast lake surface (Ding et al., 2018; Cheng et al., 2019; Tian et al., 2022).

As one of the most diverse and abundant classes of photosynthetic microalgae, diatoms are known to play an indispensable role in regulating the biogeochemical cycle of nutrients such as carbon, nitrogen and silica in lake waters (Liu et al., 2012). As the genus with the highest proportion of diatom populations, *Bacillariophyta* has strong viability due to its special carbon concentration and fixation mechanism. Studies have shown that *Bacillariophyta* are the dominant population among phytoplankton in rivers, which have physiological competitive advantages over the growth of other phytoplankton in rivers, while the growth of *Bacillariophyta* is significantly correlated with phosphorus, and the TP concentration in Lake Longhu is 0.04–0.09 mg/L, which is conducive to the growth of *Bacillariophyta* (Vello et al., 2023). In addition, Beaver et al. (2013) found that the biomass of *Bacillariophyta* increased with decreasing hydraulic residence time, which was the opposite of the adaptation of *Cyanophyta* to the environment (Beaver et al., 2013). Moreover, *Bacillariophyta* potentially take up nitrate to serve as a sink for electrons during periods of imbalance between light energy harvesting and utilization, and this mechanism is apparently not present in non-diatom species, thus *Bacillariophyta* growth well in RW ponds are associated with high nitrate supply (Berg et al., 2003; Liu H. et al., 2022; Liu X. et al., 2022). The dominant phytoplankton population varies in different months, and most species only become dominant species in a certain month, so in order to better understand the composition of phytoplankton populations in Lake Longhu, it is necessary to monitor and study the phytoplankton in Lake Longhu at different times. The lake as a whole in this study was in a poor-mesotrophic state. In terms of total phytoplankton biomass and density, the *Cyanophyta*, *Chlorophyta* and *Bacillariophyta* contributed more to the total density, and *Chlorophyta* and *Cryptophyta* contributed more to the total biomass, which may be caused by multiple influences such as the population characteristics of phytoplankton and environmental factors.

4.2. Environmental factors drive phytoplankton community succession

In lakes where eutrophication occurs frequently, different dominant populations compete with each other and undergo succession, and the mechanisms by which eutrophication occurs are always the result of the interaction of complex and environmental factors (Han et al., 2023). Phytoplankton spatial processes and environmental factors are important ecological processes for community composition and biodiversity maintenance in biological assemblages (Chase and Myers, 2011; Laland et al., 2016). The results of GAM model and VPA analysis showed that there was a significant correlation between phytoplankton community variability and geographical distance and environmental factors (Figure 6; Supplementary Figure S2). Both environmental and spatial factors significantly explained the variation of phytoplankton community, indicating that spatial processes and environmental factors play equally important roles in the construction of phytoplankton community in Lake Longhu, which breaks the conclusion that phytoplankton community structure is mainly affected by environmental processes in previous studies (Xu Q. S. et al., 2022; Xu Y. P. et al., 2022; Shuwang et al., 2023).

Further analysis of specific environmental impact factors is of great significance for exploring the formation mechanism of phytoplankton community structure and the development direction of community succession. Many previous studies have focused on the environmental influences of phytoplankton in specific lakes and reservoirs. Yang et al. (2021) found that TN, conductivity, water temperature and altitude factors affected the density of phytoplankton and the distribution of dominant species in reservoirs in the arid region of northwest China (Yang et al., 2021). Wang et al. (2022) found that water temperature, pH, COD_{Mn} and total nitrogen were the main driving factors affecting the seasonal variation of phytoplankton community structure and density in urban lakes in cold areas. And in our study, pH, water temperature, nitrite nitrogen, nitrate nitrogen and COD_{Mn} were the main drivers affecting the phytoplankton community structure in Lake Longhu (Figure 7). In addition, The number of *Gymnodinium aeruginosum Stein.* was higher at sampling site 10, its community structure was significantly different from other sampling sites by cluster analysis and SIMPROF analysis (Figure 5). The RDA analysis further showed that there was a positive correlation between phytoplankton species composition and nitrite nitrogen as well as ammonia nitrogen at sampling site 10. The monitoring results of Lake Longhu over the past 10 years showed that the eutrophication problem of Lake Longhu had a tendency to intensify year by year, with the level of nitrogen and phosphorus gradually increased (Li and Li, 2018). Furthermore, the phytoplankton survey in Lake Longhu showed that *Euglenophyta* was occasionally species, and the eutrophication process that occurred changed the species composition of the phytoplankton in Lake Longhu. The results of cluster and SIMPROF analysis showed that there were significant differences in the phytoplankton community structure between sampling site 1 and other sampling sites, and there was a positive correlation between the phytoplankton species composition and pH, TP and COD_{Mn}. COD_{Mn} is a chemically measured amount of reducing substance in the water that needs to be oxidized, representing the water body in an oxidation/reduction environment. The source of COD_{Mn} is generally the organic matter in the water, and the organic matter in the water body mainly comes from the discharge of domestic sewage and industrial wastewater, as well as the influx of animals and plants after the decomposition of decay with rainfall (Liu et al., 2023). The chemical oxygen demand reflects the degree of organic pollution in water, and the larger the COD_{Mn}, the more serious the organic pollution of the water (Wang et al., 2021). Sampling site 1 was located at the entrance of Lake Longhu, where the higher Mn content in the upstream water and organic pollution affected the species composition of phytoplankton.

4.3. Mechanisms of phytoplankton community structure formation

The results of the GAM model showed that there was a significant distance attenuation effect on phytoplankton communities, and

community heterogeneity increased with geographic distance, indicating that diffusion restriction affected phytoplankton community formation. However, environmental distances also increased with geographic distances, suggesting that there was spatial autocorrelation of environmental factors in lake and the interpretation of community structure by spatial processes may be due to environmental filtering (Ma et al., 2022). The results of VPA analysis showed that spatial processes and environmental processes together explained 7.3% of variation in community structure, which was higher than purely spatial processes, and spatial processes mainly influenced the construction of phytoplankton community structure mainly through the joint action of environmental processes. The environmental variables explained the 41.6% of the variation in phytoplankton community structure in Lake Longhu, which was higher than the interpretation rate of the spatial variables, indicating that the deterministic processes filtered by the environment were the main cause of the variation in phytoplankton community structure. Studies have also shown the importance of spatial and environmental processes as community building factors in freshwater lakes (Herrera-Silveira and Morales-Ojeda, 2009; Alahuhta et al., 2023), the relative importance of which depends on the dispersal capacity of species, environmental gradients, and spatial extent (Heino et al., 2015). Increased species dispersal capacity contributes to reducing dispersal restriction and increasing the importance of environmental processes (Shurin et al., 2009). The water exchange period in the study area was short, and the environmental gradient difference was significant, which provided diffusion conditions for phytoplankton, and the spatial distribution of phytoplankton was affected by the regional cluster effect, and the role of environmental processes was obvious (Cui et al., 2016).

5. Conclusion

Based on the investigation of water quality and phytoplankton community composition in Lake Longhu, this study further explored the formation mechanism and influencing factors of phytoplankton using methods such as cluster analysis (CA), analysis of similarities (ANOSIM), redundancy analysis (RDA) and generalized additive model (GAM). During the investigation period, a total of 7 phytoplankton species were detected in Lake Longhu, mainly *Chlorophyta*, *Bacillariophyta*, *Cyanophyta*, accounting for 42.6%, 30.9%, and 10.3% respectively, and the proportion of other species was smaller. The results of CA and ANOSIM analysis showed that there were obvious spatial differences in phytoplankton communities. The GAM and variance partitioning analysis further showed that there was a significant distance attenuation effect in phytoplankton communities and spatial autocorrelation in environmental factors, which significantly affected the construction of phytoplankton communities. In addition, pH, water temperature, nitrite nitrogen, nitrate nitrogen and COD_{Mn} were the main environmental factors affecting the composition of phytoplankton species in Lake Longhu based on the RDA analysis.

Data availability statement

The original contributions presented in the study are included in the article/Supplementary material, further inquiries can be directed to the corresponding author.

Author contributions

YJ: Conceptualization, Data curation, Formal analysis, Investigation, Methodology, Project administration, Writing – original draft, Writing – review & editing. YiW: Data curation, Formal analysis, Methodology, Software, Supervision, Writing – original draft. ZH: Data curation, Formal analysis, Methodology, Software, Supervision, Writing – review & editing. BZ: Funding acquisition, Project administration, Resources, Supervision, Validation, Writing – review & editing. YuW: Funding acquisition, Project administration, Resources, Supervision, Validation, Writing – review & editing. GL: Project administration, Supervision, Validation, Visualization, Writing – review & editing.

Funding

The author(s) declare financial support was received for the research, authorship, and/or publication of this article. The authors would like to acknowledge the Researchers Supporting Project "Science and Technology Project of Huadong Engineering (Fujian) Corporation" (ZKY2022-FJ-02-02).

Acknowledgments

We are grateful to the editors and reviewers for their constructive comments to improve the quality of the manuscript during the review process.

Conflict of interest

YJ, BZ, and YuW were employed by PowerChina Huadong Engineering Corporation Ltd.

The remaining authors declare that the research was conducted in the absence of any commercial or financial relationships that could be construed as a potential conflict of interest.

Publisher's note

Supplementary material

The Supplementary material for this article can be found online at: https://www.frontiersin.org/articles/10.3389/fmicb.2023.1267299/full#supplementary-material

References

Ajani, P. A., Davies, C. H., Eriksen, R. S., and Richardson, A. J. (2020). Global warming impacts micro-phytoplankton at a long-term Pacific Ocean coastal station. *Front. Mar. Sci.* 7:576011. doi: 10.3389/fmars.2020.576011

Alahuhta, J., Kanninen, A., Hellsten, S., Vuori, K. M., Kuoppala, M., and Hämäläinen, H. (2023). Environmental and spatial correlates of community composition, richness and status of boreal lake macrophytes. *Ecol. Indic.* 32, 172–181. doi: 10.1016/j.ecolind.2013.03.031

Anceschi, N., Hidalgo, J., Plata, C. A., Bellini, T., Maritan, A., and Suweis, S. (2019). Neutral and niche forces as drivers of species selection. *J. Theor. Biol.* 483:109969. doi: 10.1016/j.jtbi.2019.07.021

Beaver, J. R., Jensen, D. E., Casamatta, D. A., Tausz, C. E., Scotese, K. C., Buccier, K. M., et al. (2013). Response of phytoplankton and zooplankton communities in six reservoirs of the middle Missouri River (USA) to drought conditions and a major flood event. *Hydrobiologia* 705, 173–189. doi: 10.1007/s10750-012-1397-1

Berg, G. M., Balode, M., Purina, I., Bekere, S., Bechemin, C., and Maestrini, S. Y. (2003). Plankton community composition in relation to availability and uptake of oxidized and reduced nitrogen. *Aquat. Microb. Ecol.* 30, 263–274. doi: 10.3354/ame030263

Berg, M., and Sutula, M. (2015). Factors affecting the growth of cyanobacteria with special emphasis on the Sacramento-san Joaquin Delta. *SCCWRP Tech. Rep.* 869:100.

Burson, A., Stomp, M., Mekkes, L., and Huisman, J. (2019). Stable coexistence of equivalent nutrient competitors through niche differentiation in the light spectrum. *Ecology* 100:e02873. doi: 10.1002/ecy.2873

Chang, L. W., Chiu, S. T., and Hsieh, C. F. (2023). Contrasting spatial distribution of pioneer versus non-pioneer saplings in a Taiwanese forest: a multiple scale approach. *Environ. Res.* 38, 604–616. doi: 10.1111/1440-1703.12395

Chase, J. M., and Myers, J. A. (2011). Disentangling the importance of ecological niches from stochastic processes across scales. *Philos. Trans. R. Soc. Lond. Ser. B Biol. Sci.* 366, 2351–2363. doi: 10.1098/rstb.2011.0063

Chen, R., Ao, D., Ji, J., Wang, X. C., Li, Y. Y., Huang, Y., et al. (2017). Insight into the risk of replenishing urban landscape ponds with reclaimed wastewater. *J. Hazard. Mater.* 324, 573–582. doi: 10.1016/j.jhazmat.2016.11.028

Cheng, B., Xia, R., Zhang, Y., Yang, Z., Hu, S., Guo, F., et al. (2019). Characterization and causes analysis for algae blooms in large river system. *Sustain. Cities Soc.* 51:101707. doi: 10.1016/j.scs.2019.101707

Chiellini, C., Guglielminetti, L., Pistelli, L., and Ciurli, A. (2020). Screening of trace metal elements for pollution tolerance of freshwater and marine microalgal strains: overview and perspectives. *Algal Res.* 45:101751. doi: 10.1016/j.algal.2019.101751

Clarke, K. R., Somerfield, P. J., and Chapman, M. G. (2006). On resemblance measures for ecological studies, including taxonomic dissimilarities and a zero-adjusted bray–Curtis coefficient for denuded assemblages. *J. Exp. Mar. Biol. Ecol.* 330, 55–80. doi: 10.1016/j.jembe.2005.12.017

Cui, D. Y., Wang, J. T., Tan, L. J., and Dong, Z. Y. (2016). Impact of atmospheric wet deposition on phytoplankton community structure in the South China Sea. *Estuar. Coast. Shelf. S.* 173, 1–8. doi: 10.1016/j.ecss.2016.02.011

Ding, S. M., Chen, M. S., and Gong, M. D. (2018). Internal phosphorus loading from sediments causes seasonal nitrogen limitation for harmful algal blooms. *Sci. Total Environ.* 625, 872–884. doi: 10.1016/j.scitotenv.2017.12.348

Dong, Y. L., Zuo, L. M., Ma, W., Chen, Z. Y., Cui, L., and Lu, S. H. (2021). Phytoplankton community organization and succession by sea warming: a case study in thermal discharge area of the northern coastal seawater of China. *Mar. Pollut. Bull.* 169:112538. doi: 10.1016/j.marpolbul.2021.112538

Fields, F. J., Hernandez, R. E., Weilbacher, E., Garcia-Vargas, E., Huynh, J., Thurmond, M., et al. (2021). Annual productivity and lipid composition of native microalgae (Chlorophyta) at a pilot production facility in Southern California. *Algal Res.* 56:102307. doi: 10.1016/j.algal.2021.102307

Han, Y., Aziz, T. N., Del Giudice, D., Hall, N. S., and Obenour, D. R. (2021). Exploring nutrient and light limitation of algal production in a shallow turbid reservoir. *Environ. Pollut.* 269:116210. doi: 10.1016/j.envpol.2020.116210

Han, M. X., Huang, J. R., Yang, J., Wang, B. C., Sun, X. X., and Jiang, H. C. (2023). Distinct assembly mechanisms for prokaryotic and microeukaryotic communities in the water of Qinghai Lake. *J. Earth Sci.* 34, 1189–1200. doi: 10.1007/s12583-023-1812-8

Han, L. B., Li, Q. H., Chen, W. S., Wang, X., Zhou, S. H., Han, M. S., et al. (2022). The key environmental factors driving the succession of phytoplankton functional groups in Hongfeng reservoir, Southwest China. *J. Oceanol. Limnol.* 40, 1472–1484. doi: 10.1007/s00343-021-1120-z

He, Y., Liang, S. C., Jiang, Y., and Ning, W. Y. (2022). The relative importance of niche and neutral processes for the community assembly of subtropical karst forest communities at different spatial scales. *Forests* 13:1930. doi: 10.3390/f13111930

Heino, J., Melo, A. S., Siqueira, T., Soininen, J., Valanko, S., and Bini, L. M. (2015). Metacommunity organisation, spatial extent and dispersal in aquatic systems: patterns, processes and prospects. *Freshw. Biol.* 60, 845–869. doi: 10.1111/fwb.12533

Herrera-Silveira, J. A., and Morales-Ojeda, S. M. (2009). Evaluation of the health status of a coastal ecosystem in Southeast Mexico: assessment of water quality, phytoplankton and submerged aquatic vegetation. *Mar. Pollut. Bull.* 59, 72–86. doi: 10.1016/j.marpolbul.2008.11.017

Ho, T. Y., Quigg, A., Finkel, Z. V., Milligan, A. J., Wyman, K., Falkowski, P. G., et al. (2003). The elemental composition of some marine phytoplankton. *J. Phycol.* 39, 1145–1159. doi: 10.1111/j.0022-3646.2003.03-090.x

Hu, H. J., and Wei, Y. X. (2006). *The freshwater algae of China-systematic, taxonomy and ecology*. Beijing: Science Press. 79–285.

Huang, B., Marchand, J., Thiriet-Rupert, S., Carrier, G., Saint-Jean, B., Lukomska, E., et al. (2019). Betaine lipid and neutral lipid production under nitrogen or phosphorus limitation in the marine microalga Tisochrysis lutea (Haptophyta). *Algal Res.* 40:101506. doi: 10.1016/j.algal.2019.101506

Keck, F., and Lepori, F. (2012). Can we predict nutrient limitation in streams and rivers? *Freshw. Biol.* 57, 1410–1421. doi: 10.1111/j.1365-2427.2012.02802.x

Kim, S., Kim, S., Mehrotra, R., and Sharma, A. (2020). Predicting cyanobacteria occurrence using climatological and environmental controls. *Water Res.* 175:115639. doi: 10.1016/j.watres.2020.115639

Klisarova, D., Gerdzhikov, D., Nikolova, N., Gera, M., and Veleva, P. (2023). Influence of some environmental factors on summer phytoplankton community structure in the Varna Bay, Black Sea (1992–2019). *Water* 15:1677. doi: 10.3390/w15091677

Laland, K., Matthews, B., and Feldman, M. W. (2016). An introduction to niche construction theory. *Evol. Ecol.* 30, 191–202. doi: 10.1007/s10682-016-9821-z

Lewis, M. R., Carr, M. E., Feldman, G. C., Esaias, W., and Mcclain, C. (1990). Influence of penetrating solar radiation on the heat budget of the equatorial Pacific Ocean. *Nature* 347, 543–545. doi: 10.1038/347543a0

Li, B., and Li, X. (2018). Analysis on transportation and conversion of nitrogen and phosphorus during the filtration process in Longhu Lake of Jinjiang River. *Pearl River* 39, 76–80.

Lin, S. (2023). Phosphate limitation and ocean acidification co-shape phytoplankton physiology and community structure. *Nat. Commun.* 14:2699. doi: 10.1038/s41467-023-38381-0

Liu, X., Li, Y., Shen, R. J., Zhang, M., and Chen, F. Z. (2022). Reducing nutrient increases diatom biomass in a subtropical eutrophic lake, China-do the ammonium concentration and nitrate to ammonium ratio play a role? *Water Res.* 218:118493. doi: 10.1016/j.watres.2022.118493

Liu, L., Liu, D. F., Johnson, D. M., Yi, Z. Q., and Huang, Y. L. (2012). Effects of vertical mixing on phytoplankton blooms in Xiangxi Bay of three gorges reservoir: implications for management. *Water Res.* 46, 2121–2130. doi: 10.1016/j.watres.2012.01.029

Liu, H., Sun, K., Liu, X., Yao, R., Cao, W., Zhang, L., et al. (2022). Spatial and temporal distributions of microplastics and their macroscopic relationship with algal blooms in Chaohu Lake, China. *J. Contam. Hydrol.* 248:104028. doi: 10.1016/j.jconhyd.2022.104028

Liu, Z. J., Wang, X. H., Jia, S. Q., and Mao, B. Y. (2023). Multi-methods to investigate spatiotemporal variations of nitrogen-nitrate and its risks to human health in China's largest fresh water Lake (Poyang Lake). *Sci. Total Environ.* 863:160975. doi: 10.1016/j.scitotenv.2022.160975

Ma, X., Johnson, K. B., Gu, B., Zhang, H., Li, G., Huang, X. P., et al. (2022). The in-situ release of algal bloom populations and the role of prokaryotic communities in their establishment and growth. *Water Res.* 219:118565. doi: 10.1016/j.watres.2022.118565

Meunier, C. L., Boersma, M., El-Sabaawi, R., Halvorson, H. M., Herstoff, E. M., van de Waal, D. B., et al. (2017). From elements to function: toward unifying ecological stoichiometry and trait-based ecology. *Front. Environ. Sci.* 5:e2640. doi: 10.3389/fenvs.2017.00018

Mucina, L., Bültmann, H., Dierßen, K., Theurillat, J. P., Raus, T., Čarni, A., et al. (2016). Vegetation of Europe: hierarchical floristic classification system of vascular plant, bryophyte, lichen, and algal communities. *Appl. Veg. Sci.* 19, 3–264. doi: 10.1111/avsc.12257

Mutshinda, C. M., Finkel, Z. V., Widdicombe, C. E., and Irwin, A. J. (2016). Ecological equivalence of species within phytoplankton functional groups. *Funct. Ecol.* 30, 1714–1722. doi: 10.1111/1365-2435.12641

Paerl, H. W., Hall, N. S., and Calandrino, E. S. (2011). Controlling harmful cyanobacterial blooms in a world experiencing anthropogenic and climatic-induced change. *Sci. Total Environ.* 409, 1739–1745. doi: 10.1016/j.scitotenv.2011.02.001

Park, J. Y., Kug, J. S., Badera, J., Rolph, R., and Kwon, M. (2015). Amplified arctic warming by phytoplankton under greenhouse warming. *Proc. Natl. Acad. Sci. U. S. A.* 112, 5921–5926. doi: 10.1073/pnas.1416884112

Pos, E., Guevara, J. E., Molino, J. F., Sabatier, D., Banki, O. S., Pitman, N. C. A., et al. (2019). Scaling issues of neutral theory reveal violations of ecological equivalence for dominant Amazonian tree species. *Ecol. Lett.* 22, 1072–1082. doi: 10.1111/ele.13264

Rao, K., Zhang, X., Wang, M., Liu, J. F., Guo, W. Q., Huang, G. W., et al. (2021). The relative importance of environmental factors in predicting phytoplankton shifting and cyanobacteria abundance in regulated shallow lakes. *Environ. Pollut.* 286:117555. doi: 10.1016/j.envpol.2021.117555

Redfield, A. C. (1960). The biological control of chemical factors in the environment. *Sci. Prog.* 15, 203–209. doi: 10.1086/646891

Rodríguez-Gómez, C. F., Vázquez, G., Papiol, V., Marino-Tapia, I., and Enriquez, C. (2022). Phytoplankton distribution and its ecological and hydrographic controls in two contrasting areas of a stratified oligotrophic system. *Hydrobiologia* 849, 3175–3195. doi: 10.1007/s10750-022-04924-7

Shi, K., Zhang, H., Xu, H., Zhu, G., Qin, B., Huang, C., et al. (2015). Long-term satellite observations of microcystin concentrations in Lake Taihu during cyanobacterial bloom periods. *Environ. Sci. Technol.* 49, 6448–6456. doi: 10.1021/es505901a

Shurin, J. B., Cottenie, K., and Hillebrand, H. (2009). Spatial autocorrelation and dispersal limitation in freshwater organisms. *Oecologia* 159, 151–159. doi: 10.1007/s00442-008-1174-z

Shuwang, X., Zhang, G. D., Li, D. Y., Wen, Y. J., Zhang, G. C., and Sun, J. (2023). Spatial and temporal changes in the assembly mechanism and co-occurrence network of the chromophytic phytoplankton communities in coastal ecosystems under anthropogenic influences. *Sci. Total Environ.* 877:162831. doi: 10.1016/j.scitotenv.2023.162831

Šmilauer, P., and Lepš, J. (2003). *Multivariate analysis of ecological data using Canoco* Cambridge University Press.

Team, R.C (2014). *R: a language and environment for statistical computing* MSOR Connections.

Tian, J., Guo, S. L., Wang, J., Wang, H. Y., and Pan, Z. K. (2022). Preemptive warning and control strategies for algal blooms in the downstream of Han River China. *Ecol. Indic.* 142:109190. doi: 10.1016/j.ecolind.2022.109190

Valencia, R., Foster, R. B., Villa, G., Condit, R., Svenning, J. C., Hernandez, C., et al. (2004). Tree species distributions and local habitat variation in the Amazon: large forest plot in eastern Ecuador. *J. Ecol.* 92, 214–229. doi: 10.1111/j.0022-0477.2004.00876.x

Vello, V., Phang, S. M., Poong, S. W., Lim, Y. K., Ng, F. L., Shanmugam, J., et al. (2023). New report of Halamphora subtropica (Bacillariophyta) from the strait of Malacca and its growth and biochemical characterisation under nutrient deprivation. *Reg. Stud. Mar. Sci.* 62:102947. doi: 10.1016/j.rsma.2023.102947

Vergnon, R., Dulvy, N. K., and Freckleton, R. P. (2009). Niches versus neutrality: uncovering the drivers of diversity in a species-rich community. *Ecol. Lett.* 12, 1079–1090. doi: 10.1111/j.1461-0248.2009.01364.x

Wagner, D. S., Cazzaniga, C., Steidl, M., Dechesne, A., Valverde-Perez, B., and Plosz, B. G. (2021). Optimal influent N-to-P ratio for stable microalgal cultivation in water treatment and nutrient recovery. *Chemosphere* 262:127939. doi: 10.1016/j.chemosphere.2020.127939

Wang, M., Sha, C., Wu, J., Su, J., Wu, J., Wang, Q., et al. (2021). Bacterial community response to petroleum contamination in brackish tidal marsh sediments in the Yangtze River estuary, China. *J. Environ. Sci. (China)* 99, 160–167. doi: 10.1016/j.jes.2020.06.015

Wang, J., Soininen, J., Zhang, Y., Wang, B., Yang, X., and Shen, J. (2011). Contrasting patterns in elevational diversity between microorganisms and macroorganisms. *J. Biogeogr.* 38, 595–603. doi: 10.1111/j.1365-2699.2010.02423.x

Wang, S. X., Wei, L., Wang, S., Chen, L., and Huang, Q. H. (2022). Seasonal changes of phytoplankton community structure and its influencing factors in lakes and reservoirs adjacent to water sources in Shanghai. *J. Environ. Sci. (China)* 34, 1127–1139. doi: 10.18307/2022.0407

Wang, W. G., and Ye, X. (2009). Environmental significance of Longhu lake sediments in the middle and late Holocene, Jinjiang, Fujian. *J. Palaeogeogr.* 11, 348–354.

Wu, S. H., Dong, Y. Z., Stoeck, T., Wang, S. J., Fan, H. N., Wang, Y. X., et al. (2023). Geographic characteristics and environmental variables determine the diversities and assembly of the algal communities in interconnected river-lake system. *Water Res.* 233:119792. doi: 10.1016/j.watres.2023.119792

Xu, Q. S., Huang, M. Q., Yang, S., Li, X. L., Zhao, H. X., Tang, J. L., et al. (2022). Ecological stoichiometry influences phytoplankton alpha and beta diversity rather than the community stability in subtropical bay. *Ecol. Evol.* 12:e9301. doi: 10.1002/ece3.9301

Xu, Y. P., Xiang, Z. L., Rizo, E. Z., Naselli-Flores, L., and Han, B. P. (2022). Combination of linear and nonlinear multivariate approaches effectively uncover responses of phytoplankton communities to environmental changes at regional scale. *J. Environ. Manag.* 305:114399. doi: 10.1016/j.jenvman.2021.114399

Xue, J., Yao, X., Zhao, Z., He, C., Shi, Q., and Zhang, L. (2021). Internal loop sustains cyanobacterial blooms in eutrophic lakes: evidence from organic nitrogen and ammonium regeneration. *Water Res.* 206:117724. doi: 10.1016/j.watres.2021.117724

Yan, X. C., Xu, X. G., Wang, M. Y., Wang, G. X., Wu, S. J., Li, Z. C., et al. (2017). Climate warming and cyanobacteria blooms: looks at their relationships from a new perspective. *Water Res.* 125, 449–457. doi: 10.1016/j.watres.2017.09.008

Yang, S. Q., Gao, X. L., Wang, L. J., Zu, T. X., Wang, D. X., and Luo, G. H. (2021). Phytoplankton community structure and driving factors in typical reservoirs of arid region of Northwest China. *J. Environ. Sci. (China)* 33, 377–387. doi: 10.18307/2021.0207

Zhang, M., Shi, X. L., Yang, Z., Yu, Y., Shi, L. M., and Qin, B. Q. (2018). Long-term dynamics and drivers of phytoplankton biomass in eutrophic Lake Taihu. *Sci. Total Environ.* 645, 876–886. doi: 10.1016/j.scitotenv.2018.07.220

Zhang, M., Zhang, Y. C., Yang, Z., Wei, L. J., Yang, W. B., Chen, C., et al. (2016). Spatial and seasonal shifts in bloom-forming cyanobacteria in Lake Chaohu: patterns and driving factors. *Phycol. Res.* 64, 44–55. doi: 10.1111/pre.12112

Zhao, Y. D., He, X. D., Chen, L., Ding, X. F., Li, M. Q., Xu, P. Y., et al. (2019). Features on N/P ratio of plants with different functional groups between two types of steppe in semi-arid area. *Sci. Cold Arid. Reg.* 11, 371–381.

Frontiers in Marine Science

Explores ocean-based solutions for emerging global challenges

The third most-cited marine and freshwater biology journal, advancing our understanding of marine systems and addressing global challenges including overfishing, pollution, and climate change.

Discover the latest Research Topics

See more →

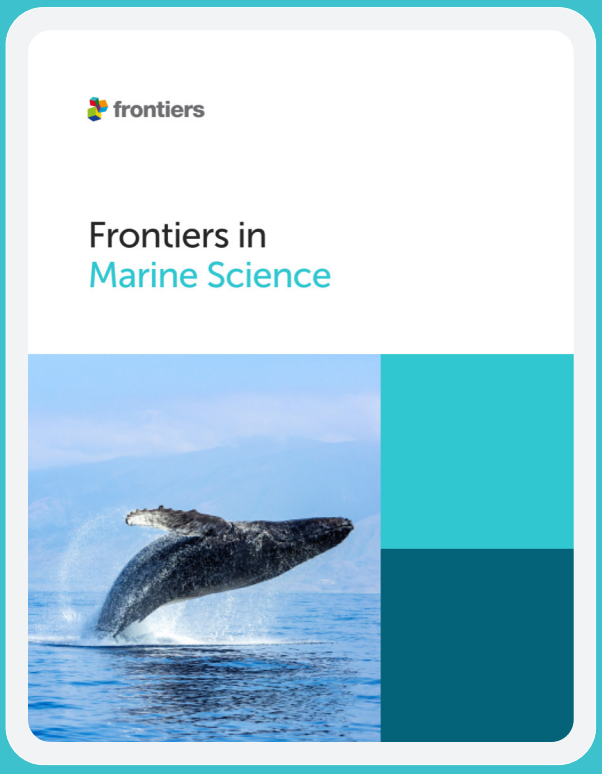

Frontiers

Avenue du Tribunal-Fédéral 34
1005 Lausanne, Switzerland
frontiersin.org

Contact us

+41 (0)21 510 17 00
frontiersin.org/about/contact